

MICHAL LEBL

# Peptides

BREAKING AWAY:  
THE PROCEEDINGS OF THE TWENTY-FIRST  
AMERICAN PEPTIDE SYMPOSIUM



INDIANA  
UNIVERSITY  
BLOOMINGTON

JUNE 7-12  
2009

21<sup>ST</sup> AMERICAN  
PEPTIDE  
SYMPOSIUM

# **Peptides: Breaking Away**

Proceedings of the Twenty-First  
American Peptide Symposium

# **Peptides: Breaking Away**

Proceedings of the Twenty-First American Peptide  
Symposium

# Peptides: Breaking Away

Proceedings of the  
Twenty-First American Peptide Symposium  
June 7-12, 2009, Bloomington, IN, U.S.A.

Edited by

***Michal Lebl***

*Prompt Scientific Publishing*

*San Diego, CA*

*michallebl@gmail.com*

**American Peptide Society**  
**San Diego**



A C.I.P. Catalogue record for this book is available from the Library of Congress.

ISBN 0-9715560-3-2

---

Published by American Peptide Society

Sold and distributed by [www.lulu.com](http://www.lulu.com)

Copyright ©2009 American Peptide Society

All rights reserved. No part of the material protected by this copyright notice may be reproduced or utilized in any form or by any means, electronic or mechanical, including photocopying, recording or by any information storage and retrieval system, without written permission from the copyright owner.

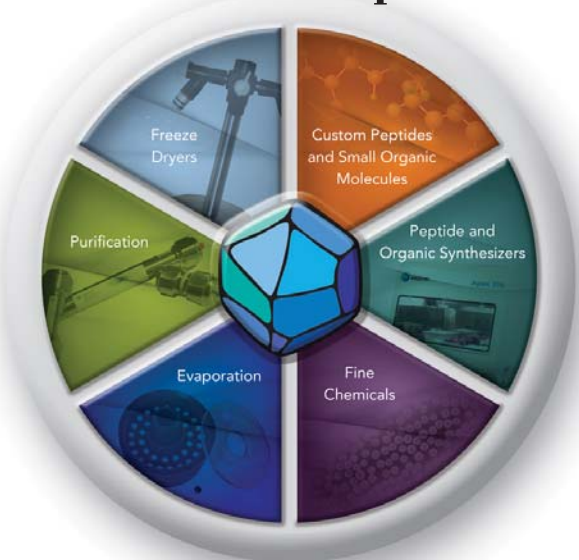
Produced by Prompt Scientific Publishing,  
[www.promptpublishing.com](http://www.promptpublishing.com), San Diego, U.S.A.



# aapptec

## aapptec – Single Source Solution for the Peptide Chemist

- Custom Peptides
- Fmoc Amino Acids (L, D, and OPfp esters)
- Boc Amino Acids (L and D)
- Z Amino Acids (L and D)
- Beta-homo Amino Acids
- Amino Acid Alcohols
- Unusual Amino Acids (Homoamino acids, Substituted Phe, Substituted Tyr, N-methyl amino acid, etc.)
- Pseudoproline Dipeptides (Ser or Thr based)
- Coupling Reagents (HATU, HBTU, HCTU, TBTU.....etc)
- Resins (Wang, Rink Amide, Merrifield, 2-Cl-Trt Chloride,.....etc.)
- Preloaded Resins (Preloaded Wang, Preloaded 2-Cl-Trt)
- Catalog Peptides (Over 3000 peptides)



aapptec also supplies HPLC columns, freeze-drying equipment, vacuum concentrators and other equipment for peptide synthesis.

**aapptec - Innovative Technology for the World of Peptide Science**

aapptec 6309 Shepherdsville Road Louisville, KY 40228

Tel: 502.968.2223 Fax: 502.968.3338 [www.aapptec.com](http://www.aapptec.com)



aapptec



Known for its quality, speed, flexibility and economic pricing, aapptec is an industrial leader in production of automated peptide synthesizers since 1983. aapptec's synthesizers offer a wide range of capabilities, from single peptide to multiple peptide synthesis, scale-up and peptide libraries. These capabilities, along with zero dead volume and no cross contamination, provide the highest quality peptides.

Call aapptec today for a FREE quote and more information on our products.

aapptec 6309 Shepherdsville Road Louisville, KY 40228

Tel: 502.968.2223 Fax: 502.968.3338 [www.aapptec.com](http://www.aapptec.com)

## Introduction

We had the distinct honor to jointly host the 21<sup>st</sup> Symposium of the American Peptide Society on the campus of Indiana University in Bloomington, Indiana. The meeting theme was “*breaking away*”, embracing the spirit of the scientific and social program we witnessed. The University setting was reminiscent of the Symposia from earlier years in the formative period of the Peptide Society. What was especially unique about this 2009 meeting was the level of commercial participation from pharmaceutical and biotechnology companies that complemented the traditional academic excellence. The unprecedented interest in the use of peptides as drugs separates this period from any other in the history of the Society and it is a direct result of the advances in core peptide chemistry and biology that have been achieved in recent years.

The meeting opened with a Sunday social gathering at the center of the Indiana University campus. Monday consisted of a full day focused on advances in chemical biology and receptor signaling. The day concluded with the Merrifield lecture given by Stephen Kent and two associated lectures that extended the scope of advances in chemical synthesis. Tuesday lectures focused predominately on advances in rational design, analysis and material aspects of peptide chemistry. It concluded with a first ever session co-sponsored by the American Association of Pharmaceutical Sciences (AAPS) pertaining to technology directed at accelerating the transition of peptides from the lab to the clinic. Wednesday was highlighted by the presentation of the Makineni lecture by William DeGrado, the first Goodman award lecture by Charles Deber, and a set of lectures pertaining to advances in biosynthesis with non-native amino acids.

The Symposium program moved to peptide biology and pharmacology in the last two days of the meeting. A particular emphasis was placed on capturing the unprecedented success currently being experienced in peptide-based therapeutics. Thursday represented an array of several therapeutic areas, most notably neuroscience, infectious diseases and cancer. Metabolic diseases with a particular emphasis on obesity and the related disorders in glucose and lipids were the focus of the last day. At the end of each of the first four days were poster sessions that stimulated communication among all participants and highlighted the importance of young investigator participation.

The social program was abundant and diverse. Whether your primary interest was the arts, athletics, or outdoor activities, there was something to meet all needs. The campus and the Bloomington community with its easily accessible open spaces and attractive architecture provided a stimulating social environment for the multiple activities. A few items of particular note were the Wednesday night social event at the Musical Arts Center where the renowned Jacobs School of Music staged a performance exclusively for Symposium guests. Additionally, the Thursday night social banquet themed, *Mix, Mingle & Move, an evening of Martinis, Moonshine and Music*, is destined to be one to that will be remembered as unlike anything previously experienced at an APS meeting.

It has been a pleasure to host this late spring week of science and entertainment. We are deeply grateful to all of the individuals who helped in the assembly, funding and operations associated with this event. The dedicated University-based conference staff, numerous volunteers and especially conference director Mary Morgan made seminal contributions to the success of this meeting. Of course, we wish to thank all of you for helping us create such a memorable Symposium.



Richard DiMarchi



Henry Mosberg

## Editor's Remarks

This year's proceedings production was a test about readiness of American Peptide Society members to accept the new technologies allowing the book to be available three months after the symposium, or earlier. On top of the speed of production, reduction of the book cost was an additional goal. Manuscripts were accepted through the internet page, entered into the database which allowed to create indexes on the fly and simplified communication with authors. Processed manuscripts were available for proofing – helping us to correct blunders made by us and authors in the rush to deliver the book as soon as possible. The finalized book was available on the website for downloading 10 weeks after the symposium. The CD version was distributed to all APS members by kind sponsorship by AAPTEC. And the “real book” is available from “just in time” printing process both in hard bound and paperback version. Due to the fact that the American Peptide Society is a nonprofit organization, there is no margin charged for the book, and all members can order it for production cost (we recommend to compare the price with the price of previous symposium volumes).

Our thanks go to all authors who delivered manuscripts of a high technical quality before the deadline. Problems with authors trying to “squeeze in” three pages of text on two pages of manuscript, or fixing their problems by modifying the template of the text file, were diligently solved by the team of technical editors, who worked very long hours to make sure that the book goes to production three weeks after the last manuscript is delivered. (Actually, the last manuscript was delivered just three days before the book went to production – you know who you are...). Due to the time constraints, we were not able to redo the graphical components of the manuscripts – graphs and illustrations – authors have to understand that some of the graphs looking good at the poster size are far from ideal for book page size. If you like the book cover, you should know that it was designed by our young perspective graphic designer, Alexandria Ferguson.

Our company, Prompt Scientific Publishing, produced the proceedings of the 17<sup>th</sup> and 18<sup>th</sup> American Peptide Symposia using the classical book printing and distribution processes. The new way of delivering the information promptly and economically, introduced by the proceedings of 21<sup>st</sup> APS, may not be universally accepted – for example, the hard bound books of the last symposia were undisputably of higher quality than paperback version of this proceedings, however, we believe that the promptness of the production and multitude of distribution avenues more than compensates for its appearance. Our ambition for the future proceeding volumes is that the book is delivered at the time of the symposium. Using the modern technologies and dedicated effort of our team, it is definitely realistic goal. We would like to hear your opinion.

Roseann Story-Lebl  
Michal Lebl

## Message from the President of the American Peptide Society

The 21<sup>st</sup> American Peptide Symposium was the most recent successful addition to the American Peptide Society's series of biennial symposia. An international group of 550 registrants contributed to the high quality scientific program documented in the present volume. Thank you to all lecturers and poster presenters for your excellent contributions. I congratulate co-chairs Richard DiMarchi and Henry Mosberg along with their staff and the organizing and program committees for a terrific meeting, and I thank them for all of their hard work and dedication. Thank you also to all of our sponsors and exhibitors. Finally, thank you to immediate Past President Richard Houghton for his oversight of this effort.

There were several special events from the Symposium that I would like to highlight. The American Peptide Society's Bruce Merrifield Award, which recognizes outstanding career achievements in peptide science, was presented to Stephen B.H. Kent of the University of Chicago. Steve's award lecture described his exciting work on "Inventing Chemistries to Reveal How Proteins Work". The Makineni Lecture, which honors long time peptide science supporter Rao Makineni, was presented by William DeGrado of the University of Pennsylvania. The inaugural Murray Goodman Award was presented to Charles Deber of Hospital for Sick Children and the University of Toronto. The meeting also featured the satellite symposium "Peptides in Metabolic Diseases." The scientific quality was high and the competition was keen in the Young Investigators Poster Competition. Symposium social events, such as "Bowling, Billiards, Movie and More," "Passport to Bloomington," "Music at the MAC," and "Mix, Mingle and Move" provided enjoyable opportunities to meet colleagues.

I will now make a few comments about the American Peptide Society, which is committed to advancing and promoting the knowledge of the chemistry and biology of peptides and proteins. I invite you to visit our web site at [www.americanpeptidesociety.org](http://www.americanpeptidesociety.org) to learn more about the Society and the benefits of membership. The Society has a dedicated Council of 15 individuals elected by Society members. Society Officers are also elected by the membership. There are several active committees, which administer areas such as awards, membership, publications, and student affairs. The official journal of the Society is *Biopolymers – Peptide Science*, and all members receive a subscription. The new editor of the journal is Joel Schneider who succeeded Lila Gierasch at the beginning of 2009. The journal publishes original research and review articles, and will feature research publication awards beginning in 2010. Dr. Schneider and I encourage you to submit your best work to our journal. The American Peptide Society also actively participates in activities of the broader research community through our associate membership in the Federation of American Societies for Experimental Biology (FASEB).

My term as President of the Society runs from June, 2009 to June, 2011. During this period, one of my priorities is to increase the membership of the Society and enhance the benefits to members. The Society will be exploring the sponsorship of peptide-focused sessions at national American Chemical Society meetings and at the annual Experimental Biology meetings. The Society will increase the visibility of its Awards. The Society will explore the representation of peptide-based research on specific study sections within the Center for Scientific Review of the NIH. Please contact me if you would like to get involved in any of these activities.

The American Peptide Society is already planning for future symposia. The 22<sup>nd</sup> American Peptide Symposium will be held June 25 - 30, 2011 at the Sheraton Hotel and Marina in San Diego. Co-chairs Phil Dawson and Joel Schneider are actively assembling the scientific program based on the theme "Peptides – The Way to Go".

It was a pleasure to interact on a scientific and personal level with many of you at the American Peptide Symposium in Bloomington. I look forward to working with you on American Peptide Society activities and to seeing you in San Diego in 2011. My best wishes for success in your professional endeavors.

Gregg B. Fields, Ph.D.  
University of Texas Health Science Center  
July 31, 2009

# **21<sup>st</sup> AMERICAN PEPTIDE SYMPOSIUM**

**June 7-12, 2009  
Bloomington, Indiana**

**Co-Chairs**

**Richard DiMarchi**  
Chemistry Department  
Indiana University  
Bloomington, IN 47405

**Henry I. Mosberg**  
College of Pharmacy  
University of Michigan  
Ann Arbor, MI 48109-1065

### **The Student Affairs Committee**

<b>Jungmo Ahn, Ph.D.</b>	University of Texas, Dallas
<b>Audrey Kelleman, Ph.D.</b>	Senn Chemical
<b>Zach Kaur</b>	Indiana University
<b>Beth Girnys</b>	University of Michigan
<b>Tae-Kyung Lee</b>	University of Texas, Dallas
<b>Wendy Hartsock</b>	Kansas University
<b>Timothy Reichart</b>	Scripps Research Institute
<b>Carine Bourguet</b>	University of Montreal
<b>Erica Haslach</b>	University of Florida
<b>Mike Giano</b>	University of Delaware

### **The Travel Award Committee**

<b>Carrie Haskell-Leuvano, Ph.D., (Chair)</b>	University of Florida
<b>Gregg Fields, Ph.D.</b>	UTHSCSA
<b>Philip Dawson, Ph.D.</b>	Scripps research Institute
<b>Jungmo Ahn, Ph.D.</b>	University of Texas, Dallas
<b>Audrey Kelleman, Ph.D.</b>	Senn Chemical



## **List of 21<sup>st</sup> American Peptide Symposium Sponsors**

The 21<sup>st</sup> American Peptide Symposium was made possible through the generous support of the following organizations:

### **MAJOR SPONSORS**

Cook Pharmica  
Eli Lilly and Company  
Indiana University College of Arts and Sciences  
Marcadia Biotech

### **DAY SPONSORS**

Roche  
Zydus Cadila Healthcare

### **GOLD SPONSORS**

aapptec  
Polypeptide Laboratories

### **SILVER SPONSORS**

Jupiter Bioscience, Ltd.  
Peptisyntha

### **BRONZE SPONSORS**

Aileron Therapeutics  
Amylin Pharmaceuticals  
AnaSpec, Inc.  
Bachem Americas  
Baxter  
Indiana University Office of the Vice-President for Engagement  
& Indiana University Research and Technology Corporation  
Midwest Bio-Tech  
New England Peptide  
Senn Chemicals

### **ADDITIONAL SPONSORS**

Escom Science Foundation  
5AM Ventures  
New England BioLabs  
Novo Nordisk  
RSP Amino Acids  
University of Michigan  
Wyeth Research

## List of 21<sup>st</sup> American Peptide Symposium Exhibitors

aapptec	FASEB
Activotec	Intavis
Almac Sciences	IRIS Biotech
AmbioPharm, Inc	Jupiter Bioscience
American Peptide Company	Neuland Laboratories
American Peptide Society	New England Peptide
AnaSpec	Peptides International/Peptide Institute
Bachem Americas	Peptisyntha
Baxter	Phenomenex
BioConvergence	Polypeptide Laboratories
Biosynthesis	Protein Technologies
Biotage	Rapp-Polymere GmbH
CBL Biopharma	Reanal
CEM Corporation	Senn Chemicals
Chem-Impex International	Student Affairs Committee
CPC Scientific	Sussex Research
Cook Pharmica	Synthetech
Covidien Mallinckrodt	Tianjin Nankai Hecheng
CreoSalus	Unigene Laboratories
Crown Bioscience	Union Biometrica
C S Bio	Wiley-Blackwell
DAISO	YMC America
EMD Chemicals	Zeochem

## **The American Peptide Society**

The American Peptide Society (APS), a nonprofit scientific and educational organization founded in 1990, provides a forum for advancing and promoting knowledge of the chemistry and biology of peptides. The approximately one thousand members of the Society come from North America and from more than thirty other countries throughout the world. Establishment of the American Peptide Society was a result of the rapid worldwide growth that has occurred in peptide-related research, and of the increasing interaction of peptide scientists with virtually all fields of science.

A major function of the Society is the biennial American Peptide Symposium. The Society also sponsors the Journal of Peptide Research and Biopolymers (Peptide Science), recommends awards to outstanding peptide scientists, works to foster the professional development of its student members, interacts and coordinates activities with other national and international scientific societies, sponsors travel awards to the American Peptide Symposium, and maintains a website at [www.ampepsoc.org](http://www.ampepsoc.org).

The American Peptide Society is administered by Officers and Councilors who are nominated and elected by members of the Society. The Officers are: President: Gregg B. Fields, University of Texas Health Science Center, President Elect: Ben Dunn, University of Florida, Secretary: Robin Offord, University of Geneva, Treasurer: Pravin Kaumaya, The Ohio State University, Past President: Richard A. Houghten, Torrey Pines Institute for Molecular Studies. The councilors are: Maria Bednarek, MedImmune Ltd, Phil Dawson, Scripps Research Institute, Charles Deber, Hospital for Sick Kids, Ernest Giralt, Barcelona Biomedical Research Institute, Carrie Haskell-Luevano, University of Florida, Jeffery W. Kelly, Scripps Research Institute, Michal Lebl, Illumina Inc., DeAnna Wiegandt Long, Peptides International, John Mayer, Eli Lilly and Co., Henry I. Mosberg, University of Michigan, Tom Muir, Rockefeller University, Joel Schneider, University of Delaware.

Membership in the American Peptide Society is open to scientists throughout the world who are engaged or interested in the chemistry or biology of peptides and small proteins. Categories of membership include Active Member, Associate Member, Student Member, Emeritus Member and Honorary Member. For application forms or further information on the American Peptide Society, please visit the Society web site at [www.americanpeptidesociety.org](http://www.americanpeptidesociety.org) or contact Becci Totzke, Association Manager, P.O.Box 13796, Albuquerque, NM 87192, U.S.A., tel (505) 459-4808; fax (775) 667-5332; e-mail "[APSmanager@americanpeptidesociety.org](mailto:APSmanager@americanpeptidesociety.org)".

## American Peptide Symposia

<i><b>Symposium Year</b></i>	<i><b>Chair (s)</b></i>	<i><b>Location</b></i>
1st 1968	Saul Lande & Boris Weinstein	Yale University New Haven, CT
2nd 1970	F. Merlin Bumpus	Cleveland Clinic Cleveland, OH
3rd 1972	Johannes Meienhofer	Children's Cancer Research Foundation, Boston, MA
4th 1975	Roderich Walter	The Rockefeller University New York, NY
5th 1977	Murray Goodman	University of California-San Diego, San Diego, CA
6th 1979	Erhard Gross	Georgetown University Washington, DC
7th 1981	Daniel H. Rich	University of Wisconsin- Madison, Madison, WI
8th 1983	Victor J. Hruby	University of Arizona Tucson, AZ
9th 1985	Kenneth D. Kopple & Charles M. Deber	University of Toronto Toronto, Ontario, Canada
10 <sup>th</sup> 1987	Garland R. Marshall	Washington University St. Louis, MO
11 <sup>th</sup> 1989	Jean E. Rivier	University of California-San Diego, San Diego, CA
12 <sup>th</sup> 1991	John A. Smith	Massachusetts Institute of Technology, Cambridge, MA
13 <sup>th</sup> 1993	Robert S. Hodges	Edmonton Convention Center Edmonton, Alberta, Canada
14 <sup>th</sup> 1995	Pravin T.P. Kaumaya	The Ohio State University Columbus, OH
15 <sup>th</sup> 1997	James P. Tam	Nashville Convention Center Nashville, TN
16 <sup>th</sup> 1999	George Barany & Gregg B. Fields	Minneapolis Convention Center, Minneapolis, MN
17 <sup>th</sup> 2001	Richard A. Houghten & Michal Lebl	Town and Country Resort Hotel, San Diego, CA
18 <sup>th</sup> 2003	Michael Chorev & Tomi K. Sawyer	Marriott Copley Place Boston, MA
19 <sup>th</sup> 2005	Jeffery W. Kelly & Tom W. Muir	Town and Country Resort Hotel, San Diego, CA
20 <sup>th</sup> 2007	Emanuel Escher & William D. Lubell	Palais des congres de Montreal, Quebec, Canada
21 <sup>st</sup> 2009	Richard DiMarchi & Hank Mosberg	Indiana University, Bloomington, Indiana

# The Merrifield Award

(previously the Alan E. Pierce Award)

The Merrifield Award was endowed by Dr. Rao Makineni in 1997, in honor of R. Bruce Merrifield (1984 Nobel Prize in Chemistry), inventor of solid phase peptide synthesis. Previously, this award had been called the Alan E. Pierce Award and was sponsored by the Pierce Chemical Company from 1977-1995.

## Stephen B. H. Kent



The American Peptide Society is very pleased to announce that Stephen Kent of the University of Chicago has been chosen to receive the R. Bruce Merrifield Award for 2009. Kent is cited for ‘the development and application of innovative and robust methods for the total chemical synthesis of enzymes’. This award will be presented during the 21st APS Symposium to be held in Bloomington, Indiana on June 7-12, 2009.

Stephen Kent has pioneered modern methods for the total chemical synthesis of proteins, and has used these novel synthetic methods for unprecedented studies of protein structure and function.

Kent’s early work focused on fundamental studies of methods for the chemical synthesis of peptides, and on the application of chemical peptide synthesis to studies of the hepatitis B virus and the human immunodeficiency virus. In 1989, this work culminated in the use of total chemical synthesis to prepare protein used for the determination, by crystallography collaborators, of the original X-ray structures of the HIV-1 protease molecule. These data were made freely available and formed the basis for the highly successful worldwide programs in structure based drug design that culminated in the development of the ‘protease inhibitor’ class of AIDS therapeutics.

The total chemical synthesis of proteins, especially enzymes, was one of the grand challenges in 20th century chemistry. In 1992, Kent effectively solved this problem by introducing the ‘chemical ligation’ principle, the use of chemoselective reaction for the covalent condensation of unprotected peptides in aqueous solution. In 1994, Kent and his colleagues at The Scripps Research Institute extended this concept to ‘native chemical ligation’, the amide-forming thioester-mediated covalent condensation of two unprotected peptides at a cysteine residue. Chemical ligation methods are a break-through in protein science and for the first time have led to practical, reproducible, and general synthetic access to the world of proteins.

In 2003, Kent and his industry colleagues reported the systematic design and total chemical synthesis of the neoglycoprotein ‘synthetic erythropoiesis protein’, an improved version of erythropoietin. Synthetic EPO contained a polypeptide chain of 166 amino acid residues and had two covalently attached branched glycan-mimetics, homogeneous polymer entities of defined molecular structure each carrying four negative charges. Synthetic erythropoiesis protein is the largest synthetic protein construct ever made, with a molecular mass of 50,825 Daltons; it displayed full biological activity and improved duration of action in vivo.

The principal focus of the Stephen Kent laboratory at The University of Chicago is to understand the chemical basis of protein function, particularly enzyme catalysis, and to demonstrate that knowledge by the design and construction of protein molecules with novel properties. Kent and his colleagues have continued to develop improved synthetic chemistries for the study of proteins. These include ‘one pot’ methods (2004), and novel catalysts for native chemical ligation based on detailed mechanistic studies (2007). In 2006, the Kent lab introduced ‘kinetically controlled ligation’, a method that has enabled the fully convergent total chemical synthesis of large protein molecules, including the crystalline fully active enzyme molecules human lysozyme and a covalent-dimer form of the HIV-1 protease containing a 203 amino acid residue polypeptide chain. In 2008, the Kent laboratory reported the use of racemic protein crystallography for the determination of novel molecular structures, using mirror image proteins prepared by total chemical synthesis to enable crystallization of difficult-to-crystallize proteins and to facilitate the determination of their X-ray structures by direct methods.

2009 – Stephen Kent, University of Chicago  
2007 – Isabella Karle, Naval Research Laboratory, D.C.  
2005 – Richard A. Houghten Torrey Pines Institute for Molecular Studies  
2003 – William F. DeGrado, University of Pennsylvania  
2001 – Garland R. Marshall, Washington University Medical School  
1999 – Daniel H. Rich, University of Wisconsin-Madison  
1997 – Shumpei Sakakibara, Peptide Institute, Inc.  
1995 – John M. Stewart, University of Colorado-Denver  
1993 – Victor J. Hruby, University of Arizona  
1991 – Daniel F. Veber, Merck Sharp & Dohme  
1989 – Murray Goodman, University of California-San Diego  
1987 – Choh Hao Li, University of California-San Francisco  
1985 – Robert Schwyzler, Swiss Federal Institute of Technology  
1983 – Ralph F. Hirschmann, Merck Sharp & Dohme  
1981 – Klaus Hofmann, University of Pittsburgh, School of Medicine  
1979 – Bruce Merrifield, The Rockefeller University  
1977 – Miklos Bodansky, Case Western Reserve University

# The 2009 Makineni Lecture Award

Endowed by PolyPeptide Laboratories and Murray and Zelda Goodman (2003)

## William F. DeGrado



The 2009 Makineni Lectureship is meant to recognize a recent scholarly contribution of broad significance, and Bill DeGrado's 2008 *Nature* paper entitled "Structural basis for the function and inhibition of an influenza virus proton channel" is a stellar example of high-impact peptide science. The M2 protein from influenza virus self-assembles in a host cell membrane to form a tetramer, which enables protons to cross the membrane. DeGrado's lab (and many others) has studied this protein for some time. The 2008 *Nature* paper reports the crystal structures of two 25-mer peptides that correspond to the membrane-spanning alpha-helical segment of the M2 protein. In both cases the peptides form a four-helix bundle that represents the proton channel region of the native M2 tetramer.

This work is highly significant because of insights regarding M2 channel assembly, function and inhibition (in one of the two crystal structures an antiviral agent blocks the center of the channel). Perhaps even more important, however, is the fact that this work represents the first example in which the transmembrane segment of an integral membrane protein has been structurally characterized at atomic resolution via crystallography. This monumental achievement is likely to inspire related studies in many groups, which will ultimately bring our understanding of membrane protein structure and function to new levels of sophistication. The first crystal structure of a membrane protein led to the award of the 1987 Nobel Prize, because this accomplishment was viewed as leading the way to many more structures of membrane proteins. Water-soluble peptides of medium length (10-40 residues) are typically much more difficult to crystallize than are full-length soluble proteins. This trend is likely to apply as well to medium-length membrane-embedded peptides, relative to membrane proteins. Thus, DeGrado's goal of growing high-quality crystals of M2 transmembrane peptides was extremely courageous (one might have said "foolhardy" at the time he began); this goal would probably not even have been imagined by most workers in the field because success seemed so unlikely.

The importance of acquiring high-resolution structural data for self-associating trans-membrane segments of embedded proteins cannot be overstated. Interactions among such segments play crucial roles in determining the identity, geometry and stoichiometry of membrane protein assemblies. These assemblies play vital roles in normal and pathological cellular physiology and in the behavior of infectious agents. Many integral membranes involved in signal transduction, for example, contain single-pass helical segments that link an extracellular receptor domain to an intracellular effector domain (e.g., a tyrosine kinase domain). There is good evidence that such helical segments have intrinsic propensities for homo- and/or heteroassociation, and these association phenomena play a crucial role in normal signaling as well in aberrant signaling that can lead to development of disease. Our understanding of physiologically important interactions among intrinsic membrane proteins has been hampered by our lack of high-resolution structural information for the associated states. DeGrado's stunning success with M2-derived integral membrane peptides suggests that this deficiency of structural data will soon be remedied.

2009 - William DeGrado, University of Pennsylvania

2007 - Ronald T. Raines, University of Wisconsin - Madison

2005 - Robin E. Offord, Centre Medical Universitaire, Switzerland

2003 - James P. Tam, Vanderbilt University

# The 2009 Murray Goodman Scientific Excellence & Mentorship Award

The Goodman Award recognizes an individual who has demonstrated career-long research excellence in the field of peptide science. In addition, the selected individual should have been responsible for significant mentorship and training of students, post-doctoral fellows, and/or other co-workers. The Awards Committee may also take into account any important contributions to the peptide science community made by the candidate, for example through leadership in the American Peptide Society and/or its journals. Endowed by Zelda Goodman (2007).

## Charles M. Deber



The announcement that Dr. Charles M. Deber, Professor of Biochemistry at the University of Toronto and Acting Head of the Division of Molecular Structure and Function at the Research Institute Hospital for Sick Children at the University of Toronto, was the first recipient of the Goodman Award of the American Peptide Society is certainly well deserved recognition of Charlie's many scientific contributions to peptide and protein science and to the American Peptide Society.

Professor Deber is known worldwide for his seminal research on the structure and function of membrane peptides and proteins, and in the examination of disease states that involve misfolding of membrane proteins. At the more fundamental level he was among the first to recognize that peptide and protein folding in membranes had fundamental differences from peptide and protein folding in aqueous environments. This led to a critical re-evaluation of the structural properties in amino acids in proteins that are in membrane environments, which has provided new tools for the design of membrane peptides and proteins. Among these tools, the web based TM Finder Program is a most valuable tool, available worldwide.

As a mentor and teacher, Dr. Deber's contributions also have been exemplary. He teaches widely acclaimed courses from large undergraduate courses, to advanced Chemistry courses for graduate students. For his excellent undergraduate teaching he received the W.T. Aikins Award from the University of Toronto. He has mentored more than 60 graduate students and postdoctoral fellows, many of who have gone on to have outstanding careers in academia and industry.

Finally, Charlie has made many outstanding contributions in service to our field worldwide. In addition to being President of the APS from 1991-1993, he has been a long time Editor of Peptide Science, on the editorial board of several international journals in our field, and has organized or helped organize several international conferences.

The Murray Goodman Scientific Excellence and Mentorship Award is well-deserved recognition for the above and many other contributions.

2009 – Charles M. Deber, University of Toronto, Hospital for Sick Children



# Young Investigators' Poster Competition

## Judges

Paul Alewood	Satish Joshi
Maria Bednarek	Ashok Khatri
Annette Beck-Sickinger	Teresa Kubiak
Ashraf Brik	Kit Lam
Ronald Bowsher	Tom Lobl
Gerardo Byk	Derek Maclean
Weibo Cai	Lenore Martin
Julio Camarero	Palgunachari Mayakonda
Erin Carlson	John Mayer
Predrag Cudic	Bradley Nilsson
Juan Del Valle	Sue O'Dorisio
Ben Dunn	Laszlo Otvos
Sebastian Dziadek	Laurie Parker
Emanuel Escher	Shai Rahimipour
Nick Fisk	Thomas Tolbert
Joseph Garlich	John Wade
Paolo Grieco	Harry Wang
Ryan Holder	Oliver Zerbe
Mark Jarosinski	Lianshan Zhang
Jiri Jiracek	

## Winners

Jessica Anand	University of Michigan, Ann Arbor
Leah Cohen	College of Staten Island, CUNY
Arnab De	Columbia University Medical Center
David Dietrich	University of British Columbia
Reena Halai	University of Queensland
Sonia Henriques	University of Queensland/ University of Lisbon
Gary Kemp	London School of Pharmacy
John Kulp	Naval Research Laboratory
Burkhardt Laufer	Technical University of Munich
Piotr Mroz	Indiana University
Radhika Nargarkar	University of Delaware
David Przybyla	Purdue University
Nir Qvit	Stanford University
Irene Shu	University of Washington
Pauline Tan	Ohio State University
A. Pernille Tofteng	University of Copenhagen
Yanyan Zhang	Ohio State University

## Peptide Society Travel Grants

Jessica P. Anand, University of Michigan (Ann Arbor)  
Emilia Antolikova, Institute of Organic Chemistry and Biochemistry  
De Arnab, Columbia University Medical Center  
Jason Arsenault, University of Sherbrooke  
Kajal A Bhimani, University of Texas (at Dallas)  
Nina Bionda, Florida Atlantic University  
Nicolas Boutard, University of Montreal  
Diego Brancaccio, University of Naples (Frederico II)  
Monica Branco, University of Delaware  
Rui Chen, Indiana University (Bloomington)  
Amit Choudhary, University of Wisconsin (Madison)  
Leah S. Cohen, College of Staten Island (CUNY)  
Matteo De Poli, University of Padova  
Channa De Silva, University of Arizona  
David J. Dietrich, University of British Columbia  
Salvatore Di Maro, University of Texas (at Dallas)  
Tatiana Moreira Domingues, Federal University of Sao Paulo  
Ebele Ezeigwe, London School of Pharmacy  
Reena Halai, University of Queensland (St. Lucia)  
Marcus P.D. Heatfield, Creighton University  
Sonia Henriques, University of Queensland (St. Lucia)  
Ziqing Jiang, University of Colorado (Denver)  
John Paul Juliano, Monash University  
Gary C. Kemp, London School of Pharmacy  
Isuru Ransiri Kumarasinghe, University of Arizona  
Huiyuan Li, University of California (Los Angeles)  
Stefania Malfi, University of Naples (Frederico II)  
Kalyaneswar Mandal, University of Chicago  
Molly Martin, University of Iowa  
Marta Natividade Crizol Martins, Federal University of Sao Paulo  
Eunice Murage, University of Texas (at Dallas)  
Radhika Nagarkar, University of Delaware  
Elke Otto, Institute of Advanced Study  
Sonalika Vijaykumar Pawar, Katholieke Universiteit Leuven  
Caroline Proulx, University of Montreal  
Hongchang Qu, University of Pennsylvania  
Nir Qvit, Stanford University  
Michal Richman, Bar-Ilan University  
Luisa Ronga, University of Montreal  
David Sabatino, University of Montreal  
Diganta Sarma, Kyoto Pharmaceutical University  
Karbalae-Mohammad Shahrbanoo, Tarbiat Modares University  
Fazel Shanbanpoor, University of Melbourne  
Irene Shu, University of Washington  
David Singer, Leipzig University

Anamika Singh, University of Florida  
Chamdao Sinthuvanich, University of Delaware  
Daniel J. Smith, University of Delaware  
Subramanyam J. Tantry, College of Staten Island (CUNY)  
Yat T. Tang, Washington University in St. Louis  
Atsuhiko Taniguchi, Kyoto Pharmaceutical University  
Theresa K. Tiefenbrunn, The Scripps Research Institute  
Vladimir Torbeev, University of Chicago  
Claire Winsor, University of Surrey  
Joanna M. Wojnar, University of Chicago  
Sandra Lynn Veech, Ramapo College of New Jersey  
Taku Yoshiya, Kyoto Pharmaceutical University

# Contents

Introduction	vii
Editor's Remarks	viii
People Behind Symposium	x
Symposium Sponsors and Exhibitors	xii
American Peptide Society	xiv
American Peptide Symposia	xv
The Merrifield Award: Stephen B.H. Kent	xvi
The Makineni Lecture Award: William F. DeGrado	xviii
The 2009 Murray Goodman Scientific Excellence & Mentorship Award: Charles M. Deber	xix
Young Investigators' Poster Competition	xx
Peptide Society Travel Grants	xxi
Contents	xxiii

## Merrifield Award Lecture

Chemical Protein Synthesis - Inventing New Chemistries to Reveal How Proteins Work <i>Stephen B.H. Kent</i>	3
--	---

## Peptide Synthesis and Biosynthesis, Peptidomimetics, Peptide Libraries and Chemical Diversity

Synthesis of Optically Active Anti-beta-Substituted gamma,delta-Unsaturated Amino Acids Via Asymmetric Thio-Claisen Rearrangement <i>Zhihua Liu, Hongchang Qu, Xuyuan Gu, Kwang-Soo Lee, Bryan Grossman, Vlad K. Kumirov, Victor J. Hruby</i>	11
O-Acyl Isopeptide Method: Toward an Efficient Chemical Preparation of Peptides/Proteins Using Racemization-Free Segment Condensation Method <i>Taku Yoshiya, Hiroyuki Kawashima, Youhei Sohma, Tooru Kimura, Yoshiaki Kiso</i>	13
Racemization of Cysteine and Histidine Residues in Automated Peptide Synthesis <i>Krzysztof Darlak, Thomas E. Hopkins, Antonio Thigpen</i>	15
Further Investigations into Microwave Assisted Solid Phase Peptide Synthesis: Synthesis of Modified Peptides <i>Sandeep K. Singh, Alicia D. Douglas, Eric J. Williamson, Grace S. Vanier</i>	17
Application of CDFSS Tools to the Oxidation of a Peptide Containing Multiple Cysteine Residues <i>Miranda Steele, Todd Osiek, Allan Casciola, Thomas Gordon</i>	19
Evaluation of Alternatives to HOBT During Solid Phase Peptide Synthesis <i>Matt Davis, Kripa Srivastava</i>	21
Development of a Novel Solid Support for the Economical Synthesis of Leuprolide Drug <i>Kripa Srivastava, Matt Davis</i>	23
<sup>1</sup> H, <sup>13</sup> C-HSQC HR-MAS NMR as a Tool for Investigating the Quality of Fmoc-AA-Wang Resins for SPPS <i>Christian Staehelin, Fritz Dick, Stefano Ferrari, Daniel Rentsch</i>	25
Spiral Countercurrent Chromatography: New Purification Technique for Peptides and Proteins <i>Martha Knight, Aprile Pilon, Melissa Winn, Thomas M. Finn</i>	27
Peptide Thioester Formation and Ligation Using a Cysteinylyl Prolyl Ester (CPE) Autoactivating Unit <i>Toru Kawakami, Saburo Aimoto</i>	29
Thioacid Capture Ligation at Valine <i>Fu-Peng Li, Chuan-Fa Liu</i>	31

Native Ligation with Post-translational Modifications Using C-terminal, N-acylurea Peptides <i>Juan B. Blanco-Canosa, Sampat Ingale, Philip E. Dawson</i>	33
Use of Native Chemical Ligation as a Tool for Polymer Construction over Solid Substrates <i>Raymond Jr Hamel, Ewa Wieczerek, Vincent Chabot, Vincent Aimez, Paul G. Charette, Michel Grandbois, Emanuel Escher</i>	35
Efficient Peptide Ligation Using Azido- and Pyruvoyl-Protected Peptides via the Ag <sup>+</sup> -Free Thioester Method <i>Hidekazu Katayama, Hironobu Hojo, Tsuyoshi Ohira, Yuko Nakahara, Yoshiaki Nakahara</i>	37
Solid Phase Chemical Synthesis of N-linked Glycopeptides <i>Rui Chen, Thomas J. Tolbert</i>	39
Synthesis of Fluorescently Labeled O-Mannosylated Glycopeptides as POMGnT1 Substrates in Clinical Assays <i>Mian Liu, Gerardo Alvarez-Manilla, Franchesca Brothers, David Live</i>	40
Synthesis of Hemopressin by [(2+2+2+1)+2] Segment Condensation <i>P. Anantha Reddy, K. Timothy McElroy, Charles J. McElhinny, Anita H. Lewin, F. Ivy Carroll</i>	42
Shorter Arginine Homologues to Stabilize Peptides Towards Tryptic Digestion <i>Petra Henklein, Thomas Bruckdorfer</i>	44
Application of Proteases in the C-terminal Modification of Peptides <i>Dirk-Jan van Zoelen, Francesca Gini, Gilbert Bours, Ivo Eggen, Guus Frissen, Carmen Boeriu</i>	46
N-Methylation as a Synthetic Resource for Increasing Stability in Depsipeptides <i>Judit Tulla-Puche, Eleonora Marcucci, Irene Izzo, Gerardo Acosta, Sara Auriemma, Chiara Falciani, Fernando Albericio</i>	48
Chemical Synthesis of Full-Length Parathyroid Hormone Related Protein-(1-141) <i>Ashok Khatri, John T. Potts, T. John Martin, Thomas J. Gardella</i>	50
Towards a Minimalist Cell-Penetrating Peptide <i>Emily Ricq, Nabila Brabez, Teresa Coppola, Solange Lavielle, Gérard Chassaing</i>	52
Acid Catalyzed Monodehydro-2,5-diketopiperazine Formation toward Natural Product Synthesis <i>Yuri Yamazaki, Yuki Mori, Akiko Oda, Yoshiaki Kiso, Yoshio Hayashi</i>	54
Solid-phase Synthesis of Aza-proline Analogs of GHRP-6 <i>Caroline Proulx, William D. Lubell</i>	56
Submonomer Solid-Phase Aza-peptide Synthesis and Circular Dichroism Spectroscopic Analysis of [aza-Phe <sup>4</sup> ]-GHRP-6 <i>David Sabatino, William D. Lubell</i>	58
Versatile Microwave Assisted Synthesis of Acyl-Tetramic Peptide Analogs <i>Gerardo Byk</i>	60
Preparation for the Ligand Peptide Probe of Heart-type Fatty Acid-binding Protein <i>Shuhua Zhang, Licheng Wang, Shuwen Guan, Yuanyuan Li, Liping Wang, Wei Li</i>	62
Cloning, Expression, and Purification of Large Fragments of a GPCR <i>Katrina E. Caroccia, Subramanyam J. Tantry, Racha Estephan, Leah S. Cohen, Boris Arshava, Oliver Zerbe, Jeffrey M. Becker, Fred Naider</i>	64
Synthesis of Bis-Benzamides as New Amphiphilic Alpha-Helix Mimetics <i>Srinivasa Marimganti, Murthy N. Cheemala, Jung-Mo Ahn</i>	66
ZY-GLP1: A Novel Peptidomimetic Glp-1 Agonist <i>R.H. Bahekar, A.A. Joharapurkar, D. Bandyopadhyay, G. Chakraborti, H. Patel, V.D. Pawar, R. Sunder, M.R. Jain, P.R. Patel</i>	68
Design and Synthesis of Novel Amphiphilic $\alpha$ -Helix Mimetics Based on a New Tris-Benzamide Scaffold <i>Murthy N. Cheemala, Jung-Mo Ahn</i>	70
Design and Synthesis of $\alpha$ -Helix Mimetics Based on a Tris-Benzamide Scaffold to Target Bcl Proteins <i>Kajal Bhimani, Myoung H. Kim, Jian Zhou, Jer-Tsong Hsieh, Jung-Mo Ahn</i>	72

Efficient Solid-Phase Synthesis of Tris-Benzamides for a Rapid Production of Alpha-Helix Mimetics <i>Tae-Kyung Lee, Jung-Mo Ahn</i>	74
Synthesis of a Radio-labelled Peptide Mimic for Examining Affinity and Activity at the Prostaglandin F2a Receptor <i>Carine B. Bourguet, William D. Lubell</i>	76
Solid-Phase Synthesis and CD Spectroscopic Conformational Analysis of $\alpha$ - and $\beta$ -Amino $\gamma$ -Lactam (Agl and Bgl) Analogs of Growth Hormone-Releasing Peptide GHRP-6 <i>Nicolas Boutard, Andrew G. Jamieson, William D. Lubell</i>	78
Design, Synthesis and Structure of Peptidomimetic Inhibitors of Eukaryotic Ribonucleotide Reductase: A Target for Cancer Chemotherapy <i>Jaskiran Kaur, Shalini Jha, Chris Dealwis, Barry S. Cooperman</i>	80
Dhhp-6 Protect H9c2 Cardiomyocyte Against Oxidative Injury Induced by Hypoxia/Reoxygenation <i>Xiaoguang Chen, Lei Huang, Shuwen Guan, Liping Wang, Wei Li</i>	82
Free Radical Scavenging Activity of Hydroxycinnamoyl Amino Acid Amides <i>Maya Spasova, Djemile Dagon, Galya Ivanova, Tsenka Milkova</i>	84
Solid-Phase Synthesis and CD Spectral Analysis of IL1R- Allosteric Modulator 101.10 Bearing Multiple Agl-Residues <i>Luisa Ronga, William D. Lubell</i>	86
From Combinatorial Chemistry to Nanomicelles to Cancer Targeting <i>Juntao Luo, Kai Xiao, Yuan-pei Li, Joyce Lee, Nianhuan Yao, Wenwu Xiao, Yan Wang, Wiley Fowler, Michael Kent, Holland Cheng, Li Xing, Kit S. Lam</i>	88
Development of One-Bead Two-Compounds Technology for the Identification of Cell Surface Acting Functional Ligands <i>Yan Wang, Yoshiko Maeda, Ming Zhu, Xiaobing Wang, Pappanaicken R. Kumaresan, Kit S. Lam</i>	91
Identification of Peptide Substrate Preference for Tyrosylprotein Sulfotransferases <i>Chao-Yu Chen, Hsing-Jien Kung, Kit S. Lam</i>	93
The Direct In Vivo Use of Mixture-Based Libraries in the Drug Discovery Process <i>Jay P. McLaughlin, Andrew Heusser, Kate J. Reilley, Marc Giulianotti, Richard A. Houghten</i>	97
Identification of Inhibitors of Protein-protein Interactions Through the Screening of Simplified Combinatorial Peptide Libraries <i>Pasqualina L. Scognamiglio, Nunzianna Doti, Carlo Pedone, Paolo Grieco, Marco Sabatella, Menotti Ruvo, Daniela Marasco</i>	98
3-Nitro-tyrosine as a Quencher of OBOC Autofluorescence <i>Jared Townsend, Babak Sanii, Alan Lehman, Andrew Do, Kit S. Lam</i>	100
Macrocyclic Peptide-Peptoid Hybrids Designed as PPII Helix Mimetics <i>Fa Liu, Andrew G. Stephen, Abdul A. Waheed, Eric O. Freed, Robert J. Fisher, Terrence R. Burke, Jr.</i>	102
Application of Oxime-Based Post Solid-Phase Diversification to Optimization of Polo Box Domain-Binding Peptides <i>Fa Liu, Jung-Eun Park, Shilpa R. Shenoy, Nak-Kyun Soung, James B. McMahon, Kyung S. Lee, Terrence R. Burke, Jr.</i>	104
A Novel Biochip System Focusing on Protein Detection by the Use of Labeled Glycopeptides Arrayed on a Novel Chip-material <i>K. Nokihara, T. Kawasaki, A. Hirata, Y. Takebayashi, Y. Oka, T. Ohyama</i>	106
<b>Peptide Therapeutics and Bioactive Substances, Peptide Antibiotics and Natural Products, Peptides and Immunity, Peptides and Membrane Proteins, Peptides as Diagnostics, Probes, and Biomarkers</b>	
Peptides As Drugs: Re-examination Perceived Wisdom in Drug Design <i>Victor J. Hruby</i>	111
Regulatory Perspectives for Early Phase Development of Protein and Peptide Biotherapeutics <i>Robert G. Bell</i>	114
New Insight into the Binding Mode of Cyclic Melanocortin Ligands at the MC4 Receptor <i>Brancaccio Diego, Alfonso Carotenuto, Paolo Grieco, Victor J. Hruby, Ettore Novellino</i>	117

The Central Melanocortin Receptors and Voluntary Exercise <i>Jay W. Schaub, Amy Andreasen, Lorraine M. Koerper, Zhimin Xiang, Carrie Haskell-Luevano</i>	119
Incorporation of a Reverse Turn Mimetic into a Chimeric AGRP- Melanocortin Peptide Template: Structure and Function Studies <i>Anamika Singh, Jerry R. Holder, Andrzej Wilczynski, Rachel M. Witek, Marvin Dirain, Arthur S. Edison, Carrie Haskell-Luevano</i>	122
Determination of Unique AGRP and MC4R Interactions: Use of Stereochemical Modifications of Ligands and Receptor Mutagenesis <i>Erica M. Haslach, Marvin L. Dirain, Carrie Haskell-Luevano</i>	124
Semi-rigid MC1 Selective Agonists Based on N-capped His-D-Phe-Arg-NH <sub>2</sub> Tripeptide Core <i>Leonid Koikov, Andrew R. Ruwe, Zalfa Abdel-Malek, Carrie Haskell-Luevano, Marvin L. Dirain, Federico Portillo, Zhimin Xiang, Matt Wortman, James J. Knittel</i>	126
Effect of New Leptin Fragments on Food Intake and Body Weight of Rats <i>Marta N. C. Martins, Jádson M. Pereira, Mônica M. Telles, Juliana C. S. Zemdeg, Iracema S. Andrade, Eliane B. Ribeiro, Antonio Miranda</i>	128
Adropin - A Novel Secreted Factor Linking Diet with Energy Homeostasis <i>K. Ganesh Kumar, Jingying Zhang, Randall L. Mynatt, Andrew A. Butler.</i>	130
Design, Synthesis and Biological Activities of New Urotensin II-Related Peptides (URP) <i>David Chatenet, Myriam Létourneau, Alain Fournier</i>	133
pSK - A Novel Amphibian Skin Bowman-Birk-like Trypsin and TMPRSS2 Inhibitor <i>Hang Chen, Susan Hawthorne, Tianbao Chen, Chris Shaw, Brian Walker</i>	135
Peptides Inhibitors of F11R/JAM-A Adhesion Molecules and Potent Anti-atherosclerosis Drugs <i>Cristina C. Clement, Anna Babinska, Yigal H. Ehrlich, Manfred Philipp, Elizabeth Kornecki</i>	137
The Human Insulin/Relaxin Superfamily: New Members and Functions <i>John D. Wade, M. Akhter Hossain, Feng Lin, Fazel Shabanpoor, Alessia Belgi, Linda Chan, Suode Zhang, Geoffrey W. Tregear</i>	139
Molecular-basis for Specificity in Biological Action at the Homologous Glucagon and GLP-1 Receptors <i>Jonathan W. Day, James T. Patterson, Vasily M. Gelfanov, Richard D. DiMarchi</i>	142
Highly Constrained Glucagon-Like Peptide-1 with Improved Biological Activity and Enzyme Stability <i>Eunice N. Murage, Guangzu Gao, Alessandro Bisello, Jung-Mo Ahn</i>	144
Discovery and Structural Optimization of High Affinity Co-Agonists at the Glucagon and GLP-1 Receptors <i>Tao Ma, Jonathan Day, Vasily Gelfanov, Richard DiMarchi</i>	146
Structural Characterization of a Novel GLP-1 Analog Taspoglutide by NMR Spectroscopy <i>Natia Tsomaia, Jundong Zhan, Andrea Piserchio, Dale F. Mierke, Jesse Z. Dong</i>	148
Oral Delivery of Peptide Hormones: Insulin, Interferon, Growth Hormone and Calcitonin <i>W. Blair Geho, John R. Lau</i>	150
Exploring the N-terminal Hydrophobic Faces of Glucagon and Glucagon-like Peptide-1 <i>Brian P. Ward, Brian P. Finan, Vasily M. Gelfanov, Richard D. DiMarchi</i>	153
Discovery of Degarelix, a Self-Depoting GnRH Antagonist with Long Duration of Action <i>Claudio Schteingart, Guangcheng Jiang, Robert Galyean, Jacek Stalewski, Jean Rivier, Richard White, Gregoire Schwach</i>	155
Development of Insulin Based Inhibitors of Human Islet Amyloid Polypeptide <i>Deborah L. Heyl, Durgaprasad Peddi, Ranadheer Reddy Pesaru</i>	158
Synthesis & Analysis of Peptide Hormone-based prodrugs <i>Arnab De, Richard D. DiMarchi</i>	160
Discovery of Peptides as Granulocyte Colony-Stimulating Factor Receptor Agonist (Series I) <i>Y. Sarah Dong, Ashok Bhandari, Kalyani Penta, Karen Leu, Peter J. Schatz, Christopher P. Holmes</i>	162
Discovery of Peptides as Granulocyte Colony-Stimulating Factor Receptor Agonist (Series II) <i>Y. Sarah Dong, Yijun Pan, Caiding Xu, Ashok Bhandari, Yvonne Angel, Karen Leu, Kalyani Penta, Bruce Mortensen, Jennifer M. Green, Peter J. Schatz, Qing Fan, Kathryn Woodburn, Christopher P. Holmes</i>	164

Role of the Guanidine Group in Position 11 of PTH(1-11) Analogues <i>Andrea Caporale, Elisabetta Schievano, Iwona Woznica, Stefano Mammi, Evaristo Peggion</i>	167
Peptide Antagonists of Human BAFF/BAFF Receptor Binding <i>Y. Sarah Dong, Erik Whitehorn, Christopher P. Holmes, Peter J. Schatz, Jennifer M. Green</i>	169
Cell Membrane Damage by the Type 2 Diabetes Associated Peptide Amylin in the Presence of Insulin <i>Joshua M. Osborne, Daniel J. Clegg, Deborah L. Heyl</i>	171
Synthesis and Analysis of Analogs of hIAPP (1-19), a Peptide Involved in Membrane Disruption <i>Deborah L. Heyl, Srikanth Reddy Konda, Anitha Jayaprakash</i>	173
Use of Peptoid-Peptide Hybrids in the Development of Shc SH2 Domain-Binding Inhibitors <i>Sung-Eun Kim, Won Jun Choi, Andrew G. Stephen, Iwona Weidlich, Alessio Giubellino, Fa Liu, Karen M. Worthy, Lakshman Bindu, Matthew J. Fivash, Marc C. Nicklaus, Donald P. Bottaro, Robert J. Fisher, Terrence R. Burke, Jr.</i>	175
Immunoglobulin Fc-based Peptide Fusion Proteins as a Basis for Optimizing In Vivo Pharmacology <i>Allison Kukuch, James T. Patterson, Richard D. DiMarchi, Thomas J. Tolbert</i>	177
Novel $\mu$ Agonist, $\delta$ Antagonist, and NK1 Antagonist Peptide Chimeras <i>Isuru R. Kumarasinghe, Victor J. Hruby, Suneeta Tumati, Shou-Wu Ma, Eva Varga, Josephine Lai, Frank Porecca</i>	179
Dynorphin A as a Novel Ligand at Bradykinin Receptors <i>Brianna Paisley, Josephine Lai, Victor Hruby</i>	181
Replacement of the Tyr1 Hydroxyl Group of TIPP Peptides with N-(Alkyl)carboxamido Groups Results in Potent and Selective Delta Opioid Agonists or Antagonists <i>Irena Berezowska, Grazyna Weltrowska, Carole Lemieux, Nga N. Chung, Brian C. Wilkes, Peter W. Schiller</i>	183
Role of Alzheimer's Amyloid- $\beta$ Peptide as a Putative Transcription Factor <i>Debmoy K. Lahiri, Bryan Maloney, Jason Bailey, Yuan-Wen Ge</i>	185
Investigation of A $\beta$ 42 C-Terminal Fragments as Inhibitors of A $\beta$ 42 Assembly and Neurotoxicity <i>Huiyuan Li, Bernhard H. Monien, Aleksey Lomakin, Erica A. Fradinger, Sean M. Spring, Brigita Urbanc, George B. Benedek, Gal Bitan</i>	187
SAR and Mechanistic Studies of Tetrapeptide Inhibitors of A $\beta$ 42-Induced Neurotoxicity <i>Huiyuan Li, Gal Bitan</i>	189
Nuclear Localization of the Amyloid b-peptide During Oxidative Stress in Neuronal Cells <i>Jason A. Bailey, Debmoy K. Lahiri</i>	191
Total Chemical Synthesis of Islet Amyloid Polypeptide and its Precursors For Membrane Interaction Studies <i>Pieter Van de Vijver, Lucie Khemtémourian, Dennis Suylen, Liesbeth Scheer, Gemma Lahoz Casarramona, Hans J.D. Meeldijk, Ben de Kruijff, J. Antoinette Killian, Jo W.M. Höppener, Tilman M. Hackeng</i>	193
"Click Peptide" Based on "O-Acyl Isopeptide Method": In Situ Production of Monomer Amyloid b Peptide from Water-Soluble Precursor Analogues <i>Atsuhiko Taniguchi, Youhei Sohma, Mariusz Skwarczynski, Yuta Hirayama, Takuma Okada, Keisuke Ikeda, Halan Prakash, Hidehito Mukai, Tooru Kimura, Yoshio Hayashi, Shun Hirota, Katsumi Matsuzaki, Yoshiaki Kiso</i>	195
Aromatic Versus Hydrophobic Contributions to Amyloid Peptide Self-Assembly <i>Charles J. Bowerman, Todd M. Doran, Xianfeng Gu, Derek M. Ryan, F. Timur Senguen, David A. Nissan, Bradley L. Nilsson</i>	197
Proteinous Microspheres Containing KLVFF Peptides Sequester Amyloid-Beta Protein and Inhibit its Aggregation <i>Michal Richman, Sara Wilk, Natalie Skirtenko, Alex Perelman, Shai Rahimpour</i>	199
The ApoE Mimetic Peptide, Ac-hE18A-NH2 Recycles in THP-1 Monocyte-derived Macrophages <i>Palgunachari Mayakonda, Manjula Chaddha, Gaurav Nayyar, Shaila P. Handattu, David W. Garber, Candyce E. Monroe, Roger C. White</i>	201
Cryptides: Discovery of Functional Cryptic Peptides Hidden in Protein Structures and Identification of Their Signaling Mechanisms <i>Hidehito Mukai, Tetsuo Seki, Eisuke Munekata, Yoshiaki Kiso</i>	203



Highly Active and Selective Integrin Ligands for Imaging Purposes <i>S. Neubauer, D. Heckmann, J. Eckardt, G. Zahn, D. Vossmeier, R. Stragies, H.-J. Wester, H. Kessler</i>	205
isoDGR: A New Sequence for Integrin Ligands <i>E. Otto, D. Heckmann, G. Zahn, D. Vossmeier, R. Stragies, H. Kessler</i>	207
PEGylation A Key Technology to Improve Solubility and Pharmacokinetic of Peptides, Proteins and other Biopharmaceuticals for Superior Drug Delivery <i>Thomas Bruckdorfer</i>	209
Pegylation of Intermediate Peptides: Thymosin $\alpha 1$ and Growth Hormone-Releasing Factor <i>Arthur M. Felix, Sandra Lynn Veech</i>	211
An Integrated Strategy for Improving Plasma Half-life of Therapeutic Peptides <i>Hongjian Li, Yi Ma, Tianhong Zhou, Xuemei Huang, Tao Zeng, Yanhong Ran, Meilan Qiu, Xi Zhou, Zhengding Su</i>	213
PEGylation of the Anorexigenic Peptide Neuromedin U Yields a Promising Candidate for the Treatment of Obesity <i>Paolo Ingallinella, Andrea Peier, Karolina Zytko, Annalise Di Marco, Kunal Desai, Ying Qian, Edith Montegudo, Ralph Laufer, Donald J. Marsh, Elisabetta Bianchi, Antonello Pessi</i>	215
Structure-Property of PEGylated Peptides in Normal and Renal Insufficient Rat Models <i>Kevin Yin, Sarah Walter, Amos Baruch, Shawn Alexander, Eiketsu Sho, Felix Karim, Steven Harrison, Derek Maclean</i>	217
Development of Compstatin Derivative-Albumin Binding Peptide Chimeras for Prolonged Plasma Half-Life <i>Hongchang Qu, Paola Magotti, Daniel Ricklin, John D. Lambris</i>	219
Peptide Regulators of Protein-Protein Interactions with Selectivity for Specific Sub-Cellular Compartments <i>Nir Qvit, Marie-Helene Disatnik, Daria Mochly-Rosen</i>	221
Potent Inhibitors of PHEX Derived From Succinic Acid Hydroxamates <i>Elaref S. Ratemi, Mostafa Hatam, Denis Gravel, Philippe Crine, Guy Boileau, Isabelle Lemire</i>	223
Design and Synthesis of Mercaptoacyl Dipeptides as Potent and Selective PHEX inhibitors <i>Elaref S. Ratemi, Denis Gravel, Philippe Crine, Guy Boileau, Isabelle Lemire</i>	225
Synthesis and Biological Activity of New Esters of Acyclovir <i>Ivanka G. Stankova, Stoyan Shishkov, Angel S. Galabov, Tsenka S. Milkova</i>	227
Engineering of Better HIV Entry Inhibitor Peptides through Chemical Modification <i>Junpeng Xiao, Thomas J. Tolbert</i>	229
Synthesis and Conformational Analysis of a Natural Peptide Inhibitor of HIV-1 Integrase <i>Marta De Zotti, Francesca Damato, Fernando Formaggio, Marco Crisma, Elisabetta Schievano, Stefano Mammi, Bernard Kaptein, Quirinus B. Broxterman, Peter J. Felock, Daria J. Hazuda, Sheo B. Singh, Jochem Kirschbaum, Hans Br��ckner, Claudio Toniolo</i>	231
Functional Reconstruction of Structurally Complex Protein Binding Sites Using CLIPS Technology <i>Peter Timmerman, Wouter C. Puijk, Jerry W. Slootstra, Peter van Dijken, Rob H. Melen</i>	233
Fusion of Bioactive Peptides to Antibody Fragments <i>Junpeng Xiao, Allison Kukuch, Mark A. Pawlicki, Brian S. Hamilton, Thomas J. Tolbert</i>	235
Exenatide Rescues Sirt1 Expression in Apoptotic RINm-5F cells <i>Xueyun Wang, Jiayi Yu, Jing Wang, Shijie Yang, Wei Li</i>	237
Towards Peptide Vasodilators as Anticancer Drug Delivery Vehicles <i>Rachel J. White, Paul G. Plieger, Nadia G. Kandile, David R. K. Harding</i>	239
Development of Selective, Exosite Binding Matrix Metalloproteinase (MMP) Inhibitors <i>Janelle L. Lauer-Fields, Gregg B. Fields</i>	241
Design of Structured gp41 N-heptad Repeat Peptides as HIV-1 Vaccine Candidates <i>Elisabetta Bianchi, Joseph Joyce, Michael D. Miller</i>	244
TMZ-BioShuttle, an Exemplary Drug Reformulation by Inverse Diels Alder Click-Chemistry <i>R. Pipkorn, M. Wiessler, W. Waldeck, H. Fleischhacker, P. Lorenz, K. Braun</i>	246

Dramatic Increase of Antiviral Potency of an HIV Peptide Fusion Inhibitor by Targeting to Lipid Rafts via Addition of a Cholesterol Group <i>Antonello Pessi, Paolo Ingallinella, Elisabetta Bianchi, Ying-Jie Wang, Renee Hrin, Alessia Santoprete, Annunziata Langella, Maria Veneziano, Fabio Bonelli, Thomas J. Ketas, John P. Moore, Michael D. Miller</i>	249
Angiogenesis Inhibition using VEGF Receptor Blockade Approach <i>Sharad V. Rawale, Daniele Vicari, Kevin C. Foy, Pravin T. P. Kaumaya</i>	252
Phase I Clinical Trial with Her-2 B-Cell Chimeric and Multi-Epitope Based Peptide Vaccines in Patients with Metastatic and/or Recurrent Solid Tumors <i>Pravin T.P. Kaumaya, Kevin Chu Foy, Joan Garrett, Sharad V. Rawale, Daniele Vicari, Tammy Lamb, Aruna Mani, Yahaira Kane, Catherine Balint, Donald Chalupa, Gregory Otterson, Charles Shapiro, Jeffrey Fowler, Michael Grever, Tanios Bekaii-Saab</i>	254
Combination Treatment with Her-2 and VEGF Peptide Mimics Induces Potent Anti-Tumor and Anti-Angiogenic Responses In Vitro and In Vivo <i>Kevin C. Foy, Zhenzhen Liu, Sharad Rawale, Gary Phillips, Megan Miller, Aravind Menon, Nina D. Osafo, Pravin T.P. Kaumaya</i>	257
Structure-Activity Relationship Study of New FK228 Analogues as Antitumor Agents <i>Salvatore Di Maro, Rey-Chen Pong, Jer-Tsong Hsieh, Jung-Mo Ahn</i>	260
DhHP-6 Extends <i>Caenorhabditis Elegans</i> Lifespan in a SIR2.1- Dependent Manner <i>Shuwen Guan, Pengfei Li, Yuanyuan Li, Shuhua Zhang, Xiaoguang Chen, Liping Wang, Wei Li</i>	262
Solid Phase Synthesis of Lipidated Peptidotriazoles as Bisubstrate Inhibitors of Protein Geranylgeranyltransferase-I <i>Animesh V. Aditya, Richard A. Gibbs</i>	264
Effect of Net Positive Charge and Charge Distribution on the Polar Face of Amphipathic $\alpha$ -Helical Antimicrobial Peptides on their Biological and Biophysical Properties <i>Ziqing Jiang, Adriana I. Vasil, Michael L. Vasil, Robert S. Hodges</i>	266
Lysine Trimethylation, a Tool for Improving the Therapeutic Index of Antimicrobial Peptides <i>Beatriz G. de la Torre, Maria Fernandez-Reyes, Dolores Diaz, Ania Cabrales-Rico, Mariona Valles-Miret, Jesus Jimenez-Barbero, Luis Rivas, David Andreu</i>	268
Design and Synthesis of New Potent Melanocortin Peptides with Candidacidal Activity <i>Luigia Auriemma, Stefania Malfi, Salvatore Di Maro, Pietro Campiglia, Ettore Novellino, Anna Catania, Paolo Grieco</i>	270
Structure-Antibacterial Activity Relationship of Cyclic Lipopeptide Antibiotic Fusaricidin A <i>Nina Bionda, Daniela Treitl, Maciej Stawikowski, Predrag Cudic</i>	272
Probing the Effect of Gomesin and its Linear Analogue on Giant Unilamellar Vesicle via Optical Microscopy <i>Tatiana M. Domingues, Sirlei Daffre, Karin A. Riske, Antonio Miranda</i>	274
Total Fmoc Solid-phase Synthesis of Naturally Occurring Dipeptide Antibiotic Katanosin B <i>Nina Bionda, Diego Binetti, Predrag Cudic, Mare Cudic</i>	276
Efficient Total Synthesis of Dipeptidic Antibiotics (+)-Negamycin and Its Derivatives <i>Yoshio Hayashi, Akihiko Taguchi, Thomas Regnier, Shigenobu Nishiguchi, Yoshiaki Kiso</i>	278
Design, Synthesis and Conformational Studies of New Analogues of Temporins A and L <i>Stefania Malfi, Maria Rosaria Saviello, Ludovica Marcellini Hercolani Gaddi, Cristina Marcozzi, Alfonso Carotenuto, Maria Luisa Mangoni, Luigia Auriemma, Isabel Gomez-Monterrey, Pietro Campiglia, Ettore Novellino, Paolo Grieco</i>	280
Novel Antimicrobial Peptides from the Venom of Eusocial Bee <i>Halictus sexcinctus</i> (Hymenoptera: Halictidae) <i>Lenka Monincová, Oldřich Hovorka, Josef Cvačka, Zdeněk Voburka, Vladimír Fučík, Lenka Borovičková, Lucie Bednářová, Miloš Buděšínský, Jiřina Slaninová, Jakub Straka, Václav Čerovský</i>	282
Role of the Strongly Helicogenic Aib Residues on the Properties of the Lipopeptide Trichogin GA IV <i>Barbara Biondi, Marta De Zotti, Cristina Peggion, Fernando Formaggio, Claudio Toniolo</i>	284
Solution and Solid-Phase Syntheses and Conformational Analysis of a Novel Medium-Length Peptaibiotic <i>Marina Gobbo, Claudia Poloni, Marta De Zotti, Cristina Peggion, Barbara Biondi, Fernando Formaggio, Claudio Toniolo</i>	286

Multivalent Antimicrobial Peptides with Enhanced Activity Against MDR Bacteria <i>Anne W. Young, Zhigang Liu, Chunhui Zhou, Po Hu, Yingkai Zhang, Neville R. Kallenbach</i>	288
Novel Peptide-based Antimicrobial Agents for the Treatment of Clostridium Difficile Associated Disease <i>David A. Kennedy, Marc Devocelle</i>	290
Virtual Screening Targeting the PhoP Response Regulator to Inhibit Bacterial Virulence <i>Yat T. Tang, Tammy Latifi, Eduardo A. Groisman, Garland R. Marshall</i>	292
Pyrazinoylation and Benzoylation of Anoplin as a Plausible Approach of Preparing Novel Potent Antibacterial Drugs <i>Maximilien Alaric O. Tan, Portia Mahal G. Sabido</i>	294
Scale-up of Antiviral Polyamide Comprising Pyrrole and Imidazole Amino Acids <i>Kam F. Fok, Kevin J. Koeller, Holly M. Pope, Terri G. Edwards, Christopher Fisher, James K. Bashkin</i>	296
Synthetic Study of Voltage-Gated Proton Channel (VSOP/Hv) <i>Ken'ichiroh Nakamura, Toshiaki Hara, Hiroko Tamagaki, Yuichi Akai, Takeshi Sato, Toru Kawakami, Tatsuki Kurokawa, Yuichiro Fujiwara, Yasushi Okamura, Saburo Aimoto</i>	298
Functional Studies of AT1 Antagonist SII Analogues Reveal Selective Cell Signaling and Inhibition of Ang-II Mediated NHE3 Activation <i>Minying Cai, Hua Xu, Zhihua Liu, Hongchang Qu, Jing Li, Fayez K. Ghishan, Victor J. Hruby</i>	300
NMR Studies on a Double Transmembrane-Containing Fragment of a G Protein-Coupled Receptor <i>Leah S. Cohen, Alexey Neumoin, Boris Arshava, Melinda Hauser, Jeffrey M. Becker, Oliver Zerbe, Fred Naider</i>	302
Photoactive Isoprenoid-containing Peptides <i>Kelly Kyro, Daniel Mullen, Surya Manandhar, Walter K. Schmidt, Mark Distefano</i>	304
Chemical Synthesis, Isolation and Assembly of c-Subunits of Human FoF1-ATP Synthase <i>Toshiaki Hara, Akira Tainosho, Takashi Sato, Ken'ichiroh Nakamura, Toru Kawakami, Hideo Akutsu, Saburo Aimoto</i>	306
Antiparallel b-Hairpin/b5.6-Helical Structures <i>John L Kulp III, Thomas D Clark</i>	308
Studies of Energy Balance and Cancer <i>Joel Nyberg, Alexander Mayorov, Min Ying Cai, Morgan Zingsheim, Victor J. Hruby</i>	310
Modulation of Function in Heme Binding Membrane Protein <i>Sandip Shinde, Jeanine Cordova, Giovanna Ghirlanda</i>	312
Temporal Analysis of Phosphopeptide Induced by Nocodazole Treatment <i>Kohji Nagano, Takashi Shinkawa, Hironori Mutoh, Osamu Kondoh, Sayuri Morimoto, Noriyuki Inomata, Motooki Ashihara, Nobuya Ishii, Yuko Aoki, Masayuki Haramura</i>	314
Regulation of Protein Binding by Photoswitchable Peptides <i>Christian Hoppmann, Sabine Seedorff, Anja Richter, Heinz Fabian, Peter Schmieder, Karola Ruck-Braun, Michael Beyermann</i>	316
Utilization of Hydrophobic Modification to Promote Internalization of a CAAX Box-containing Peptide <i>James W. Wollack, Joseph Katzenmeyer, Joshua D. Ochocki, Nicholette A. Zeliadt, Daniel G. Mullen, Edgar A. Arriaga, Elizabeth V. Wattenberg, Mark D. Distefano</i>	318
Assessment of a Tat-Derived Peptide as a Vector for Hormonal Transport <i>Brian P. Finan, Vasily M. Gelfanov, Richard D. DiMarchi</i>	321
Molecular Imaging of Angiogenesis: Cancer and Beyond <i>Weibo Cai</i>	323
Development of an Europium(III) DOTA-based Luminescence Assay for Detection of Ligand-Receptor Interactions <i>Channa R. De Silva, Josef Vagner, Ronald Lynch, Robert J. Gillies, Victor J. Hruby</i>	325
Specific Targeting of Cells by Heteromultivalent Ligands and its Implications in Cancer <i>Jatinder S Josan, Heather L. Handl, Ronald M. Lynch, Josef Vagner, Robert J Gillies, Victor J. Hruby</i>	327

LHRH-II Analog Design: Structure-Function Studies Toward the Development of a LHRH-II Based Radiotherapeutic Agent <i>Palaniappa Nanjappan, Sudha Khurana, Karen E. Linder, Natarajan Raju, Adrian D. Nunn, Edmund R. Marinelli, Bitha Narayanan, Rolf E. Swenson</i>	330
Heterobivalent Ligands Crosslink Multiple Receptors for Targeting of Pancreatic $\beta$ -cell to Monitor $\beta$ -cell Mass <i>Josef Vagner, Woo Jin Chung, Craig S. Weber, Sean W. Limesand, Channa R. De Silva, Ronald Lynch</i>	332
The Novel Cell Penetrating Peptide NrTP Exquisitely Targets the Nucleolus of Tumor Cells <i>Gandhi Rádís-Baptista, Beatriz G. de la Torre, David Andreu</i>	334
Quantum Dot-Based Dual-Modality Imaging of Integrin $\alpha v \beta 3$ Expression on Tumor Vasculature <i>Weibo Cai</i>	337
<b>Biophysical Chemistry, Folding, Recognition, and Catalysis, Peptides in Materials Science, Peptides as Research Tools</b>	
Conformation and Stability of the Helix-Loop-Helix Domain of the Id Protein Family <i>Sebastian D. Kiewitz, Yoshiaki Kiso, Chiara Cabrele</i>	343
NMR Solution Structure Analysis of the C-terminal Linear and Cyclic Peptides of Pheromone Biosynthesis-Activating Neuropeptide (PBAN) from the Silkworm <i>Bombyx mori</i> <i>Koji Nagata, Akitoshi Okada, Takeshi Kawai, Jun Ohtsuka, J. Joe Hull, Ken-ichi Moto, Shogo Matsumoto, Hiromichi Nagasawa, Masaru Tanokura</i>	345
A Donor-Acceptor Perspective on Carbonyl-Carbonyl Interactions in Proteins <i>Amit Choudhary, Ronald T. Raines</i>	347
Spectroscopic Analysis of a b-hairpin Forming Miniprotein <i>Marcus P. D. Hatfield, Richard F. Murphy, Sandor Lovas</i>	349
Hyperstable b Sheets Without Turns <i>Brandon L. Kier</i>	351
Structural Studies of Mucin Glycoprotein Motifs <i>David Live, Andrew Borgert, George Barany, Mian Liu</i>	353
Replacement of Ala by Aib Improves Structuration and Biological Stability in Thymine-Based Nucleopeptides <i>Piero Geotti-Bianchini, Alessandro Moretto, Cristina Peggion, Julien Beyrath, Alberto Bianco, Fernando Formaggio</i>	355
Do Gta(340-350) Analogs Bind Opsin Similar to its X-ray Crystal Structure? <i>Christina M. Taylor, Jiawen A. Feng, Garland R. Marshall</i>	357
The Use of Paramagnetic and Fluorescent Quenching Amino Acid TOAC for Evaluating Angiotensin I-Converting Enzyme <i>Luis G.D.Teixeira, Patricia A. Bersanetti, Shirley Schreier, Adriana K. Carmona, Clovis R. Nakaie</i>	360
A Photolabile Thiol Protecting Group for Cellular Studies <i>Daniel Abate-Pella, Nicholette Zeliadt, Daniel Mullen, Patrick McDonald, Priyanka Pathak, Timothy Dore, Joachim Mueller, Elizabeth Wattenberg, Mark D. Distefano</i>	362
Design of a Receptor Labeling Angiotensin II Analogue Containing a 3'-hydroxy-Tyrosine in Position 4 <i>H. Jarine, J. Arsenaault, M.-R. Lefebvre, D. Fillion, G. Guillemette, R. Leduc, E. Escher</i>	366
Development of Imageable Toxin A Peptide for Cellular Imaging Study <i>Wei Wang, Zhi-Dong Jiang, Arlin G. Cameron, Michel E. Mawad, Herbert L. DuPont, Shi Ke</i>	366
Synthesis and Biological Characterization of Novel Fluorescent Analogs of Vasopressin <i>Sylvia Chen, Richard Bouley, Jean-Pierre Vilardaga, Dennis A. Ausiello, Ashok Khatri</i>	368
(aMe)Pro Versus Pro b-Turn Formation Propensity <i>Matteo De Poli, Alessandro Moretto, Marco Crisma, Cristina Peggion, Fernando Formaggio, Bernard Kaptein, Quirinus B. Broxterman, Claudio Toniolo</i>	370
Anti-angiogenic Properties of a Rhegnylogically-organised Cell Penetrating Peptide Derived from Endothelial Nitric Oxide Synthase <i>John Howl, Sarah Jones</i>	372

Targeting The Nuclear Pore Complex With Cell Penetrating Peptides: A Novel Therapeutic Strategy <i>Sarah Jones, John Howl</i>	374
A Conformationally Constrained, Benzophenone Containing, $\alpha$ -Amino Acid Photophore <i>Karen Wright, Alessandro Moretto, Marco Crisma, Michel Wakselman, Jean-Paul Mazaylerat, Fernando Formaggio, Claudio Toniolo</i>	376
A Peptido[2]rotaxane Molecular Machine <i>Alessandro Moretto, Ileana Menegazzo, Marco Crisma, Stefano Mammi, Claudio Toniolo</i>	378
Effects of Controlled Gamma Irradiation upon Structures of Bradykinin and Angiotensin II <i>Daniela T. Nardi, Jose C. Rosa, Guita N. Jubilut, Murilo C. Silva, Nanci Nascimento, Clovis R. Nakaie</i>	380
Design of a Novel FRET Substrate with a Long Wavelength Fluorophore for Detection of Matrix Metalloproteinases <i>Vera Rakhmanova, Siu-Kei Lui, Fengying Li, Xiaofen Zhong, Jianjun He, Anita Hong, Xiaohe Tong</i>	382
Conformations of End-Capped Melanocortin Agonists RCO-X-Z-Arg-Trp-NH <sub>2</sub> by 2D-NMR, CD and Computations <i>Seetharama D. Satyanarayanajois, Leonid Koikov, Matt Wortman, Zalfa Abdel-Malek, Renny Kavanagh, James J. Knittel</i>	384
<sup>13</sup> C Shifts Reveal a Clear Pattern along Strands in b Hairpins <i>Irene Shu, James M. Stewart, Brandon L. Kier, Michele Scian, Niels H. Andersen</i>	386
Characterization of Octapeptide GAP as a Precise Carrier for an Imaging or Cancer Therapeutic Agent <i>Chumpol Theeraladanon, Keisuke Hamada, Nobukazu Takahashi, Ukihide Tateishi, Kazuhiro Ogata, Tomio Inoue</i>	388
Effect of Side-Chain Chirality on Peptide Helix Type and Screw Sense <i>Ivan Guryanov, Cristina Peggion, Fernando Formaggio, Ahmed Lakhani, Timothy A. Keiderling, Claudio Toniolo</i>	390
Peptide-assisted Assembly and Patterning of Carbon Nanotubes <i>Zhengding Su, John Honek</i>	392
Manipulating Solvent Exposed Residues for the Formation of a pH-Dependent Coiled Coil Peptide <i>Dawn Ernenwein, Jean Chmielewski</i>	394
Collagen Peptide Fiber Formation Triggered by Metal Ions <i>David E. Przybyla, Jean Chmielewski</i>	396
Strand Exchange of Charged Collagen-Based Peptides <i>Jeeyeon Lee, Jean Chmielewski</i>	398
Site-Specific Delivery of BMP-2 Protein via Click Chemistry Derived Bifunctional Peptides <i>Shrikumar A. Nair, Krzysztof Krajewski, Guy Orgambide, Paul T. Hamilton</i>	400
Fabrication of Efficient Dye-Sensitized Solar Cells by Using Bulky Peptides <i>Mizuki Kitamatsu, Yousuke Ooyama, Yutaka Harima, Masahiko Sisido</i>	402
<i>Author Index</i>	407
<i>Subject Index</i>	412

# **Merrifield Award Lecture**

**Stephen B. H. Kent**



# Chemical Protein Synthesis: Inventing New Chemistries to Reveal How Proteins Work

Stephen B.H. Kent

Departments of Chemistry, Biochemistry & Molecular Biology; Institute for Biophysical Dynamics;  
 University of Chicago, Chicago, IL 60637, U.S.A.

## Introduction

Proteins are the ‘natural products’ of our era, and now play the same role as targets for synthetic organic chemistry that plant and microbial natural products played in the second half of the 20<sup>th</sup> century. Millions of proteins are being discovered at the DNA level as predicted open reading frames, by highly automated genome and metagenome sequencing [1]. Numerous proteins are also being identified by mass spectrometry from a variety of natural sources such as the venoms of spiders, snakes, and cone snails [2]. It has been estimated that there are between 10<sup>5</sup> and 10<sup>6</sup> unique venom-derived proteins alone [3]. Many of these venom-derived proteins have post-translational modifications that are essential for biological activity. The challenge for chemists in the current era is to develop synthetic methods that are powerful enough to enable the straight-forward preparation of predicted proteins and post-translationally modified protein molecules, of defined structure and high purity, in order to elucidate and control the molecular basis of the diverse biological activities of protein molecules.

unprotected peptide segments

‘chemical ligation’

large polypeptides

fold/disulfides

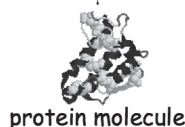


Fig. 1. Modern chemical protein synthesis.

chemistry to proteins. Selected case studies will be used to illustrate the application of synthetic chemistry to elucidate the molecular basis of protein function

## Results and Discussion

### Chemical Ligation

Modern chemical protein synthesis (Figure 1) is based on the chemoselective and regiospecific covalent condensation of *unprotected* peptide segments, a process termed ‘chemical ligation’ [4]. Chemical ligation makes use of two unique functional groups that are designed to be mutually reactive and to not react with any of the functionalities found in the twenty genetically encoded amino acids found in protein molecules (Figure 2). The key conceptual breakthrough was that the product of reaction of these two unique functional groups *does not need to be a native amide bond* [4]. Freed from this constraint, a wide range of chemoselective reactions can potentially be used to covalently join two unprotected peptide segments. The chemical ligation principle is a radical departure from the synthetic approaches that in the latter half of the 20<sup>th</sup> century dominated attempts to make proteins using chemistry. Conventional solution synthesis relied on the reaction of maximally protected peptide segments in organic solvents. Poor solubility of the protected peptides frequently led to slow and incomplete reactions, and partial racemization of the C-terminal amino acid of

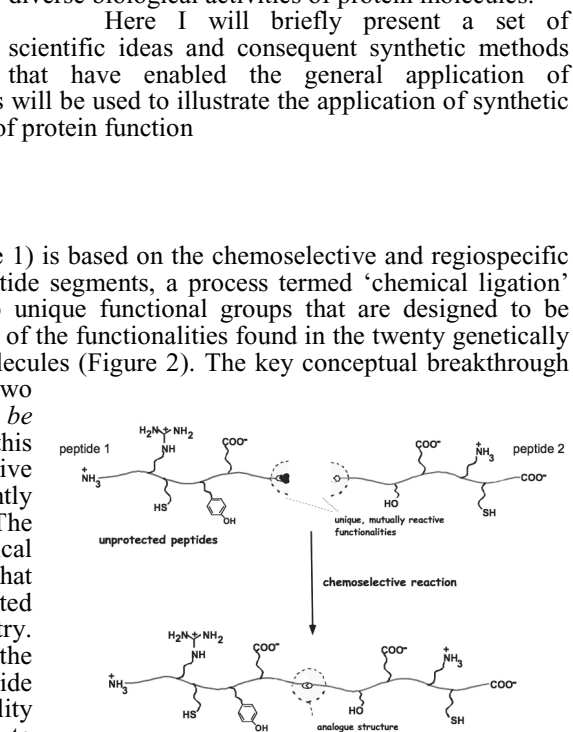


Fig. 2. The chemical ligation principle.



the activated peptide segment often compromised the chiral integrity of the synthetic products. By contrast, the chemical ligation of unprotected peptide segments is usually carried out at neutral or slightly acidic pH in aqueous solution containing a chaotrope such as 6M guanidine.HCL. Peptides are freely soluble under these conditions and millimolar concentrations of reacting peptides can be used, giving rapid and complete condensation reactions.

**Native Chemical Ligation.** The most widely used and successful of the new synthetic chemistries is 'native chemical ligation' (Figure 3) [5,6]. In native chemical ligation, one reacting peptide segment has a thioester at the C-terminal; the other peptide segment has an N-terminal cysteine residue. At neutral pH in the presence of a suitable thiol catalyst, thioester-linked products are formed by reaction of the thiol(ate) functionality of Cys side chain(s) with the thioester moiety (transthioesterification). In accord with the chemical ligation principle, the

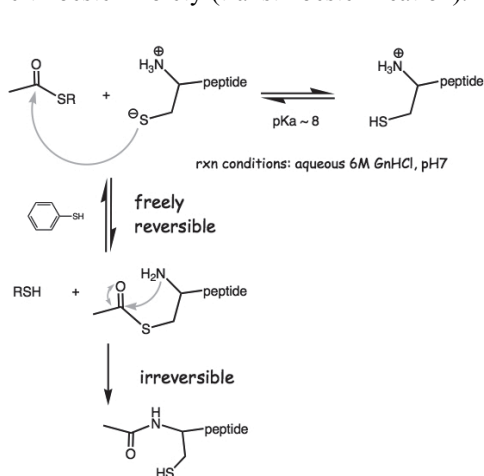


Fig. 3. Native chemical ligation.

susceptible than oxoesters to hydroxide ion-catalyzed hydrolysis, and so are stable in aqueous solution at neutral pH. However, thioesters are *10,000 times more susceptible* than esters to attack by thiolate or amine nucleophiles. The peptide-thioester thus undergoes facile transthioesterification with the thiolate side chain of an N-terminal Cys-, followed by rapid intramolecular nucleophilic attack by the free primary amine of the Cys- residue to give a stable amide-linked condensation product (Figure 3).

**Supporting Technologies.** Chemical ligation of unprotected synthetic peptides is supported by a number of key technologies. Peptide building blocks contain ~20 to ~50 amino acid residues and are readily prepared by stepwise solid phase peptide synthesis (SPPS) [7]. The versatility of polymer supported chemistry and the extraordinary purity of crude products produced by highly optimized SPPS enables the preparation in the research laboratory of hundred milligram amounts of a peptide or peptide-thioester building block in a matter of days. After an unprotected peptide building block has been assembled by SPPS in suitably derivatized form, it is purified by preparative reverse phase HPLC and characterized by analytical LC-electrospray mass spectrometry (LCMS). LCMS is also used to monitor ligation reactions, and to characterize the ligation products in terms of purity and exact mass. In conjunction with knowledge of the synthetic chemistry used, the exact mass serves as a powerful confirmation of the covalent structure of the peptide building blocks and ligation products. After the full-length target peptide – typically containing 50-200<sup>+</sup> amino acids – has been assembled from two or more starting segments, the polypeptide chain is folded (with formation of disulfides if present) to give the synthetic protein molecule. Multidimensional NMR is used to show that the protein has a unique folded structure in solution, and X-ray crystallography is used to determine the three-dimensional structure of the synthetic protein molecule.

**Impact of Chemical Ligation.** Whatever size of peptide is synthetically accessible to a researcher, chemical ligation enables that to be immediately doubled; reaction of two such ligation products gives a synthetic polypeptide chain that is four times the size of the starting peptide segments. Since its introduction ~15 years ago [4,5], chemical ligation has enabled the total chemical synthesis of a wide range of correctly folded, fully active protein molecules with masses ranging from 5 kiloDaltons to more than 50 kiloDaltons (Figure 4).

### Convergent Synthesis

A typical enzyme is a protein molecule made up of two folded domains formed from a single polypeptide chain of 250-300 amino acids. Even the smallest enzymes have more than 120 amino acid residues. In order to prepare protein molecules of 200+ amino acids, we must use at least four synthetic peptide building blocks. The most efficient way to condense four starting materials is by a fully convergent strategy, in which each starting compound is the same number of steps from the final product [8]. This strategy exposes each part of the product molecule to the fewest synthetic manipulations, and is also the most versatile synthetic route to analogues of the parent compound. In a four segment convergent synthesis, each of the two middle peptide segments contains an N-terminal Cys- and a C-terminal -thioester; under native chemical ligation reaction conditions, these two peptides would each form cyclic monomers rather than undergo the desired intermolecular ligation. The challenge is to independently control the reactivity of the N-terminal Cys- and the C-terminal -thioester in these segments, to allow reaction at either end at will.

**Kinetically Controlled Ligation.** We were able to control the reactivity of the thioester moiety by taking advantage of the large reactivity differences between a peptide<sub>1</sub>-thioarylester and a peptide<sub>2</sub>-thioalkylester, when reacted with a Cys-peptide in the *absence* of added thiol catalyst. Under these 'kinetically controlled ligation' conditions, a unique peptide<sub>1</sub>-peptide<sub>2</sub>-thioalkylester ligation product was formed [9]. We were also able to protect the N-terminal Cys as the thiazolidine (Thz), and to cleanly convert a Thz-peptide-thioalkylester to a Cys-peptide-thioalkylester by reaction with CH<sub>3</sub>ONH<sub>2</sub>.HCl at pH 4, without damage to the thioester moiety. This combination of chemistries (Figure 5) enabled us to control the reactivity of the middle pieces in a fully convergent synthesis.

### Chemical Synthesis of Enzymes

**Human Lysozyme.** To illustrate the utility of a fully convergent synthetic strategy based on a combination of native chemical ligation and kinetically controlled ligation, we undertook the total chemical synthesis of human lysozyme (Figure 6). Lysozyme was one of the classic targets for the total chemical synthesis of an enzyme molecule by conventional solution methods [10], but was never made in active form. Using a convergent chemical ligation approach, human lysozyme (130 amino acid residues, 8 Cys, 4 disulfides) was made in high purity and with the correct mass; the synthetic enzyme molecule had a unique fold in solution and had full enzymatic activity; finally, the high resolution (1.04 Angstrom) molecular structure of the crystalline synthetic enzyme was determined by X-ray diffraction [11].

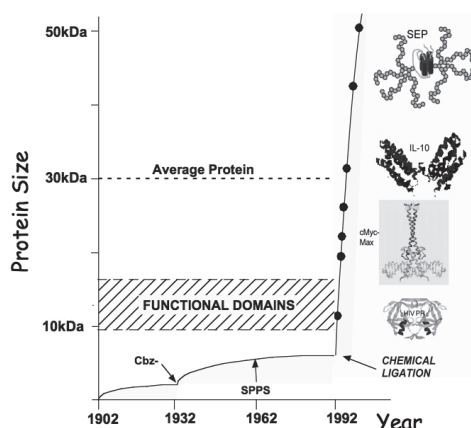


Fig. 4. Impact of chemical ligation.

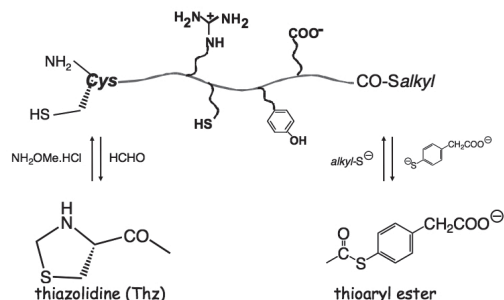


Fig. 5. Control of the reactivity of a Cys-peptide-thioester.

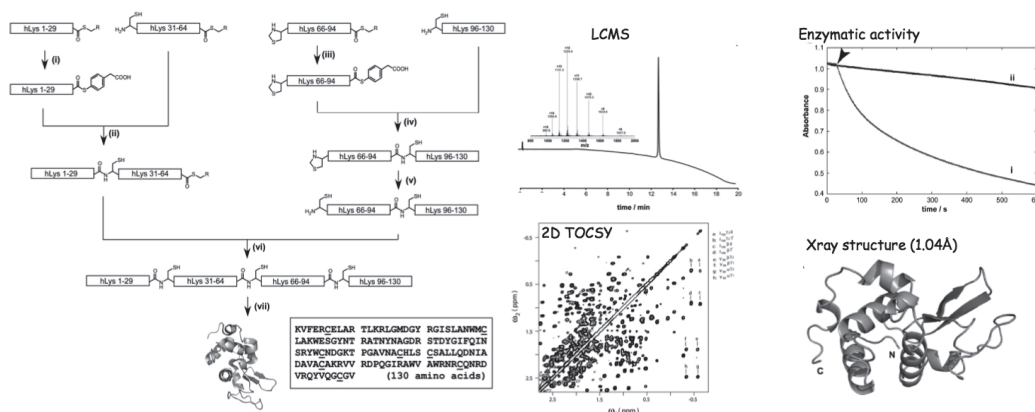


Fig. 6. Total chemical synthesis of lysozyme. (Left) Convergent synthetic strategy. (Right) Characterization.

**HIV-1 Protease.** The human immunodeficiency virus-1 protease is a homodimeric protein molecule made up of two identical 99 residue polypeptide chains. Each monomer contributes a catalytic aspartic acid side chain to the active site of the enzyme. In addition, there are two mobile ‘flap’ structures that close down over the peptide substrate, desolvating the scissile bond. The exact role of the two flaps in the catalytic mechanism of the HIV-1 protease remains to be determined; it is noteworthy that the corresponding cell-encoded aspartyl proteinases, believed to have the same catalytic mechanism, are single polypeptide chain-two domain proteins that have only one ‘flap’ structure.

In the HIV-1 protease complex with substrate-derived inhibitors, observed by X-ray crystallography [12], both flaps close down over the substrate. Gly<sup>51</sup> is the amino acid residue at the tip of each flap, and in the closed conformation adopts distinct conformations; in one flap, Gly<sup>51</sup> is in the L-amino acid region of the Ramachandran plot, while in the other flap in the same enzyme molecule Gly<sup>51</sup> adopts a D-amino acid backbone conformation. Based on this distinction between the conformations of the two flaps, we set out to establish a modular total synthesis of a covalent dimer form of the HIV-1 protease containing a 203 residue polypeptide chain (Figure 7(A)). This would then allow us to make asymmetric chemical analogues of the flaps in a single enzyme molecule. Our fully convergent synthetic strategy, by chemical ligation of four peptide segments, is shown in Figure 7(B) [13]. The left half of the target polypeptide chain was made by kinetically controlled ligation; the right half was made by native chemical ligation, followed by the conversion of the Thz-peptide product to a Cys-peptide. A final native chemical ligation step gave the full-length 203 residue polypeptide chain; the three Cys residues at the ligation sites were alkylated with bromoacetamide, and the polypeptide was folded to give high purity crystalline HIV-1 protease with full enzymatic activity (Figure 7 (C)-(E)).

The modular synthetic route to covalent dimer HIV-1 protease enabled us to design and prepare a series of analogue enzyme molecules in which the Gly<sup>51</sup> residue at the tip of each flap was replaced by L-Ala, D-Ala, or the achiral  $\alpha$ -aminoisobutyric acid (Aib). Both symmetrically substituted and asymmetric analogues were prepared. The purity and identity of each analogue was established by analytical LCMS of the synthetic proteins. High-resolution X-ray diffraction crystal structures were determined for all the synthetic enzyme molecules, complexed with the reduced isostere hexapeptide inhibitor MVT101 [12]. Enzyme assays of each analogue and the parent molecule with native Gly<sup>51</sup> in both flaps were carried out under initial velocity conditions using the fluorogenic substrate Abz-Thr-Ile-Nle-Phe(NO<sub>2</sub>)-Gln-Arg.amide (Abz = anthranilic acid) [14]. The kinetic parameters for the analogue enzymes are shown in Table 1 [15].

Substitution of Gly51 in both flaps with L-Ala51 or D-Ala51 resulted in a substantial reduction of the enzymatic activity. In contrast to this, an asymmetric analogue with L-Ala51 in one flap and D-Ala51 in the other flap in the same enzyme molecule had near-full activity, as did the enzyme molecule with Gly51 in one flap and L-Ala51 in the other flap (Table 1). Clearly, in the HIV-1 protease molecule the two flaps do not function in an equivalent manner in the enzyme-substrate complex. Further work is being undertaken on selected flap analogues with site-specific NMR and EPR probes, in order to correlate the conformational properties of the flaps with catalytic properties in the HIV-1 protease protein molecule.

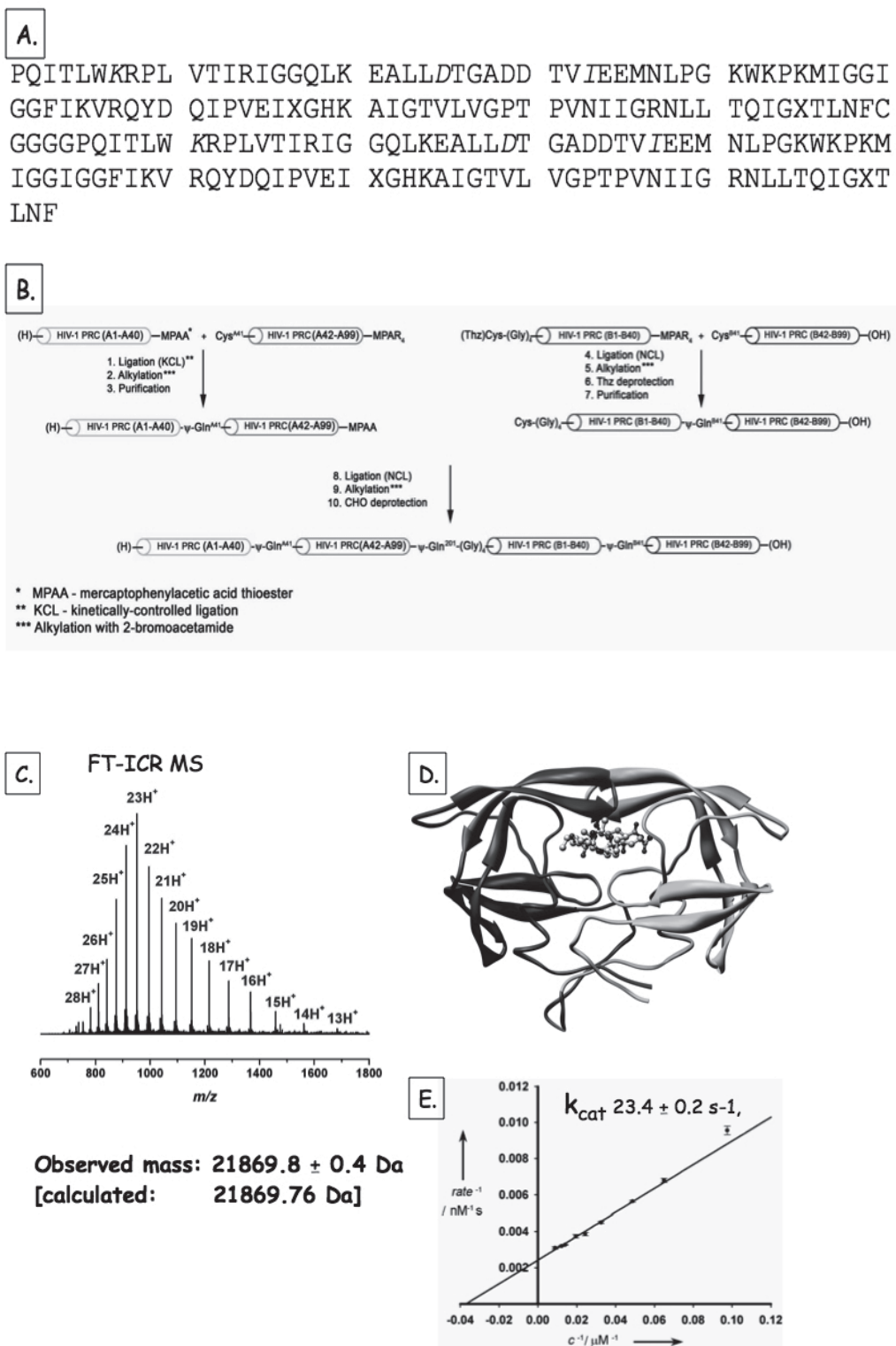


Fig. 7. Total chemical synthesis of HIV-1 protease covalent dimer. (A) 203 amino acid target sequence. (B) Fully convergent synthetic strategy. (C) Fourier transform ion cyclotron resonance electrospray MS of the synthetic protein. (D) X-ray crystal structure. (E) Enzymatic activity.

Table 1. Enzymatic activity of chemically synthesized HIV-1 protease 'flap' analogues

	51	151	$K_{cat}(S^{-1})$	$K_m(\mu M)$	$K_{cat}/K_m$
Native	Gly	Gly	<b>23.4</b>	25	<b>0.93</b>
Symmetric	L-Ala	L-Ala	3.7	50	0.07
	D-Ala	D-Ala	4.9	434	0.01
	Aib	Aib	(very low activity)		<0.001
Asymmetric	D-Ala	L-Ala	<b>17.6</b>	26	<b>0.67</b>
	Gly	L-Ala	<b>22.2</b>	47	<b>0.47</b>
	Gly	D-Ala	6.2	44	0.14
	Gly	Aib	4.0	105	0.04

## Conclusions

Robust, reproducible total chemical synthesis of proteins has been achieved by application of the chemical ligation principle: the chemo- and regio-selective covalent condensation of unprotected peptide segments, enabled by the formation of a non-native chemical structure at the ligation site. In native chemical ligation, the initial thioester-linked ligation product undergoes an intramolecular nucleophilic rearrangement to give a native peptide bond at the ligation site. Fully convergent, modular total synthesis of larger protein molecules has been achieved by a combination of native chemical ligation and kinetically controlled ligation.

Chemical synthesis gives atom-by-atom control over the molecular structure of a protein, and allows the preparation of essentially unlimited sites, number, and kinds of 'non-coded' chemical analogues. Mirror image proteins, fixed elements of secondary structure, backbone engineering, and protein molecules of novel backbone topology not found in nature are just some of the protein analogues that have been prepared. Chemical protein synthesis and the wide range of chemical protein analogues prepared by total chemical synthesis have been reviewed [16]. In combination with advanced physical techniques such as NMR, FTIR, and single molecule fluorescence spectroscopy, total chemical protein synthesis enables the systematic dissection of the molecular basis of protein function.

## Acknowledgments

First and foremost, I want to acknowledge the debt that I owe to Bruce Merrifield for the invention of SPPS. Without that ingenious and powerful technique, modern chemical protein synthesis would not be feasible. I also wish to thank my colleagues and collaborators who have contributed to the development of modern chemical protein synthesis and its applications to the total synthesis of a variety of protein targets. Supported by Office of Science (BER), U.S. Department of Energy, Grant number: DE-FG02-07ER64501.

## References

1. Yooseph, S. et al. *PLoS. Biol.* **5**, e16 (2007).
2. Ueberheide, B.M., et al. *Proc. Natl. Acad. Sci. U.S.A.* **106**, 6910-6915 (2009).
3. Ménez, A., Stöcklin, R., Mebs, D. *Toxicon*. **47**, 255-259 (2006).
4. Schnölzer, M., Kent, S.B.H. *Science* **256**, 221-225 (1992).
5. Dawson, P.E., Muir, T.W., Clark-Lewis, I., Kent, S.B.H. *Science* **266**, 776-779 (1994).
6. Hackenberger, C.P.R., Schwarzer, D. *Angew Chem. Int. Ed. Eng.* **47**, 10030-10074 (2008).
7. Merrifield, R.B. *Science* **232**, 341-347 (1986).
8. Hendrickson, J.B., *J. Am. Chem. Soc.* **99**, 5439-5450 (1977).
9. Bang, D., Pentelute, B.L., Kent, S.B.H. *Angew Chem. Int. Ed. Eng.* **45**, 3985-3988 (2006).
10. Kenner, G.W., *Proc. R. Soc. Lond. B. Biol. Sci.* **197**, 237-53 (1977).
11. Durek, T., Torbeev, V. Yu., Kent, S.B.H. *Proc. Natl. Acad. Sci. U.S.A.* **104**, 4846-4851 (2007).
12. Miller, M., et al. *Science* **246**, 1149-1152 (1989).
13. Torbeev, V. Yu., Kent, S.B.H. *Angew Chem. Int. Ed. Eng.* **46**, 1667-70 (2007).
14. Toth, M.V., Marshall, G.R. *Int. J. Pept. Protein Res.* **36**, 544-50 (1990).
15. Torbeev, V. Yu., Terechko, V.A., Kent, S.B.H. Presented at *The Protein Society*, Boston (2007).
16. Kent, S.B.H. *Chem. Soc. Reviews* **38**, 338-51 (2009).

**Peptide Synthesis and Biosynthesis**  
**Peptidomimetics**  
**Peptide Libraries and Chemical Diversity**



# Synthesis of Optically Active Anti- $\beta$ -Substituted $\gamma,\delta$ -Unsaturated Amino Acids via Asymmetric Thio-Claisen Rearrangement

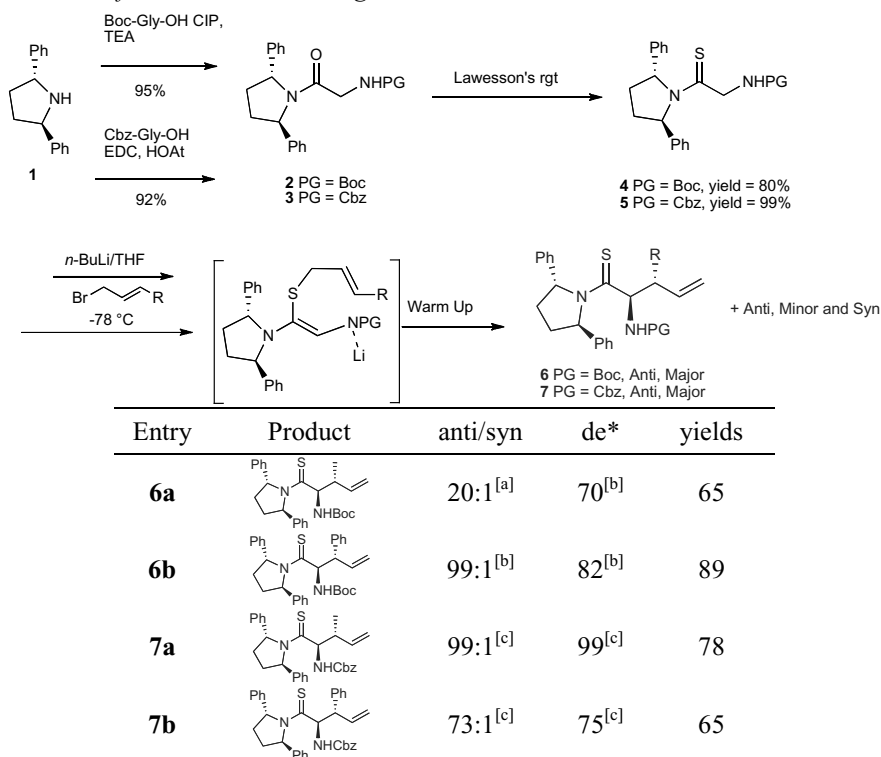
Zhihua Liu, Hongchang Qu, Xuyuan Gu, Kwang-Soo Lee,  
 Bryan Grossman, Vlad K. Kumirov, and Victor J. Hruby

Department of Chemistry, 1306 E. University Blvd, University of Arizona, Tucson, AZ 85721, U.S.A.

## Introduction

$\beta$ -Substituted  $\gamma,\delta$ -unsaturated amino acids are important unnatural amino acids. The versatile reactivity of the terminal double bond and their ability to functionalize at the  $\beta$ -position make them extremely useful in the peptide sciences. Among the methods to prepare these amino acids, the Claisen rearrangement has turned out to be a very efficient strategy due to its high asymmetric selectivity. The chelation-Claisen rearrangement has already proved to be good in producing syn- $\beta$ -substituted  $\gamma,\delta$ -unsaturated amino acids,[1] but the corresponding anti amino acids were not readily available until our recently developed novel Eschenmoser-Claisen rearrangement [2,3]. Following this success, we envisioned that the thio-Claisen could be a complementary method towards these amino acid preparations: the selectivity of forming (Z)-N, S-ketene acetal and the pseudochairlike conformations during the rearrangement could provide good asymmetric introduction. We here report the novel synthesis of anti- $\beta$ -substituted  $\gamma,\delta$ -unsaturated amino acids, which gave excellent diastereoselectivities and enantioselectivities via the thio-Claisen rearrangement [4].

Table 1. Results of thio-Claisen rearrangement



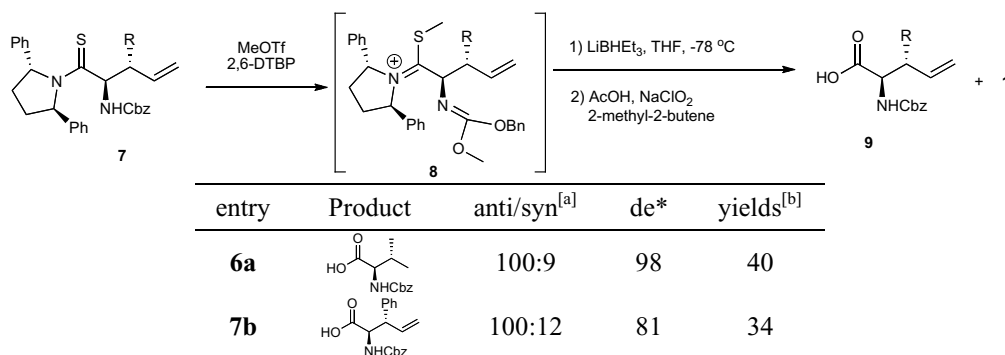
\*Diastereomer excess between two anti isomers. [a] Determined by weight. [b] Determined by <sup>1</sup>H-NMR. [c] Determined by chiral HPLC. [d] Isolated yield of total isomers



## Results and Discussion

Our amino acids synthesis started from coupling  $N^\alpha$ -protected glycine to (2*R*,5*R*) diphenylpyrrolidine (**1**), which was obtained from a literature reported method with high optical purity [5]. Despite the steric bulkiness of the amine, the coupling reaction gave excellent yields. The resulting amides **2** or **3** was treated with Lawesson's reagent at 120 °C to form the thioamides **4** or **5**. The thioamide was then treated with *n*-BuLi at -78 °C to form the thioenolate dianion, which was allylated with allylic bromides at the sulfur position. When the reaction mixture was warmed up, the thio-Claisen rearrangement took place to generate the thioamides **6** or **7** as the major products. The anti/syn ratios and diastereoselectivities were summarized in Table 1. We were happy to see that this rearrangement gave strong preference to the anti product as we expected. This is due to the use of  $C_2$  symmetric chiral auxiliary, which eliminated the C-N bond rotation problem that is known to reduce the stereoselectivities.

Table 2. Results of amino acids generation



\*Enantiomer excess between two anti isomers, determined by chiral HPLC. [a] Determined by <sup>1</sup>H-NMR. [b] Isolated yield of total isomers.

Amino acid generation was achieved by reducing the thioamide **7** to an aldehyde, and then oxidizing to the carboxylic acid. Since there is no reagent that can directly reduce a thioamide to and aldehyde or alcohol, we have to alkylate the thioamide with MeOTf first and followed by Superhydride reduction. The resulting *N,S*-acetal was then quenched to generate the aldehyde in situ and oxidized immediately to avoid the epimerization problem. Results of this three-step one-pot reaction were summarized in Table 2.

In summary, we have developed a novel methodology for synthesizing-β-substituted γ,δ-unsaturated amino acids via asymmetric thio-Claisen rearrangement, which offered excellent anti/syn ratios and diastereoselectivities. The amino acids were obtained with high optical purities.

## Acknowledgments

This work was supported by U.S. Public Health Service grant DK 17420 and the National Institute of Drug Abuse grants DA 06284, DA 13449.

## References

1. Kazmaier, U. *Angew. Chem., Int. Ed.* **33**, 998-999 (1994).
2. Qu, H., Gu, X., Min, B.J., Liu, Z., Hraby, V.J. *Org. Lett.* **8**, 4215-8 (2006).
3. Qu, H., Gu, X., Liu, Z., Min, B.J., Hraby, V.J. *Org. Lett.* **9**, 3997-4000 (2007).
4. Liu, Z., Qu, H., Gu, X., Min, B.J., Nichol, G.S., Nyberg, J., Hraby, V.J. *Org. Lett.* **10**, 4105-8 (2008).
5. Chong, J.M., Clarke, I.S., Koch, I., Olbach, P.C., Taylor, N.J. *Tetrahedron: Asymmetry* **6**, 409-418 (1995).

# **O-Acyl Isopeptide Method: Toward an Efficient Chemical Preparation of Peptides/Proteins Using Racemization-Free Segment Condensation Method**

**Taku Yoshiya, Hiroyuki Kawashima, Youhei Sohma,  
 Tooru Kimura, and Yoshiaki Kiso**

*Department of Medicinal Chemistry, Center for Frontier Research in Medicinal Science,  
 21st Century COE Program, Kyoto Pharmaceutical University, Kyoto, 607-8412, Japan*

## **Introduction**

Peptides and proteins synthesized by chemical means have been widely used in biological studies. To synthesize longer peptides and proteins, many kinds of convergent synthetic methods have been proposed. Among them, “segment condensation”, in which a side-chain protected peptide carboxylate is coupled with an amino group of another peptide segment to construct a longer peptide, has attracted attention as an important method. However, a fundamental drawback of the segment condensation is that epimerization at the C-terminal residue of an *N*-segment occurs during the condensation reaction with a *C*-segment (Figure 1A), limiting the *N*-segment to contain either a C-terminal Gly or Pro. This epimerization occurs because, in contrast to urethane-protected amino acids, peptides easily form chirally labile oxazolones upon C-terminal carboxyl activation.

Recently, we have developed “racemization-free segment condensation” based on the *O*-acyl isopeptide method (Figure 1) [1]. The idea was that an *N*-segment with a C-terminal isopeptide structure (*O*-acyl Ser/Thr residue) can be coupled to an N-terminal amino group of the *C*-segment without any epimerization, because the amino group of C-terminal isopeptide part is protected by a urethane-type protective group [2]. Activation of the carboxyl group of the isopeptide was thus expected to suppress the formation of racemization-inducing oxazolone. Toward future protein synthesis, we herein synthesized bioactive peptides by the *O*-acyl isopeptide method-based racemization-free segment condensation method.

## **Results and Discussion**

We synthesized humanin (H-MAPRGFSCLLLTSEIDLVPVKRRA-OH, **1**) to examine the advantage of the method in the synthesis of a longer peptide. Humanin is reported as a “difficult sequence”-containing peptide because of highly hydrophobic L<sup>9</sup>L<sup>10</sup>L<sup>11</sup>L<sup>12</sup> sequence. In our hand, the total isolated yield of **1** was only 6% using the conventional stepwise Fmoc-SPPS because of the poor quality of crude **1**. Thus, **1** was synthesized via sequential segment condensation using protected *O*-acyl isopeptide **2** and **3** (Scheme 1). Both *N*<sub>1</sub>-segment **2** and *N*<sub>2</sub>-segment **3** could be efficiently prepared using Fmoc SPPS, and purified by RP-HPLC (24% yield for **2** and 40% yield for **3**). Using the DIPCDI-HOAt method in NMP, *N*<sub>2</sub>-segment **3** was coupled to peptide-resin **5**, which was synthesized by standard Fmoc SPPS on a 2-chlorotrityl resin. The reaction was monitored by HPLC analysis of the deprotected/cleaved compound. In the next, *N*<sub>1</sub>-segment **2** was coupled by the HATU-HOAt method in DCM-NMP (1:4). The resulting peptide-resin **7** was subsequently treated with a TFA cocktail to give isopeptide **8**. Also, both of D-Ser<sup>7</sup> or D-Ser<sup>14</sup> derivative were not identified (<2.0%, verified by comparison with authentic samples using the analytical HPLC) in crude **8** (Figure 2). Pure **8** was then

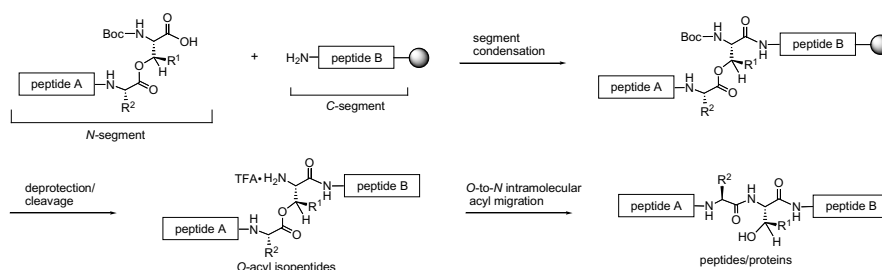
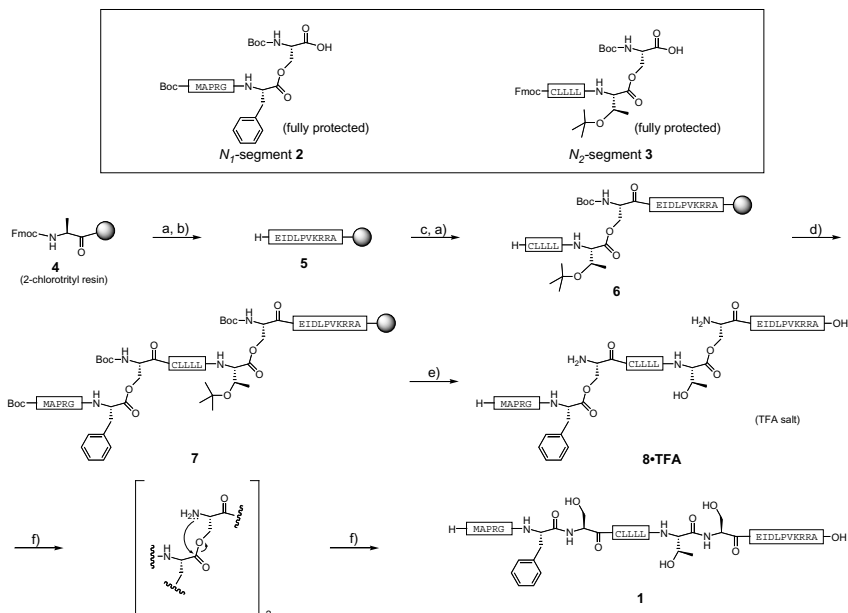


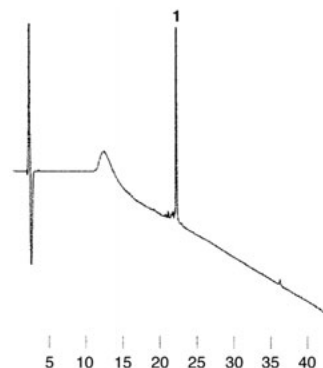
Fig. 1. *O*-Acyl isopeptide method based-racemization free segment condensation reaction.



**Scheme 1.** Reagents and conditions: a) 20% piperidine/DMF, 20 min; b) Fmoc-AA-OH, DIPCDI, HOBT, DMF, 2 h; c) 3, DIPCDI, HOAt, NMP, 2 h; d) 2, HATU, HOAt, 2,4,6-collidine, 1,8-bis(dimethylamino)-naphthalene, DCM-NMP (1:4), 4 h; e) TFA (94%), 1,2-ethanedithiol (2.5%), water (2.5%), triisopropylsilane (1%), 90 min; f) pH7.4 phosphate buffer, 37°C, overnight.

dissolved in pH 7.4 phosphate buffer to afford target peptide **1** via an *O*-to-*N* intramolecular acyl migration reaction (half time: ca. 10 min at 37°C), followed by a final HPLC purification to give pure **1** with a total yield of 41% based on the resin-bound-Ala residue. These results suggest that middle-sized peptides could be efficiently synthesized by use of the *O*-acyl isopeptide method-based segment condensation reaction.

These results suggested that the racemization-free segment condensation reaction of middle-sized peptide segments becomes possible at not only the C-terminal Gly/Pro but also Ser/Thr residues of the N-segment. In addition, final deprotected peptides and proteins were effectively purified by HPLC, because a simple isomerization to an *O*-acyl isopeptide remarkably and temporarily changed the physicochemical properties of the native peptide. Especially, higher water solubility of *O*-acyl isopeptide would enable easy purification of hydrophobic peptides. Finally, an *O*-to-*N* intramolecular acyl migration reaction triggered the native amide bond formation quantitatively under neutral conditions. These observations would be useful information for future chemical protein synthesis based on the segment condensation method [3].



**Fig. 2.** HPLC profile of crude **1**.

## Acknowledgments

T.Y. thanks APS for travel grant in the 21st APS. T.Y. and Y.S. are grateful for Research Fellowships of JSPS for Young Scientists. This research was supported in part by the “Academic Frontier” Project for Private Universities: matching fund subsidy from MEXT (Ministry of Education, Culture, Sports, Science and Technology) of the Japanese Government, and the 21st Century COE Program from MEXT.

## References

1. Sohma, Y., et al. *Chem. Commun.* 124-125 (2004).
2. Yoshiya, T., et al. *Tetrahedron Lett.* **47**, 7905-7909 (2006).
3. Yoshiya, T., et al. *Org. Biomol. Chem.* **7**, 2894-2904 (2009).

## Racemization of Cysteine and Histidine Residues in Automated Peptide Synthesis

Krzysztof Darlak, Thomas E. Hopkins, and Antonio Thigpen

*CreoSalus Incorporated, Louisville, KY 40228, U.S.A.*

### Introduction

Automated peptide synthesis allows for preparation of a large number of peptide sequences in a fairly straightforward manner. Currently, the most widely applied methodologies utilize Fmoc-protection in combination with uronium/phosphonium activating agents for synthesis of peptides. While these new and powerful activating agents can be applied to the majority of commonly used Fmoc amino acids, there are some exceptions such as cysteine and histidine. Racemization of these amino acids during activation with above listed reagents is well documented [1]. Herein we reevaluate the degree of racemization of cysteine and histidine residues using several popular currently available activating agents applied to a typical automated peptide synthesis using an in-situ activation method. Two modified model peptides [1e,1g] Z-Ile-Cys(Trt)-Pro-OH and Z-Ile-His-Pro-OH were used as a targets. HPLC analysis was used to evaluate the extent of racemization during cysteine and histidine incorporation.

### Experimental

Model peptides Z-Ile-Cys(Trt)-Pro-OH and Z-Ile-His-Pro-OH were prepared on 2-chlorotrityl resin using the Tetras (Thuramed) multiple peptide synthesizer using in-situ activation. Reagents used in the studies were: 0.6 M solution in NMP (BOP, PyBOP<sup>®</sup>, HCTU, HATU, COMU), 0.4 M solution in NMP (HBTU, PyClock<sup>®</sup>), 0.9 M solution in NMP (DIEA, NMM), 1.0 M solution in NMP (DIC, HOBt, 6-Cl-HOBt, Oxyma Pure). Coupling conditions for uronium/phosphonium reagents (order of addition to the 150 mg of resin (0.6 meq/g), no preactivation): Fmoc-amino acid 0.5 mmole, amine 0.9 mmole, reagent 0.5 mmole, mixing for 120 min; with diisopropylcarbodiimide/additive (order of addition to the resin, no preactivation): additive 0.5 mmole, Fmoc-amino acid 0.5 mmole, DIC 0.5 mmole, mixing for 120 min. Target peptides were cleaved from the resin with the mixture of TFA : water : phenol : TIPS (87.5:5:5:2.5) for 2 hours at RT or AcOH : TFE : DCM (1:2:7) for 1 hour at RT. The products were precipitated by addition of cold diethyl ether or hexane, centrifuged and dried. Chromatographic analysis of the obtained products was performed on a Waters Alliance HPLC system using a Vydac C18 column (4.6x250 mm, 218TP54) with the linear gradients (20-50 % B in 30 min for Z-Ile-His-Pro-OH and 50-80 % B in 30 min for Z-Ile-Cys(Trt)-Pro-OH in H<sub>2</sub>O/MeCN/0.05% TFA solvent system with detection at 220 nm. The content of LDL isomer was calculated as relative peak areas (Absorbance) from HPLC as: A (LDL isomer)/[A (LDL isomer + A (LLL isomer)) x 100. Results of the analysis are presented in Table 1 and 2.

*Table 1. Racemization during SPPS of Z-Ile-His-Pro-OH*

Reagent	%LDL Isomer		
	DIEA	NMM	None
BOP	1.1	3.1	-
PyBOP <sup>®</sup>	1.3	1.2	-
PyClock <sup>®</sup>	4.1	3.6	-
HBTU	2.0	2.8	-
HCTU	2.8	4.6	-
HATU	0.7	3.6	-
COMU	14.9	5.2	-
DIC/HOBt	-	-	2.3
DIC/6-Cl-HOBt	-	-	0.7
DIC/Oxyma	-	-	2.2

Table 2. Racemization during SPPS of Z-Ile-Cys(Trt)-Pro-OH

Reagent	%LDL Isomer		
	DIEA	NMM	None
BOP	5.1	13.8	-
PyBOP ®	5.0	21.0	-
PyClocK ®	7.5	16.3	-
HBTU	4.4	18.6	-
HCTU	6.5	15.4	-
HATU	2.9	16.2	-
COMU	1.5	7.3	-
DIC/HOBt	-	-	0.6
DIC/6-Cl-HOBt	-	-	0.6
DIC/Oxyma	-	-	0.1

## Results and Discussion

We have used two model peptides, Z-Ile-Cys(Trt)-Pro-OH and Z-Ile-His-Pro-OH, as targets to evaluate the degree of racemization during incorporation of Fmoc-Cys(Trt)-OH and Fmoc-His(Trt)-OH to the solid support utilizing a Tetras automated peptide synthesizer. We have selected the most popular and widely used coupling agents and bases in our experiments. We also included the recently introduced reagents: COMU [2,3], PyClock [4] and Oxyma Pure [2,3,5,6]. Published racemization results so far have covered mostly either solution or manual solid phase synthesis.

We have applied, in our studies, the in-situ activation method routinely used in batch type automated peptide synthesis. In many cases of the routine peptide synthesis the same activating method is used to prepare an entire peptide sequence. This approach is necessary due to the limitation of instrumentation (lack of sufficient number of reagents precisely delivered on board of synthesizer) or the user's choice. This strategy is acceptable for preparation of the routine peptide sequence where cysteine and histidine residues are not present. In cases where cysteine and/or histidine are present in the sequence a single activation methodology will not yield the highest quality peptide product due to extensive racemization with uronium / phosphonium chemistry.

Our studies confirmed that N-Methylmorpholine is not acceptable for activation with uronium and phosphonium type activating agents. DIEA gave better results but the level of epimerization was still too high when applied to Cys and His residues. New reagents such PyClock and COMU also are found not to be acceptable for incorporation of cysteine. COMU in the combination with DIEA gave lower level of racemization for Cys residue but still high enough (>1%) to make it unacceptable for its incorporation. Future studies of less basic and more hindered bases like TMP, as noted by Barany group [1a, 1d], may possibly reduce racemization even further.

Use of diisopropylcarbodiimide with various additives was found to be a good method for introduction of cysteine and histidine residues using an automated peptide synthesis. The new Oxyma Pure additive with DIC as activator gave the lowest racemization level observed in all tested reagents (0.1%).

## References

1. a) Han, Y., et al. *J. Org. Chem.* **62**, 4307 (1997), b) Musiol, H., et al. *Biopolymers* **34**, 1553 (1994), c) Kaiser, T., et al. *Tetrahedron Lett.* **37**, 1187 (1996), d) Angel, Y.M., et al. *J. Peptide Res.* **60**, 292 (2002), e) Mergler, M., et al. *J. Peptide Sci.* **7**, 502 (2007), f) Van den Nest, W., et al. *J. Pept. Sci.* **7**, 115 (2001), g) Loidl, G. et al., in *Peptides for Youth-Proceedings of the 20<sup>th</sup> American Peptide Symposium*, ed. Delvalle, S., et.al., Springer, New York, U.S.A., 2009, 163.
2. Albericio, F. *J. Pept. Sci., Suppl.* **14**, 57 (2008).
3. Subiros-Funosas, R., Prohens, R., Barbas, R., El-Fahan, A., Albericio, F. *Chem. Eur. J.* 2009, in press.
4. Moreno, J.A., et al. 29<sup>th</sup> European Peptide Symposium, Gdansk, Poland, 2006.
5. Itoh, M., *Bull Chem. Soc. Japan* **46**, 2219 (1973).
6. Izdebski, J. *Pol. J. Chem.* **53**, 1049 (1979).

## Further Investigations into Microwave Assisted Solid Phase Peptide Synthesis: Synthesis of Modified Peptides

Sandeep K. Singh, Alicia D. Douglas, Eric J. Williamson, Grace S. Vanier\*

CEM Corp., Bioscience Division, PO Box 200, 3100 Smith Farm Road, Matthews, NC 28106, U.S.A.

### Introduction

In solid phase peptide synthesis (SPPS), while certain peptide sequences are synthesized relatively easily, some sequences are much more difficult. Efficient couplings occur within a fully solvated peptide-polymer matrix, where reagent penetration is rapid and unhindered. Sudden decreases in reaction rates and incomplete couplings have been attributed to peptide aggregation resulting in poor solvation [1]. Microwave energy represents a fast and efficient way to enhance both the deprotection and coupling reactions hindered by aggregation. The *N*-terminal amino group and peptide backbone are polar and they constantly try to align with the alternating electric field of the microwave, this helps in breaking up the chain aggregation. The application of microwave energy has proved to be a major enabling tool for enhancing slow and difficult chemical reactions [2]. Unlike conventional heating, microwave energy directly activates any molecule with a dipole moment and allows for rapid heating at the molecular level. Microwave assisted SPPS has been successfully applied to and shown useful for the synthesis of a range of difficult peptides [3]. Microwave peptide synthesis routinely shows substantial improvements in crude purity with reduced synthesis time compared to conventional SPPS. Previous studies have investigated the effects of microwave on aspartimide formation and epimerization, and offered optimized conditions for susceptible sequences to these well-known side reactions [4]. We now report our recent results on the development of microwave assisted *N*-terminal modifications and head-to-tail on-resin cyclization.

### Results and Discussion

***N*-Terminal modifications:** Fatty acid acylation on the *N*-terminus of a peptide increases its cell permeability and affinity, and is a common post-translational modification for a wide variety of viral, bacterial and eukaryotic proteins and peptides [5]. Biotin labeled peptides have numerous biochemical and microbiological applications [6]. Under conventional conditions, these modifications often require coupling reactions of 24 h or more due to poor solubility and reactivity of the fatty acid or biotinylating reagents. We envisaged that sluggish reaction kinetics in these couplings could be overcome by the application of microwave irradiation.

The acyl carrier protein, ACP-(65-74) sequence (Val-Gln-Ala-Ala-Ile-Asp-Tyr-Ile-Asn-Gly) was selected as the test peptide for the present study. ACP-(65-74) was synthesized on Fmoc-Gly Wang resin (0.61 mmol/g) in less than 5 h using the CEM Liberty automated microwave peptide synthesizer. Fmoc deprotection with 20% piperidine in DMF for 0.5 min and 3 min at 75 °C and coupling with Fmoc-AA-OH/HBTU/DIEA for 5 min at 75 °C gave the ACP-(65-74) with a crude purity of more than 95% (Figure 1a). Double coupling of *n*-hexanoic acid to ACP for 5 min at 75 °C using HCTU/DIEA activation gave the *N*-capped peptide in 80% crude purity (Figure 1b). Similarly, microwave coupling of biotin-LC to ACP using HATU/DIEA for 5 min at 75 °C gave the biotin labeled peptide in 93% crude purity (Figure 1c). Thus, *N*-terminal modifications with a fatty acid or biotin were completed in excellent yields in less than 15 min using microwave energy.

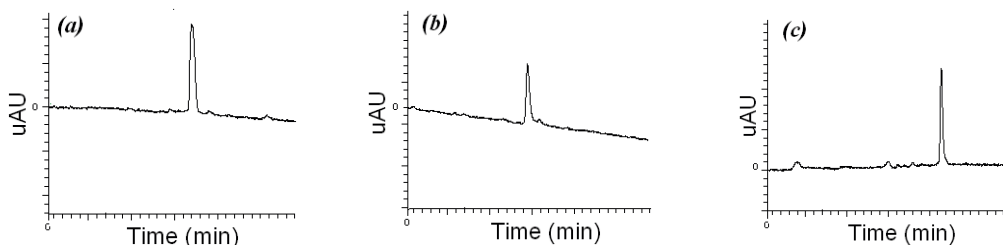
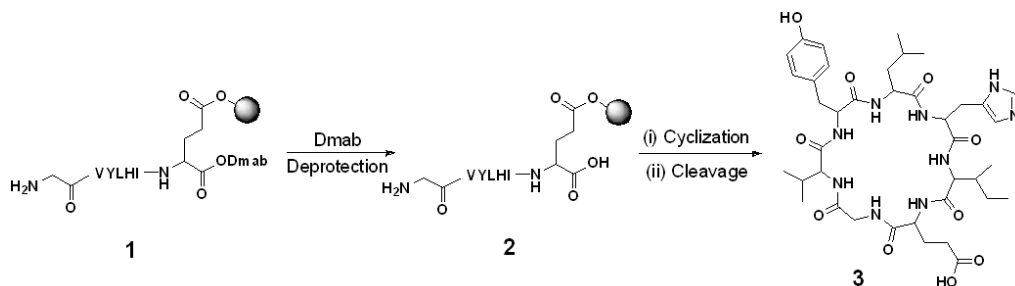


Fig. 1. HPLC crude chromatograms of (a) ACP-(65-74), (b) *n*-Hexanoic-ACP-(65-74), (c) Biotin-LC-ACP-(65-74).



Scheme 1. On-resin peptide cyclization.

**Head-to-tail on-resin cyclization:** Introduction of a conformational restraint in peptides through cyclization increases their receptor affinity. Cyclic peptides exhibit improved metabolic stability, and increased potency and bioavailability as compared to their linear counterparts [7]. Head-to-tail on-resin cyclization strategy is an important tool in SPPS that takes advantage of the resin induced pseudo-dilution effects. However, such cyclizations often require long reaction times under conventional conditions and result in a low crude purity of the cyclized peptide.

The present work describes optimized microwave reaction conditions for each step in the head-to-tail on-resin cyclization method (Scheme 1). All of the synthesis steps were carried out in a fully automated fashion using the CEM Liberty microwave peptide synthesizer. The test sequence (Gly-Val-Tyr-Leu-His-Ile-Glu) for the cyclization studies was synthesized on Fmoc-Glu(Wang resin)-ODmab (0.32 mmol/g) in which the side chain  $\gamma$ -carboxyl group is anchored to the resin and the  $\alpha$ -carboxyl is protected by Dmab orthogonal protecting group. A small amount of peptidyl resin was cleaved at the end of each step to assess the purity. Thus, Fmoc deprotection with 20% piperidine in DMF for 0.5 min and 3 min at 75 °C and coupling with Fmoc-AA-OH/HBTU/DIEA for 5 min at 75 °C assembled the backbone **1** in 91% crude purity (Scheme 1). Selective on-resin removal of Dmab protection was effected by treatment with 5% hydrazine in DMF (2 x 3 min at 75 °C) to give the linear precursor **2** in 91% crude purity. Head-to-tail cyclization of resin bound peptide **2** was accomplished using DIC/HOBt (3 x 10 min at 75 °C); cleavage of the cyclic peptide **3** from the resin followed by LC-MS analysis of the crude product indicated 77% purity.

In summary, we have developed efficient microwave assisted methods for the *N*-terminal modifications and head-to-tail on-resin cyclization of peptides. Microwave synthesis allows the completion of these transformations in high yields and purities in a fraction of the time compared to conventional peptide synthesis.

## Acknowledgments

We thank the Bioscience Division of CEM Corporation for providing the research facilities.

## References

- Quibell, M., Johnson, T. In *Fmoc Solid Phase Peptide Synthesis. A Practical Approach*; Chan, W.C., White, P.D., (Eds.), Oxford University Press, New York, 2000.
- Loupy, A., *Microwaves in Organic Synthesis*. Wiley-VCH, Weinheim, 2002.
- (a) Yu, H.-M., Chen, S.-T., Wang, K.-T. *J. Org. Chem.* **57**, 4781-4784 (1992). (b) Erdelyi, M., Gogoll, A. *Synthesis* **11**, 1592-1596 (2002). (c) Collins, J.M., Collins, M.J., Steorts, R.C. *Poster Presentation at the 18<sup>th</sup> American Peptide Symposium, Boston, MA.* (2003). (d) Matsushita, T., Hinou, H., Kurogochi, M., Shimizu, H., Nishimura, S.-I. *Org. Lett.* **7**, 877-880 (2005). (e) Bacsa, B., Desai, B., Dibo, G., Kappe, C.O. *J. Pept. Sci.* **12**, 633-638 (2006). (f) Fara, M.A., Diaz-Mochon, J.J., Bradley, M. *Tetrahedron Lett.* **47**, 1011-1014 (2006). (g) Tantry, S.J., Rao, R.V. R., Babu, V.V.S. *ARKIVOC* **1**, 21-30 (2006). (h) Grieco, P., et al. *J. Med. Chem.* **51**, 2701-2707 (2008). (i) Santagada, V., et al. *Mini Rev. Med. Chem.* **9**, 340-358 (2009). (j) Galanis, A.S., et al. *Biopolymers* **92**, 23-34 (2009).
- Palasek, S.A., Cox, Z.J., Collins, J.M. *J. Pept. Sci.* **13**, 143-148 (2007).
- Chicharro, C., et al. *Antimicrob. Agents Chemother.* **43**, 1267-1269 (1999).
- Winkler, D.F.H., McGeer, P.L. *Proteomics* **8**, 961-967 (2008).
- Rovero, P. In *Solid Phase Synthesis. A Practical Guide*; Kates, S.A., Albericio, F., (Eds.), Marcel Dekker, New York, 2000.

## Application of CDFSS Tools to the Oxidation of a Peptide Containing Multiple Cysteine Residues

Miranda Steele, Todd Osiek, Allan Casciola, and Thomas Gordon

Covidien/Mallinckrodt, St. Louis, MO 63147, U.S.A.

### Introduction

For many businesses, success and growth are measured not just by formulating quality products, but by how efficient they are at launching new products. The strategy and tools utilized during research and development directly impact the success of a product's launch. Chemical Design for Six Sigma (CDFSS) provides the methodology needed to build customer requirements into every aspect of the development process [1,2]. This systematic approach uses statistical tools to align an organization's goals with their customer's expectations by consistently providing reliable and manufacturable products in a reasonable time. Understanding the customer's expectations and correctly implementing CDFSS tools will increase the likelihood of overall success. In an effort to meet the demands of a current customer, Six Sigma tools were applied to optimize the oxidation of a peptide containing multiple cysteine residues. Tools including process maps, cause and effect (C&E) matrices, failure mode and effect analysis (FMEA) and design of experiments (DOE), as they relate to the oxidation, are outlined in this paper.

### Results and Discussion

**Process Map:** Process mapping (Figure 1) graphically outlines the steps in a process—identifying both the key process input and output variables (KPIVs and KPOVs, respectively), as well as controlled or uncontrolled variables. Once the inputs have been identified, subsequent tools are used to fully characterize the factors that impact customer satisfaction.

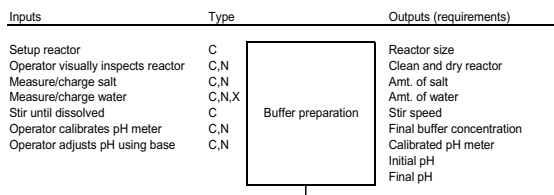


Fig. 1. Section of Process map.

**Cause and Effect Matrix:** The Cause and Effect (C&E) matrix (Figure 2) uses the process map as the primary tool to prioritize input variables that significantly impact the process and customer requirements (outputs). By using this rating system, key variables emerge, which later become inputs for the FMEA and DOEs.

Rating of Importance to Customer		1	3	5	2	1	7	7
		1	2	3	4	5	6	7
	Reactor size (buffer prep)							
	Amt. of salt							
	Amt. of water							
	Stir speed (buffer prep)							
	Initial pH (buffer prep)							
	Final pH (buffer prep)							
	Final buffer concentration							
Process Step	Process Input	9	0	0	0	0	0	0
1 Buffer preparation	Setup reactor	9	0	0	0	0	0	0
3 Buffer preparation	Measure/charge salt	0	9	0	0	9	1	9
4 Buffer preparation	Measure/charge water	3	0	9	0	3	0	0
5 Buffer preparation	Stir until dissolved	0	0	0	9	0	0	1
7 Buffer preparation	Adjust pH	0	0	0	3	0	9	9

Fig. 2. Section of C&E diagram.

**Failure Modes & Effects Analysis:** Failure Mode & Effect Analysis assesses the risk to a customer if a key process input were to fail and helps identify

Process Step	Key Process Input	Potential Failure Mode	Potential Failure Effects	S E V	Potential Causes	O C C	Current Controls	D E T	R P N
What is the process step	What is the Key Process Input?	In what ways does the Key Input go wrong?	What is the impact on the Key Output Variables (Customer Requirements) or internal requirements?	How Severe is the effect to the customer?	What causes the Key Input to go wrong?	How often does the cause or FM occur?	What are the existing controls and procedures (inspection and test) that prevent either the cause or the Failure Mode? Should include an SOP number.	How often can the defect cause or FM occur?	
Oxidation	Add buffer	Add too little salt	Unsure	5	Calculation error	1	Calculations are witnessed	1	5
Oxidation	Add buffer	Add too little salt	Unsure	5	Operator weighing error	1	Readings are witnessed	1	5
Oxidation	Add buffer	Add too much salt	Unsure	5	Calculation error	1	Calculations are witnessed	1	5

Fig. 3. Section of FMEA.



controls needed to minimize risk. The FMEA also serves as living documentation of all process improvements (Figure 3).

**Design of Experiments:** Design of Experiments (DOE) is used to understand the effects of selected input variables (factors) that impact the output variables (responses). The factors are set at selected levels of interest and in randomized combinations to determine the effects of the factors and their interactions on output variables. DOEs provide information to increase the control of the process, as well as help identify the conditions needed to yield optimal process output.

Design Layout (full factorial)

Input variables: pH, peptide concentration, buffer concentration, % solvent

Output variables: % peptide content (yield), % polymer (impurity)

Statistical analysis of the DOE data showed a normal distribution of the data ( $p > 0.05$ ) and favorable  $R^2$  adjusted values, which indicated that the model was sufficient. The response optimization plot (Figure 4) shows a composite desirability of 0.895, with the peptide content (PC) maximum at 76.0% and the polymer minimum at 10.0%. Figures 5 and 6 show the effects of the two-way interactions on peptide content and polymer, respectively.

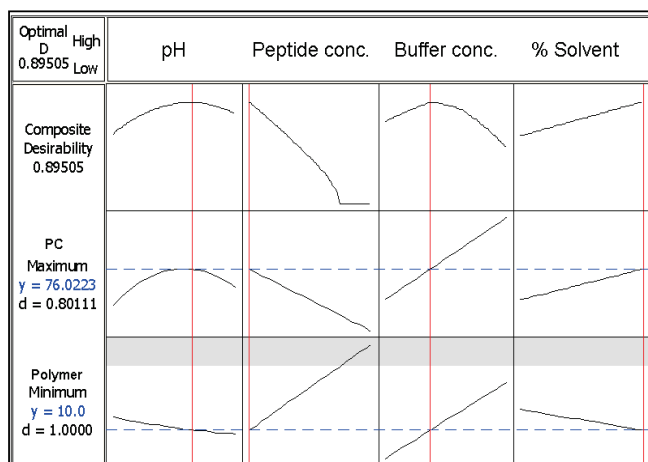


Fig. 4. Optimization plot for DOE.

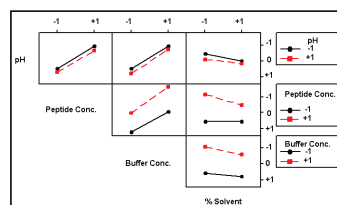


Fig. 5. PC interactions plot.

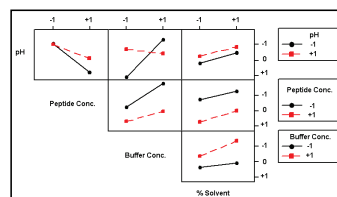


Fig. 6. Polymer interactions plot.

Implementation of selected Six Sigma tools provided a means to develop a scalable and robust oxidation process. This methodology enabled the R&D group to utilize experience from a cross-functional team, allowed for identification of critical process parameters and reduced risks associated with the process by our evaluation of key failure modes.

## Acknowledgments

The authors want to thank the Imaging/Pharma Operational Excellence (OpEx) Managers for their technical support, Peptides R&D, Peptides QA, and Mark Puett, Director of Peptides R&D, Coviden.

## References

1. Gursahaney, N., (10/17/2003). THC. DFSS Summit.
2. The Black Belt Memory Jogger: A Pocket Guide for Six Sigma Success. (2002).

## **Evaluation of Alternatives to HOBT in Solid Phase Peptide Synthesis**

**Matt Davis and Kripa Srivastava**

*Pharmaceuticals Division, Covidien, St. Louis, MO 63147, U.S.A.*

### **Abstract**

HOBT has often been used with the coupling agents to suppress racemization and to prevent side-reactions. Recently, it has been placed under explosive category and its transportation has been restricted. Due to the ongoing development of peptide-based drugs, it would be highly advantageous to have a new and efficient racemization suppressing peptide coupling additive free of the above hazardous nature. In the quest for such a coupling additive to replace HOBT, we examined 2-mercaptobenzothiazole (2-MBT) and oxymaPure (ethyl cyanoglyoxylate-2-oxime) by preparing several peptides for comparison study.

### **Introduction**

In peptide synthesis, coupling of two amino acids - one with a free acid function, and the other with a free amino group - is generally carried out with DCC or DIC carbodiimide [1, 2]. Sometimes other coupling agents such as EDC [3, 4] or CDI [5, 6] have also been used. These coupling reagents are known to suffer from high levels of racemization and other side reactions. As a consequence, coupling reactions of molecules containing various functional groups have generally been performed with HOBT [7] as a racemization suppressant. Recently, benzotriazole derivatives like HOBT, HOAT, HBTU, TBTU, etc... are considered potentially explosive and their transport/delivery, storage and handling needs special attention. More so, HOBT has been placed under an explosive category and as a result, its availability on a large quantity is not possible because of transport limitations. A few years back, replacement of HOBT by 2-MBT (2-mercaptobenzothiazole) was proposed by Reaxa Company [8]. Luxemborg Biotechnologies Ltd. is now advertising oxymaPure [9] as the most effective racemization suppressing coupling additive available. We, as a contract manufacturer of peptide API are considering substituting 2-MBT or oxymaPure for HOBT in our synthesis process. As a result, we decided to study their applicability by synthesizing several peptides of different types such as peptide-acids, peptide-amides and peptide alkylamides.

### **Synthesis of Peptides**

Several peptides were synthesized by Fmoc-SPPS method using DIC in combination with HOBT, 2-MBT, and oxymaPure. They were then released from the support by cleaving with TFA+H<sub>2</sub>O+TIS. The crude peptides were analyzed by analytical HPLC to determine their purity.

Peptide 1: Peptide-acid containing Arg, Leu, Phe, Ser, Tyr

Peptide 2: Peptide-acid containing Arg, Gly, Leu, Phe, Ser, Tyr, Trp

Peptide 3: Peptide-amide containing Ala, Gly, Gln, His, Leu, Met, Trp, Val

Peptide 4: Peptide-ethylamide.

### **Results and Discussion**

Condensation reactions of molecules containing various functional groups often require mild reaction conditions to avoid side reactions. Widely used condensing agents are DCC, DIC, or EDC but they suffer from racemization and side-reaction formation because of their high reactivity. Presently, addition of HOBT in a coupling mixture has become a very common practice. It is because of its racemization suppressing ability and minimization/elimination of by-product formation due to its participation in the conversion of over-reactive species into a milder but sufficiently reactive intermediate species. We explored the use of 2-MBT and oxymaPure to replace HOBT. Our investigation showed that both additives were found suitable but not as good as HOBT. But, because of safety and environmental concerns, when a choice of

reagents, solvents, or reactions conditions exists, the less dangerous alternative is preferred, even at the expense of the yield or the purity of the products.

## Conclusion

HOBt, 2-MBT and oxymaPure all prove to be suitable coupling additives for the avoidance of racemization during the coupling step of solid phase peptide synthesis. In fact, different additives proved to be more advantageous on a peptide to peptide basis, and dependent on the coupling conditions. HOBt, 2-MBT and oxymaPure are all suitable coupling additives. This examination was inconclusive to recommend any particular additive, and further study will be required.

## References

1. Sheehan, J.C., et al. *JACS* **77**, 1067 (1955).
2. Albericio, F., et al. *Org. Prep & Proc. Int.* **33**, 203 (2001).
3. Kopple, K.D., et al. *JACS* **84**, 4457 (1962).
4. Sheehan, J.C., et al. *JACS* **87**, 2492 (1965).
5. Bodanszky, M., et al. *Chem. Ind. London* 1597 (1966).
6. Paul, R., et al. *JACS* **82**, 4596 (1960).
7. König, W., et al. *Chem. Ber.* **103**, 788 (1970).
8. Reaxa Company, SP<sup>2</sup>, U.K., Nov. 2005.
9. Luxemborg Biotchnologies, 30EPS, Helsinki, Finland, Aug. 30-Sept. 5, 2008.

## **Development of a Novel Solid Support for the Economical Synthesis of Leuprolide Drug**

**Kripa Srivastava and Matt Davis**

*Pharmaceuticals Division, Covidien, St. Louis, MO 63147, U.S.A.*

### **Introduction**

The secretion of luteinizing hormone-releasing hormone/follicle stimulation hormone (LH-RH/FSH) is under the stimulatory control of the gonadotropin releasing hormone (GnRH), a decapeptide-amide. Leuprolide, a nonapeptide with a C-terminal alkylamide moiety is an analog of LH-RH/FSH and has been approved and marketed as a drug for prostate cancer. Leuprolide has been prepared by both solution phase and solid phase methods, employing Boc/Benzyl chemistry [1-4] and Fmoc/t-butyl methodology [5-10]. During the synthesis, the C-terminal amino acid of leuprolide either has a benzyl ester group or is attached to a solid support via a benzyl ester linkage. This requires alkylaminolysis at the end of the synthesis to yield the protected leuprolide, which after acidolysis results into leuprolide. Nowadays, the most common way to synthesize peptides quickly is via solid phase approach, where the success is heavily determined by the solid support applied and its performance. Currently, there is no general rule to decide on the most convenient and effective solid support for a particular peptide synthesis. However, it is important to consider the type of chemistry to be carried out during the synthesis, resin-reagent compatibility, swelling to solvent ratio, and the length as well as the sequence of the desired peptide.

### **Results and Discussion**

To produce leuprolide inexpensively and safely employing Fmoc-SPPS method, an intellectual effort was initiated to develop a low-cost solid support containing a few steps in its synthesis. The newly developed resin, called, "ethylaminomethyl-indolylmethyl resin" or EAM-IMR was then tested for its suitability in the synthesis of leuprolide. The yield and purity of the crude leuprolide obtained after its release from the support was appreciably high and was comparable to leuprolide synthesized on another developed support, which is also commercially available and known as, "ethylaminomethyl-indolylacetyl-aminomethyl resin" or EAM-IA-AMR. The application of this support also avoided the exposure of the constructed peptide chains to an excess ethylamine. This developed technology was able to lower the production cost of leuprolide by at least 50% compared to Boc-chemistry process on Merrifield resin.

The entire sequence of the peptide was assembled in a stepwise fashion on the solid carrier by a series of N- $\alpha$ -deprotection and amino acid coupling steps. The simultaneous removal of all the protection groups and the release of the peptide from the support was accomplished by an acid cleavage method. Leuprolide was synthesized by the linear Fmoc-solid phase method [5-7] using DIC-HOBT coupling method [8-10].

#### ***Preparation of 3-formyl-indolylmethyl resin***

A mixture of Merrifield resin (12g, sub=1.25mmol/g; 15mmol/total), 3-formylindole (3.3g, 1.5 fold) and anhydrous potassium carbonate (3.1g, 1.5 fold) or sodium methoxide/methanol solution (1.5 mole equivalents) in 100-120ml DMF was agitated for overnight. Water (100-120ml) was added and after agitation for 30 minutes, it was filtered and washed with water, 50%DMF/H<sub>2</sub>O, DMF, DCM, and MeOH (2x each) and was dried to get 13.72g (97%) of the aldehyde-resin. According to nitrogen analysis, the substitution of the aldehyde group was 1.20mmol/g.

#### ***Loading of ethylamine by reductive amination***

Aldehyde-resin (2g, sub=1.2mmol/g; 2.4mmol/total) was agitated with 40ml of THF and ethylamine (5 fold, 0.8ml) was added and agitation was continued for overnight. Sodium borohydride (10 fold, 0.91g) and EtOH (10ml) were added and agitation was continued for additional 6-7 hours. Water (~20ml) was added and after stirring for 20-30 minutes, it was filtered and washed with H<sub>2</sub>O, MeOH, DMF, and MeOH (2x each) and was dried to yield ethylaminomethyl-indolyl methyl resin with a sub=0.85mmol/g.

#### ***Preparation of Ethyl-3-formyl-indolylacetate***

A mixture of 3-formyl-indole (30g, 1 equivalent), ethylbromoacetate (34ml, 1.48 equivalents) in

300ml DMF was stirred for overnight and then at 60°C for an hour. The mixture and potassium carbonate (43g, 1.48 equivalents) were poured into stirred water (~1.5L) at 0°C and after one hour, the solid was filtered followed by washing twice with water and dried to yield 38.8g (80%) of the ethyl-3-formyl-indolylacetate.

#### **Preparation of 3-formyl-indolylacetic acid**

A mixture of ethyl-3-formyl-indolylacetate (46.3g, 1 equivalent) and KOH (16.8g, 1.5 equivalents) in 500ml MeOH was refluxed for 2 hours and then the solvent was removed by evaporation. The residue was dissolved in ~250ml of water and was washed twice with ethylacetate. The aqueous phase was acidified to pH ~1 and the solid separated and filtered followed by washing with water (3-4x) and was dried to yield 37.2g (91.5%) of the product. It was recrystallized from hot ethanol to yield 36.5g (89.8%) of the 3-formyl-indolylacetic acid.

#### **Preparation of 3-formyl-indolylacetyl-aminomethyl resin (CHO-IA-AMR)**

Aminomethyl resin (20g, sub=0.9mmol/g; 18mmol/total) was added to a stirred solution of 3-formyl-indolyl acetic acid (7.3g, 2 equivalents) and HOBt (19.5g, 8 equivalents) in 140ml of 50% DCM/DMF followed by the addition of DIEA (9.4ml, 3 equivalents) and then DIC (22.6ml, 8 equivalents). The agitation was continued for 3-4 days and then the resin was filtered and washed with DCM, MeOH, DMF, MeOH, and DCM (1x each). It was dried to yield 26.5g of indole resin.

#### **Loading of ethylamine by reductive amination**

The ethylamine was loaded on the resin by reductive amination using different reducing agents [11-15] to get amine substitution from 0.2mmol/g to 0.9mmol/g.

#### **Synthesis of leuprolide**

EAM-IMR=22.0g(sub=0.5mmol/g; 11mmol/total).

Fmoc-AA-OH, HOBt, DIC=1.5 mole equivalents; Coupling solvent=DMF+DCM (3:1).

Yield of peptide-resin=38.9g (92.7%).

Cleavage: 2.0g (0.5mmol) of the peptide resin was cleaved with 10ml of TFA+H<sub>2</sub>O+TIS (95+2.5+2.5) for 3 hours to yield 0.48g (78.7%) of the crude leuprolide with a purity of >69.34% (TFA method).

EAM-IA-AMR=18.6g (sub=0.54mmol/g; 10mmol/total); Fmoc-AA-OH, HOBt, DIC=1.5 mole equivalents; Coupling solvent=DMF+DCM (3:1).

Yield of peptide-resin=37.3g (99.5%).

Cleavage: 2.0g (0.53mmol) of the peptide-resin was cleaved with TFA+H<sub>2</sub>O+TIS (95+2.5+2.5) to yield 0.53g (82.2%) of the crude peptide with a HPLC purity of 69.53% (TFA method).

## **Conclusion**

We examined several solid supports and subsequently developed a new solid support. The suitability and the effectiveness of the support developed was tested by synthesizing leuprolide. The process was found efficient, reproducible and economical.

## **References**

1. Merrifield, R.B. *JACS* **85**, 1249 (1963).
2. Rivier, J., et al. *IJPPR* **25**, 414 (1985).
3. Ajayagosh, A., et al. *JOC* **55**, 2826 (1990).
4. Coy, D.H., et al. *Biochem.* **13**, 303 (1974).
5. Carpino, L.A., et al. *JOC* **37**, 3404 (1972).
6. Field, G.B., et al. *IJPPR* **35**, 161 (1990).
7. Meienhofer, J., et al. *IJPPR* **11**, 246 (1978).
8. Schmidt, E., et al. *Justus Liebigs Ann. Chem.* **571**, 83 (1951).
9. Ripkorn, R., et al. *IJPPR* **21**, 100, (1983).
10. Sheehan, J.C., et al. *JACS* **77**, 1067, (1955).
11. Sarantakis, D., et al. *Tetrahedron Letters* **38**, 7325 (1997).
12. Bhattacharya, S., et al. *Tetrahedron Letters* **44**, 6099 (2003).
13. Sabramanyam, C., et al. *Tetrahedron Letters* **43**, 6313 (2002).
14. Swayze, E.E. *Tetrahedron Letters* **38**, 84645 (1992).
15. Estep, K.G., et al. *JOC* **63**, 5300 (1998).
16. Ramage, R., et al, *Tetrahedron Letters* **34**, 6599 (1993).
17. Bui, C.T., et al. *Tetrahedron Letters* **40**, 3471 (1999).
18. Chan, W.C., et al. *JCS Chem. Commun.* **1475** (1995).

## $^1\text{H}$ , $^{13}\text{C}$ -HSQC HR-MAS NMR as a Tool for Investigating the Quality of Fmoc-AA-Wang Resins for SPPS

C. Stähelin,<sup>1</sup> F. Dick,<sup>1</sup> S. Ferrari,<sup>1</sup> and D. Rentsch<sup>2</sup>

<sup>1</sup>Bachem AG, Bubendorf Switzerland and <sup>2</sup>Swiss Federal Laboratories for Materials Testing and Research (EMPA), Dübendorf Switzerland

### Introduction

The use of high quality starting materials in SPPS is a prerequisite to obtain peptides of high purity and with high yields [1]. Beside AA derivatives and reagents, the quality of employed resins like Fmoc-AA-Wang is also of crucial importance. Due to the insolubility of resins, the range of analytical methods suitable to assess their quality directly is restricted. Many attempts have been described in literature to overcome this difficulty [2-4]. Nevertheless, the quality control of resin beads still remains challenging compared to building blocks and reagents.

MAS NMR enables direct analysis of resin beads without prior cleavage and sample preparations. 1D  $^{13}\text{C}$  MAS NMR with conventional MAS probes has already been used successfully to determine quantitatively the loading of resins using internal references [5]. The significantly better resolution of HR-MAS probes enabled quantitative results from 1D  $^1\text{H}$  MAS NMR spectra as well [6,7]. Owing to overlap of resonances, the 1D NMR methods cannot always be successfully applied, particularly in cases with weak resonances. Herein, results obtained with the much more powerful HSQC tool on the generic example Fmoc-Ala-Wang resin are presented.

### Results and Discussion

Wang resin (1.3 mmol/g) was loaded with a substoichiometric amount of Fmoc-Ala-OH via the standard esterification method (DCCl/DMAP in DMF/THF at 0°C), aiming at an incomplete loading. The resulting Fmoc-Ala-Wang resin (0.43 mmol/g, corresponding to approx. 33% of the theoretical full loading) was subsequently treated with benzoylchloride/pyridine in THF to cap the remaining active sites leading to a 33:67 mixture of Fmoc-Ala-Wang resin and benzoyl-Wang resin. Characteristic signals of Fmoc-Ala-Wang can be identified at 172.2 ppm (C-(11)), 155.0 ppm (C-(14)), 66.4 ppm (C-(10)), 49.1 ppm (C-(12)) and 18.0 ppm (C-(13)) (Figure 1). As a result of endcapping the residual hydroxyl groups of Wang to benzoyl-Wang, a second signal of carboxyl C-(11) can be observed at 165.8 ppm. The integral ratio of the Fmoc-Ala-Wang signals C-(11), (12), (13) and (14) to C-(11) of benzoyl-Wang enables to determine quantitatively the proportions of Fmoc-Ala- and benzoyl-Wang. For the resin shown in Figure 1, a

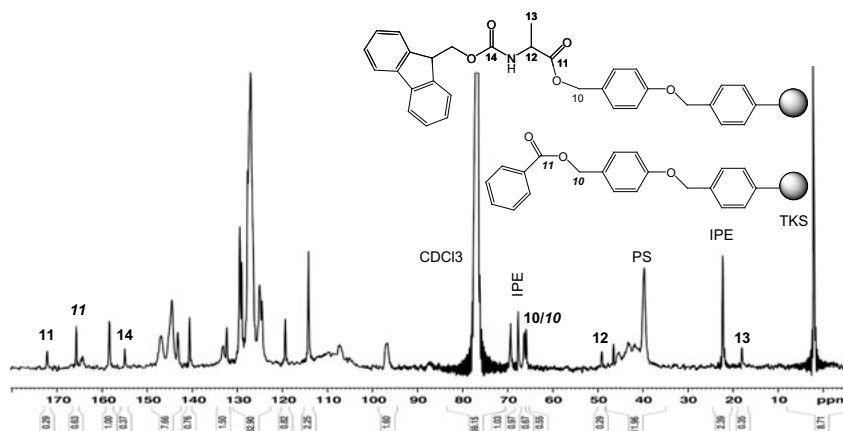


Fig. 1. Structure and 1D  $^{13}\text{C}$  MAS NMR spectrum of Fmoc-Ala-Wang resin with benzoyl endcapped residual Wang sites recorded at 100.6 MHz (Bruker Avance 400, MAS rate 2 kHz).

content of 34% Fmoc-Ala-Wang versus 66% benzoyl-Wang has been determined which corresponds well with the substitution determined by Fmoc cleavage / UV absorption.

In order to avoid free hydroxyl groups of Wang and thus the formation of side products, endcapping of Fmoc-AA loaded Wang resins is an important synthesis step. Therefore, a direct and sensitive detection method to verify the completeness of the endcapping is of high interest.

1D  $^{13}\text{C}$  MAS NMR is principally able to distinguish between C-(10) of unloaded Wang and the corresponding C-(10) of Fmoc-Ala-Wang resin. However, 10% Wang resin or more had to be spiked to Fmoc-Ala-Wang in order to detect a Wang-C-(10) signal.

A significantly lower LOD of unreacted Wang hydroxyl groups can be achieved by  $^1\text{H}$ ,  $^{13}\text{C}$ -HSQC HR-MAS NMR. The 2D spectrum of Fmoc-Ala-Wang spiked with 2% Wang resin shows a characteristic cross-signal of H-(10) / C-(10) at 4.7/64.1ppm (Figure 2). The intensity of the cross signal depends directly on the amount of Wang resin spiked. Quantitative determinations using calibration curves are therefore possible.

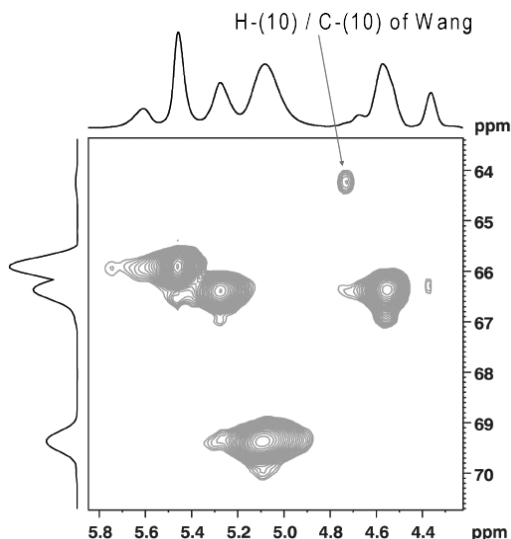


Fig. 2. Expansion of the  $^1\text{H}$ ,  $^{13}\text{C}$ -HSQC HR-MAS NMR spectrum of benzoyl endcapped Fmoc-Ala-Wang spiked with 2% Wang (Bruker Avance 400, MAS rate 4 kHz).

## Conclusion

The NMR method presented here is considered to be a powerful tool for investigating quality aspects of resins used in SPPS. The main advantage of the method is that significant structural information can be acquired directly from the resins without the need for cleavage and sample preparation. The quantitative determination of residual unreacted Wang in Fmoc-Ala-Wang resin is shown as an example. Further investigations will be performed with the aim to improve the analytical method (lower LOD for unreacted Wang) and to extend its application to other resins used in SPPS.

## References

1. Vorherr, T., Dick, F., Mergler, M., Sax, B., Schwindling, J., Vizzavona, J., Weiler, P.; Proceedings of the 7th Chinese Peptide Symposium 236–240; eds: Du, Y.-C., Zhang, Y.-S., Tam, J.P. (2002).
2. Yan, B. *Analytical Methods in Combinatorial Chemistry*; Technomic Publishing (2000).
3. Anderson, R.C., Stokes J.P., Shapiro, M.J. *Tetrahedron Lett.* **36**, 5311–5314 (1995).
4. Egner, B.J., Bradley, M. *Drug Discovery Today* **2**, 102–109 (1997).
5. Hany, R., Rentsch, D., Dhanapal, B., Obrecht, D. *J. Comb. Chem.* **3**, 85–89 (2001).
6. Blas, J., Rivera-Sagredo, A., Ferritto, R., Espinosa, J.F. *Magn. Reson. Chem.* **42**, 950–954 (2004).
7. Lucas, L.H., Cerny, M.A., Koen, Y.M., Hanzlik, R.P., Larive, C.K. *Anal. Bioanal. Chem.* **380**, 627–631 (2004).

## Spiral Countercurrent Chromatography: New Purification Technique for Peptides and Proteins

Martha Knight,<sup>1</sup> Aprile Pilon,<sup>2</sup> Melissa Winn,<sup>2</sup> and Thomas M. Finn<sup>1</sup>

<sup>1</sup>CC Biotech LLC and <sup>2</sup>APC Biotechnology Services, Inc. 9700 Great Seneca Highway,  
Rockville, MD 20850-3307, U.S.A.

### Introduction

Countercurrent chromatography (CCC), a liquid-liquid partitioning method carried out in flow-through tubing coils mounted in planetary centrifuges, has served well in laboratory-scale preparative purification of small molecules, including peptides. A recent breakthrough in the design of the CCC rotor has enabled the use of aqueous-organic solvent systems containing the heavy alcohols (polar solvent systems) and the aqueous 2-phase solvent systems which extend the technique to the large molecules such as proteins, other polymers and many more types of peptides. Here we present application of the new spiral tubing support (STS) separation rotor to the preparative purification of peptides and proteins.

### Results and Discussion

In a centrifuged rotor consisting of coiled tubing due to the Archimedean screw, the upper phase



Fig. 1. The STS rotor made of nylon polymer plastic mounted in a planetary centrifuge [3].

(of a 2-phase solvent system) goes to the head end and the lower phase goes to the tail. The centrifugal force field induces hydrodynamic mixing of the phases. When the mobile phase is passed into the system against the stationary phase direction the stationary phase is retained. Yoichiro Ito coupled this discovery to the design of continuous-flow entry and outflow to create the coil planet centrifuge. This countercurrent chromatography instrument is used for purification of compounds with high sample load capacity due to the high volume of the stationary liquid phase. Heretofore instruments with the multi-layer tubing coils have successfully provided synthesis and natural product purification. The organic-aqueous solvent system phases were well retained as stationary phases,

except for the heavy alcohol organic solvents—the very ones more suitable for polar, larger MW substances, such as peptides and proteins. Recently, Ito introduced a frame support rotor with channels wherein the tubing is placed in 4 loops per layer resulting in a spiral flow pathway of higher pitch [1,2]. This increases stationary phase retention from 40% to over 70% for all the 2-phase solvent systems including the polyethylene glycol / aqueous salt solutions.

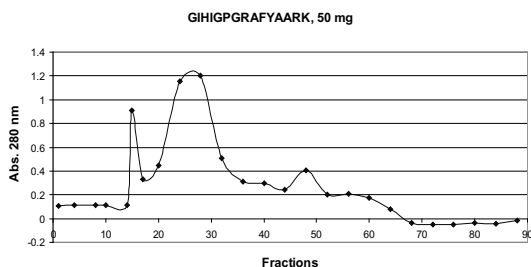


Fig. 2. Separation of a peptide in *sec*-butanol/0.1%aq. TFA with the lower phase mobile at 1ml/min, 830rpm. Mobile phase emerged at fraction 15 (solvent front).

phases were well retained as stationary phases, except for the heavy alcohol organic solvents—the very ones more suitable for polar, larger MW substances, such as peptides and proteins. Recently, Ito introduced a frame support rotor with channels wherein the tubing is placed in 4 loops per layer resulting in a spiral flow pathway of higher pitch [1,2]. This increases stationary phase retention from 40% to over 70% for all the 2-phase solvent systems including the polyethylene glycol / aqueous salt solutions.

We manufactured the rotor in lightweight material using laser sintering. The 1.6 mm ID FEP tubing is wound inside the rotor frame and a top is affixed with tubing union holders to connect the tubing to 0.85 mm ID PTFE in/outflow tubing (Figure 1). The STS rotor has been operated in experiments of separating small molecules, peptides and protein mixtures [4]. In Figure 2 is shown a CCC chromatogram of the purification of 50 mg of a synthetic peptide. The major peak (fractions 23-31) contained 25 mg pure peptide as determined by HPLC. Stationary phase retention was 76%.



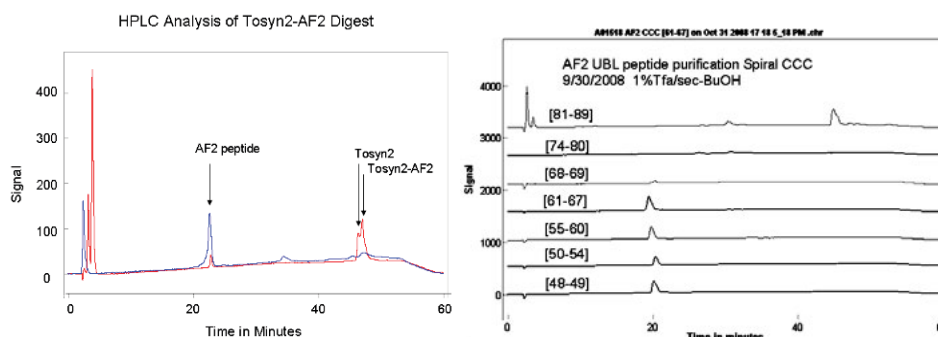


Fig. 3. Left. Identification of the AF2 peptide (HDMNKVLDL, antflammin) in a UBL fusion biosynthesis product digestion. Right. HPLC analysis of CCC separation of UBL protease digestion. Early pooled fractions contain the peptide isolated from other products. (Color version available on the CD.)

Similar results were obtained with a sample load of 100 mg in the 135-ml volume rotor.

A peptide produced as a UBL fusion (called Tosyn2) expressed in *E.coli* was isolated from the fusion protein cleavage by CCC in the sec-butanol/1% TFA-water solvent system with lower phase mobile (Figure 3). The fractions identified with peptide were lyophilized to a dry powder. Experiments are underway to directly isolate the fusion protein from the cell lysate prior to the protease digestion step to reduce multiple filtration and column steps.

A non-denaturing 2-phase aqueous solvent system described in Figure 4 consists of the polyethylene glycol rich upper phase and phosphate buffer rich lower phase. The lower phase

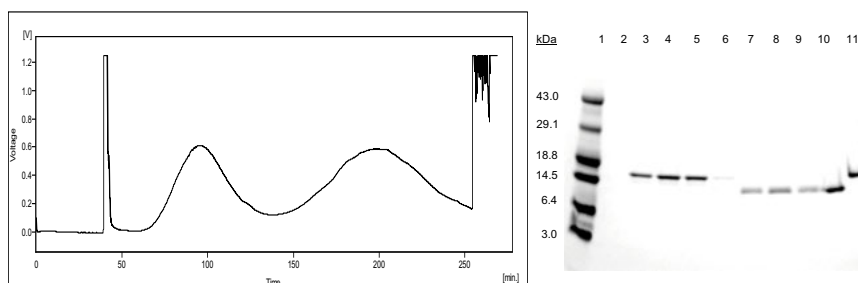


Fig. 4. Left. Spiral CCC separation of proteins, 24 mg myoglobin (17.67kD) and 31 mg lysozyme (14.39kD) Solvent system: PEG (MW=1000) 12.5%/K<sub>2</sub>HPO<sub>4</sub> 12.5% in water. Right. PAGE analysis lane 3-5 100-min peak, 7-9 200-min peak. Standards: MW 1, lysozyme 10 and myoglobin 11.

was used as the mobile phase at a flow of 1 ml/min. The online UV detection showed the elution of solvent front at approximately 40 ml, indicating a stationary phase retention of 70%, followed by the two protein peaks that were baseline separated. These results indicate the potential of spiral CCC in the STS rotor to be a useful and highly versatile tool for laboratory separations.

## Acknowledgments

CC Biotech LLC has an exclusive license L-144-2007-1 from the National Institutes of Health. This research was supported by the National Science Foundation (SBIR 0638082) and the Maryland Technology Development Corporation (TEDCO).

## References

1. Ito, Y., U.S. Patent Appl. WO 2009/073746 A1, filed Dec 7, 2007.
2. Ito, Y., Clary, R., Powell, J., Knight, M., Finn, T.M. *J. Liq. Chrom. & Rel. Tech.* **31**, 346-1357 (2008).
3. Finn, T.M., Knight, M., U.S. Prov. Patent 61/199,587, filed Nov. 18, 2008.
4. Knight, M. *Gen. Eng. Biotechnol. News* **28**, 58 (2008).

## Peptide Thioester Formation and Ligation Using a Cysteinyl Prolyl Ester (CPE) Autoactivating Unit

Toru Kawakami and Saburo Aimoto

Institute for Protein Research, Osaka University, Suita, Osaka 565-0871, Japan

### Introduction

Peptide thioesters are key building blocks in the ligation strategy for polypeptide synthesis. In the thioester method, partially protected peptide thioesters are used as building blocks and are condensed in the presence of silver ions, which function as an activating reagent for the thioester [1]. In native chemical ligation, chemoselective ligation of an unprotected peptide thioester with a peptide having a cysteine residue at the N-terminus is carried out in an aqueous buffer solution [2]. During the course of our investigations directed toward new, potentially more efficient ligation methods, our research focused on an *N* to *S* acyl shift reaction of a thiol auxiliary- or a cysteine-containing peptide, to ultimately produce an *S*-peptide (peptide thioester) [3,4]. It is noteworthy that, in 1985, Zanotti *et al.* reported that the peptide *p*-nitrophenyl (Np) ester, PhCH<sub>2</sub>CO-Cys(S<sup>t</sup>Bu)-Pro-ONp (**1**), was transformed into a diketopiperazine thioester, *cyclo*-(Cys(COCH<sub>2</sub>Ph)-Pro-) (**2**) in the presence of tributylphosphine, under aqueous conditions [5]. The thioester **2** would be formed *via* the intramolecular *N*-*S* acyl shift reaction followed by diketopiperazine (DKP) formation. Consistent with these observations, we found that a peptide containing a cysteinyl prolyl ester (CPE) at the C-terminus (CPE-peptide) **3** is transformed into a peptide thioester containing a DKP moiety **4** *via* an intramolecular reaction in neutral aqueous solution [6,7]. In this paper, we describe peptide thioester formation and the ligation of the CPE-peptide (Figure 1).

### Results and Discussion

We assumed that a peptide containing a CPE unit at the C-terminus would be spontaneously transformed into a DKP thioester in a neutral buffer solution and on the addition of a Cys-peptide, the ligation reaction would occur in one pot. The CPE peptide, Fmoc-His-Pro-Ile-Arg-Gly-Cys-Pro-OCH<sub>2</sub>CONH<sub>2</sub> (**3a**), was reacted with a Cys-peptide, Cys-Asp-Ile-Leu-Leu-NH<sub>2</sub> (**5**) in phosphate buffer solution (pH 8.3, 37 °C). The ligated product, Fmoc-His-Pro-Ile-Arg-Gly-Cys-Asp-Ile-Leu-Leu-Gly-NH<sub>2</sub> (**6a**), was produced in a yield of 90% after 24 h. A small peak (5%), corresponding to the hydrolysis product, Fmoc-His-Pro-Ile-Arg-Gly-OH (**8a**), was observed in the RP-HPLC elution profile. CPE-peptides (Fmoc-His-Pro-Ile-Arg-*Xaa*-Cys-Pro-OCH<sub>2</sub>CONH<sub>2</sub>) containing different amino acid residues, denoted as *Xaa* (*Xaa* = Ala, **3b**; Val, **3c**; and Ser, **3d**) were reacted with Cys-peptide **5** in phosphate buffer at pH 8.4 and 37 °C for 24 h. The ligated products **6b-d** (**6a**, Ala; **6b**, Val; and **6c**, Ser) were all obtained in good yields (70-80%) similar to that for the ligation at the Gly residue. A small amount of epimerization at the ligation site was observed: 1% (D-Ala), 2% (D-Val), or 5% (D-Ser), respectively.

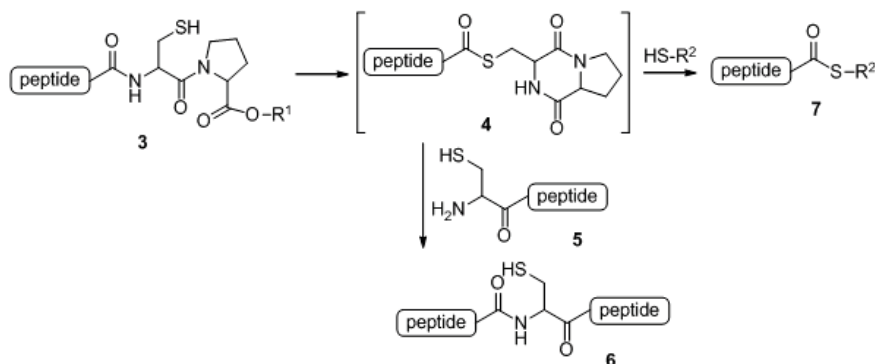


Fig. 1. Peptide thioester formation and ligation of CPE-peptide.

Epimerization of the Ser residue during the ligation was slightly higher than that for amino acids containing aliphatic side chains. It has been reported that the highly reactive His-thioester also undergoes slight epimerization during ligation [8,9], but that this can be suppressed by conducting the reaction at a lower pH (*vide infra*).

The CPE peptides containing four different amino-acid residues, Gly, Ala, Val, and Ser at the thioesterification sites were applied to the formation of the peptide thioesters **7** by reaction with sodium 2-mercaptoethanesulfonate. At pH 8.2 and 37 °C, the rates of thioester formation were very similar for all of the different amino acid residues used, and the yield of thioester reached about 70% after 6 h. The thioesters of Gly, Ala, and Ser residues underwent gradual hydrolysis with increasing reaction time, but the Val-thioester was stable for reaction periods of up to 24 h. Epimerization was observed to some extent in amino acid residues adjacent to the thioester moiety. The extent of epimerization was determined to be as follows: 5% (**7b**, Ala), 1% (**7c**, Val), and 26% (**7d**, Ser), respectively, after a 6-h reaction. The extent of epimerization of the Ser residue was exceptionally high and, when examined more closely, it was found to increase with reaction time. The epimerization of Ser-thioester **7d** increased from 12% (2 h) to 26% (6 h). The isolated peptide thioester of L-Ser **7d** underwent epimerization in a buffer solution at pH 8.2. These findings clearly indicate that epimerization occurs after thioester formation. The  $\alpha$ -proton of the thioester is slightly acidic, is deprotonated in the presence of a base and, as a result, the amino acid undergoes racemization [10]. Amino acid residues with aliphatic side chains, such as a Val residue, would be expected to be more resistant to deprotonation, and, in the case of an electron-withdrawing group such as a Ser residue, deprotonation would be accelerated. When the CPE peptide **3d** was reacted with sodium 2-mercaptoethanesulfonate at pH 7.3, Ser-thioester **7d** was formed in 65% yield after 10 h and in 80% yield after 24 h, and the degree of epimerization was determined to be 9% and 16%, respectively. Under lower pH conditions, the thioester was relatively stable to hydrolysis, and epimerization was suppressed somewhat, even in the case of the sensitive Ser-thioester. Furthermore, when the peptide thioester is immediately reacted with a Cys-peptide, these undesirable reactions are suppressed to minimum levels, and the desired ligated product can be obtained in good yield (*vide supra*).

In conclusion, a peptide containing a CPE unit at the C-terminus (CPE peptide) is spontaneously transformed into a peptide thioester through an *N-S* acyl shift reaction, followed by DKP formation. Ligation proceeds spontaneously when the CPE peptide is mixed with a Cys-peptide, and the ligation can be carried out using a variety of amino acid residues with minimal epimerization. The CPE peptide can be readily prepared by Fmoc solid phase peptide synthesis, and can be used as an alternative building block to the peptide thioester, for use in the synthesis of polypeptides by the ligation strategy. The CPE peptide can also be transformed into the corresponding peptide thioester *via* an intermolecular thiol-thioester exchange reaction after C <sup>$\alpha$</sup> -DKP thioester formation. Hydrolysis of thioester bond and epimerization of the amino acid residue adjacent to the thioester moiety are suppressed when lower pH reaction conditions are employed. Further investigations are currently in progress. At this stage, the CPE peptide is the reagent of choice for use as a building block in one-pot thiol-mediated ligation reactions.

## Acknowledgments

This research was supported, in part, by Grants-in-Aid for Scientific Research from the Ministry of Education, Culture, Sports, Science and Technology, Japan, and by the Naito Foundation.

## References

1. Hojo, H., Aimoto, S. *Bull. Chem. Soc. Jpn.* **64**, 111-117 (1991).
2. Dawson, P.E., Muir, T.W., Clark-Lewis, I., Kent, S.B.H. *Science* **266**, 776-779 (1994).
3. Kawakami, T., Sumida, M., Nakamura, K., Vorherr, T., Aimoto, S. *Tetrahedron Lett.* **46**, 8805-8807 (2005).
4. Nakamura, K., Sumida, M., Kawakami, T., Vorherr, T., Aimoto, S. *Bull. Chem. Soc. Jpn.* **79**, 1773-1780 (2006).
5. Zanotti, G., Pinnen, F., Lucente, G. *Tetrahedron Lett.* **26**, 5481-5484 (1985).
6. Kawakami, T., Aimoto, S. *Chem. Lett.* **36**, 76-77 (2007).
7. Kawakami, T., Aimoto, S. *Tetrahedron* **65**, 3871-3877 (2009).
8. Haase, C., Rohde, H., Seitz, O. *Angew. Chem. Int. Ed.* **47**, 6807-6810 (2008).
9. Hackeng, T.M., Griffin, J.H., Dawson, P.E. *Proc. Natl. Acad. Sci. U.S.A.* **96**, 10068-10073 (1999).
10. Amyes, T.L., Richard, J.P. *J. Am. Chem. Soc.* **114**, 10297-10302 (1992).

## Thioacid Capture Ligation at Valine

Fu-Peng Li and Chuan-Fa Liu

School of Biological Sciences, Nanyang Technological University, Singapore, 637551

### Introduction

Thioester-mediated peptide ligation at valine was reported recently [1]. The method utilizes an N-terminal penicillamine to mediate the ligation reaction, similar to the Cys-mediated native chemical ligation [2]. Subsequent desulfurization gives a Val residue at the ligation site. However, the steric hindrance of the tertiary thiol group in penicillamine significantly slows down the ligation reaction, which limits the practical value of this method. Herein, we report that thioacid capture ligation can overcome this problem and be used for ligation at Phe-Val, Leu-Val and even Pro-Val junctions. Using thioacid capture ligation, we successfully synthesized a histone protein H2B. Moreover, a new strategy was developed for the purification of the ligation product.

### Results and Discussion

Thioacid capture ligation (TCL) was developed in 1996 [3]. It works through acyl disulfide-mediated intramolecular acylation for peptide bond formation. In order to test the efficiency of TCL at Val, several peptide thioacids were prepared with the last residue as Gly, Ala, Leu, Pro and Phe, respectively. The results showed that the TCL worked very well in all cases (Figure 1). The ligation was performed at 37 °C for only 1 h. The ligation efficiency was very high with a C-ter Gly or Ala thioacid. The efficiency was also good with a C-ter Leu, Phe or even Pro thioacid.

Next, the synthesis of a histone protein H2B was attempted using both native chemical ligation and thioacid capture ligation. For NCL, after 24 h of ligation at 37 °C with benzyl mercaptan as the catalyst, only the hydrolyzed protein was found with no ligation product detected (Figure 2A). On the other hand, TCL gave a ligation yield of 60 % after 2 h reaction at 37 °C (Figure 2B).

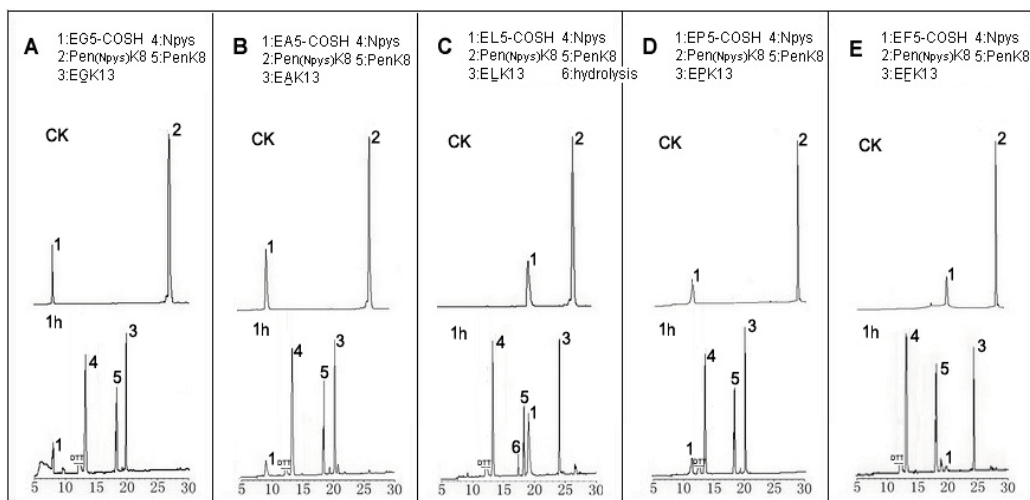


Fig. 1. Results of peptides ligation by thioacid capture ligation for 1 h at 37 °C

EG5-COSH: H-Glu-Gly-Thr-Lys-Gly-SH; EA5-COSH: H-Glu-Gly-Thr-Lys-Ala-SH;

EL5-COSH: H-Glu-Gly-Thr-Lys-Leu-SH; EP5-COSH: H-Glu-Gly-Thr-Lys-Pro-SH

EF5-COSH: H-Glu-Gly-Thr-Lys-Phe-SH; Pen(Npys)K8: H-Pen(Npys)-Thr-Lys(Ac)-Tyr-Thr-Ser-Ala-Lys-OH

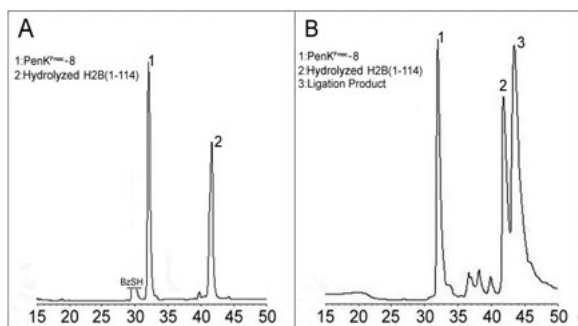


Fig. 2. Results of protein ligation.

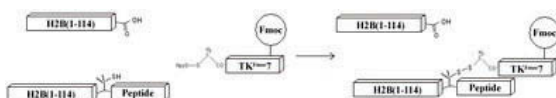


Fig. 3. A new strategy for purifying the ligation product from the hydrolyzed protein fragments.

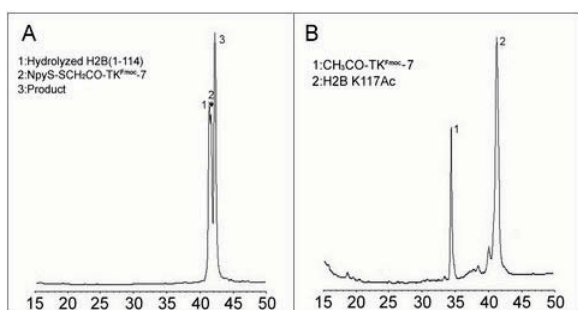


Fig. 4. Synthesis and purification of H2B K117Ac.

But the removal of Fmoc group in solution was difficult due to the insolubility of the protein in DMF and other solvents used for Fmoc removal. We therefore devised another method to help isolate the protein ligation product (Figure 3). The idea is to modify the ligation product with a hydrophobic moiety via the formation of a S-S bridge. For this purpose, NpyS-SCH<sub>2</sub>CO-TK<sup>Fmoc</sup>-7 was prepared and used to modify the H2B ligation product to facilitate its purification. The disulfide formation step was very fast and finished within several minutes, as the HPLC results showed in Figure 4A. The ligation product was easily separated from the hydrolyzed H2B(1-114). After purification, Raney nickel was used to remove the thiol in the presence of TCEP [4] and the final product H2B K117Ac was purified (Figure 4B). This new purification method can be generally useful for the isolation of ligation products which are difficult to separate from the other reaction components.

## Acknowledgments

We thank the Ministry of Education (MoE) of Singapore and Nanyang Technological University for financial support.

## References

1. Haase, C., et al. *Angew. Chem. Int. Ed.* **47**, 6807-6810 (2008).
2. Dawson, P.E., et al. *Science* **266**, 776-779 (1994).
3. Liu, C.F., et al. *Tet. Lett.* **37**, 933-936 (1996).
4. Yan, L.Z., Dawson, P.E. *J. Am. Chem. Soc.* **123**, 526-533 (2001).

The tertiary thiol group in penicillamine would impose considerable steric hindrance on its engagement with the thioester, making the NCL reaction much less efficient than in the case of Cys ligation. In thioacid capture ligation, the first step is a very efficient thiol exchange reaction between a thioacid, a super nucleophile and a highly activated disulfide with a much better leaving group. Although steric hindrance of the tertiary thiol of penicillamine would slow down the capture reaction to some degree, its highly efficient feature would still allow the ligation to proceed at a reasonable rate. Our results indicate that thioacid capture ligation is particularly useful for ligation at sterically unfavourable junctions.

For the protein ligation, because the C-ter peptide was small and hydrophilic, after the ligation the ligation product would elute together with the hydrolyzed H2B(1-114). For this reason, the C-ter peptide with an Fmoc group PenK<sup>Fmoc</sup>-8 was used first.

The hydrophobic Fmoc group made the ligation product more separable and easily purified from the hydrolyzed H2B(1-114) (Figure 2B).

## Native Ligation with Post-translational Modifications Using C-Terminal, *N*-Acylurea Peptides

Juan B. Blanco-Canosa, Sampat Ingale, and Philip E. Dawson

Department of Chemistry and Department of Cell Biology, The Scripps Research Institute,  
 10550 N Torrey Pines Road, La Jolla, CA 92037, U.S.A.

### Introduction

Proteins with post-translational modifications, e.g. glycoproteins and phosphoproteins, play important roles in many biological processes. Dysfunctions in their attachment or removal from proteins lead to illness, including autoimmune diseases and cancer. Detailed analysis of these modifications requires the use of homogeneous samples that, so far, can only be obtained by chemical peptide synthesis. With these considerations, reliable synthetic methods for post-translational modified peptides have gained considerable attention.

### Results and Discussion

Recently, we have described a method to synthesize C-terminal, *N*-acylurea peptides using Fmoc-SPPS and we have shown their utility as precursors of peptide thioesters [1], which are key intermediates for Native Chemical Ligation (NCL) [2]. Synthesis of *N*-acylureas involves the post assembly acylation of diaminobenzoic moiety **1** with *p*-nitrochloroformate (**2**), followed by intramolecular cyclization (**3**) (Scheme 1). Final cleavage of the resin affords the C-terminal, *N*-acylurea peptides **4**, which can undergo thiol exchange (**5**) or direct ligation with N-terminal cysteine peptides (**6**). Several C-terminal amino acids (Gly, Ala, Tyr, Phe, Leu), including those with high steric hindrance (Pro, Val), have been successfully incorporated in *N*-acylurea peptides and yielded efficient NCL (Table 1).

Scheme 1. Key steps in the synthesis of C-terminal, *N*-acylureas.

In order to span the applicability of this new strategy, we have pursued the synthesis of glyco- and phosphopeptides. Therefore, we synthesized the glyco-

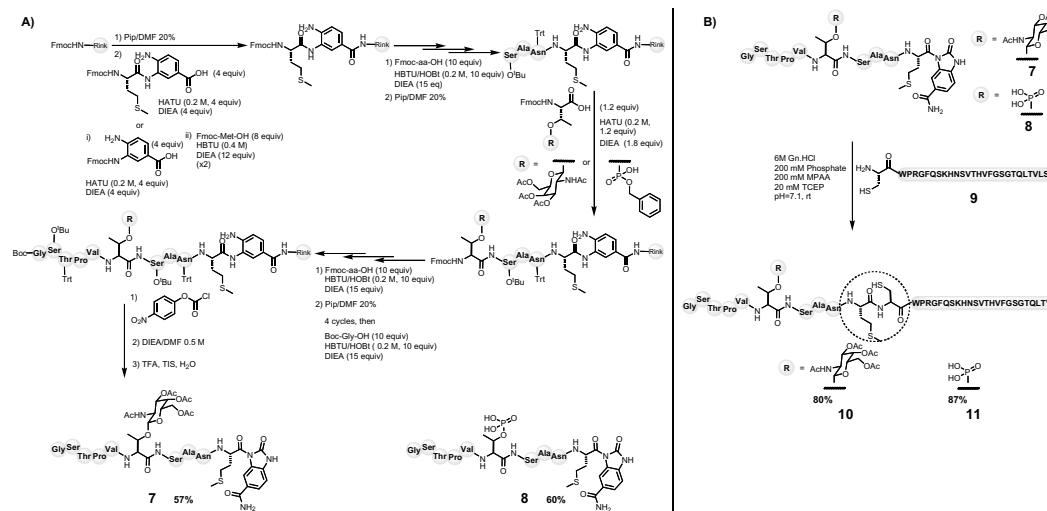


Fig. 2. A) Synthesis of CKII-OGalNAc (**7**) and CKII-OPO3H2 (**8**). B) Native Chemical Ligation of peptides **7** and **8** with cys-peptide **9**. Ligations were carried out at 2 mM of **7** or **8** and a slight excess of **9** (1.2 and 1.03 equiv).

Table 1. Synthesis and ligation yields for a set of several N-acylureas

Peptide-Nbz	Recovered yield (%)	Ligation with CRAFS (%) <sup>a</sup>
LYRAG-Nbz	90	LYRAGCRAFS 97
LYRGA-Nbz	70	LYRGACRAFS 93
LARGY-Nbz	90	LARGYCRAFS 95
LARGF-Nbz	88	LARGFCRAFS 98
AYRGL-Nbz	87	AYRGLCRAFS 96
LYRAP-Nbz	71	LYRAPCRAFS 90
LYRGV-Nbz	77	LYRGVCRAFS 95

<sup>a</sup>Calculated by integration of HPLC signal at 280 nm

and phosphoforms of CKII (GSTPVTSANM), a 10-mer substrate for *O*-GlcNAc transferase (OGT), which is a nuclear and cytosolic glycosyltransferase [3]. Synthesis of CKII-OGalNAc (**7**) was undertaken by coupling Fmoc-Met-Dbz-OH to the resin, whereas for the CKII-OPO<sub>3</sub>H<sub>2</sub> (**8**), Fmoc-Met-OH was coupled on solid phase to the Dbz linker already attached to the resin (Figure 2A).

NCL could be efficiently carried out in presence of the polypeptide **9**, a peptidic fragment of the immunoglobulin light chain, which is part of the pre-B-cell receptor, at pH 7.0 using 4-mercaptophenyl acetic acid to form in situ the thioester peptide [5] (Figure 2B). Under these conditions, reactions were completed under 2h affording the desired products **10** and **11** in high yields (80 and 87%, respectively).

In summary, we have shown that:

1. Synthesis and Native Chemical Ligation of glyco- and phosphopeptides was accomplished using C-terminal, N-acylureas.
2. No appreciable side reactions were observed in the glycosylated and phosphorylated amino acids.
3. The acylurea method is compatible with all amino acids and with no needs for extra protecting groups.

These accomplishments have motivated to us to pursue the synthesis of another post-translational modifications, e.g. lipidation and cyclization.

## Acknowledgments

J. B. Blanco-Canosa is grateful to the Marie Curie Program for a postdoctoral fellowship.

## References

1. Blanco-Canosa, J.B., Dawson, P.E. *Angew. Chemie, Int. Ed.* **47**, 6851-6855 (2008).
2. Dawson, P.E., Muir, T.W., Clark-Lewis, I., Kent, S.B. *Science* **266**, 776-779 (1994).
3. Kreppel, L.K., Hart, G.W. *J. Biol. Chem.* **274**, 32015-32022 (1999).
4. Karasuyama, H., Kudo, A., Melchers, F. *J. Exp. Med.* **172**, 969-972 (1990).
5. Johnson, E.C.B., Kent, S.B.H. *J. Am. Chem. Soc.* **128**, 6640-6646 (2006).

## Use of Native Chemical Ligation as a Tool for Polymer Construction over Solid Substrates

Raymond Jr Hamel,<sup>1,2</sup> Ewa Wiczerzak,<sup>1</sup> Vincent Chabot,<sup>1</sup> Vincent Aimez,<sup>2</sup>  
Paul G. Charette,<sup>2</sup> Michel Grandbois,<sup>1</sup> and Emanuel Escher<sup>1</sup>

<sup>1</sup>Department of Pharmacology, Université de Sherbrooke, Sherbrooke, QC, Canada; Department of

<sup>2</sup>Electrical and Computer Engineering, Université de Sherbrooke, Sherbrooke, QC, Canada

### Introduction

We previously showed [1] that polypeptides can be rapidly immobilized on glass substrates by means of thiol catalyzed native chemical ligation (NCL) [2]. The aim of the present contribution is to build long unordered molecules on glass surfaces for biosensors application. Linear  $\omega$ -amino-PEG thioesters of 10 kDa (PEG = polyethylene glycol) were to be attached on glass surfaces and to be extended to 20 kDa oligomers. NCL proved to be a useful method to attach PEG-thioester over cysteine modified substrate.

In this study, surface plasmon resonance (SPR) has been used to follow attachment of these PEG to the substrate. Native chemical ligation reaction rates of 5 and 10 kDa  $\alpha$ -Boc-PEG- $\omega$ -thioester were monitored and compared. Using the same strategy 20 kDa oligomers were created using successive NCL. For this purpose, first  $\alpha$ -Boc-Cys(Boc)-PEG- $\omega$ -thioester was synthesized and coupled to cysteine modified glass surfaces by NCL. A second PEG unit was then attached by the same procedure after acid deprotection of the Boc group of the first Boc-Cys(Boc)-PEG unit.

In order to measure the length of the attached constructions,  $\alpha$ -biotinyl PEG (10kDa)- $\omega$ -thioester modified surfaces were probed by atomic force microscopy (AFM). AFM cantilevers were coated with biotinyl BSA and then with avidin. PEG length was measured by pulling perpendicularly and the pulling force was recorded.

### Results and Discussion

SPR substrates were prepared using metal evaporation and plasma enhanced chemical vapor deposition (PECVD) to create glass-chromium-gold-silicon oxyde substrates. Final SiO<sub>2</sub> layer allowed to graft 3-aminopropyltrimethoxysilane (APTS) followed by Boc-Cys(Boc)-OH (DCC, 1h30). After acid deprotection, native chemical ligation was carried out. At first, NCL of  $\alpha$ -Boc-PEG- $\omega$ -thioester of 5kDa and 10Kda (1mM in 0,5M phosphate buffer, pH=7,2) were monitored. Reactions were conducted in the presence of 4-mercaptophenylacetic acid [2] (MPAA, 24 mM) and Tris[2-carboxyethyl] phosphine (TCEP, 20 mM) as a reducing agent.

The time-dependent measurement of the SPR signal shift allows a direct determination of NCL reaction kinetics (Figure 1). Both PEG showed similar kinetic though the 10kDa PEG NCL seems to proceed slightly slower. This might be due to the diffusion rate in the medium.

Following successful attachment of one PEG-thioester to the surface, we proceeded to extend to double length PEG constructions. The progression of the construction starts with the Boc-Cys(Boc) and is followed by deprotection (Figure 2). The first NCL (Boc-Cys(Boc)-PEG-SR, 10kDa) was successfully realised. Remaining uncapped amino groups were acetylated prior to second cysteine deprotection with 40% TFA-DCM. A second NCL with Boc-PEG-SR (10 kDa) was carried out. A right shift is observed meaning that PEG thioester

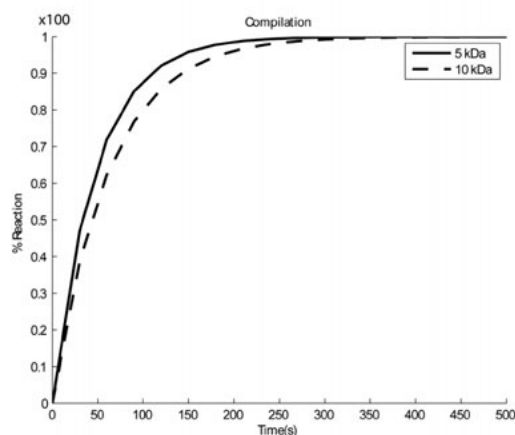


Fig. 1. Comparison of the normalised kinetic curves of NCL of 5kDa and 10Kda  $\alpha$ -Boc-PEG- $\omega$ -thioesters.



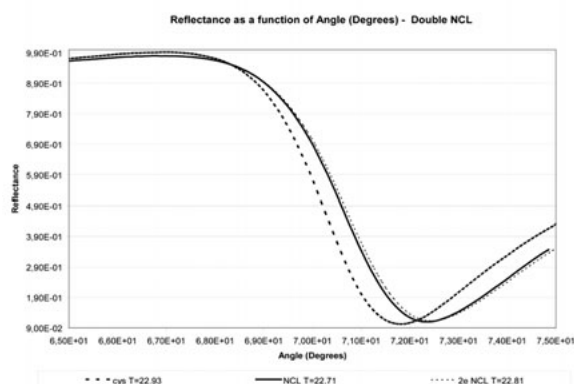


Fig. 2. SPR spectrum showing steps of construction of 20 kDa oligomers with appropriate angular shifts.

bind to the tip and stretch the PEG until rupture of the Avidin-Biotin bond. Multiple approach-retraction cycles were recorded and rupture length were measured. Figure 3 shows a compilation of values collected over 4 samples ( $n=179$ ).

According to literature, a single ethylene glycol unit has a length of  $2.8\text{\AA}$  [5]. Therefore a 10kDa PEG (which contains 227 ethylene glycol units) should measure around 64 nm. This theoretical value is in excellent accordance with the mean experimental value. Similar experiments were conducted on non-SPR glass substrates and showed equivalent length values.

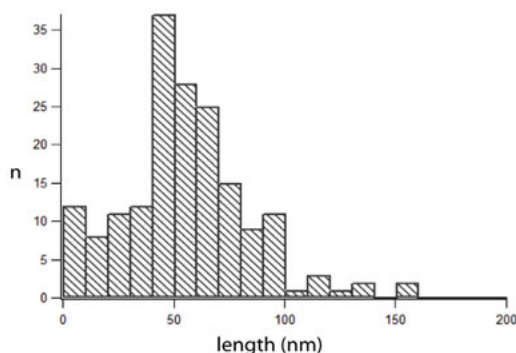


Fig. 3. Compilation of measured rupture length of  $\alpha$ -biotinyl-PEG(10kDa)- $\omega$ -thioester by atomic force spectroscopy ( $n=179$ ).

has been attached. The smaller shift after the second NCL can be explained either by a lower reaction yield or the increased distance of the second PEG from the metal interface or a combination of both. SPR sensitivity is decaying exponentially with increasing distance from the surface.

In order to assess the length of the introduced PEG unit an identical but differently functionalized PEG-thioester was attached, SPR monitored and then probed by AFM in Force Spectroscopy mode [3]. A 10kDa  $\alpha$ -biotinyl-PEG- $\omega$ -thioester was ligated by NCL. Using avidin coated AFM tips [4], the functionalized surface was probed in PBS medium. Biotin functionality in terminaison of the PEG allowed it to

We showed that it is possible to covalently attach to solid surfaces suitably modified polyethylene glycol amino acid through native chemical ligation. SPR allowed us to follow each step sequentially as well as to evaluate the kinetic process. These modified surfaces were probed by atomic force microscopy in force spectroscopy mode for length and end-cap functionality. Such combined techniques showed the capacity to create molecular tethers of desired length (50-100nm or more) and their functionality.

## Acknowledgments

This work was supported by funds from the Canadian Institute of Health Research and the Fonds Québécois de Recherche sur la Nature et les Technologies.

## References

1. Wieczerszak, E., Hamel, R. Jr, Chabot, V., Aimez, V., Grandbois, M., Charette, P.G., Escher E. *Biopolymers/PeptideScience* **90**, 415 (2008).
2. Dawson, P.E., Muir, T.W., Clark-Lewis, I., Kent, S.B.H. *Science* **266**, 776-779 (1994).
3. Johnson, E.C.B, Kent, S.B.H. *J.Am.Chem.Soc.* **128**, 6640-6646 (2006).
4. Ludwig, M., Moy, V.T., Rief, M., Florin, E.-L., Gaub, H.E. *Microsc. Microanal. Microconstruct.* **5**, 321-328 (1994).
5. Oosterhelt, F., Rief, M., Gaub, H.E. *New Journal of Physics* **1**, 6.1-6.11 (1999).

## Efficient Peptide Ligation Using Azido- and Pyruvoyl-Protected Peptides via the Ag<sup>+</sup>-Free Thioester Method

Hidekazu Katayama,<sup>1</sup> Hironobu Hojo,<sup>1</sup> Tsuyoshi Ohira,<sup>2</sup> Yuko Nakahara<sup>1</sup>  
and Yoshiaki Nakahara<sup>1</sup>

<sup>1</sup>Department of Applied Biochemistry, Institute of Glycotechnology, Tokai University, Kanagawa, 259-1292, Japan; <sup>2</sup>Department of Biological Sciences, Faculty of Science, Kanagawa University, Kanagawa, 259-1293, Japan

### Introduction

Thioester method [1] is one of the ligation methods useful for (glyco)protein synthesis. This method has the advantage that there is no limitation on selecting the ligation site, whereas the coupling by the native chemical ligation [2] is almost exclusively carried at Xaa-Cys site. Instead, the side chain amino and thiol groups have to be protected to achieve the chemoselective ligation in the thioester method. To realize this, the Boc groups have to be reintroduced to the side chain amino groups, which are made free during the deprotection step after SPPS. In this paper, we examined the direct preparation of the side chain-N-protected peptide segments by introducing azido- and pyruvoyl (Pyr)-protected Fmoc-lysine (Figure 1) during SPPS to overcome the inconvenience for segment preparation. Using pigment dispersing hormone (PDH)-I and glycopeptide toxin, Contulakin-G as models, the usefulness of these protecting groups were examined.

### Results and Discussion

Fmoc-Lys(N<sub>3</sub>)-OH **1** was synthesized from Fmoc-Lys-OH by the copper(II)-catalyzed diazo transfer method [3] with slight modifications. Fmoc-Lys(Pyr)-OH **2** was prepared by reacting Fmoc-Lys-OAll with dimethylhydrazonopropionic acid by DCC-HOBt method, followed by the removal of allyl ester by Pd(PPh<sub>3</sub>)<sub>4</sub> and dimedone in dimethoxyethane. These amino acids were then introduced during the synthesis of PDH-I (Asn-Ser-Glu-Leu-Ile-Asn-Ser-Leu-Leu-Gly-Ile-Pro-Lys-Val-Met-Thr-Asp-Ala-NH<sub>2</sub>) by the thioester method. First, the N-terminal peptide thioester, Fmoc-PDH-I (1-10)-SC<sub>6</sub>H<sub>4</sub>CH<sub>2</sub>COOH **3** was synthesized by the N-alkylcysteine (NAC)-assisted thioesterification method developed in our previous study [4]. Fmoc-N-ethyl-S-trityl-cysteine was introduced to Rink Amide MBHA resin and the peptide chain was elongated by ordinary Fmoc-based SPPS. After cleavage from the resin, the peptide was dissolved in aq CH<sub>3</sub>CN and thioesterified by the addition of 4-mercaptophenylacetic acid. This reaction was almost completed within 24 h giving the desired peptide thioester **3**. C-Terminal segments having azido- or Pyr-protected Lys<sup>12</sup> (peptide **4a**, **4b**) were prepared by introducing **1** or **2** during the Fmoc SPPS. The azido and Pyr groups were stable during the SPPS. Final deprotection was achieved by thiol-free (for the preparation of **4a**) or thiol- and silane-free (for **4b**) TFA cocktail.

The peptide segments were condensed by the Ag<sup>+</sup>-free thioester method [5] as shown in Figure 2. Peptides **3** and **4a** or **4b** were dissolved in DMSO containing 5% HOObt. Then the coupling reaction was initiated by adding DIEA at a concentration of 5%. The reaction was almost completed within 2 h without decomposition of azido or Pyr group to give peptide **5a** or **5b**. The N-terminal Fmoc group was removed by adding piperidine to the solution at a concentration of 20%. After the product was precipitated by adding ether to the solution, side chain amino protecting group was removed. In the case of the peptide derived from **5a**, the precipitate was dissolved in 50% aq AcOH and treated with Zn for 30 min. The azido group was readily converted to the amino group without serious side reaction and the desired PDH-I **6** was successfully obtained in 47% isolated yield based on peptide **3**. On the other hand, the removal of Pyr group from the peptide derived from **5b** was carried out by treating the peptide by

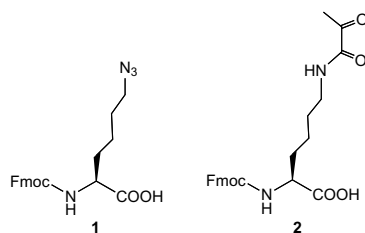


Fig. 1. Azido- and pyruvoyl-protected lysine.

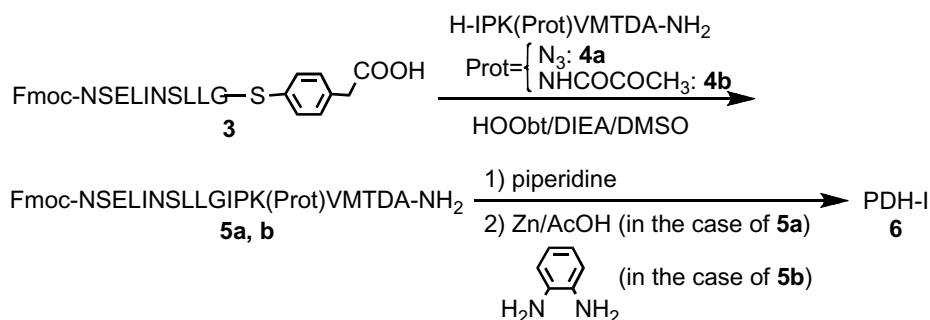
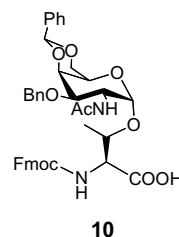


Fig. 2. Synthetic route for PDH-I.

*o*-phenylenediamine in 2 M acetate buffer (pH 6) following the reported conditions [6]. However, almost complete oxidation of Met residue as well as conversion of Pyr to formyl group were observed. We found that the addition of 10% dimethylsulfide effectively suppressed the oxidation of Met and increase in the acidity of the solution to pH 5 prevented the latter side reaction. Using this modified condition, the desired product **6** was obtained in 30% yield.

The efficiency of the new amino protecting group was further demonstrated by the synthesis of Contulakin-G: pGlu-Ser-Glu-Glu-Gly-Gly-Ser-Asn-Ala-Thr\*-Lys-Lys-Pro-Tyr-Ile-Leu **7**, where Thr\* denotes O-glycosylated Thr residue. The peptide was divided at Gly<sup>6</sup>-Ser<sup>7</sup> and the N-terminal peptide thioester, Contulakin-G (1-6)-SC<sub>6</sub>H<sub>4</sub>CH<sub>2</sub>COOH **8** was prepared in the same manner as described for peptide **3**. The C-terminal peptide carrying *N*-acetylgalactosamine at Thr<sup>10</sup> **9** was synthesized starting from Fmoc-Leu-CLEAR-Acid resin by the Fmoc strategy. Thr<sup>10</sup> was introduced using compound **10** by DCC-HOBT method. Lys<sup>11</sup> and Lys<sup>12</sup> were introduced using compound **2**. After the completion of the peptide chain assembly, the peptide was cleaved from the resin by TFA cocktail, followed by low-TfOH treatment [7, 8] to remove benzyl group on the glycan moiety. After RPHPLC purification, the desired Contulakin-G (7-16) **9** was obtained. Then the segment coupling by the thioester method was carried out following the procedure for PDH-I synthesis. After removal of Pyr group by *o*-phenylenediamine at pH 5, the desired Contulakin-G carrying GalNAc **7** was successfully obtained in 32% yield.



In conclusion, azido- and Pyr-groups were successfully used as the amino protecting groups in the thioester method. Peptide segments carrying these protecting groups can be directly prepared by the SPPS and thus, the inconvenience for the segment preparation in the thioester method was overcome by the use of these protecting groups.

## References

1. Hojo, H., Aimoto, S. *Bull. Chem. Soc. Jpn.* **64**, 111-117 (1991).
2. Dawson, P.E., Muir, T.W., Clark-Lewis, I., Kent, S.B. *Science* **266**, 776-779 (1994).
3. Speers, A.E., Cravatt, B.F. *Chem. Biol.* **11**, 535-546 (2004).
4. Hojo, H., Onuma, Y., Akimoto, Y., Nakahara, Y., Nakahara, Y. *Tetrahedron Lett.* **48**, 25-28 (2007).
5. Hojo, H., Murasawa, Y., Katayama, H., Ohira, T., Nakahara, Y., Nakahara, Y. *Org. Biomol. Chem.* **6**, 1808-1813 (2008).
6. Kawakami, T., Hasegawa, K., Teruya, K., Akaji, K., Horiuchi, M., Inagaki, F., Kurihara, Y., Uesugi, S., Aimoto, S. *Tetrahedron Lett.* **41**, 2625-2628 (2000).
7. Tam, J.P., Heath, W.F., Merrifield, R.B. *J. Am. Chem. Soc.*, **108**, 5242-5251 (1986).
8. Hojo, H., Haginoya, E., Matsumoto, Y., Nakahara, Y., Nabeshima, K., Toole, B.P., Watanabe, Y. *Tetrahedron Lett.* **44**, 2961-2964 (2003).

## Solid Phase Chemical Synthesis of N-linked Glycopeptides

Rui Chen and Thomas J. Tolbert

Department of Chemistry, Indiana University, Bloomington, IN 47408, U.S.A.

### Introduction

In order to study the effects of N-linked glycosylation and develop N-linked glycopeptide based vaccines and therapeutics [1-2], it is important to have an efficient and rapid strategy of synthesizing glycopeptides containing large N-linked oligosaccharides. However, the difficulty of obtaining sufficient amounts of N-linked oligosaccharides [3] and the problematic aspartimide side reaction [4-6] have seriously limited and slowed down the development of N-linked glycopeptide synthesis. As an alternative to solution phase synthesis, solid-phase synthesis can avoid repetitive purification steps which reduce yield, and has the possibility of achieving higher yields with excesses of materials and reagents. Herein, we studied the chemical synthesis of N-linked glycopeptides containing the high mannose oligosaccharide Man<sub>8</sub>GlcNAc<sub>2</sub> on solid phase using both the glycosyl asparagine building block approach and the on-resin glycosylamine coupling approach, and applied it to the synthesis of HIV gp120 glycopeptides and HIV gp41 C34 glycopeptides.

### Results and Discussion

The traditional use of preformed glycosyl asparagine as building blocks on solid phase has proven to be a reliable method [7], yet, we found that the coupling of the glycosyl building block was not satisfying both on PEG-polyacrylamide-based (PEGA) and polystyrene-based (PS) Rink amide resins, and the building block synthesis itself is inefficient resulting in losses of precious oligosaccharide precursors during their synthesis. However, in the on-resin glycosylamine coupling strategy, we found that the 2-phenyl-isopropyl protecting group was an excellent handle on Aspartic acid for the introduction of N-glycosylation, not only allowing selective deprotection of aspartic acid residues for creation of glycosylation sites but also efficiently suppressing aspartimide formation during peptide synthesis. The key step of on-resin glycosylamine coupling to an aspartic acid residue was first optimized for a small sugar, N-acetylglucosamine, and then applied to a much larger high mannose oligosaccharide, Man<sub>8</sub>GlcNAc<sub>2</sub>. Satisfying yields were obtained for both small and large sugars on aspartimide prone peptides. The use of on-resin glycosylamine coupling simplifies purification of N-linked glycopeptides, and also allows convenient recovery of un-reacted, valuable large oligosaccharides. This approach has been successfully applied to the solid phase synthesis of HIV gp120 glycopeptides and different glycosylated forms of the 34 amino acid HIV-1 gp41 C34 glycopeptide.

### Acknowledgments

We thank Prof. DiMarchi for generously support on solid phase peptide synthesis. We thank Dr. Jonathan A. Karty and Angela M. Hanson for assistance with mass spectrometry. We thank Mr. Junpeng Xiao for the help with the in-vitro HIV entry inhibition assay. This research was supported by Indiana University, Bloomington.

### References

1. Dove, A. *Nature Biotech.* **19**, 913 (2001).
2. Scanlan, C.N., Offer, J., Zitzmann, N., Dwek, R.A. *Nature* **446**, 1038 (2007).
3. Chen, R., Pawlicki, M.A., Hamilton, B.S., Tolbert, T.J. *Adv. Synth. & Catal.* **350**, 1689 (2008).
4. Kan, C., Trzuppek, J.D., Wu, B., Wan, Q., Chen, G., Tan, Z., Yuan, Y., Danishefsky, S.J. *J. Am. Chem. Soc.* (2009).
5. Tan, Z., Shang, S., Halkina, T., Yuan, Y., Danishefsky, S.J. *J. Am. Chem. Soc.* (2009).
6. Kaneshiro, C.M., Michael, K. *Angew. Chem. Int. Ed. Engl.* **45**, 1077 (2006).
7. Yamamoto, N., Tanabe, Y., Okamoto, R., Dawson, P.E., Kajihara, Y. *J. Am. Chem. Soc.* **130**, 501 (2008).

## Synthesis of Fluorescently Labeled *O*-Mannosylated Glycopeptides as POMGnT1 Substrates in Clinical Assays

Mian Liu, Gerardo Alvarez-Manilla, Franchesca Brothers, and David Live

Complex Carbohydrate Research Center, University of Georgia, Athens, GA 30602, U.S.A.

### Introduction

Glycopeptides are valuable tools for studying the enzyme activities involved in the process of post-translational protein glycosylation, particularly for *O*-linked glycosylation. They can also be useful diagnostics for detecting disease related glycosylation defects. One such case relates to the function of the enzyme POMGnT1 which attaches an *N*-acetyl-glucosamine to a mannose in assembling the tetrasaccharide epitope on the glycoprotein  $\alpha$ -dystroglycan, (DG) important in the proper organization of muscles [1]. Defects in this enzyme prevent proper glycan assembly and lead to muscle-eye-brain disease, one of the congenital forms of muscular dystrophy. We have prepared several *O*-Man glycopeptides based on  $\alpha$ -DG sequences as substrates for the enzyme to study this process. Towards extending the application of these *O*-Man glycopeptides to improving diagnostic assays with patient tissue extracts [2], we report here preparation of forms with fluorescent tags for sensitive detection of glycopeptide products.

### Results and Discussion

Since intermediate glycoprotein or glycopeptide substrates for POMGnT1 are not accessible from natural sources, we have turned to solid-phase methods in preparing several DG related *O*-Man glycopeptides, as reported previously [3]. They have now been evaluated as substrates for the POMGnT1 enzyme. Of these, VEPT( $\alpha$ -D-Man)AV, had the advantages of both good substrate properties, and only one site of mannosylation, and was therefore chosen for further optimization as a fluorescent assay substrate. Data suggest that the Thr residue is mannosylated in the native glycoprotein [4]. In optimizing the fluorescent glycopeptide assay construct, several related structures were prepared with sequences successively shortened by one or two amino acid residues, or lengthened by one (Tyr) from the *N*-terminus, and their substrate properties examined.

Glycopeptide assembly was carried out with coupling of Fmoc-Thr(Ac<sub>4</sub>- $\alpha$ -D-Man)-OPfp for the glycosylated residue [3]. Incorporation of fluorescent probes at the *N*-terminus of the glycopeptides was accomplished in aqueous solution of NaHCO<sub>3</sub> (pH ~9) in the dark with fluorescein isothiocyanate (FITC) dissolved in acetone. Four FITC-labeled glycopeptides, with mannose attached to Thr through side chain hydroxyl group, FITC-PT( $\alpha$ -D-Man)AV, FITC-EPT( $\alpha$ -D-Man)AV, FITC-VEPT( $\alpha$ -D-Man)AV, and FITC-YVEPT( $\alpha$ -D-Man)AV (Figure 1) were synthesized by this route.

Derivatization of EPT( $\alpha$ -D-Man)AV with FITC was also evaluated in DMF adjusted to pH ~8.5 using DIEA, and compared to the NaHCO<sub>3</sub>/acetone system. While the former reached completion more rapidly, 3 h, than the latter, usually complete in 24 h, the reaction in NaHCO<sub>3</sub>/acetone was much cleaner as monitored by RP-HPLC and the products were easier to purify by semi-preparative RP-HPLC. Surprisingly, with the NaHCO<sub>3</sub>/acetone conditions, the labeling of PT( $\alpha$ -D-Man)AV and PT(Ac<sub>4</sub>- $\alpha$ -D-Man)AV with FITC was faster than for EPT( $\alpha$ -

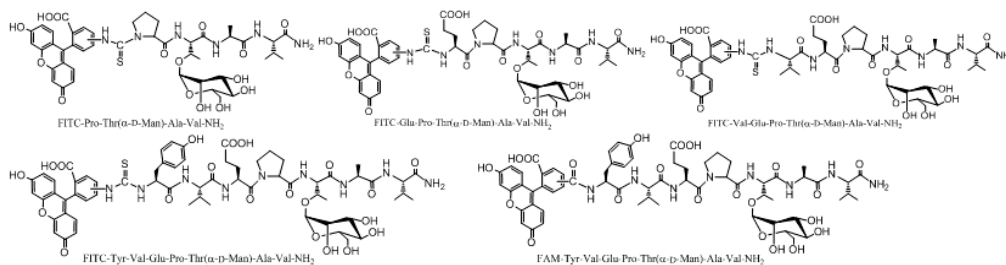


Fig. 1. FITC/FAM-labeled glycopeptides.

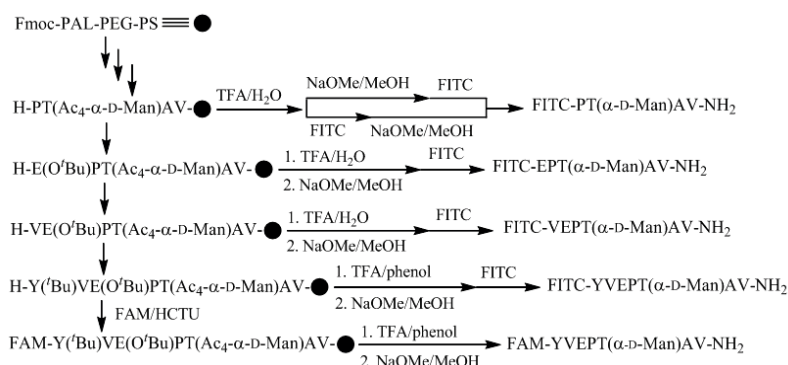


Fig. 2. Synthesis of fluorescently labeled glycopeptides.

D-Man)AV, VEPT( $\alpha$ -D-Man)AV, or YVEPT( $\alpha$ -D-Man)AV in spite of the terminal secondary amine. The reaction with PT(Ac<sub>4</sub>- $\alpha$ -D-Man)AV was complete in 2 h, followed by deacetylation of the acetyl groups on mannose residue to give FITC-PT( $\alpha$ -D-Man)AV quantitatively. Decomposition of FITC was observed during the labeling process in the presence of a base, *i.e.* NaHCO<sub>3</sub>, and in an extreme condition, FITC completely decomposed within a few hours at a high base concentration ( $>> 1$  mg/ml) and high molar ratio of NaHCO<sub>3</sub> to FITC ( $> 10:1$ ), giving rise to slow and incomplete FITC labeling.

In an alternative approach, carboxyfluorescein (FAM) was coupled on-resin to the N-terminus of Tyr residue after peptide assembly (Figure 2), *via* HCTU-mediated coupling in the presence of HOBt and DIEA, followed by peptide cleavage using a TFA-phenol cocktail. The acetyl groups were then removed by NaOMe in methanol to give FAM-YVEPT( $\alpha$ -D-Man)AV. Coupling of FAM on the solid-phase support, followed by washing the resin with piperidine-DMF (1:4,  $2 \times 2$  min) presumptively precluded the formation of acylated by-product from carboxyfluorescein [5]. In practice, mixtures of 5(6)-isomers of FITC and FAM were used in labeling the mannosylated glycopeptides, and the labeled glycopeptide isomers were not distinguishable before or after deacetylation (one single peak) by analytical RP-HPLC, except for 5(6)-FAM-YVEPT( $\alpha$ -D-Man)AV ( $t_R$  32.4, 32.8 min respectively).

Fluorescamine was also tested for labeling mannosylated glycopeptides, due to its efficient coupling with primary amines at room temperature, but the fluorophor rapidly deteriorates in acidic solution, making it incompatible with analysis and purification using RP-HPLC. Even in neutral or mildly alkaline solution, the fluorophor has limited stability to light at ambient temperature, and survives for only several days in the dark, limiting its usefulness in this application. The fluorescently labeled mannosylated-glycopeptides have the wavelength for maximum excitation at 484 nm and emission at 516 nm.

Initial determination of reaction kinetics for POMGnT1 action on FAM-YVEPT( $\alpha$ -D-Man)AV shows good substrate properties, consistent with what was previously observed for unmodified VEPT( $\alpha$ -D-Man)AV. Thus, addition of FAM does not compromise the activity. The  $K_m$  is 1,000 times more favorable for the FAM glycopeptide compared to benzyl-Man, that had been used conventionally as a substrate for POMGnT1 in the clinical assay [2].

## Acknowledgments

This research was supported by NIH grant R21-AR056055.

## References

- Barresi, R., Campbell, K.P. *J. Cell Sci.* **119**, 199-207 (2006).
- Vajsar, J., Zhang, W.L., Dobyns, W.B., Biggar, D., Holden, K.R., Hawkins, C., Ray, P., Olney, A.H., Burson, C.M., Srivastava, A.K., Schachter, H. *Neuromusc. Disord.* **16**, 132-136 (2006).
- Liu, M., Borgert, A., Barany, G., Live, D. *Biopolymers* **90**, 358-368 (2008).
- Manya, H., Suzuki, T., Akasaka-Manya, K., Ishida, H-K., Mizuno, M., Suzuki, Y., Inazu, T., Dohmae, N., Endo, T. *J. Biol. Chem.* **282**, 20200-20206 (2007).
- Fischer, R., Mader, O., Jung, G., Brock, R. *Bioconjugate Chem.* **14**, 653-660 (2003).

## Synthesis of Hemopressin by [(2+2+2+1)+2] Segment Condensation

**P. Anantha Reddy, K. Timothy McElroy, Charles J. McElhinny,  
 Anita H. Lewin, and F. Ivy Carroll**

*Center for Organic and Medicinal Chemistry, Discovery and Analytical Sciences.  
 Research Triangle Institute, Research Triangle Park, NC 27709, U.S.A.*

### Introduction

Hemopressin (HP), a naturally occurring nonapeptide (Pro-Val-Asn-Phe-Lys-Phe-Leu-Ser-His-OH) derived from the  $\alpha$ -chain of hemoglobin [1] has recently been identified as an endogenous selective CB1 antagonist [2]. Because of widespread interest [3] in this bioactive nonapeptide, which is reported to have been synthesized using solid phase Fmoc chemistry [1b], the National Institute on Drug Abuse (NIDA) authorized the solution phase synthesis of HP as part of its Drug Synthesis Program. The fragment condensation approach involves peptides fragments derived from synthetic intermediates that can also be used in possible structure-activity studies.

### Results and Discussion

Our synthesis of HP involved appropriately N-protected acids and C-protected amines (Figures 1 and 2). Specifically, the N-protected dipeptide Boc-Pro-Val-OH (**4**) and C-protected dipeptide H-Asn(Trt)-Phe-OBn (**8**) were prepared by coupling of Boc-Pro-OH (**1**) with HCl•Val-OBn (**2**) and Fmoc-Asn(Trt)-OH (**5**) with HCl•Phe-OBn (**6**) respectively, followed by deprotection of intermediates **3** and **7** (Figure 1).

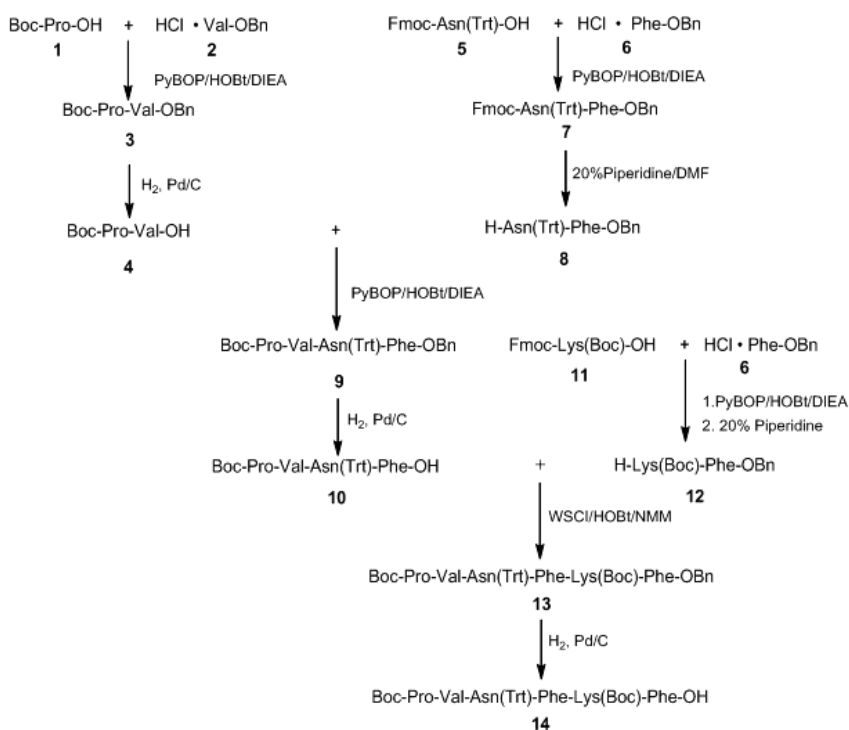


Fig. 1. Synthesis of hemopressin (part 1).

A (2+2) condensation of **4** with **8**, followed by hydrogenolysis of intermediate **9**, afforded the tetrapeptide Boc-Pro-Val-Asn(Trt)-Phe-OH (**10**), the N-terminal tetrapeptide fragment. Similarly, the dipeptide H-Lys(Boc)-Phe-OBn (**12**) was prepared by coupling Fmoc-Lys(Boc)-OH (**11**) with HCl-Phe-OBn (**6**), followed by exposure to piperidine. Subsequent (4+2) condensation of the tetrapeptide Boc-Pro-Val-Asn(Trt)-Phe-OH (**10**) with the dipeptide H-Lys(Boc)-Phe-OBn (**12**) furnished the corresponding hexapeptide Boc-Pro-Val-Asn(Trt)-Phe-Lys(Boc)-Phe-OBn (**13**). Hydrogenolysis of **13** to the N-terminal hexapeptide Boc-Pro-Val-Asn(Trt)-Phe-Lys(Boc)-Phe-OH (**14**), followed by conversion of **14** to the N-terminal heptapeptide Boc-Pro-Val-Asn(Trt)-Phe-Lys(Boc)-Phe-Leu-OH (**17**) by coupling to p-Tos Leu-OBn (**15**) gave **16**, which was hydrogenolyzed to **17** (Figure 2). Condensation of Cbz-Ser(Bu<sup>t</sup>)-OH (**18**) with His(Trt)-OBu<sup>t</sup> (**19**), followed by hydrogenolysis of the resulting dipeptide intermediate Cbz-Ser(Bu<sup>t</sup>)-His(Trt)-OBu<sup>t</sup> (**20**) gave the C-terminal dipeptide fragment H-Ser(Bu<sup>t</sup>)-His(Trt)-OBu<sup>t</sup> (**21**) (Figure 2). With heptapeptide **17** and dipeptide **21** on hand the protected nonapeptide Boc-Pro-Val-Asn(Trt)-Phe-Lys(Boc)-Phe-Leu-Ser(Bu<sup>t</sup>)-His(Trt)-OBu<sup>t</sup> (**22**) was assembled using WSCI/HOBt/NMM in a (7+2) condensation. Finally, the protecting groups were removed by exposure to TFA to afford HP (TFA•Pro-Val-Asn-Phe-Lys-Phe-Leu-Ser-His-OH, **23**), which was purified by preparative reversed phase HPLC. Purified HP trifluoroacetate was characterized by TLC, HPLC, <sup>1</sup>H NMR, amino acid analysis and was identical with a reference sample [1b].

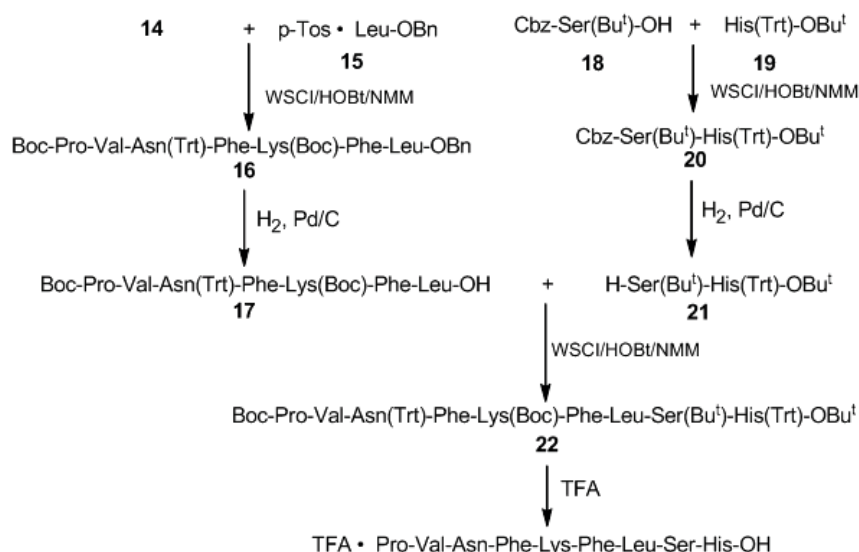


Fig. 2. Synthesis of hemopressin (part 2).

## Acknowledgments

Supported by National Institute on Drug Abuse (NIDA), Contract No. N01DA-8-7763.

## References

1. a) Dale, C.S., et al. *Mem Inst. Oswaldo. Cruz*, **100** (suppl. 1), 105-106 (2005); b) Rioli, V., et al. *J. Biol. Chem.* **278**, 8547-8555 (2003).
2. Heimann, A.S., et al. *Proc. Natl. Acad. Sci. U.S.A.* **104**, 20588-20593 (2007).
3. Blais, P-A., et al. *Peptides* **26**, 1317 (2005); Dale, C.S., et al. *Peptides* **26**, 431 (2005).



## Shorter Arginine Homologues to Stabilize Peptides Towards Tryptic Digestion

Petra Henklein,<sup>1</sup> and Thomas Bruckdorfer<sup>2</sup>

<sup>1</sup>Charité - Universitätsmedizin Berlin, Institute for Biochemistry, Monbijoustr. 2, D-10117 Berlin, Germany; <sup>2</sup>IRIS Biotech GmbH, Waldershofer Str. 49-51, D-95615 Marktredwitz, Germany, [thomas.bruckdorfer@iris-biotech.de](mailto:thomas.bruckdorfer@iris-biotech.de)

### Introduction

Trypsin (EC 3.4.21.4), an endopeptidase and natural protease cleaves peptide chains and proteins predominantly at the carboxyl side of the amino acids Lys and Arg (except when followed by Pro). Because shorter homologues of arginine with appropriate protecting groups for conventional Fmoc/tBu peptide synthesis are now available, three model peptides containing arginine and two shorter homologues of arginine were synthesized. They were incubated with trypsin in order to explore how stable the corresponding peptides are towards enzymatic degradation. It could be demonstrated that a peptide gains significant stability if arginine is being exchanged by a homologue containing one methylene group less. If arginine is substituted by a homologue with two methylene groups less the model peptide was almost fully stable over 24h towards enzymatic degradation.

### Results and Discussion

Peptides and proteins are gaining importance as modern biopharmaceuticals, due to their high specificity and efficacy. One drawback, however, is their low stability and resulting unfavourable pharmacokinetics. Proteases such as trypsin degrade peptides and proteins rather rapidly

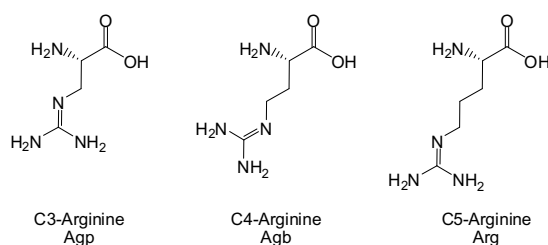


Fig. 1. Arginine homologues.

decreasing in this way their bioavailability. Many efforts have been made, in order to improve the stability of peptides and proteins, like modifying their structure by forming cyclic structures or altering the surface of biopharmaceuticals through PEGylation [1]. It is well known that side chain modification of Arg in the substrate has a definite influence on the activity of trypsin [2]. As cleavage typically happens at the C-terminal position of Lys and Arg,

exchange of these amino acids with longer and shorter homologues could have an effect on the protein resistance towards digestion [3]. As we developed the protected derivatives of shorter homologues of Arg (Figure 1) (having a chain of 5 carbons)  $\alpha$ -amino-4-guanidino-butyric acid (Agb), having 4 carbon chain, and  $\alpha$ -amino-3-guanidino-propionic acid (Agp), consisting of a 3 carbon chain - that are suitable for Fmoc/tBu SPP synthesis strategy - we were interested in whether substituting Arg with these shorter homologues

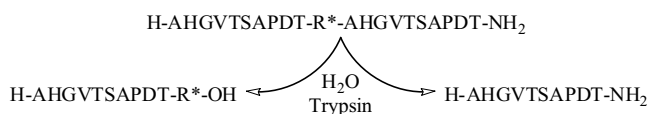


Fig. 2. Model sequence.

would have an influence on tryptic digestion of a peptide containing these building blocks. Therefore the sequence in Figure 2 was selected, which contains one Arg that can be exchanged with Agb and Agp; the corresponding peptides would then be hydrolysed into two fragments that would easily be detected by mass spectrometry and well separated by HPLC. The original three peptides contain Arg and Arg-like amino acid in the middle of the sequence [4].

As expected, the natural Arg (C=5) containing peptide is being completely digested even at a low concentration of trypsin. The concentration of original sequence and digested fragments of each peptide was determined by HPLC. Identity was confirmed by MS. These experiments were carried out with two different peptide/trypsin ratios. If the side chain of Arg is

reduced by one methylene group (C=4), digestion after 24h has hydrolyzed approx. 50% of the peptide at a peptide:trypsin ratio of 50:1. This digestion is a function of the concentration, i.e. lower relative concentrations of enzyme resulting in a lower extent of hydrolysis. In the case of C=3, the  $\alpha$ -amino-3-guanidino-propionic acid, trypsin appears almost inactive. At a low concentration of trypsin (1:100) no fragmentation can be observed, at all. At a higher concentration even after 24 h hydrolysis is observed only to a level of approx. 1%. The consequences from these results are if Arg is substituted by its shorter homologues Agb and Agp, Arg containing peptides can be stabilized towards proteolysis. The stability of biologically active peptides or peptide drugs can therefore be improved by appropriate substitution of Arg, if this substitution is not resulting in a lower biological activity of the peptide sequence. Although the C4 analogue Agb containing peptide is not fully resistant towards digestion, it is still much more stable compared to the natural Arg containing peptide. Thus, the half life of peptide drugs in biological media can be significantly improved and therefore can further help to establish peptides as standard drugs in pharmacological applications. Laminin YIGSR fragments containing Agp and Agb have already been synthesized, however, via different chemistry. The advantage of the developed building block Fmoc-L-Agp(Boc)<sub>2</sub>-OH is that it can be incorporated in standard peptide synthesis procedures and enables researchers to explore new sequences in a very convenient way. Current commercial productions can manufacture Agp containing sequences in a very economic way. However, Fmoc-L-Agb(Boc)<sub>2</sub>-OH is better coupled using a manual strategy. Presumably, the active ester tends to cyclize forming the corresponding pyrrolidone. Currently, synthetic strategies are being developed in our laboratories, to incorporate Agb in peptide sequences.

*Table 1. Summary of the degree of digestion of all three model peptides with two different trypsin concentrations*

	<i>HPLC (retention time) and MS (m/z)</i>	<i>trypsin:peptide 1/50</i>	<i>trypsin:peptide 1/100</i>
<b>Arg-Peptide</b>	21.3min (m/z = 955)	48.4%	48.4%
C = 5	22.1min (m/z = 1112)	51.6%	51.6%
	Approx. 26min	0%	0%
% Digested		complete	complete
<b>Agb-Peptide</b>	21.3min (m/z = 955)	33%	21.0%
C = 4	21.6min (m/z = 1098)	35.4%	21.9%
	26.0min (m/z = 2032)	31.6%	57.1%
% Digested		52%	27.0%
<b>Agp-Peptide</b>	20.6min (m/z = 1084)	1.0%	
C = 3	21.2min (m/z = 955)	1.1%	
	25.9min (m/z = 2018)	97.9%	100%
% Digested		approx. 1%	none

## Acknowledgments

This work is dedicated to Dr. Peter Henklein to the occasion of his 65th birthday. The authors thank Dr. Peteris Romanovskis (Bapeks sia, Latvia) and Prof. Fernando Albericio (Parc Científic de Barcelona, Spain) for helpful discussions.

## References

1. Bruckdorfer, T. *European Pharmaceutical Review*; Spring 2008, 96-104.
2. Schwegler, F. Influence on the trypsin activity by the side chain of arginine homologues in *Cellular and Molecular Life Sciences*, Verlag Birkhäuser Basel, Vol. 32 Nr. 11 (1976).
3. Witkowska, E., Orlowska, A., Izdebski, J. *Acta Biochimica Polonica* **51**, 51-56 (2004).
4. Henklein, P., Bruckdorfer, T. *Chemistry Today* **26**(6), 12-15 (2008).

## Application of Proteases in the C-terminal Modification of Peptides

Dirk-Jan van Zoelen,<sup>1</sup> Francesca Gini,<sup>1</sup> Gilbert Bours,<sup>1</sup> Ivo Eggen,<sup>1</sup>  
Guus Frissen,<sup>2</sup> and Carmen Boeriu<sup>2</sup>

<sup>1</sup>Schering-Plough, Molenstraat 110, 5342 CC Oss, The Netherlands; and  
<sup>2</sup>AFSG - Biobased Products, Wageningen University and Research Centre,  
Bornsesteeg 59, 6708 PD Wageningen, The Netherlands

### Introduction

In the past years the research directed toward protease-catalysed synthesis of small therapeutic peptides and oligopeptides received increasing attention. Obvious advantages of enzymatic synthesis over chemical approaches are the minimal protection required, the virtual absence of undesired side reactions and the easy separation of the products, features that make enzymatic processes really appealing, also from an industrial point of view. However, this approach has still not been thoroughly explored. Recently, we published the protease-catalysed selective deprotection of the C-terminal *tert*-butyl esters of peptides [1]. In this paper, we present recent developments by our groups in new synthetic applications for the modification of the carboxy-terminus of peptides, such as the C-terminal amidation and the synthesis of various esters by transesterification.

### Results and Discussion

#### *Selective enzymatic C-terminal amidation*

Many biological active peptides, *e.g.* gonadorelin, oxytocin and arginine vasopressin, contain an amide as the C-terminal functionality. Their synthesis can start from the free C-terminal amino acyl amide. However, this approach often entails serious solubility problems in solution-phase synthesis. Alternatively, the C-terminal amide function can be protected, though this approach is limited by the poor (commercial) availability of the precursors. The synthesis from amino acyl esters, followed by hydrolysis, activation of the free acid and amidation, includes considerable risks of racemization in both the esterification and the amidation steps. On the other hand direct ammonolysis of the amino acyl esters can lead to many side reactions. Considering the good results obtained in the ester hydrolysis, it was envisaged to use proteases in combination with an ammonium source to achieve amidation under mild reaction conditions. The screening of different ammonium sources was carried out with Alcalase-CLEA on the dipeptide Z-Ala-Phe-OMe. Among the ammonium sources tested, NH<sub>2</sub>COONH<sub>4</sub> afforded the best results leading to complete conversion in 2 hours in a Bu'OH/DMF (82.5/17.5, v/v) mixture at 30°C. However, a certain degree of hydrolysis of the ester starting material could not be avoided, since extremely dry conditions were not contemplated due to the possible inactivation of the enzyme. Under the optimized reaction conditions several peptides were screened and the results are listed in Table 1.

The amidation was also tested with several substituted amines, resulting in high chemoselectivity and little formation of the hydrolysis products (Table 2). However, diethylamine gave selectively Z-Ala-Phe-OH, probably due to sterical hindrance.

#### *Transesterification of peptide esters*

To further expand the scope the use of other nucleophiles was investigated. It was demonstrated that transesterification of methyl esters with Alcalase-CLEA could be achieved. Up to quantitative conversions could be achieved for alcohols such as Tmse-OH, EtOH, *n*-pentanol and *i*-propanol. Ester hydrolysis could, however, not be completely suppressed. Thiols on the other hand proved to be poor nucleophiles.

Table 1. Reactivity of different dipeptides in the presence of  $\text{NH}_2\text{COONH}_4$

Peptide	Time (h)	P-OMe (a/a%)	P-OH (a/a%)	P-NH <sub>2</sub> (a/a%)
Z-Val-Phe-OMe	75	0.0	13.3	86.7
Z-Val-Tyr-OMe	75	0.8	40.0	59.2
Z-Val-Leu-OMe	4	0.0	26.5	73.5
Z-Val-Thr-OMe	4	0.0	9.2	90.8
Z-Val-Ala-OMe	2	0.0	11.2	88.8
Z-Val-Met-OMe	4	0.0	27.3	72.7
Z-Val-Lys(Boc)-OMe	75	1.3	24.0	74.7
Z-Ala-Phe-OMe	4	0.5	6.7	92.8
Z-Ala-Phe-Ala-OMe	4	1.0	6.9	92.1
Z-Ala-Phe-D-Ala-OMe	75	54.3	10.4	35.4
Boc-Pro-Pro-Ala-Phe-Ala-OMe	21	0.0	0.0	> 99

Table 2. Reactivity with different amines (10 moleq) in  $\text{Bu}^t\text{OH}/\text{DMF}$  (82.5/17.5, v/v) after 24 h at 30°C

Amine	P-OH (a/a%)	P-Nu (a/a%)
$\text{EtNH}_2 \text{ HCl} + \text{TEA}^a$	10.8	88.9
DMAPA <sup>b</sup>	2.4	97.6
<i>n</i> BuNH <sub>2</sub>	1.4	98.6
<i>n</i> HepNH <sub>2</sub>	2.8	97.2
$\text{Et}_2\text{NH}$	95.7	4.2

<sup>a</sup> Without the addition of triethylamine (TEA) incomplete conversion was obtained after 96 h

## Conclusion

Subtilisin is a powerful enzyme for the conversion of C-terminal peptide methyl esters into primary and secondary amides. Transesterification of methyl esters of peptides can also be achieved with alcohols, but further optimization is needed. In view of the possible industrial applicability, patents have been filed [2,3].

## References

1. Del Valle, S., Esher E., Lubell W.D. (Eds.) *Peptides: Peptides for Youth (Proceedings of the 20<sup>th</sup> American Peptide Symposium)*, Springer, New York, 2009, 115-116.
2. Eggen, I.F., Boeriu, C.G. WO 2007/082890A1
3. Eggen, I.F., Boeriu, C.G. WO 2009/000814A1

## N-Methylation as a Synthetic Resource for Increasing Stability in Depsipeptides

Judit Tulla-Puche,<sup>1,2</sup> Eleonora Marcucci,<sup>1,2</sup> Irene Izzo,<sup>1</sup> Gerardo Acosta,<sup>1,2</sup>  
Sara Auriemma,<sup>1</sup> Chiara Falciani,<sup>1</sup> and Fernando Albericio<sup>1,2,3</sup>

<sup>1</sup>Institute for Research in Biomedicine, Barcelona Science Park, University of Barcelona, Barcelona, Spain; <sup>2</sup>CIBER-BBN, Networking Centre on Bioengineering, Biomaterials and Nanomedicine, Barcelona Science Park, Barcelona, Spain; and <sup>3</sup>Department of Organic Chemistry, University of Barcelona, Spain

### Introduction

Many depsipeptides of natural origin display high biological activities. [1] However, only a few of these compounds have entered clinical trials because of problems associated with bioavailability as well as low stability in plasma favored by the presence of the ester bonds. Another key feature of natural peptides and depsipeptides is the presence of *N*-methylated residues in their sequence. Cyclosporin, for example, bears six *N*-methyl amino acids. [2] Since the presence of *N*-methyl groups confers resistance to proteolytic cleavage, [3] the introduction of these groups has been widely used to prevent enzymatic degradation. Nevertheless, to date, *N*-methylation has been limited mostly to the backbone but has not been extensively studied as the replacement of the ester bond into a depsipeptide [4].

Here we describe the application of this strategy to two distinct depsipeptides of marine origin: (i) thiocoraline, [5] a bicyclic thiodepsipeptide which acts as bisintercalator to DNA; and (ii) kahalahide F, [6] which is now in preclinical stage.

### Results and Discussion

Following previous experience in solid-phase synthesis of some thiocoraline analogues and natural product kahalahide F, *N*Me-azathiocoraline and *N*Me-kahalahide F (Figure 1) were built on 2-chlorotrityl (CTC) resin. *N*Me amino acids were synthesized in solution using protocols previously optimized. In the case of *N*Me-azathiocoraline, *N*-methylation of the side-chain of Dap was carried out on solid-phase under Mitsunobu conditions of the *o*-nosyl(*o*-NBS)-

protected amine. The synthesis followed a [4+4] fragment coupling strategy (Scheme 1, A). Fmoc-Gly-OH was loaded as a first amino acid, followed by Fmoc removal and coupling of Boc-D-Dap(Fmoc)-OH. After performing the *N*-methylation, the tetrapeptide was obtained in good purity. Coupling between consecutive *N*Me amino acids was accomplished by using HATU/HOAt/DIEA in DMF. At this point the resin was split in two portions: in 1/3 of the resin, the Alloc group was removed whereas protected peptide from the remaining 2/3 of the resin was cleaved, lyophilized, and coupled to the unprotected tetrapeptidyl resin using PyAOP and DIEA. After obtaining the disulfide bridge with I<sub>2</sub> in DMF, the peptide was cleaved, and cyclized in solution by using PyBOP, HOAt, DIEA, in CH<sub>2</sub>Cl<sub>2</sub>-DMF. Finally, the Boc groups were removed using TFA-CH<sub>2</sub>Cl<sub>2</sub> (1:1), and the

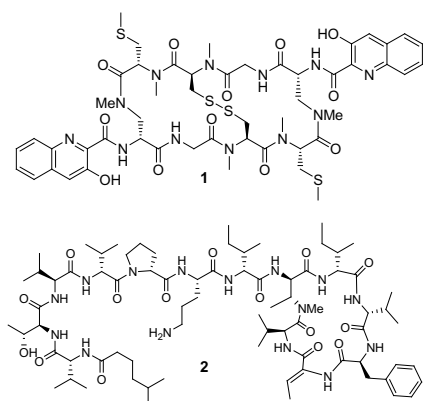
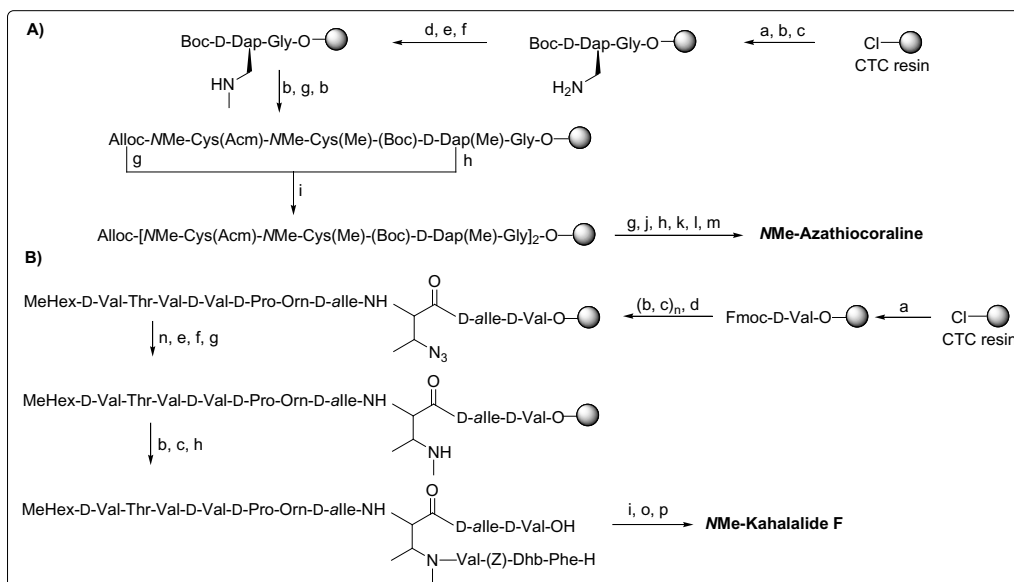


Fig. 1. Structures of **1** *N*Me-azathiocoraline and **2** *N*Me-kahalahide F

3-hydroxyquinaldic units introduced with the aid of EDC·HCl and HOSu, and purified by reversed-phase HPLC.

For *N*Me-Kahalahide F, solid-phase synthesis started by anchoring Fmoc-D-Val-OH on CTC resin (Scheme 1, B). Elongation of the linear chain was performed by using DIPCDI, HOAt in DMF, including the coupling of (2*R*,3*R*)-2-amino-3-azidobutanoic acid. Afterwards, reduction of the azide group was carried out with a freshly prepared solution of 0.2 M SnCl<sub>2</sub>, 0.8 M PhSH and 1.0 M DIEA in THF.



*Scheme 1. Solid-phase synthesis of (A) NMe-azathiocoraline and (B) NMe-kahalalide F: (a) Fmoc-AA-OH, DIEA, DCM; (b) PG<sub>1</sub>-AA(PG<sub>2</sub>)-OH, HATU, HOAt, DIEA, DMF; (c) piperidine-DMF (1:4); (d) *o*-NBS-Cl, DIEA, DCM; (e) PPh<sub>3</sub>, MeOH, DIAD, THF; (f) OH-CH<sub>2</sub>-CH<sub>2</sub>-SH, DBU, DMF; (g) Pd(PPh<sub>3</sub>)<sub>4</sub>, PhSiH<sub>3</sub>, DCM; (h) TFA-DCM (1:99); (i) PyAOP, DIEA, DMF; (j) I<sub>2</sub>, DMF; (k) PyBOP, HOAt, DIEA, DMF-DCM (1:1); (l) TFA-H<sub>2</sub>O (1:1); (m) 3-hydroxyquinaleic acid, EDC·HCl/HOSu/DIEA, DCM; (n) SnCl<sub>2</sub>, PhSH, DIEA, THF; (o) DIPCDI, HOBT, DIEA, DCM; (p) TFA-DCM (19:1).*

After 4 treatments (4 × 1 h), 66% of the amine was obtained. *N*-Methylation following Mitsunobu conditions proceeded well and after coupling of the two remaining amino acids using Alloc chemistry, cleavage, and cyclization, a crude NMe-kahalalide F of 35% purity was obtained, which was purified by semi-preparative HPLC.

Stability assays in human serum for a period of 120 h showed more resistance to degradation, with a half-life of 23.1 h for NMe-azathiocoraline compared to 14.4 h for thiocoraline. [7]

## Acknowledgments

Supported by CICYT (CTQ2006-03794/BQU), the ISCIII (CIBER, nanomedicine), the Institute for Research in Biomedicine, and the Barcelona Science Park.

## References

1. Sarabia, F., Shammaa, S., Sanchez Ruiz, A., Martin Ortiz, L., Lopez Herrera, F. *J. Curr. Med. Chem.* **11**, 1309–1332 (2004), and references therein.
2. Ruegger, A., Kuhn, M., Lichti, H., Loosli, H.R., Huguenin, R., Quiquerez, C., von Wartburg, A. *Helv. Chem. Acta* **59**, 1075–1092 (1976).
3. Yu, J., Butelman, E.R., Woods, J.H., Chait, B.T., Kreek, M.J. *J. Pharmacol. Exp. Ther.* **280**, 1147–1151 (1997).
4. Cavelier, F., Jacquier, R., Mercadier, J.-L., Verducci, J. *Tetrahedron* **52**, 6173–6186 (1996).
5. (a) Romero, F., Espliego, F., Pérez-Baz, J., García de Quesada, T., Gravalos, D., De la Calle, F., Fernández-Puentes, J.L. *J. Antibiot.* **50**, 734–737 (1997); (b) Pérez-Baz, J., Cañedo, L.M., Fernández-Puentes, J.L., Silva Elipe, M.V. *J. Antibiot.* **50**, 738–741 (1997).
6. (a) Hamann, M.T., Scheuer, P.J. *J. Am. Chem. Soc.* **115**, 5825–5826 (1993); (b) López-Macia, A., Jimenez, J.C., Royo, M., Giralt, E., Albericio, F. *J. Am. Chem. Soc.* **123**, 11398–11401 (2001).
7. Tulla-Puche, J., Marcucci, E., Prats-Alonso, E., Bayó-Puxan, N., Albericio, F. *J. Med. Chem.* **52**, 834–839 (2009).

## Chemical Synthesis of Full-Length Parathyroid Hormone-Related Protein-(1-141)

Ashok Khatri,<sup>1</sup> John T. Potts,<sup>1</sup> T. John Martin,<sup>2</sup> and Thomas J. Gardella<sup>1</sup>

<sup>1</sup>Massachusetts General Hospital and Harvard Medical School, Boston, MA 02114, U.S.A.;

<sup>2</sup>St. Vincent's Institute of Medical Research, Fitzroy, Australia

### Introduction

Parathyroid hormone-related protein (PTHrP) is a 141-residue long protein (Figure 1) that plays a critical role in bone and tissue development. The intact protein can be obtained by recombinant methods, but shorter-length synthetic fragments, such as PTHrP(1-36), are used in most studies. Knowledge on the structural and functional properties of intact PTHrP is thus limited. No attempt at chemical synthesis of full-length PTHrP has so far been reported. We thus sought to produce full-length PTHrP(1-141) by chemical synthesis methods.

<sup>1</sup>AVSEHQLLHDKGKSIQDLRRRFFLHHLIAEIHAEIRATSEVSPNSKPSNTKN  
HPVRFSGDDEGRYLTQETNKVETYKEQPLKTPGKKKGKPKGRKEQEKKKR  
RTRSAWLDSGVTGSGLEGDHLSDTSTTSLELDSRRH<sup>141</sup>

Fig. 1. Sequence of full length PTHrP.

### Results and Discussion

To produce full length PTHrP(1-141), we used an Applied Biosystems Model 431A automated peptide synthesizer. We started assembly of the peptide chain using 370mg (74 micromoles) of a preloaded Fmoc-His(Trt)-NovaSyn-TGT resin. Residues 140 through 61 were sequentially coupled at the 0.25mmol scale (HBTU/HOBt/DIEA activation) [1]. The synthesis was continued with ten micromoles of this peptide resin using 0.1 mmole-scale cycles and HOBt/DIC activation. A one-hundred-fold molar excess of Fmoc amino acid and activator was employed at each coupling cycle. During synthesis, the peptide resin was selectively capped with HOBt/DIC-activated acetic acid after the coupling cycles of G60, R37, S14 and A1. The final Fmoc group on A1 was left intact until the final purification step. The completed peptide, with the A1 Fmoc group intact, was cleaved from the resin by treatment for 4 hours at room temperature with Reagent K [2]; the crude protein was then precipitated in cold MTBE, and the precipitate was washed twice with MTBE, dissolved in 20% CH<sub>3</sub>CN/0.1%TFA.dH<sub>2</sub>O, and freeze-dried.

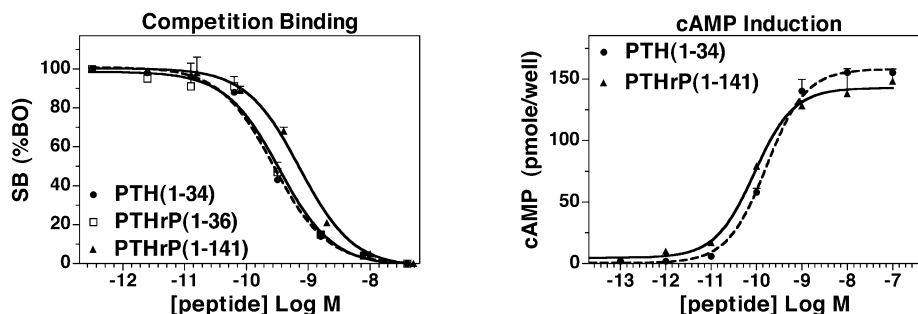
Sixteen mg of the crude Fmoc-PTHrP(1-141)-OH was dissolved in 20% CH<sub>3</sub>CN/0.1%TFA.dH<sub>2</sub>O and purified by reversed-phase HPLC using a 250 x 20 mm column (Higgins Targa C18 Semi-Preparative) and a 2-72% gradient of Buffer B (0.1%TFA in CH<sub>3</sub>CN) in Buffer A (0.1% TFA in dH<sub>2</sub>O) run over 35 minutes at a flow rate of 15 ml/min. Eluted fractions containing peptide were collected, freeze-dried, and assessed for Fmoc-PTHrP(1-141)-OH content by mass-spec analysis. The yield of the Fmoc-containing product was 1.7mg. The Fmoc group was then removed by treating the product with 25% piperidine in DCM for 30 minutes and then precipitating the peptide in cold MTBE. The dried protein was then reconstituted and purified by a second RP-HPLC step.

Matrix-assisted Laser Desorption Ionization Time of Flight mass spectrometry (MALDI-TOF/MS) analysis of the final product confirmed the mass expected for full-length PTHrP(1-141) (~16kD). Tryptic digest peptide mass finger print analysis, performed in tandem with recombinant PTHrP(1-141), further confirmed identity.

Of note, in HPLC-processing of the crude peptide, intact Fmoc-PTHrP(1-141) eluted considerably later than the internally deleted or truncated failed peptides; the product could thus be obtained at near homogeneity by a single HPLC step. Isolation of this later-eluting peak followed by removal of the Fmoc group and a second HPLC step resulted in the final product at approximately 95% purity. The final yield was 220 micrograms.

The chemically synthesized PTHrP was tested for activity in cells or cell membranes expressing the PTH/PTHrP receptor. Competition binding studies performed in COS-7 cell membranes expressing the rat PTHR using  $^{125}\text{I}$ -PTH(1-15) analog as tracer radioligand revealed an affinity comparable to that of PTH(1-34) and PTHrP(1-36) (Figure 2, left). The synthetic PTHrP(1-141) was also comparably potent to PTH(1-34) for stimulating cAMP production in mouse preosteoblastic MC3T3-E1 cells (Figure 2 right).

Fig. 2. Functional properties of synthetic PTHrP(1-141).



An 11Kd protein has been synthesized using a similar strategy; however this work involved utilizing a specialized removable lipophilic probe at the N-terminus [3]. By using the N-terminal Fmoc group alone for aiding the purification process, we were successful in the synthesis of a longer, 16Kd protein by a simpler process.

This work shows that peptides longer in length than previously appreciated can be approached via the automated synthesis route, and opens new avenues of investigation into PTHrP biology.

## Acknowledgment

This work was supported in part by NIH program project grant. DK-11794.

## References

1. Fields, C.G., Lloyd, D.H., Macdonald, R.L., Otteson, K.M., Noble, R.L. *Peptide Res.* **4**, 95-101 (1991).
2. King, D., Fields, C., Fields, G. *Int. J. Pept. Protein Res.* **36**, 255-266 (1990).
3. Ball, H.L., Mascagni, P. *Int. J. Pept. Protein Res.* **48**, 31-47 (1996).



## Towards a Minimalist Cell-Penetrating Peptide

Emily Ricq,<sup>1</sup> Nabila Brabez,<sup>2</sup> Teresa Coppola,<sup>3</sup> Solange Lavielle,<sup>2</sup>  
 and Gérard Chassaing<sup>2</sup>

<sup>1</sup>Department of Chemistry and Biochemistry, University of Arizona, Tucson, AZ 85721, U.S.A.;

<sup>2</sup>Laboratoire des BioMolécules, Université Pierre et Marie Curie-CNRS-ENS, Paris, 75252, France; and

<sup>3</sup>Dipartimento di Chimica delle Sostanze Naturali, Università di Napoli Federico II, Napoli, 80131, Italy

### Introduction

Cell-penetrating peptides (CPPs) are known to internalize exogenous macromolecules and have received much attention for their pharmaceutical potential. The most commonly studied natural and synthetic CPPs include Penetratin, Tat, and (Arg)<sub>9</sub>; these CPPs are between 9-30 amino acid residues, feature multiple positive charges, and can efficiently internalize cargo without cell-type specificity or chiral receptors [1]. Although their secondary structure and amphipathicity varies, it is thought that the presence of multiple positively-charged residues is critical to achieve uptake into the cell [1]. In addition to the presence of positive charges, past research shows that myristoylation of peptides increases their uptake into cells [2]. Our research suggests that pseudopeptides much simpler than the commonly studied CPPs can also efficiently internalize cargo, so long as the critical cationic and lipophilic features are conserved [3]. The solution-phase synthesis of a novel, minimalist CPP which encapsulates these core features is presented here (Figure 1).

### Results and Discussion

The central feature of our minimalist CPP is the pseudo-amino acid bis-ornithine [4], which is formed from a double Michael addition on the  $\alpha$ -carbon of glycine methyl ester, **1**. In order for both additions to occur, the  $\alpha$ -carbon protons must be sufficiently acidic. This is achieved by the formation of a Schiff base at the amino terminus from *para*-chlorobenzaldehyde, **2**. This imine allows for the efficient double-addition of acrylonitrile, **3**; the nitrile of acrylonitrile acts a protecting group yet can be conveniently converted to a number of nitrogen-based functional groups. Removal of the Schiff base in aqueous acid yields the methyl ester of bis-ornithine, **4**. When in its reduced form, the bis-ornithine will allow for two positive charges on a single amino acid residue, and its achirality simplifies the synthesis of the minimalist CPP.

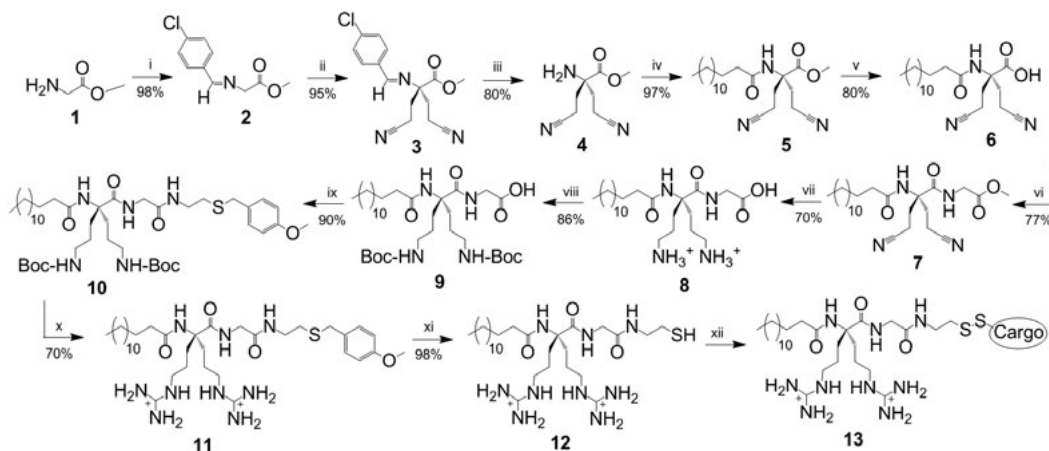


Fig. 1. Synthesis of the minimalist CPP. i. *p*-chlorobenzaldehyde, Et<sub>3</sub>N, MgSO<sub>4</sub>, DCM; ii. acrylonitrile, K<sub>2</sub>CO<sub>3</sub>, MeOH; iii. 1 N HCl, THF, 0° C; iv. myristoyl chloride, DIEA, DCM, 0° C; v. 2 M NaOH, 1:3 THF/EtOH; vi. 1. HBTU, DIEA, DMF; vii. 1. 2 M NaOH, 1:3 THF/EtOH, 2. 5 atm H<sub>2</sub>, PtO<sub>2</sub>, MeOH; viii. Boc<sub>2</sub>O, 1:1 H<sub>2</sub>O/dioxane, pH 8-9; ix. *p*-methoxybenzyl-protected cysteamine, HCTU, DIEA, DMF; x. 1. trifluoroacetic acid, DCM, 2. 1-*H*-pyrazole-1-carboxamide HCl, DIEA, DMF; xi. HF; xii. cargo-SH.

A lipid chain is added *via* N-acylation with myristoyl acid chloride, **5**. This myristoyl chain should increase the minimalist CPP's ability to cross the cell membrane [2,4]. Hydrolysis of the bis-ornithine from ester to acid, **6**, in aqueous base allows for subsequent coupling reactions at the carboxy-terminus. Next, a glycine spacer is introduced using HBTU as a carboxyl activating agent, **7**. The glycine spacer serves two purposes. First, it increases the distance between the sterically-hindered  $\alpha$ -carbon of the bis-ornithine, thus improving yields in subsequent reactions. Second, it prevents intramolecular lactam formation upon reduction of the nitriles. Following the hydrolysis of the terminal glycine from ester to acid, the nitriles are reduced to amines using 5 atmospheres of hydrogen gas and a platinum oxide catalyst, **8**. The free amines are immediately protected with *tert*-butoxycarbonyl (Boc) groups to minimize unwanted side reactions in the next steps, **9**. Next, a *para*-methoxybenzyl (PMB) protected cysteamine is coupled to the terminal glycine using HCTU as a carboxyl activating group, **10**. This thioether was introduced so that the cargo could later be linked to the CPP *via* disulfide bond, a common method of linking the cargo to the carrier [1]. Next, the Boc protecting groups are cleaved in aqueous acid and the resulting amines are guanylated, affording their final cationic character essential for uptake into the cell, **11**. Finally, the PMB protecting group is removed using HF, **12**, the cargo is linked to the carrier *via* a disulfide bond, **13**, and the CPP-cargo complex is purified by HPLC.

We have presented the efficient synthesis of a novel, minimalist CPP which will serve as a simplified model for CPP activity. Future studies will quantify CPP-cargo uptake into Chinese hamster ovary (CHO) cells using matrix-assisted laser desorption/ionization time-of-flight (MALDI-TOF) mass spectrometry [5], and measure the thermodynamic properties of interactions between the minimalist CPP and artificial membranes using Plasmon Waveguide Resonance (PWR) spectrometry and microcalorimetry [6].

## Acknowledgments

We thank the National Science Foundation's International Research Experience for Undergraduates (iREU) program, the Howard Hughes Medical Institute, the Flinn Foundation, and the Science for Life program coordinators at the University of Florida.

## References

1. Derossi, D., Chassaing, G., Prochiantz, A. *Trends Cell Bio.* **8**, 84-87 (1998).
2. Aussedat, B., Dupont, E., Sagan, S., Joliot, A., Lavielle, S., Chassaing, G., Burlina, F. *Chem. Comm.* **12**, 1398-1400 (2008).
3. Aussedat, B., Chassaing, G., Lavielle, S., Burlina, F. *Tetrahedron Lett.* **47**, 3723-3726 (2006).
4. Pham, W., Kircher, M.F., Weissleder, R., Tung, C.H. *ChemBioChem.* **5**, 1148-1151 (2004).
5. Burlina, F., Sagan, S., Bolbach, G., Chassaing, G. *Angew. Chem. Int. Ed.* **44**, 4244-4247 (2005).
6. Alves, I.D., Correia, I., Jiao, C.Y., Sachon, E., Sagan, S., Lavielle, S., Tolin, G., Chassaing, G. *J. Pept. Sci.* **15**, 200-209 (2009).

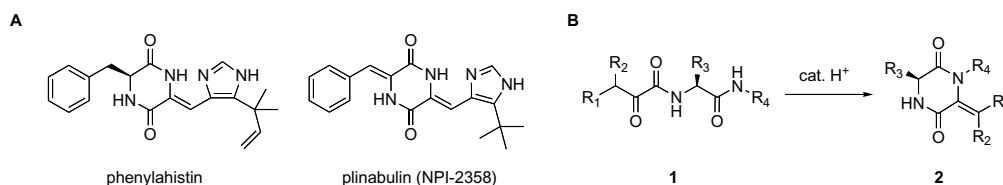
## Acid Catalyzed Monodehydro-2,5-diketopiperazine Formation toward Natural Product Synthesis

Yuri Yamazaki,<sup>1</sup> Yuki Mori,<sup>1</sup> Akiko Oda,<sup>2</sup> Yoshiaki Kiso,<sup>2</sup>  
and Yoshio Hayashi<sup>1</sup>

<sup>1</sup> Department of Medicinal Chemistry, Tokyo University of Pharmacy and Life Sciences, Hachioji, Tokyo, 192-0392, Japan; <sup>2</sup> Department of Medicinal Chemistry, Center for Frontier Research in Medicinal Science, 21st Century COE Program, Kyoto Pharmaceutical University, Kyoto 607-8412, Japan

### Introduction

There are many naturally occurring monodehydro-2,5-diketopiperazines (monodehydroDKPs) possessing biological activity such as phenylahistin (PLH) with microtubule depolymerization activity, which is a lead compound of plinabulin (NPI-2358) under Phase II clinical trials as a vascular disrupting agent (VDA) [1]. Additionally, monodehydroDKPs are useful building blocks and templates for combinatorial chemistry. However, racemization at the  $\alpha$ -position of the amino acid moiety is often observed during cyclization of the corresponding dipeptide unit, or introduction of the dehydromoiety in the synthesis of monodehydroDKPs [2]. In order to develop a new method that reduces such unfavorable racemization and to provide a new efficient synthetic route of monodehydroDKPs, in our previous study, we focused our work on Gladiali *et al.*'s report [3] that the reaction of  $\alpha$ -ketoester and Boc-NH<sub>2</sub> in the presence of a catalytic amount of *p*-TsOH resulted in the formation of dehydroamino acid, and successfully applied this method to *N*- $\alpha$ -ketoacyl-Phe-NH<sub>2</sub> to synthesize monodehydroDKPs in a reasonable yield with no racemization [4]. In the present study, we have also expanded this method to other amino acid residues such as Leu and Ser(Bzl) in case that  $\beta$ -aliphatic- $\alpha$ -keto acid derivatives were used. Additionally, the effect of acids was examined on this reaction and the reaction condition was optimized. Then, we successfully synthesized a derivative of natural microtubule depolymerization agent PLH, (-)-*t*Bu-oxa-PLH, by using this reaction as a key step.

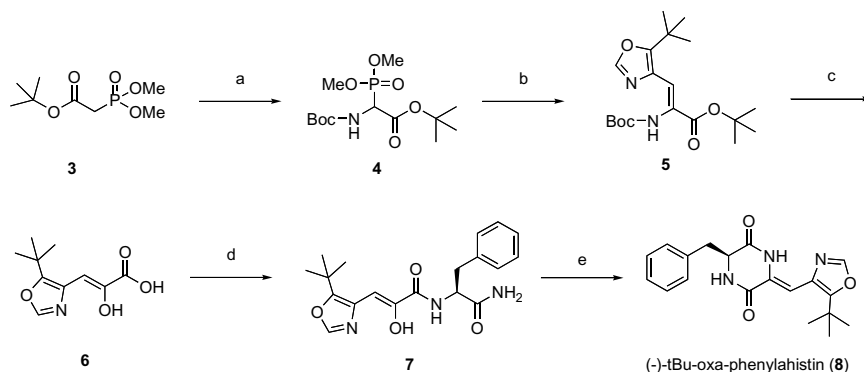


Scheme 1 (A) Structures of phenylahistin and plinabulin (NPI-2358), (B) New synthetic strategy of monodehydroDKP

### Results and Discussion

In order to expand this method to other amino acid residues such as Leu and Ser(Bzl) in place of Phe residue, corresponding  $\alpha$ -ketoacyl amino acid allylamides were refluxed in toluene in the presence of 5 mol % *p*-TsOH. As a result, similar chemical yield to the L-Phe derivative (92%, >99% ee) was obtained in the case of L-Leu derivative (96%, >99% ee). In the case of L-Ser(Bzl) derivative, it needed longer reaction time and showed moderate chemical yield (69%, >99% ee) probably due to some steric effect. No racemization was observed in both cases.

Then, to understand the effect of acids, which were required in the cyclization reaction, a model substrate pyruvoyl-Phe-NH-allyl was refluxed in the presence of a variety of acids. The reaction did not proceed with a catalytic amount (3 mol%) of TFA (pK<sub>a</sub> = -0.25) or MSA (pK<sub>a</sub> = -2.6). However, in the catalytic use of stronger acids *p*-TsOH (pK<sub>a</sub> = -6.57) and TFMSA (pK<sub>a</sub> = -14), a corresponding monodehydroDKP was produced with no racemization. Especially, the use of *p*-TsOH resulted in the highest chemical yield (92%) of the desired product. Alternatively, the effect of the large amount of TFA or AcOH as a weaker acid was evaluated. 1% TFA solution (corresponding to 50 mol%) in toluene, promoted the production of



**Scheme 2** Synthesis of a phenylahistin derivative (**8**) via acid-catalyzed monodehydroDKP synthesis. Reagents and conditions; (a) i) NaH, TsN<sub>3</sub>, rt, 2 h, ii) Boc-NH<sub>2</sub>, cat. Rh<sub>2</sub>(OAc)<sub>4</sub>, toluene, reflux, 1 h, 51% in 2 steps; (b) 5-tert-butyl-4-oxazolecarboxaldehyde, Cs<sub>2</sub>CO<sub>3</sub>, DMF, rt, 14 h, 47%; (c) 4M HCl/dioxane, rt, 1 h, 76%; (d) HCl·H-Phe-NH<sub>2</sub>, EDC·HCl, HOBT·H<sub>2</sub>O, Et<sub>3</sub>N, DMF, rt, 14h, 43%; (e) 5 mol% *p*-TsOH, toluene, reflux, 6 h, 20%.

corresponding monodehydroDKP in 26% yield and a higher chemical yield of 62% was obtained in 10% TFA. AcOH (10%, pK<sub>a</sub> = 4.76) was not effective in this cyclization reaction. As a result, the catalytic use of *p*-TsOH with a pK<sub>a</sub> value of -6.57 was superior for this cyclization reaction. Additionally, we found that 5 mol% *p*-TsOH and 6 h reflux was the best reaction condition on this *p*-TsOH catalyzed cyclization reaction from the examinations using *N*-phenylpyruvoyl Phe-NH<sub>2</sub>.

We applied this optimized reaction condition to the synthesis of (–)-*tert*-butyl-oxa-phenylahistin **8**, which is a derivative of natural anti-microtubule agent phenylahistin. The key amino acid intermediate **7** was synthesized from *tert*-butyl-*P,P*-dimethylphosphonoacetate **3** in five steps as shown in Scheme 2. Then, the acid catalyzed intramolecular cyclization reaction in the presence of 5 mol% *p*-TsOH for 6 h was performed to give desired compound **8** with no racemization (>99% ee), although the chemical yield of the final step was low (20%). Observed low reactivity in β-aryl-α-keto acid derivative was surely caused by keto-enol tautomerism at the α-keto acid moiety with β-aromatic ring, i.e., an unfavorable enol form for the cyclization was stabilized by conjugation with the aromatic ring. Reaction conditions that are able to accelerate the keto formation might be effective to solve this problem, which should be considered in the future study. However, it is certain that this method is beneficial for the synthesis of monodehydroDKPs from β-aliphatic-α-ketoacyl amino acid derivatives, likely to be applied to combinatorial synthesis of monodehydroDKP derivatives in the future [5].

## Acknowledgments

This research was supported by grants from MEXT (Ministry of Education, Culture, Sports, Science and Technology), Japan, including Grant-in Aid for Young Scientists (B) 21790118 and Grant-in Aid for Scientific Research (B) 20390036.

## References

- Kanoh, K., Kohno, S., Katada, J., Takahashi, J., Uno, I. and Hayashi, Y. *Bioorg. Med. Chem.* **7**, 1451-1457 (1999).
- Hayashi, Y., Orikasa, S., Tanaka, K., Kanoh, K. and Kiso, Y. *J. Org. Chem.* **65**, 8402-8405 (2000).
- Gladiali, S. and Pinna, G. *Tetrahedron: Asymmetry*, **2**, 623-632 (1991).
- Hayashi, Y., Oda, A., Yamazaki, Y., Okuno, Y., Kiso, Y. In Blondelle, S. E. (Ed.) *Peptides: Understanding Biology Using Peptides, (Proceedings of the 19<sup>th</sup> American Peptide Symposium)*, 2005, p. 98-99.
- Yamazaki, Y., Mori, Y., Oda, A., Okuno, Y., Kiso, Y., Hayashi, Y. *Tetrahedron* **65**, 3688-3694 (2009).

## Solid-Phase Synthesis of Aza-Proline Analogs of GHRP-6

Caroline Proulx and William D. Lubell

Département de Chimie, Université de Montréal, Montréal, H3C 3J7, Canada

### Introduction

Incorporation within the peptide sequence of an aza-amino acid, in which the alpha-carbon is substituted for a nitrogen atom, has been shown to induce a  $\beta$ -turn conformation as a direct consequence of lone pair – lone pair repulsion [1]. Particularly, aza-proline has been shown to enhance *cis*-amide conformation, thereby favoring type VI  $\beta$ -turns [2] (Figure 1). Whereby native GHRP-6 shows affinity for both the CD36 and GHS-R1a receptors, [3] AzaPro-containing GHRP-6 azapeptide analogs were anticipated to introduce conformational rigidity that could allow for preferential binding towards the CD36 receptor, and constituted promising targets for the treatment of angiogenesis related diseases.

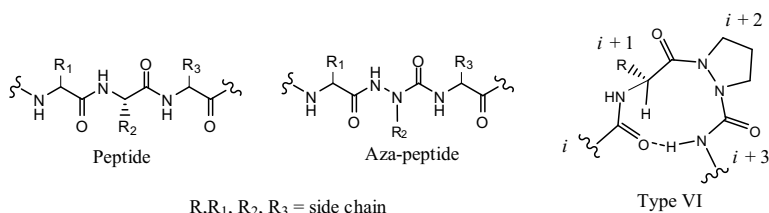


Fig. 1. Representative peptide, aza-peptide and azaPro peptide with type VI  $\beta$ -turn.

### Results and Discussion

Peculiarities of the azaPro moiety give rise to conformational preferences biasing  $\beta$ -VI folding of Xaa-AzaPro sequences, as observed by X-ray crystallography [2]. Previously synthesized biologically active peptide analogs possessing AzaPro include thyrotropin-releasing hormone analogs [4], and FKBP12 ligands [5] which were synthesized via *tert*-butyl pyrazolidine-1-carboxylate and di-*tert*-butylpyrazolidine-1,2-dicarboxylate intermediates, respectively. In the context of our research, an Fmoc approach was developed to introduce aza-proline into analogs of GHRP-6 (His-D-Trp-Ala-Trp-D-Phe-Lys-NH<sub>2</sub>), a ligand with dual receptor affinity, in order to modulate turn geometry and introduce selectivity for the CD36 receptors as opposed to the GHS-R1a receptors.

Synthesis of aza-proline containing peptides was previously achieved via *tert*-butyl pyrazolidine-1-carboxylate intermediate, which can be used to couple with an amino-ester derived isocyanate to form N-Boc-aza<sup>1</sup>-depipetides in solution [6]. In contrast, Fmoc protected aza-amino acid chlorides intermediates were shown to be effective for incorporation of aza-amino acids onto growing peptides on rink amide resin [7]. Extending this methodology for the synthesis and incorporation of aza-proline, we prepared Fmoc carbazate building block 2 by acylation of *tert*-butyl pyrazolidine-1-carboxylate [4] with Fmoc succinamide, followed by Boc group removal using a 1:1 TFA:DCM mixture. Phosgene activation of 2 allowed incorporation of Fmoc protected aza-amino acid chloride intermediate 3 onto resin-bound peptide. Coupling of the next amino acid was achieved using BTC as the acylating agent. Further peptide chain elongation, cleavage and purification were conducted according to general solid-phase peptide synthesis protocols [8] (Figure 2).

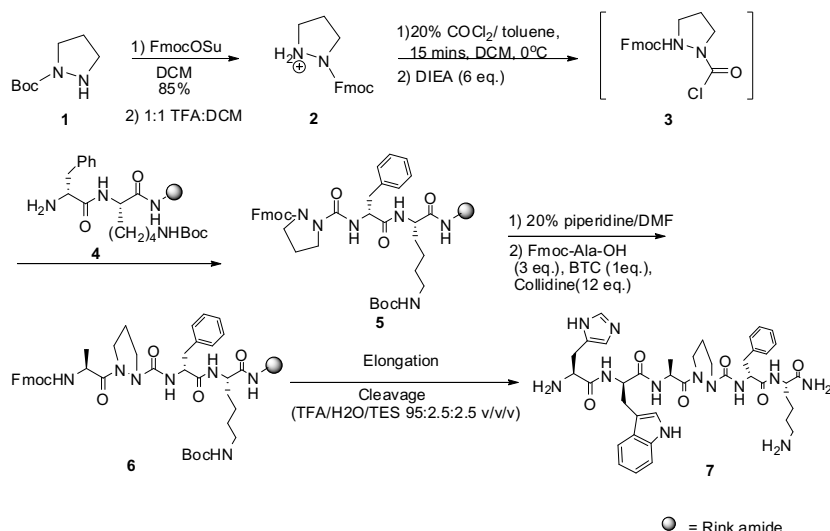


Fig. 2. Representative synthesis of GHRP-6 aza-proline containing aza-peptide analogues.

Systematic incorporation of aza-proline within the D-Trp<sup>2</sup>-Ala<sup>3</sup>-Trp<sup>4</sup>-D-Phe<sup>5</sup> region GHRP-6 sequence afforded four [aza-Pro]GHRP-6 analogs, which were prepared in parallel using a split-and-mix approach with IRORI kans. Briefly, macrokans undergoing identical reactions were combined in a single reaction vessel, into which reagents passed through the walls of the macrokans. Following reaction completion, kans were separated and pooled accordingly for the next reaction. A radiofrequency (Rf) tag associated to a unique ID number allowed for identification of each IRORI kan. The IC<sub>50</sub> binding values of the aza-peptides for affinity to both the GHS-R1a and CD36 receptors will be presented in the near future.

## Acknowledgments

This work was funded by the Natural Sciences and Engineering Research Council of Canada.

## References

- (a) André, F., Boussard, G., Bayeul, D., Didierjean, C., Aubry, A., Marraud, M. *J. Peptide Res.* **49**, 556-562 (1997). (b) André, F., Vicherat, A., Boussard, G., Aubry, A., Marraud, M. *J. Peptide Res.* **50**, 372-381 (1997).
- (a) Didierjean, C., Del Duca, V., Benedetti, E., Aubry, A., Zouikri, M., Marraud, M., Boussard, G. *J. Pept. Res.* **50**, 451-457 (1997). (b) Zouikri, Vicherat, A., Aubry, A., Marraud, M., Boussard, G. *J. Pept. Res.* **52**, 19-26 (1998). (c) Lecoq, A., Boussard, G., Marraud, M., Aubry, A. *Biopolymers* **33**, 1051-1059 (1993). (d) Lecoq, A., Boussard, G., Marraud, M. *Tetrahedron Letters* **33**(36), 5209-5212 (1992).
- Demers, A., McNicoll, N., Febbraio, M., Servant, M., Marleau, S., Silverstein, R., Ong, H. *Biochem J.* **382**, 417-424 (2004).
- Zhang, W.-J., Berglund, A., Kao, J.L.-F., Couty, J.-P., Gershengorn, M.C., Marshall, G.R. *J. Am. Chem. Soc.* **125**, 1221-1235 (2003).
- Wilkinson, D.E., Thomas, B.E., Limburg, D.C., Holmes, A., Sauer, H., Ross, D.T., Soni, R., Chen, Y., Guo, H., Howorth, P., Valentine, H., Spicer, D., Fuller, M., Steiner, J.P., Hamilton, G.S., Wu, Y.-Q. *Bioorg. Med. Chem.* **11**, 4815-4825 (2003).
- Melendez, R.E., Lubell, W.D. *J. Am. Chem. Soc.* **126**, 6759-6764 (2004).
- Boeglin, D., Lubell, W.D. *J. Comb. Chem.* **7**, 864-878 (2005).
- Lubell, W.D., Blankenship, J.W., Fridkin, G., Kaul, R. (2005) "Peptides" Science of Synthesis 21.11, Chemistry of Amides. Thieme, Stuttgart, 713-809.

## Submonomer Solid-Phase Aza-peptide Synthesis and Circular Dichroism Spectroscopic Analysis of [aza-Phe<sup>4</sup>]-GHRP-6

David Sabatino and William D. Lubell

Department of Chemistry, Université de Montréal, C.P. 6128, Succursale Centre-Ville,  
 Montréal Québec, H3C 3J7, Canada

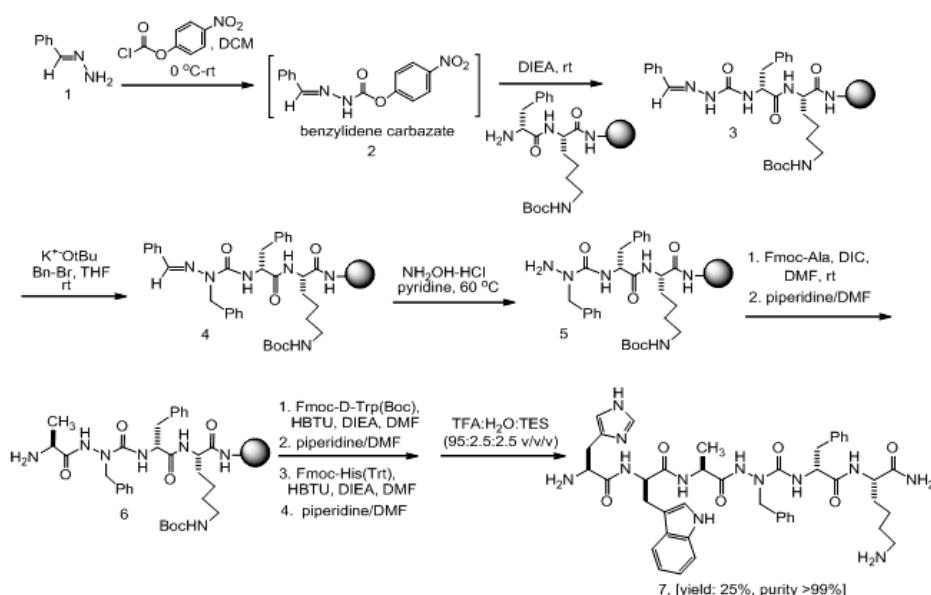
### Introduction

Aza-peptides incorporate an aza-amino acid residue (in which N replaces the alpha-CH) into the peptide backbone. They have improved peptide pharmacokinetic properties and enhanced substrate activity and specificity towards receptor targets [1], likely because of lone pair interactions of the hydrazine nitrogen causing a pre-organized backbone secondary structure related to  $\beta$ -turn types [2]. Aza-peptides are useful probes for exploring the influences of peptide backbone configuration and conformation on the biological activity of the native peptide.

### Results and Discussion

Solid-phase aza-peptide synthesis has typically necessitated synthesis of a hydrazine building-block in solution prior to incorporation on solid-phase [3]. By building the aza-residue directly on the supported peptide during solid-phase synthesis, our submonomer approach circumvents tedious hydrazine synthesis in solution and paves the way for broader diversity to be added at the aza-residue side-chain [4]. To a standard Fmoc protection strategy for SPPS, we've incorporated a 3-step procedure for the construction of the aza-residue directly on resin: (a) acylation of peptide-bound resin with a benzylidene carbazate, (b) regioselective semicarbazone alkylation and (c) chemoselective semicarbazone deprotection. Completion of SPPS is performed as usual to provide aza-peptide (Scheme 1). [aza-Phe<sup>4</sup>]-GHRP-6 (**7**) related to the growth hormone releasing peptide GHRP-6 (His-D-Trp-Ala-Trp-D-Phe-Lys-NH<sub>2</sub>, **8**) was synthesized by selective aza-residue incorporation at the Trp<sup>4</sup> position of the sequence in good yield (25%) and high purity (>99%) as confirmed by LCMS analyses.

The conformations of aza-peptide **7** and the native GHRP-6 sequence **8** were studied using circular dichroism (CD) spectroscopy in three solvents (water, 2,2,2-trifluoroethanol (TFE) and methanol, Figure 1). In water, aza-peptide **7** exhibited a CD curve indicative of an ordered  $\beta$ -



Scheme 1. Submonomer synthesis of [aza-Phe<sup>4</sup>]-GHRP-6 (**7**).

turn conformer with characteristic negative maximum values at around 190 and 230 nm and a positive maximum band near 215 nm; whereas, the parent peptide displayed a random coil structure with characteristic negative maximum band observed at 190 nm [5]. The solvent effected the conformations of **7** and **8** which both gave curves indicating ordered structure in TFE, and disorder in MeOH. In TFE, the parent peptide **8** and aza-peptide **7** possessed comparable traces with negative maximum values at around 230 nm and 205 nm and a maximum band near 210 nm. Methanol destabilized the ordered peptide conformation, rendering both **7** and **8** with curves absent of strong intensity nor characteristic bands in the spectra.

Although GHRP-6 **8** and aza-Phe<sup>4</sup> counter-part **7** exhibited conformational liberty contingent on solvent system, both showed potential to adopt conformations that exhibited characteristic CDs for turn geometry in TFE. Moreover, aza-peptide **7** favored an organized turn conformation in water as well as TFE.

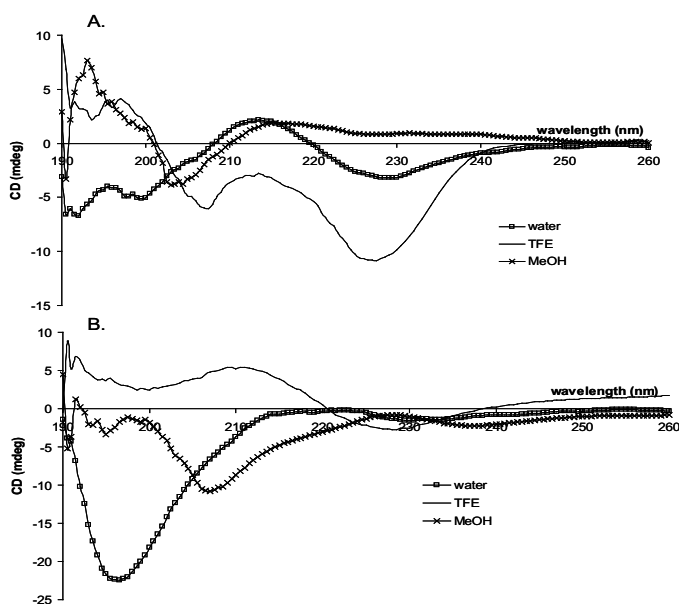


Fig. 1. Circular dichroism spectra of: A. [aza-Phe<sup>4</sup>]-GHRP-6 (**7**) and B. GHRP-6 (His-D-Trp-Ala-Trp-D-Phe-Lys-NH<sub>2</sub>, **8**); in water (squared line), TFE (line) and MeOH (crossed line).

## Acknowledgments

Financial Support from the Natural Sciences and Engineering Research Council (NSERC) of Canada, le Fond Québécois de la Recherche sur la Nature et les Technologies (FQRNT) and the CIHR Team Grant Program (funding no: CTP79848) in G-Protein Coupled Receptor Allosteric Regulation (CTIGAR) is gratefully acknowledged.

## References

1. Zega, A. *Curr. Med. Chem.* **12**, 589-597 (2005).
2. Gante, J. *Synthesis* 405-413 (1989).
3. Boeglin, D., Lubell, W.D., *J. Comb. Chem.* **7**, 864-878 (2005) and references therein.
4. Sabatino, D., Proulx, C., Kloczek, S., Bourguet, C.B., Boeglin, D., Ong, H., Lubell, W.D. *Org. Lett. asap* **11** (2009).
5. Kelly, S.M., Jess, T.J., Price, N.C. *Biochim. Biophys. Acta* **1751**, 119-139 (2005).



## Versatile Microwave Assisted Synthesis of Acyl-Tetramic Peptide Analogs

Tamar Mozes,<sup>1</sup> Randi Diestel,<sup>2</sup> Florenz Sasse,<sup>2</sup> and Gerardo Byk<sup>1</sup>

<sup>1</sup> Department of Chemistry, Bar-Ilan University, Ramat-Gan 52900 Israel and <sup>2</sup> Department of Chemical Biology, Helmholtz Centre for Infection Research, Inhoffenstrasse 7, Braunschweig D-38124, Germany

### Introduction

C-3 Acyl-tetramic acids are key structural motifs in many natural products (Figure 1). They exhibit a wide range of biological activities including antibiotic, antiviral, antifungal, cytotoxic and enzyme inhibitory activities. Thus, the synthesis of such compounds represents a worthwhile and challenging goal for the organic chemist.

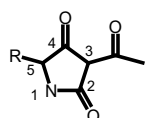


Fig. 1. Acyl-tetramate privileged structure.

We have recently presented an improved method based on previous works [1] for the microwave assisted acylation of tetramic acid derivatives in solution which allowed the access to a variety of acyl-tetramic derivatives [2]. As an effort for improving the versatility of this method, we have designed and synthesized a novel acyl-tetramic building block as “privileged scaffold” that can be easily reacted with many aliphatic compounds in solution or introduced into peptides in solid phase using classical coupling methods. Synthetic results demonstrate that introduction of acyl-tetramic acid building block into peptides and other small molecules is an attractive approach for discovering novel anticancer and antibacterial candidates. Products are currently being screened in a panel of bioassays including a series of bacteria and cancer cell lines, additionally some of them were submitted to high content screening revealing interesting morphological changes in cells treated with some of the products.

### Results and Discussion

Diglycolic anhydride was reacted in solution with various tetramic acid derivatives adding DMAP and TEA (one equivalent of each) in DMF. The reaction was performed under microwave irradiation (Biotage). Reaction times varied depending on the starting tetramic acid: 5 min for Val and Leu scaffold, and 10 min for Phe scaffold, at 80°C (Figure 2). Yields were about 25 %. This strategy opens the gate to acyl-tetramate building blocks that can be directly coupled to peptides as any classical amino acid. In order to demonstrate the versatility of the new building blocks, they were coupled to a series of aliphatic amines such as hexylamine, tetradecylamine and 1, 6-hexamethylenediamine, activated by BOP and TEA in acetonitrile solution at room temperature (Figure 3).

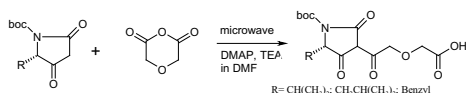


Fig. 2. Acylation of tetramic acid using diglycolic anhydride.

Finally, the scaffolds were coupled to model peptide RRKK (an antiviral tetramer peptide) using solid phase peptide synthesis (SPPS). Each coupling reaction was conducted according to known SPPS procedures at room temperature, and lasted 1.5 h. Cleaved peptides were purified by HPLC and characterized by HRMS and some of them by NMR (Figure 4). Derivative TMM-1062 showed anti-proliferative activity against L929 mouse fibroblasts (IC50: 21 µg/ml).

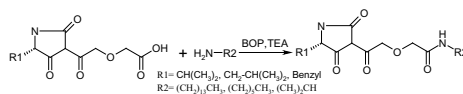


Fig. 3. Coupling of acyl-tetramates building blocks to aliphatic amines.

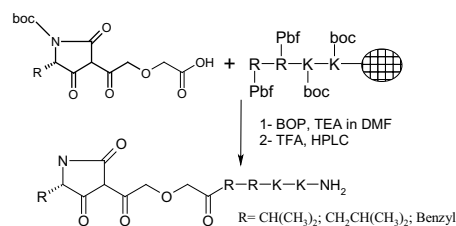
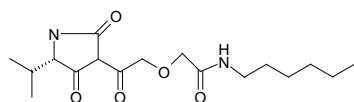
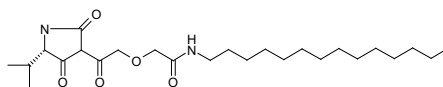


Fig. 4. Coupling of acyl-tetramate building blocks to RRKK using SPPS.

Compound TMM-1116 showed toxicity in U-937 leukemia cells (IC<sub>50</sub>: 10 µg/ml).



TMM-1062



TMM-1116

Both compounds were submitted to phenotypic screening as follows: PtK2 potoroo kidney cells (*Potorous tridactylis*) were incubated at a concentration of 40 µg/ml overnight. At the end of incubation cells were fixed and stained for endoplasmic reticulum by immunostaining of GRP-94, a marker protein of the ER, and for the nuclei by DAPI. Figure 5 (left panel) shows control cells stained green (ER) and blue (nuclei). Cells treated with TMM-1116 are shown in the right panel. We see cells with more than one nucleus, and in the middle one giant multinuclear cell with four nuclei. In some of the cells we observe that the nuclei have the tendency to decay into pieces (e.g., cell at the top of the right panel, see arrow). The reason for these phenotypical changes might be an interference with cell division. We did not observe these effects with TMM-1062.

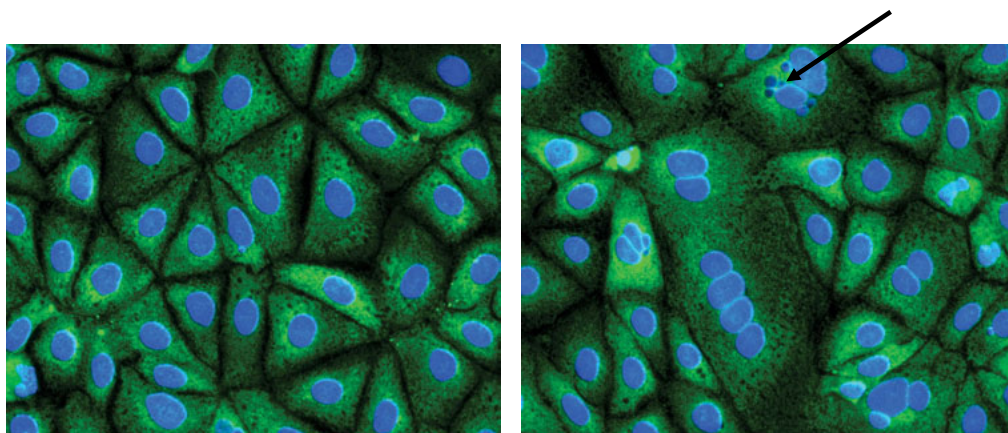


Fig. 5. Potoroo kidney cells were incubated with TMM-1116 and stained for nuclei (blue in electronic, grey in printed) and Endoplasmic Reticulum (green in electronic, around nuclei). Clear morphological changes are observed when the treated cells in the right panel are compared to control cells of the left panel. Arrow indicates nuclei decay into pieces.

## Conclusions

We have developed a versatile method for the acylation of tetramic acid derivatives, a privileged scaffold has been synthesized using microwave energy and was introduced into a variety of compounds. The method is suitable for synthesizing lipid, amino acid and peptide derivatives both in solution and on solid phase. Product TMM-1116 displayed interesting toxicity in leukemia cell line and induced phenotypic changes that might indicate cytokinesis impairment, maybe by action of the compound on actin polymerization. Positional libraries using the new building blocks are currently being synthesized and their biological results will be discussed soon.

## Acknowledgments

The work was supported by the Marcus Center for Medicinal Chemistry, Bar Ilan University, Israel.

## References

- Schobert, R., Jagusch, C. *Tetrahedron* **61**, 2301-2307 (2005).
- Davidov, G., Mozes, T., Khandadash, R., Byk, G. *J. Pept. Sci.* **14**(8), Suppl. S, 59 (2008).

## Preparation of the Ligand Peptide Probe of Heart-type Fatty Acid-binding Protein

Shuhua Zhang,<sup>1,2</sup> Licheng Wang,<sup>1</sup> Shuwen Guan,<sup>1</sup> Yuanyuan Li,<sup>3</sup>  
 Liping Wang,<sup>1\*</sup> and Wei Li<sup>1</sup>

<sup>1</sup>Life Science Institute, Jilin University, Changchun; <sup>2</sup>Life Science Institute, Changchun University of Science and Technology, Changchun, P.R. China.; <sup>3</sup>Jilin Province Product Quality Supervision Test Institute, Changchun, 130021, P.R. China

\* Corresponding author Tel: +86-431-88499505; Fax: +86-431-88921591; Email: [wanglp@jlu.edu.cn](mailto:wanglp@jlu.edu.cn)

### Introduction

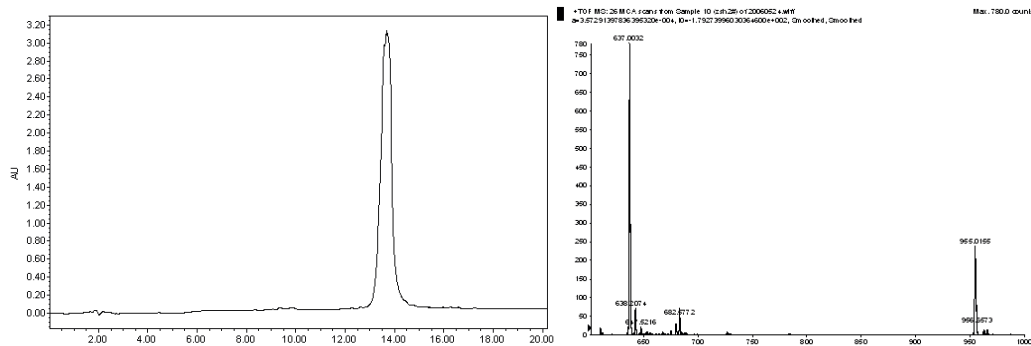
Heart-type fatty acid-binding protein (H-FABP) is a cytoplasmic protein with a molecular weight of 14-15KDa [1]. It was initially identified in heart tissue and subsequently shown to be present in several other tissues such as skeletal muscle, kidney and brain [2]. Because H-FABP levels are highly elevated in blood and urine during the hyperacute phase of acute myocardial infarction (AMI), it can be used as a good biological marker for detection of AMI [3]. Up-to-date, there are several monoclonal antibodies prepared for the determination of H-FABP level in the diagnosis of AMI. Although these antibodies have high specificity to the serum H-FABP, they are not easy to prepare and relatively expensive. To overcome these defects, we have developed a ligand peptide probe of H-FABP using 12-mer phage display peptide libraries. The small peptide probe we synthesized is specific to H-FABP and the process of synthesizing this peptide is much less time consuming and less costly. This peptide probe could be applicable to the purpose of diagnosis of AMI in the emergency room.

### Results and Discussion

Panning the ligand peptide of H-FABP was carried out by incubating the phage-displayed peptide library which carries random 12-mer peptides with a plate coated with H-FABP. After washing off the non-specific binding peptide-containing phage, the phage that carry peptides which specifically bind to H-FABP were eluted. This pool of phage were then amplified and subjected to the second and third round of panning. Three rounds of panning were conducted. The amino acid sequences of the peptide displayed on selected phage were determined by DNA sequencing which displayed a related pattern. The selected 12-mer peptide sequences are shown in Table 1. From this table, we can see some similarity in individual sequences. Some conserved motifs such as W~P and H-H-R are found also. We selected one sequence of W-P-N-H-H-M-L-H-K-R-W-P as target sequence to synthesize.

Table 1. The comparison of peptide sequences of selected phage clones

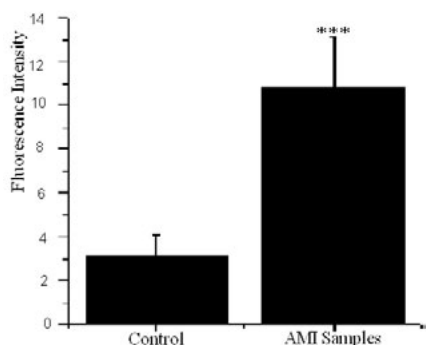
Clones	Sequences	Conserved sequences
1	N-Y-S-A-H-L-Y-N-H-L-R	H~H; N-H~R
1	H-W-K-H-N-R-H-D-P-S-P-P	H-W~H~S; N-R~H; W~P
1	A-R-L-H-D-H-H-W-H-P-R-M	H~H~R; W-H-P
1	K-H-M-H-W-H-P-P-A-L-N-T	H~W-H; W-H-P
1	<b>W-P-N-H-H-M-L-H-K-R-W-P</b>	<b>W-P; N-H~H~R</b>
1	V-P-H-N-F-H-W-H-P-R-H-Y	W-H-P; H~H~R
1	H-K-M-H-S-H-P-R-L-T-S-P	H~H~R; H~S
1	E-E-W-R-C-R-Q-E-I-H-R-L	R~H-R
1	K-L-W-H-C-P-P-Y-H-A-M-R	W-H~P; H~R



**Fig. 1. Purification of the Peptide Probe by HPLC. B MS Spectrum of the Peptide Probe Buffer A:** 0.1%Trifluoroacetic Acid (TFA)/H<sub>2</sub>O. Buffer B: 90%CH<sub>3</sub>CN, 0.1%TFA. Loaded peptide was washed first with 10% buffer B for 2.5 minutes, then eluted by 10% to 90% gradient of buffer B at flow rate of 1 ml/min for 20 minutes.

This sequence was synthesized by the solid-phase method using Fmoc chemistry. Briefly, each amino acid in DMF (dimethylformamide) was activated in situ with PyBOP (benzotriazole-1-yl-oxy-tris-pyrrolidinophosphonium) and NMM (N-methylmorpholine) using Rink Resin. Dicarboxylate pyrene (Mw 290, Excitation wavelength: 310nm, Emission wavelength: 400 nm) as a fluorescent marker was coupled to the target peptide at N-terminus by the same method. The target peptide probe marked with dicarboxylate pyrene was cleaved from resin. It was purified by reverse phase HPLC on a C<sub>18</sub> column at with detection at 400nm (Figure 1A). As determined by mass spectrometry (Figure 1B), its molecular mass was 1908 as was expected.

In this work, fifty serum samples of AMI patients were collected to 96-well plates and coated by overnight incubation at 4°C, while forty-five serum samples of healthy volunteers were used as negative control. The wells were blocked with 1% bovine serum albumin in 50mM PBS for two hours at room temperature and washed six times with 0.1%Tween-20 in PBS buffer. The synthesized peptide probe in PBS with 20µg/ml was added to each well and incubated for two hours at room temperature. After washed off excess peptide probe, the fluorescence intensity was measured at 400nm. The result is shown in Figure 2.



**Fig. 2. Conjunction Activity of the Probe to Serum Samples by ELISA. Mean  $\pm$  S.D.;** n=50. p\*\*\*<0.001 indicates significantly different from control.

In this study, the ligand peptides binding to H-FABP were selected in 12-mer phage display peptide libraries. After sequence determination and comparison, the target peptide sequence was defined. The target peptide coupled with dicarboxylate pyrene was then synthesized to be used as the biological probe. It was purified and identified by reverse phase HPLC (high pressure liquid chromatography) and mass spectrometry. The peptide probe was used to analyze the serum samples of AMI patients. The peptide probe we prepared has some advantages such as easy preparation, convenient testing and high sensitivity. The result suggests that the target peptide probe we have synthesized has potential in clinical application for diagnosis of AMI.

## References

1. Keagten, J.A., Nieuweuhoven, F.A.V., Biejen Visser, M.P.V. *Clin. Chem.* **42**, 337-338 (1996).
2. Paulussen, R.J.A., Moerkerk, H.T.B., Veerkamp, J.H. *Biochem.* **22**,393-398 (1990).
3. Ohkaru, Y., Asayama, K., Ishii, H. *Journal of Immunological Methods* **178**, 99-111 (1995).
4. Kaufman, D.B., Hentsch, M.E., Baumbach, G.A. *Biotechnol. Bioengineering* **77**, 278-289 (2002).

## **Cloning, Expression, and Purification of Large Fragments of a GPCR**

**Katrina E. Caroccia,<sup>1,2</sup> Subramanyam J. Tantry,<sup>1</sup> Racha Estephan,<sup>1</sup>  
Leah S. Cohen,<sup>1,2</sup> Boris Arshava,<sup>1</sup> Oliver Zerbe,<sup>3</sup> Jeffrey M. Becker,<sup>4</sup>  
and Fred Naider<sup>1,2</sup>**

<sup>1</sup>*Department of Chemistry, The College of Staten Island, City University of New York (CUNY), Staten Island, NY 10314, U.S.A.*; <sup>2</sup>*Department of Biochemistry, The Graduate Center, CUNY*; <sup>3</sup>*Institute of Organic Chemistry, University of Zurich, Switzerland*; and <sup>4</sup>*Department of Microbiology, University of Tennessee, Knoxville, TN 37996, U.S.A.*

### **Introduction**

G protein-coupled receptors (GPCRs) are a class of proteins, involved in cellular signaling cascades, which are composed of seven transmembrane (TM) domains connected by intra- and extracellular loops (IL and EL, respectively). Structural information regarding these proteins is extremely valuable, but characterization of these proteins is difficult due to their hydrophobicity, flexibility and large size. Smaller fragments of GPCRs are useful for studying membrane protein folding and NMR structural analysis.

Our group has been focusing on NMR analysis of fragments of the yeast  $\alpha$ -factor receptor, Ste2p. We have recently published an NMR structure for a fragment containing the first two TMs of the receptor in LPPG micelles and have also conducted biophysical analysis of this 80-residue peptide in TFE/water mixtures [1,2]. Here, we report the cloning, expression and purification of two larger fragments of Ste2p for biophysical investigations. A 3TM fragment containing 130 residues of Ste2p, G31-R161, including 19 residues from the N-terminal domain, the first TM through the third TM with connecting loops and five residues of the second IL was cloned downstream of the Trp $\Delta$ LE fusion protein. Similarly, a 5TM fragment containing 212 residues of Ste2p, I128-L340, including 13 residues of the first EL, the third TM through the seventh TM with connecting loops, and 40 residues of the C-terminal domain was cloned into the same plasmid. The 3TM fragment was chosen because it may prove to be more stable than the TM1-TM2 fragment. An unsatisfied Arg residue in the TM1-TM2 fragment may form a salt bridge with a Glu residue in the TM1-TM3 fragment. The 5TM fragment was chosen because we wish to mix the TM1-TM2 fragment with the unlabeled 5TM fragment and perform NMR experiments on the reconstituted receptor. Expression for both constructs was optimized in *E. coli* and CNBr and thrombin cleavages and purification of the target peptides from the fusion tag were attempted. The 3TM peptide has been isolated, characterized by MS and biophysical analysis has begun. The 5TM fusion protein has proven to be more challenging and attempts at purification are in progress.

### **Results and Discussion**

The DNA sequences corresponding to Ste2p TM1-TM3 (G31-R161) and TM3-TM7 (I128-L340) were cloned into a Trp $\Delta$ LE vector with an N-terminal His-Tag by PCR amplification, restriction enzyme digestion and ligation. The resulting plasmids were named pKC01 and pST01 respectively. The plasmids were transformed into the BL21-AI *E. coli* expression vector and expression of the Trp $\Delta$ LE fusion proteins was optimized in both rich and minimal media.

The <sup>15</sup>N labeled TM1-TM3 fusion protein was expressed in both rich and M9 minimal media containing <sup>15</sup>NH<sub>4</sub>Cl, and the fusion protein was isolated in inclusion bodies. The inclusion bodies were solubilized in 70% TFA and CNBr cleavage was performed in order to release the TM1-TM3 peptide. The resulting cleaved peptide was purified by RP-HPLC on a Zorbax 300SB-C3 Prep HT column using a 50-90% acetonitrile gradient with 20% isopropanol at 60°C. The yield of purified <sup>15</sup>N labeled TM1-TM3 was 15-20mg/L. The unlabeled TM1-TM3 gave the expected mass as judged using electron spray ionization MS, and <sup>15</sup>N labeled TM1-TM3 had a mass of 14580.5 indicating 95% incorporation of the <sup>15</sup>N isotope.

The purified peptide was subject to CD analysis in order to determine the helicity of the peptide. Analysis was done in both TFE:water mixtures (Figure 1) and lipid micelles. In TFE:water, the spectra contained a maximum at 192 nm and two minima at 208 nm and 222

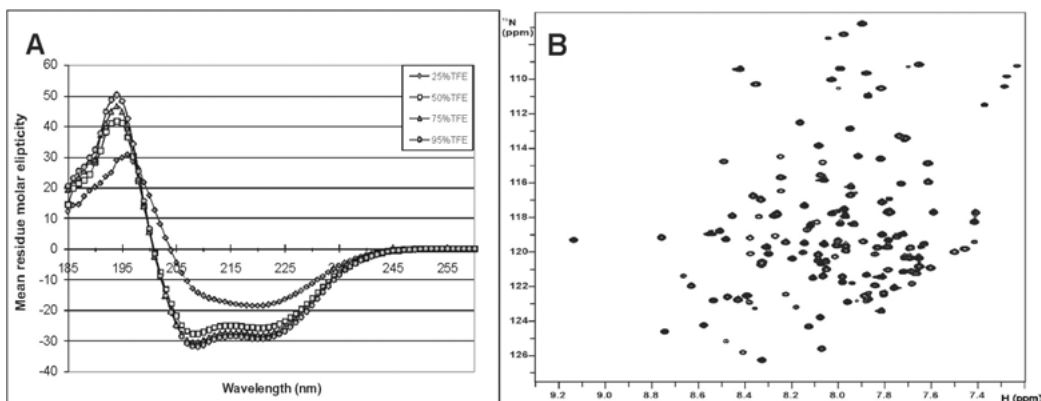


Fig. 1. Biophysical analysis of TM1-TM3.

nm, which are indicative of a helical peptide. The helicity increased with increasing percentage of TFE and the peptide was highly helical at TFE concentrations of greater than 50% v/v. Similar spectra were observed in several lipid micelles, including 1-myristoyl-2-hydroxy-*sn*-glycero-3-[Phospho-*rac*-(1-glycerol)] (LMPG) (data not shown). [ $^{15}\text{N}$ ,  $^1\text{H}$ ]-HSQC spectra were obtained for the  $^{15}\text{N}$  labeled fragment in 50% TFE (Figure 1B) and a [ $^{15}\text{N}$ ,  $^1\text{H}$ ]-HSQC-TROSY spectrum was obtained in LMPG micelles (data not shown). In both cases, well-dispersed chemical shifts and narrow crosspeaks were obtained.

The 5TM fusion protein proved to be more challenging to express, purify and subject to biophysical analysis. The fusion protein was successfully expressed, and the identity of the protein was verified by Western Blot using anti-His antibodies. Initial attempts at purification were conducted by RP-HPLC on a Zorbax 300SB-C3 column with a 36-81% acetonitrile gradient with 10% isopropanol. However, the protein did not efficiently elute from the column. A fraction containing a small amount of purified fusion protein was collected and subject to MS analysis. The obtained mass was very close to the expected mass. Subsequent attempts at purification of this construct have been unsuccessful, and sufficient quantities for biophysical analysis have yet to be obtained. Optimization of the purification protocol for this construct is underway.

## Acknowledgments

Supported by grant GM22087 (National Institutes of Health).

## References

1. Neumoin, A., Cohen, L.S., Arshava, B., Tantry, S., Becker, J.M., Zerbe, O., Naider, F. *Biophys. J.* **96**, 3187-3196 (2009).
2. Cohen, L.S., Arshava, B., Estephan, R., Englander, J., Kim, H., Hauser, M., Zerbe, O., Ceruso M., Becker, J.M., Naider, F. *Biopolymers* **90**, 117-130 (2008).

## Synthesis of Bis-Benzamides as New Amphiphilic $\alpha$ -Helix Mimetics

Srinivasa Marimganti, Murthy N. Cheemala, and Jung-Mo Ahn\*

Department of Chemistry, University of Texas at Dallas, Richardson, TX 75080, U.S.A.

### Introduction

$\alpha$ -Helices are one of the most commonly found protein secondary structures and often play a vital role in mediating protein-protein interactions. However, helical peptide segments are prone to be damaged by entropy effect when taken out of proteins, and fall in to random coil or other structure [1]. Several approaches have been developed in order to stabilize  $\alpha$ -helices in short peptides, such as lactam, salt and disulfide bridge formations between the  $i$  and  $i+4$  positions of a helix [2]. An alternative approach is to achieve small molecules that mimic  $\alpha$ -helices by using

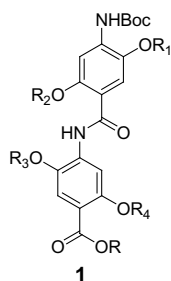


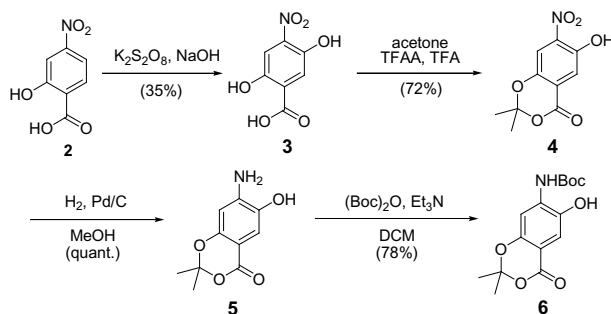
Fig. 1. Bis-benzamides as amphiphilic  $\alpha$ -helix.

rigid and pre-organized scaffolds including terphenyls [3], trispyridylamides [4], polycyclic ethers [5], pyridazines [6], and trisbenzamides [7]. These  $\alpha$ -helix mimetics focus on presenting only one side of a helix that comprises of the side chains of amino acids found at the  $i$ ,  $i+3$  (or  $i+4$ ), and  $i+7$  positions. On the contrary,  $\alpha$ -helix mimetics that have a capability to represent two opposing helical faces have not been reported yet. Hence, we report a new bis-benzamide scaffold that can place four side chain functional groups, two found at the  $i$  and  $i+7$  positions on one helical face; and the other two from the  $i+2$  and  $i+5$  positions on the opposite side (Figure 1). The spatial arrangement of the four substituents was fixed by two hydrogen bonds between a benzamide proton and two adjacent alkoxy groups that promote high structural rigidity and superior  $\alpha$ -helix mimicry.

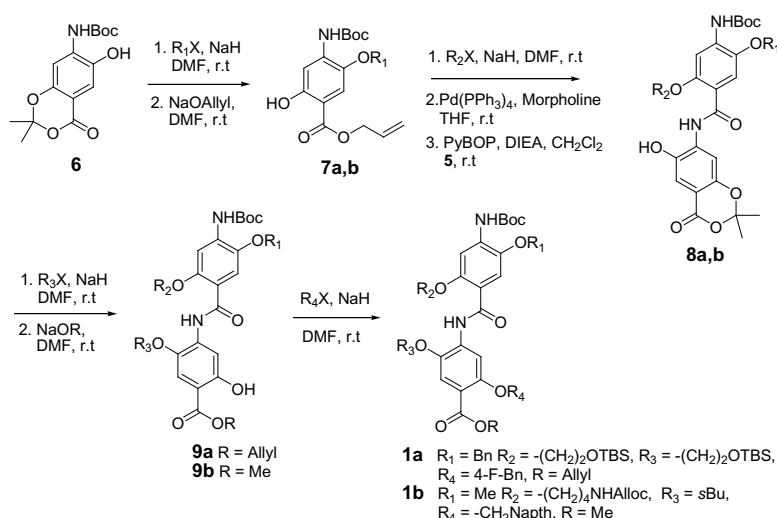
### Results and Discussion

For the construction of bis-benzamides as amphiphilic  $\alpha$ -helix mimetics, we have first focused on the synthesis of an amphiphilic subunit **5**. A persulfate oxidation of a benzoic acid **2** provided a hydroquinone **3**, and the 2-hydroxyl group was protected as a ketal **4** together with the 1-carboxylic acid group by reacting with acetone and trifluoroacetic anhydride. The reduction of the nitro group produced the amphiphilic subunit **5** (Scheme 1).

To evaluate  $\alpha$ -helix mimicry of the bis-benzamide scaffold, we have sought to emulate a helical region of a peptide hormone, glucagon-like peptide-1 (GLP-1). GLP-1 is a 30 amino acid-containing peptide and plays an important role in glucose homeostasis by stimulating insulin secretion and restoring pancreatic  $\beta$ -cell mass, which are highly favored for treating type 2 diabetes [8]. 2D-NMR studies showed that GLP-1 has two  $\alpha$ -helical segments between residues 11-21 and 24-35, and the significance of two helices in receptor interaction was confirmed by our recent cyclization scanning study [9]. These helices in GLP-1 present key functional groups on both helical sides, indicating the importance of helical amphiphilicity [9c].



Scheme 1. Synthesis of an amphiphilic subunit.



Scheme 2. Synthesis of amphiphilic  $\alpha$ -helix mimetics based on a bis-benzamide scaffold.

To emulate two helical segments in the N- and C-terminal regions of GLP-1, two amphiphilic  $\alpha$ -helix mimetics (**1a,b**) were designed by using the bis-benzamide scaffold described above. The bis-benzamide **1a** mimics the N-terminal helix and presents side chain functional groups of Phe<sup>12</sup>, Ser<sup>14</sup>, Ser<sup>17</sup>, and Tyr<sup>19</sup>, whereas the C-terminal  $\alpha$ -helix mimetic **1b** represents Ala<sup>24</sup>, Lys<sup>26</sup>, Ile<sup>29</sup>, and Trp<sup>31</sup>. Starting from the ketal **6**, a series of *O*-alkylation, ester hydrolysis, and coupling reactions were carried out to synthesize the two amphiphilic  $\alpha$ -helix mimetics (Scheme 2).

## Acknowledgments

Supported by grant 7-07-JF-02 (American Diabetes Association), AT-1595 (Welch Foundation), and 009741-0031-2006 (Texas Advanced Research Program).

## References

- Schneider, J.P., Kelly, J.W. *Chem. Rev.* **95**, 2169-2187 (1995).
- (a) Ospay, G., Taylor, J.W. *J. Am. Chem. Soc.* **112**, 6046-6051 (1990). (b) Marqusee, S., Baldwin, R.L. *Proc. Natl. Acad. Sci. U.S.A.* **84**, 8898-8902 (1987). (c) Jackson, D.Y., King, D., S., Chmielewski, J., Singh, S., Schultz, P.G. *J. Am. Chem. Soc.* **113**, 9391-9392 (1991).
- Orner, B.P., Ernst, J.T., Hamilton, A.D. *J. Am. Chem. Soc.* **123**, 5382-5383 (2001).
- Ernst, J.T., Becerril, J., Park, H.S., Yin, H., Hamilton, A.D. *Angew. Chem. Int. Ed.* **42**, 535-539 (2003).
- Oguri, H., Oomura, A., Tanabe, S., Hiram, M. *Tetrahedron Lett.* **46**, 2179-2183 (2005).
- Volonterio, A., Moisan, L., Rebek, J. *Org. Lett.* **9**, 3733-3736 (2007).
- Ahn, J-M., Hang, S-Y. *Tetrahedron Lett.* **48**, 3543-3547 (2007).
- Baggio, L.L., Drucker, D.J. *Gastroenterology* **132**, 2131-2157 (2007).
- (a) Neidigh, J.W., Fesinmeyer, R.M., Prickett, K.S., Andersen, N.H. *Biochemistry* **40**, 13188-13200 (2001); (b) Murage, E.N., Schroeder, J.C., Beinborn, M., Ahn, J-M. *Bioorg. Med. Chem.* **16**, 10106-10112 (2008); (c) Adelhorst, K., Hedegaard, B.B., Knudsen, L.B., Kirks, O. *J. Biol. Chem.* **269**, 6275-78 (1994).



## **ZY-GLP1: A Novel Peptidomimetic Glp-1 Agonist**

**R.H. Bahekar, A.A. Joharapurkar, D. Bandyopadhyay, G. Chakraborti,  
H. Patel, V.D. Pawar, R. Sunder, M.R. Jain, and P.R. Patel**

*Zydus Research Centre, Moraiya, Ahmedabad 382210, Gujarat, India*

### **Introduction**

Type-2 diabetes mellitus (T2DM) is characterized by increased blood glucose levels, either because of defect in insulin secretion or due to insulin resistance or a combination of both [1]. During the last decade, incretin hormones such as Glucagon-Like Peptide (GLP-1) have been extensively explored in order to develop new therapeutic agents for the safe and effective treatment of T2DM [2]. GLP-1 stimulates insulin secretion from the pancreatic  $\beta$ -cells in a glucose-dependent manner, prevents pre- and post-prandial hyperglycemia, suppresses glucagon secretion from pancreatic  $\alpha$ -cells, delays gastric emptying, reduces food intake and stimulates  $\beta$ -cell proliferation [3]. The native GLP-1 has an extremely short half-life as it is rapidly degraded by the enzyme DPP-IV. Although continuous infusions of GLP-1 could be useful for the short-term control of hyperglycemia, the long-term treatment of T2DM would require a more feasible approach to achieve sustained activation of GLP-1 receptors. Exendin-4 was discovered as the first clinically relevant, potent and metabolically stable GLP-1 receptor (GLP-1R) agonist. Exendin-4 at 10  $\mu$ g (sc twice a day) dose effectively reduces elevated plasma glucose level and HbA1c levels [4]. Under clinical regime, Exendin-4 treatment causes incidences of nausea and vomiting, immunogenicity, pancreatitis, hypoglycemia (in combination therapy) and reaction at the site of injection [5]. Thus Exendin-4 represents a potent GLP-1 agonist with several safety concerns. Considering these side-effects of Exendin-4, we decided to develop ZY-GLP1, a short-chain peptidomimetic based novel GLP-1 agonists, for long-term treatment of T2DM.

### **Results and Discussion**

Structurally, ZY-GLP1 consists of optimal activation and binding components, which were linked together by suitable spacer and it exhibits close homology with the native GLP-1 peptide. Classically, in a membrane-mimetic environment, ZY-GLP1 showed helix formation, similar to the native peptide [6]. In general, the ZY-GLP1 is a highly water soluble (150 mg/ ml) molecule and was found to be stable in plasma, blood, PBS and water for more than 24 h. Under accelerated stability testing, ZY-GLP1 was found to be stable up to 6 months at 25°C.

ZY-GLP1 is a potent and selective agonist of GLP-1 receptors. In an in vitro assay using CHO cells stably transfected with human GLP-1R, ZY-GLP1 showed a GLP-1R-mediated concentration-dependent cAMP production with an  $EC_{50}$  of 34nM. The maximum cAMP stimulation by ZY-GLP1 was similar to native GLP-1 indicating full receptor agonism. ZY-GLP1 was also tested for its selectivity over 75 common molecular targets comprising of receptors, ion-channels and drug transporters. These experiments showed that ZY-GLP1 is a highly selective to GLP-1 R and showed no significant affinity to other molecular targets at 10 $\mu$ M. Significantly, ZY-GLP1 showed a glucose-dependent insulin secretion in RIN5F cells in a concentration-dependent manner [7].

Various in vivo experiments revealed that ZY-GLP1 has similar antidiabetic actions as that of native GLP-1 peptide. Acute ZY-GLP1 treatment in various diabetic animal models resulted in consistent and dose-dependent reduction in plasma glucose. In C57 mice subjected to intraperitoneal glucose load, subcutaneous ZY-GLP1 administration produced significant anti-hyperglycemic effect with an  $ED_{50}$  of 0.116 mg/kg (Table 1). Studies in ob/ob mice demonstrated that the reduction in plasma glucose was mediated via stimulation of insulin secretion in a glucose-dependent manner (Table 1). Similar observations were made in db/db mice. Secondary pharmacodynamic effect such as delayed gastric emptying was observed, which was of lesser magnitude than one seen at efficacy doses of Exendin-4 [8]. In repeated-dose efficacy studies in diabetic db/db mice, ZY-GLP1 reduced HbA1c levels, food intake and body weight at doses, which produced efficacy in acute studies (Table 2). In this context, ZY-GLP1 is quite distinct from Exendin-4, which is reported to produce chronic metabolic effects such as reduction in body weight and HbA1c at significantly higher doses (24X) than those required for its acute antihyperglycemic effects [9].

*Table 1. Acute antihyperglycemic effect of subcutaneous ZY-GLP1 treatment in male C57 and ob/ob mice.*

Animal Model : C57 mice		Animal Model: ob/ob mice		
Treatment (dose mg/kg)	Percent change against vehicle control AUC glucose (mg/dL*240 min)	Treatment (dose mg/kg)	Percent change against vehicle control in AUC glucose (mg/dL*240 min)	Percent change against vehicle control in AUC insulin (ng/mL*240 m in)
ZY-GLP1 (0.075)	-16.6 ± 2.4	ZY-GLP1 (0.015)	-11.2 ± 5.7	59.9 ± 7.5
ZY-GLP1 (0.1)	-27.0 ± 3.3*	ZY-GLP1 (0.045)	-20.9 ± 7.3*	42.4 ± 12.4
ZY-GLP1 (0.15)	-43.6 ± 3.3*	ZY-GLP1 (0.15)	-24.1 ± 2.0*	113.7 ± 5.3*
ZY-GLP1 (0.3)	-50.4 ± 4.8*	ZY-GLP1 (0.45)	-46.4 ± 6.5*	145.8 ± 27.6*
ZY-GLP1 (0.6)	-51.3 ± 6.0*	ZY-GLP1 (1.5)	-39.0 ± 4.6*	90.4 ± 9.6*
ZY-GLP1 (1.2)	-51.3 ± 6.2*	Exendin-4 (0.008)	-45.2 ± 3.0*	105.1 ± 9.4*

Data are mean ± SE from 6 mice in each group. Results indicate changes in glucose and insulin in the intraperitoneal glucose tolerance test after 2g/kg glucose load administered at 0 min. AUC glucose and insulin calculated based on the 0-240 min changes. \*, P<0.05 as compared to vehicle control group.

*Table 2. Effects of ZY-GLP1 on metabolic parameters in male db/db mice after repeated-dose sc treatment for 50 days*

Treatment (dose)	Body Weight (g) on Day-0	Body Weight (g) on Day-50	Fed glucose (mg/dL) on Day-0	Fed glucose (mg/dL) on Day-50	Percent change Vs vehicle control in serum glucose on Day-50	Difference in % HbA1c (Day 50- Day 0)
Vehicle Control	44.5 ± 1.6	42.4 ± 1.7	520.8 ± 19.2	595.7 ± 20.9		1.6 ± 0.5
ZY-GLP1 (1.5mg/kg/day)	46.0 ± 1.8	41.4 ± 1.4*	522.2 ± 19.2	398.4 ± 50.2*	-33.1 ± 8.4	-0.8 ± 0.8
ZY-GLP1 (3 mg/kg/day)	44.5 ± 1.8	35.7 ± 2.4*	521.4 ± 17.9	417.4 ± 30.9*	-29.9 ± 5.2	-1.4 ± 0.5
ZY-GLP1 (6 mg/kg/day)	47.7 ± 1.8	33.2 ± 2.0*	520.4 ± 18.0	423.0 ± 12.3*	-29.0 ± 2.1	-1.1 ± 0.9

Data expressed as mean ± SE from 9 mice in each group. \*, P<0.05 as compared to vehicle control group.

Pharmacokinetic studies of ZY-GLP1 were conducted in rats and dogs using subcutaneous (sc) route of administration. ZY-GLP1 showed rapid T<sub>max</sub> (15 min) and extended T<sub>1/2</sub> (3.8h in rats and 15h in dogs). ZY-GLP1 was found to be eliminated via non-renal pathways.

In preclinical safety studies, ZY-GLP1 showed good margin of safety (the NOAEL was more than 500X of the acute efficacy dose). In repeated dose toxicity studies, it did not show any adverse effects on cardiovascular & CNS functions and was found to be non immunogenic. The observed untoward effects at very high doses were limited to GLP-1R-mediated exaggerated pharmacodynamic effects. Unlike Exendin-4, ZY-GLP1 did not cause emetic effect in dogs and nausea-like symptoms in rats in conditioned taste aversion model, even at very high doses, whereas, Exendin-4 produces nausea-like symptoms at efficacy doses [10].

In summary, ZY-GLP1 represents a novel short-chain peptidomimetic GLP-1 agonist. It has shown desirable incretin effect and antidiabetic activity in different non-clinical screening models. Unlike many other GLP-1 agonists, ZY-GLP1 treatment is less likely to be associated with nausea or immunogenic effects. The overall pre-clinical profile of ZY-GLP-1 was found to be very promising with significantly higher safety index, for the safe and effective treatment of T2DM.

## References

- DeFronzo, R.A. *Med. Clin. North Am.* **88**, 787–835 (2004).
- Meier, J.J., Nauck, M.A. *Diabetes Metab. Res. Rev.* **21**, 91–117 (2005).
- Chia, C.W., Egan, J.M. *Drug Discovery Today: Disease Mechanisms* **2**, 295-301 (2005).
- DeFronzo, R.A., et al. *Diabetes Care* **28**, 1092–1100 (2005).
- Kim, D., et al. *Diabetes* **55**(Suppl 1),116 (2006).
- Adelhorst, K. *J. Biol. Chem.* **269**, 6275-6278 (1994).
- Wang, X., et al. *Endocrinology* **142**, 1820-1827 (2001).
- Chelikani, P.K., et al. *Am. J. Physiol. Regul. Integr. Comp. Physiol.* **288**, R1695-R1706 (2005).
- Young, A.A. *Diabetes* **48**, 1026–1034 (1999).
- Seeley, R.J. *J. Neurosci.* **20**,1616-1621 (2000).

## Design and Synthesis of Novel Amphiphilic $\alpha$ -Helix Mimetics Based on a New Tris-Benzamide Scaffold

Murthy N. Cheemala and Jung-Mo Ahn\*

Department of Chemistry, University of Texas at Dallas, Richardson, TX 75080, U.S.A.

### Introduction

As the most abundant structural motif in proteins, an  $\alpha$ -helix often involves in the formation of protein complexes. To modulate such protein-protein interaction,  $\alpha$ -helix mimetics have been designed by using rigid and pre-organized scaffolds with low molecular weights and high synthetic efficiency. During the past decade, a handful of  $\alpha$ -helix mimetics were reported including terphenyls [1], trispyridylamides [2], polycyclic ethers [3], pyridazines [4], and tris-

benzamides [5]. However, all of them focus on representing only one side of an  $\alpha$ -helix organized by side chains at the *i*, *i*+3/*i*+4 and *i*+7 positions. Compared to these "one-sided"  $\alpha$ -helix mimetics, engineering a molecule to mimic two opposing helical faces is still a formidable task. Amphiphilic  $\alpha$ -helix mimetics that present side chains from both hydrophobic and hydrophilic surfaces of a helix, will strongly interact with target proteins, which in turn leads to high binding affinity and potent biological activity. Thus, we have designed new amphiphilic  $\alpha$ -helix mimetics by using our recently developed tris-benzamide scaffold [5] as a template due to its high structural rigidity, synthetic efficiency, and easy derivatization (Figure 1). The new scaffold places five side-chain functionalities, three found at the *i*, *i*+3/*i*+4, *i*+7 positions on one helical face and two at the *i*+2, *i*+5 positions on the opposite side.

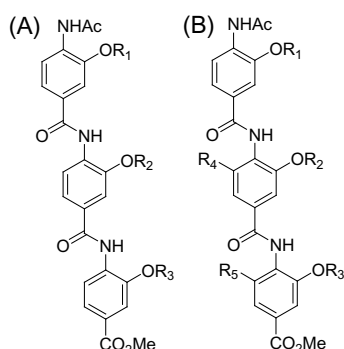


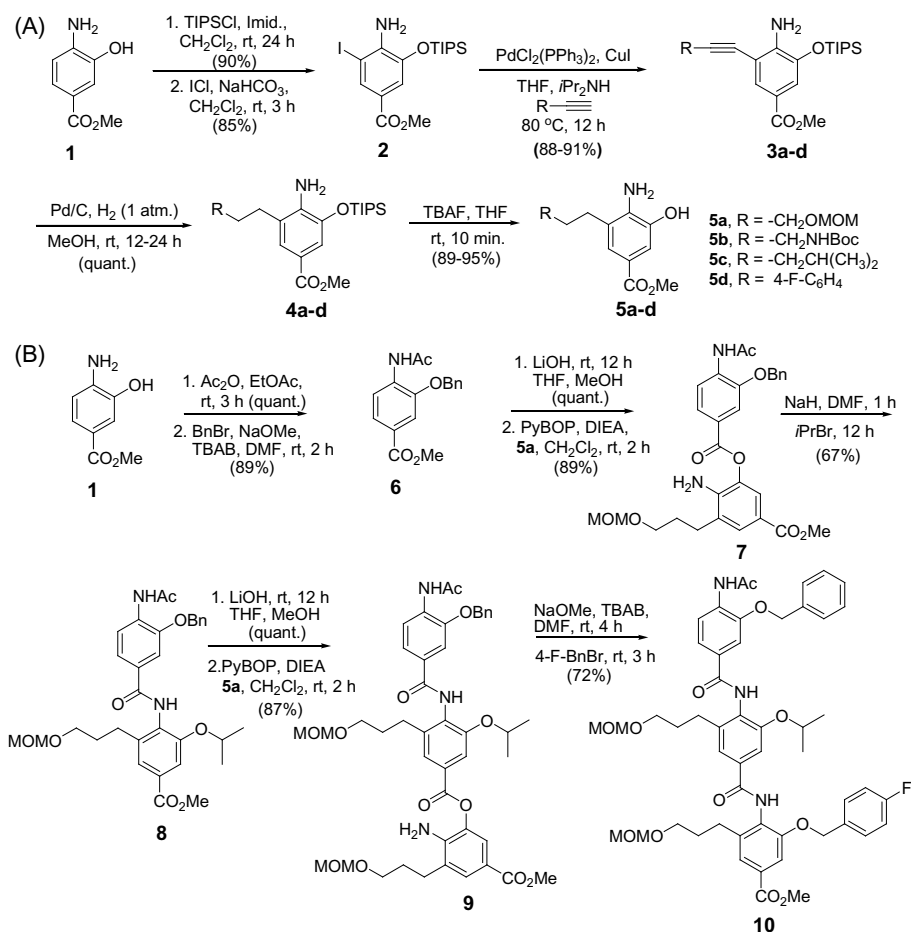
Fig. 1. Structures of tris-benzamides as (A) one-sided and (B) amphiphilic  $\alpha$ -helix mimetics.

### Results and Discussion

To facilitate the synthesis of amphiphilic  $\alpha$ -helix mimetics, we have first developed an efficient synthetic method for amphiphilic subunits (**5**). After iodination of an aniline **1**, a Sonogashira cross-coupling reaction was carried out with a variety of alkynes. An amphiphilic subunit **5** was produced in high yield by hydrogenation of the triple bond of the alkyne **3** (Scheme 1A).

Then, an amphiphilic  $\alpha$ -helix mimetic was constructed to emulate a helical segment in glucagon-like peptide-1 (GLP-1). GLP-1 is a 30 amino acid-containing peptide hormone and plays an important role in stimulating insulin secretion and restoring pancreatic  $\beta$ -cell mass, which are highly beneficial to treat type 2 diabetes [6]. 2D-NMR studies of GLP-1 revealed the presence of two  $\alpha$ -helical segments [7], and their significance in receptor binding and activation was confirmed by our recent cyclization scanning study [8]. Based on the sequence of the N-terminal helix of GLP-1 (residues 12-19), an amphiphilic tris-benzamide **10** was designed to hold side chains of Phe<sup>12</sup>, Ser<sup>14</sup>, Val<sup>16</sup>, Ser<sup>17</sup> and Tyr<sup>19</sup> that correspond to the *i*, *i*+2, *i*+4, *i*+5 and *i*+7 positions of the helix, respectively.

The synthesis of the amphiphilic tris-benzamide **10** was outlined in Scheme 1B. After acetylation of the aniline **1**, an *O*-alkylation of the 3-hydroxyl group was carried out with benzyl bromide and NaOMe. Saponification of the ester **6** and a subsequent coupling reaction with an amphiphilic subunit **5a** resulted in an ester intermediate **7** that was rearranged to a bis-benzamide during a next *O*-alkylation reaction. Repeating the steps of ester hydrolysis, coupling of an amphiphilic subunit **5a**, and an *O*-alkylation successfully synthesized the designed compound **10** in high yield (Scheme 1B).



Scheme 1. Synthetic schemes for (A) amphiphilic subunits and (B) amphiphilic  $\alpha$ -helix mimetics.

## Acknowledgments

Supported by grant 7-07-JF-02 (American Diabetes Association), AT-1595 (Welch Foundation), 009741-0031-2006 (Texas Advanced Research Program).

## References

- Orner, B.P., Ernst, J.T., Hamilton, A.D. *J. Am. Chem. Soc.* **123**, 5382-5383 (2001).
- Ernst, J.T., Becerril, J., Park, H.S., Yin, H., Hamilton, A.D. *Angew. Chem. Int. Ed.* **42**, 535-539 (2003).
- Oguri, H., Oomura, A., Tanabe, S., Hiram, M. *Tetrahedron Lett.* **46**, 2179-2183 (2005).
- Volonterio, A., Moisan, L., Rebek, J. *Org. Lett.* **9**, 3733-3736 (2007).
- Ahn, J.-M., Han, S.-Y. *Tetrahedron Lett.* **48**, 3543-3547 (2007).
- Baggio, L.L., Drucker, D.J. *Gastroenterology* **132**, 2131-2157 (2007).
- Neidigh, J.W., Fesinmeyer, R.M., Prickett, K.S., Andersen, N.H. *Biochemistry* **40**, 13188-13200 (2001).
- Murage, E.N., Schroeder, J.C., Beinborn, M., Ahn, J.-M. *Bioorg. Med. Chem.* **16**, 10106-10112 (2008).

## Design and Synthesis of $\alpha$ -Helix Mimetics Based on a Tris-Benzamide Scaffold to Target Bcl Proteins

Kajal Bhimani,<sup>1</sup> Myoung H. Kim,<sup>2</sup> Jian Zhou,<sup>3</sup> Jer-Tsong Hsieh,<sup>3</sup> and Jung-Mo Ahn<sup>1\*</sup>

<sup>1</sup>Department of Chemistry, University of Texas at Dallas, Richardson, TX 75080, U.S.A.;

<sup>2</sup>Department of Molecular Biology and Immunology, University of North Texas Health Science Center, Fort Worth, TX 76107, U.S.A.; <sup>3</sup>Department of Urology, University of Texas Southwestern Medical Center, Dallas, TX 75390, U.S.A.

### Introduction

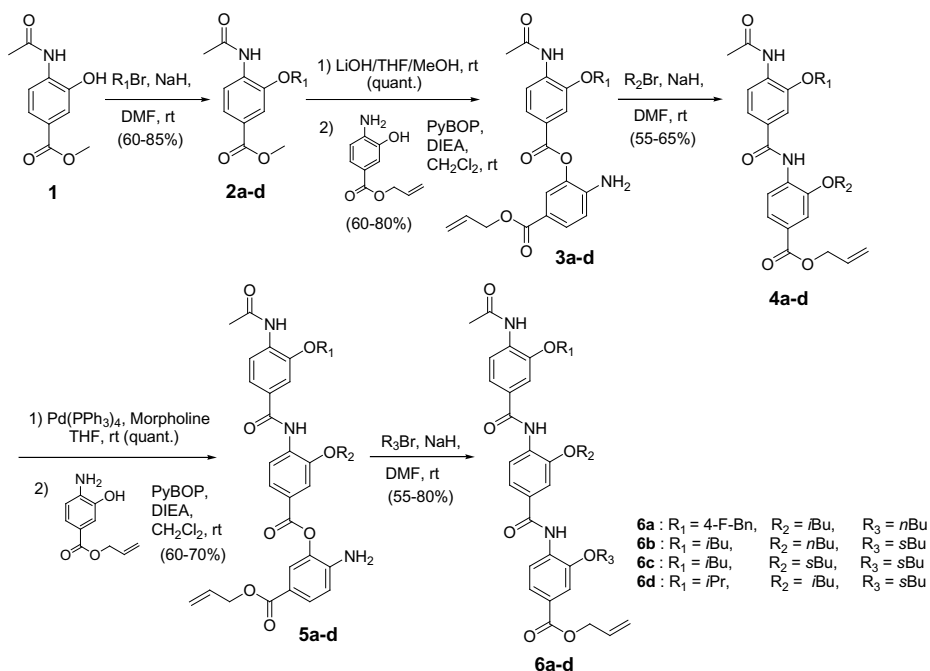
Regulation of cell death relative to cell proliferation is crucial for tissue homeostasis, and any impairment in this process may lead to life-threatening diseases like cancer. Among numerous genes and proteins involving in apoptosis, members of a Bcl-2 family play a pivotal role in the control of cell death. The Bcl-2 family is divided into two groups, anti-apoptotic proteins like Bcl-2 and Bcl-x<sub>L</sub> that inhibit programmed cell death, and pro-apoptotic proteins like Bak, Bad, and Bax that promote the process of apoptosis [1]. The formation of heterodimers between pro- and anti-apoptotic proteins regulates cell death since unbound pro-apoptotic proteins trigger the formation of pores in mitochondrial membrane, resulting in the release of cytochrome c, which in turn activates caspase cascade that ultimately leads to cell death. Since over-expression of anti-apoptotic proteins are commonly observed in many cancers, small molecules that can inhibit Bcl protein complex formation would be of high potential for cancer treatment.

### Results and Discussion

Pro-apoptotic proteins (e.g., Bak, Bad, Bax, Bid, Bik) interact with anti-apoptotic proteins through BH3 domains, and the structure of a peptide derived from a BH3 domain of Bak was determined by 2D-NMR when it was bound to Bcl-x<sub>L</sub> [2]. It was found that the Bak BH3 domain adopts  $\alpha$ -helical structure and interacts with a hydrophobic cleft in Bcl-x<sub>L</sub> by using Val<sup>74</sup>, Leu<sup>78</sup>, and Ile<sup>81,85</sup>. Since these residues organize one side of the helical BH3 domain, they have been targeted by small molecules that mimic  $\alpha$ -helices [3,4]. Recently, we have designed new  $\alpha$ -helix mimetics based on a tris-benzamide scaffold that places three functional groups found at the *i*, *i*+3 (or *i*+4), and *i*+7 positions in two helical turns [5]. In addition to proper  $\alpha$ -helix mimicry demonstrated by molecular modeling, the tris-benzamide scaffold allows facile synthesis that uses straightforward and high-yielding reactions.

Thus, we have designed four tris-benzamides to mimic helical BH3 domains of Bak and Bad proteins. Since the important hydrophobic amino acids span over three helical turns of the BH3 domain, two tris-benzamides were prepared to represent its hydrophobic surface. For the N-terminal two helical turns of the Bad BH3 domain, a tris-benzamide (**6a**) contains 4-fluorobenzyl, isobutyl, and *n*-butyl groups that correspond to the side chain functional groups of Tyr<sup>147</sup>, Leu<sup>151</sup>, and Met<sup>154</sup>, respectively. Due to an unexpected synthetic difficulty, 4-fluorobenzyl group was used as a surrogate for the side chain of Tyr. For the C-terminal two helical turn of the Bad BH3 domain, another tris-benzamide (**6b**) was designed to present isobutyl, *n*-butyl, and benzyl groups for Leu<sup>151</sup>, Met<sup>154</sup>, and Phe<sup>158</sup>, respectively. In the same manner, two tris-benzamides were designed for the Bak BH3 domain comprising of isopropyl, isobutyl, and *s*-butyl groups for Val<sup>74</sup>, Leu<sup>78</sup>, and Ile<sup>81</sup>, respectively (**6c**); and isobutyl, *s*-butyl, and *s*-butyl groups for Leu<sup>78</sup>, and Ile<sup>81,85</sup>, respectively (**6d**).

The synthesis of the four tris-benzamides was summarized in Scheme 1. Starting from a methyl 4-acetamido-3-hydroxybenzoate (**1**), an alkylation reaction was carried out with a variety of alkyl halides and NaH. After hydrolysis of a methyl ester (**2a-d**), an allyl 4-amino-3-hydroxybenzoate was coupled to the release benzoic acid with PyBOP to produce an ester intermediate (**3a-d**) resulting from significantly low nucleophilicity of the 4-aminobenzoate. However, the ester intermediate was rearranged to a bis-benzamide during a subsequent alkylation reaction with NaH and an alkyl halide. After an allyl ester (**4a-d**) was removed with Pd<sup>0</sup>, coupling and alkylation reactions were repeated to yield a final tris-benzamide (**6a-d**).



Scheme 1. Synthesis of  $\alpha$ -helix mimetics for BH3 domains of Bak and Bad proteins.

Inhibitory effects of the tris-benzamides (**6a-d**) were evaluated by PARP cleavage and MTT assays by using a prostate cancer cell line (PC3) grown in RPMI medium with 1% FBS (Figure 1). As a downstream indicator of apoptosis, the observed PARP cleavages confirm that the tris-benzamides well emulated the hydrophobic helical faces of the BH3 domains and indeed disrupted the heterodimer formation of anti- and pro-apoptotic proteins. Among the four  $\alpha$ -helix mimetics designed for the BH3 domains, the tris-benzamide **6c** was found to be the most effective in PARP cleavage as well as inhibiting cell growth of the prostate cancer cells.

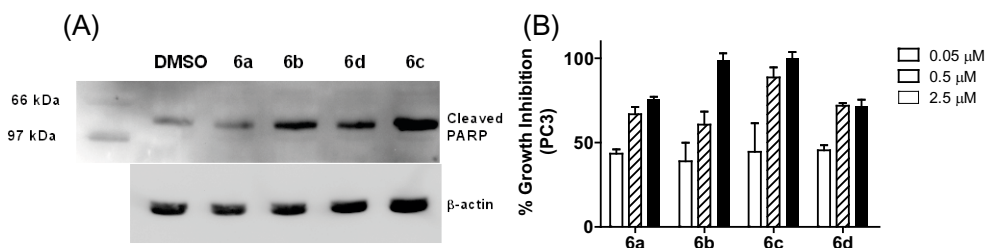


Fig. 1. Inhibitory effects of  $\alpha$ -helix mimetics designed for BH3 domains of pro-apoptotic proteins on a prostate cancer cell line, PC3. (A) PARP cleavage and (B) MTT assay.

## Acknowledgments

Supported by grant AT-1595 (Welch Foundation) and 009741-0031-2006 (Texas Advanced Research Program).

## References

1. Chao, D.T., Korsmeyer, S.J. *Annu. Rev. Immunol.* **16**, 395-419 (1998).
2. Sattler, M., et al. *Science* **275**, 983-986 (1997).
3. Ernst, J.T., et al. *Angew. Chem. Int. Ed.* **42**, 535-539 (2003).
4. Yin, H., et al. *J. Am. Chem. Soc.* **127**, 10191-10196 (2005).
5. Ahn, J.M., Han, S.Y. *Tetrahedron Lett.* **48**, 3543-3547 (2007).

## Efficient Solid-Phase Synthesis of Tris-Benzamides for a Rapid Production of $\alpha$ -Helix Mimetics

Tae-Kyung Lee and Jung-Mo Ahn\*

Department of Chemistry, University of Texas at Dallas, Richardson, TX 75080, U.S.A.

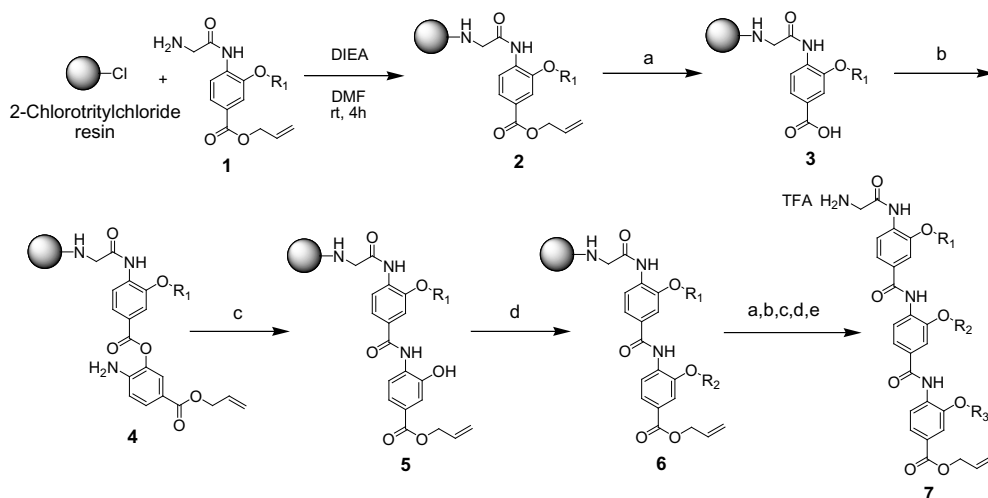
### Introduction

$\alpha$ -Helix is the most common structural motif in proteins and frequently plays an important role in protein-protein interactions [1,2]. Thus, small molecules that can modulate this fundamental process would be of great value in studying numerous key biochemical pathways. Whereas short peptide fragments derived from helical segments in proteins have been employed to regulate protein complex formations, their effective use has been limited by high conformational flexibility in solution, rapid enzymatic degradation, and difficulty in penetrating membrane.

To overcome these issues, non-peptidic  $\alpha$ -helix mimetics have been developed by using rigid and pre-organized scaffolds to interact with target proteins [2-7]. Although rational design of  $\alpha$ -helix mimetics has been successful in modulating protein-protein interaction, it is still difficult to arrange all functional groups of  $\alpha$ -helix mimetics as accurately as found in an ideal  $\alpha$ -helix. Therefore, it is often necessary to produce a number of analogues for rapid identification of initial leads with high biological activity. Recently, we have designed a tris-benzamide scaffold to present side chain functional groups found at the *i*, *i*+4, and *i*+7 positions in a helix [7], and report herein an efficient solid-phase synthetic strategy to construct a library of tris-benzamides.

### Results and Discussion

The solid-phase synthesis of a tris-benzamide started from anchoring the first benzoate (**1**) on a 2-chlorotrityl-chloride polystyrene resin (Scheme 1). To achieve high loading efficiency, a glycine was used as a linker between a 3-alkoxy-4-aminobenzoate and the resin. The allyl ester of the resin-bound benzoate (**2**) was removed with  $\text{Pd}(\text{PPh}_3)_4$  and phenylsilane, and the second benzoate was coupled to the released carboxylic acid (**3**) to give an ester intermediate (**4**) that was rearranged to a bis-benzamide (**5**) by treating  $\text{NaH}$ . Then, an alkyl group ( $\text{R}_2$ )



Scheme 1. Solid-phase synthesis of  $\alpha$ -helix mimetics based on a tris-benzamide scaffold. Reagents and conditions: <sup>a</sup>  $\text{Pd}(\text{PPh}_3)_4$ ,  $\text{PhSiH}_3$ ,  $\text{CHCl}_3$ , rt, 1 h; <sup>b</sup> allyl 4-amino-3-hydroxybenzoate, PyBOP, DIEA, DMF, rt, 20 h; <sup>c</sup>  $\text{NaH}$ ,  $n\text{Bu}_4\text{NBr}$ , DMF, rt, 1 h; <sup>d</sup>  $\text{R}_2\text{-X}$  (or  $\text{R}_3\text{-X}$ ),  $\text{Cs}_2\text{CO}_3$ ,  $n\text{Bu}_4\text{NBr}$ , DMF, rt, 12 h (or 24 h); <sup>e</sup> 10%  $\text{TFA}/\text{CH}_2\text{Cl}_2$ , rt, 10 min.

Table 1. Tris-benzamides produced by the solid-phase synthesis

$R_1$	$R_2$	$R_3$	Purity (%)
Bn	<i>i</i> Pr	<i>i</i> Pr	87
Bn	<i>i</i> Pr	<i>i</i> Bu	90
Bn	<i>i</i> Pr	Bn	93
Bn	<i>i</i> Bu	<i>i</i> Pr	96
Bn	<i>i</i> Bu	<i>i</i> Bu	92
Bn	<i>i</i> Bu	Bn	89
Bn	Bn	<i>i</i> Pr	83
Bn	Bn	<i>i</i> Bu	99
Bn	Bn	Bn	88
<i>i</i> Pr	CPr <sup>a</sup>	CPr	99
<i>i</i> Pr	CPr	ABu <sup>a</sup>	81
<i>i</i> Pr	ABu	CP	91
<i>i</i> Pr	ABu	ABu	99

<sup>a</sup> CPr=3-carboxypropyl, ABu=4-aminobutyl

corresponding to the *i*+4 position of a helix was introduced to the 3-hydroxyl group of the bis-benzamide (**5**) by treating with a variety of alkyl halides and a base. After screening bases to optimize the reaction condition, cesium carbonate along with tetrabutylammonium bromide as a catalyst was found to be the most effective. Reactive benzyl bromides showed faster completion of the reaction (<12 h) compared to less reactive alkyl halides (e.g., 2-bromopropane, 1-bromo-2-methylpropane) that typically require 24 h. The alkylation reaction was repeated to ensure complete conversion to a bis-benzamide with two alkoxy substituents (**6**).

After ester cleavage, *O*-acylation, and *O*→*N* acyl migration reactions were carried out, an alkyl group ( $R_3$ ) corresponding to the *i*+7 position of a helix was installed in the same manner described above. Each step in the synthesis was carried out with high yield, and a tris-benzamide (**7**) was finally released from the resin as a TFA salt. In addition to hydrophobic alkyl groups, tris-benzamides with hydrophilic functionalities like 3-carboxypropyl and 4-aminobutyl groups were also assembled in high yields.

To demonstrate the synthetic efficiency, a small library of 13 tris-benzamides was constructed (Table 1). Hydrophobic functional groups like *i*-propyl, *i*-butyl, and benzyl groups were used to represent Val, Leu, and Phe, respectively, whereas 3-carboxypropyl and 4-aminobutyl groups were used for the hydrophilic side chains of Glu and Lys, respectively.

In summary, an efficient synthetic route to produce  $\alpha$ -helix mimetics based on the tris-benzamide scaffold was developed by using allyl ester cleavage, amide bond formation via *O*→*N* acyl migration, and *O*-alkylation reactions. A small library of tris-benzamides was produced in high purity (>80%). This solid-phase synthetic strategy will facilitate rapid production of a number of  $\alpha$ -helix mimetics that can be broadly applied to numerous protein targets where  $\alpha$ -helical structure plays an important role.

## Acknowledgments

Supported by grant 07-07-JF-02 (American Diabetes Association), AT-1595 (Welch Foundation), and 009741-0031-2006 (Texas Advanced Research Program).

## References

- Barlow, D.J., Thornton, J.M. *J. Mol. Biol.* **201**, 601-619 (1998).
- Davis, J.M., Tsou, L.K., Hamilton, A.D. *Chem. Soc. Rev.* **36**, 326-334 (2007).
- Orner, B.P., Ernst, J.T., Hamilton, A.D. *J. Am. Chem. Soc.* **123**, 5382-5383 (2001).
- Ernst, J.T., Becerril, J., Park, H.S., Yin, H., Hamilton, A.D. *Angew. Chem. Int. Ed.* **42**, 535-539 (2003).
- Biros, S.M., Moisan, L., Mann, E., Carella, A., Zhai, D., Reed, J.C., Rebek, J., Jr. *Bioorg. Med. Chem. Lett.* **17**, 4641-4645 (2007).
- Rodriguez, J., Hamilton, A.D. *Angew. Chem. Int. Ed.* **46**, 8614-8617 (2007).
- Ahn, J.-M., Han, S.-Y. *Tetrahedron Lett.* **48**, 3543-3547 (2007).



## Synthesis of a Radio-labelled Peptide Mimic for Examining Affinity and Activity at the Prostaglandin F2 $\alpha$ Receptor

Carine B. Bourguet and William D. Lubell

Département de Chimie, Université de Montréal, Montréal, Québec H3C 3J7, Canada

### Introduction

The occurrence of prematurity has increased significantly over the three last decades and constitutes an unmet medical need with the highest per patient cost per year in the USA [1]. Actually, two hormones are known to be implicated in the initiation of parturition and labor. On one hand, oxytocin, a nona-cyclopeptide, is routinely used to induce labor in mammals [2] and its antagonist, Atosiban [3] is used in clinic to stop preterm uterine contractions. On the other hand, labor, parturition and consequently preterm labor, all can be initiated by the prostaglandin F2 $\alpha$  (PGF2 $\alpha$ ) receptors in uterine muscles [4,5] making this receptor an ideal complementary target for designing new tocolytic agents. (Knock out mouse for PGF2 $\alpha$  receptor never go into labor.) The FP receptor is a member of the GPCR family receptors and may be regulated by allosterism. In our laboratory, peptides and mimics were designed as allosteric antagonists [6,7] of the PGF2 $\alpha$  receptor. For example, peptide THG113 and peptide mimic THG113.824 (Figure 1) were synthesized and exhibited selective non competitive inhibition on PGF2 $\alpha$  receptor with good specificities (IC<sub>50</sub> 340 nM and 1.1 nM respectively) [6,7].

Phenacetamido mimic THG113.824, features an indolizidin-2-one (I<sup>2aa</sup>) of 3*S*,6*S*,9*S* configuration which induces an active type II'  $\beta$ -turn geometry and enhances lipophilicity such that it serves as a probe for cell based assays. [8,9] A protocol for the synthesis of radio-labelled THG113.824, iodide **1** has now been developed for the goal of studying its affinity for the PGF2 $\alpha$  receptor.

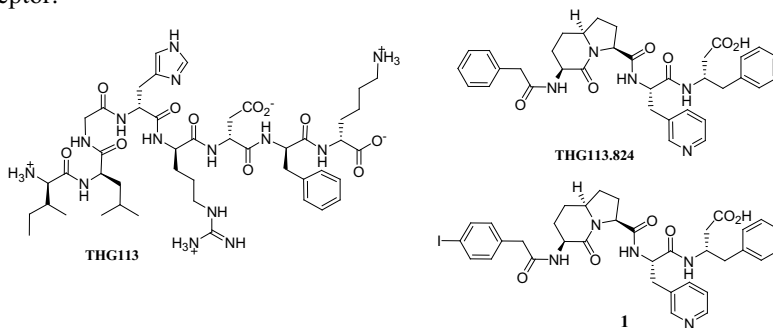


Fig. 1. Peptide and peptide mimics active against uterine contractions.

### Results and Discussion

Iodide **1** was synthesized employing Boc-protection in solution, using TBTU and HOBT as coupling agents in the presence of DIEA in dichloromethane (Figure 2). First, Boc-PyAla-OH **2** was coupled to  $\beta$ -Phe-OBn **3** [10]. After removal of the Boc group with 20% TFA in DCM for 1h and a salt exchange to the hydrochloride, the dipeptide was coupled to (3*S*,6*S*,9*S*)-Boc-I<sup>2aa</sup>-OH [11]. After TFA treatment and salt exchange, phenylacetic and *p*-*N*-(Boc)aminophenylacetic acid (synthesized from benzylocyanide in 4 steps, Figure 3) were respectively coupled, and the protected peptide mimics were hydrogenated in EtOH to give THG 113.824 and its respective aniline **5** which were purified by preparative HPLC. Iodide incorporation was performed by submitting **5** to sodium nitrate treatment to afford the diazonium salt, which was substituted by sodium iodide *in situ* to give cold **1** in 80% yield.

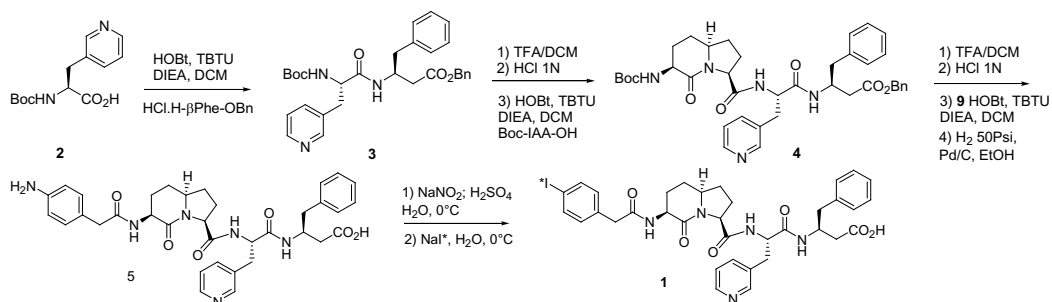


Fig. 2. Synthesis of radiolabelled mimic 1.

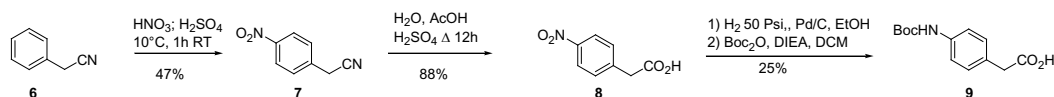


Fig. 3. Synthesis of Boc-aminophenylacetic acid.

Iodinated THG113.824 was thus synthesized to develop a method for preparing radioactive mimics for binding and dissociation assays on the PGF2 $\alpha$  receptor.

## Acknowledgments

This research was supported by the Canadian Institutes of Health Research (CIP-79848) for the financial support. We thank Dr. Alexandra Fürtös of the Université de Montréal Mass Spectrometry facility for mass spectral analyses, and Ms. Sylvie Bilodeau and Mr. Cedric Malveau of the Regional High-Field NMR Laboratory for aid with NMR spectroscopy.

## References

1. Lam, F., Istwan, N.B., Jacques, D., Coleman, S.K., Stanziano, G.J. *Manag. Care* **12**, 39-46 (2003).
2. Schröder, E., Lübke, K. *The Peptides* vol. II: Synthesis, Occurrence, and Action of Biologically Active Polypeptides, Acad. Press, NY 281, (1966).
3. a) Melin P. Development of an oxytocin antagonist - Atosiban. *Res. Clin. Forums* 1994; 16: 155-168.  
b) Brownstein, M.J.; in *Peptides: Chemistry, Structure and Biology*, Hodges, R.S., Smith, J.A. Eds.; ESCOM Leiden, The Netherlands 571 (1994).
4. Pathe-Neushäfer-Rube, A., Neushäfer-Rube, F., Püschel, G. P. *Biochem. J.* **388**, 317 (2005).
5. Presland, J. *Cur. Opinion Drug Discovery Development* **8**, 567 (2005).
6. Peri, K.G., Quiniou, C., Hou, X., Abran, D., Varma, D.R., Lubell, W. D., Chemtob, S. *Seminars in Perinatology* **67**, 389 (2002).
7. Peri, K.G., Polyak, F., Thouin, E., Lubell, W.D., Chemtob, S. *PCT Int. Appl. Ser. No. 60/387, 424*, Jun 11 (2002).
8. Bourguet, C.B., Hou, X., Chemtob, S., Lubell, W.D. *Proceeding Book of the 29th European Peptide Symposium*, 215, (2006).
9. Bourguet, C.B., Hou, X., Chemtob, S., Lubell, W.D. *Proceeding Book of the 20th American Peptide Symposium*, 271, (2009).
10. Linder, M.R., Steurer, S., Podlech, J. *Org. Synth.* **79**, 154 (1998).
11. Lombart, H.G., Lubell, W.D. *J. Org. Chem.* **61**, 9437 (1996).

# Solid-Phase Synthesis and CD Spectroscopic Conformational Analysis of $\alpha$ - and $\beta$ -Amino $\gamma$ -Lactam (Agl and Bgl) Analogs of Growth Hormone-Releasing Peptide GHRP-6

Nicolas Boutard, Andrew G. Jamieson, and William D. Lubell

Département de Chimie, Université de Montréal, C.P. 6128, Succursale Centre-Ville,  
 Montréal, Québec H3C 3J7, Canada

## Introduction

GHRP-6 (HwAWfK) is a member of the growth hormone-releasing peptides (GHRPs) family [1]. It stimulates GH liberation from somatotrophs in a dose dependent manner in different species including humans [2] by its interaction with the ghrelin receptor GHS-R1a. Through their interaction with the scavenger receptor CD36, GHRP-6 analogs are able to exert protective effects on ischemia/reperfusion injury and anti-atherosclerotic activity [3,4]. A  $\beta$ -turn conformation around Ala<sup>3</sup> is suspected to be an important feature for binding and differentiating the CD36 from the GHS-R1a receptor [5,6]. Thus, preparation of analogs bearing  $\beta$ -turn mimics in position 3 would provide information about the structural requirements to achieve activity and/or selectivity. In that context, analogs of GHRP-6 bearing  $\alpha$ - and  $\beta$ -amino  $\gamma$ -lactam (respectively Agl **1** and Bgl **2**, Figure 1) residues in this position, in both (*S*)- and (*R*)-forms, have been synthesized using suitably configured cyclic sulfamidate reagents **3** and **4**. These reagents are respectively derived from homoserine, and aspartate [6].

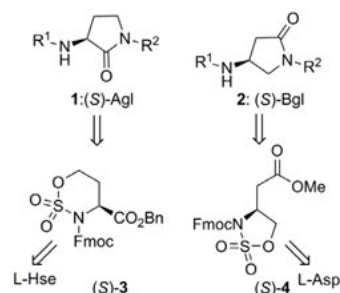
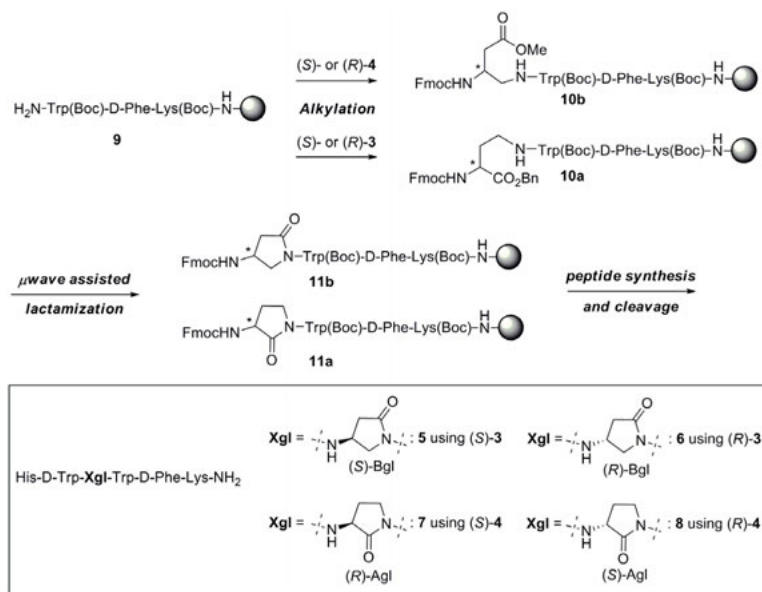


Fig. 1. Agl **1**, Bgl **2** and cyclic sulfamidates **3** and **4**.

## Results and Discussion

Four lactam analogs of GHRP-6 (**5-8**, Scheme 1) were prepared on Rink amide resin according to a recently reported Fmoc-based protocol relying on two key steps [6]: (1) selective monoalkylation of the free N-terminal amine of the supported tripeptide precursor **9** with (*S*)- and (*R*)-configured reagents **3** and **4** and (2) microwave assisted lactam formation. Conventional Fmoc peptide synthesis was then pursued to elongate the peptide and TFA cleavage provided the lactam GHRP-6 analogs with crude purities ranging from 22% to 46%. Purification by preparative RP-HPLC furnished 99% pure peptides **5-8** in 4% to 25% yields.



Scheme 1. Synthetic strategy for preparation of Agl<sup>3</sup> and Bgl<sup>3</sup> GHRP-6 analogs **5**, **6**, **7** and **8**.

Circular dichroism (CD) spectra of the four GHRP-6 analogs were measured in water and TFE (Figure 2). In water, GHRP-6 displayed a random coil characteristic curve (maximum negative band at 190 nm). The curve shapes of the lactam analogs indicated an equilibrium between disorder and a  $\beta$ -turn structure, with a negative maximum at 230 nm [7]. The lactam curves also featured a smaller negative maximum at 215 nm particularly apparent for (S)-Agl<sup>3</sup> **5** and (R)-Bgl<sup>3</sup> **8** suggesting similarities in their conformations in water. The double negative curve shape in water was similar to that of Gramicidin S, albeit with a 10 nm blue shift compared to **5** and **8** and may indicate type II'  $\beta$ -turn geometry [8]. In TFE, GHRP-6 and its lactam analogs **5**–**8** all gave curves indicative of ordered  $\beta$ -turn conformers with negative maxima around 225–235 nm, the most intense being displayed by the (S)-Agl and (R)-Bgl analogs **5** and **8**. Bgl<sup>3</sup> peptides **7** and **8** also had curves with a positive maximum around 210–220 nm. Agl<sup>3</sup> analogs **5** and **6** exhibited a shoulder in that region, underlining the differences of geometry induced by Agl and Bgl in TFE.

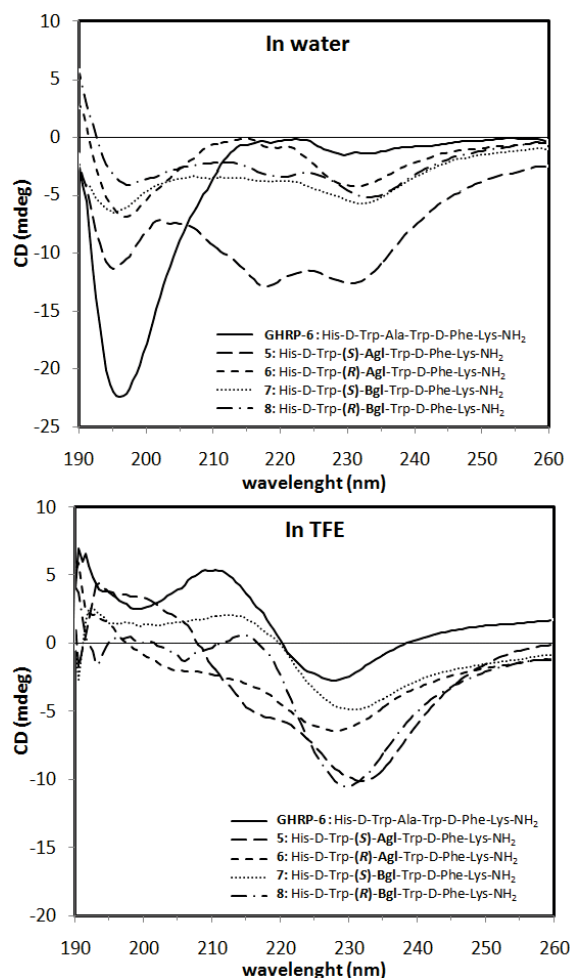


Fig. 2. CD spectra of GHRP-6, **5**, **6**, **7** and **8** (20  $\mu$ M).

This CD study confirms that Agl and Bgl residues are able to induce  $\beta$ -turn conformations at position 3 of GHRP-6. Although the two types of lactams bring about differences in geometry, some similarities seem to arise from lactams of both different types and configuration as exemplified by (S)-Agl and (R)-Bgl peptides **5** and **8**.

## Acknowledgments

We acknowledge financial support from NSERC, UdeM, CIHR, CIHR-Team in GPCR allosteric regulation (CTiGAR), FQRNT.

## References

1. Bowers, C.Y. *Cell. Mol. Life Sci.* **54**, 1316-29 (1998).
2. Bowers, C.Y., Sartor, A.O., Reynolds, G.A., et al. *Endocrinology* **128**, 2027-35 (1991).
3. Torsello, A., Bresciani, E., Rossoni, G., et al. *Endocrinology* **144**, 1787-92 (2003).
4. Bodart, V., Febbraio, M., Demers, A., et al. *Circ. Res.* **90**, 844-9 (2002).
5. Momany, F.A., Bowers, C.Y., In Bercu B.B., Walker R.F. (Eds.) *Growth Hormone Secretagogues*, Springer-Verlag, New-York, 1996, p. 73.
6. Jamieson, A.G., Boutard, N., Beaugerard, K., et al. *J. Am. Chem. Soc.* **131**, 7917-27 (2009).
7. Bush, C.A., Sarkar, S.K., Kopple, K.D. *Biochemistry* **17**, 4951-4 (1978).
8. Urry, D.W., Ruiter, A.L., Starcher, B.C., Hinners, T.A. *Antimicrob. Agents Chemother.* **8**, 87-93 (1968).

## Design, Synthesis and Structure of Peptidomimetic Inhibitors of Eukaryotic Ribonucleotide Reductase: A Target for Cancer Chemotherapy

Jaskiran Kaur,<sup>1</sup> Shalini Jha,<sup>2</sup> Chris Dealwis,<sup>3</sup> and Barry S. Cooperman<sup>4</sup>

<sup>1,4</sup> Department of Chemistry, University of Pennsylvania, Philadelphia, PA 19104, U.S.A.

<sup>2,3</sup> Department of Pharmacology, Proteomics and Bioinformatics Center Case Western Reserve University, Cleveland, OH 44016, U.S.A.

### Introduction

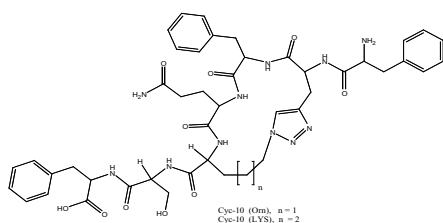
Eukaryotic ribonucleotide reductase (RR) catalyzes nucleoside diphosphate conversion to deoxynucleoside diphosphate. Crucial for rapidly dividing cells, RR is a well-recognized target for cancer therapy. Active mammalian RR (mRR) depends on the association of two different subunits, mR1 and mR2 in which the mR2 C-terminal peptide binds to mR1. Inhibitors of human RR (hRR) currently in clinical use or in clinical trial, target either the active site or an allosteric site within mR1, or the diferric-tyrosyl radical center within mR2/p53R2 [1]. A potential problem with these hRR inhibitors has been their relative lack of specificity. In contrast, inhibitors that target quaternary structure, because of their higher intrinsic specificity, have the potential to be effective with fewer side effects. mRR can be inhibited by competitive binding at the mR1 subunit by hR2 C-terminal heptapeptide, NAcFTLDADF, P7, and its peptidomimetic, Fmoc(Me) PhgLDChaDF, denoted P6 [2,3].

Recently, we reported crystal structures of heterocomplexes containing P7 or P6 bound to *Saccharomyces cerevisiae* R1 (ScR1) at a locus consisting of residues that are highly conserved between yeast, mouse, and human R1 [4,5]. ScR2 and ScR4 C-terminal peptides (ScR2pep and ScR4pep, respectively), P7 and P6 (K<sub>d</sub> 300 nM) bind to ScR1 in three distinct conformations, those adopted by: (i) P7/ScR2pep, (ii) P6, and (iii) ScR4pep. Both P7 and ScR4 bind with a reverse turn, although the turn is in opposite directions for each, whereas P6 binds in an extended fashion. These three conformations demonstrate the inherent flexibility of the eukaryotic R1 peptide binding site, and provide the basis for the design and synthesis of peptidomimetics reported here.

### Results and Discussion

#### Design of peptidomimetic inhibitors:

Based on the structure of ScR1 complexed with ScR2-pep, ScR4-pep, P7, P6; binding site was created using the PROTOMOL module and then COMBIMAKER module allowing facile alterations of different sites of these molecules by varying diverse R-groups. Best fit molecules were docked and energy minimized with the SURFLUX module in SYBYL8.0. This led to the design of [1,2,3]-triazolyl containing cyclic peptides (Figure 1) with the potential of very tight binding to R1. The cyclic backbone rigidifies the reverse turn as seen in P7, ScR2 and ScR4 while improving the interactions in the spacer region.



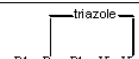
Intramolecular triazoles			
	X <sub>1</sub>	X <sub>2</sub>	X <sub>3</sub>
Compound			
Cyc7 (Orn)	His	Orn	Asp
Cyc7 (Lys)	His	Lys	Asp
Cyc9 (Orn)	His	Orn	Ser
Cyc9 (Lys)	His	Lys	Ser
Cyc10 (Orn)	Gln	Orn	Ser
Cyc10 (Lys)	Gln	Lys	Ser

Fig. 1. Structure of Cyc10 and table of cyclic peptides synthesized.

### Synthesis of Peptidomimetic inhibitors:

The cyclic peptides were synthesized by solid phase peptide synthesis using Fmoc chemistry. NovaSyn TGA resin with a loading of 0.2 mmoles/g was used as the solid support. Lower loading capacity facilitated intra-molecular 1,3-dipolar cycloaddition. For Cyc10 (lys), the linear precursor Phe1-Pra2-Phe3-Gln4-Lys5-Ser6-Phe7 was assembled with propargylglycine (Pra) and Lys in positions *i* and *i*+3 respectively. Alloc protecting group on Lys was selectively removed using Pd(PPh<sub>3</sub>)<sub>4</sub> to provide free amine which upon reaction with triflic azide was converted to azide. Both the diazotransformation of Lys residue into Nle( $\epsilon$ -N<sub>3</sub>) and the Cu(I) catalysed 1,3-dipolar addition of azido and alkynyl functionalities, leading to the conversion of linear precursor into the 1,4-disubstituted [1,2,3]triazolyl containing peptide were carried out efficiently on resin. Disappearance of the characteristic azide IR band (KBr) at 2100 cm<sup>-1</sup> was used to monitor azide conversion to triazole (Figure 2). All the peptides were purified by HPLC and their structure confirmed by ESI-mass spectroscopy.

### Crystal Structure of Cyc10(lys):

The crystal structure of Cyc10(lys) at 2.7 Å resolution as bound to ScR1 (Figure 3) shows two strong interaction sites, denoted subsites 1 and 2, separated by a spacer region which interacts only weakly with the inhibitor. Subsite 1 is predominantly hydrophobic and interacts with the N-terminus up until residue three. The hydrophobic pocket is well occupied by two phenylalanines. Subsite 2 is partially polar/hydrophobic and has strong interactions with the Phe and Ser. Cyclization via the triazole ring connects the two sites; thus rigidifying the turn between residues 2-5 [<sup>1</sup>PhePraPheGlnLysSerPhe<sup>7</sup>] and enhancing the interactions in the spacer region. It appears from the structure of Cyc10, that some side-chains do not make extensive interactions with R1. Removing these groups may have little impact on binding while reducing the molecular weight. Also efforts will be made to enhance the interactions at subsite 1 by the introduction of hydrophobic groups at the N-terminal and altering the spacer region.

This structure of Cyc10(Lys) will be used for a new round of modeling, synthesis, testing, and structural characterization, and the process will continue until no further improvements are seen. We plan to test the best compounds emerging from this iterative process for *in vivo* efficacy in mice containing human breast cancer tumors, optimizing for both efficacy in reducing tumor size and low toxicity.

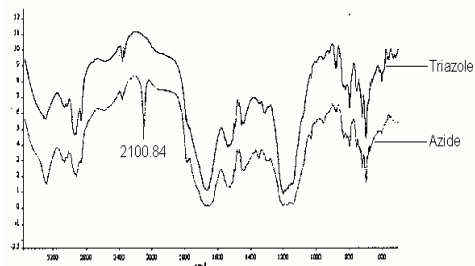


Fig. 2. Conversion of azide to triazole as monitored by IR.

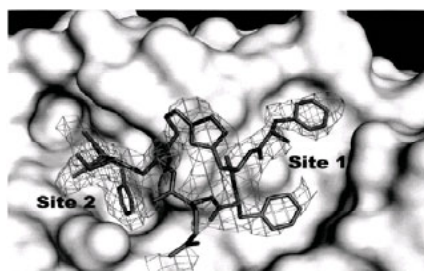


Fig. 3. Structure of Cyc10(Lys) bound to ScR1. The 2Fo-Fc electron density map is contoured at 0.8  $\sigma$ . Subsites 1 and 2 are shown as surfaces.

### Acknowledgments

Supported by grants 4100043202 from the Commonwealth of Pennsylvania (to B.S.C.) and CA 100827 from the National Institutes of Health (to C. D.).

### References

1. Silva, D.J., Stubbe, J., Samano, V., Robins, M.J. *Biochemistry* **37**(16), 5528-5535 (1998).
2. Yang, F.D., et al. *FEBS Lett.* **272**, 61-64 (1990).
3. Cooperman, B.S., Gao, Y., Tan, C., Kashlan, O.B., Kaur, J. *Adv. Enzyme Regul.* **45**, 112-115 (2005).
4. Xu, H., et al. *J Med Chem.* **51**(15), 4653-4659 (2008).
5. Xu, H., Faber, C., Uchiki, T., Racca, J., Dealwis, C. *Proc. Natl. Acad. Sci. U.S.A.* **103**(11), 4028-4033 (2006).

## DhHP-6 Protect H9c2 Cardiomyocyte Against Oxidative Injury Induced by Hypoxia/Reoxygenation

Xiaoguang Chen,<sup>1,2</sup> Lei Huang,<sup>1</sup> Shuwen Guan,<sup>1</sup> Liping Wang,<sup>1\*</sup>  
and Wei Li<sup>1</sup>

<sup>1</sup>College of Life Science, Jilin University; <sup>2</sup>Department of Pharmaceutical Engineering, College of Humanities & Information, Changchun University of Technology, Changchun, PR China

\* Corresponding author Tel: +86-431-88499505; Fax: +86-431-88921591; Email: wanglp@jlu.edu.cn

### Introduction

Myocardial infarction is the major cause of death in the world. Reperfusion of ischemic tissue is necessary to terminate the processes of ischemic injury. However, abrupt reperfusion may results in the so-called ischemia/reperfusion (IR)-injury that can provoke further tissue injury and myocardial cell death. There is great interest in the development of adjunct therapies, which might attenuate reperfusion injury and thereby maximize the benefits of reperfusion. Therefore, studies on the safe and effective new cardioprotective agents used to prevent IR injury are still a pivotal issue [1].

DhHP-6 (Deuterohaemin – Ala-His-Thr-Val-Glu-Lys) is a novel peptide mimic of peroxidases designed and synthesized in our laboratory. The *in vitro* peroxidase activity of DhHP-6 is very similar to that of microperoxidase-11 (MP-11), but DhHP-6 has very good water solubility, stability and its chemical synthesis is much simpler. DhHP-6 has been demonstrated to exert anti-cataract activity *in vitro* and significant cardio protective effects against myocardial ischemia reperfusion injury in rats previously. In this study, we investigate the protective effects and potential molecular mechanism of DhHP-6 on cardiomyocytes against oxidative injury induced by hypoxia/reoxygenation.

### Results and Discussion

In hypoxia/reoxygenation-induced H9c2 cardiomyocytes injury model, the H9c2 cardiomyocytes were exposed to hypoxia/reoxygenation (1 h of reoxygenation after 13 h of

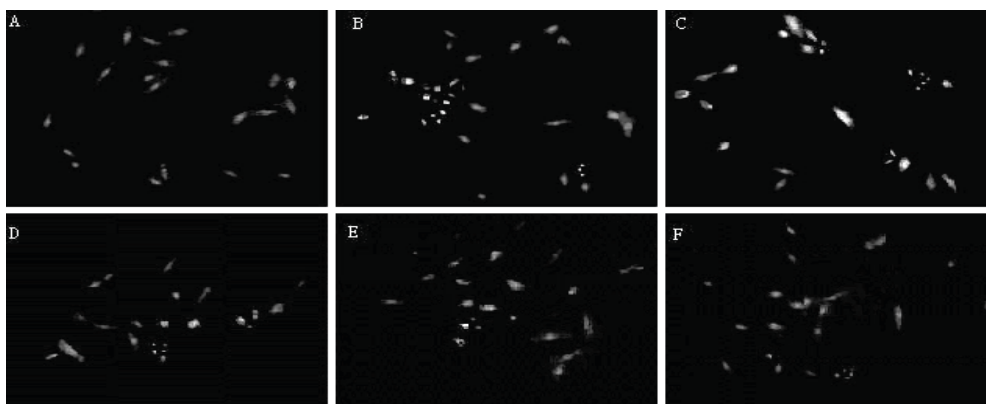


Fig. 1. The fluorescence microscope observation by AO/EB staining. A: Control, H9c2 cells were cultured in a low volume of substrate-free medium (serum-free, glucose-free and sodium pyruvate-free DMEM) in 5% CO<sub>2</sub> humidified atmosphere, at 37° C for 13 h. Simulated ischemia was followed by a simulated “reperfusion” period during which the cells were exposed to normoxic fresh culture medium at 37° C for 60 min. B: IR injury group, H9c2 cells were cultured in a low volume of substrate-free medium (serum-free, glucose-free and sodium pyruvate-free DMEM) into an anaerobic Plexiglas chamber, saturated with 95% N<sub>2</sub> and 5% CO<sub>2</sub>, at 37° C for 13 h. Simulated ischemia was followed by a simulated “reperfusion” period during which the cells were exposed to normoxic fresh culture medium at 37° C for 60 min. C,D,E and F: H9c2 cells were pretreated with 0.08, 0.41, 0.82, 4.10 μmol·L<sup>-1</sup> DhHP-6 for 30 min before IR injury.



hypoxia), with or without DhHP-6-treatment. Cell viability was assessed by the Trypan blue exclusion and 3-(4,5-dimethyl-thiazol-2yl)-2,5-diphenyl tetrazolium bromide(MTT) uptake assay. A clear increase in cell death was observed when the cells were exposed to hypoxia/reoxygenation. Pretreatment with DhHP-6 significantly increased the viability of hypoxia/reoxygenation-induced H9c2 cardiomyocytes by 20% in the model injury group compared with the normal group ( $P<0.01$ ). Besides, the alleviation of DhHP-6 on the morphologic changes of myocardial cells, swelled, shrank and fell off in model injury group, was observed. The fluorescence microscope observation by AO/EB staining showed that there were many apoptosis and necrosis cells in model injury group, but there was little apoptosis and necrosis cells in DhHP-6 treated groups (Figure 1).

Hypoxia followed by reoxygenation caused a significant increase in LDH release, DhHP-6 significantly lowered LDH release in a dose-dependent manner, with  $4.10\mu\text{mol}\cdot\text{L}^{-1}$  DhHP-6 reducing LDH release to 50% of control. DhHP-6 also significantly increased the SOD activity and decreased the MDA level in the model injury cells. This suggests that DhHP-6 protect myocardial cells via an antioxidant effect. Furthermore, in severely ischemic myocardium, subsequent reperfusion will lead to calcium overload due to the amplified sequestration of the elevated  $\text{Ca}^{2+}$  into the endoplasmic reticulum by  $\text{Ca}^{2+}$ -ATPase as ATP synthesis begins to resume [2]. Therefore, reduction of  $[\text{Ca}^{2+}]$  during ischemia can greatly alleviate calcium overload during reperfusion. Our data (not shown) showed that DhHP-6 significantly improved  $\text{Ca}^{2+}$ -ATPase activity in the model injury cardiomyocytes compared with in normal group ( $P<0.01$ ). This indicates that alleviating calcium accumulation during myocardial ischemia and reperfusion may be one of the mechanisms of the cardioprotective effect of DhHP-6.

The previous study results indicate that some cardioprotectors inhibit hypoxia-induced apoptosis via the activation of SIRT1 in H9c2 cells [3]. Therefore, to investigate the potential molecular mechanism of DhHP-6 protect cardiomyocytes injury, we studied the expression of SIRT1 both in mRNA and protein levels in DhHP-6 treated cardiomyocytes. The mRNA expression level of sirt1 by real time RT-PCR is 24 times higher in treatment groups (Figure 2).

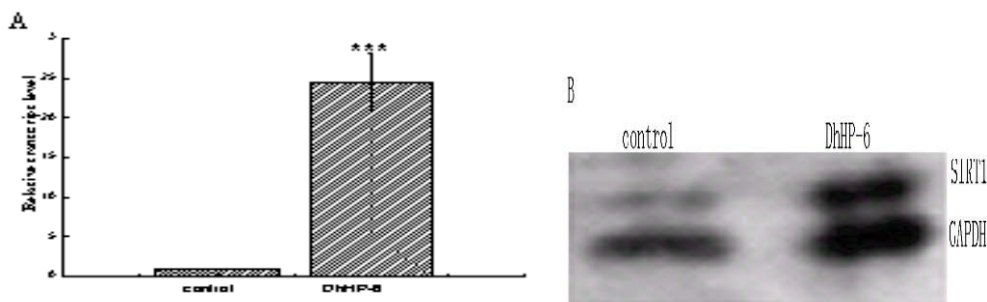


Fig. 2. DhHP-6 increases the expression of SIRT1. A: mRNA expression of SIRT1 relative to housekeeping gene gapdh, were determined by real time RT-PCR. DhHP-6:  $0.82\mu\text{mol}\cdot\text{L}^{-1}$  DhHP-6 treated 24 hours. Control: no treated. \*\*\*:  $p<0.001$ ,  $n=4$ . B: Western blot of SIRT1. DhHP-6:  $0.82\mu\text{mol}\cdot\text{L}^{-1}$  DhHP-6 treated 24 hours. Control: no treated.

Western blot analysis showed that SIRT1 expression was higher in DhHP-6 treatment groups than in control groups. These results indicated that exposures of the cells to DhHP-6 caused increase the expression of SIRT1. This may be one of mechanisms of DhHP-6 protect H9c2 cardiomyocytes injury.

In summary, DhHP-6 exerts significant protective effects on cardiomyocytes against oxidative injury induced by hypoxia/reoxygenation. This function may be related to its antioxidant properties and activation of SIRT1.

## References

1. Yellon, D.M., Hausenloy, D.J. *N. Engl. J. Med.* **357**, 1121-1135 (2007).
2. Tani, M. *Annu. Rev. Physiol.* **52**, 543- 59.(1990).
3. Chen, C.J., et al. *Biochem. Biophys. Res. Commun.* **378**, 389-393 (2009).



## Free Radical Scavenging Activity of Hydroxycinnamoyl Amino Acid Amides

Maya Spasova,<sup>1</sup> Djemile Dagon,<sup>1</sup> Galya Ivanova,<sup>2</sup> and Tsenka Milkova<sup>1</sup>

<sup>1</sup>South-West University "Neofit Rilski" Blagoevgrad 2700, Bulgaria,

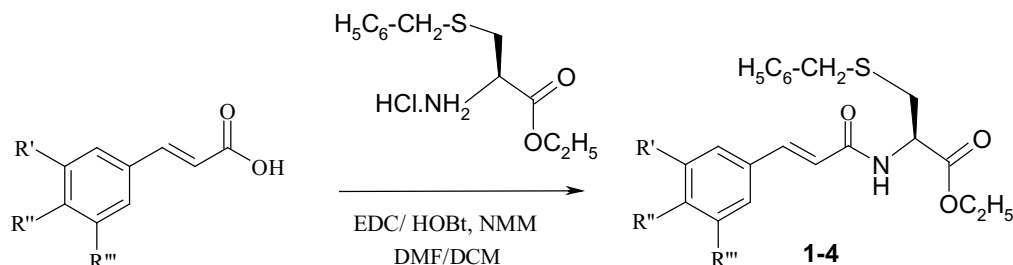
<sup>2</sup>Institute of Organic Chemistry with Centre of Phytochemistry,  
 Bulgarian Academy of Sciences, Sofia 1113, Bulgaria

### Introduction

The hydroxycinnamic acid compounds are an important source of antioxidants [1] due to their ubiquitous occurrence in the plant kingdom. They usually exist as esters of organic acid, glycosides, or amides. Only a small number of them exist as free acids in nature [2,3]. As the quantity of hydroxycinnamoyl amides in the nature is very low and their enzyme stability is higher than esters, we decided to synthesize series of cinnamoyl-, feruloyl-, caffeoyl- and sinapoyl- cysteine amides in order to define their antioxidant activity.

### Results and Discussion

Four hydroxycinnamoyl amides (1-4) were prepared by condensation of the corresponding phenylpropenoic acids with H-Cys(Bzl)-OEt using 1-(3-dimethylaminopropyl)-3-ethylcarbodiimide hydrochloride (EDC), 1-hydroxybenzotriazole (HOBT), and N-methylmorpholine in methylene chloride and dimethylformamide in 52-70% yields (Scheme 1). The products were purified by CC on silica gel with CH<sub>2</sub>Cl<sub>2</sub>:CH<sub>3</sub>COCH<sub>3</sub>.



Scheme 1. Synthesis of amides of cinnamic ( $R'$ ,  $R''$ ,  $R'''=H$ ), ferulic ( $R'=OCH_3$ ,  $R''=OH$ ,  $R'''=H$ ), sinapic ( $R'=OCH_3$ ,  $R''=OH$ ,  $R'''=OCH_3$ ) and caffeic acids ( $R'=OH$ ,  $R''=OH$ ,  $R'''=H$ ).

The structure of the amides **1** – **4** has been characterized using UV, <sup>1</sup>H NMR, <sup>13</sup>C NMR, <sup>1</sup>H-<sup>1</sup>H COSY and EI-MS spectroscopy. All <sup>1</sup>H-NMR spectra are referenced to tetramethylsilane (TMS) in CDCl<sub>3</sub> in  $\delta$  units ppm. The values of the proton-proton vicinal coupling constants (<sup>3</sup>J<sub>H/H</sub> about 15.6 Hz) measured for the olefinic protons of cinnamoyl-, feruloyl-, caffeoyl- and sinapoyl residues define E configuration of the double bond of the studied compounds.

The model of scavenging stable DPPH free radical was used to evaluate the antioxidant activities of synthesized amides in relatively short time compared to previously used method against lipid peroxidation [4]. The DPPH test was determined according to the method of Pekkarinen *et al.*[5]. As shown in Table 1, the scavenging activities of N-hydroxycinnamoyl cysteine amides (1-4) were compared to the standard antioxidants as quercetin, eugenol, isoeugenol, sinapic acid, ferulic acid and D,L  $\alpha$ -Tocopherol. It has been established that feruloyl-, sinapoyl- and caffeoyl amides exert higher antioxidant activity than the standards-eugenol and isoeugenol, but lower than the free hydroxycinnamic acid and quercetin, tocopherol.

Table 1. Radical scavenging activity of hydroxycinnamoyl amides against DPPH\* test

AH	(%) RSA					
	0.9 mM		1.8 mM		3.6 mM	
	Reaction time ( min )					
	10'	20'	10'	20'	10'	20'
Quercetin	49.0	54.0	80.1	86.2	85.2	87.8
Eugenol	9.0	11.4	17.1	21.2	30.4	37.6
Isoeugenol	7.8	8.6	13.5	14.7	23.8	25.3
Sinapic acid	16.1	17.2	26.5	31.9	69.0	69.6
Ferulic acid	12.0	13.8	21.0	25.1	36.7	44.3
D,L $\alpha$ -Tocopherol	15.5	15.9	34.9	38.4	53.0	58.1
CA-Cys(Bzl)-OEt ( <b>1</b> )	2.9	3.7	2.9	3.7	2.9	3.7
FA-Cys(Bzl)-OEt ( <b>2</b> )	11.9	14.9	22.7	28.1	31.0	38.4
SA-Cys(Bzl)-OEt ( <b>3</b> )	14.9	16.6	25.9	28.6	42.3	47.3
CafA-Cys(Bzl)-OEt ( <b>4</b> )	12.3	13.2	21.5	22.8	42.8	44.9

% RSA—percent radical scavenging activity; % RSA =  $[Abs_{516nm}(t = 0) - Abs_{516nm}(t = t')] \times 100 / Abs_{516nm}(t = 0)$ , as proposed by Pekkarinen et al.[5]; quercetin, eugenol, isoeugenol, tocopherol, sinapic-and ferulic- acids were used as standards.

## Acknowledgments

This investigation was funded by South-West University "N.Rilski"-Blagoevgrad, Bulgaria.

## References

1. Chen, J.H, Ho, Chi-Tang, *J. Agric. Food Chem.* **45**, 2374 (1997).
2. Herrmann, K. *Gordian* **93**, 92 (1993).
3. Herrmann, K. *Fluess. Obst.* **59**, 66 (1992).
4. Spasova, M., Kortenska-Kancheva, V., Totseva, I., Ivanova, G., Georgiev, L., Milkova, T.S. *J. Peptide Sci.* **12**, 369 (2006).
5. Pekkarinen, S., Stockmann, H., Schwarz, K., Heinonen, I.M., Hopia, A.I., *J. Agric. Food. Chem.* **47**, 3036 (1999).

## **Solid-Phase Synthesis and CD Spectral Analysis of IL1R-Allosteric Modulator 101.10 Bearing Multiple Agl-Residues**

**Luisa Ronga and William D. Lubell**

*Département de Chimie, Université de Montréal, C.P. 6128 Succursale Centre-Ville,  
Montréal (Qc), H3C 3J7, Canada*

### **Introduction**

Agl ( $\alpha$ -amino  $\gamma$ -lactam) residues in peptides have stabilized  $\beta$ -turn structures and have enhanced potency and receptor selectivity [1], underlining their importance as synthetic tools in conformational analysis and drug discovery [2]. The solid-phase synthesis of Agl peptide sequences has been performed on SynPhase lanterns [3] using a six-member cyclic sulfamidate derived from homoserine to annulate the amino lactam residue onto the peptide chain. Parallel synthesis of Agl analogs of the allosteric modulator 101.10 (D-Arg-D-Tyr-D-Thr-D-Val-D-Glu-D-Leu-D-Ala, rytvela) of the interleukin-1 receptor (IL-1R) [4] was performed by split and mix chemistry on the lanterns, including analogs with two Agl residues in the same peptide sequence. Conformational analysis of the Agl analogs of rytvela by CD spectroscopy is now reported and shows the pronounced influence of the lactam constraint on peptide conformation.

### **Results and Discussion**

With the goal to better understand the conformational preferences responsible for the biological activity of 101.10, six (*R*)-Agl analogs were synthesized on Rink amide resin and their efficacy in inhibiting IL-1 induced TF-1 cell proliferation was examined [5]. Substitution of (*R*)-Agl for either D-Thr<sup>3</sup> or D-Val<sup>4</sup> in rytvela caused respectively the complete loss and retention of the activity of the parent peptide. In addition, replacement of the N-terminal D-Arg<sup>1</sup> residue by (*R*)-Agl led to a 2.2 fold increase in efficacy compared to the parent peptide [5]. In light of the improved activity of the (*R*)-Agl<sup>1</sup> analog **1** and the retained potency of (*R*)-Agl<sup>2</sup>, (*R*)-Agl<sup>4</sup> and (*R*)-Agl<sup>5</sup> analogs of rytvela [5], combinations of two (*R*)-Agl residues, one at position 1 as well as one at either position 2, 4 or 5, respectively, were synthesized to give bis-Agl rytvela analogs **2-4** [6].

The circular dichroism (CD) spectrum of the parent peptide rytvela in water was compared with that of (*R*)-Agl<sup>1</sup> analog **1** and double Agl analogs **2-4**. The D-peptide rytvela and (*R*)-Agl-analogs exhibited curve shapes that were inverted indicative of mirror image secondary structures of those formed by L-peptides [7]. The insertion of an Agl motif into the rytvela core had a pronounced influence on the shape of the CD spectra (Figure 1). The CD spectrum of rytvela exhibited a curve shape indicative of a disordered structure, as suggested by the maximum around 198 nm [8]. The replacement of the D-Arg<sup>1</sup> residue by (*R*)-Agl caused the spectrum of the parent peptide to change into a predominant  $\alpha$ -helical conformation, as suggested by the maximum around 200 nm and the presence of a shoulder at about 220 nm [7]. The better-defined maximum around 200 nm in the spectra of bis-Agl analogs **2-4** suggests that the insertion of the second Agl motif increases the  $\alpha$ -helical-like character of the mono-Agl analog **1** which may be important for the activity of this peptide.

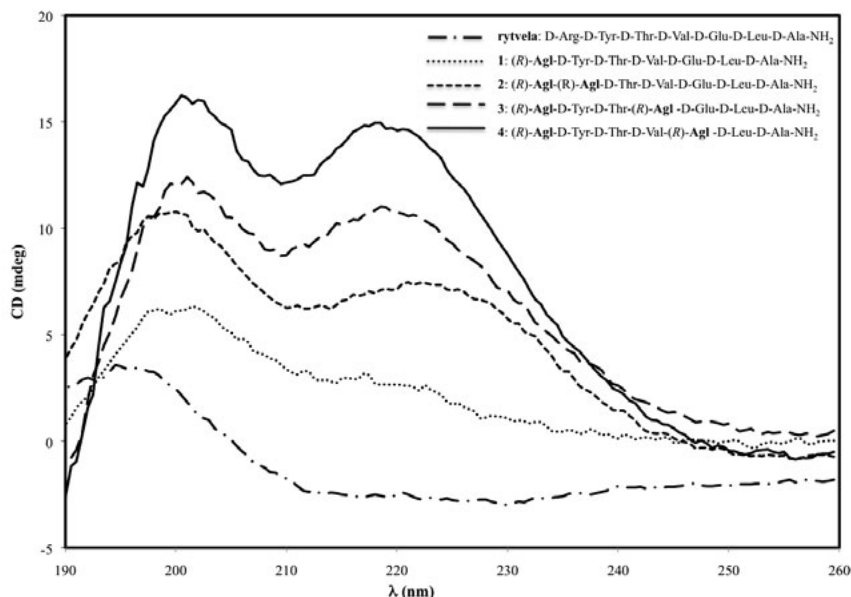


Fig. 1. Far UV CD spectra in water at 20  $\mu$ M of rytvela and its mono-Agl analog **1** and bis-Agl analogs (**2-4**).

## Acknowledgments

The authors acknowledge financial support from the Natural Sciences and Engineering Research Council of Canada (NSERC), Université de Montréal, Canadian Institutes of Health Research (CIP-79848) CIHR-Team in GPCR allosteric regulation (CTiGAR), The Fonds Québécois de la Recherche sur la Nature et les Technologies (FQRNT), and equipment made possible from the Canadian Foundation for Innovation. L.R. thanks the Foreign Affairs and International Trade, Canada (DFAIT) and the Fonds de la recherche en santé Québec for post-doctoral research fellowships.

## References

1. Freidinger, R.M. *J. Med. Chem.* **46**, 5553-5566 (2003) and references within.
2. Perdih, A., Kikelj, D. *Curr. Med. Chem.* **13**, 1525-1556 (2006) and references within.
3. Ede, N.J. *J. Immunol. Methods* **267**, 3-11 (2002).
4. Quiniou, C., Przemyslaw, S., Lahaie, I., Hou, X., Brault, S., Beauchamp, M., Leduc, M., Rihakova, L., Joyal, J-S., Nadeau, S., Heveker, N., Lubell, W.D., Sennlaub, F., Gobeil, Jr. F., Miller, G., Pshezhtsky, A.V.; Chemtob, S. *J. Immunol.* **180**, 6977-87 (2008).
5. Jamieson, A.G., Boutard, N., Beauregard, K., Bodas, M.S., Ong, H., Quiniou, C., Chemtob, S., Lubell, W.D. *J. Am. Chem. Soc.* **131**, 7917-7927 (2009).
6. Ronga, L., Jamieson, A.G., Beauregard, K., Quiniou, C., Chemtob, S., Lubell, W.D. *Biopolymers Pept. Sci.*, accepted (2009).
7. Sakurai, K., Chung, S.H., Kahne D. *J. Am. Chem. Soc.* **126**, 16288-16289 (2004).
8. Kelly, S.M., Jess, T.J., Price, N.C. *Biochim. Biophys. Acta* **1751**, 119-139 (2005).

## From Combinatorial Chemistry to Nanomicelles to Cancer Targeting

Juntao Luo,<sup>1</sup> Kai Xiao,<sup>1</sup> Yuan-pei Li,<sup>1</sup> Joyce Lee,<sup>1</sup> Nianhuan Yao,<sup>1</sup>  
Wenwu Xiao,<sup>1</sup> Yan Wang,<sup>1</sup> Wiley Fowler,<sup>2</sup> Michael Kent,<sup>3</sup>  
Holland Cheng,<sup>4</sup> Li Xing,<sup>4</sup> and Kit S. Lam<sup>1\*</sup>

<sup>1</sup>Division of Hematology & Oncology, Department of Internal Medicine, UC Davis Cancer Center,

<sup>2</sup>Division of Gynecologic Oncology, <sup>3</sup>Veterinarian School of Medicine,

<sup>4</sup>College of Biological Sciences, University of California Davis, CA 95817, U.S.A.

\*Corresponding author (Kit.Lam@ucdmc.ucdavis.edu)

### Introduction

Abraxane® and Doxil® are the first two nanotherapeutic agents approved by the FDA for cancer treatment. However, because of their relatively large sizes (130 and 150 nm, respectively), it is doubtful that they can penetrate deep inside the tumor mass [1]. Furthermore, they have a propensity to be trapped in the reticuloendothelial system (RES), liver, and lung [2,3]. To take full advantage of the enhanced permeability and retention effect (EPR) [4,5] and to ensure deep penetration of these nanotherapeutic agents into a tumor mass, the size of the nanoparticles needs to be smaller. We have recently developed novel biocompatible telodendrimers (PEG-block-dendritic oligomer of cholic acids) that can self-assemble, in the presence or absence of hydrophobic drug such as paclitaxel, into stable micelles (~50 nm). *In vivo* optical imaging studies in xenograft models demonstrated preferential uptake of the paclitaxel-loaded nanoparticles in tumor compared to normal organs. When decorated with cancer targeting ligands identified from the one-bead-one-compound (OBOC) combinatorial library methods, the drug-loaded nanoparticles were rapidly taken up by the target tumor cells causing cell death.

### Results and Discussion

Using Fmoc-chemistry, we have synthesized a number of amphiphilic polymers, comprised of a cluster of cholic acids (4 to 16) linked by a series of lysines and attached to one end of a linear polyethylene glycol chain (PEG, 2000-10,000 Dalton) (Table 1). PEG<sup>5k</sup>CA<sub>8</sub> is a representative telodendrimer and the structure is shown in Figure 1. Under aqueous condition, it self-assembles to form highly stable nanomicelles in a size of 21 nm. The proportional increase in the molecular weight of telodendrimers with the increasing number of cholic acids was observed with MALDI-TOF mass spectrometry analysis. The measured molecular weights by <sup>1</sup>H NMR were also almost identical to the theoretical molecular weights of the telodendrimers (Table 1), indicating the well-defined structure of the telodendrimers. The

size of the final nanocarriers loaded with paclitaxel (15-150 nm in diameter) and their loading capacities are tunable depending on the size of the PEG chain and the number and arrangement of cholic acid molecules in the dendrimer (Table 1). Unlike Abraxane®, a paclitaxel-loaded human serum albumin nanoparticles (130 nm diameter), which aggregate in saline and serum

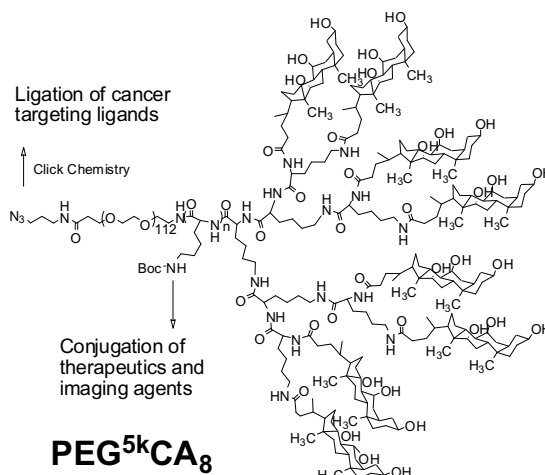


Fig. 1. Chemical structure of the representative telodendrimer (PEG<sup>5k</sup>CA<sub>8</sub>).

over time, our paclitaxel-loaded nanomicelles are highly stable in normal saline and 50% serum. We can readily load hydrophobic drugs, radionuclides, and fluorochromes, as well as quantum dots, and iron nanoparticles into the hydrophobic core of these nanomicelles. We have also compared the therapeutic efficacy and toxicity profile of our paclitaxel-loaded nanomicelles with the two FDA approved formulations of paclitaxel (Taxol® and Abraxane®) in nude mice bearing ovarian cancer xenograft, and determined that the nanomicelles had superior anti-tumor activity and toxicity profile. Using near infra-red optical imaging techniques, we were able to show that nanomicelles smaller than 64 nm preferentially targeted xenografts with great efficiency and with low liver and lung uptake (Figure 2), whereas those nanomicelles at 154 nm targeted the tumor poorly but with very high liver and lung uptake (data is not shown).

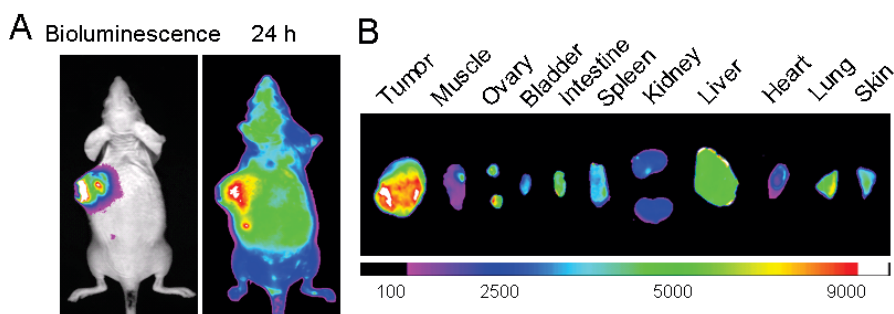
*Table 1. The physical properties of telodendrimers with different PEG chain length, number of cholic acids and lipophilic molecules*

<i>Telodendrimers</i>	<i>M<sub>w</sub></i> ( <i>theo.</i> )	<i>M<sub>w</sub></i> <sup><i>a</i></sup> ( <i>MS</i> )	<i>M<sub>w</sub></i> <sup><i>b</i></sup> ( <i>NMR</i> )	<i>CMC</i> ( $\mu$ <i>M</i> ) <sup><i>c</i></sup>	<i>Size</i> (nm) <sup><i>d</i></sup>	<i>Size with</i> <i>PTX</i> (nm) <sup><i>d</i></sup>	<i>PTX</i> <sup><i>e</i></sup> (mg/mL)
PEG <sup>2k</sup> -CA <sub>4</sub>	3914	4105	4511	7.9	11.5	15	5.2
PEG <sup>3k</sup> -CA <sub>4</sub>	5250	5606	5251	12.5	15	141	5.6
PEG <sup>5k</sup> -CA <sub>4</sub>	6644	6313	6082	67	10	131	2.3
PEG <sup>2k</sup> -CA <sub>8</sub>	5986	5985	6127	1.3	302/6000	96/348/1863	N/D
PEG <sup>3k</sup> -CA <sub>8</sub>	7322	7624	8025	5.9	20	58	4.7
PEG <sup>5k</sup> -CA <sub>8</sub>	8716	8814	8805	5.3	21	61	7.3
PEG <sup>10k</sup> -CA <sub>16</sub>	8172	N/D	N/D	0.97	42.7/2163	102/602/2435	0.6

<sup>*a*</sup> Obtained via MALDI-TOF MS analysis, -cyano-hydroxyl-cinnamic acid as a matrix compound.

<sup>*b*</sup> Obtained via <sup>1</sup>H NMR method. The molecular weight was calculated based on the ratio of proton signals of the methyl groups on cholic acid to the proton signals from PEG in the <sup>1</sup>H NMR spectra.

<sup>*c*</sup> CMC was measured by fluorescence spectrometry using pyrene ( $2 \times 10^{-6}$  M) as a probe; <sup>*d*</sup> Measured by dynamic light scattering particle sizer (Nanotrac®); <sup>*e*</sup> PTX loading, in the presence of 20 mg/mL of telodendrimers, were measured by HPLC after passing through an 0.22  $\mu$ m filter. N/D means not detectable.



*Fig. 2. In vivo and ex vivo NIR optical imaging. (A) Left: Bioluminescence signal of the athymic nude mice bearing SKOV3-luc ovarian cancer xenograft; right: In vivo NIR fluorescence images of the same mouse was obtained with Kodak imaging system 24 hr after i.v. injection of PEG<sup>3k</sup>-CA<sub>8</sub> NP co-loaded with hydrophobic dye (DID) and paclitaxel. (B) Ex vivo NIR image of dissected organs and tumor was obtained at 24 h after i.v. injection. Tumor exhibited strong NIR fluorescence intensity, whereas the fluorescence signal in normal organs and tissues was low. (Color version available on CD.)*

This nanoplatform is multifunctional and highly versatile. We can also conjugate cancer-targeting peptides to the distal end of the telodendrimer such that these peptides will be displayed on the surface of the final drug-loaded nanoparticles. When decorated with cancer targeting ligands identified from the OBOC combinatorial library methods, the drug-loaded

nanoparticles were rapidly taken up by the target tumor cells causing cell death. These ligands include LLP2A [6], OA02 [7], LXY3 [8] and LXW7 which target the  $\alpha 4\beta 1$ ,  $\alpha 3\beta 1$ ,  $\alpha 3\beta 1$ , and  $\alpha v\beta 3$  integrins, respectively. *In vitro* cellular uptake of FITC-labeled OA02-PEG-<sup>5k</sup>CA<sub>8</sub> (ligand-conjugated) was observed to be more significant compared with the unconjugated micelles (Figure 3). *In vivo* near infra-red optical imaging studies with hydrophobic fluorescent dye demonstrated that xenograft uptake of the nanomicelles was greatly enhanced by the cancer targeting peptide. Confocal microscopy revealed that the targeted nanomicelles, unlike the naked nanomicelles, were distributed throughout the entire tumor mass and not just at the perivascular space (data is not shown).

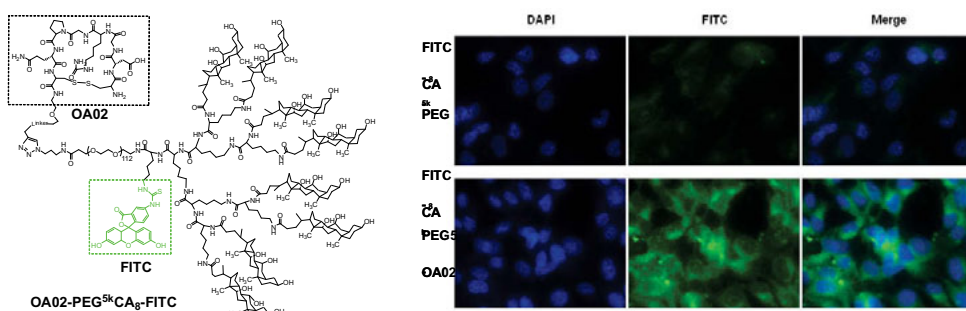


Fig. 3. (A) Chemical structure of FITC-labeled telodendrimer conjugated to OA02 ovarian cancer targeting ligand. (B) Fluorescent microscopy of FITC-labeled paclitaxel-loaded nanoparticles with or without decoration with OA02, the ovarian cancer targeting ligand. It is evident that the tumor targeting ligand greatly facilitates the uptake of the nanoparticle into the SKOV3 ovarian cancer cells. OA02 is related to LXY3, a ligand against  $\alpha_3\beta_1$  integrin.

In addition to paclitaxel, we have also successfully loaded SN-38, etoposide, doxorubicin and vincristine into these nanocarriers with high efficiency. This novel nanoplatfrom, in conjunction with cell surface targeting ligands, shows great promise in future cancer therapy and imaging. In addition, it could also be exploited as a highly efficient intracellular delivery tool for basic research.

## Acknowledgments

The authors thank the financial support from NIH grants U19CA113298, R21CA128501, and RO1CA115483.

## References

1. Unezaki, S., et al. *International Journal of Pharmaceutics* **144**, 11-17 (1996).
2. Oku, N. *Adv. Drug Deliv. Rev.* **40**, 63-73 (1999).
3. Senior, J.H. *Crit. Rev. Ther. Drug Carrier Syst.* **3**, 123-193 (1987).
4. Maeda, H. *Adv. Enzyme Regul.* **41**, 189-207 (2001).
5. Jain, R.K. *Cancer Metastasis Rev.* **9**, 253-266 (1990).
6. Peng, L., et al. *Nat. Chem. Biol.* **2**, 381-389 (2006).
7. Aina, O.H., Marik, J., Gandour-Edwards, R., Lam, K.S. *Mol. Imaging* **4**, 439-447 (2005).
8. Yao, N., et al. *J. Med. Chem.* **52**, 126-133 (2008).

## Development of One-Bead Two-Compounds Technology for the Identification of Cell Surface Acting Functional Ligands

Yan Wang, Yoshiko Maeda, Ming Zhu, Xiaobing Wang,  
 Pappanaicken R. Kumaresan,<sup>\*</sup> and Kit S. Lam<sup>\*</sup>

Division of Hematology & Oncology, Department of Internal Medicine, UC Davis Cancer Center,  
 University of California, Davis, Sacramento, CA 95817, U.S.A.; <sup>\*</sup>Corresponding Authors  
 (Kit.Lam@ucdmc.ucdavis.edu, Pappanaicken.Kumaresan@ucdmc.ucdavis.edu)

### Introduction

The one-bead-one-compound (OBOC) combinatorial technology [1] allows one to efficiently generate thousands to millions of chemical entities on tiny beads (100 microns), such that each bead displays  $10^{13}$  copies of only one chemical entity. In the last decade, we have successfully used this enabling technology to identify targeting ligands against specific cell surface receptors [2,3] or intracellular proteins. We have modified the OBOC method to a one-bead-two-compounds (OBTC) cell-based screening strategy which enables easy identification of cell surface acting functional molecules. In the OBTC library, every bead has two compounds on its outer layer: (i) a known adhesion ligand for cell binding and (ii) a random library compound constructed with “split-mix” synthesis technique [1]. Screening methods for OBTC libraries to identify cell surface acting signaling ligands are relatively simple, inexpensive, robust and can be easily adapted to academic laboratories.

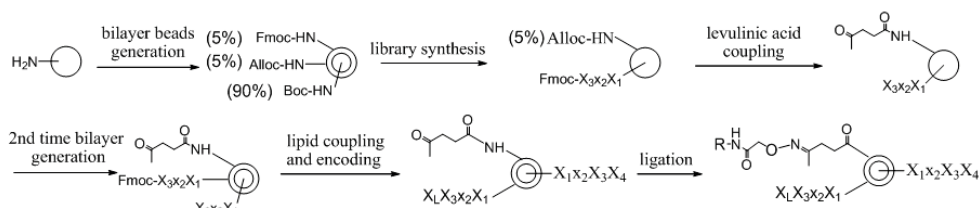


Fig. 1. Synthetic scheme of an OBTC combinatorial library using topographically segregated bilayer beads. R: known cell adhesion ligand, in this case LLP2A, against Jurkat T-lymphoma cell;  $X_1$ : lipid building blocks;  $X_4$ : amino acids which encode lipids.

### Results and Discussion

**One-bead two-compounds concept:** Meldal et al first reported the use of an OBTC strategy to identify specific protease inhibitors through screening bead libraries with each bead displaying a random library compound and a fixed fluorescence quench substrate [4,5]. We have exploited this concept by developing cell-based screening methods that allow us to identify cell-surface acting molecules which induce specific cell signaling. In our OBTC method, topographically segregated bilayer beads were generated with the outer layer displaying both a cell specific adhesion ligand and a random combinatorial library compound, and an inner layer with a coding tag. Under this configuration, when mixed with living cells, each library bead will be coated with a monolayer of cells, and the many receptors displayed on the outer surface of the cell membrane will be placed in close proximity to the tethered library compounds. Using this strategy, we synthesized two OBTC combinatorial libraries: a random hexamer peptide library and a lipo-tripeptide library, both of which displayed LLP2A as the peptidomimetic cell adhesion ligand against activated  $\alpha 4 \beta 1$  integrin of malignant lymphoma cells (Figure 1). The OBTC libraries were screened for bioactive ligands that trigger specific cell functions such as proliferation, necrosis, apoptosis and specific tyrosine phosphorylation of signaling proteins.

**Screening for pro-apoptotic, anti-proliferative and cell signaling activating ligands:** Fluorescence quenched caspase-3 substrates (D2R) and propidium iodide were used as probes to detect cells that undergo early or late apoptosis, respectively. For example, after 72 hours of incubation, Jurkat lymphoma cell coated OBTC hexapeptide library beads were stained with propidium iodide (1  $\mu\text{g/mL}$ ). Beads coated with apoptotic cells (fluorescent red, Figure 2) were



isolated for Edman microsequencing. Using this method, six hexapeptides were identified, some of which were able to induce apoptosis when added in solution form to Jurkat lymphoma cells.

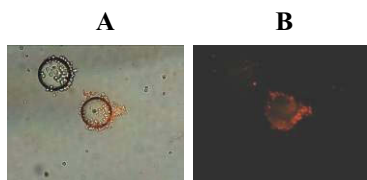


Fig. 2. Screening for pro-apoptotic beads: Jurkat cells were incubated with OBTC library for 3 days and propidium iodide staining was then performed. (A) Under the white field two beads were shown to cover with cells but only one was found to induce apoptosis. (B) Fluorescent micrograph of the propidium iodide stained cells covering the positive bead.

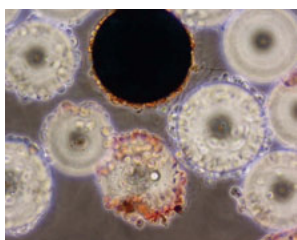


Fig. 3. The use of immunohistochemistry to screen OBTC library with Jurkat lymphoma cells for cell surface acting hexapeptides that activate JNK. One positive bead covered with brown colored cells, indicating JNK activation (tyrosine phosphorylation) was detected in this field. The rest of the beads were also coated with cells but no JNK activation was detected. The positive control bead (stained by charcoal) was coated with cells that underwent JNK activation. (Color version of the figure available on the CD.)

**Screening OBTC libraries for specific cell signaling with immunohistochemistry:** Beads coated with cells that undergo specific cell signaling can be easily identified with antibodies against specific phosphorylated intracellular signaling proteins. After incubation with living cells, the bead library was treated briefly with formaldehyde, permeated with non-ionic detergent, and stained with specific antibodies such as anti-phospho-JNK antibody-horse radish peroxidase conjugate. Upon addition of colorimetric substrate, cells that underwent JNK phosphorylation turned brown (Figure 3). Since numerous antibodies against various forms of cell signaling proteins are commercially available, this ultra-high-throughput immunohistochemical screening strategy will allow rapid discovery of cell surface acting molecules that trigger specific cell signaling pathways of interest.

## Acknowledgments

This study is supported by funds from NIH-R01CA115483, DOD-CML064046 and Children's Miracle Network of UC Davis Health System.

## References

1. Lam, K.S., et al. *Nature* **354**, 82-84 (1991).
2. Aina, O.H., et al. *Mol. Pharm.* **4**(5), 631-51 (2007).
3. Li, P., et al. *Nature Chem. Biol.* **2**(7), 381-389 (2006).
4. Meldal, M., et al. *Biopolymers* **66**, 93-100 (2002).
5. Meldal, M., et al. *Curr. Opin. Chem. Biol.* **8**, 238-244 (2004).

## Identification of Peptide Substrate Preference for Tyrosylprotein Sulfotranferases

Chao-Yu Chen,<sup>1</sup> Hsing-Jien Kung,<sup>2</sup> and Kit S. Lam<sup>1</sup>

<sup>1</sup>Division of Hematology and Oncology, <sup>2</sup>Department of Internal Medicine, <sup>2</sup>Department of Biological Chemistry and Molecular Medicine, University of California Davis Cancer Center, 4501 X Street, Sacramento, CA 95817, U.S.A.

### Introduction

Protein tyrosine sulfation is a common post-translational protein modification in eukaryotic cells, catalyzed by tyrosylprotein sulfotransferase (TPST). It has been reported that almost 1% of the total protein tyrosine is sulfated in *Drosophila melanogaster* [1]. TPST1 and TPST2 are Golgi-membrane bound proteins and exist in many different tissues [2]. Protein tyrosine sulfation affects homeostasis, chemokine receptor functions, leukocyte adhesion and peptide bioactivities [3]. For example, the chemokine receptor CCR5 tyrosine sulfation is responsible for co-receptor binding to glycoprotein 120 (gp120) on HIV for its cell entry [4]. These observations indicate that protein tyrosine sulfation plays an important role in protein-protein interactions. Leary and her colleagues have developed elegant mass spectrometric methods to determine tyrosine sulfation sites of selected peptides and proteins [5]. However, experimental determination of protein sulfation sites at the proteomic level is challenging; only about 60 proteins have been confirmed to be sulfated. Here we report the use of one-bead-one-compound (OBOC) combinatorial peptide library method [6] to map the substrate specificities of TPSTs.

### Results and Discussion

A random OBOC heptapeptide library with a fixed tyrosine in the middle, XXXYXXX- PEGA bead (X=L-19 amino acids, Y=L-Tyrosine), was synthesized by using the "split and mix synthesis" method [6]. 10<sup>5</sup> beads were incubated with TPST1 or TPST2, isolated from culture supernatants of CHO-K1 cells transfected with TPST1-HPC4 or TPST2-HPC4, in the presence of PAPS as the sulfate donor (Figure 1). After 2 hr, the sulfated peptide beads were identified with a 2 step image subtraction screening method [7] using anti-sulfotyrosine antibody and BCIP substrate to colorize the background beads in the first step, followed by incubation with anti-sulfotyrosine antibody and anti-mouse antibody-alkaline phosphatase conjugate in the second step. The beads were then immobilized in 1% agarose, the image of the plate was then captured prior to the addition of BCIP. Beads that turned turquoise color after 2 hr incubation with BCIP in the second step were the true-positive beads and isolated for automatic Edman microsequencing.

Based on the amino acid sequences of known sulfation sites, Rosenquist et al has developed software that allows one to predict sulfation sites on proteins [8]. Such sites contain at least 3 acidic residues within the -5 to +5 positions, and typically with an acidic residue at the -1 position. Although our OBOC heptapeptide library was designed to only scan -3 to +3 positions, the sulfation sites derived from the positive beads (Table 1) closely resemble those reported by Rosenquist but with some exceptions. First, almost all the 30 peptides shown in Table 1 have an acidic residue at the -1 position. Second, most of the peptide substrates are acidic with 5 acidic residues in 1 peptide, 4 acidic residues in 3 peptides, 3 acidic residues in 10 peptides, and 2 acidic residues in 14 peptides. There are 2 peptide substrates (WHEYPGM and YYMYPEP) identified for TPST1 that contain only 1 acidic residue and do not fit the general

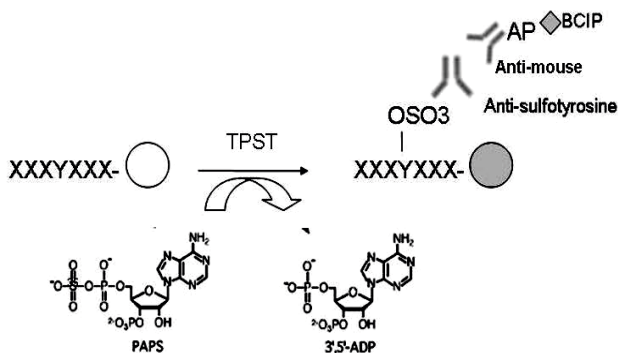


Fig. 1. Using anti-sulfotyrosine antibody to identify peptide substrate beads.

motif reported. Interestingly, 11 of the 30 peptides contain 2 or 3 tyrosine residues in their sequence. It is not clear at this time which of these tyrosines are sulfated. Data from Table 1 suggests that -DYD- is the preferred motif for TPST1, whereas, -DYX- is the preferred motif for TPST2.

Table 1. Peptide sequence of positive beads identified from OBOC library screening

TPST1													TPST2														
Y	Y	D	Y	D	G	Y	T	W	D	Y	G	D	V	E	L	D	Y	Y	W	T	F	D	D	Y	E	W	T
F	Y	D	Y	D	D	L	E	D	D	Y	D	D	K	F	G	D	Y	G	W	D	D	Y	A	Y	L	D	Y
F	F	D	Y	D	G	L	I	E	Y	Y	F	D	N	E	H	D	Y	D	E	W	V	Y	D	Y	E	F	V
H	L	D	Y	F	E	D	F	T	D	Y	F	D	A	D	Y	A	Y	A	D	A	N	D	E	Y	S	D	Y
E	E	D	Y	A	W	L	D	E	D	Y	D	W	S	W	G	D	Y	E	D	D	D	F	D	Y	G	D	H
W	Q	D	Y	D	V	D	W	H	E	Y	P	G	M	Y	F	D	Y	E	G	I	F	D	Y	Y	G	E	E
W	S	E	Y	D	Y	A	Y	Y	M	Y	P	E	P	W	A	D	Y	W	M	D	V	W	D	Y	T	D	D
H	D	Y	Y	D	V	P								I	F	D	Y	A	W	E							

Table 2. Previously identified sulfated proteins whose sequences are similar to the peptide substrates identified from OBOC library screening

Sequence	Matched protein	Description	Sequence matched
YYDYDGY	LUM_HUMAN	Lumican	1 YYDYD 5 20 YYDYD 24
VDYDEFV	LUM_HUMAN	Lumican	2 YDYEF 6 21 YDYDF 25
FFDYDGL	CCR2_HUMAN	Chemokine (C-C motif) receptor 2	1 FFDYD 5 23 FFDYD 27
DYAYLDY	SELPL_HUMAN	P-selectin glycoprotein ligand 1	1 YAYLDY 7 45 EYEYLDY 51
FDYYGEE	GP1BA_HUMAN	Platelet glycoprotein Ib alpha chain	1 FDYYGEE 7 292 YDYYPPEE 298
DEDYDWS	NID1_HUMAN	Nidogen 1	1 DEDYD 5 293 DEDYD 297

The OBOC combinatorial library method enables us not only to determine in a non-bias manner the substrate recognition elements by the TPST enzymes, but also predict potential sulfation sites of native proteins. Through searching the protein database with our identified sequences with NCBI BLAST [9], we discovered that 6 out of 30 peptides in Table 1 are either identical or very similar to the previously identified sulfation sites (Table 2).

In summary, we have demonstrated that the primary sequence of a short linear tyrosyl peptide is necessary and sufficient for TPST1 and TPST2 recognition, and that OBOC combinatorial library methods can be used to identify peptide substrates specific for these enzymes.

## Acknowledgments

We would like to thank Dr. K.L. Moore for the generous gift of CHO-K1 cells transfected with TPST1 or TPST2, Dr. G. Rosenquist for the stimulating discussion on the project, and financial support from NIH grant CA098116.

## References

- Baeuerle, P.A., Huttner, W.B. *J. Biol. Chem.* **260**, 6434-6439 (1985).
- Baeuerle, P.A., Huttner, W.B. *J. Cell Biol.* **105**, 2655-2664 (1987).
- Monigatti, F., Hekking, B., Steen, H. *Biochim. Biophys. Acta.* **1764**(12):1904-1913 (2006).
- Farzan, M., et al. *Cell* **96**, 667-676 (1999).
- Yu Y., Hoffhines, A.J., Moore, K.L., Leary, J.A. *Nat. Methods* **4**, 583-588 (2007).
- Lam, K.S., et al. *Nature* **354**, 82-84 (1991).
- Lehman, A., Gholami, S., Hahn, M., Lam, K.S. *J. Comb. Chem.* **8**, 562-570 (2006).
- Rosenquist, G.L., Nicholas, H.B., Jr. *Protein Sci.* **2**(2):215-222 (1993).
- Altschul, S.F., Gish, W., Miller, W., Myers, E.W., Lipman, D.J. *J. Mol. Biol.* **215**, 403-410 (1999).

## The Direct *In Vivo* Use of Mixture-Based Libraries in the Drug Discovery Process

Jay P. McLaughlin,<sup>1,2</sup> Andrew Heusser,<sup>2</sup> Kate J. Reilley,<sup>1</sup>  
 Marc Giulianotti,<sup>1</sup> and Richard A. Houghten<sup>1</sup>

<sup>1</sup>Torrey Pines Institute for Molecular Studies, Port St. Lucie, FL 34987, U.S.A.; <sup>2</sup>Department of Psychology, Northeastern University, Boston, MA 02115, U.S.A.

### Introduction

Using a mixture-based synthetic combinatorial approach, libraries composed of tens of thousands to millions of different compounds have been produced in a fraction of the time and cost of equivalent individual compound arrays [1,2]. Two approaches have evolved over the past two decades to screen and evaluate the large numbers of compounds now available. These are: 1) the massive parallel screening of large individual compound arrays; and 2) the generation and screening of extremely large, focused mixture-based libraries. The first approach, testing individual compounds, has been successfully utilized for decades to identify useful therapeutics. However, while the use of this method is common in large pharmaceutical companies, it remains impractical for the majority of academic and small research organizations to screen such large numbers of samples. Additionally, the harsh reality is that many drug candidates resulting from combinatorial approaches lack desirable drug-like properties at later stages of testing, thereby suffering a high rate of attrition due to poor physicochemical properties [2].

To circumvent the limitations of existing screening methods, we sought to directly test samples from a mixture-based combinatorial library *in vivo* for analgesic properties, thereby simultaneously increasing the evaluation of compounds while decreasing the failure rate inherent in the traditional drug discovery process [2]. Previous screening of a library of 400 separate mixtures each of 132,000 hexapeptides by monitoring blood pressure and heart rate in rats and dogs [3] demonstrated the feasibility of this approach, identifying useful therapeutic candidates while simultaneously eliminating compounds with poor absorption, distribution,

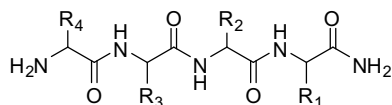


Fig.1. Core scaffold for the combinatorial tetrapeptide library. Scaffold is a tetrapeptide with an amide C-termini synthesized using standard Boc chemistry on mBHA resin.

metabolism and pharmacokinetic properties [3]. We hypothesized that direct *in vivo* antinociceptive screening would identify potentially useful analgesics from a mixture-based combinatorial library of tetrapeptides consisting of 7,311,616 compounds derived from the substitution of 52 different Boc-amino acids at each of the four positions of a core scaffold (Figure 1). Notably, these samples included the high affinity, high potency mu opioid receptor (MOR) agonists DALDA and Dmt-DALDA [4,5]. As MOR agonists are useful therapeutics

Table 1. List of examined samples from combinatorial tetrapeptide library

Sample	R4	R3	R2	R1
DALDA	L-Tyr	D-Arg	L-Phe	L-Lys
Dmt-DALDA	L-(2,6)-dimethyl-Tyr	D-Arg	L-Phe	L-Lys
1575-1	L-Tyr	X	X	X
1575-3	L-(2,6)-dimethyl-Tyr	X	X	X
1702-2	L-Tyr	D-Arg	X	X
1702-4	L-(2,6)-dimethyl-Tyr	D-Arg	X	X
1826-269	L-Tyr	D-Arg	L-Phe	X
1826-270	L-(2,6)-dimethyl-Tyr	D-Arg	L-Phe	X

"X" refers to an equal molar mixture of 52-Boc-amino acids. Therefore, sample 1702-2 contains an approximately equal molar mix of 2704 (52x52) tetrapeptides.

for the treatment of pain [6], we used these structures as comparative standards to prove the validity of our *in vivo* screening of library samples for novel analgesics. Specifically, this preliminary study sought experimental proof of the hypothesis by testing *in vivo* a series of samples from the mixture-based combinatorial library that became progressively more defined as the active compounds, DALDA and Dmt-DALDA (Table 1).

## Results and Discussion

Six mixture-based samples from this library progressively based on the structures of DALDA and Dmt-DALDA (Table 1) were evaluated in this study, along with morphine and Dmt-DALDA as positive controls, using C57Bl/6J mice in the 55°C warm-water tail-withdrawal assay [7]. Following intraperitoneal (i.p.) administration, antinociception was measured repeatedly up to 24 hr later. Morphine produced antinociception up to 2 hr, but Dmt-DALDA produced a dose-dependent analgesia up to 24 hr later (Figure 2A). Mixture samples from the combinatorial library fixed at the R4, N-termini position (1575-1, Figure 2B, and 1575-3, Figure 2C) also produced significant, if less potent, dose-dependent antinociception lasting up to 5 hr. Importantly, mixture samples fixed at the R4 and R3 position with amino acids corresponding to the structures of DALDA (1702-2, Figure 3A) and Dmt-DALDA (1702-4, Figure 3B) resulted in a progressively more robust, longer-lasting antinociception. This increase in analgesic potency was further improved with additional samples fixed at the R4, R3 and R2 positions with amino acids corresponding to DALDA and Dmt-DALDA (1826-269 and 1826-270, respectively, Figure 3C). Notably, the antinociception produced by 1575-1 and 1702-4 was determined to be mediated by activation of opioid receptors, as pre-treatment with the opioid receptor antagonist naloxone blocked the analgesic effects (triangles, Figures 2B and 3B, respectively).

In conclusion, the data suggests a correlation of increasing antinociceptive potency with the progressive definition of the mixture-based samples as they approach the

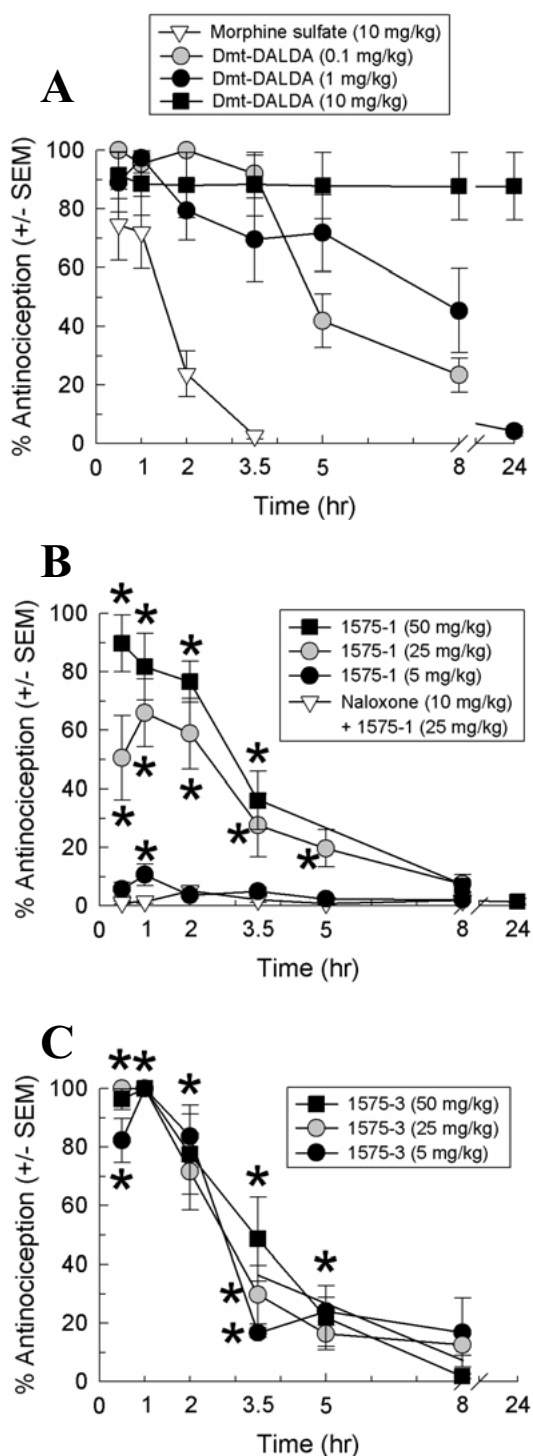


Fig. 2. Dose- and time-dependent antinociception. **A:** MOR agonists morphine and Dmt-DALDA; **B:** 1575-1; **C:** 1575-3. \* = sig. diff. ( $p < 0.05$ ) from baseline response.

structures of the comparative MOR agonists, DALDA and Dmt-DALDA. These findings demonstrate that direct *in vivo* testing of mixture-based library samples can identify analgesics of varying potency, and supports the validity of this approach for screening the library for additional novel analgesic compounds. Moreover, the potency of the tetrapeptide library samples screened here promises potentially valuable lead compounds for future development, a set of studies which are currently underway in our laboratories.

## Acknowledgments

This research was supported by grants from NIH-NIDA (R21-DA019620, to RAH) and by the State of Florida, Executive Office of the Governor's Office of Tourism, Trade, and Economic Development.

## References

1. Houghten, R.A., Pinilla, C., Giulianotti, M.A., Appel, J.R., Dooley, C.T., Nefzi, A., Osteresh, J.M., Yu, Y., Maggiora, G.M., Medina-Franco, J.L., Brunner, D., Schneider, J. *J. Comb. Chem.* **10**, 3-19 (2007).
2. Carroll, F.I., Houghten, R.A. *Neuropsychopharmacology* **34**, 251-252 (2009).
3. Houghten, R.A. *Methods Companion Methods Enzymol.* **6**, 354-360 (1994).
4. Schiller, P.W., Nguyen, T.M., Berezowska, I., Dupuis, S., Weltrowska, G., Chung, N.N., Lemieux, C. *Eur. J. Med. Chem.* **35**, 895-901 (2000).
5. Shimoyama, M., Shimoyama, N., Zhao, G.M., Schiller, P.W., Szeto, H.H. *J. Pharmacol. Exp. Ther.* **297**, 364-371, 2001.
6. Gutstein, H., Akil, H., Opioid analgesics. In *Goodman and Gilman's The Pharmacological Basis of Therapeutics*, 10<sup>th</sup> edition. McGraw-Hill, New York, 2001.
7. McLaughlin, J.P., Hill, K.H., Jiang, Q., Sebastian, A., Archer, S., Bidlack, J.M. *J. Pharmacol. Exp. Ther.* **289**, 304-311 (1999).

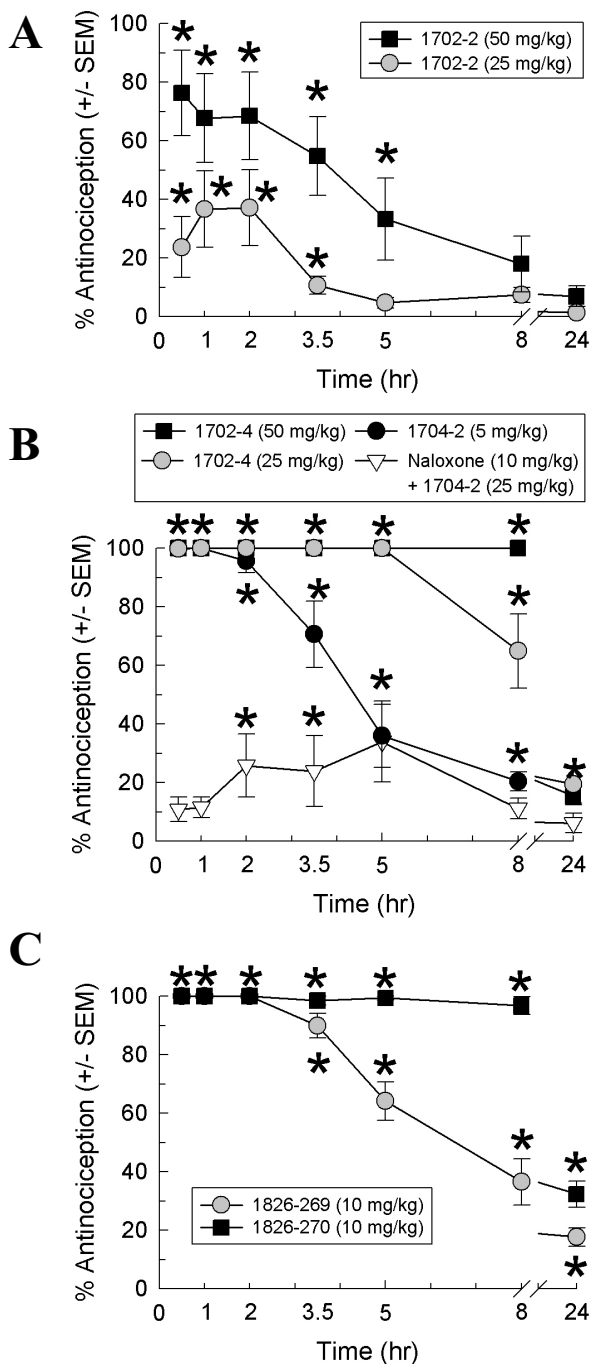


Fig. 3. Dose- and time-dependent antinociception. **A:** 1702-2; **B:** 1702-4; **C:** 1826-269 and 1826-270. \* = sig. diff. ( $p < 0.05$ ) from baseline response.

# Identification of Inhibitors of Protein-Protein Interactions Through the Screening of Simplified Combinatorial Peptide Libraries

**Pasqualina L. Scognamiglio,<sup>1,2</sup> Nunzianna Doti,<sup>3</sup> Carlo Pedone,<sup>2</sup>  
 Paolo Grieco,<sup>1</sup> Marco Sabatella,<sup>3</sup> Menotti Ruvo,<sup>3</sup> and Daniela Marasco<sup>2,3</sup>**

<sup>1</sup>Dept. of Pharmaceutical and Toxicological Chemistry, University of Studies of Naples "Federico II", Via Montesano 49, Naples, Italy; <sup>2</sup>Dept. of Biological Sciences, University of Studies of Naples "Federico II", via Mezzocannone, 16, 80134, Naples, Italy; <sup>3</sup>IBB-CNR, Via Mezzocannone 16, 80134, Naples, Italy.

## Introduction

In the field of drug discovery through the combinatorial preparation and HTS of arrays of compounds, peptide libraries play a pivotal role for the rapid identification of high- or medium-affinity target ligands that can be subsequently optimized in terms of potency, selectivity and stability [1]. Our novel approach is based on the use of simplified synthetic peptide libraries (SSPL) composed by a minimum number of non redundant amino acids for the assembly of short peptides. This approach offers the advantage of simplifying the synthesis and deconvolution of libraries and provides new active compounds with a molecular size similar to that of small molecules, to which they can be easily converted [2].

PED/PEA15 (Phosphoprotein Enriched in Diabetes/in Astrocytes) is an ubiquitously expressed protein regulating different biological processes and over-expressed in several tissues of a consistent population of individuals affected by type 2 diabetes. It has been observed that increasing PED/PEA15 abundance in human cell lines, favours its interaction with PLD1 (phospholipase D) and alters a downstream signaling that controls glucose transport [3]. Previous studies have demonstrated that the inhibition of PLD1/PED-PEA15 complex restores glucose transport in PED-PEA15-overexpressing cells, thereby validating this protein-protein interaction as an important target for type 2 diabetes [4].

## Results and Discussion

In order to find new antagonists for PLD1/PED-PEA15 interaction, we have prepared two simplified synthetic peptide libraries of general formula: (K or E)-G-G-X1-X2-X3-X4, whereby X indicates random residues and the two glycines are spacers for the charged residues. Employed building blocks were 12 different amino acids (instead of 20) selected preserving a wide distribution of hydrophobicity, charges, pKa, aromaticity (Table 1).

In our strategy libraries are generated in the Positional Scanning format, this allows to assay all the sub-libraries in one round of screening in which, each variable position is tested separately, permitting the selection of the most active sequence at the end. This format also provides a general applicability of these libraries to different targets. Assays are carried out in high throughput mode, with fully automated station for the handling and storage of samples, employing different assays based on several techniques (FRET, Chemiluminescence, Fluorescence, Absorbance, Surface Plasmon Resonance). In particular the identification of

*Table1. Selection of the building blocks for a simplified synthetic peptide library*

<i>Side Chain</i>	<i>Selected aa</i>
Basic	Arg
Acidic	Asp
Amide	Gln
Polar	Ser
Hydrophobic	Ala, Pro, Met
Aliphatic	Leu, Cys (Acm)
Hydrophobic, Polar, Aromatic	Tyr
Hydrophobic, Aromatic	Phe
Hydrophobic, Polar	His

Table 2. EC50 values of most active peptides selected from competitive ELISA screening of the interaction PED-PEA15/D4 $\alpha$

Peptide sequence	EC50 ( $\mu$ M)
EGGYPHY	79.2 $\pm$ 1.4
KGGSPFY	105.5 $\pm$ 1.6
KGGSPFQ	261.5 $\pm$ 1.4

inhibitors of protein-protein interaction is carried out by competition experiments, then direct binding experiments are developed in order to investigate the entity and the molecular basis of binding.

The search for inhibitors of the complex between PED/PEA-15 and a subdomain of PLD1 named D4 $\alpha$  [5] has been carried out through the screening of two peptide combinatorial libraries, having at their N-termini a charged residue, alternatively, positive and negative (Lys and Glu (library I and library II, respectively)), introduced in order to evaluate charge effects in this region and to enhance peptide solubility. Four positions were randomized providing an overall complexity of 12<sup>4</sup>=20736 divided, for PS format, in 48 sub-libraries each containing 1728 peptides. The first competitive screening allowed to selected: residue Ser for P1, Pro for P2, Phe for P3 and Tyr and Gln for P4 for the library I, while for library II residue Tyr for P1, Pro and Asp for P2, His for P3 and Tyr for P4. From all the possible combinations several single peptides were synthesized and analyzed by competitive ELISA, in particular dose-response competitive ELISAs carried out on them provided EC50 values in the high micromolar range, as reported in Table 2.

In conclusion, our combinatorial approach led to the selection of a consensus inhibitor sequence for PED/PEA-15/D4 $\alpha$ , indeed the selected residues for each position present similar chemical-physical features, in particular an H-bonding residue in position P1 (Ser, Tyr), a sterically hindered side chain in P2 (Pro) and aromatic groups at P3 (His, Phe) and P4 (Tyr). Further, the presence of different charged residues at the N-terminal position seem not crucially affect peptide recognition, even if EC50 values presented from this first generation of inhibitors are in the high micromolar range.

On this basis the ability of these peptides to inhibit the binding between the protein PED/PEA-15 and D4 $\alpha$  will investigate at molecular level, employing other techniques such as SPR and NMR. Deriving from these sequences, second generation peptides will be designed to enhance their biological activity and several of them will be submitted to cellular assays in lines overexpressing PED/PEA-15 to establish their ability to restore physiological conditions on glucose uptake.

## Acknowledgments

The technical assistance of Dr. Giuseppe Perretta is gratefully acknowledged. Supported by FIRB n RBRN07BMCT.

## References

1. Houghten, R.A., Wilson, D.B., Pinilla, C. *Drug Discovery Today* **5**(7), 276- 285 (2000).
2. Marasco, D., Perretta, G., Sabatella, M., Ruvo, M. *Curr. Protein Pept. Sci.* **9**(5):447-67 (2008).
3. Condorelli, G., Vigliotta, G., Trencia, A., Maitan, M.A., Caruso, M., Miele, C., Oriente, F., Santopietro, S., Formisano, P., Beguinot, F. *Diabetes* **50**, 1244-1252 (2001).
4. Viparelli, F., Cassese, A., Doti, N., Paturzo, F., Marasco, D., Dathan, N.A., Monti, S.M., Basile, G., Ungaro, P., Sabatella, M., Miele, C., Teperino, R., Consiglio, E., Pedone, C., Beguinot, F., Formisano, P., Ruvo, M. *J. Biol. Chem.* **283**, 21769-21778 (2008).
5. Doti, N., Cassese, A., Marasco, D., Monti, S.M., Viparelli, F., Dathan, N.A., Paturzo, F., Miele, C., Beguinot, F., Formisano, P., Ruvo, M., *submitted*.



## 3-Nitro-Tyrosine as a Quencher of OBOC Autofluorescence

Jared Townsend, Babak Sanii, Alan Lehman, Andrew Do, and Kit S. Lam\*

Div. of Hematology & Oncology, UC Davis Cancer Center, Univ. of California Davis, CA 95817, U.S.A.

### Introduction

One-bead-one-compound (OBOC) combinatorial libraries have been used to identify a diverse range of ligands against a broad spectrum of biological targets [1]. Many screening methods have been developed: e.g. enzyme-linked colorimetric assays and fluorescent assays for protein binding, fluorescent-quench assays and radioactive assays for protease and kinase substrates respectively, and whole cell binding assays. In principle, the use of fluorescent-tagged target proteins as probes to screen OBOC libraries could permit highly efficient automated screening via high speed fluorescent-activated bead sorting. However, such assays are limited by strong autofluorescence emission (AFEM) due to the intrinsic properties of the bead resin, the covalently attached library compound, as well as residual coupling reagents from chemical synthesis. AFEM increases false positive frequency, decreases sensitivity, and renders automated screening techniques highly impractical. Previous studies have described methods by which one can theoretically circumvent the AFEM dilemma by restricting the screening process to the use of high-intensity probes with minimal fluorescence emission (FEM) overlap with the substrate and/or by secondary analysis of the probe binding characteristics at the bead surface [2-4]. Nonetheless, a method that enables one to lower the AFEM of the resin/compound across a broad range of the quantum spectra would greatly enhance the versatility and compatibility of fluorescent-based screening of OBOC libraries. 3-Nitro-tyrosine [Y(NO<sub>2</sub>)], has previously been characterized as an efficient energy acceptor pair in FRET techniques and has been used extensively in protein characterization [5]. We show here that the addition of Y(NO<sub>2</sub>) to the interior of TentaGel (TG) bead resin (Rapp Polymere) in a topologically segregated fashion [6] dramatically reduces the AFEM of both the bead resin as well as the covalently attached random peptide library. This modification to the screening process greatly enhances the sensitivity and efficiency of performing fluorescent-based screens using OBOC libraries. By dramatically reducing AFEM we demonstrate the potential this modification presents to automated high-throughput fluorescent-based OBOC screening.

### Results and Discussion

Spectral scans were obtained using a confocal microscope (405 nm  $i_{ex}$ ). These scans were performed on a random sampling of blank TG beads and TG beads with interior-coupled (95%) Y(NO<sub>2</sub>) [Y(NO<sub>2</sub>)-TG].

The resulting spatially resolved spectra obtained exhibited the characteristic AFEM for TG between the 420 nm to 600 nm (Figure 1a) [4]. The levels of AFEM were even more pronounced with the addition of a random 5-mer peptide (XXXXX-TG) (Figure 1c). The spectra obtained for the internally quenched TG beads had near indistinguishable levels of fluorescence across the analysis spectrum compared to background emission (Figure 1b).

Furthermore, the addition of Y(NO<sub>2</sub>) to 95% of the interior of beads displaying 5-mer natural amino acid peptide-bead library [XXXXX-Y(NO<sub>2</sub>)-TG] dramatically reduced the AFEM detected across the wavelengths analyzed (Figure 1d). The reduction in AFEM intensity can also be seen in the fluorescent photomicrographs in Figure 2.

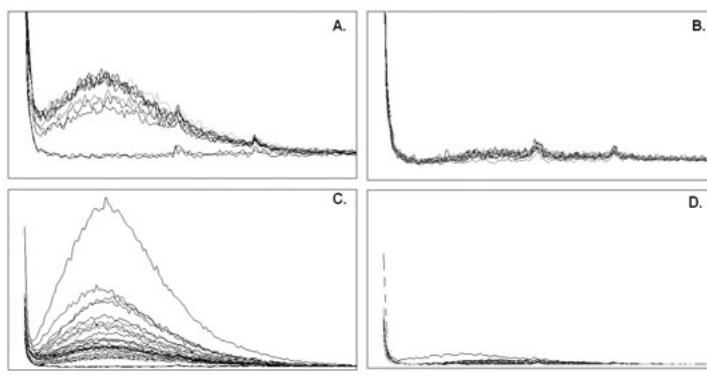


Fig. 1. Fluorescence emission intensity ( $y$ ) vs.  $\lambda(x)$  plots from TG resin.

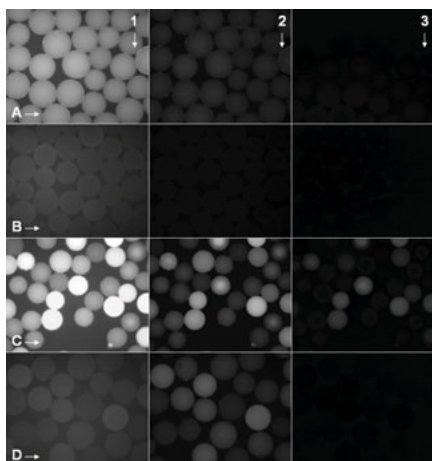


Fig. 2. Fluorescence photomicrographs of quenched and unquenched TG resin.

nm  $\lambda_{em}$ ) 2. “green” ( $535 \pm 20$  nm  $\lambda_{em}$ ) and 3. “red” ( $585 \pm 20$  nm  $\lambda_{em}$ ) range photomultiplier tubes (PMT). Biotinylated beads were incubated with STVD-conjugated fluorescent probes (1. Alexa Fluor® 405, 2. Qdot® 525, and 3. Qdot® 585) and mixed with equal amounts of unlabeled beads. The presence of Y(NO<sub>2</sub>) on the bead interior permitted concise separation of labeled and unlabeled

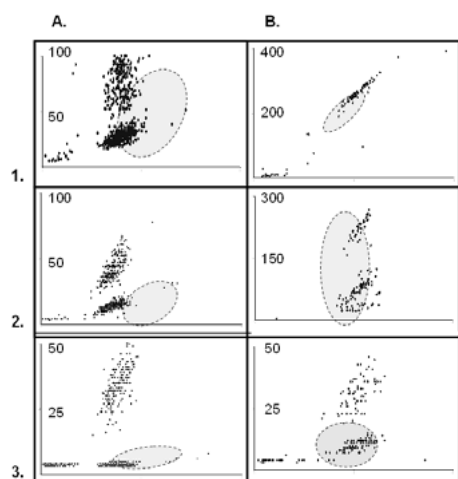


Fig. 3. Fluorescence emission (y) vs. TOF (x) plots of TG.

TG (A), Y(NO<sub>2</sub>)-TG (B), XXXXX-TG (C) and XXXXX-Y(NO<sub>2</sub>)-TG (D) were imaged using 3 filter sets [(1.  $\lambda_{ex}$  330-385;  $\lambda_{em}$  420+), (2.  $\lambda_{ex}$  437, 501;  $\lambda_{em}$  475, 545), and (3.  $\lambda_{ex}$  360;  $\lambda_{em}$  590+), to determine the quenching capacity of Y(NO<sub>2</sub>) at multiple  $\lambda_{ex}$  /  $\lambda_{em}$  settings.

Fluorescent-based automated flow sorting of bead-bound combinatorial libraries such as the Complex Object Parametric Analyzer and Sorter (COPAS) (Union Biometrica) greatly enhances the high-throughput capabilities of the OBOC combinatorial method. However, the AFEM dilemma reduces the feasibility and versatility of utilizing this platform. Figure 3 is comprised of a series of TOF (x) vs. FEM (y) plots compiled by data obtained from COPAS analysis. These plots depict quenched (A) and unquenched (B) populations of biotinylated TG beads as well as observed data point acquisition regions of quenched (A) and unquenched (B) pentapeptide libraries (shown in gray) excited with UV laser diode ( $375$  nm  $\lambda_{ex}$ ) and detected through 1. “blue” ( $420 \pm 10$  nm  $\lambda_{em}$ ) 2. “green” ( $535 \pm 20$  nm  $\lambda_{em}$ ) and 3. “red” ( $585 \pm 20$  nm  $\lambda_{em}$ ) range photomultiplier tubes (PMT). Substantial overlap was observed between labeled biotinylated beads and unlabeled libraries when detected through “blue” range PMT. While no library overlap was observed for unquenched beads detected through “red” range PMT, quenched populations afforded increased separation of bound and unbound bead states.

## Conclusions

Due to AFEM, the feasibility and functionality of performing high-throughput combinatorial solid-state screening is limited. Accordingly, there exists the need to circumvent the problems that arise when dealing with the AFEM properties of both the solid state resin and attached target. Consequently, quenching properties of Y(NO<sub>2</sub>) greatly enhance the versatility and functionality of the OBOC combinatorial approach.

## Acknowledgments

This work was supported by NIH R01CA098116, R01CA115483, and R21CA128501.

## References

1. Lam, K.S., et al. *Nature* **354**, 82-84 (1991).
2. Kodadek, T., Bachhawat-Sikder, K. *Mol. Biosyst.* **2** (1), 25-35 (2006).
3. Marani, M.M., et al. *J. Comb. Chem.* **11**(1), 146-150 (2009).
4. Olivos, H.J., Bachhawat-Sikder, K., Kodadek, T. *ChemBiochem.* **4**(11), 1242-5 (2003).
5. Meldal, M., Breddam, K. *Anal. Biochem.* **195**, 141-147 (1991).
6. Liu, R., et al. *QSAR Comb. Sci.* **24**(10), 1127 – 1140 (2005).

## Macrocyclic Peptide-Peptoid Hybrids Designed as PPII Helix Mimetics

Fa Liu,<sup>1</sup> Andrew G. Stephen,<sup>2</sup> Abdul A. Waheed,<sup>3</sup> Eric O. Freed,<sup>3</sup>  
 Robert J. Fisher,<sup>2</sup> and Terrence R. Burke,<sup>1</sup>

<sup>1</sup>Laboratory of Medicinal Chemistry, CCR, NCI-Frederick, NIH, Frederick, MD 21702, U.S.A.; <sup>2</sup>Protein Chemistry Laboratory, SAIC-Frederick, Inc. Frederick, MD 21702, U.S.A.; and <sup>3</sup>HIV Drug Resistance Program, CCR, NCI-Frederick, NIH, Frederick, MD 21702, U.S.A.

### Introduction

HIV-1 budding represents a potentially promising yet under-exploited target for new anti-HIV-1 therapeutics. The UEV (ubiquitin E2 variant) domain of the human protein Tsg101 (tumor susceptibility gene 101) facilitates viral budding through recruitment by the Gag p6 protein, a major structural component of HIV-1 [1]. We had previously improved the Tsg101-binding affinity of p6-derived peptoid-peptide hybrids by applying hydrazone and hydrazide chemistries [2]. We had also reported a promising oxime-based post solid-phase diversification approach to peptide library construction [3,4]. However, the peptide mimetics resulting from this earlier work showed poor cellular uptake. Furthermore, conjugation of ligands with antennapedia and HIV-Tat (48-60)-derived membrane carrier peptides, seriously disrupted binding affinity. Published NMR solution studies of the interaction between the p6-derived "wild-type" (WT) 9-mer peptide, P<sup>1</sup>E<sup>2</sup>P<sup>3</sup>T<sup>4</sup>A<sup>5</sup>P<sup>6</sup>P<sup>7</sup>E<sup>8</sup>E<sup>9</sup> and Tsg101, indicated that the key "A<sup>5</sup>P<sup>6</sup>" dipeptide region binds to Tsg101 in a PPII helix-like conformation [5]. In the current study, ring-closing metathesis (RCM) macrocyclization strategies were applied to a parent Tsg101-binding peptide to investigate effects on conformational stabilization and Tsg101-binding affinity and bioavailability. This study is of particular interest because it provides new insights into the use of RCM macrocyclization to stabilize PPII helix conformations. Since the overall macrocycle ring size and the insertion locations of the alkenyl chains needed to produce the most effective binding conformations were not known at the outset, an empirical "scanning" approach to macrocycle design was taken. This involved situating the needed ring-closing *N*-alkenylglycine residues within the N-terminal and C-terminal "P<sup>1</sup>E<sup>2</sup>" and "E<sup>8</sup>E<sup>9</sup>" sequences, respectively. In this fashion RCM macrocyclization would occur with maintenance of the critical "P<sup>3</sup>T<sup>4</sup>A<sup>5</sup>P<sup>6</sup>" recognition region. By employing a range of chain lengths in the *N*-alkenyl side chains, four series of macrocycles (**1-4**) were constructed that varied in ring size and location of ring-closing junctions (Figure 1).

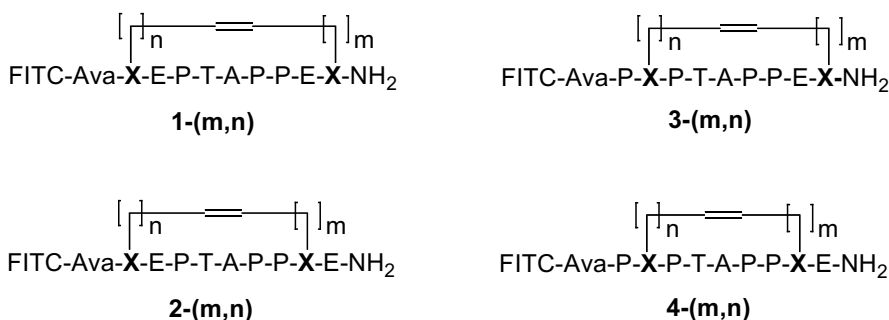


Fig. 1. Macrocyclic Tsg101-derived ligands prepared in the current study: X = *N*-substituted glycine.

### Results and Discussion

The synthesis of macrocycles **1-4** was achieved using standard Fmoc-based solid-phase protocols. The precursor open-chain peptides **5** were built up on the NovaSyn<sup>®</sup> TGR resin and amino-terminally acylated with an *N*-Fmoc 5-aminovaleic acid (*N*-Fmoc Ava) group.

Macrocyclizations of intermediates **5** were conducted on the resin at room temperature in CH<sub>2</sub>Cl<sub>2</sub> using Hoveyda-Grubbs 2<sup>nd</sup> generation catalyst. The *N*-Fmoc Ava groups were then deprotected and the peptides were acylated using fluorescein isothiocyanate (FITC). Cleavage of the peptides from the resin (TFA) followed by HPLC purification provided final macrocycles (Figure 2).

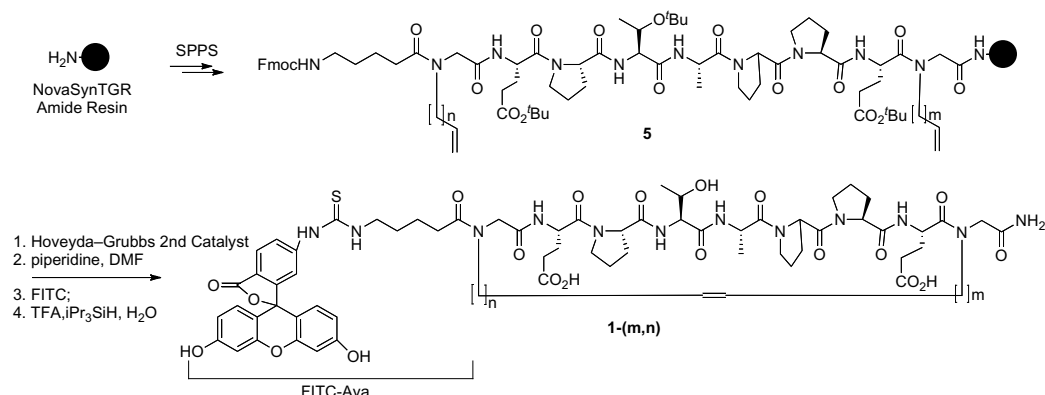


Fig. 2. Solid-phase synthesis of macrocyclic Tsg101-based ligands.

In order to explore a variety of binding conformations, four series of macrocycles were prepared as defined by the locations of the ring-closing segments (Figure 1). For each series, the ring-closing alkenyl chains varied in length to provide a total of 11 gradually expanding macrocycles, with overall ring sizes from 23 to 39 members. In this fashion, in excess of 50 macrocyclic peptide-peptoid hybrids were prepared. Stabilization of left-handed PPII helix conformations was evident for members of series **2** and **4** macrocycles as indicated by CD spectral data. Unexpectedly, series **2** and **4** macrocycles that showed the greatest degree of PPII helix stabilization, also exhibited significantly diminished Tsg101-binding affinities. In contrast, series **1** and **3** macrocycles that displayed helicities similar to those of the WT 9-mer peptide showed higher affinities. It was also found that macrocycles showing greater PPII helix character exhibited enhanced resistance to protease digestion. The best cellular uptakes were shown by macrocycles with larger ring sizes. Compared to the WT 9-mer peptide, peptide-peptoid hybrid **1-(6,6)**, with a total ring size of 39 members, showed the best combination of Tsg101-binding affinity ( $K_d = 19 \mu\text{M}$ , 3-fold enhancement) and cellular uptake (4.5 fold enhancement). Work is in progress to evaluate the antiviral efficacy in whole cell systems of macrocycles such as **1-(6,6)**.

## Acknowledgments

This Work was supported in part by the Intramural Research Program of the NIH, Center for Cancer Research, NCI-Frederick and the National Cancer Institute, National Institutes of Health, under contract HHSN261200800001E. The content of this publication does not necessarily reflect the views or policies of the Department of Health and Human Services, nor does mention of trade names, commercial products, or organizations imply endorsement by the U.S. Government.

## References

1. Freed, E.O. *Trends Microbiol.* **11**(2), 56-59 (2003).
2. Liu, F., Stephen, A.G., Adamson, C.S., Gousset, K., Aman, M.J., Freed, E.O., Fisher, R.J., Burke, T.R., Jr. *Org. Lett.* **8**, 5165-5168 (2006).
3. Liu, F., Stephen, A.G., Waheed, A.A., Aman, M.J., Freed, E.O., Fisher, R.J., Burke, T.R., Jr. *Chembiochem* **9**, 2000-2004 (2008).
4. Liu, F., Stephen, A.G., Fisher, R.J., Burke, T.R., Jr. *Bioorg. Med. Chem. Lett.* **18**, 1096-1101 (2008).
5. Pornillos, O., Alam, S.L., Davis, D.R., Sundquist, W.I. *Nature Struct. Biol.* **9**, 812-817 (2002).

## Application of Oxime-Based Post Solid-Phase Diversification to Optimization of Polo Box Domain-Binding Peptides

Fa Liu,<sup>1</sup> Jung-Eun Park,<sup>2</sup> Shilpa R. Shenoy,<sup>3</sup> Nak-Kyun Soung,<sup>2</sup>  
James B. McMahon,<sup>4</sup> Kyung S. Lee,<sup>2</sup> and Terrence R. Burke, Jr.<sup>1</sup>

<sup>1</sup>Laboratory of Medicinal Chemistry, CCR, NCI-Frederick, NIH, Frederick, MD 21702, U.S.A.;

<sup>2</sup>Laboratory of Metabolism, CCR, NCI, NIH, Bethesda, MD 20892, U.S.A.; <sup>3</sup>Molecular Targets Development Program, SAIC-Frederick, Inc., Frederick, MD 21702, U.S.A. and <sup>4</sup>Molecular Targets Development Program, CCR, NCI-Frederick, NIH, Bethesda, MD 20892, U.S.A.

### Introduction

Peptides modeled on consensus recognition sequences provide valuable starting points for the development of protein-protein binding inhibitors. We have recently incorporated aminooxy handles into consensus recognition sequences and used these for post-solid phase construction of libraries bearing tethered components. These libraries can be easily assembled and directly evaluated without intermediate purification. We have previously reported the application of this approach to the discovery of TSG101-directed HIV-1 budding antagonists [1]. The current study applies this technique to an entirely unrelated system. Over-expression of the serine/threonine polo-like kinase 1 (Plk1) is tightly associated with oncogenesis in several human cancers [2]. Interference with Plk1 function induces apoptosis in tumor cells but not in normal cells. Accordingly, Plk1 is a potentially attractive anti-cancer chemotherapeutic target. Plk1 possesses a unique phosphopeptide-binding "polo box domain" (PBD) that is essential for its intracellular localization and mitotic functions. Unlike kinase domains, PBDs are found only in the four members of Plks. Therefore, they represent ideal targets for selectively inhibiting the function of Plks. By examining various PBD-binding phosphopeptides, we previously found that a 5-mer phosphopeptide "PLHSpT" (**1**, Figure 1) specifically interacts with the Plk1 PBD with high affinity, whereas it fails to significantly interact with the PBDs of two closely-related kinases, Plk2 and Plk3 [3]. The crystal structure of the 5-mer peptide bound to the Plk1 PBD has also recently been solved. This structure shows that the *N*-terminal Pro residue, which is critical for high affinity and specificity, binds in a pocket formed by two aromatic amino acids, Trp414 and Phe535 [3]. The current report describes our use of oxime-based post solid-phase diversification to optimize binding interactions originating from this Pro residue.

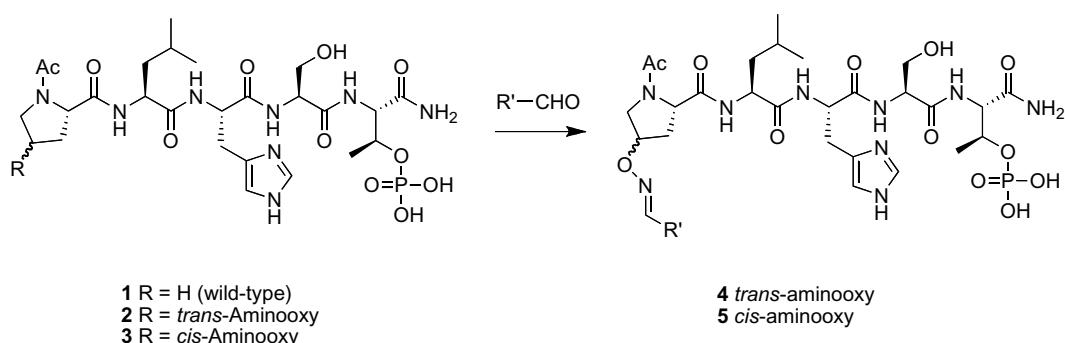


Fig. 1. PBD-binding peptide libraries obtained by diversification of an *N*-terminal aminooxy-containing Pro residue.

### Results and Discussion

Oxime-containing peptide libraries were prepared by conjugating parent peptides **2** and **3** with a collection of aldehydes (Figure 1). Without purification, the resulting oxime peptide libraries (**4** and **5**) were directly evaluated for PBD binding affinity in an ELISA-based competition assay

using an immobilized PLHSpT-containing peptide (**1**) and cell lysates expressing a recombinant full-length Plk1 [3]. Certain of the oxime peptides (**4** and **5**) exhibited enhanced PBD-binding affinity as compared to the wild-type 5-mer sequence (**1**). Further PBD binding experiments were also conducted using isothermal titration calorimetry (ITC). These latter experiments confirmed the earlier data from the ELISA-based competition binding assays. ITC data indicated that relative to the wild-type peptide (**1**), certain oxime peptides **4** and **5** exhibit more enthalpically-driven binding with Plk1 PBD. However, these advantages are also accompanied by large entropic penalties. This could potentially indicate that further binding enhancement may be achieved by induction of conformational constraint.

## Acknowledgments

This Work was supported by the Intramural Research Program of the NIH, Center for Cancer Research, NCI-Frederick and the National Cancer Institute, National Institutes of Health. This work was funded in part by HHSN261200800001E. The content of this publication does not necessarily reflect the views or policies of the Department of Health and Human Services, nor does mention of trade names, commercial products, or organizations imply endorsement by the U.S. Government.

## References

1. Liu, F., Stephen, A.G., Waheed, A.A., Aman, M.J., Freed, E.O., Fisher, R.J., Burke, T.R., Jr. *Chembiochem* **9**, 2000-2004 (2008).
2. Strebhardt, K., Ullrich, A. *Nat. Rev. Cancer* **6**(4), 321-330 (2006).
3. Yun, S-M., Moulaei, T., Lim, D., Bang, J.K., Shenoy, S.R., Park, J-E., Liu, F., Kang, Y.H., Liao, C., Soung, N-K., Lee, S., Yoon, D-Y., Lim, Y., Lee, D-H., Otaka, A., Appella, E., McMahon, J.B., Nicklaus, M.C., Burke, T.R., Jr., Yaffe, M.B., Wlodawer, A., Lee, K.S. *Nat. Struct. Mol. Biol.* **16**(18), 876-882 (2009).

## A Novel Biochip System Focusing on Protein Detection by the Use of Labeled Glycopeptides Arrayed on a Novel Chip-material

Kiyoshi Nokihara,<sup>1</sup> Takayasu Kawasaki,<sup>1</sup> Akiyoshi Hirata,<sup>1</sup>  
 Yasushi Takebayashi,<sup>2</sup> Yasuo Oka,<sup>2</sup> and Takafumi Ohyama<sup>1</sup>

<sup>1</sup>HiPep Laboratories, Kyoto, 602-8158, Japan, <sup>2</sup>Nippon Light Metal Company, Ltd.,  
 Shizuoka 421-3291, Japan

### Introduction

The major goal of biochips is their use for rapid and economical characterization of biological samples. We have devoted considerable effort to the development of practical bio-detection systems. Most of protein-chips, in which proteins (antibodies) are immobilized as capture molecules, are impractical especially with regard to their stability. We have proposed a novel biochip-concept for a protein detection system involving labeled structured peptides as capture molecules that are arrayed on the chip surface. Visualization of interactions is not in a "one to one" manner, but as bar-code like patterns with fluorescent intensities generating "protein fingerprints", while the protein-protein interaction can be mimicked by a protein-peptide interaction [reviewed in 1]. Peptide array has greater potential, as even after drying immobilized peptides recognized analytes in a dose dependent manner [2]. Important factors for peptide micro-arrays are the construction of peptide libraries, the use of chip materials with a suitable surface chemistry, the deposition of peptide solutions by an arrayer, detection and data mining. In practice our system has been shown to discriminate the structures of a number of different proteins. As several toxic proteins, such as *Ricinus communis* agglutinin (RCA), cholera toxin, staphylococcal enterotoxin B, and *Pseudomonas aeruginosa* lectin (PA-I) recognize cell-surface carbohydrates of the host cells, these carbohydrate-binding species with protein-structure recognition may be applied for detection. The present paper describes the construction of glycopeptide libraries in addition to fluorescently labeled structured peptides ( $\alpha$ -helical,  $\beta$ -loop and  $\beta$ -strand) and the development of the novel chip-material made from amorphous carbon with a special surface chemistry. The loading amounts on this amino-carbon plate were calculated ca 4 pmol/mm<sup>2</sup> [3]. This novel microarray, designated PepTenChip<sup>®</sup>, satisfies all the requirements for protein detection, specificity, reproducibility, sensitivity, easy handling, stability (storage/transport) and production economics.

### Results and Discussion

Peracetylated glucose, mannose, galactose and lactose were successfully attached to the hydroxyl group of Fmoc-Thr in good yields using BF<sub>3</sub>OEt<sub>2</sub>-mediated glycosylation and resulting Thr-building blocks were manually incorporated into the automatically assembled peptide chains and further elongated by the synthesizer to generate protected glycopeptidyl resins. Their diversity arises from the use of four different glycosides, their position and number (one or two) in addition to the backbone amino acid sequence. The architecture of the present glycopeptides is shown in Figure 1. After deacetylation with hydrazine hydrate, fluorescent dye (TAMRA) was incorporated at the N- $\alpha$ -amino group and then cleaved. The desired glycopeptides were purified by preparative HPLC and characterized by LCMS. CD spectra indicated that the sugar moieties did not significantly influence their secondary structures. Thus, a total number of ca 100 O-glycosylated peptides have been successfully prepared by the improved SPPS [4]. The Ac<sup>m</sup> group of the Cys residue was removed with silver trifluoromethanesulfonate in a mixture of TFA/anisole just before arraying. The peptide (350 picoLiter, ca. 2.1 femtomole) was immobilized on the chip-surface through N- $\epsilon$ -maleimido-

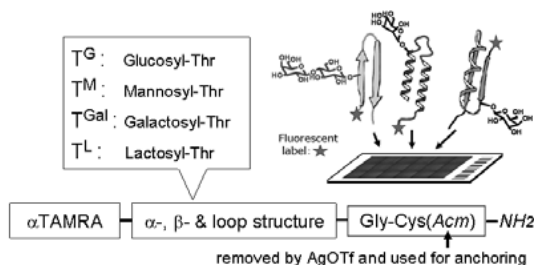


Fig. 1. Architecture of present glycopeptides.

caproic acid to form a ca 100 micron spot on the above PepTenChip® by a Piezorray™. The prepared amorphous carbon plates were chemically inert, not self-fluorescent, easily manufactured by laser drawing, and mechanically stable. The surface chemistry we have developed produces extremely low background and non-specific adsorption, uniform distribution of functional groups on the plate surface and a much higher concentration on the surface than conventional materials, thereby making immobilization much easier. The toxic protein solutions (RCA from Vector lab. and PA-I from Sigma) were added onto this array and the fluorescent responses were measured. The experiments were performed twice and the peptides that showed reproducible responses were picked out for fingerprint imaging (Figure 2.).

One of the most important issues in bio-chips for protein detection is quantitative analysis. Bio-detection of toxicant proteins has been achieved by application of *O*-glycopeptides libraries as capture molecules. Significant differences have been observed in the responses against RCA and PA-I. The fluorescent changes ( $\Delta I/I_0$ ) of the  $\alpha$ -helical peptides (19, 21, 22, and 23) are decreased against RCA upon increasing the concentration, in contrast they increased against PA-I. The  $\beta$ -sheet peptides (30, 41, 42, and 52) responded more strongly against RCA than against PA-I. The results reflect differential recognition between RCA and PA-I, due to different sugar-side chains and the secondary structures of the backbone peptide sequences. As is well known RCA and PA-I have affinities for galactose (peptides: 21, 22, 23) and lactose (peptides 52), hence the proteins should bind to these carbohydrates in the glycopeptides. In contrast, peptides 19, 30, 41, and 42 have mannosyl residues, which should be recognized by lectins in a non-specific manner. The response was dose dependent and fingerprints have been generated. In fact, assays using microtiter plates require larger amounts of capture molecules and analytes. At the present the optimized amounts of arrayed peptides on a chip was 9 femtomoles and toxic protein as an analyte was ca 20 ng. The assay has also been performed in the presence of 2% milk to simulate practical conditions, hence the range of fluorescence changes ( $\Delta I/I_0$ ) in milk solution was within - 0.3 ~ +0.3. These results suggested that glycopeptide arrays show promising applications as a toxin detection tool.

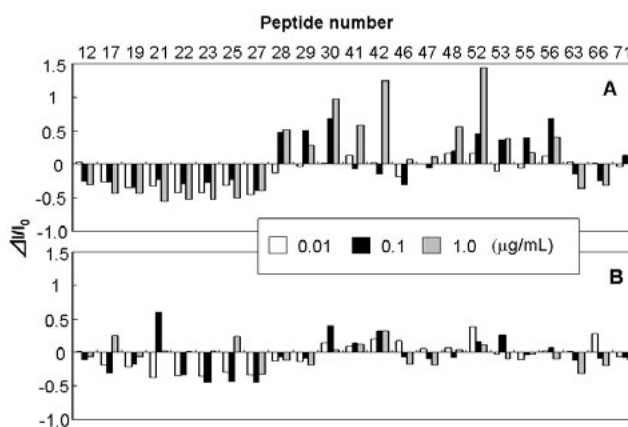


Fig. 2. The fluorescent responses and their fingerprints of toxic proteins (A: RCA, B: PA-I) using selected glycopeptides. Each protein in PBS was added to the array at three different concentrations. Peptides 27 and 53 are non glycosylated (controls).

## Acknowledgments

Supported by grants, the Bio-VB R&D Support Project of Okinawa Prefecture (MIC, Japan), the Bio-Venture Project (NEDO/METI, Japan) and the Research and Development Program for New Bio-industry Initiatives (BRAIN/NARO, Japan).

## References

1. Nokihara, K., Ohyama, T., Usui, K., Yonemura, K., Takahashi, M., Mihara, H. in *Solid-Phase Synthesis and Combinatorial Chemical Libraries*, Epton, R.(Ed) Mayflower Scientific, UK, 2004, p. 83-88.
2. Usui, K., Tomizaki, K., Ohyama, T., Nokihara, K., Mihara, H. *Mol. BioSyst.* **2**, 113-121 (2006).
3. Nokihara, K., Hirata, A., Takebayashi, Y., Ohyama, T., Kawasaki, T., Miyazato, N., Kodama, Y., Ono, N., Sogon, T., Suzuki, K., Miyajima, M., Kawahira, N., Oka, Y. in *Peptide Science 2008*, Nomizu, M. (Ed) Japanese Peptide Society, 2009, p 95-98.
4. Kawasaki, T., Miyajima, M., Kawahira, N., Hirata, A., Ohyama, T., Nokihara, K. in *Peptides 2008*, Lankinen, H. (Ed.) Finnish Peptide Society, 2008, p 184-185.





**Peptide Therapeutics and Bioactive Substances**  
**Peptide Antibiotics and Natural Products**  
**Peptides and Immunity**  
**Peptides and Membrane Proteins**  
**Peptides as Diagnostics, Probes, and Biomarkers**



## **Peptides as Drugs: Re-examination Perceived Wisdom in Drug Design**

**Victor J. Hruby**

*Department of Chemistry and Biochemistry, University of Arizona, Tucson, AZ 85721, U.S.A.*

### **Introduction**

The development of safe and effective drugs always has been a challenge. Indeed most drugs have LD<sub>50</sub>'s, and many have additional toxicities. Many small molecular scaffolds which possess "drug-like" properties have inherent toxicities and their uses are coupled with the development of tolerance. It is increasingly evident that the "classical" approach to drug design is limiting, and in general these drugs do not address the problems of treating most of our major diseases (prolonged and neuropathic pain, diabetes, cancer, heart disease, etc.) but only their symptoms. A new paradigm for drug design and development is needed, and given the lessons we are learning from comparative genomics and proteomics of normal vs. disease states, drug design and development will require new approaches. From this perspective, peptides offer many advantages. Currently there are over 40 peptide drugs on the market and many additional peptide mimetics; about 270 peptides are in various phases of clinical trials, and over 400 peptides are in advanced preclinical studies [1]. Among the advantages of peptides are: 1) non-toxic scaffold; 2) remarkable chemical landscape; 3) easily modified for proteolytic stability; 4) inherent manipulation for bioavailability; and 5) readily designed to cross the blood brain barrier and other barriers. Here we will re-examine perceived wisdom regarding peptide drug design, with special emphasis on those common beliefs that are wrong, and provide an illustrative example of the design of a family of multivalent peptide ligands that may treat prolonged and neuropathic pain states that currently have no effective treatment.

It is interesting that in going from unicellular to multicellular life, especially animal life, most "small molecule chemistry" was dropped, probably due to their inherent toxicities. Instead amino acids, amino acid derivatives and peptides were chosen for intercellular communication. We should learn from Mother Nature! Despite the ubiquitous use of peptides for intracellular communication and maintenance of homeostasis, there is perceived wisdom that peptides have poor pharmacokinetic and pharmacodynamic properties. Of course many do, and were designed by Nature that way. But many do not, and Nature uses various chemical approaches to enhance these properties. We should learn from Mother Nature! Similarly perceived wisdom is that peptides do not cross the BBB. There are many solutions to this problem including: 1) stabilization of 3-D conformations, e.g.  $\alpha$  helix or  $\beta$ -turns; 2) N-methylation; 3) glycopeptides; 4) amphipathic peptides; 5) cell penetrating peptides; and 6) pegylation etc.

### **Results and Discussion**

***New Paradigms for Drugs Discovery Using Peptides:*** A key observation from genomics and proteomics is that disease states such as chronic pain, cancer, addiction, CNS diseases, diabetes etc. involve changes in gene expression. Drug design should consider these system level adaptations which involve increased complexity and more than one target. Advantage can be taken of these changes in drug design (e.g. 2, 3). We will illustrate the use of peptides for design of novel ligands that utilize this new paradigm for drug design and discovery, with an example of novel drugs for pain states for which there is no current treatment methods.

Though there generally are good drugs for the treatment of acute pain, treatment of prolonged pain states leads to many problems including: 1) high levels of toxicity; 2) low levels of efficacy; and 3) system changes leading to more pain during prolonged use, etc. This is particularly the case for neuropathic pain states such as hyperalgesia and allodynia.

Table 1. Structure of design peptides with potent mu and delta opioid receptor agonist activities and potent NK-1 receptor antagonist activities

TY005	H-Tyr-D-Ala-Gly-Phe-Met-Pro-Leu-Trp-0-3:5'- Bn(CF <sub>3</sub> ) <sub>2</sub>
TY027	H-Tyr-D-Ala-Gly-Phe-Met-Pro-Leu-Trp-NH-3:5'-Bn(CF <sub>3</sub> ) <sub>2</sub>
TY025	H-Tyr-D-Ala-Gly-Phe-Met-Pro-Leu-Trp-NH-BN

In these cases, our most potent analgesics such as opioids are ineffective. There is much evidence that in these pain states, in ascending and descending pain pathways, there is up regulation of neuropeptides and their receptors that can cause pain (e.g. substance P and the neurokinin-1 receptor). Treatment attempts with e.g. morphine leads to up-regulation of neurotransmitters and their receptors in pain pathways that can cause more pain. Based on these and other observations, we hypothesized that the design of a ligand with delta and mu opioid receptor agonist activity, and selective NK1 receptor antagonist activity would provide a ligand that was efficacious in neuropathic pain states and in prolonged pain, where morphine has very little effect. Designing multiple pharmacophores in one molecule that would have a single metabolism, enhanced proximity effects due to multivalent activity, and greatly enhanced efficacy *in vivo* is our goal.

The design involved placing the pharmacophore for the delta/mu ligand at the N-terminal and the pharmacophore for the NK-1R at the C-terminal with an intervening address residue(s) between the two pharmacophores such as in H-Tyr-D-Ala-Gly-Phe-Met-Pro-Leu-Trp-0-3,5'-Bn(CF<sub>3</sub>)<sub>2</sub> (TY005, Table 1) which was a nanomolar agonist at  $\mu$  and  $\delta$  opioid receptors and a nanomolar antagonist at the neurokinin-1 receptor [4] and has potent *in vivo* antinociceptive activities. However, when examined for stability in serum it was found that the ester functionality was readily hydrolyzed. For this reason we modified the structure at the N-terminal to an amide to give analogues such as TY027 and TY025 (Table 1).

These compounds had superior binding affinities, and second messenger activities as agonists at  $\delta$  and  $\mu$  receptors, and especially in the NK-1 receptor binding assay [5]. Most importantly they have  $T_{1/2}$ 's, in serum of 5 hours or more compared to the  $T_{1/2}$ 's of 1 minute for the ester derivatives. Based on BBB penetration studies *in vivo*, and antinociception assays following i.v. administration, the amide compounds crossed the blood brain barrier (BBB) well. Ordinarily such linear peptides are not expected to cross the BBB well. So why do these cross well? To examine this question we evaluated the conformations of the peptides in aqueous solution and in the presence of lipid micelles using NMR methods. In aqueous solution these peptides showed no secondary structure, but they showed well defined helix or  $\beta$ -turn structures in the presence of lipid micelles [6]. We suggest that the ready formation of a helical structure or successive  $\beta$ -turn structures in the presence of lipids provides these peptides with the three - dimensional structural features to cross the BBB.

We have begun extensive studies of the *in vivo* biological properties of TY005 and TY027 using a variety of experimental models of pain. A summary of the results of these studies for TY005 are given in Table 2. In acute antinociceptive experiments TY005 was found to have potent antinociceptive effects. The SNL rat model was used for neuropathic pain. In the anti-allodynic and antihyperalgesic assays in SNL rats, TY005 was a potent analgesic (Table 2), whereas in the same model morphine has only minor or no antinociceptive effects. An undesirable side effect of morphine is its impairment of motor skills. TY005 was tested at high doses, and it did not impair motor skills of rats in the Rotarod test (Table 2). These results suggest that many of the undesirable side effects of opioid may not obtain for this novel class of ligands. A hallmark of long term administration of opioids is the development of tolerance. In our studies to date we have found that these new ligands do not develop tolerance. These very exciting results suggest that these novel class of ligands will be especially useful for treatment of long-term neuropathic without the development of tolerance.

Table 2. Summary of some *in vivo* activities of trifunctional opioid receptor agonist, NK-1 receptor antagonist activities of TY005\*

A	Potent Though Short Lived Antinociceptive Effects in Naïve Rats (acute pain model)
B	Potent – Short Lived Anti-allodynic Effects in SNL Rats
C	Potent – Short Lived Anti-hyperalgesic Effects in SNL Rats
D	No Impaired Performance in Rotarod Test
E	No Development of Tolerance

\*administration either *i.t.* or *i.v.* with comparable results

## Concluding Remarks

The studies briefly discussed above clearly establish this new paradigm for drug design. Its hallmarks are: 1) consider the evolutionary changes that account for the development of the disease, and then use these findings for drug design; 2) target the changes that have resulted in disease while simultaneously targeting symptoms – design of ligands for multiple targets generally needed; and 3) consider efficacy, tolerance and toxicities as a part of the design. The trifunctional ligands we have discussed address all of these issues, and furthermore do not appear to have undesirable side effects such as sedation or motor impairment associated with current analgesics. Preliminary studies suggest that these compounds will have little or no addiction liabilities. Clearly there is still much to do and learn to enhance *in vivo* potency and efficacy, enhanced bioavailability, and develop smart drug delivery systems, but the peptides designed thus far have most of the desired properties for a drug.

Considering how evolution has increasingly utilized peptides for maintaining homeostasis in multicellular life we believe that peptides can be readily developed with all of the desired activities, distribution properties, low toxicities, and maximal efficacies of good drugs. We look forward to continued development and promotion of peptides as safe drugs.

## Acknowledgments

We thank our biological colleagues whose research has stimulated us to design ligands with novel biological properties, especially Frank Porreca, Henry Yamamura (deceased), Todd Vanderah and Josephine Lai, and their colleagues and students who did the *in vivo* assays. A special thanks to Takashi Yamamoto and Padma Nair who prepared and determined the structural properties of the compounds, and Tally Largent-Milnes who did most of the *in vivo* assays. This work was supported by grants from the U.S. Public Health Service, NIDA, P01 DA00284 and R01 DA13449.

## References

1. Marx, V. *Chem. & Eng. News* **83**(11), 17-24 (2005).
2. Hruby, V.J., Agnes, R.S., Davis, P., Ma, S.-W., Lee, Y.S., Vanderah, T.W., Lai, J., Porreca, F. *Life Sciences* **73**, 699-704 (2003).
3. Hruby, V.J., Porreca, F., Yamamura, H.I., Tollin, G., Agnes, R.S., Lee, Y.S., Cai, M., Alves, I., Cowell, S., Varga, E., Davis, P., Salamon, Z., Roeske, W., Vanderah, T.W., Lai, J. *Am. Assoc. Pharm. Sci. J.* **8**(3), E450-E460 (2006).
4. Yamamoto, T., Nair, P., Davis, P., Ma, S.-W., Navratilova, E., Moye, S., Tumati, S., Lai, J., Vanderah, T.W., Yamamura, H.I., Porreca, F., Hruby, V.J. *J. Med. Chem.* **50**, 2779-2786 (2007).
5. Yamamoto, T., Nair, P., Vagner, J., Largent-Milnes, T., Davis, P., Ma, S.-W., Navratilova, E., Moye, S., Tumati, S., Lai, J., Yamamura, H.I., Vanderah, T.W., Porreca, F., Hruby, V.J. *J. Med. Chem.* **51**, 1369-1376 (2008).
6. Yamamoto, T., Nair, P., Jacobsen, N.E., Davis, P., Ma, S.-W., Navratilova, E., Moye, S., Lai, J., Yamamura, H.I., Vanderah, T.W., Porreca, F., Hruby, V.J. *J. Med. Chem.* **51**, 6334-6347 (2008).

## **Regulatory Perspectives for Early Phase Development of Protein and Peptide Biotherapeutics**

**Robert G. Bell**

*Drug & Biotechnology Development, LLC, Clearwater, FL 33765, U.S.A.*

### **Introduction**

Developing meaningful Chemistry and Manufacturing Controls (CMC) specifications for early phase development of therapeutic proteins and peptides can be a difficult task. Many times, the scientist developing these specifications is limited by the amount of investigational product available to conduct the appropriate testing and the evolving manufacturing process. It is during this early development of the product that understanding of the critical specifications of the product's life-cycle begins to take form. Early product specifications should be based on the knowledge, experience and mechanistic understanding of the process and formulation factors on the product performance quality characteristics. The aspect of building quality into the process and products (quality by design) at this early stage assures that the appropriate identity, strength, quality, purity and potency of the product is achieved on a consistent basis. This ensures the safety, efficacy, product consistency and stability of the clinical supplies. As drug development proceeds from the pilot-scale to larger-scale production, the information on the active and finished product specifications submitted in the IND should be strengthened and refined. These early quality assessments lay the groundwork for the stability and release specifications for the FDA registration of therapeutic proteins and peptides.

### **Regulations Overview**

Early phase product development (Phase 0, Phase 1) of biopharmaceuticals must assure the safety and quality of the investigational new drug (IND) products. Current good manufacturing practices (CGMP) are required under section 501(a)(2)(B) of the Federal Food, Drug, and Cosmetic Act (FD&C Act) in the manufacture of most investigational new drugs (IND) used in phase 2 and 3 clinical trials [1]. However, phase 0 or 1 investigational drugs, which include proteins and peptides, are exempt from complying with 21 Codes of the Federal Registrar (CFR) part 211 [2] under 21 CFR 210.2(c). This does not except the sponsor from Good Scientific Practices and Principles, and interpreting and implementing CGMP consistent with good scientific practices and methodology. The Food and Drug Administration's (FDA) review of Phase 1 IND submissions will focus primarily on assessing the safety of Phase 1 clinical investigation ([21 CFR § 312.22(a)]). The amount of information that must be submitted in an IND to assure the accomplishments of the objectives of safety and quality have been met will depend upon such factors as the novelty of the product, the extent to which it has been studied previously, the known or suspected risks and the phase of development of the product ([21 CFR § 312.22(b)]). Although in each phase of the investigation sufficient information is required to be submitted to assure the proper identification, quality, purity, and strength of the investigational product, the amount of information needed to make that assurance will vary with the phase of the investigation, the dosage form, and the amount of information otherwise available ([21 CFR § 312.23 (a)(7)(i)]). Phase 2 and 3 investigational products are required to be manufactured in accordance with CGMPs. If not, the products are considered adulterated [501(a)(2)(B) FD&CA]. This applies to all components, raw materials, actives and final products.

It is the sponsor's responsibility, in all phase of development, to assure the safety and rights of subjects. Failure to comply can result clinical holds and termination. If human subjects are or would be exposed to an unreasonable and significant risk of illness or injury [21 CFR § 312.42 (b) (1) (i)] or the IND does not contain sufficient information required under 312.23 to assess the risks to subjects of the proposed studies, the clinical studies may be placed on "hold" (clinical hold [21 CFR § 312.42 (b) (1) (iv)]) or terminated (21 CFR § 312.44). A clinical hold is an order issued by FDA to the sponsor to delay a proposed clinical investigation or to suspend an ongoing investigation (21 CFR § 312.42(a)). Absent, inadequate or incomplete CMC information can lead to clinical holds. Examples of CMC deficiencies that could result in clinical holds include (a) incomplete description of the manufacturing process, (b) inadequate

information regarding animal-derived components, (c) incomplete information regarding source material and history, (d) lack of detailed testing procedures (active, in-process, final product), and (e) inadequate product release testing (assay, viral clearance, endotoxin, mycoplasma, sterility, stability, etc.). A clinical study can be terminated for CMC issues if the methods, facilities, and controls used for the manufacturing, processing, and packing of the investigational biologic are inadequate to establish and maintain appropriate standards of identity, strength, quality, and purity as needed for subject safety.

### **GMPs for Phase 1 Studies**

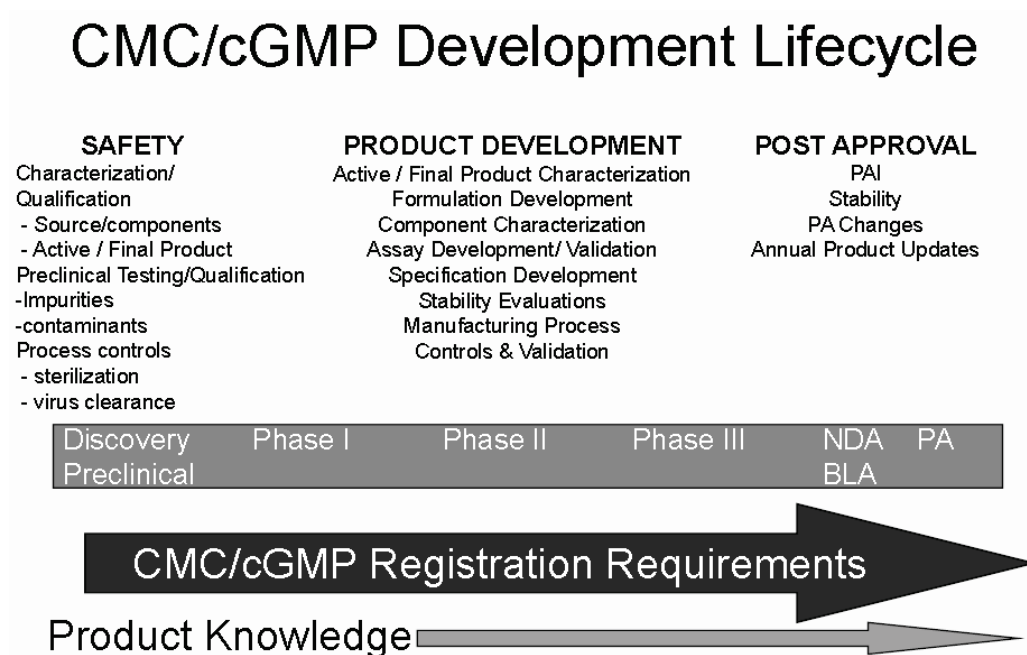
Adherence to GMPs during manufacture of phase 1 investigational drugs occurs mostly through well-defined written procedures, the use of adequately qualified equipment, controlled manufacturing environment, and accurately and consistently recorded data from manufacturing (including testing). The FDA issued July 2008 guidance for industry for CGMP for Phase 1 Investigational Drugs [3]. The guidance describes an approach sponsors may use to implement manufacturing controls that are appropriate for the phase 1 clinical trial stage of development. Sponsors are expected to implement manufacturing controls that reflect product history, knowledge and experiences gained during the evolving development process. The guidance recommends the sponsor have sufficient controls regarding the personnel, quality systems, facility, equipment, components, manufacturing records, laboratory controls, packaging, labeling and record keeping. The sponsor should assure that the personnel involved in the product development have the education, experience, and training (including quality) to enable each individual to perform their assigned function. The sponsor should establish a written plan that describes the role of and responsibilities for quality functions including release and testing of all components used in the manufacture of the investigational product. It is preferred to assign an individual to perform QC functions independent of manufacturing responsibilities, especially for the cumulative review and release of phase 1 investigational drug batches. The facility and equipment should be adequately qualified and calibrated. Typical categories of systems and equipment which require performance qualification include HVAC, room classification, autoclave, compressed air, depyrogenation oven, steam, lyophilizer, centrifuge, purified water, WFI, central vacuum, etc. Each IQ, OQ, and PQ protocol should provide the specific procedure to follow, information to be recorded, a set of acceptance criteria, and a list of materials, equipment and documents needed to perform the validation.

The components, containers and closures should have acceptance criteria, release testing and batch traceability. The sponsor should keep detailed manufacturing records (including microbiology) that details the materials, equipment, procedures used, and any problems encountered during manufacturing, including any change controls and out of specification (OOS) results. Additional assurances for sterile and aseptically processed products should be demonstrated and documented. Laboratory tests used in manufacture of the investigational product (e.g., testing of materials, in-process material, packaging, drug product) should be scientifically sound (e.g., specific, sensitive, and accurate), suitable and reliable to assess (and document) the identity, strength, potency, purity of the investigational product. Any methodology changes should be documented by change control. Early phase specifications should be based on clinical relevance, safety considerations, process capabilities, product development history and knowledge. Laboratory equipment should be qualified, calibrated and maintained. Clinical supplies should be adequately released and stability data generated. Adequate investigational samples and products should be retained. The sponsor should establish written procedures for controlling packaging, labeling, and distribution operations. The investigational product should be suitably packaged to protect it from alteration, contamination, and damage during storage, handling, and shipping. The sponsor should keep complete records relating to the quality and operation of the manufacturing processes, including but not limited to equipment maintenance and calibration, manufacturing records and related analytical test records, distribution records, quality functions, component records, deviations, investigations and complaints. Under 21 CFR § 312.57(c), sponsors must retain records for at least two years after a marketing application is approved for the drug, or if an application is not approved for the drug, until two years after shipment and delivery of the drug for investigational use is discontinued and FDA is notified.

In summary, GMP adherence applies to all clinical IND studies. This is consistent with good scientific practices and principles that are applicable to product quality development. It is important that the sponsor assess risks and take appropriate actions during early product



development. This is the beginnings of the product lifecycle and it is important to address and integrate product quality (quality by design). Documentation of early phase observations, processes and testing is critical to the success of the investigational product and product's lifecycle (Figure 1).



*Fig. 1. CMC / GMP development lifecycle.*

### References

1. Federal Food, Drug, and Cosmetic Act Section 501(a)(2)(B).
2. Codes of the Federal Registrar parts 210 and 211.
3. Guidance for Industry - CGMP for Phase 1 Investigational Drugs, U.S. Department of Health and Human Services, Food and Drug Administration, (July 2008).

## New Insight into the Binding Mode of Cyclic Melanocortin Ligands at the MC4 Receptor

Diego Brancaccio,<sup>1</sup> Alfonso Carotenuto,<sup>1</sup> Paolo Grieco,<sup>1</sup> Victor J. Hruby,<sup>2</sup>  
 and Ettore Novellino<sup>1</sup>

<sup>1</sup>Department of Pharmaceutical and Toxicological Chemistry, University of Naples, Naples, Italy; and

<sup>2</sup>Department of Chemistry, University of Arizona, Tucson, AZ 85721, U.S.A.

### Introduction

The melanocortin receptors are involved in many physiological functions, including pigmentation, sexual function, feeding behavior, and energy homeostasis, making them potential targets to treat obesity, sexual dysfunction, etc. [1]. Understanding the basis of the ligand-receptor interactions is crucial for the design of potent and selective ligands for these receptors.

Table 1. Sequences of the ligands

Peptide	Sequence
MTII	Ac – Nle <sup>4</sup> –c[Asp <sup>5</sup> – His <sup>6</sup> – <b>D</b> Phe <sup>7</sup> – Arg <sup>8</sup> – Trp <sup>9</sup> – Lys <sup>10</sup> ]-NH <sub>2</sub>
SHU9119	Ac – Nle <sup>4</sup> –c[Asp <sup>5</sup> – His <sup>6</sup> – <b>D</b> Nal <sup>7</sup> – Arg <sup>8</sup> – Trp <sup>9</sup> – Lys <sup>10</sup> ]-NH <sub>2</sub>

### Results and Discussion

**NMR and Conformational Analysis.** The conformational preferences of the cyclic melanocortin agonists MTII, and antagonists SHU9119 (Table 1) were comprehensively investigated by solution NMR spectroscopy in a 200 mM aqueous solution of DPC (dodecylphosphocholine). DPC was used as a membrane mimetic environment. For both peptides, NMR parameters (<sup>3</sup>J<sub>HN-Hα</sub> coupling constants, Hα chemical shifts, and NOE pattern) point to a helical structure of the N-terminal residues (4-7) and extended conformation of C-terminal residues.

NMR data obtained in DPC solution were used as input data for a restrained molecular dynamic calculation. Lowest energy conformer of MTII is shown in Figure 1a. Two β-turns that involve Nle4 to D-Phe7 and Asp5 to Arg8, respectively, can be identified in MTII. Conversely, residues 8 to 10 are in an extended conformation. Peptide surface has amphipathic nature. In

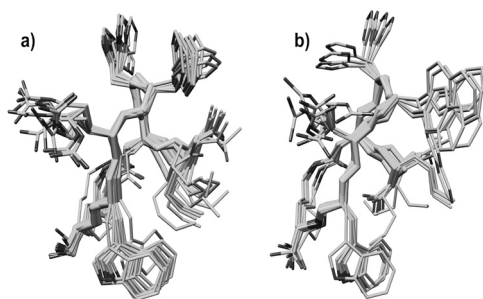


Fig. 1. Superposition of the 10 lowest energy conformers of **MTII** (a), **SHU9119** (b).

fact, considering the pseudo-plane defined by the backbone atoms hydrophobic residues Nle4, D-Phe7 and Trp9 lie on one side (right in Figure 1a) while positively charged residues His6 and Arg8 lie on the other side. 3D structure of SHU9119 is very similar to that obtained for MTII (Figure 1b). The main difference is that D-Nal7 side chain of SHU9119 is more flexible than D-Phe7 side chain of MTII.

**Docking.** The theoretical structures of the hMC4 receptor both in the active (hMC4R<sub>a</sub>) and inactive (hMC4R<sub>i</sub>) state were those proposed by Mosberg [2]. Since the currently available docking programs may not



Fig. 2. Superposition of the of hMC4 models in the inactive and active conformations complexed with SHU9119 and MTII, respectively.

work very well for peptide compounds, manual docking was conducted. The NMR-derived MTII and SHU9119 structures were placed in between the trans-membrane domains of the hMC4R<sub>a</sub> and hMC4R<sub>i</sub>, respectively. The following criteria were employed to achieve meaningful docking modes: (i) The positively charged side of the amphipathic surface of the peptides had to be close to the carboxylate groups of Asp122, Asp126, and Glu100, as suggested by several mutagenesis studies; (ii) No steric clashes should occur between any atom. Starting from 10 initial poses for both complexes, after optimization steps we could select one representative complex model for MTII/hMC4R<sub>a</sub> and one for SHU9119/hMC4R<sub>i</sub> (Figure 2). Interactions between the message segment His6-Trp9 and the receptors are shown

in Figure 3. As shown, the two ligands have similar interactions apart for Phe/Nal7 side chains which occupy different hydrophobic pockets.

The conformational behaviour of MTII and SHU9119 were studied in the presence of DPC micelles. The peptides show a well defined structure: two consecutive  $\beta$ -turns encompassing residues 4-7 (distorted type VIII) and 5-8 (distorted type II) and a brief extended C-terminal segment (residues 8-10) are observed. An amphipathic surface is defined by hydrophobic residues Nle4, D-Phe7 and Trp9 and positively charged residues His6 and Arg8. Docking studies indicate a similar binding modes of MTII and SHU9119 within hMC4R, with the exception of Phe/Nal7 side chains which are differently oriented.

Understanding the conformational preferences of hMC4R peptide ligands, combined with information regarding their interactions with the receptor in both the active and inactive state, is crucial to increase the knowledge of structure-activity relationships aimed to the design of new potent MC4 receptor ligands.

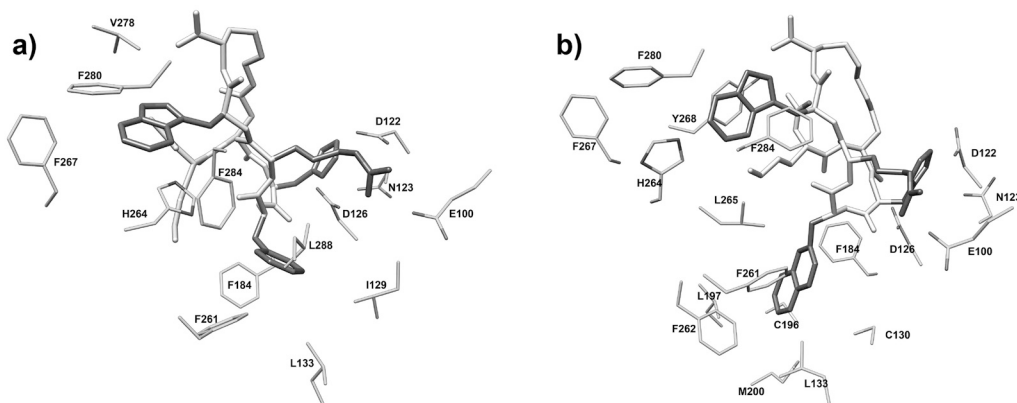


Fig. 3. (a) MTII within the binding pocket of hMC4<sub>a</sub>. (b) SHU9119 within the binding pocket of hMC4<sub>i</sub>.

## References

1. Gantz, I., Fong, T.M. *J. Physiol. Endocrinol. Metab.* **284**, E468-E474 (2003).
2. Fowler, C.B., Pogozeva, I.D., Lomize, A.L., LeVine, H., Mosberg, H.I. *Biochemistry* **43**, 15796-15810 (2004). [http://mosberglab.phar.umich.edu/resources/models/OPSD\\_BOVIN\\_AD.pdb](http://mosberglab.phar.umich.edu/resources/models/OPSD_BOVIN_AD.pdb).

## The Central Melanocortin Receptors and Voluntary Exercise

Jay W. Schaub, Amy Andreasen, Lorraine M. Koerper, Zhimin Xiang, and  
 Carrie Haskell-Luevano

Department of Pharmacodynamics, University of Florida, Gainesville, FL 32610-0487, U.S.A.

### Introduction

The melanocortin system is made up of five G-Protein Coupled receptors (GPCRs), MC1-5R, involved in the regulation and signaling processes of a wide range of physiological functions from skin and hair pigmentation (MC1R), steroidogenesis (MC2R), energy homeostasis (MC3R and MC4R), and exocrine gland function (MC5R) [1-4]. The receptors are bound and activated by a series of endogenous agonists and inhibited by the only known endogenous antagonists of GPCRs, agouti (ASP) and agouti related protein (AGRP) [5]. The melanocortin agonists are derived from post-translational cleavage and modification of the proopiomelanocortin (POMC) gene product [6]. The melanocyte stimulating hormones (MSH),  $\alpha$ -MSH,  $\beta$ -MSH,  $\gamma$ -MSH, and adrenocorticotropin hormone (ACTH) are capable of binding and activating each of the receptors with the notable exception of the MC2R, which is only capable of being stimulated by ACTH [1]. The melanocortin-3 and -4 receptors are expressed in the brain and are postulated to play important roles in the regulation of food intake and energy homeostasis [2,3,7]. The role of the MC4R in energy homeostasis has been well established with the generation of MC4R knockout (KO) mice which have an obese phenotype [8] and the identification of a subset of the obese human population which possess genetic mutations of their MC4R [9,10].

Previous data has shown that if provided with the means to voluntarily exercise (free access to a running wheel in the home cage), melanocortin-4 knockout mice do not develop the obese phenotype seen in sedentary littermates [11,12]. Over the course of the experiment a variety of parameters were monitored including body weight, body composition (fat mass as determined by quantitative MRI), and the plasma concentrations of the adiposity factors insulin and leptin. At the conclusion of the experiment hypothalamic gene expression levels were evaluated. Herein data is presented to support the hypothesis that voluntary exercise can prevent the onset of obesity and diabetes of the MC4R knockout mice.

### Results and Discussion

MC4R<sup>+/-</sup> heterozygous knockout mice were generously provided by Dr. Dennis Huszar at Millennium Pharmaceuticals. Knockout (MC4R<sup>-/-</sup>) and wild-type (MC4R<sup>+/-</sup>) mice were generated using a heterozygous breeding scheme. Mice were housed in a room with a reverse light cycle room (12-h light/12-h dark). All animals had *ad libitum* access to food and water for the duration of the experiment. Male mice were housed in standard conventional (Conv) or in cages equipped with a running wheel (RW) at 6 weeks of age. Data was recorded starting at 7 weeks of age for a duration of 8 weeks.

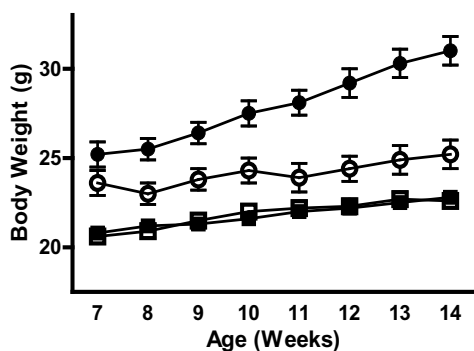


Fig. 1. Body weight in grams. Key – ■-WT Conv; □-WT RW; ●-MC4R KO Conv; ○-MC4R KO RW.

Food intake and body weight were measured twice a week. Body composition of the mice was determined once a week, measured in terms of fat and lean mass (grams), using an EchoMRI-100 (Echo Medical Systems LLC, Houston, TX). Plasma hormone concentrations of insulin and leptin were determined using a commercially available mouse endocrine panel kits (Linco Research, Millipore) on a Luminex 200 platform (Austin, TX). Hypothalami were dissected out of the brain at sacrifice, homogenized, and RNA

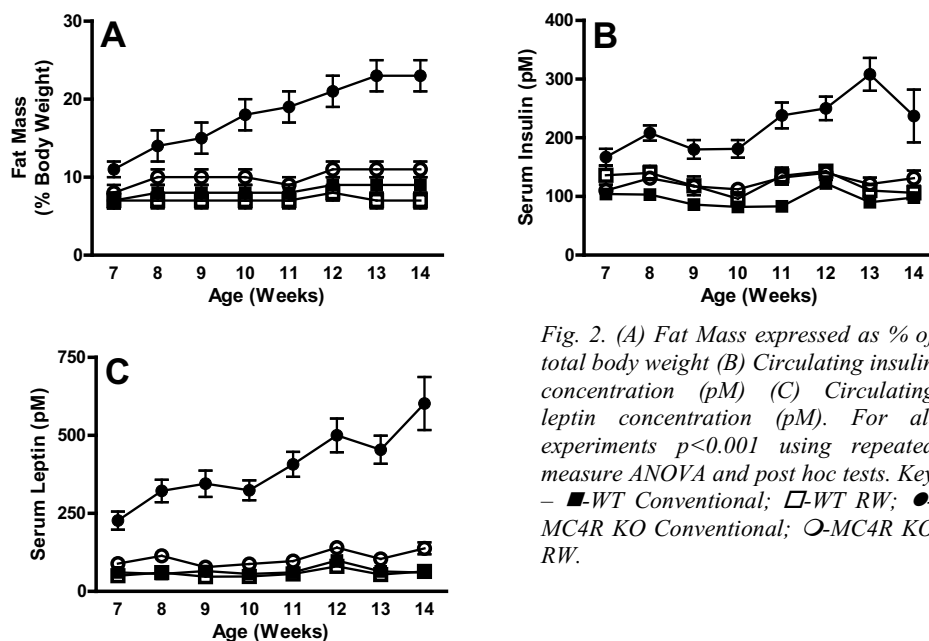


Fig. 2. (A) Fat Mass expressed as % of total body weight (B) Circulating insulin concentration (pM) (C) Circulating leptin concentration (pM). For all experiments  $p < 0.001$  using repeated measure ANOVA and post hoc tests. Key – ■-WT Conventional; □-WT RW; ●-MC4R KO Conventional; ○-MC4R KO RW.

was extracted using the Trizol method (Invitrogen). cDNA was synthesized from 2  $\mu$ g of total RNA using a High Capacity cDNA Archive Kit (Cat. # 4322171, Applied Biosystems) according to manufacturer instructions. Quantitative, real-time PCR was performed using 100 ng of sample cDNA with Taqman primers and reagents on an ABI 7300 System (Applied Biosystems). Samples were run in duplicate on a single 96-well plate for each Taqman probe to confirm the consistency of gene level expression. The Hprt1 gene was used as an internal housekeeping gene to correct for differences in starting amounts of cDNA and for data normalization across groups. mRNA levels are expressed as fold differences as compared to wild-type conventionally housed mice. The data was analyzed using two-way ANOVA with Bonferroni post hoc test (Prism 4 statistical software (GraphPad, La Jolla, CA)). Values of  $p < 0.05$  were considered to be significant.

At the start of the experiment, both the MC4R KO and wild-type littermate group body weights were not statistically different between the conventionally housed vs. running wheel-housed groups. At 6 weeks of age, the MC4R KO mice ( $23.1 \pm 0.5$  g) weighed significantly more than the wild-type mice ( $19.9 \pm 0.3$  g) ( $p < 0.001$ ). Differences in body weight between the MC4R KO groups were observed 2 weeks after running wheel exercise began and continued for the remainder of the experiment as seen in Figure 1. No statistically significant differences were observed between the wild-type groups at any time. Even though the exercised MC4R KO mice experienced a significant reduction in body weight compared to the MC4R KO conventional animals, they remained heavier than the wild-type mice throughout the study.

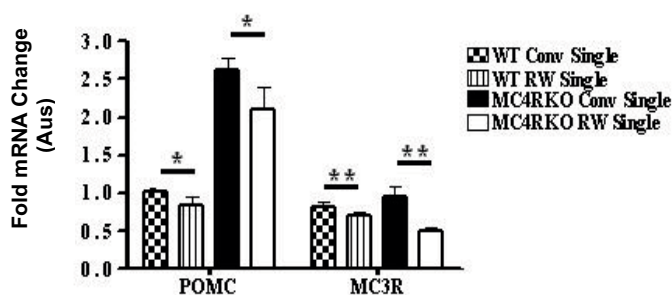


Fig. 3. Hypothalamic POMC and MC3R Expression levels. Significant differences in gene expression level were seen between exercised and sedentary animals of both genotypes. (\*  $p < 0.05$ , \*\* $p < 0.01$ ).

Statistically significant differences were seen in fat mass (expressed as the percentage of total body weight) between the MC4R KO conventionally housed mice and the exercising MC4R KO mice after two weeks of being allowed to voluntarily exercise (Figure 2A). No statistically significant differences were seen between the MC4R KO exercised mice and the wild-type conventionally housed mice.

The plasma concentrations of leptin and insulin (Figures 2B and 2C respectively) were analyzed to determine if exercise prevents the hyperinsulinemia and hyperleptinemia seen in obese MC4R KO mice. Significant differences between the sedentary and exercising MC4R KO animals were observed after only 1 week ( $p<0.01$ ) for both insulin and leptin. No significant differences in either insulin or leptin concentrations were seen between the MC4R KO exercised mice and either of the wild-type groups.

Hypothalamic levels of POMC and MC3R mRNA were quantified to establish if there was a change in expression level caused by exercise, the data is shown in Figure 3. For the POMC gene, there was found to be a significant difference for both the MC4R KO and wild-type animals between the groups with access to the running wheel equipment and conventionally housed animals ( $p<0.05$ ). Additionally, significant differences between the sedentary and exercise groups were also seen for levels of MC3R expression ( $p<0.01$ ).

In conclusion, the beneficial effects of voluntary exercise in the MC4R KO mouse model, including prevention of the obese and hyperinsulinemic phenotype that corresponds to type II diabetes, were found to be supported by the data. Since the area of voluntary exercise is a relatively young field of research, studies in this area are increasing at a rapid pace as scientific technologies continue to improve in sensitivity and selectivity. As such, determination of the mechanisms associated with the positive benefits of exercise will continue to be an important task in hopes of developing human therapeutic agents. Toward these goals, this study presented provides further physiological characterization of the genetic MC4R KO obese mouse model and the effects of voluntary exercise, and supports the hypothesis that voluntary exercise can prevent the genetic predisposition of obesity and diabetes associated with MC4R dysfunction.

## Acknowledgments

We would like to thank Dr. Dennis Huszar and Millennium Pharmaceuticals/Genelogic for use of the MC4RKO mice. This work was supported by National Institutes of Health Grants RO1DK57080 and an American Diabetes Association Research Award.

## References

1. Mountjoy, K.G., Robbins, L.S., Mortrud, M.T., et al. *Science* **257**, 1248-1251 (1992).
2. Roselli-Rehfuess, L., Mountjoy, K.G., Robbins, L.S., et al. *Proc. Natl. Acad. Sci. U.S.A.* **90**, 8856-8860 (1992).
3. Gantz, I., Miwa, H., Konda, Y., et al. *J. Biol. Chem.* **268**, 15174-15179 (1993).
4. Gantz, I., Shimoto, Y., Konda, Y., et al. *Biochem. Biophys. Res. Commun.* **200**, 1214-1220 (1994).
5. Ollmann, M.M., Wilson, B.D., Yang, Y.K., et al. *Science* **278**(5335), 135-138 (1997).
6. Lerner, A.B., McGuire, J.S. *Nature* **189**, 176-179 (1961).
7. Chhajlani, V., Wikberg, J.E. *FEBS Lett.* **309**, 417-420 (1992).
8. Huszar, D., Lynch, C.A., Fairchild-Huntress, V., et al. *Cell* **88**, 131-141 (1997).
9. Marti, A., Corbalan, M., Forga, L., et al. *Int. J. Obes. Relat. Metab. Disord.* **27**, 385-388 (2003).
10. Vaisse, C., Clement, K., Guy-Grand, B., et al. *Nature Genetics* **20**, 113-114 (1998).
11. Haskell-Luevano, C. et al. *FASEB J.* **23**, 642-655 (2009).
12. Irani, B.G., et al. *Biochem. Biophys. Res. Commun.* **326**, 638-644 (2005).

## Incorporation of a Reverse Turn Mimetic into a Chimeric AGRP-Melanocortin Peptide Template: Structure and Function Studies

Anamika Singh,<sup>1</sup> Jerry R. Holder,<sup>1</sup> Andrzej Wilczynski,<sup>1</sup> Rachel M. Witek,<sup>1</sup> Marvin Dirain,<sup>1</sup> Arthur S. Edison,<sup>2</sup> and Carrie Haskell-Luevano<sup>1</sup>

<sup>1</sup>Department of Pharmacodynamics and <sup>2</sup>Department of Biochemistry & Molecular Biology, College of Pharmacy, University of Florida, Gainesville, FL 32610, U.S.A.

### Introduction

The melanocortin receptor (MCR) family consists of five receptor subtypes (MC1R-MC5R) identified to date [1]. Agouti-related protein (AGRP) is one of two known naturally occurring antagonists of the brain melanocortin receptors MC3R and MC4R. The melanocortin peptides ( $\alpha$ -,  $\beta$ -,  $\gamma$ - melanocyte stimulating hormones and adrenocorticotropin, ACTH) are the endogenous ligands for these melanocortin receptors [1]. All of these hormones possess a central His-Phe-Arg-Trp motif, which is responsible for receptor recognition and binding and is referred to as the “message” sequence. It is postulated that the bioactive conformation of melanocortin ligands involve  $\beta$  - turn structures in this region [2]. Centrally located MC3R and MC4R have been identified in knockout mice to play important role in regulating energy homeostasis, obesity, and metabolism and are potential drug targets for treatment of obesity and related diseases [3]. MC4R knockout mice are obese and hyperphagic which demonstrate the involvement of MC4R in feeding regulation [3]. The discovery of new selective and potent MC4R ligands will help in further investigation of the physiological role of this receptor subtype. It was hypothesized that insertion of reverse turn mimetics into a known peptide template will result in receptor selective and potent analogues by restricting the peptide template into its bioactive conformation.

### Results and Discussion

A thioether cyclized peptidomimetic scaffold was postulated to mimic a reverse turn structure and resulted in a potent ligand (Figure 1) with 650 nM agonist potency at mMC4R [4]. Using the hypothesis that a reverse turn in the melanocortin agonist His-Phe-Arg-Trp core sequence results in ligands that have increased potency, a thioether cyclized mimetic was inserted into the potent chimeric AGRP-Melanocortin template (AMW3-130; Yc[CHdFRWNAFC]Y-NH<sub>2</sub>) (Figure 2) [4,5]. The 10-membered macrocycle was generated on the resin by: i) synthesizing a linear peptide on solid polymer support; ii) reductive alkylation of an aldehyde amino acid derivative; iii) coupling of cysteine; iv) chloroacetylation of amine moiety;

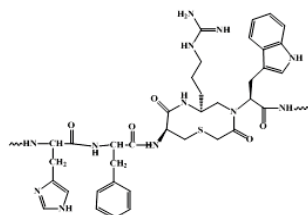


Fig. 1. Small molecule reverse turn mimetic.

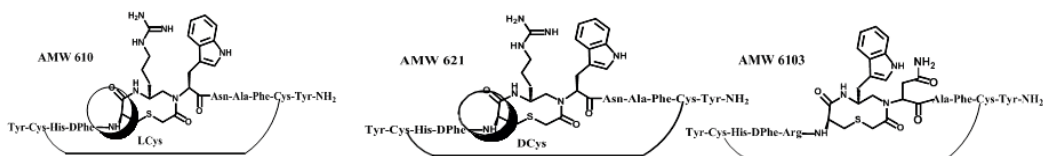


Fig. 2. Incorporation of small molecule reverse turn mimetic into AMW3-130 template.

Table 1. Agonist  $EC_{50}$  (nM) pharmacology of the modified peptides at the mouse MC4R

Peptide	Agonist $EC_{50}$ (nM)
	mMC4R
$\alpha$ -MSH	5.37 $\pm$ 0.62
NDP-MSH	0.21 $\pm$ 0.03
AMW3-130	0.27 $\pm$ 0.09
AMW610	85
AMW621	780
AMW6103	440

and v) formation of a thioether linkage and disulfide bridge formation within the linear peptide chain [4]. This methodology enabled the generation of ligands in which the cyclic mimetic scaffold was walked down the His-DPhe-Arg-Trp sequence. The “positional walking” approach allowed conformational scanning of the tetrapeptide residues that have been identified as key to binding and affinity for the melanocortin receptor subtypes [6].

Peptide synthesis was performed using standard Fmoc methodology in a manual reaction vessel [7] or with microwave. The peptides were assembled on Rink amide MBHA resin with repeated cycles of deprotection and coupling. Synthesis of thioether cyclized peptidomimetic scaffold was done on solid support according to the literature procedure [2]. Disulfide bridge formation was obtained by stirring the peptides in 20 % DMSO/H<sub>2</sub>O solution at room temperature for 2 days. Progress of the reaction was monitored by HPLC. All peptides were purified by RP-HPLC, and analyzed and characterized by HPLC and MS. The purified peptides were at least >95% pure as determined by RP-HPLC in two diverse solvent systems. The synthesized peptides were pharmacologically characterized by the  $\beta$ -galactosidase reporter gene assay at the mouse melanocortin receptor isoforms [5]. By using microwave-assisted stepwise protocols, the synthesis time of template can be reduced to 1 day vs. 4 days using conventional methods. Synthesis was performed using a polypropylene reaction vessel on a Discover SPS synthesizer (CEM Corp). The Discover SPS is equipped with fiber-optic temperature probe for controlling the microwave power delivery. Agitation is accomplished by inert gas bubbling through external setup. A separate vacuum manifold is provided with the assembly for solvent drainage.

This study resulted in the discovery that compound AMW610, having Arg and Trp in the reverse turn, was the most potent MC4R agonist (85 nM) (Table 1) ligand in the series. Moreover, it was observed that change in stereochemistry of thioether ring closure play an important role as change from L-Cys (AMW610) to D-Cys (AMW621) resulted in substantial change in potency. These results support the hypothesis that reverse turn mimetic into chimeric AGRP-melanocortin template results in ligands with varying potency.

## Acknowledgments

This work was supported by NIH Grant RO1DK064250. AS is an APS 2009 Travel Grant Recipient.

## References

1. Irani, B.J., et al. *Curr. Pharma. Design* **10**, 3443-3479 (2004).
2. Haskell-Luevano, C., et al. *J. Med. Chem.* **42**, 4380-4387 (1999).
3. Huszar, D., et al. *Cell* **88**, 131-141 (1997).
4. Bondebjerg, J., et al. *J. Am. Chem. Soc.* **124**, 11046-11055 (2002).
5. Hruby, V.J., et al. *Peptide Protein Rev.* **3**, 1-64 (1984).
6. Xiang, Z., et al. *Biochemistry* **46**, 8273-8287 (2007).
7. Wilczynski, A., et al. *J. Med. Chem.* **47**, 2194-2207 (2004).



## Determination of Unique AGRP and MC4R Interactions: Use of Stereochemical Modifications of Ligands and Receptor Mutagenesis

Erica M. Haslach, Marvin L. Dirain, and Carrie Haskell-Luevano

Department of Pharmacodynamics, University of Florida, Gainesville, FL 32610 U.S.A.

### Introduction

The melanocortin system belongs to a superfamily of GPCRs and consists of endogenous agonists, antagonists and five receptor subtypes [1]. The MC4R has been shown to be involved weight and energy homeostasis and feeding behavior [2]. MC4R deficient mice exhibit an obese and hyperphagic phenotype proposing that the MC4R is involved in the regulation of feeding behavior.[2] The antagonist, AGRP, is a target of interest because is involved in the regulation of food intake and is a competitive antagonist of the MC4R [3]. Therefore, it is postulated that AGRP mediates its effects through the MC4R in the CNS [1-3]. The C-terminus of AGRP is a cysteine-rich region of the protein and has receptor binding affinity and antagonism comparable to the full length protein. This region contains five disulfide bridges with a conserved Arg-Phe-Phe motif that has been identified as being important for the antagonistic activity of AGRP [4-5]. Truncation of this domain has led to the identification of monocyclic and bicyclic derivatives of AGRP that provide support to the hypothesis that not all five disulfide bridges are necessary for molecular recognition and receptor antagonism [6-8]. The stereochemical inversion of the Arg-Phe-Phe region led to the discovery of a new melanocortin agonist template [6]. Previous studies have shown that the incorporation of DArg<sup>111</sup> in the monocyclic compound (EMH1-100) converts an antagonist into an agonist at the MC4R [6]. Within the homology model of the mMC4R complexed with hAGRP(87-132) [9], a putative interaction was observed that may explain the pharmacology [6]. It is postulated that DArg<sup>111</sup> interacts with MC4R Asn115 [8]. Previous studies showed that the bicyclic peptide (EMH2-93) displayed equipotent binding affinity to that of hAGRP (87-132) at the mMC4R [7]. However, it was an 80-fold less potent antagonist at the mMC4R [7]. Homology modeling demonstrated a postulated interaction of Arg<sup>111</sup> of the bicyclic compound interacting with Asn115 of mMC4R. This Arg<sup>111</sup>-mMC4R Asn115 interaction was not observed for hAGRP (87-132) and may attribute to the change in antagonist potency observed for the bicyclic compound [8]. It is hypothesized that similar pharmacological results will be observed when Arg<sup>111</sup> is stereochemically inverted in the bicyclic compound as seen with the monocyclic compounds.

### Results and Discussion

Monocyclic and bicyclic derivatives of AGRP and their DArg<sup>111</sup> analogues were synthesized and tested at the mouse melanocortin receptors in this study. Table 1 displays the agonist EC<sub>50</sub> and antagonist pA<sub>2</sub> values obtained for the peptides synthesized in this study. As previously reported, the DArg analogue (EMH1-120) became a full  $\mu$ M agonist at the mMC4R. As hypothesized, the incorporation of DArg into the bicyclic template (EMH3-45) caused a conversion of pharmacology from antagonist to agonist at the mMC4R (EC<sub>50</sub> = 21  $\mu$ M). Figure 1 displays the micromolar agonist activity of EMH3-45 at the mMC4R. The data obtained supports the hypothesis that the incorporation of DArg into the bicyclic AGRP derivative caused a conversion of pharmacology from antagonist to agonist resulting in a new agonist template at the mMC4R. AGRP and the MC4R are important therapeutic targets for both the understanding and treatment of obesity

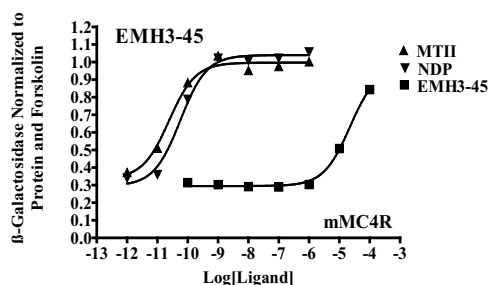


Fig. 1. Dose response curve displaying agonist activity of EMH3-45 at the mMC4R.

Table 1. Functional Activity at the mMC4R

Name	Peptide Sequence	Agonist <i>EC</i> <sub>50</sub> (nM) mMC4R	Antagonist <i>pA</i> <sub>2</sub> mMC4R
MTII	Ac-Nle-c[DH-DPhe-RWK]-NH <sub>2</sub>	0.020	-
NDP-MSH	Ac-SYS-Nle-EH-DPhe-RWGKPV-NH <sub>2</sub>	0.052	-
EMH1-100	DPAATAYc[CRFFNAFC]YARKL	-	6.1
EMH1-120	DPAATAYc[C-DArg-RFFNAFC]YARKL	37700*	-
EMH2-93	c <sub>1</sub> [CUDPUATUYc <sub>2</sub> [CRFFNAFC] <sub>2</sub> YC] <sub>1</sub> RKL	-	8.2
<b>EMH3-45</b>	c <sub>1</sub> [CUDPUATUYc <sub>2</sub> [C-DArg-FFNAFC] <sub>2</sub> YC] <sub>1</sub> RKL	21 μM	-

\**EC*<sub>50</sub> values obtained from published work [6]

related diseases and the involvement of the melanocortin system in the neuroendocrine regulation of energy homeostasis. Therefore, it is important to undertake further studies to examine ligand-receptor interactions. Receptor mutagenesis will be performed in future experiments to explore specific putative AGRP Arg<sup>111</sup> interactions with the MC4R.

## Acknowledgments

This study has been supported by NIH grant DK57080. EMH was supported by travel awards from the APS Student Affairs Committee, University of Florida College of Pharmacy, and Graduate Student Council.

## References

1. Wilson, K., et al. *Cell. Mol. Bio.* **52**, 3-20 (2006).
2. Huszar, D., et al. *Cell* **88**, 131-141 (1997).
3. Ollmann, M., et al. *Science* **278**, 135-138 (1997).
4. Yang, K., et al. *Biochemistry* **39**, 14900-14911 (2000).
5. Tota, M., et al. *Biochemistry* **38**, 897-904 (1999).
6. Joseph, C., et al. *J. Med. Chem.* **47**, 6702-6710 (2004).
7. Wilczynski, A., et al. *J. Med. Chem.* **47**, 5662-5673 (2004).
8. Wilczynski, A., et al. *J. Med. Chem.* **47**, 2194-2207 (2004).
9. Jackson, P., et al. *Biochemistry* **41**, 7565-7572 (2002).

## Semi-rigid MC1 Selective Agonists Based on N-capped His-D-Phe-Arg-NH<sub>2</sub> Tripeptide Core

Leonid Koikov,<sup>2</sup> Andrew R. Ruwe,<sup>1</sup> Zalfa Abdel-Malek,<sup>2</sup>  
Carrie Haskell-Luevano,<sup>4</sup> Marvin L. Dirain,<sup>4</sup> Federico Portillo,<sup>4</sup>  
Zhimin Xiang,<sup>4</sup> Matt Wortman,<sup>3</sup> and James J. Knittel<sup>1</sup>

<sup>1</sup>University of Cincinnati, James L. Winkle College of Pharmacy, Cincinnati, OH 45267, U.S.A.;

<sup>2</sup>University of Cincinnati, College of Medicine, Cincinnati, OH 45267, U.S.A.; <sup>3</sup>University of Cincinnati, College of Medicine, Genome Research Institute, Cincinnati, OH 45237, U.S.A.; and

<sup>4</sup>University of Florida, College of Pharmacy<sup>4</sup>, Gainesville, FL 32610, U.S.A.

### Introduction

Melanocortin receptors (MCRs) found in different tissues are a target of intensive pharmacological research. Five MCRs (MC1R – MC5R) have been cloned and design of their selective ligands is very challenging. Activation of MC1R in skin by UV-induced paracrine factors stimulates pigmentation and DNA damage repair, thus confers natural photoprotection. We proposed that MC1R selective ligands can be used for prevention of the most fatal skin cancer-melanoma [1]. Based on the minimum melanocortin core sequence **HfRW** and our superpotent hMC1R selective agonist LK-184 Ph(CH<sub>2</sub>)<sub>3</sub>CO-**HfRW**-NH<sub>2</sub> (**1**) [EC<sub>50</sub> (nM): hMC1R 0.009±0.004, hMC3R 4.7±1.2, hMC4R 4.6±2.8] and its less potent truncated analog LK-394 Ph(CH<sub>2</sub>)<sub>3</sub>CO-**HfR**-NH<sub>2</sub> (**2**) [hMC1R 5.0±0.6, weak partial agonist for hMC3R and hMC4R] [2], a new series of 30 RCO-**HfR**-NH<sub>2</sub> derivatives was designed and tested on mMC1R, MC3R-MC5R. All N-capping groups had an aromatic ring attached to a C<sub>2</sub>, C<sub>3</sub> or C<sub>4</sub> spacer (saturated, unsaturated or 1,4-diene) or directly, with special attention to cinnamic derivatives providing a shorter more rigid link compared to the saturated C<sub>3</sub> chain in **1** and **2**. Substituents in the phenyl rings offered an extended conjugated  $\pi$  system overlapping in space with the  $\pi$  system of the phenyl in **2** (Figure 1).

### Results and Discussion

In contrast to hMCRs, **1** was more potent at mouse MC4R and MC5R [EC<sub>50</sub> (nM): mMC1R 1.60±0.29, mMC3R 26.0±4.0, mMC4R 0.54±0.19, mMC5R 0.33±0.14], while **2** showed some MC1R selectivity albeit with 590-fold loss in potency [EC<sub>50</sub> (nM): mMC1R 940±260, mMC3R 43700±1370, mMC4R 15140±8800, mMC5R 11800±5950; selectivity 1:46:16:12]. All synthesized tripeptides had very low or no activity at mMC3R-MC5R. At this time it is not clear, if this consistent increase in MC1 selectivity in the tripeptide series is caused by shortening of the molecule due removal of the Trp or linked to interaction with Trp specifically. The direct unsaturated 4-phenylbuten-3-oyl analog of the parent tripeptide **2** was equipotent to **2** at mMC1R but showed some loss of selectivity (MC1/3/4/5Rs ratio 1:24:5:3). Potency of the

simple cinnamoyl derivative at mMC1R was close to that of **2** and its selectivity improved (MC1/4/5Rs 1:44:25 and no activity at mMC3R). Several derivatives of 3- or 4-substituted cinnamic acids (3-Cl, 3-CF<sub>3</sub>, 3-OH, 4-MeO, 4-NO<sub>2</sub>) were more potent than LK-394 at mMC1R with *trans*-4-HOC<sub>6</sub>H<sub>4</sub>CH=CHCO-**HfR**-NH<sub>2</sub> (**3**) being the most active [EC<sub>50</sub> (nM): mMC1R 83.3±13.7, mMC3R 20500±12600, mMC4R 18130±3258, mMC5R 935±310; selectivity 1:246:217:11]. Shifting position of the OH, O-methylation, CH=CH reduction or inclusion in a cyclic system (Figure 1c, d) leads to a 3-7 fold drop in potency at mMC1R. Elongation of the C2 spacer or addition of polarizable non-hydrogen bonding substituents into 3- or 4-position to the cinnamic moiety (Figure 1a, b) weakened or abolished binding at

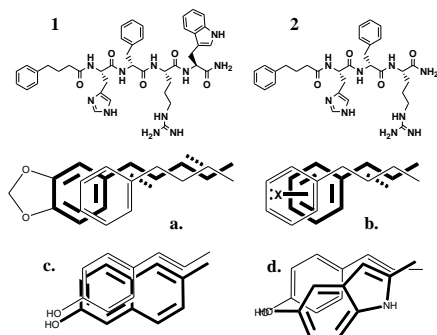


Fig. 1. N-capping group rational. Parent structures in thin lines: phenylbutyryl (a, b) and *trans*-4-HOC<sub>6</sub>H<sub>4</sub>CH=CH (c, d).

mMC3R. The elongation of the end-capping group due to spacer extensions (Figure 1a) or aromatic substituents (Figure 1b) elicited a weak mMC3R response, although polar groups on aryl in some cases could cancel it.

The observed biological activity correlates with increased conformational rigidity of the **HfR** core (the backbone and side chains) stabilized by the semi-rigid cinnamoyl tail

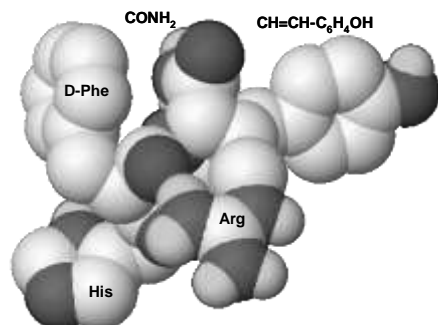


Fig. 2. Global minimum of **3** (CPK without non-polar H, heteroatoms in dark grey).

(modeled with MacroModel, OPLS\_2005 in water, the Monte Carlo Multiple Minimum (MCMM) mixed torsional/low-frequency sampling in MacroModel [3]). Although the number of conformers for **2** (108 within 3 kcal/mol, 293 within 5 kcal/mol) and **3** (55 within 3 kcal/mol, 221 within 5 kcal/mol) does not vary drastically their 3D distribution is totally different - **2** has no preferred conformation, while all 221 conformers of **3** are very well aligned [4]. Polar basic Arg and His are situated on the same side of the molecule opposite to the non-polar aromatic D-Phe and cinnamoyl. The existence of **3** in multiple but similar conformations that can convert into the biologically active conformation upon binding and this “pre-alignment” is beneficial for initial recognition of the ligand by the mMC1R that contains compact acidic (Glu-94, Asp-117 and

121) and aromatic hydrophobic (Phe-175, 179, 196, and 257) binding pockets [5]. Distribution of the conformations for the cyclic analogs of **3** (Figure 1c, d) are similar to **3**, which demonstrates that their lower potency relative to **3** is due to misplacement of HO in the active site and not an increase in width or rigidity of the end-capping group.

Thus, based on targeted screening, molecular modeling and a “soft” control of the peptide conformation without restricting dihedral angles of the backbone or side chains favorable for interaction with an active site of MC1R, we were able to reduce the minimum melanocortin sequence to the tripeptide **HfR** (previously known minimum melanocortin tetrapeptide Ac-**HfRW**-NH<sub>2</sub> elicits full agonist response but with low potency [6]). The resulting flexible tripeptide **3** was much more selective than the native melanocortin tridecapeptide  $\alpha$ -MSH [EC<sub>50</sub> (nM): mMC1R 7.20 $\pm$ 3.73, mMC3R 10.20 $\pm$ 2.53, mMC4R 19.3 $\pm$ 3.59, mMC5R 6.72 $\pm$ 2.01] and only 11 times less potent at mMC1R. These findings provide an insight into the structure on the active site of MCRs that could be useful for future design of low molecular weight synthetic drugs acting only on targeted MCRs subtypes.

## Acknowledgments

Supported by grants RO1CA114095 (NIH) for Z.A-M, RO1DK057080 (NIH) for C.H-L and a Skin Cancer Foundation Henry W. Menn Memorial Award for JJK.

## References

1. Abdel-Malek, Z. *Cell. Molec. Life Sci.* **58**, 434-441 (2001); Hadley M.E., et al. *Pigment Cell Res.* **9**, 213-234 (2006); Abdel-Malek, Z.A., et al. *The FASEB Journal*, **20**, 1561-1563 (2006); Abdel-Malek, Z.A., et al. *Photochem. Photobiol.* **84**, 501-508 (2008); Abdel-Malek, Z., et al. *Pigment Cell & Melanoma Res.* **22**, in print (2009).
2. Koikov, L.N., et al. *Bioorg. Med. Chem. Lett.* **13**, 2647-2650 (2003); *ibid.*, 3997-4000 (2004).
3. Schrodinger Suite 2008 (Schrodinger LLC, New York, NY, 2008).
4. Ruwe, A.R., et al. *Bioorg. Med. Chem. Lett.* **19**, in print (2009).
5. Haskell-Luevano, C., et al. *J. Med. Chem.*, **44**, 2247-2252 (2001).
6. Yang, Y., et al. *J. Biol. Chem.* **272**, 23000-23010 (1997); Haskell-Luevano C., et al. *J. Med. Chem.* **40**, 2133-2139 (1997).

## Effect of New Leptin Fragments on Food Intake and Body Weight of Rats

Marta N.C. Martins,<sup>1</sup> Jádson M. Pereira,<sup>1</sup> Mônica M. Telles,<sup>2</sup> Juliana C.S. Zemdegs,<sup>2</sup> Iracema S. Andrade,<sup>2</sup> Eliane B. Ribeiro,<sup>2</sup> and Antonio Miranda<sup>1</sup>

<sup>1</sup>Department of Biophysics, Federal University of São Paulo, São Paulo, SP, 04044-020, Brazil;

<sup>2</sup>Department of Physiology, Federal University of São Paulo, São Paulo, SP, 04023-062, Brazil

### Introduction

The protein hormone produced by the *ob*-gene and denominated leptin (LEP), is a product originating from adipose tissue, circulates in the plasma and affects the energy balance by interacting with the hypothalamus. Leptin plays a key role in regulating energy intake and energy expenditure, including appetite and metabolism. Total absence or resistance to leptin causes morbid obesity, diabetes and hypogonadism. In order to identify regions of the leptin molecule responsible for its bioactivity, we studied a series of decapeptides fragments encompassing the region of the amino acids residues 98-122 present in the leptin molecule [1,2] (Table 1). The effect caused by the fragments on body weight and food intake were assessed when administered into the lateral cerebroventricle of normal Wistar rats during four consecutive days [3]. LEP and cerebrospinal fluid (CSF) were used as positive and negative control, respectively.

Table 1. Human leptin fragments synthesized and tested

#	Name	Sequence
I	Ac-LEP <sub>98-122</sub> -NH <sub>2</sub>	Ac-S-N-D-L-E-N-L-R-D-L-L-H-V-L-A-F-S-K-S-C-H-L-P-W-A-NH <sub>2</sub>
II	Ac-LEP <sub>98-107</sub> -NH <sub>2</sub>	Ac-S-N-D-L-E-N-L-R-D-L-NH <sub>2</sub>
III	Ac-LEP <sub>101-110</sub> -NH <sub>2</sub>	Ac-L-E-N-L-R-D-L-L-H-V-NH <sub>2</sub>
IV	Ac-LEP <sub>104-113</sub> -NH <sub>2</sub>	Ac-L-R-D-L-L-H-V-L-A-F-NH <sub>2</sub>
V	Ac-LEP <sub>107-116</sub> -NH <sub>2</sub>	Ac-L-L-H-V-L-A-F-S-K-S-NH <sub>2</sub>
VI	Ac-LEP <sub>110-119</sub> -NH <sub>2</sub>	Ac-V-L-A-F-S-K-S-C-H-L-NH <sub>2</sub>
VII	Ac-LEP <sub>113-122</sub> -NH <sub>2</sub>	Ac-F-S-K-S-C-H-L-P-W-A-NH <sub>2</sub>
VIII	Ac-[Ser <sup>117</sup> ]-LEP <sub>113-122</sub> -NH <sub>2</sub>	Ac-F-S-K-S-S-H-L-P-W-A-NH <sub>2</sub>

### Results and Discussion

Our results indicated that leptin induced a reduction of body weight and of food intake gain of 6.3% and 36.0% respectively (Figure 1). Among the fragments studied we observed that with fragments Ac-LEP<sub>98-122</sub>-NH<sub>2</sub> (I), Ac-LEP<sub>98-107</sub>-NH<sub>2</sub> (II), Ac-LEP<sub>107-116</sub>-NH<sub>2</sub> (V) and Ac-[Ser<sup>117</sup>]-LEP<sub>113-122</sub>-NH<sub>2</sub> (VIII) no significative changes of body weight gain and also on the food intake were observed. Interestingly, with fragments Ac-LEP<sub>101-110</sub>-NH<sub>2</sub> (III), Ac-LEP<sub>104-113</sub>-NH<sub>2</sub> (IV) and Ac-hLEP<sub>113-122</sub>-NH<sub>2</sub> (VII) we observed a great increase on the food intake, intriguingly, without any significant change in the body weight of the treated animals. Differently of the other leptin fragments behavior, fragment Ac-hLEP<sub>110-119</sub>-NH<sub>2</sub> (VI) was able to induce a significant reduction of the food intake (39.8%) and a reduction of the body weight (6.0%) similarly as observed with leptin. Peptide fragments [3-5] design approach may offer the basis for the development of leptin-related compounds with potential application in human and veterinary obesity understanding.

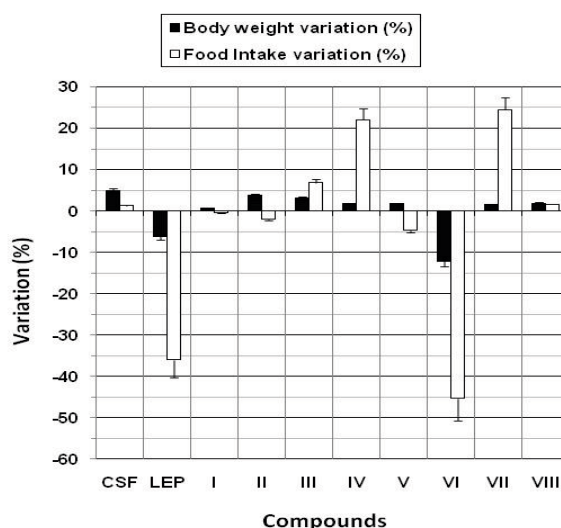


Fig. 1. Body weight and food intake variations after intracerebroventricular administration of the peptide in Wistar rats during four days.

## Acknowledgements

The work was supported by FADA-UNIFESP, FAPESP, CNPq and CAPES.

## References

1. Oliveira, V.X. Jr., et al. *Reg. Pep.* **127**,123-132 (2005).
2. Oliveira, V.X. Jr., et al. *J. Pep. Sci.* **14**, 617-625 (2008).
3. Martins, M., et al. *Reg. Pep.* **153**, 77-82 (2009).
4. Grasso, P., et al. *Reg. Pep.* **101**, 123-129 (2001).
5. Novakovic, Z.M., et al. *Reg. Pep.* **154**, 107-111 (2009).

## Adropin – A Novel Secreted Factor Linking Diet with Energy Homeostasis

K. Ganesh Kumar,<sup>1</sup> Jingying Zhang,<sup>2,3</sup> Randall L. Mynatt,<sup>2,3</sup> and Andrew A. Butler<sup>1,3</sup>

<sup>1</sup>Neuropeptides laboratory, <sup>2</sup>Transgenic Core Facility and <sup>3</sup>Clinical Nutrition Research Unit, Pennington Biomedical Research Center, Baton Rouge, LA 70808, U.S.A.

### Introduction

Organisms must adapt substrate preference and energy expenditure to daily changes in dietary macronutrient intake and energy status. An impaired capacity for metabolic adaptation may increase risk for weight gain and insulin resistance [1,2]. The adaptive response involves an integrated response involving the central nervous system and several peripheral organ systems, with the liver having a central role in coordinating processing and distribution of metabolites [3]. Endocrine signals play a role in this process. Classical examples include insulin, glucagon, leptin, and adiponectin. We recently identified a novel liver secreted factor named adropin which is encoded by the *Energy Homeostasis Associated* transcript (*Enho*). *Enho* expression is altered by macronutrient content of the diet and fasting, and is proposed to have important role in maintaining energy homeostasis by regulating lipid and glucose metabolism [4]. Here we briefly summarize the identification of the *Enho* transcript and adropin, and present some of unpublished data from the analysis of FVB/NJ mice over expressing adropin.

### Results and Discussion

**Identification of the *Enho* transcript:** Our laboratory has a long standing interest in the regulation of energy homeostasis by the hypothalamic melanocortin system. While melanocortin receptor knockout (*Mc3r*<sup>-/-</sup> and *Mc4r*<sup>-/-</sup>) mice exhibit obesity, they differ in the severity of insulin resistance (IR) and nonalcoholic fatty liver disease (NAFLD) [5]. While investigating the differential sensitivity of melanocortin receptor knockout mice to obesity-induced IR and NAFLD, we identified a transcript containing a high conserved open reading frame predicted to express a small 76 aa secreted protein (RIKEN cDNA 2310040A07). The transcript, highly expressed in liver, exhibited a decline in expression secondary to obesity. Based on our preliminary data from studies assessing function, we named the protein Adropin (derived from latin root “aduro” – to set fire, and “pinquis” – fats or oils).

**Regulation of *Enho* expression:** Obesity induced by genetic mutation (*A<sup>Y/a</sup>*, *Lep<sup>ob</sup>/Lep<sup>ob</sup>*, *Mc4r*<sup>-/-</sup>, *Mc3r*<sup>-/-</sup>) or diet is associated with reduced hepatic *Enho* expression. Prevention of obesity by calorie restriction or improvement of insulin sensitivity using  $\beta$ 3 agonist improves hepatic *Enho* expression. Reduced *Enho* expression in *Mc4r*<sup>-/-</sup> mice is secondary to obesity and insulin resistance. Together, these observations suggested an inverse association of *Enho* expression with obesity and diabetes.

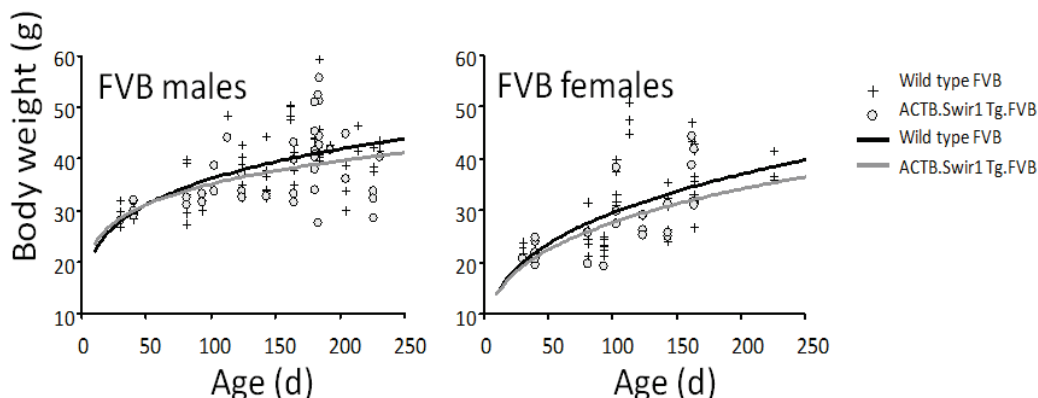


Fig. 1. Analysis of body weight as a functional of age in FVB-Tg mice maintained in chow showed a modest reduction in both sexes.

To investigate whether nutritional status regulates hepatic *Enho* expression, we examined C57BL/6J (B6) mice subject to fasting-refeeding using low or high fat diets. Fasting is associated with reduced *Enho* expression in liver. While diet induced obesity induced by 3 months of high fat diet (HFD) feeding is associated with reduced liver *Enho* expression, short term exposure to HFD actually increases expression. 2d of HFD feeding resulted in a 9-fold increase in liver *Enho* expression; 7d, 14d and 28d of HFD feeding resulted in a complex pattern of regulation, however altogether a significant increase expression was still observed compared to low fat fed groups. Presumably, long term HFD feeding sufficient to develop obesity and severe insulin resistance impairs normal regulation of the *Enho* transcript in liver. Collectively, these results suggested that adiponin could be a secreted factor linking dietary macronutrient content and energy status with metabolic regulation.

***Adiponin transgenic mice are protected against obesity induced metabolic disorders:***

As *Enho* level declines with obesity and insulin resistance, we investigated whether transgenic over-expression of *Enho* in mice could protect them against metabolic disorders associated with obesity. A transgenic line expressing the adiponin open reading frame controlled by the human  $\beta$ -actin promoter was created by Dr. Robert Kesterson at the University of Alabama School of Medicine on the B6 background. A second line on the FVB/NJ background was created by the Transgenic Core Pennington Biomedical Research Center. Overall, both strains appear grossly normal with no mortality associated with overexpression. We have already reported the phenotype of B6 adiponin transgenics, which exhibit improvements in glucose homeostasis, protection from obesity-induced NAFLD, and delayed diet-induced obesity [4]. Here we present some of the phenotype data of FVB/NJ adiponin transgenics [FVB-Tg(adiponin)]. Overall, the phenotype is similar to that of the B6-Tg(adiponin) strain, suggesting conservation of function on a different genetic backgrounds.

Regression analysis of body weight in male and female FVB-Tg(adiponin) and control mice over a period of age ranging from weaning to 6 months indicated a modest reduction associated with adiponin overexpression (Figure 1). In females, a significant reduction in fat mass (FM) and body weight of was observed in FVB-Tg(adiponin) mice at 9 wk of age compared to controls (Figure 2 – *left panel*). Female FVB-Tg(adiponin) mice also exhibited

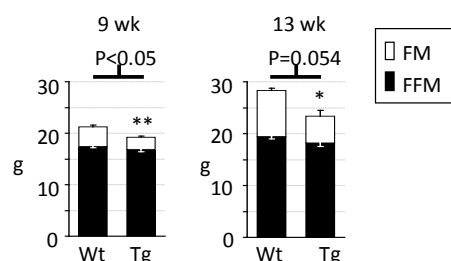


Fig. 2. Body composition analysis revealed FVB-Tg mice have significantly reduced fat mass at 9 weeks and significantly reduced gain in FM after one month of HFD feeding.

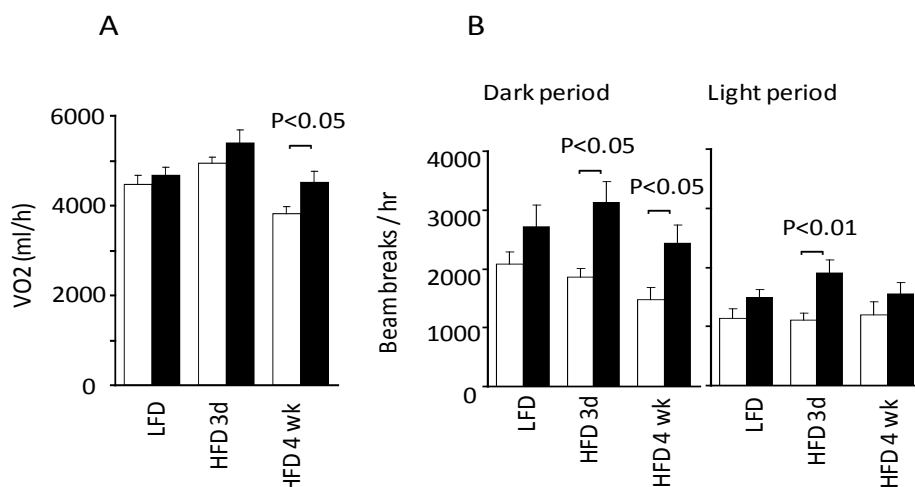


Fig. 3. FVB-Tg mice (DARK BAR) exhibit increased oxygen consumption (A) and spontaneous physical activity (B) compared to WT controls (LIGHT BAR).



protection from increased adiposity associated with 4 wk ingestion of a HFD (Figure 2 – right panel).

We next evaluated whether FVB-Tg(adropin) mice would exhibit improvements in glucose homeostasis observed in B6-Tg(adropin) mice. Female FVB-Tg(adropin) mice fed HFD for 4 wk exhibited lower fasting insulin ( $0.06 \pm 0.02$  vs.  $0.22 \pm 0.04$  ng/ml,  $P < 0.05$ ), with no significant difference in blood glucose ( $123 \pm 5$  vs  $128 \pm 8$  mg/dL,  $P = 0.6$ ). Insulin resistance promotes hepatic steatosis in part by stimulating hepatic lipogenesis [6,7]. Expression of a key lipogenic enzyme, stearoyl CoA desaturase was lower in liver of female FVB-Tg(adropin) mice compared to controls (expression in AU: WT  $1.00 \pm 0.27$ ; Tg  $0.25 \pm 0.04$ ,  $P < 0.05$ ,  $n = 8/\text{group}$ ).

Delayed diet-induced obesity in B6-Tg(adropin) mice is due to altered metabolism, with no difference in food intake [4]. Oxygen consumption ( $\text{VO}_2$ ) of female FVB-Tg(adropin) mice was significantly elevated compared to controls at 13 wk of age after exposure to HFD for 4 wk, but was not significantly different at 8 wk of age (Figure 3 – panel A). Female but not male B6-Tg(adropin) mice exhibit increased movement [4]. Female FVB-Tg(adropin) mice also exhibited increased activity during the dark phase (Figure 3 - panel B). Activity of male FVB-Tg(adropin) mice was normal (data not shown).

In summary, we have observed that FVB-Tg(adropin) mice exhibit a phenotype suggesting protection from metabolic disorders associated with diet induced obesity. As reported for B6-Tg(adropin) mice, these improvements are primarily due to altered metabolism and not altered food intake, while females also exhibited an increase in spontaneous physical activity.

## Conclusion

Adropin is a novel secreted peptide that is regulated by nutrient content of the diet and energy status of the body. Characterization of the function of adropin using transgenic mouse models in two different backgrounds suggests an important role in regulating glucose homeostasis. The adropin peptide may have potential for developing a novel therapy for treating metabolic disorders associated with obesity.

## Acknowledgments

Funding was provided by grants from the American Diabetes Association and Biomeasure Inc., IPSEN (to AAB). AAB and RLM are partially supported by Clinical Nutrition Research Unit Center Grant (1P30 DK072476) entitled "Nutritional Programming: Environmental and Molecular Interactions" sponsored by National Institute of Diabetes and Digestive and Kidney Diseases.

## References

1. Heilbronn, L.K., Gregersen, S., Shirkhedkar, D., Hu, D., Campbell L.V. *Diabetes* **56**, 2046 (2007).
2. Ravussin, E., Smith, S.R. *Ann. N.Y. Acad. Sci.* **967**, 363 (2002).
3. Reitman, M.L. *Cell. Metab.* **5**, 405 (2007).
4. Kumar, K.G., et al. *Cell. Metab.* **8**, 468 (2008).
5. Sutton, G.M., et al. *Endocrinology* **147**, 2183 (2006).
6. Browning, J.D., Horton, J.D. *J. Clin. Invest.* **114**, 147 (2004).
7. Yki-Jarvinen, H. *Ann. Med.* **37**, 347 (2005).

## Design, Synthesis and Biological Activities of New Urotensin II-Related Peptides (URP)

David Chatenet, Myriam Létourneau, and Alain Fournier

Laboratoire d'études moléculaires et pharmacologiques des peptides (LEMPP), INRS –  
Institut Armand-Frappier, Ville de Laval, Québec, H7V 1B7 Canada; Laboratoire  
International Associé INSERM – INRS Samuel de Champlain

### Introduction

Several studies have demonstrated that the urotensinergic system, composed of two cyclic peptides namely urotensin II and urotensin II-related peptide, was involved in numerous biological processes in normal and pathological states [1,2]. Both peptides mediate their actions through the activation of a specific G-protein coupled receptor (UT), belonging to the 1A subclass of the GPCR family, originally designated as sensory epithelial neuropeptide-like receptor (SENr) or GPR14 [3]. Up to now, the urotensin II peptides are being considered as the most potent vasoconstrictors identified so far. Based on their blood pressure-independent trophic and mitogenic actions, it has been suggested that UII and URP exert specific functions in pathological processes such as myocardial hypertrophy and fibrosis, vascular smooth muscle cell proliferation, atherosclerosis, and diabetic nephropathy [4]. Spectroscopic analysis of hU-II minimal active fragment, hUII(4-11), in which only the amino acid adjacent to the cyclic core differs from URP (Asp in hUII(4-11) versus Ala in URP), revealed a highly structured compound in SDS with a type II'  $\beta$ -turn structure [5]. Conversely, the conformation of URP, investigated in aqueous solution, demonstrated the presence of an inverse  $\gamma$ -turn centered on the Trp<sup>4</sup>-Lys<sup>5</sup>-Tyr<sup>6</sup> sequence, and an intramolecular hydrogen bond (i, i+2) between the C=O of Trp<sup>4</sup> and the NH of Tyr<sup>6</sup> [3].

### Results and Discussion

Apart from a D-isomer substitution, modifications of the Trp residue in UII or URP have always generated analogs with weak potency or affinity demonstrating its crucial role for biological activity. In this study, we investigated the impact of side chain modification or structural constrain introduction (Figure 1) on the biological activity of URP. These URP analogs have been evaluated for their binding affinity on hUT-transfected CHO cells and for their contractile activity on rat aortic rings stripped of endothelium (Table 1).

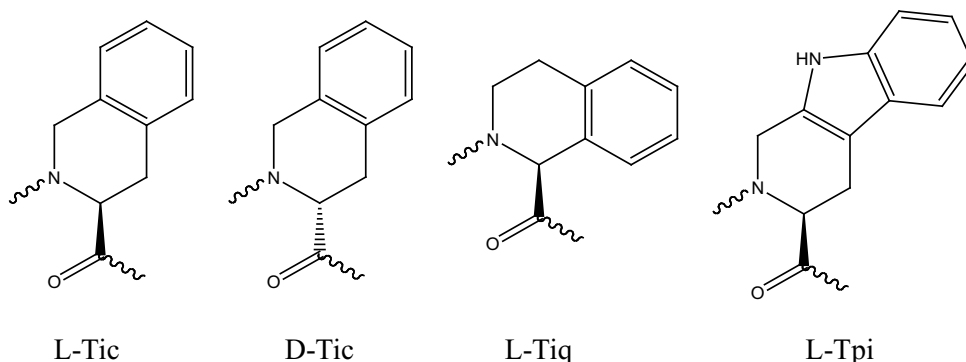


Fig. 1. Chemical structure of L/D 1,2,3,4-tetrahydroisoquinoline-3-carboxylic acid (Tic), L-1,2,3,4-tetrahydroisoquinoline-1-carboxylic acid (Tiq) and L-1,2,3,4-tetrahydronorharman-3-carboxylic acid (Tpi).

As shown in Table 1, substitution of the Trp<sup>4</sup> residue with Tiq or Tpi yielded two compounds ([Tiq<sup>4</sup>]URP (3) and [Tpi<sup>4</sup>]URP (6) that retained high binding affinity and almost equipotent contractile activity compared to URP (2) in the rat aortic ring assay. In contrast, replacement of the Trp<sup>4</sup> residue by the L-1,2,3,4-tetrahydroisoquinoline-3-carboxylic acid (4) reduced by 500-fold the binding affinity and almost 2-fold the biological activity. Surprisingly, inversion of configuration

of the Tic residue produced an analog which is able to bind and to fully activate UT though its binding for the receptor is reduced. NMR studies are in progress to assess the impact of such modifications on the secondary structure. Interestingly, replacement of the Trp moiety by the para-iodo-phenylalanine amino acid did not dramatically modify the pharmacological profile of the peptide suggesting that this particular compound might be used for further modifications *via* the Suzuki-Miyaura and Sonogashira cross-coupling reaction. Although we expected that the aromatic feature was a critical requirement to ensure biological activity, we observed that the [D-tBu-Gly<sup>4</sup>]URP was able to exert the same contractile activity as the native peptide whereas its L-enantiomer was not able to bind the receptor. Besides, replacement by a non-aromatic moiety reduced both the binding ability and contractile potency (but not efficacy) of the compound suggesting that steric hindrance might induce a favourable environment to trigger biological activity. Other substitutions such as Tyr(PO<sub>4</sub>), Tyr(SO<sub>3</sub>), Sta, Sar, Deg, Tic(OH) or Hyp generated analogs totally devoid of binding affinity.

Table 1. Pharmacological profile of URP derivatives

	Compounds	Binding	Aortic ring contraction	
		IC <sub>50</sub> (nM) <sup>a</sup>	pEC <sub>50</sub>	E <sub>max</sub> (%) <sup>b</sup>
1	hUII	13 (7.7-22.1)	9.9 ± 0.5	92.3
2	URP	21 (5.5-82.8)	8.1 ± 0.2	90.3
3	[Tiq <sup>4</sup> ]URP	12 (7.0-19.8)	7.6 ± 0.1	96.3
4	[Tic <sup>4</sup> ]URP	> 10 <sup>-5</sup>	5.8 ± 0.7	49.0
5	[D-Tic <sup>4</sup> ]URP	137 (28.6-653)	6.4 ± 0.1	122.0
6	[Tpi <sup>4</sup> ]URP	30 (10.9-84.5)	7.4 ± 0.2	138.9
7	[1-Nal <sup>4</sup> ]URP	23 (10.7-49.7)	7.3 ± 0.2	73.4
8	[D-1-Nal <sup>4</sup> ]URP	52 (34.1-80.4)	6.1 ± 0.1	43.9
9	[p-iodo-Phe <sup>4</sup> ]URP	74 (33-167)	6.3 ± 0.5	108.4
10	[Cha <sup>4</sup> ]URP	250 (132-476)	5.5 ± 0.2	138.8
11	[tBu-Gly <sup>4</sup> ]URP	> 10 <sup>-5</sup>	-	-
12	[D-tBu-Gly <sup>4</sup> ]URP	3681 (1671-8110)	6.8 ± 0.6	84.1

<sup>a</sup>Competitive binding assays using the <sup>125</sup>I-labeled hUII. Values in parentheses are 95% confidence limits.

<sup>b</sup>The maximum effect is expressed as a percentage of the amplitude of the contraction induced by 40 mM KCl

In summary, the present study has provided a detailed analysis of the structure-activity relationships of a series of URP analogs and suggested the presence of a very tight and well define hydrophobic binding pocket for the Trp residue inside UT. Using these *in vitro* and *ex vivo* assays, we were able to design and characterize new constrained URP agonists. These data should be useful for the development of selective UT antagonists.

## References

1. Douglas, S.A., Dhanak, V.R. *Trends Pharmacol. Sci.* **25**, 76-85 (2004).
2. Mori, M., Fujino, M. *Peptides* **25**, 1815-1818 (2004).
3. Chatenet, D., et al. *Peptides* **25**, 1819-1830 (2004).
4. Kemp, W., Roberts, S., Krum, H. *Curr. Vasc. Pharmacol.* **2**, 159-168 (2005).
5. Carotenuto, A., et al. *J. Med. Chem.* **47**, 1652-1661 (2004).

## pSK - A Novel Amphibian Skin Bowman-Birk-like Trypsin and TMPRSS2 Inhibitor

Hang Chen, Susan Hawthorne, Tianbao Chen, Chris Shaw,  
and Brian Walker

Molecular Therapeutics Research, School of Pharmacy, Queen's University, McClay Research Centre, 97  
Lisburn Road, Belfast BT9 7BL, Northern Ireland, UK

### Introduction

For centuries, extracts of amphibian skin has been widely used as folk medicines. Amphibian skin is a morphologically, biochemically and physiologically multifunctional organ which subserves general survival roles, such as anti-predator, anti-microbial and anti-fungal defense [1,2]. The complex cocktails of bioactive molecules which constitute defensive secretion in the highly-specialized dermal granular glands contain proteins, biogenic amines, alkaloids and a plethora of bioactive peptides. Serine proteases are one of the most well studied grouping of proteins and are involved in key regulatory processes such as peptide hormone precursor processing and release, blood coagulation and complement fixation, and additionally, for their intimate involvement in the pathogenesis of numerous diseases, including cancer, pulmonary emphysema and inflammation [3,4]. TMPRSS2, a type II transmembrane-bound serine protease, has gained interest due to its highly localized expression in the prostate and its overexpression in neoplastic prostate epithelium [5]. Once activated, the serine protease domain of TMPRSS2 is released from the cell surface into the extracellular space. TMPRSS may contribute to the prostate tumor metastasis via the activation of PAR (protease-activated receptor)-2 which belongs to a family of G-protein coupled receptors (PAR-1–4) activated by specific serine proteases expressed in many normal and malignant cell types.

### Results and Discussion

Here we describe a novel C-terminally amidated heptadecapeptide, isolated from the skin secretion of the frog of the genus *Rana pipiens*, {SAPRGCWTK SYPPKPCK-amide (pSK)} which contains a disulphide loop between Cys6 and Cys16. pSK shares a high degree of homology with the core inhibitory motif found in Bowman-Birk type protease inhibitors (BBI) such as sunflower seed trypsin inhibitor (aSFTI) (Acyl-SAPRGCWTKSYPPKPCK-amide). A synthetic replicate of pSK, was found to be a potent inhibitor of trypsin with a  $K_i$  just slightly less than 96 nM, a value falling between those determined for aSFTI (2.2 nM) and the core inhibitory loop of BBI (CTKSIPPQC)(119.0 nM). pSK also exhibited inhibitory activity ( $K_i$  = 6.85  $\mu$ M) against TMPRSS2 (type II transmembrane-bound serine protease), a trypsin-like serine protease involved in tumor proliferation. This compares very favorably with the degree of inhibition observed with aSFTI ( $K_i$  = 6.97  $\mu$ M) and BBI ( $K_i$  = 19.55  $\mu$ M). The kinetic data for each peptide are summarized in Table 1.

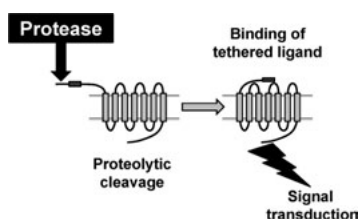


Fig. 1. Mechanism of activation of PARs.

and tissue inhibitors of metalloproteases (TIMPS)) [6-8]. Amphibian skin secretions have been

Table 1. Inhibitor constants for *Rana-cyclinE-Amide*, *BBI-Amide* and a *SFTI-Amide* against trypsin and TMPRSS2.

Peptide	Ki (nM) (trypsin)	Ki (μM)(TMPRSS2)
Acyl-GRCTKSIPPICFPD- amide	2.2	6.97
CTKSIPPQC	119	6.85
SAPRGCWTKSYPPKPCCK-amide	96	19.55

found to contain protease inhibitors from several different classes. Kunitz-type protease inhibitors have been isolated and structurally-characterized from the skin secretion of the North American crawfish frog, *Rana areolata*, and the Madagascan tomato frog, *Dyscophus guineti*. Additionally, *R. areolata*, in common with four species of bombinid toad investigated (*Bombina bombina*, *variegata*, *orientalis* and *maxima*), contained a novel inhibitor of trypsin/thrombin in defensive skin secretions that shared a common motif with an inhibitor from the parasitic nematode, *Ascaris suum*. More recently, a Kasal-type inhibitor of post-proline cleaving enzyme was found in the skin secretions of the South American phyllomedusid [9]. Due to the tissue-specific expression of TMPRSS2, and its location on the cell membrane, it provides a potential therapeutic target for prostate cancer. Treatment of invasive cancer depends increasingly more on therapeutic strategies for prevention and intervention before metastatic dissemination. pSK is one of the first examples of a naturally occurring inhibitor of TMPRSS2 and could prove useful in delineating the role of this protease in tumor proliferation and invasion.

## Acknowledgments

Hang Chen is in receipt of an Overseas Studentship at Queen's University, Belfast, UK.

## References

1. Clarke, B.T. *Biol. Rev. Camb. Philos. Soc.* **72**, 365–379 (1997).
2. Horl, H., Heidland, A. *Proteases: potential role in health and disease*, in: *Advances in Experimental Medicine and Biology*, vol. 167, Plenum Press, New York, 2004.
3. Bode, W., Huber, R. *Eur. J. Biochem.* **204**, 433–451 (1992).
4. Lambert, E., Dassé, E., Haye, B., Petitfrère, E. *Crit. Rev. Oncol. Hematol.* **49**, 187–198 (2004).
5. Paoloni-Giacobino, A., Chem, H., Peitsch, M.C., Rossier, C., Antonarakis, S.E. *Genomics* **44**, 309–3203 (1997).
6. Conlon, J.M. *Rev. Med. Microbiol.* **15**, 1–9 (2004).
7. Tyler, M.J., Stone, D.J.M., Bowie, J.H. *J. Pharmacol. Toxicol. Methods* **28**, 199–200 (1992).
8. Gettins, P.G. *Chem. Rev.* **102**, 4751–4804 (2002).
9. Song, G., et al. *Biochem. Biophys. Res. Commun.* doi:10.1016/j.bbrc.2008.05.035 (2008).

## Peptides Inhibitors of F11R/JAM-A Adhesion Molecules and Potent Anti-atherosclerosis Drugs

Cristina C. Clement,<sup>1</sup> Anna Babinska,<sup>2</sup> Yigal H.Ehrlich,<sup>3</sup> Manfred Philipp,<sup>4</sup>  
and Elizabeth Kornecki<sup>2</sup>

<sup>1</sup>Chemistry Department, Lehman College, City University of New York (CUNY), 250 Bedford Park BLVD West, Bronx, New York City, NY 10468, U.S.A.; <sup>2</sup>Department Anatomy and Cell Biology, and Dept. of Medicine, SUNY, Down State Medical Center, Brooklyn-NYC, NY 11203, U.S.A.; <sup>3</sup>Program in Neuroscience, CUNY at Staten Island, NY 10314; <sup>4</sup>Chemistry Department, Lehman College and Biochemistry Ph.D. Program, City University of New York, New York City, NY 10016-430, U.S.A.

### Introduction

The F11 receptor (F11R) was characterized as an adhesion protein, aka JAM-A, which under normal physiological conditions is expressed constitutively on the surface of platelets and localized within tight junctions of endothelial cells. The utilization of specific F11R/JAM-A peptide antagonists and recombinant proteins demonstrated a role for F11R/JAM-A in the process of platelets adhesion to inflamed endothelial cells which initiates plaque formation leading to inflammatory thrombosis and atherosclerosis, where the platelets have a critical influence in the progression and development of cardiovascular disease [1]. Thus, the development of new drugs antagonizing the F11R/JAM-A function could evolve as an effective new strategy for the treatment of atherosclerosis, heart attacks and stroke [2]. We present one of the first trials toward development of peptide-based inhibitors of F11R/JAM-A function. Among many trials, the peptide D-Lys-Ser-Val-Ser-D-Arg-Glu-Asp-Thr-Gly-Thr-Tyr-Thr-Cys-CONH<sub>2</sub> proved to be a potent inhibitor of human platelets aggregation *in vitro*. Further molecular docking experiments showed that this peptide makes favorable hydrophobic and electrostatic interactions within the proposed binding site of JAM-1 (X-Ray structure 1nbq.pdb was used as a template in docking experiments).

### Results and Discussion

The utilization of specific F11R/JAM-A peptide antagonists and recombinant proteins has begun to reveal the role of F11R/JAM-A in the process of platelet adhesion to inflamed endothelial cells and identified F11R/JAM-A as a potentially important molecule in platelet plaque formation leading to inflammatory thrombosis and atherosclerosis, with platelets as critical factors involved in the progression and development of cardiovascular disease [1,2]. The peptides were originally developed from the L-amino acid sequence (H<sub>2</sub>N-Lys-Ser-Val-Ser-Arg-Glu-Asp-Thr-Gly-Thr-Tyr-Thr-Cys-COOH) predicted to be involved in the interaction between the two adhesion molecules, F11R and JAM-A (1), and were further modified with D-amino acids to increase their stability to proteolysis *in vivo*. *In silico* modeling using the docking software SCULPT from MDL, predicted four different conformations for the new lead peptide H<sub>2</sub>N-D-Lys-Ser-Val-Ser-D-Arg-Glu-Asp-Thr-Gly-Thr-Tyr-Thr-Cys-CONH<sub>2</sub> (peptide-4-D), that are characterized with the lowest free energy of interaction with the target protein, the F11 receptor (1nbq.pdb) All predicted conformers are characterized by both van der Waals and electrostatic interactions with the target protein, the F11 receptor (1nbq.pdb) (Table 1).

Table 1. The predicted free energy of interaction (based on van der Waals and Van der Waals+Electrostatics) between the lead peptide D-Lys-Ser-Val-Ser-D-Arg-Glu-Asp-Thr-Gly-Thr-Tyr-Thr-Cys-CONH<sub>2</sub> (peptide-4-D) and its target, the F11 receptor, together with its four different conformations adopted in the proposed active site of F11R/JAM-A receptor (1)

Conformation	Van der Waals (kcal/mol)	Van der Waals+ Electrostatic (kcal/mol)	Active site contacts (based on Van der Waals and electrostatic interactions)
1	-138.6	-556.0	Val38, Ile40, Asn44, Pro45, Val46, Lys47, Ser49, Gly93, Thr95
2	-145.7	-591.6	Ser82, Tyr83, Asp85, Arg86, Val87, Phe96, Lys97, Ser98, Val99, Thr100, Arg101, Glu102, Asp103
3	-151.7	-593.6	Lys47, Cys50, Tyr52, Val60, Asn77, Thr88, Phe89, Leu90, Pro91, Thr92, Gly93, Ile94, Thr95
4	-142.2	-531.8	Ser34, Glu35, Val38, Ile40, Asn44, Pro45, Val46, Lys47, Leu48, Ser49, Gly93, Thr95

All four conformations of the peptide-4-D are fitted within the steric active site of F11-R (1) (Table 1). The data from the docking experiments prompted us to further synthesize the lead compound and to analyze its efficacy as an inhibitor of platelets aggregation *in vitro*. Solid phase peptide synthesis was used for the synthesis of peptide-4-D on a Rink-Amide resin and by employing standard Fmoc chemistry. The ability of peptide-4-D to inhibit the platelets aggregation was determined using a standard platelets aggregation assay developed originally by Babinska et al. [1]. Platelets aggregation was initiated by the addition of a monoclonal antibody anti-F11R (0.65 ug/assay) which was shown previously to activate the platelets aggregation [1]. At 210 uM, peptide-4-D inhibited completely the platelets aggregation, as compared with the peptide-4-L (its L-analog), which had the same effect at a concentration two fold higher (~410 uM). This is the first report of a peptide containing D-amino acids at selective positions, potential inhibitor of platelets adhesion to the inflamed endothelium and can be used as a new scaffold for developing new anti-atherosclerosis and anti-thrombosis drugs. The new lead compound was stable to hydrolysis by different proteases (such as trypsin and thrombin) and had two fold higher efficiency to inhibit the platelets aggregation *in vitro*.

## Acknowledgments

We thank to Dr. Manfred Philipp's lab, at Lehman College-CUNY for the assistance with the peptide synthesis.

## References

1. Babinska, A., et al. *Thromb. Haemost.* **88**, 43-50, (2002).
2. Babinska, A., et al. *Thromb. Haemost.* **97**, 272-81, (2007).

## The Human Insulin/Relaxin Superfamily: New Members and Functions

John D. Wade,<sup>1,2</sup> M. Akhter Hossain,<sup>1</sup> Feng Lin,<sup>1</sup> Fazel Shabanpoor,<sup>1</sup>  
 Alessia Belgi,<sup>1</sup> Linda Chan,<sup>1</sup> Suode Zhang,<sup>1</sup> and Geoffrey W. Tregear<sup>1</sup>

<sup>1</sup>Howard Florey Institute, <sup>2</sup>School of Chemistry, University of Melbourne, Parkville,  
 Victoria 3010, Australia

### Introduction

Some twenty years after Sanger's landmark report of the primary structure of bovine insulin, it was shown that porcine relaxin also consisted of two chains that were cross bridged by three disulfide bonds in an identical arrangement to that of insulin [1]. This established the concept of the insulin superfamily of peptides and led to a vigorous search for additional members in not only the human but other mammals as well. With the emergence of novel DNA sequencing methods, analysis of human DNA showed the presence of not one but two genes for relaxin which were named genes 1 and 2 [2]. Subsequent work has since shown that gene 1 relaxin is only found in humans and higher primates and has an unknown function. Shortly afterwards, gene 2 relaxin was identified and is now recognized to be the major circulating form of relaxin in all mammals and is simply called relaxin. The next two members of the superfamily to be identified were insulin-like growth factors 1 and II which, unlike all other members are single-disulfide chain peptides that possess the insulin-like crosslinks. Differential screening of testis-specific transcripts led to the identification of insulin-like peptide 3 (INSL3) and analysis of human placental cDNA library resulted in the discovery of the gene for insulin-like peptide 4 (INSL4). It has not yet been confirmed that INSL4 is expressed *in vivo* and, if so, whether it consists of a one or two-chain structure. EST databases were used to identify the presence of both insulin-like peptide 5 (INSL5) and insulin-like peptide 6 (INSL6). Finally, the availability of the Celera Genomic database in the early 2000s allowed the most unexpected discovery of the final member of the superfamily, relaxin-3 [2]. Membership thus numbers ten peptides. The primary structure varies considerably between these members; only seven residues are invariant with six of these being the cysteine residues that make up the three disulfide bonds (Figure 1).

### Phylogeny of the human insulin superfamily

The availability of comprehensive genomic sequence databases has allowed a detailed phylogenetic analysis of the insulin superfamily and an elucidation of the evolution of its members. The ancestral insulin gene is that of insulin itself. It is the precursor to the genes for IGFs I and II. However, the next gene to evolve was that of relaxin-3 followed closely by that of INSL5 at a time before the evolution of the fish. The genes of the remaining members of the family have evolved from this relaxin-3 ancestor [3]. Indeed, these are collectively classified as members of the relaxin sub-family of peptide hormones.



Fig. 1. Primary structures of members of the human insulin superfamily. Conserved residues are shaded.



## Receptors for the relaxin family peptides

The recognition that the receptors for insulin and IGFs I and II are tyrosine kinases led to a long, concerted search by several laboratories for similar receptors for relaxin. Finally, as recently as 2002, it was shown that relaxin bound to and activated a G-protein coupled receptor known as LGR7 (leucine-rich GPCR7). It also interacts with the related receptor LGR8 with high affinity [4]. However, subsequent work showed this latter receptor to be that for INSL3. These two receptors are class C LGRs which share 60% amino acid sequence identity. Both contain the typical seven transmembrane spanning regions of GPCRs together with a large ectodomain containing leucine-rich repeat strands and a LDL class A module at the terminus. In contrast, the receptors for relaxin-3 and INSL5 have been determined to be conventional GPCRs that lack the LRR and LDLa module, and which are closely related to the receptors for somatostatin and angiotensin II. These have been termed GPCRs 135 and 142 respectively. To date, the receptors for INSLs4 and 6 remain unknown [5].

## Biological functions

Relaxin was first discovered in 1926 and it was soon identified to be a substance that had key roles in the preparation of the birth tract for the delivery of the young. In higher primates, however, relaxin has evolved to assume a pleiotropic role. It is expressed in many tissues and is now recognized to be important for protecting several organs from the onset of fibrosis [6]. It is also a potent vasodilator and has significant cardiovascular actions including increasing cardiac output and heart rate. It has recently passed Phase II clinical trials for the treatment of acute heart failure [7]. INSL3 is expressed in both the male testes and the female ovary where it is known to regulate germ cell maturation. It is also involved in mediating testes descent during foetal development. In contrast, little is known about a possible function for INSL4. Its gene is principally expressed in placental tissue but it is not yet known whether a processed INSL4 peptide is produced *in vivo* and, if so, if this has a single-chain IGF-like or two-chain structure. Highest expression of human INSL5 is in the gut, particularly the colon, leading to the speculation that it may play a role in appetite regulation. INSL6 is highly expressed in the male testis and a recent study has identified a role in the regulation of spermatogenesis [8]. The nature of the peptide *in vivo* remains unknown as does its receptor. The final member of the human insulin superfamily to be identified, relaxin-3, is highly expressed in the brain, more specifically in the neurons of the nucleus incertus. It is now clear that it has key roles in appetite regulation and in stress and anxiety [6].

## Contribution of chemical synthesis to the study of insulin-like peptides

A great deal of our current knowledge of the biological roles of these peptides has stemmed from their availability via chemical synthesis. Their two-chain three disulfide bond structure has long been a technical challenge. The pioneering work of the Shanghai Insulin Synthesis group in the early 1960s showed that the individual A- and B-chains of insulin could be combined together in solution at high pH to produce correctly linked and folded peptide [9]. The same approach has enabled the provision of numerous analogues of insulin as well as relaxin and INSL3. However, it was soon apparent that the loss of secondary structure that accompanies truncated or mutated chains of INSLs was detrimental to the efficiency of folding, often completely so. The subsequent development of efficient solid phase synthesis strategies together with regioselective disulfide bond formation methods now provides a means of obtaining virtually any analogue of an INSL peptide [10]. It has been employed to systematically Ala-scan the receptor binding site of human INSL3 which is defined by just five key residues within the B-chain (Figure 2) [10]. To date, the data suggest that, despite these relaxin family members sharing a common insulin core structure, their respective binding sites are exquisitely dictated by few residues, seemingly all within their B-chains.

Much remains to be understood about this fascinating superfamily of peptides. Given that insulin-like peptides are present in all classes of vertebrates including the dog, cat and rabbit and also in amphibians, fish and birds. Remarkably, such peptides are also present in invertebrates including insects, mollusks and nematodes which highlights that insulin is an evolutionarily ancient molecule that is present in all metazoa. The ongoing studies on the human

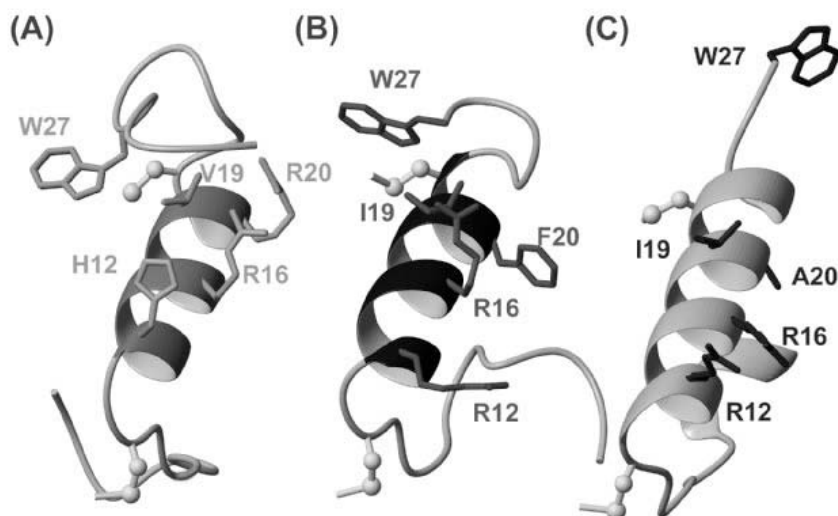


Fig. 2. The tertiary structures of the B-chains of (A) human INSL3, (b) human relaxin-3, and (C) human relaxin showing the key residues involved in the binding of the native molecules to their receptors.

insulin/relaxin superfamily will undoubtedly contribute to our understanding of the molecular evolution of this fascinating class of molecule.

## Acknowledgments

We thank our many colleagues, past and present, including those within the Neuropeptides Team at the Howard Florey Institute for their considerable support and collaboration. Supported in part by grants 508995 and 509048 (NHMRC of Australia) to JDW.

## References

1. Schwabe, C. and McDonald, J.K. *Science* **197**, 914-915 (1976).
2. Shabanpoor, F., Separovic, F. and Wade, J.D., In Litwack, G. (Ed.) *Vitamins and Hormones* Elsevier, The Netherlands, 2009, p. 1.
3. Wilkinson, T.N., Speed, T.P. and Bathgate, R.A.D. *BMC Evol. Biol.* **5**, 14 (2005).
4. Hsu, S.Y. et al. *Science* **295**, 671-674 (2002).
5. van der Westhuizen, E. et al. *Drug Discov. Today* **13**, 640-651 (2008).
6. Samuel, C.S. et al. *Cell Mol. Life Sci.* **64**, 1539-1557 (2007).
7. Dschietzig, T. et al. *J. Card. Fail.* **15**, 182-190 (2009).
8. Burnicka-Turek, O. et al. *Endocrinol.* (in press).
9. Wade, J.D., In Buchner, J. and Moroder, L. (Eds.) *Oxidative Folding of Peptides and Proteins* RSC Publishing, UK, 2009, p. 345.
10. Rosengren, K.J. et al. *J. Biol. Chem.* **281**, 28287-28295 (2006).

## **Molecular-basis for Specificity in Biological Action at the Homologous Glucagon and GLP-1 Receptors**

**Jonathan W. Day, James T. Patterson, Vasily M. Gelfanov, and  
Richard D. DiMarchi**

*Department of Chemistry, Indiana University, Bloomington, IN 47405, U.S.A.*

### **Introduction**

Glucagon and glucagon-like peptide-1 (GLP-1) are two highly homologous hormones involved in the maintenance of glucose homeostasis and of sizable importance to the clinical management of diabetes. These two peptides are highly specific in association with their native receptors through structural elements within different regions of their sequences that confer biological specificity. We explored the structure-activity relationship of these two hormones through the use of single residue substitutions and hybrid peptides. We have identified a set of novel 29-residue peptides which exhibit high potency and balanced co-agonism at the glucagon and GLP-1 receptors. Modifications to the glucagon C-terminal sequence resulted in a nearly complete loss of specificity, with minimal change to inherent activity. Three modifications to native glucagon and addition of a C-terminal amide produced a peptide with a 100-fold increase in potency at the GLP-1 receptor and potency equivalent to glucagon. The significant increase in potency at the GLP-1 receptor can be attributed to an increase in alpha helicity as well as enhanced positional interactions at the receptor. These high potency glucagon-based co-agonists represent a refined set of peptides that vary in selectivity within a dynamic range that spans a ten-fold preference for one or the other receptor while maintaining full potency at one of the two receptors. The analogs identified provide the basis for investigating through *in vivo* studies the relative efficacy and safety obtainable at each receptor for purposes of optimizing metabolism and body weight.

### **Results and Discussion**

**Glucagon/GLP-1 chimeric peptides:** Chimeric peptides of glucagon and GLP-1 were synthesized around an E16 Glucagon-NH<sub>2</sub> nucleus (Table 1). Substitution of the N-terminal half of E16 Glucagon-NH<sub>2</sub> yielded GLP-E16-Glucagon-NH<sub>2</sub>. This peptide was equipotent at the GLP-1R and 1000-fold less potent at the GCGR relative to E16 Glucagon-NH<sub>2</sub> (Table 1). Replacement of the C-terminal half of E16 Glucagon-NH<sub>2</sub> yielded Chimera 1 (Table 1). C-terminal GLP-1 sequence reduced potency 10-fold at the GCGR and enhanced potency at the GLP-1R by almost 12-fold relative to E16 Glucagon-NH<sub>2</sub>. This aligns with previously published glucagon/GLP-1 hybrid data that showed the N-terminal half of GLP-1 to be highly selective for the GLP-1R while C-terminal GLP-1 sequence provided less specificity [1]. Chimera 1 is a highly potent GLP-1R agonist, but is 14-fold more selective for the GLP-1R. We replaced the three C-terminal GLP-1 residues of Chimera 1 with glucagon residues resulting in Chimera 2 sequence. Chimera 2 exhibited less than 2-fold selectivity for the GLP-1R and potency greater than 100% relative to the native ligands at the glucagon and GLP-1 receptors. From the six divergent residues between E16 Glucagon-NH<sub>2</sub> and Chimera 2, Ala18 and Lys20 provided the molecular basis for the 6.5-fold increase in potency at the GLP-1R.

Our work demonstrates that GLP-1 derives the majority of its specificity in biological action for the GLP-1R from its divergent N-terminal residues Ala2, Glu3, Val10, and Ser12. Our work also shows the importance of Val27, Lys28, and Gly29 for selective activation at GLP-1R. Key features of glucagon that confer selectivity for the GCGR are the C-terminal acid and positions 17-24, more specifically Arg18 and Gln20. Starting with highly selective native glucagon, we designed a peptide (Chimera 2) equipotent to glucagon at GCGR that showed a greater than 100-fold increase in potency at the GLP-1R.

Table 1. Data summary of glucagon/GLP-1 chimeric peptides

Peptide	Glucagon Receptor EC50(nM)±s.d.	GLP-1 Receptor EC50(nM)±sd	Relative % GCGR	Relative % GLP-1R	Selectivity GCGR:GLP-1R
Glucagon	0.071±0.036	3.3±0.5	100	0.99	101
GLP-1	>1000	0.033±0.017	<0.008	100	<10 <sup>-4</sup>
Glucagon-NH <sub>2</sub>	0.15±0.10	0.60±0.37	47	5.5	8.5
E16 Glucagon-NH <sub>2</sub>	0.049±0.019	0.18±0.11	145	18	8.1
E16 K20 Glucagon-NH <sub>2</sub>	0.077±0.026	0.071±0.034	92	46	2.0
Chimera 1	0.47±0.19	0.015±0.009	15	220	0.07
Chimera 2	0.068±0.029	0.026±0.012	104	127	0.82
E16 A18 K20 Glucagon-NH <sub>2</sub>	0.087±0.018	0.028±0.019	82	118	0.69
GLP-E16-Glucagon-NH <sub>2</sub>	50±17	0.18±0.10	0.15	18	0.008
E16 GLP-1(1-29)-NH <sub>2</sub>	-	0.011±0.003	-	300	-

## Acknowledgments

We thank Jay Levy, David Smiley, Angela Hansen and Jonathan Karty for their support in synthesis, purification and analysis.

## References

1. Runge, S., et al. *Br J Pharmacol.* **138**, 787-794 (2003).

## Highly Constrained Glucagon-Like Peptide-1 with Improved Biological Activity and Enzyme Stability

Eunice N. Murage,<sup>1</sup> Guangzu Gao,<sup>2</sup> Alessandro Bisello,<sup>2</sup> and Jung-Mo Ahn<sup>1</sup>

<sup>1</sup>Department of Chemistry, University of Texas at Dallas, Richardson, TX 75080, U.S.A.; <sup>2</sup>Departments of Medicine and Pharmacology, University of Pittsburgh School of Medicine, Pittsburgh, PA 15260, U.S.A.

### Introduction

Glucagon-like peptide-1 (GLP-1) is a peptide hormone secreted from intestine upon food intake and stimulates insulin release by acting on pancreatic  $\beta$ -cells [1]. In addition, it was found to restore pancreatic  $\beta$ -cell mass and function, thus has been regarded as a potent therapeutic agent for treating type 2 diabetes. However, its clinical application is severely limited by rapid degradation by enzymes that result in a short half life [1]. Thus, developing enzymatically stable and potent GLP-1 agonists is of considerable interest.

A solution structure of GLP-1 determined by 2D-NMR showed two  $\alpha$ -helical segments between residues 13-20 and 24-35 connected by a short linker region between residues 21-23 [2]. To confirm the presence and locations of the two helices when GLP-1 binds to its receptor, we have scanned a lactam bridge throughout the sequence of GLP-1 [3]. A lactam bridge was formed between Lys<sup>1</sup> and Glu<sup>1+4</sup> to induce and stabilize  $\alpha$ -helical conformation at various regions of GLP-1. A series of the cyclic GLP-1 analogues were synthesized and assessed on GLP-1 receptors, and confirmed that the receptor-bound conformation of GLP-1 has two helical segments between residues 11-21 and 23-34, similar to the NMR structure.

Based on these findings, a number of GLP-1 analogues containing multiple lactam bridges between Glu<sup>1</sup> and Lys<sup>1+4</sup> were synthesized and evaluated for their capability to activate the receptor. Simultaneous stabilization of both helices in GLP-1 is anticipated to enhance receptor interaction. In addition, these cyclic GLP-1 analogues were also examined for enzyme stability against dipeptidyl peptidase-IV (DPP-IV) and neutral endopeptidase (NEP) 24.11 that are found to rapidly degrade GLP-1.

DPP-IV is a serine protease that cleaves protein substrates with Pro or Ala at the penultimate N-terminus, and cleaves GLP-1 between Ala<sup>8</sup> and Glu<sup>9</sup> [4] resulting in an inactive metabolite GLP-1(9-36)-NH<sub>2</sub> [5]. On the other hand, NEP 24.11 is a membrane-bound zinc metallopeptidase that cleaves peptide bonds immediately after amino termini of hydrophobic residues. NEP 24.11 cleaves multiple sites of GLP-1, in particular Asp<sup>15</sup>-Val<sup>16</sup>, Ser<sup>18</sup>-Tyr<sup>19</sup>, Tyr<sup>19</sup>-Leu<sup>20</sup>, Glu<sup>27</sup>-Phe<sup>28</sup>, Phe<sup>28</sup>-Ile<sup>29</sup>, and Trp<sup>31</sup>-Leu<sup>32</sup>, all leading to inactive metabolites [6]. Although stability of GLP-1 against DPP-IV has been achieved by N-terminal modifications or DPP-IV inhibitors, limited studies have been reported for NEP 24.11 [7]. Thus, the cyclic GLP-1 analogues were examined for enzyme stability since the lactam bridges installed to stabilize  $\alpha$ -helical conformation may also shield them from degradation by DPP-IV and NEP 24.11.

### Results and Discussion

All of the cyclic GLP-1 analogues were synthesized by using a standard *N* $^{\alpha}$ -Fmoc/*t*-butyl solid-phase peptide synthesis protocol. Glu and Lys used to form a lactam bridge were orthogonally protected with allyl protecting groups. After selective removal of the allyl groups with Pd(PPh<sub>3</sub>)<sub>4</sub> and an allyl scavenger like *N,N'*-dimethylbarbituric acid, a lactam bridge was created with PyBOP while the peptide was still bound to the resin. The synthesized peptides were then purified with RP-HPLC and analyzed by ESI-MS. The peptides were then examined for their capability to activate the GLP-1 receptor in subconfluent cultures of HEK293 cells stably expressing human GLP-1 receptors in the presence of a phosphodiesterase inhibitor, 3-isobutyl-1-methylxanthine [8].

As summarized in Table 1, the introduction of a lactam bridge led to increase or no significant loss in potency, and all of the monocyclic GLP-1 analogues **1-3** showed high receptor activation presumably resulting from the stabilized  $\alpha$ -helical conformation by placing a lactam bridge. In particular, the cyclic peptide **2** with a lactam bridge between Glu<sup>18</sup> and Lys<sup>22</sup>

Table 1. Summary of efficacy and half life of GLP-1 and its cyclic analogues against DPP-IV and NEP 24.11

	Sequence	EC <sub>50</sub> (nM)	Relative Efficacy	DPP-4 t <sub>1/2</sub>	NEP t <sub>1/2</sub>
GLP-1	HAEGTFTSDVSSYLEGQAAKEFIAWLVKGR	4.7	100	2.5	3.5
1	c[E <sup>16</sup> , K <sup>20</sup> ] GLP-1(7-36) NH <sub>2</sub> -----E---K-----	4.0	120	2	nd <sup>a</sup>
2	c[E <sup>18</sup> , K <sup>22</sup> ] GLP-1(7-36) NH <sub>2</sub> -----E---K-----	0.5	940	2.5	8
3	c[E <sup>30</sup> , K <sup>34</sup> ] GLP-1(7-36) NH <sub>2</sub> -----E---K-----	5.8	80	4	nd <sup>a</sup>
4	c[E <sup>16</sup> , K <sup>20</sup> ] c[E <sup>30</sup> , K <sup>34</sup> ] GLP-1(7-36) NH <sub>2</sub> -----E---K-----E---K---	3.3	140	3	4.5
5	c[E <sup>18</sup> , K <sup>22</sup> ] c[E <sup>30</sup> , K <sup>34</sup> ] GLP-1(7-36) NH <sub>2</sub> -----E---K-----E---K---	1.2	390	4	>24

<sup>a</sup> Not determined

exhibited superior potency (10-fold increase) compared to GLP-1. No significant loss of potency was observed by placing a lactam bridge at the C-terminal region.

In order to stabilize both helices at the N- and C-terminal regions simultaneously, bicyclic GLP-1 analogues **4** and **5** were synthesized by combining lactam bridges found effective in the monocyclic peptides **1-3**. The additional helix stabilization by the lactam bridge at the N-terminal region improved the potency of the monocyclic peptide **3** with a lactam bridge at the C-terminal region. Remarkably, this approach led to develop a highly constrained GLP-1 analogue **5** with significantly higher potency compared to GLP-1 (4-fold increase).

The potent bicyclic GLP-1 analogue **5** was incubated with DPP-IV and found to have higher stability against the enzyme despite its native N-terminal sequence. It is interesting that the lactam bridge located in the N-terminal region did not protect GLP-1 analogues from DPP-IV degradation whereas the C-terminal one did (peptide **2** vs. **3**). On the other hand, the bicyclic GLP-1 analogue **5** was found to be quite stable against NEP 24.11. This superior NEP stability appears to be acquired from the lactam bridges placed in the sequence that protected the peptide from being recognized by the enzyme.

In summary, we have designed and synthesized GLP-1 analogues containing multiple lactam bridges, and the conformational restriction improved potency by stabilizing binding determinants, two  $\alpha$ -helices. In addition, the lactam bridges used to create the bicyclic structure are found to enhance enzyme stability, especially against NEP 24.11.

## Acknowledgments

Supported by grant 37-2009-103 (Juvenile Diabetes Research Foundation), AT-1595 (Welch Foundation), and 7-07-JF-02 (American Diabetes Association).

## References

1. Deacon, C.F. *Diabetes* **53**, 2181 (2004).
2. Thorton, K., Gorenstein, D.G. *Biochemistry* **33**, 3532-3539 (1994).
3. Murage, E.N., Schroeder, J.C., BeinBorn, M., Ahn, J.-M. *Bioorg. Med. Chem.* **16**, 10106-10112 (2008).
4. Mentlein, R. *FEBS Lett.* **234**, 251-256 (1988).
5. Knusden, L.B., Pridal, L. *Eur. J. Pharmacol.* **318**, 429-435 (1996).
6. Turner, A.J., Isaac, R.E., Coates, D. *Bioessays* **23**, 261-269 (2001).
7. Gallwitz, B., Ropeter, T., Morys-Wortmann, C., Mentlein, R., Siegel, E.G., Schmidt, W.E. *Regulatory Peptides* **86**, 103-111 (2000).
8. Syme, C.A., Zhang, L., Bisello, A. *Mol. Endocrinol.* **12**, 3400-3411 (2006).

## **Discovery and Structural Optimization of High Affinity Co-Agonists at the Glucagon and GLP-1 Receptors**

**Tao Ma, Jonathan Day, Vasily Gelfanov, and Richard DiMarchi**

*Department of Chemistry, Indiana University, Bloomington, IN 47405, U.S.A.*

### **Introduction**

Glucagon, which consists of 29 amino acid residues, is a peptide hormone secreted by the  $\alpha$ -islet cells of pancreas and has a central function in glucose homeostasis. It is used as a critical care medicine in the treatment of insulin-induced hypoglycemia. Glucagon-like peptide-1 (GLP-1) is an incretin hormone that is secreted from intestinal L-cells, and it enhances insulin secretion, stimulates insulin biosynthesis, and decreases glucagon secretion. GLP-1 receptor is an attractive target for the treatment of hyperglycemia.

Through the analysis of their native sequence, glucagon and GLP-1 are structurally homologous but of apparent opposite physiological function (Figure 1). We have pioneered the use of co-agonists of appropriate balance to obtain improved management of obesity and the associated diseases, such as Type II Diabetes. A thorough understanding of the respective chemical and physical elements involved in each receptor's activation remains our goal as a means to a more informed design of new drug candidates. Starting from the native glucagon sequence, a series of receptor co-agonists have been prepared through insertion of specific helix-favoring amino acid substitutions and peptide backbone conformational constraints. Specifically in this report we studied backbone stabilization by using covalent lactam bridge formation at various positions and with differing linker size. In certain peptides, non-coded amino acids (Orn, and Dab) and D-amino acid isomers have been applied to further our structure-function analysis.

### **Results and Discussion**

Helix-favoring amino acid substitutions in the central sequence of glucagon and GLP-1 have been associated with enhanced biopotency [1,2]. We have observed that co-agonism can be achieved through careful selection of the peptide sequence and site-selective optimization of secondary structure [3]. These results emphasize the importance of lactam ring location and size in the achievement of balanced co-agonism (Table 1). The central region of the peptide is the preferred location for backbone stabilization, with 16-20 and 17-21 being of similar character (peptides 1 & 7). Interestingly, the open and lactam forms of the 17-21 linear peptide was comparably potent and balanced in its co-agonism (peptides 1 & 2). The C-terminal was of considerable importance to achieving balanced co-agonism with GLP-1 activity diminished in the C-terminal acids. Shortening the size of the lactam-bridge in the 16-20 lactams (peptides 4-6) decreased the potency at both receptors. Similar chemical changes in the N-terminus of the peptide (peptides 12-19) were uniformly less potent at both receptors. We conclude that glucagon C-terminal amides that are appropriately stabilized in the central region of the peptide can provide potent and balanced co-agonism.

Glucagon: HSQGT FTSDY SKYLD SRRAQ DFLVQW LMNT  
GLP-1: HAEGT FTSDV SSYLE GQAAK EFLAW LVKGR

*Fig. 1. Sequence homology of native glucagon and GLP-1.*

Table 1. Bioactivity of glucagon analogues

Peptide	Glucagon Receptor		GLP-1 Receptor	
	EC <sub>50</sub> , nM	Std.	EC <sub>50</sub> , nM	Std.
Glucagon	0.14	0.01	7.12	0.442
1. K <sup>17</sup> ,E <sup>21</sup> -glucagon amide	0.14	0.02	0.13	0.11
2. c[K <sup>17</sup> ,E <sup>21</sup> ]-glucagon amide	0.12	0.00	0.12	0.10
3. c[K <sup>16</sup> ,E <sup>20</sup> ]-glucagon acid	0.34	0.05	1.15	0.35
4. c[E <sup>16</sup> ,Orn <sup>20</sup> ]-glucagon acid	1.27	0.12	23.82	0.32
5. c[E <sup>16</sup> ,Dab <sup>20</sup> ]-glucagon acid	3.51		26.10	
6. c[E <sup>16</sup> ,Orn <sup>20</sup> ] <sub>G</sub> -glucagon acid	0.61		2.38	
7. E <sup>16</sup> ,Orn <sup>20</sup> -glucagon amide	0.21		0.15	
8. D <sup>16</sup> ,Orn <sup>21</sup> -glucagon acid	1.76	0.05		
9. D <sup>17</sup> ,Orn <sup>20</sup> -glucagon acid	6.71	0.44	14.64	0.23
10. c[D <sup>17</sup> ,Orn <sup>20</sup> ]-glucagon acid	6.80	0.38	16.15	0.13
11. c[E <sup>17</sup> ,Orn <sup>20</sup> ]-glucagon acid	0.90		5.79	
12. K <sup>-1</sup> ,A <sup>0</sup> ,E <sup>3</sup> -glucagon amide	85.88		41.73	
13. c[K <sup>-1</sup> ,E <sup>3</sup> ]A <sup>0</sup> -glucagon amide	30.66		14.35	
14. dK <sup>0</sup> ,dE <sup>4</sup> -glucagon amide	329.14		33.00	
15. c[dK <sup>0</sup> ,dE <sup>4</sup> ]-glucagon amide	19.42		73.42	
16. K <sup>4</sup> ,E <sup>8</sup> -glucagon amide			120.51	
17. c[K <sup>4</sup> ,E <sup>8</sup> ]-glucagon amide	861.57		147.94	
18. E <sup>8</sup> -glucagon amide	719.31		116.60	
19. c[E <sup>8</sup> ,K <sup>12</sup> ]-glucagon amide	78.97		10.05	
GLP-1			0.023	0.002

## References

1. Ahn, J-M., Gitu, P.M., Medeiros, M., Swift, J.R., Trivedi, D., Hruby, V.J. *J. Med. Chem.* **44**, 3109-16 (2001).
2. Miranda, L.P., Winters, K.A., Gegg, C.V., et al. *J. Med. Chem.* **51**, 2758-2765 (2008).
3. Day, J., Patterson, J., Gelfanov, V., DiMarchi, R.D. poster 21<sup>st</sup> APS.



## Structural Characterization of a Novel GLP-1 Analog Taspoglutide by NMR Spectroscopy

Natia Tsomaia,<sup>1</sup> Jundong Zhang,<sup>1</sup> Andrea Piserchio,<sup>2</sup> Dale F. Mierke,<sup>2</sup> and  
Jesse Z. Dong<sup>1</sup>

<sup>1</sup>IPSEN /Biomeasure Incorporated, 27 Maple Street, Milford, MA 01757, U.S.A.;

<sup>2</sup>Department of Chemistry, Dartmouth College, Hanover, NH 03755, U.S.A.

### Introduction

Glucagon-like peptide-1 (GLP-1) is a glucose-dependent insulinotropic agent. It stimulates insulin secretion and inhibits glucagon release in a strictly glucose-dependent manner. GLP-1 also promotes insulin gene expression and biosynthesis, induces pancreatic  $\beta$ -cell proliferation, slows gastric emptying and suppresses appetite. These unique properties make GLP-1 a potentially important treatment of type 2 diabetes. However, native GLP-1 is rapidly degraded by proteases *in vivo* and the short circulating half-life greatly hampers its clinical utility [1].

After the extensive investigation on the GLP-1 structural elements that influence the potency and enzymatic stability, a novel human GLP-1 analog [Aib<sup>8,35</sup>]hGLP-1(7-36)-NH<sub>2</sub> (Taspoglutide) was designed [1-3]. The introduction of  $\alpha$ -aminoisobutyric acid (Aib) at positions 8 and 35 protects both N- and C- terminal peptide bonds from enzymatic cleavage and results in increased circulating half-life [3]. In addition, the Aib<sup>8,35</sup> mutations enhance  $\alpha$ -helical content, especially in the C-terminal region. The combination of the high enzymatic stability and stronger C-terminal  $\alpha$ -helix makes the analog highly efficacious in stimulating the insulin release *in vivo*. In this particular study, we analyzed the impact of Aib<sup>8,35</sup> substitutions on the secondary structure of the peptide using NMR spectroscopy.

### Results and Discussion

To characterize the membrane associated structure of the peptide, our NMR study was carried out in the presence of zwitterionic micelles formed by dodecylphosphocholine. All 2D TOCSY and NOESY experiments were recorded on a Burkert 600 MHz at 308K. The calculated secondary shift values of  $\alpha$ -protons ( $H_{\alpha}$ ) suggest the presence of two helical segments in the peptide. Namely, large negative deviations (-0.7 ppm) in the C-terminal part describe a well-defined helix, while N-terminus is more consistent with a poorly ordered helical conformation. The mid-region of the peptide around Gly<sup>22</sup> displays chemical shifts close to random coil values.

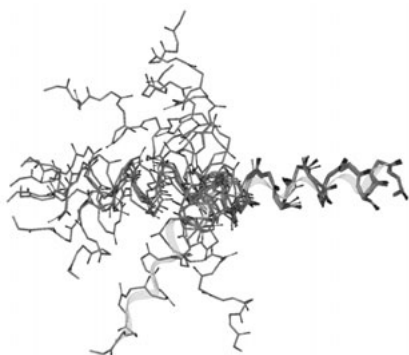


Fig. 1. Superposition of the C-terminal segment (Ala<sup>24</sup> to Arg<sup>36</sup>) of the resulting structures from the DG calculations. One random structure is depicted with a ribbon.

(backbone RMSD = 0.3 Å). Consistent with  $H_{\alpha}$  secondary shift calculations, a poorly defined N-terminal helical segment is connected to C-terminal helix via a flexible region centered on Gly<sup>22</sup>.

To refine the structural features of Taspoglutide, an NOE-restrained MD simulation in a water/decane membrane mimetic solvent box was carried out using OPLS force field within GROMACS software [7]. An average conformation of [Aib<sup>8,35</sup>]hGLP-1(7-36)-NH<sub>2</sub> peptide (Figure 2) clearly shows a well-defined  $\alpha$ -helical structure in the C-terminal region, a flexible

mid-region around Gly<sup>22</sup>, and a poorly defined N-terminal  $\alpha$ -helix. The stronger C-terminal  $\alpha$ -helix is clearly due to the presence of the helix promoting Aib substitution at position 35 and is consistent with the higher potency observed in the biological studies.

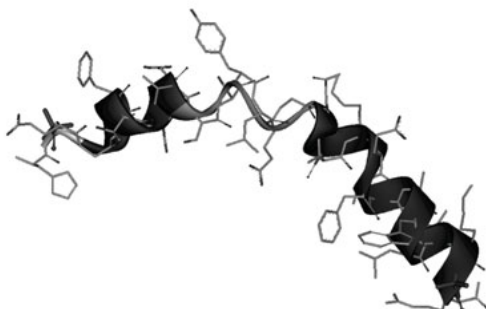


Fig. 2. One representative structure of the Taspoglutide while associated with the membrane environment as determined by NMR. Solvent is not shown for simplicity.

## References

1. Dong, J., Shen, Y., et al. *Proceedings of the 17<sup>th</sup> American Peptide Symposium*, 2001, p. 670.
2. Dong, J., Zhang, J., et al. *Proceedings of the 27<sup>th</sup> European Peptide Symposium*, 2002, p 88.
3. Dong, J., Shen, Y., et al. *Proceedings of the 18<sup>th</sup> American Peptide Symposium*, 2003, p. 625.
4. Wüthrich, K., *NMR of Proteins and Nucleic acids*, Wiley, New York, 1986.
5. Havel, T.F., *Prog. Biophys. Mol. Biol.* **56**, 43-78 (1991).
6. Mierke, D.F., Geyer, A., Kessler, H. *Int. J. Pept. Protein Res.* **44**, 325-331 (1994).
7. Berendsen, H.J.C., van der Spoel, D., van Buuren, R. *Comput. Phys. Commun.* **95**, 43-56 (1995).

## **Oral Delivery of Peptide Hormones: Insulin, Interferon, Growth Hormone and Calcitonin**

**W. Blair Geho and John R. Lau**

*SDG, Inc., Cleveland, OH 44106, U.S.A.*

### **Introduction**

Peptides and proteins are routinely administered by parenteral injection and their delivery to specific sites in the body are a function of random delivery. Peptide hormone efficacy has been studied in model bio-nano formulations in which peptides are carried to specific cell receptors by means of a bipolar lipid membrane fragment which is “targeted” to receptors by specific receptor target molecules. The leading example is HDV-Insulin (hepatocyte directed vesicle insulin). HDV-Insulin has been shown in animals and humans to be effective in activating hepatocyte insulin responses by both injection and oral routes of administration, at very low doses. HDV-Insulin is in Phase 2b studies in type 2 diabetes mellitus subjects. The same formulation approach has been taken with other peptide hormones such as interferon alfa, calcitonin, growth hormone and IgG antibodies. All of these formulations have been successfully shown to be bioavailable by the oral route of administration. This formulation technology may represent a major advance in developing oral peptide products.

### **Formulation Description**

SDG’s Bio-nano formulations use a 20-50 nm bipolar phospholipid membrane fragment as a basic structure to which targeted molecules and RES (reticuloendothelial system) masking molecules such as sialic acid can be attached to give the carrier both receptor specificity and immune cell anonymity. HDV is a membrane consisting of lecithin, cholesterol and dicetyl phosphate. Hepatocyte specificity is by means of inserting biotin as a hepatocyte receptor targeting molecule. Human recombinant insulin is attached passively by means of association of insulin with the combined electrical and membrane hydrophobic regions. Large scale manufacturing of cGMP HDV-Insulin has been completed and is suitable for oral formulations by means of a specific complex with gelatin, which is then filled into standard hard gelatin capsules. Without gelatin, the formulation is suitable for injection.

HDV-Insulin for subcutaneous administration is a mixture of 1% of total insulin bound to HDV, with the remaining 99% being non-HDV, or “free” insulin. Oral HDV-Insulin has 100% of the insulin bound to HDV.

The bio-nano cGMP oral HDV-Insulin capsules have extended stability even at elevated temperatures and humidity for six months. Injectable HDV-Insulin has the same stability profile as recombinant human insulin for injection.

Other peptides, such as growth hormone, interferon, and calcitonin may be substituted for insulin, with similar kinetics of attachment to the basic membrane. The peptide-carrier structures can either be targeted or non-targeted. Extended circulation times and hepatic bypass characteristics can be achieved by adding sialic acid to the membrane carrier.

### **Results and Discussion**

Therapeutic peptides and proteins have been administered parenterally because oral delivery did not work: the proteins and peptides were both digested in the gastrointestinal tract and they were also not absorbed across the gut into the portal circulation. HDV is an example of a bio-nano delivery particle that both protects peptides and proteins from digestion, and also facilitates their gut absorption. The effect of subcutaneously injected HDV-Insulin on oral glucose tolerance tests (OGTT) has been studied in dogs [1] and humans [2], and orally administered to type 1 and type 2 [3] diabetes mellitus patients. Results of an OGTT in pancreatectomized dogs is shown in Figure 1 and humans with type 1 diabetes in Figure 2. HDV-I treatment in insulin deficient dogs normalized OGTT, with the blood glucose levels closely approximating the normal control curves of intact dogs. This is in contrast to the abnormal curves of the insulin deficient dogs receiving equal subcutaneous doses of regular, non hepatic targeted insulin. A similar effect on OGTT was observed in the human study. Peripheral plasma insulin levels as well as blood

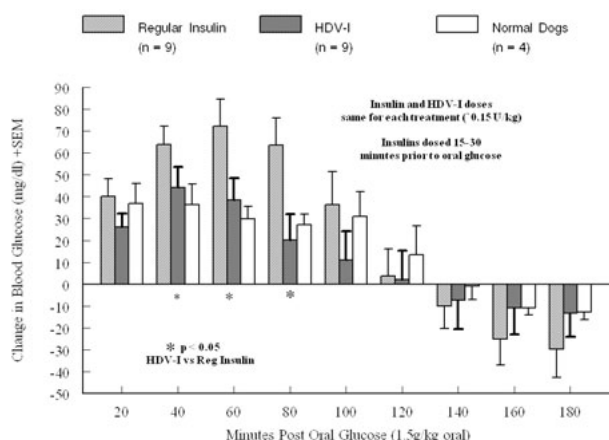


Fig. 1. OGTT in normal dogs and pancreatomectomized dogs treated subcutaneously with either regular insulin or HDV-Insulin.

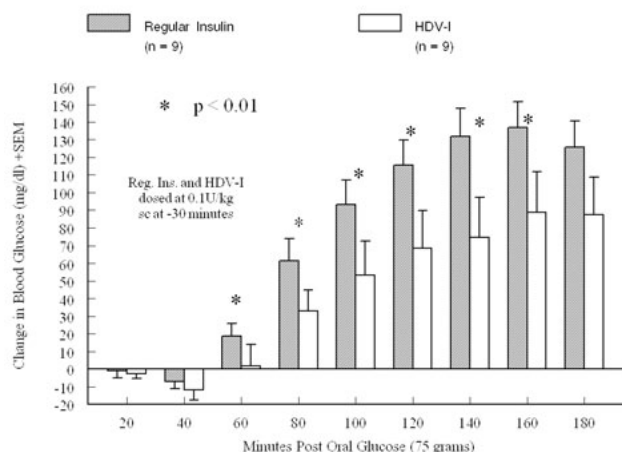


Fig. 2. OGTT in human type 1 diabetic subjects treated with subcutaneously administered regular insulin or HDV-Insulin.

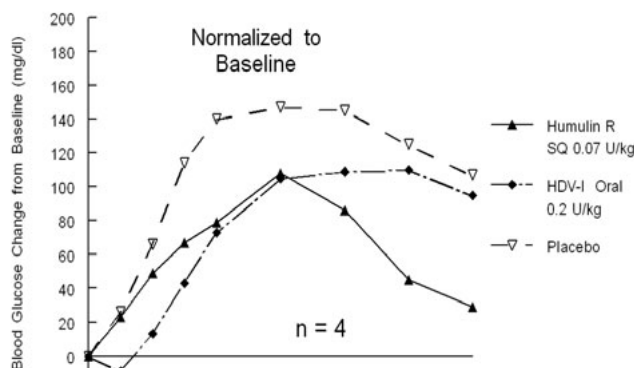


Fig. 3. OGTT in type 1 diabetes treated with subcutaneous regular insulin or oral placebo or HDV-Insulin.

levels of relevant counter regulatory hormones such as glucagon and cortisol were the same for both forms of injected insulin, strongly suggesting that the improved OGTT curves were due to hepatic glucose retention and not a peripheral effect of insulin on fat and muscle tissues.

HDV-Insulin (100% of insulin bound to HDV) was then formulated into an oral dose form by complexing aqueous HDV-Insulin with pharmaceutical grade gelatin powder. The resultant dry granulation was put into small hard gelatin capsules containing 5 IU human recombinant HDV-Insulin. In an open label crossover trial in which subcutaneous regular insulin at 0.07 IU/kg body weight was compared to 0.1 IU Oral HDV-Insulin/ kg body weight, administered 30 minutes prior to meals to type 1 diabetes mellitus patients resulted in similar significant reductions for both forms of insulin in the post-prandial area under the curve (AUC) analyses (Figure 3) compared to placebo control. Type 2 diabetics [3] on background metformin therapy were administered Oral HDV-Insulin dosed over a dose range of 0.05 to 0.4 IU HDV-insulin/kg body weight, following a baseline

OGTT with metformin alone and an oral placebo. All responses were significantly different from placebo treatment (Figure 4). The "flat" dose response was predicted by earlier animal studies. The "flat" dose response suggested that a 5 IU oral HDV-Insulin dose would be sufficient for human diabetes subjects weighing 50-120 kg. This 5 IU Oral Insulin dose form in a size 2 gelatin capsule is now in a large double-blind phase 2b clinical trial in type 2 diabetes mellitus subjects. Phase 2a data from a number of studies all confirm this remarkable oral activity. The success of oral delivery with human recombinant insulin suggested using similar

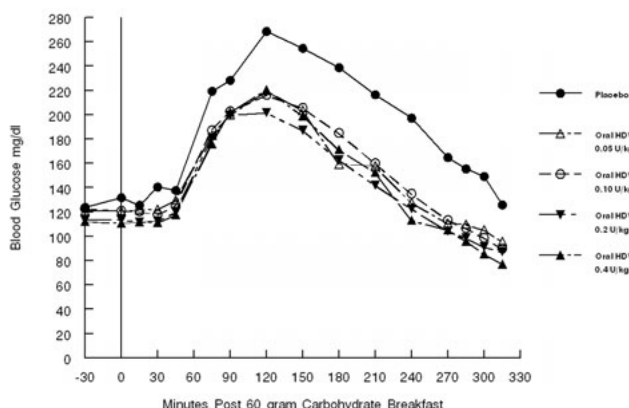


Fig. 4. Post-Breakfast Blood Glucose levels in 6 type 2 diabetics on metformin treated with oral placebo capsules or increasing doses of oral HDV-Insulin.

#### Oral vs SQ Growth Hormone in Hypox Rats

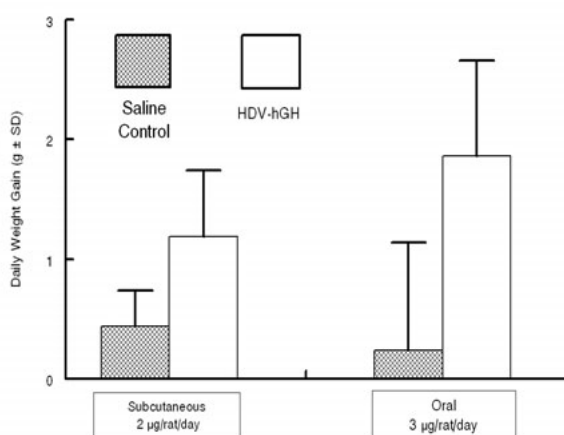


Fig. 5. Effect of Oral delivery of hGH in 6 Hypox rats on weight gain.

delivery particles to deliver other materials to the liver by the oral route. Interferon alfa has been formulated with HDV for hepatocyte delivery. Pre-clinical studies in mice in which PKR RNA markers that are responsive to interferon alfa have been used as indicators of hepatocyte delivery of interferon. Equal doses HDV-Interferon alfa were administered by intravenous and oral routes. The RNA markers of interferon activity were equally stimulated by HDV-Interferon administered by both routes of administration.

HDV has also been used, in a similar manner, to carry human growth hormone (hGH), administered both orally and parenterally at 1 and 3 ug/kg body weight per day, to hypophysectomized rats for a week to determine growth hormone efficacy on growth. HDV-hGH stimulated of the rats significantly compared to placebo treated rats (Figure 5).

The bio-nanoparticle delivery system exemplified by HDV is a versatile vehicle for both parenteral and oral delivery of a variety of peptides and protein hormones. The pharmacodynamic efficacy of several therapeutic proteins has been shown to be similar by both parenteral and oral administration. The SDG bio-nanoparticle delivery system is a potential mechanism for the delivery of many protein and peptide base pharmaceutical products.

#### Acknowledgments

These studies were funded by SDG, Inc., and AMDG, Inc., both of Cleveland, Ohio, and Diasome Pharmaceuticals, Inc., Conshohocken, Pennsylvania.

#### References

1. Geho, B., Lau, J., Rosenberg, L. *Diabetes* **57**(Suppl 1):A126 (2008).
2. Davis, S.N., Geho, B., Tate, D., Galassetti, P., Lau, J., Granner, D., Mann, S. *J. Diabetes Complications* Sep-Oct; **15**(5):227-233 (2001).
3. Schwartz, S., Geho, B., Rosenberg, L., Lau, R., *Diabetes* **57** (Suppl 1): A127 (2008).

## Exploring the N-terminal Hydrophobic Faces of Glucagon and Glucagon-like Peptide-1

Brian P. Ward, Brian P. Finan, Vasily M. Gelfanov,  
 and Richard D. DiMarchi

Department of Chemistry, Indiana University, Bloomington, IN 47405, U.S.A.

### Introduction

Glucagon, Glucagon-like Peptide-1 (GLP-1), as well as human (hCT) and salmon calcitonin (sCT) are all members of the secretin family of hormones that act on distinct G protein-coupled receptors in what are believed to be largely  $\alpha$ -helical conformations [1-5]. Approximately 50% sequence homology exists between the two glucagon-related peptides and among the two calcitonins. The amino acid sequences and  $\alpha$ -helical projections of these four peptides reveals a strong sequence and structural similarity between three N-terminal hydrophobic residues in GLP-1 (F<sup>6</sup>, V<sup>10</sup> and Y<sup>13</sup>) and glucagon (F<sup>6</sup>, Y<sup>10</sup> and Y<sup>13</sup>) and a set of equally-spaced, aromatic residues in hCT (Y<sup>12</sup>, Y<sup>16</sup> and F<sup>19</sup>). The sCT sequence differs from this trend with a triad of leucine residues (L<sup>12</sup>, L<sup>16</sup> and L<sup>19</sup>). Structural studies have indicated that both of these regions (6, 10, 13 for glucagon & GLP-1 and 12, 16, 19 in hCT & sCT) exhibit  $\alpha$ -helical secondary structure. This structure is purported to be the most probable receptor-active conformation for these two regions [2-5].

Fowler *et al.* (2005) reported the characterization of hCT-sCT chimeric peptides [1]. Most crucial to the design of our study was a H<sup>17</sup>R-hCT peptide substituted with residues K<sup>11</sup>, L<sup>12</sup>, E<sup>15</sup>, L<sup>16</sup> and L<sup>19</sup> of sCT. The resulting peptide (6CH-R) showed a ten-fold increase in receptor binding potency and a two-fold increase in cAMP production when compared to native hCT. This hCT analog was reported to be equipotent with sCT [1]. Given these results and the structural similarities in the aromatic regions of CT and the glucagon-related peptides, we questioned whether a L<sup>6</sup>, L<sup>10</sup> and L<sup>13</sup> variant of GLP-1 or glucagon would provide an analog with enhanced receptor potency. We characterized this assertion as the leucine hypothesis. The strategy was two-fold; if L<sup>6,10,13</sup> analogs proved more potent *in vitro* we would explore the possibility of using aliphatic residues at these positions, and if not, we would determine the extent that these three residues could be modified with aromatic character.

### Results and Discussion

The tri-substituted L<sup>6,10,13</sup> GLP-1 and glucagon analogs showed a large decrease in receptor potency in our cell-based cAMP production assay, negating the leucine hypothesis derived from homology to calcitonin. Select mono- and di-substituted leucine analogs at position 6, 10 and 13 for each peptide were made to interrogate the substitutions most responsible for the reduced

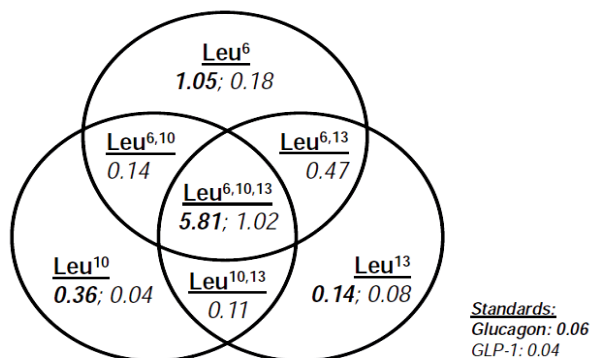


Fig. 1. Venn-diagram of EC<sub>50</sub> (nM) values for leucine analogs of Glucagon at the GluReceptor followed by the leucine analogs of GLP-1 at the GLP-1Receptor.

Table 1: Bioactivity of aromatic analogs

Residue #	Amino Acid	Receptor Potency $EC_{50}$ (nM) Values	
		Glucagon Analogs	GLP-1 Analogs
Residue 6	Phe	0.06	0.05
	Tyr	0.39	0.08
	Trp	0.27	0.14
Residue 10	Phe	0.06	0.05
	Tyr	0.04	0.15
	Trp	0.05	0.05
Residue 13	Phe	0.05	0.11
	Tyr	0.06	0.05
	Trp	0.11	0.13

bioactivity. Receptor activation potency for the entire set of leucine analogs is presented in a Venn-diagram (Figure 1). Leucine substitution at position 6 inflicted the greatest loss in potency at both receptors but of sizably greater magnitude at the glucagon receptor. Substitutions at position 10 and 13 also reduced the potency at both receptors, but to a lesser magnitude than position 6. The results indicate that the native aromatic residues at positions 6, 10 and 13 for glucagon and GLP-1 are required for full receptor activation.

A series of aromatic substitutions in both hormones where residues 6, 10 and 13 were substituted with phenylalanine, tyrosine or tryptophan was synthesized and characterized. *In vitro* potency values for this set of aromatic analogs are shown in Table 1. Substitutions made at position 6 in glucagon (Y<sup>6</sup> and W<sup>6</sup>) yielded the greatest reduction in potency of all the analogs, stressing the importance of the native phenylalanine in glucagon receptor interaction. W<sup>10</sup> and F<sup>13</sup> substitutions in glucagon provided variants with slight increases in receptor potency. All other position 10 and 13 analogs were of reduced potency but less so than observed for position 6, which is consistent with other work [6]. GLP-1 position 6 aromatic analogs (Y<sup>6</sup> and W<sup>6</sup>) showed reductions in potency and were equally destructive with their position 13 counterparts (F<sup>13</sup> and W<sup>13</sup>). Position 10 in GLP-1 proved to be most capable of allowing changes without loss of receptor potency. The F<sup>10</sup> and W<sup>10</sup> substitutions possess native hormone potency. In total, non-native aromatic residues at the three N-terminal region aromatic amino acids of glucagon diminished this ligand's receptor potency more than the analogous change in GLP-1.

While the leucine hypothesis based upon homology to calcitonin did not prove correct, our findings clarify the importance of the N-terminal hydrophobic faces of GLP-1 and glucagon for full receptor potency. The role of Y<sup>12</sup>, F<sup>16</sup> and F<sup>19</sup> in calcitonin receptor activation appears to differ from that of the comparably spaced hydrophobic ligand sequences in association with the glucagon-related receptors. The aromatic structure at position 6 in both GLP-1 and glucagon is most sensitive to modification of the native residue. Additionally, position 10 and to a lesser extent 13, have revealed themselves as tolerant to substitution with minimal losses in receptor potency for both peptides. Ongoing studies are exploring the depth and breath of structural modification that can be managed successfully at these sites for the two glucagon-related hormones.

## References

1. Fowler, S.B., Poon, S., Muff, R., Chiti, F., Dobson, C.M., Zurdo, J. *PNAS* **102**, 10105-10110 (2005).
2. Andreotti, G., Méndez, B.L., Amodeo, P., Castiglione Morelli, M.A., Nakamuta, H., Motta, A. *J. Biol. Chem.* **281**, 24193-24203 (2006).
3. Neidigh, J.W., Fesinmeyer, R.M., Prickett, K.S., Andersen, N.H. *Biochemistry* **40**, 13188-13200 (2001).
4. Thornton, K., Gorenstein, D.G. *Biochemistry* **33**, 3532-3539 (1994).
5. Blundell, T., Wood, S. *Ann. Rev. Biochem.* **51**, 123-154 (1983).
6. Azizeh, B.Y., Ahn, J.M., Caspari, R., Shenderovich, M.D., Trivedi, D., Hruby, V.J. *J. Med. Chem.* **40**, 2555-2662 (1997).

## Discovery of Degarelix, a Self-Depoting GnRH Antagonist with Long Duration of Action

Claudio Schteingart,<sup>1</sup> Guangcheng Jiang,<sup>1</sup> Robert Galyean,<sup>1</sup>  
Jacek Stalewski,<sup>1</sup> Jean Rivier,<sup>2</sup> Richard White,<sup>1</sup> and Gregoire Schwach<sup>3</sup>

<sup>1</sup>Ferring Research Institute Inc., San Diego, CA 92121, U.S.A.; <sup>2</sup>Salk Institute for Biological Studies, San Diego, CA 92037, U.S.A.; and <sup>3</sup>Ferring Pharmaceuticals A/S, Copenhagen, 2300, Denmark

### Introduction

Prostate cancer is the second leading cause of cancer death after lung cancer in the Western world. Even in its locally advanced or metastatic phase, tumor growth is sensitive to the presence of testosterone, and androgen deprivation therapy is one important modality of treatment. Testosterone is produced by the testes in response to circulating luteinizing hormone (LH), in turn produced by the pituitary gland when hypothalamic gonadotropin releasing hormone (GnRH or LHRH) activates the corresponding GnRH receptor in gonadotrophs. Current treatment is by the use of GnRH superagonists incorporated in slow release formulations. During the initial two to three weeks after dosing, these actually increase LH and testosterone levels, a phenomenon termed “testosterone surge”, before gonadotrophs desensitize and LH and testosterone production ceases. During the surge, there is a transient increase in tumor growth, possible exacerbation of existing symptoms, and an overall delay in initiation of treatment [1]. By contrast, treatment with a GnRH antagonist directly blocks the receptor, resulting in fast reduction of circulating levels of LH and testosterone, avoidance of the surge, and the immediate initiation of treatment.

The most effective known GnRH antagonist pharmacophore incorporates three lipophilic amino acids [Ac-D-Nal<sup>1</sup>, D-(Cl)Phe<sup>2</sup>, D-3Pal<sup>3</sup>] at the N-terminus of a nona- or decapeptide, which typically results in compounds with low solubility and limited duration of action after injection. The two antagonists in clinical use, cetrorelix and ganirelix, are administered by daily injection for the prevention of premature LH surges in assisted reproductive techniques. Cetrorelix, ozarelix, and teverelix are currently in clinical trials for the treatment of benign prostatic hyperplasia (BPH) by two separate injections, each one partially suppressing testosterone for a few days. Only one peptidic GnRH antagonist, abarelix, was introduced, as a CMC complex, for the treatment of very advanced prostate cancer by monthly i.m. injection, but it was withdrawn due to serious allergic reactions and lack of efficacy over time.

In 1996, Ferring initiated a program to discover a peptidic GnRH antagonist with physicochemical properties suitable for the treatment of prostate cancer by monthly injection or at longer dosing intervals.

### Results and Discussion

Most of the classical pharmacophore [Ac-D-Nal<sup>1</sup>, D-(X)Phe<sup>2</sup>, D-AA<sup>3</sup>] was maintained (Figure 1), but aliphatic and aromatic amino acids were explored in position 3 as well as the R<sub>2</sub>

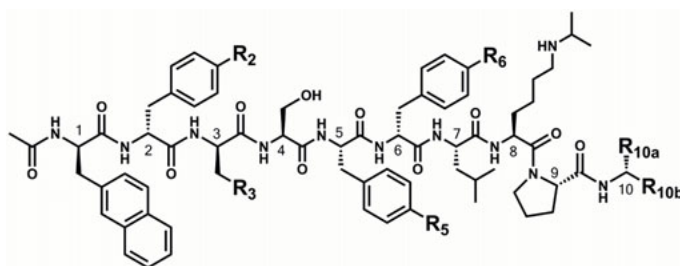


Fig. 1. The basic structure and modifications explored in Ferring's GnRH antagonists program.



substituent in position 2. An N-isopropyl lysine replaced Arg<sup>8</sup> with the intention of minimizing histamine release, and variations in position 10 were also examined. Crucially, aromatic amino acids were selected for positions 5 and 6 (the last one with D configuration) decorated with a variety of moieties (R<sub>5</sub>, R<sub>6</sub>) carrying hydrogen bond donors and acceptors, to encourage intermolecular interactions between peptide molecules and between peptide and the components of the interstitial space with the idea that these would modulate the release rate of the antagonist from the injection site.

The primary screening assay was performed following the duration of LH suppression in castrated Sprague Dawley male rats after one subcutaneous administration of peptide at a dose of 0.25 mg/kg injected at a concentration of 0.5 mg/ml. This assay integrated solubility, pharmacokinetics, and potency of the antagonists at the rat GnRH receptor.

A campaign of synthesis and testing of approximately 150 analogues resulted in the discovery of degarelix (Figure 2), which had the longest duration of action in the screening assay [2]. The distinguishing features of degarelix, possibly responsible for its unique physicochemical properties, are acylation of the side chain nitrogen of aminophenylalanine<sup>5</sup> with L-hydroroctic acid (Hor) and the presence of a carbamoyl moiety acylating the side chain nitrogen of D-aminophenylalanine<sup>6</sup> to form a urea. Very small variations in the structure of these decorating groups resulted in substantial differences in duration of action in the rat screening assay. There was no simple SAR correlating duration of action with peptide structure,

suggesting that the physicochemical properties of the peptides may be exquisitely dependent on fine details of the spatial arrangement of the groups involved in intermolecular hydrogen bonding, or of other moieties involved in peptide aggregation, like aromatic or lipophilic groups.

When degarelix was injected s.c. to intact male rats at a dose of 2 mg/kg in 5% mannitol (5%M) (20 µl/rat) testosterone was suppressed for 42 days [3], pointing at the formation of a drug reservoir at the injection site with slow release of the antagonist over time. Indeed, after injection of 0.25 ml of a 10 mg/ml solution of degarelix in 5%M in the subcutaneous space of rats, a depot containing the injected material could be easily seen in the internal side of the skin structure.

To investigate the factors responsible for this extraordinary behavior solutions of degarelix acetate, 10 mg/ml in 5%M, were incubated at room

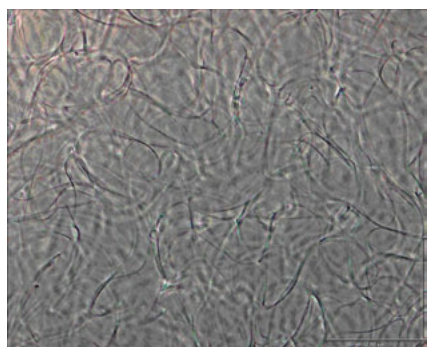
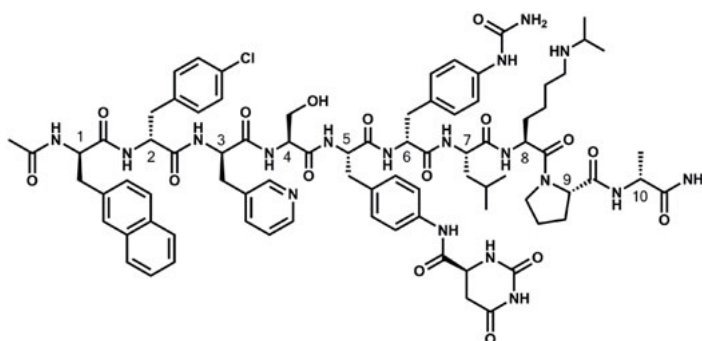


Fig. 3. Phase contrast micrograph (x200) of degarelix aggregates in 5% mannitol at 10 mg/ml. The scale bar on the bottom right is 100 µm.

temperature and samples examined by phase contrast microscopy. Over a period of hours, small aggregates appeared, which elongated over time to form a fine stranded network with increasing density of aggregates (Figure 3).



Ac-D-2Nal-D-Cpa-D-Pal-Ser-Aph(Hor)-D-Aph(Cbm)-Leu-Lys(iPr)-Pro-D-Ala-NH<sub>2</sub>

Fig. 2. Structure and sequence of degarelix.

The possible interactions of degarelix with the subcutaneous milieu were examined by introducing a drop of a degarelix solution into 20% diluted human plasma to simulate the protein content of interstitial fluid. Under microscopy (Figure 4), the same network of degarelix strands was observed to form inside the drop of peptide solution, but a new layer formed at the interface between the peptide solution and diluted plasma, possibly containing degarelix and protein.

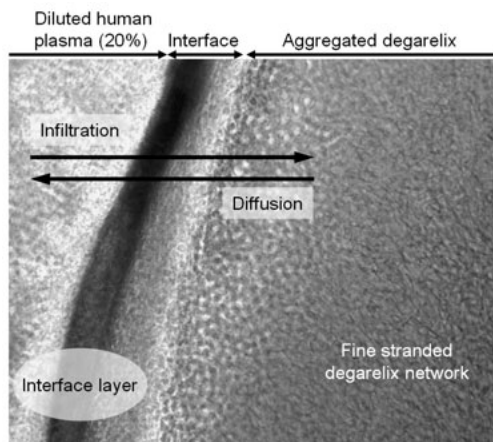


Fig. 4. Micrograph of a degarelix microdepot prepared by addition of a drop of degarelix solution to diluted human plasma.

We hypothesize that ions and other components of interstitial fluid infiltrate the depot contributing to its maturation and consolidation, whereas degarelix is able to slowly diffuse out through the depot surface at a rate sufficient to achieved complete GnRH receptor blockade for a long period of time.

In clinical trials, degarelix had an i.v. elimination half life of 11-16 hs, and a s.c. terminal half life between 35 and 76 days, depending on the concentration injected [4]. The combination of depotting behavior, slow release, and low clearance (2.9 L/h [5]) makes possible to use degarelix to antagonize the GnRH receptor in prostate cancer patients by s.c. monthly administration. After a s.c. induction dose of 240 mg as 40 mg/ml solution, testosterone levels decrease to castration levels (<50 ng/dL) in 96% of patients by day 3 and in 99% of patients by day 7. Testosterone levels are maintained below castration levels

by monthly injection of a maintenance dose of 80 mg at a concentration of 20 mg/ml. Degarelix (FIRMAGON) was approved by FDA in December 2008 and by EMEA in February 2009 for the treatment of advanced prostate cancer.

Degarelix is probably the first example of a peptidic drug designed to rely on the spontaneous formation of a subcutaneous depot containing aggregates upon injection, followed by slow release of the drug to achieve very long duration of action, without the aid of polymeric formulations.

## Acknowledgments

We would like to thank Ms. Pernille Rosted for the micrographs of degarelix aggregates.

## References

1. Gittelman, M., et al. *J. Urol.* **180**, 1986-1992 (2008).
2. Jiang, G., et al. *J. Med. Chem.* **44**, 453-467 (2001).
3. Broqua, P., et al. *J. Pharmacol. Exp. Ther.* **301**, 95-102 (2002).
4. Balchen T., et al. Pharmacokinetics, pharmacodynamics, and safety of a novel fast-acting gonadotropin-releasing hormone receptor blocker degarelix, in healthy men. 8<sup>th</sup> International Symposium on GnRH Analogues In Cancer and Human Reproduction, Salzburg, February 10-13, 2005.
5. Jadhav, P., et al. *J. Pharmacokinet. Pharmacodyn.* **33**, 609-634 (2006).

## Development of Insulin Based Inhibitors of Human Islet Amyloid Polypeptide

Deborah L. Heyl, Durgaprasad Peddi, and Ranadheer Reddy Pesaru

Department of Chemistry, Eastern Michigan University, Ypsilanti, MI 48197, U.S.A.

### Introduction

Human islet amyloid polypeptide (hIAPP) is a 37 amino acid peptide, co-secreted along with insulin in the islets of Langerhans of pancreatic beta cells. Postmortem exams show plaques of hIAPP found in the pancreas of 97 % of type 2 diabetic patients. Therefore, aggregation of hIAPP fibrils is believed to be toxic to beta cells and responsible for beta cell dysfunction and death associated with type 2 diabetes [1-2]. Insulin has been found to act against the actions of hIAPP. The internal sequence of insulin, HLVEALYLVC, recognizes and binds the 10-19 region of hIAPP [3]. Since insulin reportedly blocks the formation of amyloid fibers, insulin analogs may protect cell membranes from damage. In an effort to study this effect, truncated analogs of hIAPP, namely VEALYLV and LVEALYLVC, were synthesized and tested in the presence of hIAPP 1-19, which has been found to have similar activity to the full length analog [4]. Carboxyfluorescein-encapsulating vesicles which mimic the  $\beta$ -cell were created using a 7:3 ratio of the lipids 1,2-dioleoyl-sn-glycero-3-phosphocholine (DOPC) and 1,2-dioleoyl-sn-glycero-3-(phospho-L-serine) (DOPS), respectively, and the percent leakage of fluorescent dye from the vesicles in the presence of the peptides was calculated as compared to a 100% Triton-X detergent-treated control. Assays were run in triplicate in a 96-well plate, and average values are reported. Fluorescence values were recorded by an FLx fluorescence microplate reader. The activity of the truncated analogs was compared to that of insulin under the same conditions.

### Results and Discussion

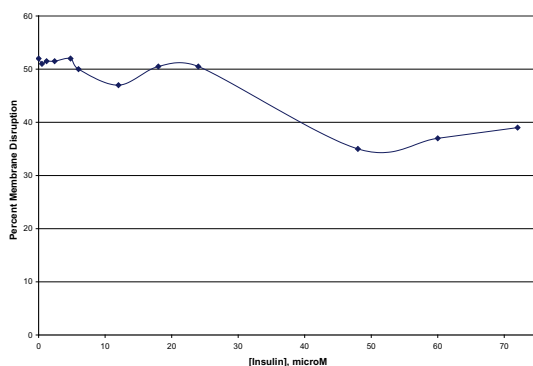


Fig. 1. Percent dye leakage from vesicles in the presence of 9.1 micromolar hIAPP 1-19 and varying insulin concentration.

The results of the preliminary experiment depicted in Figure 1 show that at a 9.1  $\mu\text{M}$  constant concentration of hIAPP 1-19, increasing insulin reduces membrane damage after a threshold is reached. The greatest inhibition is exhibited when the insulin concentration is greater than or equal to 48  $\mu\text{M}$ , or in five-fold excess to hIAPP 1-19. The maximal inhibition (change in extent of dye leakage) observed was 17%. It should be noted that intermediate concentrations between 24 and 48  $\mu\text{M}$ , and concentrations greater than 72  $\mu\text{M}$ , still need to be tested.

For the nonapeptide insulin analog LVEALYLVC (Figure 2), preliminary data surprisingly indicate that this shorter analog optimally inhibits membrane disruption (same extent as insulin, about 15%) at only 13.5  $\mu\text{M}$ . The increase in liposome damage after that point warrants further investigation. The shorter heptapeptide analog, VEALYLV, which is missing both the N- and C-termini relative to the nonapeptide, reduces membrane disruptive activity in a roughly concentration dependent manner (Figure 3). Membrane damage is reduced by 13% at 44.5  $\mu\text{M}$ , which is similar to the activity exhibited by insulin. At the highest concentration tested (177  $\mu\text{M}$ , a 20:1 ratio of inhibitor to hIAPP 1-19), dye leakage is reduced by about 65%, making it more effective than the nonapeptide inhibitor in this assay. It should be noted that insulin itself remains to be tested at this concentration, so a clear comparison to insulin cannot yet be drawn.

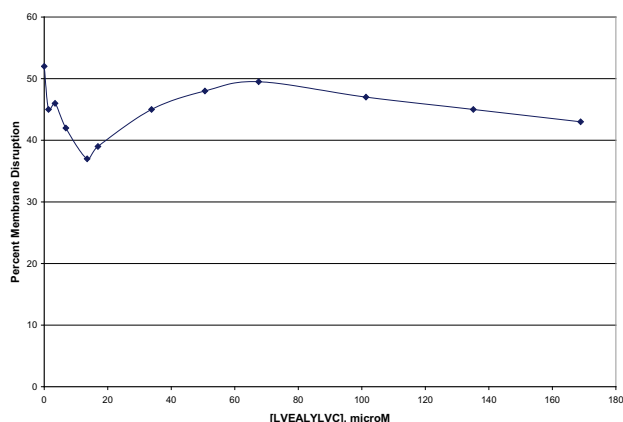


Fig. 2. Percent dye leakage from vesicles in the presence of 9.1 micromolar hIAPP 1-19 and varying concentration of LVEALYLVC.

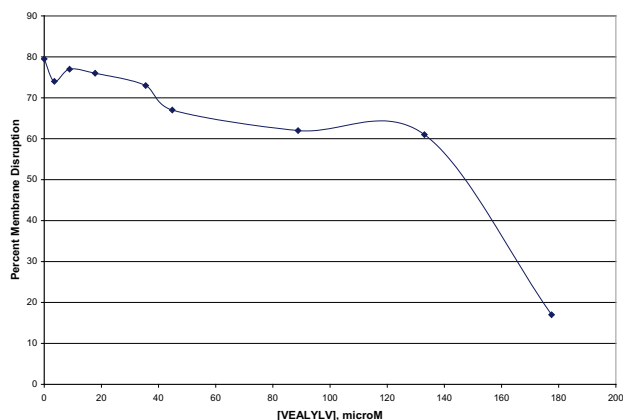


Fig. 3. Percent dye leakage from vesicles in the presence of 9.1 micromolar hIAPP 1-19 and varying concentration of VEALYLV.

Overall, the truncated insulin analogs LVEALYLVC and VEALYLV show similar activity to insulin in reducing dye leakage from model membranes in this initial study. The nonapeptide is optimally effective at lower concentration than insulin. The heptapeptide is the most effective inhibitor analog of the two at high concentration in reducing liposome damage. These results are promising in that truncated analogs may be able to mimic the action of insulin in reducing cell damage caused by hIAPP. Future work will include expanding the concentration range and testing these analogs against full length hIAPP.

## Acknowledgments

This research was supported by an award from Research Corporation.

## References

1. Nilsson, M.R., Nguyen, L.L., Raleigh, D. *Anal. Biochem.* **288**, 76-82 (2001).
2. Engel, M., Khemtémourian, L., Kleijer, C.C., Meeldijk, H.J.D., Jacobs, J., Verkleij, A.J., deKruijff, B., Killian, J.A., Hoppener, J.W.M. *PNAS*, **105**, 6033–6038 (2008).
3. Gilead, S., Wolfenson, H., Gazit, E. *Angew. Chem.* **45**, 6476- 6480 (2006).
4. Brender, J.R., Lee, E.L., Cavitt, M.A., Steel, D.G., Ramamoorthy, A. *J. Am. Chem. Soc.* **130**, 6424-6429 (2008).

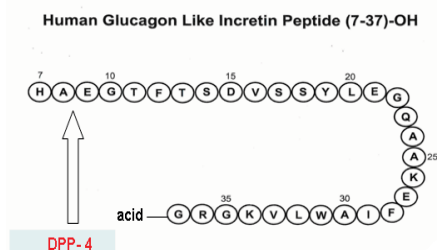
## Synthesis and Analysis of Peptide Hormone-based Prodrugs

Arnab De and Richard D. DiMarchi

Department of Chemistry, Indiana University, Bloomington, IN 47405, U.S.A.

### Introduction

Peptides represent a rich natural source of potential medicines with one notable pharmaceutical limitation being their relatively short duration of action. A particularly good example of this phenomenon is glucagon-like peptide 1 (GLP), a hormone of appreciable interest for the treatment of Type II diabetes. This is because GLP has been reported to enhance the endogenous secretion of insulin [1] only when blood glucose is elevated, significantly minimizing the risk of hypoglycemia. However, native GLP demonstrates an extremely short plasma half-life (~2 min) caused by the combined effect of rapid degradation by Dipeptidyl



Peptidase IV (DPP-IV) and renal clearance [2]; along with a relatively narrow therapeutic index. Structure-function studies have shown that the N-terminal histidine is especially important for high potency of GLP [3]. Our work focuses on the assembly of GLP-prodrugs as a mean to extend the duration of action and broaden the therapeutic index. The design is directed at the conversion of GLP amide and ester prodrugs that differentially convert to the parent drug under physiological conditions, strictly

by structural propensity for intramolecular cyclization of dipeptide-based amide/ester extensions. This conversion, driven by the inherent chemical instability of the prodrug eliminates the intrinsic variability in enzymatic cleavage within and across patient use. In a set of dipeptide extended GLP-analogs, we explored the rate of diketopiperazine (DKP) and diketomorpholine (DMP) formation, and the release of the active peptide at pH 7.2 and 37°C. These experimental conditions are virtually invariant in a chemical sense and should be translatable for use with other peptides where the N-terminus or the hydroxyl group (serine/threonine) is vital to bioactivity. Our goal is to identify a set of dipeptide prodrugs of different structures that might offer cleavage in the range 1-200 hrs.

### Results and Discussion

Various dipeptide prodrugs were prepared through modification of side chain functionality using standard solid phase protocols utilizing Boc chemistry. The conversion of the prodrug to the parent drug was analyzed by HPLC and MALDI. The half lives of the degradation of the various prodrugs were then calculated by using the formula  $t_{1/2} = 0.693/k$  where 'k' is the dissociation rate constants of the prodrug. The ability of each GLP analog or prodrug to induce cAMP was measured in a luciferase-based reporter assay [4]. Percent potency calculations were done by comparing the mean  $EC_{50}$  of the parent with that of the prodrug. Our initial analysis had shown that amide-based prodrugs of GLP are appreciably stable under physiological conditions rendering them of little pharmaceutical utility [4]. Consequently, we replaced the N-terminal amine with an  $\alpha$ -hydroxyl group and ester prodrugs were prepared at this site. We also previously demonstrated the utility of phenylalanine as a suitable synthetic and bioactive replacement for the N-terminal histidine [4]. A nine amino acid extendin-4 C-terminal extension (CEX) was linked to our GLP peptides as these analogs proved to be appreciably more soluble in physiological buffers than analogs of native GLP. Thus, the parent peptide used in this study was generated by changing the native N-terminal histidine to an  $\alpha$ -hydroxyl-phenylalanine (OH-Phe) and adding a CEX extension peptide. The resulting HO-F<sup>7</sup>,GLP(8-36)-CEX, used in this study was determined to be of high potency ( $EC_{50}$  of 0.008nM comparable to native GLP with  $EC_{50}$  of 0.011nM).

Table 1. Rates of prodrug ester cleavage

Peptide #	Dipeptide extension	$T_{1/2}(\text{hrs})$	Peptide #	Dipeptide extension	$T_{1/2}(\text{hrs})$
1	NH <sub>2</sub> -Gly-Gly	0.9	11	HO-Phe-Gly	2.5
2	HO-Gly-Gly	1.1	12	HO-Phe-Ala	2.8
3	HO-Gly-Phe	0.7	13	HO-Phe-dAla	2.4
4	HO-Gly-dPhe	0.9	14	HO-Phe-Phe	33.3
5	HO-Gly-Val	4.7	15	HO-Phe-dPhe	7.7
6	HO-Gly-dVal	5.1	16	HO-Phe-Val	NA
7	HO-Gly-tBu	NA	17	HO-Phe-dVal	50.6
8	HO-Gly-PhG	0.5	18	NH <sub>2</sub> -Phe-Val	64.0
9	HO-Gly-AIB	0.8			
10	NH <sub>2</sub> -Gly-Val	20.4			

Tables 1 show the rates of ester cleavage in HO-F<sup>7</sup>, GLP(8-36)CEX ester-based prodrugs with a glycine/ glycolic acid and phenylalanine/ phenyllactic acid in the first positions, respectively. The rate was observed to be a function of both the stereochemistry (14 vs 15 and 16 vs 17), and the steric bulk of the dipeptide side chains, with  $\beta$  branching having a greater effect than  $\gamma$  branching (14 and 15 vs 16 and 17). The rate depends on the hybridization of the  $\beta$  carbon as demonstrated in 5 and 6 where the  $\beta$  carbon is  $sp^3$  hybridized leading to enhanced steric crowding relative to peptide 8 where the  $\beta$  carbon is  $sp^2$  hybridized. Finally, the strength of the cyclization nucleophile also plays a role and the amine is generally a stronger nucleophile. Four longer duration prodrugs were studied in the *in vitro* bioassay and in each instance the potency is much reduced relative to the parent peptide. A steady increase in bioactivity as a function of time was demonstrated for prodrug 10 (48% of the parent bioactivity restored after 24 hours, consistent with previously measured half-life using MS and HPLC detection). This peptide was selected based upon the ability to examine more than five half-lives in a one week experiment.

This work demonstrates the ability of a dipeptide-based ester to reversibly inactivate GLP-agonism. We also observed that addition of similar ester-linked dipeptides to the hydroxyl group of a bioactive serine in GLP significantly reduces its potency (data not shown). Through the careful selection of chemical functionality, a set of GLP ester prodrugs of variable half-lives have been identified. The observed rate in conversion of prodrugs to parent peptides has been extended to 64 hours and additional prolongation is envisioned through further chemical optimization. This represents a highly attractive range of options for prolonging peptide action to once-a-day and once-a-week formulations. Additional *in vivo* elements for minimizing premature renal clearance are likely to be required to achieve sustained action.

## Acknowledgments

We acknowledge the contributions of Jay Levy, David Smiley, Vasily Gelfanov, and Jonathan Karty.

## References

1. Daniel, J., et al. *The Lancet* **368** (9548), 1696-17052 (2006).
2. Ørskov, C., Wettergren, A., Holst, J.J. *Diabetes* **42**, 658–661 (2006).
3. Adelhorst, K., et al. *Journal of Biological Chemistry* **269**(9), 6275-6278 (1994).
4. De, A., DiMarchi, R.D. *Intl. Journal of Peptide Research and Therapeutics* **14**, 255-262 (2008).

## Discovery of Peptides as Granulocyte Colony-Stimulating Factor Receptor Agonist (Series I)

Y. Sarah Dong, Ashok Bhandari, Kalyani Penta, Karen Leu,  
 Peter J. Schatz, and Christopher P. Holmes

Affymax, Inc., 4001 Miranda Avenue, Palo Alto, CA 94304, U.S.A.

### Introduction

Granulocyte colony-stimulating factor (G-CSF) [1] is the major physiological regulator of granulopoiesis. Recombinant G-CSF has become a valuable supportive agent in the clinic that permits the administration of high dose chemotherapy by stimulating the production of granulocytes, and as a result, shortens the neutropenia associated with chemotherapy [2,3]. Screening against Affymax recombinant peptide display (RPD) libraries yielded one hit series which displayed tight binding affinity and agonist activity against the G-CSF receptor. More importantly, these peptide sequences have shown no homology to either the natural G-CSF ligand or the receptor [4]. This hit series containing three cysteines, after being allowed to dimerize via disulfide bond formation, acted as an antagonist with a single digit nM activity. Creating a tetramer version of this peptide (i.e., a dimer of dimers) has afforded a full agonist in a cell proliferation assay with similar activity to recombinant G-CSF. Further optimization of the lead peptide including selected amino acid mutations, architecture modifications, as well as various PEGylation strategies was conducted to increase the activity in the more relevant CFU-G colony assay.

### Results and Discussion

An extensive RPD effort resulted in the discovery of a peptide with agonist activity as an MBP (Maltose Binding Protein) fusion. Possibly, the MBP fusion peptide may have formed inter-molecular disulfide bonds through three cysteines within each peptide chain. Peptide monomer behaved as a weak antagonist with an  $IC_{50}$  of 10 mM, when separated from the MBP fusion or produced synthetically. The competition binding assay identified the most active form of the dimers as the parallel linked dimer as an antagonist with an  $IC_{50}$  of 2 nM. Figure 1 shows the oxidation condition to the parallel triple cysteine linked dimer and structural determination. All related fragments by both enzymatic digestions were observed in Figure 1; therefore, the disulfide linkages were confirmed to be in parallel.

Dimerization of the parallel disulfide linked dimer has afforded a full agonist in a cell proliferation assay with similar activity to recombinant G-CSF. Subsequently, different tetrameric forms and PEGylations were explored for agonist activity in the proliferation assay with Hu-GCSFR cell lines. The  $EC_{50}$  of peptides were reported as ratios compared to the recombinant GCSF as a reflection of activity.

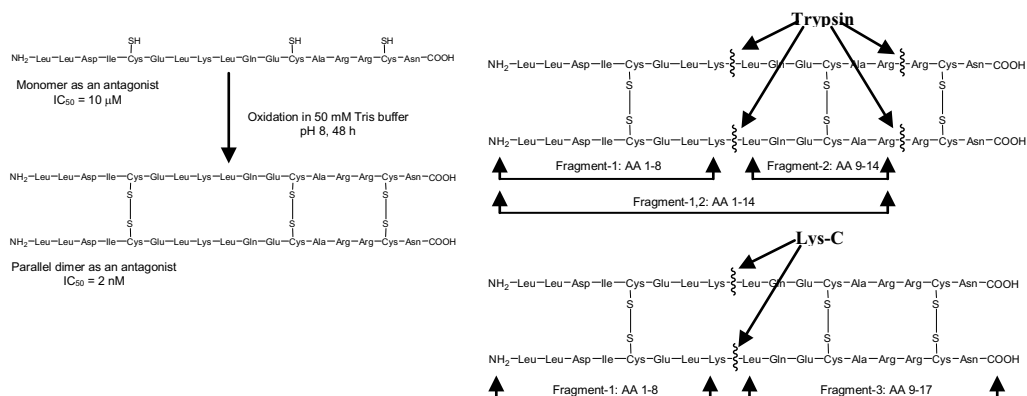

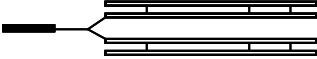


Fig. 1. Oxidation of monomer to the parallel disulfide linked dimer and its structural determination.

Table 1. PEG size and position impact on agonist activity and efficacy

Architectures	Size & Position of PEG	% Efficacy	EC <sub>50</sub> Ratio (peptide to rhG-CSF)
	2 x 20 kDa	110	620
	2 x 10 kDa (linear)	61	170
	2 x 10 kDa (branched)	84	2007
	2 x 5 kDa	81	16
	2 x 20 kDa	103	182
	30 kDa	44	72

Shown in Table 1, both activity and efficacy of PEGylated peptides were affected by the size, position, and nature (branched/linear) of the PEG.

Further mutagenesis of the lead sequence indicated high sequence conservation except for the Leu2, Asp4, Arg16, and Asn18 positions. Ala scan analysis agreed with mutagenesis results, and confirmed that only a few substitutions could be made while maintaining activity. As a result, there were no significant differences in activity of tetramers with substitutions in positions Leu2, Asp4, and Asn18. Arg16 substitutions such as Phe and Tyr, however, resulted in more active PEGylated lead peptides with similar activity to recombinant G-CSF.

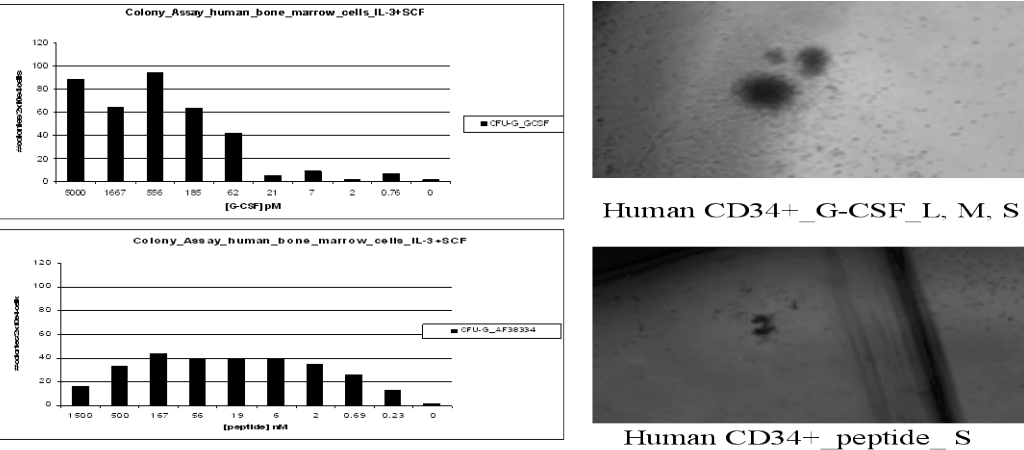


Fig. 2. Colony Assay Results.

Colony assay [5,6] results (Figure 2) indicate that G-CSF shows a clear dose response and yields large and dense colonies, while the lead PEGylated tetramer is able to form CFU-G colonies, but does not show full efficacy either by size or numbers, and a dose-response is not clearly evident.

## References

1. Aritomi, M., et al. *Nature* **401**, 713-718 (1999).
2. Tkatch, L.S., Tweardy, D.J. *Lymphokine and Cytokine Research* **12**, 477-488 (1993).
3. Eliason, J.F. *BioDrugs* **15**, 705-711 (2001).
4. Reidaar-Olson, J.F., De Souza-Hart, J.A., Selick, H.E. *Biochemistry* **35**, 9034-9041 (1996).
5. Technical manual, human colony-forming cell assays using MethoCult®. StemCell Technologies, Catalog #28404, version 3.0 (2004).
6. Miller, C.L., Lai, B. Human and mouse hematopoietic colony-forming cell assays, Basic Cell Culture Protocols 3, *Methods in Molecular Biology* **290**, Humana Press, Totowa, NJ. 71-89, 2005.



## Discovery of Peptides as Granulocyte Colony-Stimulating Factor Receptor Agonist (Series II)

Y. Sarah Dong, Yijun Pan, Caiding Xu, Ashok Bhandari, Yvonne Angel, Karen Leu, Kalyani Penta, Bruce Mortensen, Jennifer M. Green, Peter J. Schatz, Qing Fan, Kathryn Woodburn, and Christopher P. Holmes  
 Affymax, Inc., 4001 Miranda Avenue, Palo Alto, CA 94304, U.S.A.

### Introduction

Granulocyte colony-stimulating factor (G-CSF) is the principal growth factor regulating the maturation, proliferation, and differentiation of the precursor cells of neutrophilic granulocytes. G-CSF is used to treat neutropenia (low neutrophil count) caused by chemotherapy [2,3]. The crystal structure of GCSF complexed to the BN-BC domains, the principal ligand-binding region of the GCSFR, shows that the two receptor domains form a complex in a 2:2 ratio with the ligand [1].

A novel synthetic peptide, which has no homology to either G-CSF ligand or the G-CSF receptor (G-CSFR) [4], was discovered using proprietary Affymax peptide libraries. This peptide, which contains a disulfide bond, bound to the G-CSFR with an  $IC_{50}$  of 5 mM. Upon dimerization with a chemical crosslinker, the dimeric peptide was an agonist in the cell proliferation assay with an  $EC_{50}$  of ~ 100 nM. Optimization of this initial dimeric peptide, including mutations, different chemical linkers, and position of dimerization, has resulted in a significant enhancement of activity in a cell proliferation assay. Further mutagenesis based on this initial hit has lead to a new optimized series. After further optimization, several lead peptides were shown to have comparable activity to recombinant G-CSF with full efficacy in a cell proliferation assay. Selected lead PEGylated peptides were also shown to induce granulopoiesis in normal mice and several mouse models of neutropenia [7,8].

### Results and Discussion

The initial peptide, discovered from Affymax peptide libraries, was a 17-amino acid long peptide containing a disulfide bond loop. All peptides resulting from optimization of the initial hit suffered from < 100% efficacy compared to recombinant G-CSF in the cell proliferation assay. The best N-terminal dimeric peptides with N-terminal extensions combined with Q15A or Q15G have agonist activity with  $EC_{50}$  ranging from 0.5 – 5 nM with ~ 60% efficacy. The SAR information, such as intolerable changes of residues within the cysteine loop, Gln15 substitutions, and amino acid extensions, was beneficial for the optimization of new lead series.

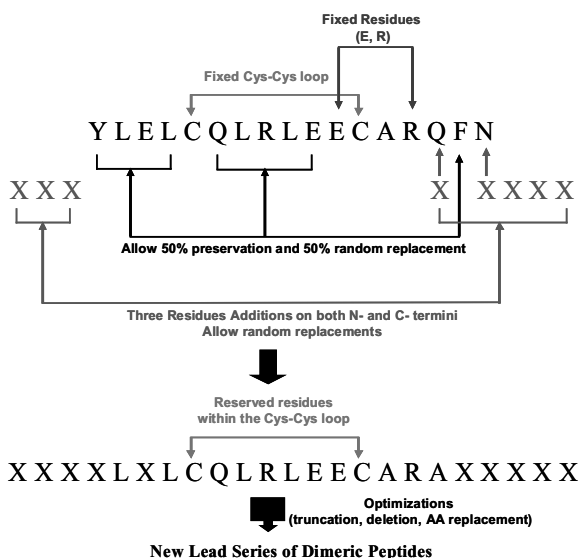


Fig. 1. Discovery of new lead peptides.

The lead series of peptides were discovered by mutagenesis of the initial hit followed by chemical optimizations (Figure 1). Table 1 is a summary of *in vitro* activity of PEGylated lead peptides.

Table 1. Biological results of PEGylated lead peptides in the cell proliferation assay

Peptide	Architecture	PEG size	Hu G-CSF (2G2)			Mu NFS-60			Difference
			EC <sub>50</sub> (nM)	Efficacy (%)	Ratio (peptide to GCSF)	EC <sub>50</sub> (nM)	Efficacy (%)	Ratio (peptide to GCSF)	
<b>Peptide -636<sup>a</sup></b>	N-terminal dimer through Lys side- chain amine	30 kDa on Linker	3.6	70	10	0.30	84	112	Higher efficacy on MuGCSF
<b>Peptide -145<sup>b</sup></b>	N-terminal dimer through β-Ala	30 kDa on Linker	0.63	104	16	0.30	92	145	Same on HuGCSFR and MuGCSF
<b>Peptide -259<sup>b</sup></b>	N-terminal dimer through Lys α- amine	2 x 10 kDa on Lys side- chain amine	0.60	99	16	0.35	95	154	Same on HuGCSFR and MuGCSF

<sup>a</sup> Peptide sequence: Asp-Arg-Leu-Phe-Leu-Cys-Gln-Leu-Arg-Leu-Glu-Glu-Cys-Ser-Arg-Arg-Leu-Gln-Met-Phe

<sup>b</sup> Peptide sequence: Ser-Arg-Leu-Phe-Leu-Cys-Gln-Leu-Arg-Leu-Glu-Glu-Cys-Ala-Leu-Asn

Ex-vivo Colony Assay [5,6] results are shown in Figure 2. Bone marrow harvested from 5-fluorouracil-induced neutropenic mice on day-8 was evaluated in a colony forming assay compared to bone marrow from untreated animals in the normal group. Both lead peptides produced robust colonies.

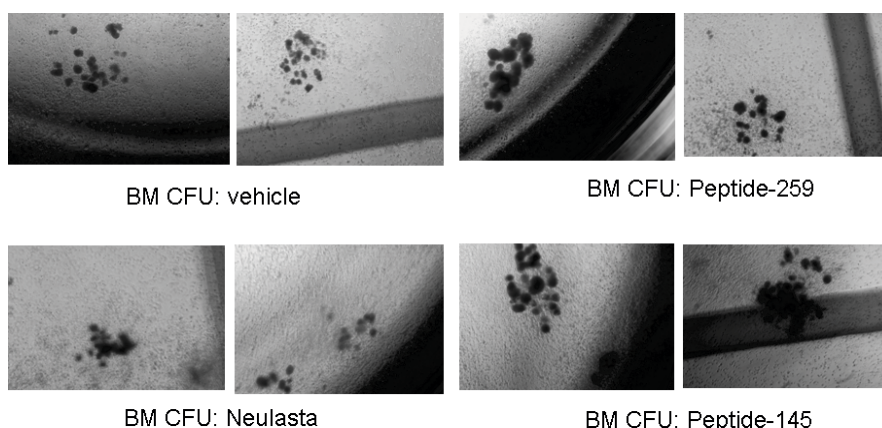
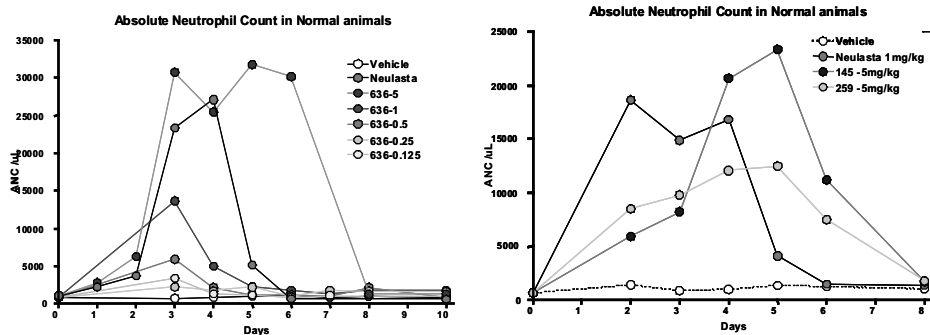


Fig. 2. Ex-vivo colony assay results.

Neutrophilic activity of G-CSF receptor peptide agonists (Peptide-636, Peptide-145, and Peptide-259) was studied in normal mice [7,8] (Figure 3, top graphs). The study groups of animals received a single subcutaneous injection of vehicle, or 1 mg/kg Neulasta, or lead peptides. Peptide-636 showed a clear dose-response as the most active peptide and induced a dramatic rise in neutrophils. Peptide-259 with 2 x 10 kDa PEG showed a similar response at the earlier days as the 30 kDa PEGylated Peptide-145, but did not have the same response at later time points. This supports the hypothesis that a larger PEG size increases the circulating half life of the peptide.

Neutrophilic activity of peptide-145 and peptide-259 was studied in 5-fluorouracil-induced neutropenic mice [7,8] (Figure 3, bottom graph). The animals were dosed with 150 mg/kg 5-FU by IV injection on Day 0 to induce neutropenia. On Day 2, the animals were treated with vehicle, or 1 mg/kg Neulasta<sup>TM</sup>, peptide-145 or peptide-259 at 1 or 5 mg/kg by a single subcutaneous injection. Both peptides at 5 mg/kg clearly corrected neutropenia in this animal model. Peptide-259, being the less favored candidate in the normal mice model, had a comparable activity at a 5 mg/kg dose to Neulasta<sup>TM</sup> at a 1 mg/kg dose.

### *in vivo* study in normal mice



### *in vivo* study in 5-FU induced neutropenic mice

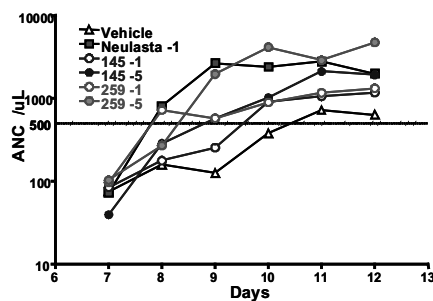


Fig. 3. *In vivo* study results.

## References

1. Aritomi, M., et al. *Nature* **401**, 713-718 (1999).
2. Tkatch, L.S., Tweardy, D.J. *Lymphokine and Cytokine Research* **12**, 477-488 (1993).
3. Eliason, J.F. *BioDrugs* **15**, 705-711 (2001).
4. Reidaar-Olson, J.F., De Souza-Hart, J.A., Selick, H.E. *Biochemistry* **35**, 9034-9041 (1996).
5. Technical manual, human colony-forming cell assays using MethoCult®. StemCell Technologies, Catalog #28404, version 3.0 (2004).
6. Miller, C.L., Lai, B. Human and mouse hematopoietic colony-forming cell assays, Basic Cell Culture Protocols 3, *Methods in Molecular Biology* **290**, Humana Press, Totowa, NJ. 71-89, 2005
7. Lord, B.I., Woolford, L.B., Molineux, G. *Clinical Cancer Research* **7**, 2085-2090 (2001).
8. Molineaux, G., et al. *Experimental Hematology* **27**, 1724-1734 (1999).

## Role of the Guanidine Group in Position 11 of PTH(1-11) Analogues

A. Caporale<sup>1</sup>, E. Schievano<sup>1</sup>, I. Woznica<sup>2</sup>, S. Mammi<sup>1</sup> and E. Peggion<sup>1</sup>

<sup>1</sup>Dept. of Chemical Sciences, Univ. of Padova, Institute of Biomolecular Chemistry, CNR,  
Via Marzolo 1, 35131 Padova, Italy, <sup>2</sup>Dept. of Physiology, Tufts Univ. School of Medicine,  
136 Harrison Avenue, Boston, MA 02111, U.S.A.

### Introduction

The N-terminal 1-34 fragment of parathyroid hormone (PTH) is fully active *in vitro* and *in vivo* and it can reproduce all the biological responses characteristic of the native intact PTH. Recent studies [1] have demonstrated that helicity-enhancing substitutions yielded potent analogues of PTH(1-11) and PTH(1-14). The role of  $\alpha$ -helicity on biological potency is well known [2]. Recently, we performed a D-scan in the PTH(1-11) sequence [3]; the analogue [Aib<sup>1,3</sup>, Nle<sup>8</sup>, Gln<sup>10</sup>, D-Har<sup>11</sup>] PTH(1-11) was the one which retained the highest activity. In the context of searching the pharmacological properties of PTH(1-11) analogues, we studied the role of a positive charge at the C-terminal position, which was identified to play an essential role in bioactivity and binding. A series of modified peptide analogues of PTH(1-11) were synthesized and characterized:

1. H-Aib-Val-Aib-Glu-Ile-Gln-Leu-Nle-His-Gln-Har-NH<sub>2</sub>
2. H-Aib-Val-Aib-Glu-Ile-Gln-Leu-Nle-His-Gln-Lys-NH<sub>2</sub>
3. H-Aib-Val-Aib-Glu-Ile-Gln-Leu-Nle-His-Gln-NH(CH<sub>2</sub>)<sub>4</sub>NH<sub>2</sub>
4. H-Aib-Val-Aib-Glu-Ile-Gln-Leu-Nle-His-Gln-NH(CH<sub>2</sub>)<sub>5</sub>NH<sub>2</sub>
5. H-Aib-Val-Aib-Glu-Ile-Gln-Leu-Nle-His-Gln-NH(CH<sub>2</sub>)<sub>6</sub>NH<sub>2</sub>
6. H-Aib-Val-Aib-Glu-Ile-Gln-Leu-Nle-His-Gln-NArgNH<sub>2</sub>  
[NArg is the N-alkylglycine corresponding to Arg]
7. H-Aib-Val-Aib-Glu-Ile-Gln-Leu-Nle-His-Gln-D-Har-NH<sub>2</sub>

### Results and Discussion

As a reference [4], we synthesized an analogue peptide containing Lys in position 11: [Aib<sup>1,3</sup>, Nle<sup>8</sup>, Gln<sup>10</sup>, Lys<sup>11</sup>]PTH(1-11)NH<sub>2</sub>, to avoid the final guanylation reaction. This analogue exhibited an activity similar to that of [Ala<sup>1,3</sup>, Nle<sup>8</sup>, Gln<sup>10</sup>, Har<sup>11</sup>]PTH(1-11)NH<sub>2</sub>. Then, the synthesis of Fmoc  $\omega$ -benzyloxy carbonyl aminoalkylglutamic acid amides [Fmoc-GluNH(CH<sub>2</sub>)<sub>n</sub>NHZ] was carried out in solution by modifying glutamic acid (Glu). Fmoc-GluNH(CH<sub>2</sub>)<sub>n</sub>NHZ was coupled to the resin and the stepwise elongation of the peptide was carried out on the solid support following published procedures. The coupling of Aib and Val residues was carried out by employing the HOAt/HATU/collidine system.

A circular dichroism (CD) study of the synthesized peptides was performed in water containing 20% TFE to compare their conformation with biological activity. From the CD spectra, a reduced ellipticity was observed for analogues containing diamines. We found a reduced activity, too, for analogues containing diamines with  $n = 5$  and  $n = 6$ , which could be justified by the role of the C-terminal amide group (Table 1). In fact, a residual activity of the H-Aib-Val-Aib-Glu-Ile-Gln-Leu-Nle-His-Gln-NArgNH<sub>2</sub> analogue was detected and the activity of the analogue containing Lys<sup>11</sup> was similar to those of the most active PTH(1-11) analogues.

Table 1. Parameters of PTH(1-11) analogs

Entry	MW calc. [M+1]	MW found [M+1]	Rt (min) <sup>a</sup>	Yield (%)	EC50 (nM) <sup>b</sup>
1	1317.7	1317.7	12.07	35.4	1.0
2	1276.7	1276.4	12.63	10	50
3	1219.7	1219.4	13.29	7	Not active
4	1233.7	1233.4	13.68	11	100
5	1247.7	1247.4	13.95	12	200
6	1303.7	1303.6	13.85	10	2130
7	1317.73	1317.72	12.47	38.5	75

<sup>a</sup> Determined with a linear gradient of 20-45 (v/v) B over 20 min (A: water + 0.1% TFA; B: 90% acetonitrile + 0.1% TFA)

<sup>b</sup> Defined as the half maximal effective concentration and is referred to the concentration of peptide which induces a response halfway between the baseline and the maximum. The experimental error on the measurement is  $\pm 7.5\%$

These initial results demonstrate that homoarginine plays an important role to anchor PTH(1-11) to the receptor. In particular, the 100-fold reduction in potency observed for mimetic analogues containing diamines with n = 5 and n = 6 in position 11, compared to the same analogue containing homoarginine (or lysine), highlights the critical role this charged residue (which replaces leucine of native PTH) in receptor binding [6]. Molecular modelling suggests that this role might involve the insertion of the guanidinium side-chain group between the extracellular ends of TM1 and TM7 [7].

## References

1. Shimizu, N., Petroni, B.D., Khatri, A., et al. *Biochemistry* **42**, 2282-2290 (2003); Tsomaia, N., Pellegrini, M., Hyde, K., et al. *Biochemistry* **43**, 690-699 (2004).
2. Caporale, A., Fiori, N., Schievano E., et al. *3rd IPS and 28th EPS*, Prague, Czech Republic, Sept. 2004, 926-927; Caporale, A., Fiori, N., Schievano E., et al. *19th APS*, San Diego, CA, U.S.A., June 2005, 38-39; Caporale, A., Fiori, N., Wittelsberger A., et al. *29th EPS*, Gdansk, Poland, Sept. 2006, 424-425.
3. Caporale, A., Biondi, B., Schievano, E., Wittelsberger, A., Mammi, S., Peggion, E. *European Journal of Pharmacology* **611**, 1-7 (2009).
4. Shimizu, M., Potts, J.T. Jr, Gardella, T.J. *J. Biol. Chem.* **275**, 21836-21843 (2000).
5. Barazza, A., Wittelsberger, A., Fiori, N., Schievano, E., Mammi, S., Toniolo, C., Alexander, J.M., Rosenblatt, M., Peggion, E., Chorev, M. *J. Pept. Res.* **65**, 23-35 (2005).
6. Shimizu, M., Carter, P.H., Khatri, A., Potts, J.T. Jr., Gardella, T.J. *Endocrinology* **142**, 3068-3074 (2001).
7. Monticelli, L., Mammi, S., Mierke, D.F. *Biophys. Chem.* **95**, 165-172 (2002).

## Peptide Antagonists of Human BAFF/BAFF Receptor Binding

Y. Sarah Dong, Erik Whitehorn, Christopher P. Holmes, Peter J. Schatz,  
 and Jennifer M. Green

Affymax, Inc., 4001 Miranda Avenue, Palo Alto, CA 94304, U.S.A.

### Introduction

BAFF (B cell Activating Factor of the Tumor Necrosis Factor family), a soluble plasma membrane cleaved homotrimer, is a key regulator of B lymphocyte maturation [1-3]. BAFF binds to three cell surface receptors of the TNF receptor family, BCMA, TACI, and BAFF-R. Studies using B cells purified from BCMA, TACI, or BAFF-R knockout mice have demonstrated that the BAFF-R is the primary mediator of the effects of BAFF on B cell survival and maturation [1]. The application of Phage Display and Affymax Peptides on Plasmids technologies has identified a series of peptide sequences which bind specifically to human and murine BAFF. Furthermore, novel peptides with sequence features similar to these selected sequences have also been shown to antagonize BAFF binding to the BAFF-R in an ELISA assay. Importantly, these peptides were also shown to inhibit the proliferation of primary B cells when cultured in the presence of human BAFF. The structure activity relationships of the lead sequence, including an Ala scan, various architectures, and different sites and sizes of PEGylations, have been explored to enhance antagonist activity in the proliferation assay. A selected lead peptide, that shows equal potency to a BAFF antagonist currently in the clinic [4], was shown to significantly inhibit B cell proliferative responses in Balb/c mice stimulated with BAFF.

### Results and Discussion

Among a series of BAFF-specific clones from phage display, a total of seven selected peptide sequences were extensively evaluated as GFP fusion proteins in BAFF-R competition and binding assays. All of them bind to hBAFF-R specifically with EC<sub>50</sub>s ranging from 14 nM to 188 nM, listed in Table 1.

Table 1. Binding affinity to hBAFF and mBAFF

Clones	3A4	2G91	3G12	3G11	4G5	3C9	4F5
EC <sub>50</sub> /hBAFF	57 nM	188 nM	140 nM	36 nM	28 nM	14 nM	107 nM
EC <sub>50</sub> /mBAFF	363 nM	>10 mM	109 nM	23 nM	14 nM	72 nM	136 nM

Synthetic peptides based on selected sequences (3A4, 4G5, and 3C9) were prepared as monomers and dimers. The monomers based on 3C9 sequence showed an IC<sub>50</sub> of 1-2 mM inhibition of rhBAFF in the primary murine splenic B cell proliferation assay, while other monomers showed activity of an IC<sub>50</sub> > 10 mM. Upon dimerization, the dimeric peptides, Peptide-311 (C-terminal dimer) and Peptide-312 (N-terminal dimer), exhibited increased activity as antagonists of rhBAFF with IC<sub>50</sub>s of 7-22 nM in Table 2.

Table 2. Inhibition activity of peptides derived from 3C9

Peptides	Sequence	IC <sub>50</sub> (nM)
Peptide-286	Ac-T-R-S-C-Y-D-A-L-T-Y-L-E-L-P-C-H-L-M-K-NH <sub>2</sub>	738
Peptide-287	Ac-K-T-R-S-C-Y-D-A-L-T-Y-L-E-L-P-C-H-L-M-NH <sub>2</sub>	2114
Peptide-311	Linker-[Ac-K-T-R-S-C-Y-D-A-L-T-Y-L-E-L-P-C-H-L-M] <sub>2</sub>	7
Peptide-312	[Ac-T-R-S-C-Y-D-A-L-T-Y-L-E-L-P-C-H-L-M-K] <sub>2</sub> -Linker	22

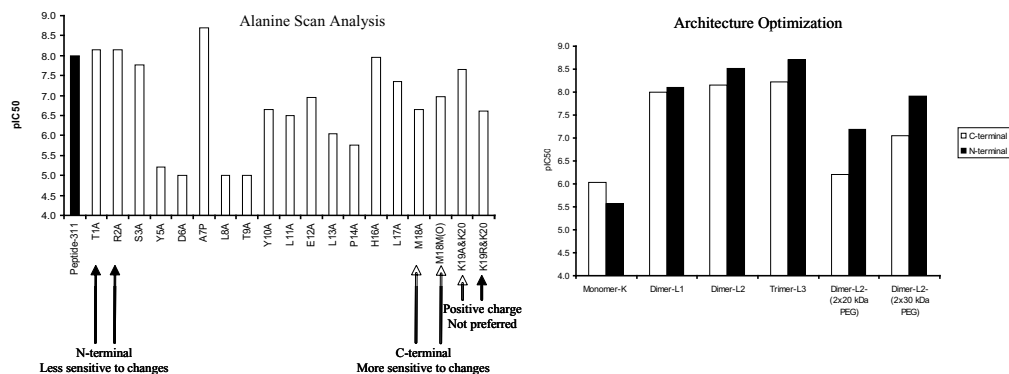


Fig. 1. The structure activity relationships of the lead sequence.

The alanine scan analysis of hit peptide-311 (Figure 1, left) reveals that the N-terminal residues such as threonine and arginine can be replaced with alanine without losing activity, while the C-terminal residues are more critical. The D-X-L-T residues within the Cys-Cys loop are the key residues for biological activity.

Shown in Figure 1 (right), there is no significant difference in activity between peptide dimer and trimer architectures, despite the fact that the natural ligand configuration is a homotrimer. Peptide dimerization was demonstrated to enhance the antagonist activity of monomeric peptides 100-fold in the B cell proliferation assay.

Linker2 has been chosen for easy assembly of two linear PEG conjugates. Since peptide activity is more tolerant of N-terminal amino acid changes, the N-terminal PEGylated dimers are more active than their corresponding C-terminal PEGylated dimers. The bis-30 kDa PEGylated N-terminal dimer (total MW 65 kDa) (Peptide-662) has shown excellent activity as a BAFF antagonist with an IC<sub>50</sub> of 12 nM in the B cell proliferation assay. The t<sub>1/2</sub> of the 40 kDa PEGylated peptide in the plasma stability study was determined to be ~ 4 hours, and the 60 kDa PEG size is known to increase t<sub>1/2</sub>. Peptide-662 was chosen for evaluation in an animal model.

The lead peptide Peptide-662 was evaluated in Balb/c mice stimulated with rhBAFF [4]. The animals were dosed with 0.3 mg/kg rhBAFF s.c. and 10 mg/kg Peptide-662 by IV *bid* on days 1, 2, 3, and 4. Spleen weight, serum IgG and IgA, and B cell subset analysis on splenocytes by flow cytometry was performed on day 5. Peptide-662 does not significantly alter blood chemistries of Balb/c mice. Hematopoiesis was observed in the animal group receiving Peptide-662.

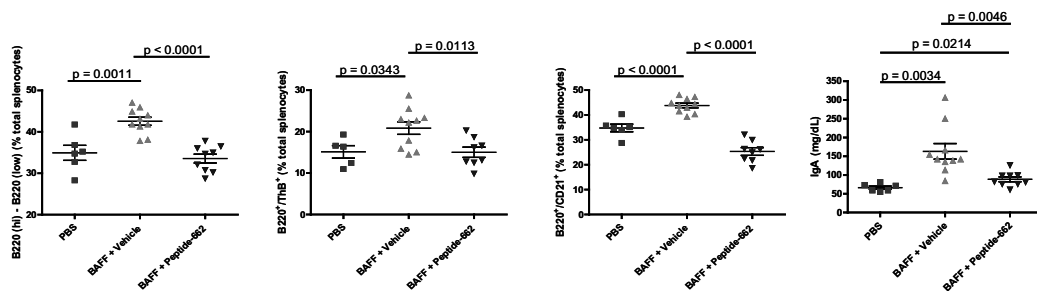


Fig. 2 Peptide-662 inhibits the rise of Splenic B cell populations and Serum IgA levels.

## References

1. Schneider, P., et al. *Current Opinion in Immunology* **17**, 282-289 (2005).
2. Mackay, F., Browning, J.L., *Nature Reviews Immunology* **2**, 465-475 (2002).
3. Patke, A., et al. *Current Opinion in Immunology* **16**, 251-255 (2004).
4. Baker, K.P., et al. *Arthritis and Rheumatism* **48**, 3253-3265 (2003).

## Cell Membrane Damage by the Type 2 Diabetes Associated Peptide Amylin in the Presence of Insulin

Joshua M. Osborne, Daniel J. Clegg, and Deborah L. Heyl

Department of Chemistry, Eastern Michigan University, Ypsilanti, MI 48197, U.S.A.

### Introduction

Amylin (human Islet Amyloid Polypeptide, hIAPP) and insulin are both stored and secreted from the  $\beta$ -cells of the pancreas. In Type 2 diabetics, insulin resistance leads to an increase in both insulin and amylin release. This excess amylin is known to cause damage to the  $\beta$ -cells of the pancreas, and plaques of the peptide are found in these patients post-mortem [1-2]. The purpose of this study was to determine if insulin, which has been shown to limit amylin fiber formation [3], would protect against its damaging effects on cell membranes. Carboxy-fluorescein-encapsulating vesicles which mimic the  $\beta$ -cell were created using a 7:3 ratio of the lipids DOPC and DOPS, respectively. Different concentrations of amylin and insulin were added alone and together, and the percent leakage of fluorescent dye from the vesicles was calculated as compared to a 100% Triton-X detergent-treated control. Assays were run in triplicate in a 96-well plate, and fluorescence values were recorded by an FLx fluorescence microplate reader.

### Results and Discussion

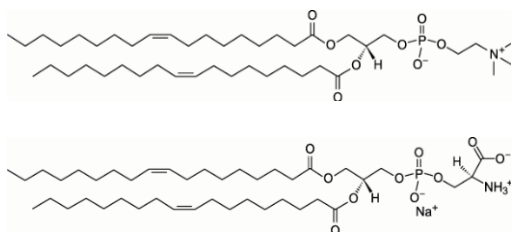


Fig. 1. 1,2-Dioleoyl-*sn*-Glycero-3-Phosphocholine (DOPC, top) and 1,2-Dioleoyl-*sn*-Glycero-3-[Phospho-L-Serine] (Sodium Salt) (DOPS, bottom).

causing greater than 80% dye leakage at 50  $\mu$ M, the highest concentration tested. A logarithmic regression is shown with a correlation coefficient of 0.87. It should be noted that membrane leakage also increased over the time period observed (data not shown), indicating the possibility of aggregate formation.

The data displayed in right graph in Figure 2 was gathered through a dye leakage assay where twelve concentrations of insulin ranging from 0  $\mu$ M to 100  $\mu$ M were run against a constant 10  $\mu$ M hIAPP concentration, and fluorescence readings were recorded every minute for three hours. The plot was produced by averaging the percent membrane disruption over time at each insulin concentration and displayed as percent leakage *versus* the ratio of the concentration of insulin to the concentration of hIAPP. It can be observed that the trial without any insulin produces the greatest membrane disruption (46% leakage, which is comparable to that obtained at 10  $\mu$ M hIAPP in the graph on the left). This confirms that insulin does inhibit membrane damage in this assay. However, the relationship between membrane disruption and the ratio of insulin to hIAPP is variable. A sharp spike can be noted at the ratio of 0.2[Insulin]:1[hIAPP]. This ratio maximizes the extent of inhibition induced by insulin. At this ratio, insulin inhibits membrane disruption by 13% (reducing percent leakage from 46% to 33%). As the insulin:hIAPP ratio is increased beyond this point, membrane disruption quickly increases to varying degrees but never surpasses the level of damage caused by hIAPP by itself.

Figure 1 shows the structures of the lipids used to create the vesicles. The data in Figure 2 was gathered through a dye leakage assay showing the interaction between the  $\beta$ -cell mimics and twelve concentrations of hIAPP. Fluorescence values were recorded every minute for three hours, and the graph was produced by averaging the percent membrane disruption at each time point and plotting these values against hIAPP concentration.

Concentration dependent damage to the  $\beta$ -cell membrane mimics by hIAPP was observed, as displayed in Figure 2, left graph. The peptide was very destructive,



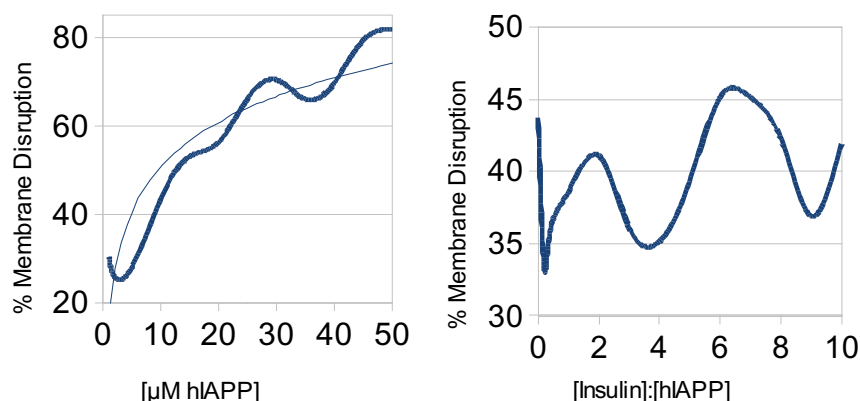


Fig. 2. Left: Percent of dye leakage in model membranes caused by hIAPP. Right: Percent of dye leakage from model membranes in the presence of varying ratios of insulin to hIAPP.

One possible explanation of this observation is that hIAPP forms a five unit complex to which one molecule of insulin binds. This six unit complex is less toxic than free hIAPP, perhaps reducing its ability to interact with the membrane in a fully aggregated form. This result is conserved over many trials and is particularly interesting given that insulin is stored in secretory cells as a hexamer, so the six unit complex may have some physiological significance. However, even at the optimal ratio, membrane damage as measured by this assay is only reduced by ~15%. This suggests that membrane disruption may be mediated by more than simply hIAPP aggregation and fiber formation, perhaps transient deformations in the acyl chain arrangements induced by interaction of the positively charged peptide with the overall negatively charged membrane surface. Indeed, two phases of damage have been reported by some investigators [4].

The relationship between membrane damage, hIAPP, and insulin will be further studied by assays probing the 0.2:1 ratio more closely. In addition, Thioflavin T assays will be run to determine the ratio of insulin to hIAPP needed to inhibit fibrillogenesis in this model system. This value can then be compared to that required to inhibit dye leakage from the vesicles, in order to obtain a clearer picture of the mechanism of this effect.

## Acknowledgments

This research was supported by an award from Research Corporation. We would also like to thank the EMU Chemistry Department and Seller's Fund for financial support. DJC is a student at Ann Arbor Huron High School who completed a science project at EMU.

## References

1. Nilsson, M.R., Nguyen, L.L., Raleigh, D.P. *Anal. Biochem.* **288**, 76-82 (2001).
2. Engel, M., Khemtournian, L., Kleijer, C.C., Meeldijk, H.J.D., Jacobs, J., Verkleij, A.J., deKruijff, B., Killian, J.A., Hoppener, J.W.M. *PNAS* **105**, 6033-6038 (2008).
3. Gilead, S., Wolfenson, H., Gazit, E. *Angew. Chem.* **45**, 6476- 6480 (2006).
4. Brender, J.R., Lee, E.L., Cavitt, M.A., Steel, D.G., Ramamoorthy, A. *J. Am. Chem. Soc.* **130**, 6424-6429 (2008).

## Synthesis and Analysis of Analogs of hIAPP (1-19), a Peptide Involved in Membrane Disruption

Deborah L. Heyl, Srikanth Reddy Konda, and Anitha Jayaprakash

Department of Chemistry, Eastern Michigan University, Ypsilanti, MI 48197, U.S.A.

### Introduction

Human islet amyloid polypeptide (hIAPP) is co-secreted with insulin in the  $\beta$ -cells of the pancreas. Capable of forming amyloid fibers and causing membrane disruption, this 37 amino acid peptide is cytotoxic to  $\beta$ -cells in type II diabetic patients [1,2]. The N-terminus of hIAPP (residues 1-19, KCNTATCATQRLANFLVHS) has been shown to bind to membranes and induce damage despite lacking the amyloidogenic (20-29) region [3]. These results indicate that the N-terminal (1-19) region of hIAPP can be used as a model in drug target studies, in place of the expensive and synthetically challenging full length hIAPP. It has been proposed that aggregation of hIAPP is mediated by  $\pi$ -stacking interactions between phenylalanine residues [4]. In this study, two analogs of hIAPP 1-19 were synthesized by standard solid phase methods in which Phe<sup>15</sup> was replaced with Ala (to reduce aromaticity) and 1-naphthylalanine (1-Nal, to increase aromaticity), respectively. These analogs were then purified by reverse phase high performance liquid chromatography and tested in a model system that mimics the pancreatic  $\beta$ -cell membrane, namely vesicles comprised of a 7:3 ratio of the lipids 1,2-dioleoyl-sn-glycero-3-phosphocholine (DOPC) and 1,2-dioleoyl-sn-glycero-3-(phospho-L-serine) (DOPS). The percent leakage of fluorescent carboxyfluorescein dye from the vesicles in the presence of the peptides was calculated as compared to a 100% Triton-X detergent-treated control. Assays were run in triplicate in a 96-well plate, and average values are reported. Fluorescence values were recorded by an FLx fluorescence microplate reader.

### Results and Discussion

Figure 1 shows the effect of varying the concentration of hIAPP 1-19 on carboxyfluorescein-encapsulating vesicles over time. Dye leakage is roughly concentration dependent. The maximal disruption observed was 80%, which was slightly higher than that produced by full length hIAPP (data not shown).

In DOPC:DOPS (7:3), the membrane disruptive activity of both the modified hIAPP 1-19 analogs (Figures 2 and 3) were found to be lower when compared to the original hIAPP 1-19 sequence, by roughly 3-10 fold. Again concentration dependence was observed, as well as time dependence for the naphthylalanine analog at higher concentrations. The hIAPP sequence modified with naphthylalanine (Figure 3) had slightly higher activity when compared to the sequence modified with alanine (Figure 2) at equal concentrations, especially at the higher concentrations tested. The Nal<sup>15</sup> analog required a threshold concentration of 15  $\mu$ M to induce

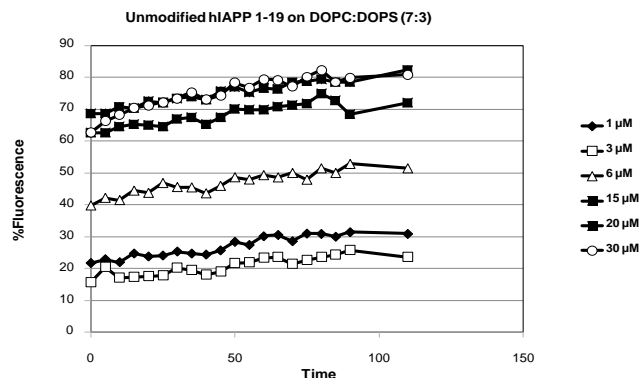


Fig. 1. Percent dye leakage from vesicles in the presence of varying hIAPP 1-19 over time.

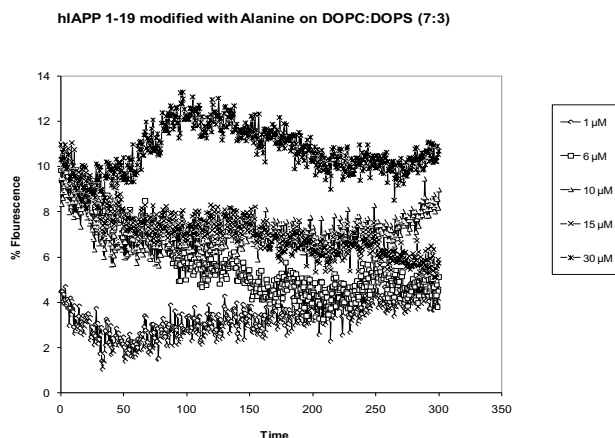


Fig. 2. Percent dye leakage from vesicles in the presence of varying Ala<sup>15</sup> hIAPP 1-19 over time.

more than 10% leakage, whereas the Ala<sup>15</sup> analog did not reach that mark even at the highest concentration tested (30  $\mu$ M). In contrast, only 1  $\mu$ M hIAPP 1-19 induced comparable ( $\geq 10\%$ ) leakage of dye from the vesicles.

Overall, these results indicate that the mechanism of membrane disruption may be more than just fibril formation, since these peptides lack the 20-29 region commonly thought to

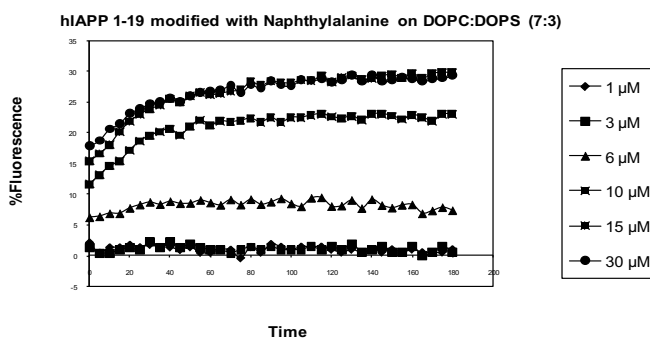


Fig. 3. Percent dye leakage from vesicles in the presence of varying Nal<sup>15</sup> hIAPP 1-19 over time.

mediate fibrilization and still induce damage. However, the activity of both of the modified peptides was found to be less than that of the original hIAPP 1-19 sequence, suggesting that aromatic character or pi-stacking in this region has no significant influence on the aggregation of the peptide and/or that the membrane disruption might be due to other mechanisms. It is also possible that pi-stacking is important, but the naphthylalanine analog is unable to adapt to the appropriate structural conformation for aggregation or membrane damage. The native sequence shows optimal activity and modification is detrimental. These modified analogs will eventually be tested as possible inhibitors of membrane damage induced by full length hIAPP. Possible interactions with insulin also will be investigated.

## Acknowledgments

This research was supported by an award from Research Corporation. We would also like to thank the EMU Chemistry Department and Seller's Fund for financial support.

## References

1. Nilsson, M.R., Nguyen, L.L., Raleigh, D.P. *Anal. Biochem.* **288**, 76-82 (2001).
2. Engel, M., et al. *PNAS* **105**, 6033-6038 (2008).
3. Brender, J.R., et al. *J. Am. Chem. Soc.* **130**, 6424-6429 (2008).
4. Gazit, E. *FASEB* **16**, 77-83 (2008).

## Use of Peptoid-Peptide Hybrids in the Development of Shc SH2 Domain–Binding Inhibitors

Sung-Eun Kim,<sup>1</sup> Won Jun Choi,<sup>1</sup> Andrew G. Stephen,<sup>2</sup> Iwona Weidlich,<sup>1</sup>  
Alessio Giubellino,<sup>3</sup> Fa Liu,<sup>1</sup> Karen M. Worthy,<sup>2</sup> Lakshman Bindu,<sup>2</sup>  
Matthew J. Fivash,<sup>4</sup> Marc C. Nicklaus,<sup>1</sup> Donald P. Bottaro,<sup>3</sup>  
Robert J. Fisher,<sup>2</sup> and Terrence R. Burke, Jr.<sup>1</sup>

<sup>1</sup>Laboratory of Medicinal Chemistry, CCR, NCI-Frederick, NIH, Frederick, MD 21702, U.S.A.;

<sup>2</sup>Protein Chemistry Laboratory, Advanced Technology Program, SAIC-Frederick, Frederick, MD 21702, U.S.A.; <sup>3</sup>Urologic Oncology Branch, CCR, NCI, NIH, Bethesda, MD 20892, U.S.A. and

<sup>4</sup>Data Management Services, Inc., NCI-Frederick, Frederick, MD 21702, U.S.A.

### Introduction

Shc is a non-catalytic adapter molecule that participates in RAS activation and mitogenic signal transduction by promoting the formation of multimeric protein complexes through the recognition and binding of its Src homology 2 (SH2) domain to phosphotyrosyl (pTyr)-containing sequences [1]. We have undertaken a program to develop Shc SH2 domain-binding antagonists as potential non-kinase directed signaling inhibitors. Using a fluorescence anisotropy (FA)-based competition assay that employs the high affinity fluorescein isothiocyanate (FITC)-containing reference peptide **1** (Figure 1), the *N*-homoallyl-glycine-containing peptide-peptoid hybrid **2** was identified as a preferred binding motif [2]. The importance of *C*-terminal hydrophobic character for high Shc SH2 domain-binding affinity was also shown. To further explore this latter observation, a series of peptoid-peptide hybrids (**3**) were prepared in which the original Leu residue in **2** was replaced by both natural and unnatural lipophilic amino acid residues (Figure 1).

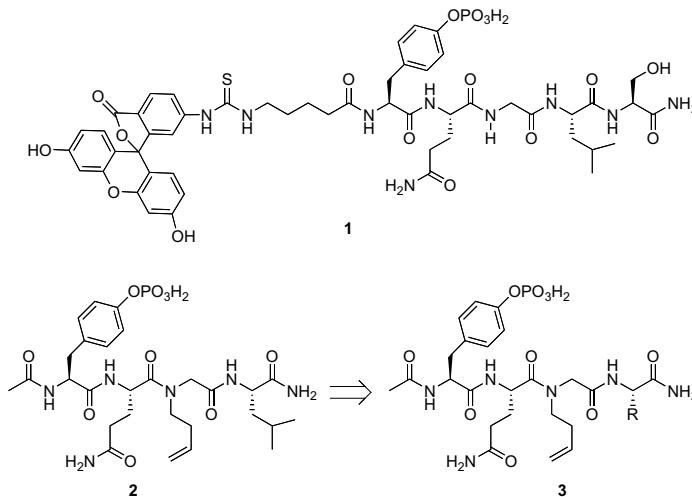
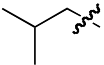
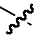
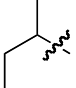
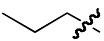
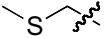
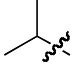
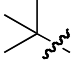
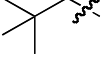
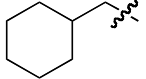


Fig. 1. Structures of Shc SH2 domain-binding peptides discussed in the text: R = hydrophobic functionality.

### Results and Discussion

Peptides (**3**) were prepared by solid-phase protocols using reported procedures [2]. Shc SH2 domain-binding affinities were determined using the previously reported (FA)-based competition assay employing peptide **1** as a reference [2]. Binding data expressed as IC<sub>50</sub> values are provided in Table 1.

Table 1. Shc SH2 domain-binding affinities<sup>a</sup>

No	R <sup>b</sup>	IC <sub>50</sub> (μM)
<b>2</b>		48
<b>3a</b>		286
<b>3b</b>		35
<b>3c</b>		30
<b>3d</b>		80
<b>3e</b>		53
<b>3f</b>		50
<b>3g</b>		77
<b>3f</b>		64

<sup>a</sup> Determined in a fluorescence anisotropy competition assay using peptide **1** as a reference ligand; <sup>b</sup> C-terminal side chain functionality as indicated for peptide **3**

Our previous work had suggested that hydrophobic character C-proximal to the peptoid N-homoallylglycine residue was beneficial to binding affinity [2]. Consistent with this, replacing the C-terminal Leu residue (**2**, IC<sub>50</sub> = 48 μM) with an Ala residue (**3a**, IC<sub>50</sub> = 286 μM), resulted in a significant loss of binding affinity. In contrast, replacement of Leu with Ile (**3b**, IC<sub>50</sub> = 35 μM) or Nle (**3c**, IC<sub>50</sub> = 30 μM) resulted in slight increases in affinity. Replacement of the Nle residue with an isosteric Met residue (**3d**, IC<sub>50</sub> = 80 μM) gave a two-fold loss of affinity. Replacement of Leu with Val (**3e**, IC<sub>50</sub> = 53 μM) and the closely related *tert*-butyl-containing **3f** (IC<sub>50</sub> = 50 μM) resulted in nearly equal affinities for all three. Increasing steric bulk by employing neopentyl (**3g**, IC<sub>50</sub> = 77 μM) or cyclohexylmethyl (**3f**, IC<sub>50</sub> = 64 μM) side chains resulted in slight affinity losses. In summary, the best affinities were obtained with side chains 3-carbons in length (**2**, **3b** and **3c**). Branching by addition of a single methyl group resulted in reduction of affinity, with higher affinity being shown when the branching occurred closer to the peptide backbone (**3b** versus **2** and **3g**).

## Acknowledgments

This Work was supported in part by the Intramural Research Program of the NIH, Center for Cancer Research, NCI-Frederick and the National Cancer Institute, National Institutes of Health, under contract HHSN261200800001E. The content of this publication does not necessarily reflect the views or policies of the Department of Health and Human Services, nor does mention of trade names, commercial products, or organizations imply endorsement by the U.S. Government.

## References

1. Kodi, S.R. *Oncogene* **20**, 6322-6330 (2001).
2. Choi, W.J., et al. *J. Med. Chem.* **52**, 1612-1618 (2009).

## **Immunoglobulin Fc-based Peptide Fusion Proteins as a Basis for Optimizing *In Vivo* Pharmacology**

**Allison Kukuch, James T. Patterson, Richard D. DiMarchi, and  
Thomas J. Tolbert**

*Department of Chemistry, Indiana University, Bloomington, IN 47405, U.S.A.*

### **Introduction**

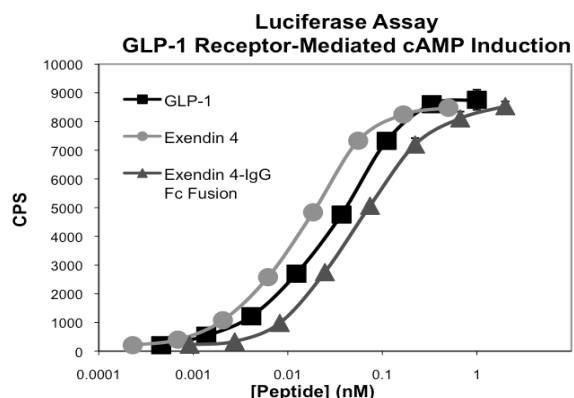
Immunoglobulin G (IgG) is the most abundant antibody class found circulating in human blood. Peptide fusions to the Fc portion of IgG are being explored for multiple research purposes and as a means to optimize pharmacology of certain medicinal agents. When fused to biologically active peptides, the Fc can improve pharmacological action by multiple mechanisms. Peptide Fc-based chimeric proteins increase the duration of action by decreasing in vivo clearance. Since the peptide is presented as a dimer, the Fc-fusion protein can also serve to increase inherent potency through an increase in the avidity of interaction with a target peptidyl-receptor. Lastly, the Fc-domain can stabilize peptides during biological-based synthesis and facilitate purification to dramatically increase the total yield. We have conducted studies directed at the production of peptide Fc-fusions in engineered yeast cells. Yeast expression, unlike bacteria, provides glycosylation, and yet it is faster and less costly than biosynthesis with mammalian or insect cells. Furthermore yeast expression is less expensive than chemical synthesis and, when produced as an Fc-fusion, does not require additional chemical modification to extend duration of action. We have produced a fusion of a glucagon-like peptide 1 (GLP-1) agonist to a specific IgG Fc as an example of this approach to medicinal peptide chemistry.

### **Results and Discussion**

The Exendin-4-IgG-Fc fusion was cloned using standard vector restriction sites. When proteolysis was found within the EcoRI cloning site, a silent mutation was used to create a second restriction site within the IgG-Fc sequence. This removed two amino acids at the fusion site, which eliminated the proteolytic processing. Yeast growth conditions of time, pH, and temperature were altered until an average of 10 mg/L was expressed.

A luciferase-based reporter gene assay was used to compare the effectiveness and potency of native synthetic GLP-1, Exendin-4, and the biosynthetic Exendin-4-IgG-Fc fusion. The native peptide proved to be extremely potent and slightly more so than the peptide fusion protein. The  $EC_{50}$  the peptide-Fc fusion protein of 0.057nM is only 2.2 fold less potent than GLP-1 and 4.5 fold less than the Exendin-4 peptide alone (Figure 1). These initial results are highly encouraging since the peptide has been increased in molecular size by more than tenfold and yet it retains subnanomolar potency as an Fc-dimer.

GLP-1 and related peptides have proven in vivo pharmacology in lowering body weight and hyperglycemia in multiple species, including humans. We report here the biosynthesis and in vitro characterization of a highly potent Exendin-4-IgG-Fc fusion protein. We are currently exploring the in vivo evaluation of this fusion protein and related peptides in rodent models of the metabolic syndrome. This slight reduction in inherent receptor potency measured in the engineered reporter cells is only a portion of in vivo pharmacology. The increased serum half-life of the fusion protein should provide a relative increase in potency. Recently a fusion of Exendin-4 fused to human serum albumin of high in vitro potency demonstrated a half-life of 70-80 hours in rodents. This represents a dramatic increase relative to the native ligands. [1] To be presented in depth later, subsequent in vivo testing done in rodents has indicated that the fusion of IgG-Fc to the GLP-1 agonist to be as effective as other modifications.



	Average EC <sub>50</sub> (nM)	Stdev
GLP-1	0.026	0.005
Exendin-4	0.013	0.002
Exendin-4-IgG-Fc	0.057	0.009

Fig. 1. Mammalian cells displaying receptors for GLP-1 were exposed to GLP-1, Exendin-4, and Exendin-4 fused to IgG-Fc. Each of these peptides proved to be full agonists with comparably shaped dose titrations.

## Acknowledgments

A special thanks to the Tolbert Lab (Brian Hamilton, Mark Pawlicki, Junpeng Xiao, and Rui Chen). Thanks to the DiMarchi Lab for support in biochemical analysis (Vasily Gelfanov, James Ford). Thanks to the IU support staff, especially the Mass Spec facility (Jonathan Karty).

## References

1. Huang, Yan-Shan, et al. *J. Peptide Science* **14**:588-595, (2008).

## Novel $\mu$ Agonist, $\delta$ Antagonist, and NK1 Antagonist Peptide Chimeras

Isuru R. Kumarasinghe,<sup>1</sup> Victor J. Hruby,<sup>1</sup> Suneeta Tumati,<sup>2</sup>  
Shou-Wu Ma,<sup>2</sup> Eva Varga,<sup>2</sup> Josephine Lai,<sup>2</sup> and Frank Porecca<sup>2</sup>

<sup>1</sup>Department of Chemistry, The University of Arizona, 1306 E University Boulevard, Tucson, AZ 85721, U.S.A.; <sup>2</sup>Department of Pharmacology, The University of Arizona, Tucson, AZ 85721, U.S.A.

### Introduction

To date, there are no efficient drugs available for neuropathic pain, which can arise from the nerve injuries resulting from inflammation. At the inflammatory site, due to the inflammation, there can be a large release of different types of neurotransmitters e.g. bradykinin, prostaglandins, substance P, etc., which can sensitize the nociceptors. These changes can lead to hyperalgesia and allodynia which are common symptoms associated with neuropathic pain. Opioids are considered to be the first line of treatment, e.g. fentanyl and morphine for pain. Their analgesic effect is helpful to overcome moderate to severe pain. Prolonged treatment is hampered by their side effects such as tolerance, withdrawal effects, constipation and nausea. The development of tolerance can occur for many reasons. For example, it has been found that chronic morphine administration increases release of the pain sensitizing neurotransmitter substance P [1,2], and decreased pain sensitizing thresholds in patients, which results in the development of tolerance. In addition, the literature indicates that the co-administer of a delta antagonist with a mu agonist decrease tolerance development [3].

These observations prompted us to create novel analgesics which act as agonists at mu Opioid receptors, antagonists at delta Opioid receptors and antagonists at the Neurokinin1 receptor. In this study we have made a series of trifunctional molecules which may have potential to reduce the development of tolerance and improve analgesic efficacy by combining the mu agonist and delta antagonist pharmacophore based on the DIPP-NH<sub>2</sub> scaffold [4] (H-Dmt-Tic-Phe-Phe-OH) and NK1 antagonist pharmacophore [5,6] (Phe-Pro-Leu-Trp-CONHBzl(CF<sub>3</sub>)<sub>2</sub>) (see Figure 1 for initially designed molecule).

### Results and Discussion

Several trifunctional molecules were made with overall reduced length of the peptides in order to understand the importance of each residue for the biological activities. This was done by systematically eliminating residues one by one at the center of the peptide. In addition, the first residue of the peptides which was initially made was replaced by the Dmt residue in order to observe the first residue effect on the biological activities.

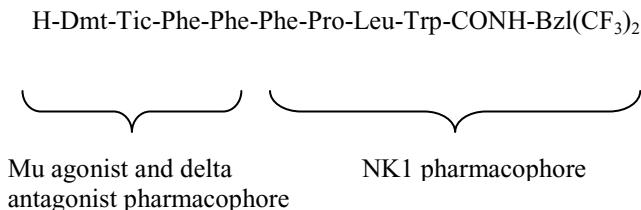


Fig. 1. Initially designed molecule.

A combined N<sup>α</sup>-Fmoc solid phase synthesis and solution phase synthesis were used to construct the trifunctional molecules. Boc-Dmt-OH was coupled to the H-Tic-OMe in the presence of the coupling reagent PyBOP, HOBt and the base NMM. The methyl ester of the dipeptide was hydrolyzed with 1N NaOH, and the product was coupled to the N<sup>α</sup>-Fmoc deprotected peptide synthesized on the chlorotrityl resin. It was cleaved by 1% TFA in DCM, precipitated from solution with either petroleum ether or diethyl ether to gain the crude peptide,



Table 1. Preliminary affinity results of trifunctional molecules

#	Peptide sequence	<i>hDOR</i> , [ <sup>3</sup> H] -DPDPE	<i>n</i>	<i>rMOR</i> , [ <sup>3</sup> H] -DAMGO	<i>n</i>	<i>hNK1</i> , [ <sup>3</sup> H] substance P	<i>n</i>
		<i>Ki</i> (nM)		<i>Ki</i> (nM)		<i>Ki</i> (nM)	
39b6	H <sub>2</sub> N-Tyr-Tic-Trp-CONH-Bzl(CF <sub>3</sub> ) <sub>2</sub>	10	2	2300	2	63	3
35b6	H <sub>2</sub> N-Dmt-Tic-Phe-Phe-Phe-Pro-Leu- Trp-CONH-Bzl(CF <sub>3</sub> ) <sub>2</sub>	13	2	1200	2	41	3

Boc-Dmt-Tic-Phe-Phe-Phe-Pro-Leu-Trp(Boc)-OH. The crude peptide was coupled to 3,5-Bis(trifluoromethyl)benzylamine in the presence of HOBT, PyBOP and NMM and the product was deprotected with 90% TFA in DCM to obtain the desired final product. The final deprotected peptide was purified by semiprep high performance liquid chromatography and was characterized by mass spectrometry and NMR.

The designed molecules were subjected to competitive radio ligand binding assay to measure affinity for the mu, delta receptors and NK1 receptor. Binding affinities of the ligands for the human  $\delta$  opioid receptor (hDOR), rat  $\mu$  opioid receptor (rMOR) and human neurokinin 1 (hNK1) were determined by using the radioligands [<sup>3</sup>H]-DPDPE/[<sup>3</sup>H]-Deltorphan, [<sup>3</sup>H]-DAMGO and [<sup>3</sup>H]-Substance P respectively in cell membrane preparations from transfected cells that stably expresses the respective receptors. Ligands which had promising affinities for the mu and delta receptors were further probed for their efficacy using the GTP-S second messenger assay.

Preliminary results have revealed that Mu affinities vary significantly depending on the chain length. Further mu affinities were shown to be the highest for smaller peptides compared to the longer peptides (Table1). The first residue of the peptide plays a vital role in maintaining the highest affinities towards the mu receptor.

In our study, preliminary results suggest that the delta affinities are not as affected by the chain length compared to the mu affinities. Also Dmt residues at position one of the peptide are important for the delta affinities. In addition, peptides show the best delta affinities for delta receptors when the length of the peptide is shorter. Also, preliminary studies suggest that peptides with shorter lengths provide lower peptide affinities for the NK1 receptor.

## Acknowledgments

The work was supported by a grant from the National Institute on Drug Abuse, DA-13449.

## References

1. Kalso, E. *Eur. J. Pain* **9**, 131-135 (2005).
2. Datar, P., Desai, P., Coutinho, E., Iyer, K. *Current Topics Med. Chem.* **4**, 75-103 (2004).
3. Fundytus, M.E., et al. *Eur. J. Pharmacol.* **286**, 105-108 (1995).
4. Schiller, P.W., Fundytus, M.E., Merovitz, L., Weltrowska, G., Nguyen, T., Lemieux, C., Chung, N.N., Coderre, T.J. *J. Med. Chem.* **42**, 3520-3526 (1999).
5. Yamamoto, T., Nair, P., Vagner, J., Largent-Milnes, T., Davis, P., Ma, S., Navratilova, E., Moye, S., Tumati, S., Lai, J., Yamamura, H.I., Vanderah, T.W., Porreca, F., Hruby, V.J. *J. Med. Chem.* **51**, 1369-1376 (2008).
6. Yamamoto, T., Nair, P., Davis, P., Ma, S., Navratilova, E., Moye, S., Tumati, S., Lai, J., Vanderah, T.W., Yamamura, H.I., Porreca, F., Hruby, V.J. *J. Med. Chem.* **50**, 2779 -2786 (2007).

## Dynorphin A as a Novel Ligand at Bradykinin Receptors

Brianna Paisley,<sup>1</sup> Josephine Lai,<sup>2</sup> and Victor Hruby<sup>3</sup>

<sup>1</sup>Department of Pharmacology, University of Arizona, Tucson, AZ 85721, U.S.A.; <sup>2</sup>Department of Pharmacology, University of Arizona, Tucson, AZ 85721, U.S.A.; and <sup>3</sup>Department of Chemistry, University of Arizona, Tucson, AZ 85721, U.S.A

### Introduction

Dynorphin A has classically been referred to as an endogenous opioid peptide. However, when a high dose injection of either dynorphin A or des-tyrosyl dynorphin A is administered into the spinal cord of rats, long-lasting allodynia is produced. The allodynia is not reversible by administering naloxone indicating that dynorphin A induced allodynia is non-opioid mediated [1]. In 2006 Lai and her colleagues determined that dynorphin A-induced intracellular  $\text{Ca}^{2+}$  increase and hyperalgesia are blocked by HOE140, a bradykinin 2 antagonist [2]. These findings have led to our hypothesis that dynorphin A promotes pain ultimately via the Bradykinin receptor.

### Results and Discussion

To better understand what amino acids in dynorphin A's structure are essential for its non-opioid effects and binding to the bradykinin receptor several dynorphin A fragments of varying length and end groups were synthesized. The fragments synthesized are shown in Figure 1 below. Each fragment synthesized also had variations of itself synthesized with either acetylation of the N-terminus, amidation of the C-terminus or both. All compounds were synthesized using solid phase peptide synthesis methods and either Rink Amide AM or 2-cholotrityl resins were used to synthesize these compounds.

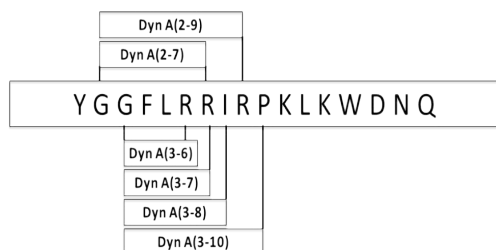


Fig. 1. Dynorphin fragments synthesized.

*In vitro* competition binding assays of these compounds were then done to determine the affinity for bradykinin 2 receptors. For the assays we competed 1.50 nM [<sup>3</sup>H] Kallidin binding against  $10^{-4}$  to  $10^{-13}$  M concentrations of the compounds. 10  $\mu\text{M}$  of the bradykinin 2 selective agonist bradykinin was used to determine non-specific binding. Fresh rat brains from male S-D rats that were stored at  $-80^\circ\text{C}$  were used to prepare the membranes used in these experiments. Once the results from the assays were obtained, a one-site competition

analysis was used and the  $K_i$  value was corrected for using the  $K_D$  value of 2000 nM and the ligand concentration of 1500 nM. The results are shown in Table 1.

Table 1. Dynorphin A fragment competition binding analysis data

Compounds	$K_i$ (nM)	$\text{Log } [\text{IC}_{50} \pm \text{s.e.m}]$	Compounds	$K_i$ (nM)	$\text{Log } [\text{IC}_{50} \pm \text{s.e.m}]$
Ac-DynA(2-7)-H	6700	$-4.93 \pm 0.15$	Ac-DynA(3-10)-H	1900	$-5.49 \pm 0.26$
H-DynA(2-7)-H	1400	$-5.62 \pm 0.21$	Ac-DynA(3-10)-OH	5900	$-4.98 \pm 0.15$
Ac-DynA(2-9)-H	1000	$-5.75 \pm 0.31$	Ac-DynA(3-6)-OH*	1300	$-5.65 \pm 0.14$
H-DynA(2-9)-H	4700	$-5.08 \pm 0.18$	H-DynA(3-7)-OH*	5600	$-5.01 \pm 0.10$

As shown in Table 1, the compounds assayed vary in length from four to eight amino acids in length. Even though the fragments varied in length, which amino acids were at the N- and C-termini and end groups the  $K_i$  and log IC50 values were all fairly similar to each other. This indicates that analogues of shorter fragments, such as Dynorphin A(4-8), should be synthesized and analyzed by competition binding analysis to better understand how their structure affects their affinity for bradykinin receptors. These studies are currently in progress.

## Acknowledgments

We would like to thank the U.S. Public Health Service, National Institute of Drug Abuse for support. Grant numbers DA06284 and DA13449.

## References

1. Vanderah, T.W., Laughlin, T., Lashbrook, J.M., Nichols, M.L., Wilcox, G.L., Ossipov, M.H., Malan T.P., Jr, Porreca, F. *Pain* **68**, 275-281 (1996).
2. Lai, J., Luo, M.C., Chen, Q., Ma, S., Gardell, L.R., Ossipov, M.H., Porreca, F. *Nature Neuroscience* **9**, 1534-1540 (2006).

## Replacement of the Tyr<sup>1</sup> Hydroxyl Group of TIPP Peptides with *N*-(Alkyl)carboxamido Groups Results in Potent and Selective $\delta$ Opioid Agonists or Antagonists

Irena Berezowska, Grazyna Weltrowska, Carole Lemieux, Nga N. Chung,  
 Brian C. Wilkes, and Peter W. Schiller

Laboratory of Chemical Biology and Peptide Research, Clinical Research Institute of Montreal,  
 Montreal, Quebec, Canada H2W 1R7

### Introduction

Substitution of a carboxamido ( $-\text{CONH}_2$ ) group for the Tyr<sup>1</sup> hydroxyl group in opioid peptides, as achieved by replacement of the tyrosine with *p*-carboxamidophenylalanine (Cpa), resulted in compounds that retained high opioid activity in vitro [1,2]. Replacement of the phenolic hydroxyl group in cyclazocine with a  $-\text{CONH}_2$  group had previously been shown to lead to a compound that also retained high  $\mu$  receptor binding affinity [3]. Furthermore, introduction of a (4'-phenyl)-phenethyl substituent at the  $-\text{CONH}_2$  group of 8-carboxamido-cyclazocine resulted in a compound with unaltered  $\mu$  receptor binding affinity [4]. Interestingly, a cyclic enkephalin analog containing 4'-[*N*-((4'-phenyl)-phenethyl)carboxamido]phenylalanine (Bcp; Figure 1) in place of Tyr<sup>1</sup>, H-Bcp-c[D-Cys-Gly-Phe(*p*NO<sub>2</sub>)-D-Cys]NH<sub>2</sub>, also showed high  $\mu$  receptor binding affinity and turned out to be a potent,  $\mu$ -selective opioid agonist [5]. Here we describe analogs of the  $\delta$  opioid antagonists TIPP (H-Tyr-Tic-Phe-Phe-OH) and H-Tyr-Tic-OH, in which the Tyr<sup>1</sup> residue was replaced by derivatives of Cpa containing various substituents at the *p*-carboxamido group, including Bcp, 4'-[*N*-(hexyl)carboxamido]phenylalanine (Hcp), 4'-[*N*-(2-(naphthalen-2-yl)ethyl)carboxamido]phenylalanine (Ncp) and 2',6'-dimethyl-4'-[*N*-((4'-phenyl)-phenethyl)carboxamido]phenylalanine (Dbcp) (Figure 1).

### Results and Discussion

The novel amino acids Bcp, Hcp, Ncp and Dbcp were synthesized by coupling the respective alkylamines to the  $-\text{COOH}$  group of Boc-Phe(4'-COOH)-OMe or Boc-Phe(2',6'-Me<sub>2</sub>,4'-COOH)-OEt, and peptides were prepared by solid-phase synthesis. The in vitro opioid activities of the compounds were determined in  $\mu$ -,  $\delta$ - and  $\kappa$ -opioid receptor binding assays and in the functional guinea pig ileum (GPI) and mouse vas deferens (MVD) assays, as described [2].

The Bcp<sup>1</sup>-tetrapeptide analog H-Bcp-Tic-Phe-Phe-OH showed 2-fold higher  $\delta$  receptor binding affinity ( $K_i^\delta = 0.605$  nM) than the TIPP parent and retained high  $\delta$  receptor binding selectivity (Table 1). Surprisingly, this compound turned out to be a potent full  $\delta$  opioid agonist in the MVD assay. The Hcp<sup>1</sup>- and Ncp<sup>1</sup>-TIPP analogs showed even higher  $\delta$  opioid agonist potency. Most impressive was H-Hcp-Tic-Phe-Phe-OH (HIPP) which displayed subnanomolar  $\delta$  receptor binding affinity, extraordinary  $\delta$  receptor selectivity and subnanomolar  $\delta$  agonist potency. HIPP is a more potent and more selective  $\delta$  agonist than DPDPE (H-Tyr-c[D-Pen-Gly-Phe-D-Pen]OH) and is of interest as a pharmacological tool. [Cpa<sup>1</sup>]TIPP retained  $\delta$  opioid antagonist activity, indicating that the presence of the large alkyl substituents attached to the *p*-CONH<sub>2</sub> group in the Bcp<sup>1</sup>-, Hcp<sup>1</sup>- and Ncp<sup>1</sup>-analogs are responsible for the  $\delta$  agonist behavior of these compounds. Interestingly, the Dbcp<sup>1</sup>-tetrapeptide analog also turned out to be a  $\delta$  opioid antagonist, having somewhat higher  $\delta$  receptor binding affinity than [Cpa<sup>1</sup>]TIPP and somewhat

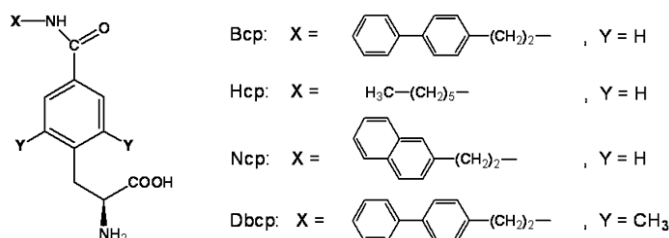


Fig. 1. Structural formulas of Bcp, Hcp, Ncp and Dbcp.

Table 1. In vitro opioid activity profiles of TIPP peptide analogs

Compound	$\delta$ receptor binding		MVD	
	$K_i^\delta$ (nM)	$K_i$ ratio ( $\delta/\mu/\kappa$ )	$IC_{50}$ (nM)	$K_e^\delta$ (nM)
H-Bcp-Tic-Phe-Phe-OH	0.605	1/145/446	3.42	
H-Hcp-Tic-Phe-Phe-OH	0.369	1/1370/25500	0.392	
H-Ncp-Tic-Phe-Phe-OH	1.01	1/247/>10000	0.950	
H-Cpa-Tic-Phe-Phe-OH	0.978	1/2240/>5000		18.3
H-Tyr-Tic-Phe-Phe-OH (TIPP)	1.22	1/1410/>1000		4.80
H-Dbcp-Tic-Phe-Phe-OH	0.783	1/181/762		3.07
H-Cdp-Tic-Phe-Phe-OH	0.532	1/4150/>2000		0.627
H-Dmt-Tic-Phe-Phe-OH	0.248	1/569/>4030		0.196
H-Bcp-Tic-OH	0.646	1/3510/7370		17.8
H-Dbcp-Tic-OH	0.825	1/745/3330		1.76
H-Dmt-Tic-OH	1.84	1/739/>543		6.55
H-Tyr-Tic-OH	242	1/>1000/>1000		263

lower  $\delta$  receptor affinity than the Dmt<sup>1</sup>- and Cdp<sup>1</sup>-tetrapeptide antagonists [Dmt = Tyr(2',6'-Me<sub>2</sub>); Cdp = Phe(4'-CONH<sub>2</sub>,2',6'-Me<sub>2</sub>)]. These results indicate that the biphenylethyl substituent of [Dbcp<sup>1</sup>]TIPP does not significantly contribute to  $\delta$  receptor binding. Using Mosberg's  $\delta$  opioid receptor models [6] and the software program Glide (Schrödinger LLC), the tetrapeptides H-Bcp-Tic-Phe-Phe-OH ( $\delta$  agonist) and H-Dbcp-Tic-Phe-Phe-OH ( $\delta$  antagonist) were docked to the activated and the inactive form of the  $\delta$  receptor, respectively. The obtained results indicated that the two peptides overall had similar modes of binding, except for the large biphenyl group which in the case of the Bcp<sup>1</sup>-agonist was positioned such as to interact with an accessory binding site of the activated receptor distinct from the binding site of the biphenyl group of the Dbcp<sup>1</sup>-antagonist bound to the receptor in the inactive state. The differential positioning of the biphenyl group of the two peptides is due to additional hydrophobic interactions of the 2',6'-dimethyl groups of the Dbcp<sup>1</sup>-antagonist peptide with the receptor.

The dipeptide H-Bcp-Tic-OH is a  $\delta$  opioid antagonist with a low efficacy  $\delta$  partial agonist component. The H-Dbcp-Tic-OH dipeptide showed subnanomolar  $\delta$  receptor binding affinity, very high  $\delta$  receptor binding selectivity and very high  $\delta$  antagonist activity ( $K_e^\delta$  = 1.76 nM). In comparison with H-Tyr-Tic-OH and H-Dmt-Tic-OH, it has 150-fold and 4-fold higher  $\delta$  antagonist activity, respectively, indicating that the biphenylethyl moiety of H-Dbcp-Tic-OH strengthens binding to the  $\delta$  receptor significantly. H-Dbcp-Tic-OH obeys most of Lipinski's and Veber's rules and is of interest as a pharmacological tool and as a potential therapeutic agent. Receptor docking studies performed with H-Bcp-Tic-OH and H-Dbcp-Tic-OH revealed that the biphenyl moieties of these dipeptides assume a completely different orientation as compared to the one in the Dbcp<sup>1</sup>-tetrapeptide and interact with the same receptor region as the phenyl rings of Phe<sup>3</sup> and Phe<sup>4</sup> in the tetrapeptide.

## Acknowledgments

Supported by grants from the NIH (DA-004443) and the CIHR (MOP-89716).

## References

1. Dolle, R.E., et al. *Bioorg. Med. Chem. Lett.* **14**, 3545-3548 (2004).
2. Weltrowska, G., et al. *J. Pept. Res.* **65**, 36-41 (2005).
3. Wentland, M.P., et al. *Bioorg. Med. Chem. Lett.* **11**, 623-626 (2001).
4. Wentland, M.P., et al. *J. Med. Chem.* **49**, 5636-5639 (2006).
5. Weltrowska, G., et al. *Chem. Biol. Drug Des.* **72**, 337-340 (2008).
6. Fowler, C.B., et al. *Biochemistry* **43**, 15796-15810 (2004).

# Role of Alzheimer’s Amyloid-β Peptide as a Putative Transcription Factor

Debomoy K. Lahiri, Bryan Maloney, Jason Bailey, and Yuan-Wen Ge

Dept. of Psychiatry, Inst. of Psychiatric Res., Indiana Univ. School Med., Indianapolis, IN 46202, U.S.A.

## Introduction

The amyloid plaque invariably deposited in Alzheimer’s disease (AD) is mostly composed of a 40-42 amino acid β-amyloid peptide (Aβ) [1]. Our goal is to understand the physiological and pathological function of Aβ, including its interaction with other molecules. While non-pathological function for this peptide is poorly understood, Aβ has been shown to induce an increase in levels of the p53 apoptosis-associated protein (gene name P53). Furthermore, this induction was due to direct action of Aβ upon the P53 promoter, with Aβ binding located to a specific decamer within a known heat shock element (HSE) [2]. We undertook a search for similar sequences in the 5’-flanking sequence of the Aβ precursor protein (APP), apolipoprotein E (APOE), and β-site APP-cleaving enzyme (BACE1) genes, which are intimately involved in pathogenesis of AD [1]. We generated specific oligomers, and investigated interaction with the Aβ1-42 and 1-40 peptides. The sequences of interacting oligomers were used to generate a consensus sequence “GGATKGGGGT” and a similarity matrix. A single-base mutation in one of the Aβ-binding APP oligomers markedly reduced binding with the Aβ1-42 and 1-40 peptides. We investigated the regions of the Aβ peptide that would bind the DNA decamer and determined that maximum binding was obtained with the cytotoxic Aβ25-35 peptide.

## Results and Discussion

The APOE [3], APP [4], and BACE1 [5] 5’-flanking regions were compared to the 5’-GGATTGGGGT-3’ Aβ-interacting decamer from the P53 HSE site. Sites with at least 80% homology were accepted as potential Aβ-interacting sequences. Within the APOE 5’-flanking region, 11 decamers were located. The APP sequence had 7 such decamers. The BACE1 sequence had 4. To determine specificity of an Aβ-binding DNA motif, Aβ1-42 peptides were incubated with radiolabeled double-stranded oligomers corresponding to putative binding sites in the APOE (+899, +171, +284, +660/+665), APP (-3833, -3364, -2871, -1682), BACE1 (-1939, -1766, -119, +36) and P53 (+104) 5’-flanking regions. Mixtures were run on 5% native polyacrylamide-TGE gel, which was subjected to radiography. Interaction was visualized as a slow migrating radioactive band on the gel. Of the 13 oligomers tested, six interacted with Aβ1-42, specifically APOE +171 and +660/+665; APP -3833, -2871, and -1862; BACE1 -119; and P53 +104. To test specificity of this binding with these particular oligomers, each binding reaction was repeated in the presence of high molar excess of unlabeled homologous oligomer (Figure 1). In all cases, self-competition visibly reduced Aβ-DNA interaction.

Further specificity was shown by repeating the assay with all APP, APOE, and BACE1 derived oligomers plus additional oligomers from the APP 5’-flanking region. The Aβ1-40 peptide was screened with these oligomers, as well as reacting “reverse” (Aβ42-1, 40-1) peptides against the APP-3833 oligomer. Interactions and their lack were similar between Aβ1-42 and Aβ1-40. The Aβ42-1 oligomer had no apparent DNA-protein interaction, while the 40-1 oligomer interacted with the APP-3833 DNA oligomer. The -3833 APP oligomer is of particular interest as its putative Aβ-binding site includes an APP promoter single nucleotide polymorphism (SNP) at -3829 associated with a familial AD (FAD) [6]. This G→A substitution reduced Aβ binding with both the 1-42 and 1-40 peptides.

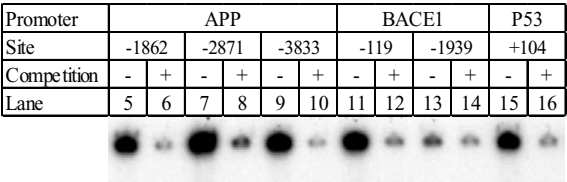


Fig. 1. Competition gel shift assay. Each of 6 different double-stranded oligomers from APP, BACE1 and P53 promoters was incubated with Aβ1-42 peptide in the absence or presence of unlabeled oligomer (140x molar excess). DNA-peptide complexes appeared as dark signal near the top of the gel and were reduced by competition.

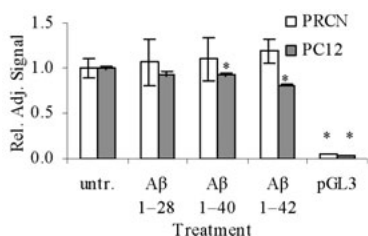


Fig. 2. APP promoter activity in transfected PC12 and PRCN cell cultures, treated with A $\beta$  peptides. “\*” indicates significant difference from untreated cultures at  $p < 0.05$ .

specifically 1-42, 1-40, 1-28, 20-29, 25-35, 29-40, 31-35, 41-1, 40-1, and 35-25, were reacted with the oligomers for the A $\beta$ -binding sites at APOE +171, APOE +660, and APP-3833. Of the peptides tests, the 1-28, 20-29, 31-35, 35-25, and 42-1 peptides had no apparent DNA-binding capacity. Of the remaining peptides, extent of binding capacity was, from lowest to highest, 40-1 < 1-42 < 1-40 < 29-40 < 25-35.

To determine if A $\beta$ -DNA interaction occurred in a concentration-dependent manner typical of transcription factors, the A $\beta$ 1-42, 1-40, 42-1, 1-28, and 25-35 peptides were reacted with the APP-3833 oligomer pair at 5 different amounts. The 1-40 and 1-42 peptides both showed concentration dependent increases in apparent interaction as measured by the gel shift assay. In addition, the 1-40 peptide showed a greater interaction at any given amount of peptide when compared to the 1-42 peptide. These traits did not appear for the 25-35 peptide.

Treatment of primary neuronal cultures transiently transfected with a 1.2kb fragment of the APP promoter fused to luciferase showed that A $\beta$ 1-28 had no significant effect on APP promoter activity, while 1-40, and 1-42 were capable of downregulating the apparent activity of the APP promoter in rat neuronal PC12 cells but not in primary rat cortical neuron (PRCN) cultures (Figure 2).

A $\beta$  modulates glutamatergic transmission in the rat basal forebrain [7]. It has also been noted that A $\beta$  is likely to contain a helix-loop-helix structure common to certain transcription factors [8]. A $\beta$  has been shown to locate intracellularly in response to conditions such as oxidative stress [2]. These aspects of A $\beta$  structure and location suggest that some of A $\beta$ 's pathological activity may be related to direct peptide-DNA interaction with genes such as those that determine apoptosis. Ohyagi et al determined that A $\beta$  regulated p53 protein levels through direct interaction with a decamer on the P53 gene promoter/5'-UTR sequence [2].

These recent data from our laboratory and other groups lead us to propose that the A $\beta$  peptide functions as a transcription factor that may regulate its own production through negative feedback on its precursor protein and the BACE1 enzyme. Thus, the possibility of intracellular amyloid  $\beta$ -protein as a therapeutic target for treating AD warrants further investigation [9].

## Acknowledgments

This work was supported by grants from the Alzheimer's Association and NIH AG18379 and AG18884.

## References

1. Lahiri, D.K., et al. *Curr. Drug Targets* **4**, 97-112 (2003).
2. Ohyagi, Y., et al. *FASEB J.* **19**, 255-257 (2005).
3. Du, Y., et al. *Brain Research Molecular Brain Research* **136**, 177-188 (2005).
4. Ge, Y.-W., et al. *J. Neurochem.* **90**, 1432-44 (2004).
5. Sambamurti, K., et al. *FASEB J.* **18**, 1034-1036 (2004).
6. Lahiri, D.K., et al. *Neurobiol. Aging* **26**, 1329-1341 (2005).
7. Chin, J.H., Ma, L., MacTavish, D., Jhamandas, J.H. *J. Neurosci.* **27**, 9262-9269 (2007).
8. Durell, S.R., et al. *Biophys. J.* **67**, 2137-2145 (1994).
9. Ohyagi, Y. *Curr. Alzheimer Res.* **5**, 555-61 (2008).

## Investigation of A $\beta$ 42 C-Terminal Fragments as Inhibitors of A $\beta$ 42 Assembly and Neurotoxicity

Huiyuan Li,<sup>1</sup> Bernhard H. Monien,<sup>1,4</sup> Aleksey Lomakin,<sup>2</sup>  
 Erica A. Fradinger,<sup>1,5</sup> Sean M. Spring,<sup>1</sup> Brigita Urbanc,<sup>3</sup>  
 George B. Benedek,<sup>2</sup> and Gal Bitan<sup>1</sup>

<sup>1</sup>Department of Neurology, David Geffen School of Medicine, University of California, Los Angeles, CA 90095, U.S.A.; <sup>2</sup>Department of Physics, Massachusetts Institute of Technology, Cambridge, MA 02139, U.S.A.; <sup>3</sup>Physics Department, Drexel University, Philadelphia, PA 19104, U.S.A.; <sup>4</sup>Current address: Deutsches Institut für Ernährungsforschung Potsdam-Rehbrücke, 14558 Nuthetal, Germany; <sup>5</sup>Current address: Department of Biology, Whittier College, Whittier, CA 90608, U.S.A.

### Introduction

Alzheimer's disease (AD) is characterized by aging-associated deterioration of learning and memory leading to dementia. A key event in AD etiology is the assembly of amyloid  $\beta$ -protein (A $\beta$ ) into neurotoxic oligomers [1]. Two predominant forms of A $\beta$  are produced *in vivo*, comprising 40 (A $\beta$ 40) or 42 (A $\beta$ 42) amino acid residues. A $\beta$ 42 has been shown to be more neurotoxic than A $\beta$ 40 [2]. Disruption of A $\beta$  oligomerization is a promising approach for developing therapeutics for AD. We have prepared a series of A $\beta$ 42 C-terminal fragments (CTFs), evaluated their bioactivity, and identified lead inhibitors of A $\beta$ 42 assembly and neurotoxicity [3]. Of 12 CTFs tested (Table 1), A $\beta$ (31–42) and A $\beta$ (39–42) were found to be the most potent inhibitors of A $\beta$ 42-induced toxicity. To decipher the mechanisms by which CTFs

affect A $\beta$  assembly and neurotoxicity, we investigated the solubility, self-aggregation, secondary structure, morphology, and interaction with full-length A $\beta$ 42 of the CTFs and of 4 control, A $\beta$ -derived fragments, including Ac- A $\beta$ (16–22)-NH<sub>2</sub>, A $\beta$ (21–30), A $\beta$ (30–40), and A $\beta$ (34–40). The first two peptides are derived from A $\beta$  regions that are involved in A $\beta$  aggregation and nucleation, which enable to test if the inhibition of A $\beta$ 42-induced toxicity required CTF derived from A $\beta$ 42 itself or whether sequences derived from other regions also had inhibitory activity. The latter two peptides are CTFs derived from A $\beta$ 40. These fragments test the importance of the C-terminal dipeptide, I41–A42, in A $\beta$ 42 for the inhibitory activity.

Table 1. Sequence of A $\beta$ 42 CTFs and control A $\beta$ -derived fragments

Peptide	Sequence
A $\beta$ (39–42)	VVIA
A $\beta$ (38–42)	GVVIA
A $\beta$ (37–42)	GGVVIA
A $\beta$ (36–42)	VGGVVIA
A $\beta$ (35–42)	MVGGVVIA
A $\beta$ (34–42)	LMVGGVVIA
A $\beta$ (33–42)	GLMVGGVVIA
A $\beta$ (32–42)	IGLMVGGVVIA
A $\beta$ (31–42)	IIGLMVGGVVIA
A $\beta$ (30–42)	AIIGLMVGGVVIA
A $\beta$ (29–42)	GAIIIGLMVGGVVIA
A $\beta$ (28–42)	KGAIIIGLMVGGVVIA
A $\beta$ (30–40)	AIIGLMVGGVV
A $\beta$ (34–40)	LMVGGVV
Ac- A $\beta$ (16–22)-NH <sub>2</sub>	Ac-KLVFFAE-NH <sub>2</sub>
A $\beta$ (21–30)	AEDVGSNKGA

### Results and Discussion

#### *Biophysical properties of CTFs and control peptides*

(1) *Solubility.* CTFs up to 10-amino acids long were found to be soluble at concentrations between 100–200  $\mu$ M. Longer peptides were soluble at concentrations between 8–85  $\mu$ M. The longest CTF, A $\beta$ (28–42), was found to have the lowest solubility ( $\sim$ 1  $\mu$ M) of all the CTFs. All four control peptides were soluble between 120–200  $\mu$ M. (2) *Self aggregation.* We used dynamic light scattering (DLS), a method commonly used for studying protein aggregation non-invasively, to study particle size. Consistent with the solubility data described above, A $\beta$ (35–42) and shorter CTFs at 100–200  $\mu$ M showed no change in scattering intensity over 96 h, suggesting no aggregation within the experimental timeframe. A $\beta$ (33–42), A $\beta$ (31–42) and



longer peptides produced strong scattering signals, indicating that these peptides aggregated over time. The aggregation rates roughly correlated with the solubility, i.e., fast aggregation correlated with low solubility and *vice versa*. A $\beta$ (30–40) did not show aggregation in the same timeframe, suggesting that the C-terminal dipeptide, I41–A42, is important for CTFs aggregation. (3) *Secondary structure*. We used circular dichroism (CD) spectroscopy as a complimentary method to investigate the correlation between aggregation and  $\beta$ -sheet formation. A $\beta$ (35–42) and shorter CTFs did not show  $\beta$ -sheet formation over 96 h, whereas longer peptides formed  $\beta$ -sheet with similar kinetics to the aggregation observed by DLS. (4) *Morphology*. Samples of CTF and control peptides were examined by electron microscopy (EM) directly after dissolution and following incubation for 7 days. Electron micrographs of A $\beta$ (35–42) and shorter CTFs did not show fibril formation within 7 days, whereas the longer CTFs, and A $\beta$ (30–40) and Ac- A $\beta$ (16–22)-NH<sub>2</sub>, formed fibrils. Substantial variability was observed in the morphology of fibrils formed by these peptides.

### **CTF interaction with A $\beta$ 42**

To study the effect of CTFs on early-forming A $\beta$  oligomers, LMW A $\beta$ 42 [4] was mixed with CTFs, cross-linked immediately, and analyzed by SDS-PAGE. CTF-mediated inhibition of A $\beta$ 42 oligomerization in PICUP [3] experiments correlated with the tendency of CTFs to form  $\beta$ -sheet and self-aggregate. A $\beta$ (36–42) and shorter peptides did not inhibit A $\beta$ 42 hexamer formation, whereas A $\beta$ (35–42) and longer CTFs showed inhibitory activity.

To study the effect of CTFs on A $\beta$  assembly, the particle size in solutions of A $\beta$ 42, DLS was measured in the presence or absence of CTFs. The data suggest that three strong inhibitors of A $\beta$ 42-induced toxicity, A $\beta$ (39–42), A $\beta$ (31–42) and A $\beta$ (30–40), interact with A $\beta$ 42 in a manner that perturbs the structure of relatively small oligomers (*P1*) and stabilizes a non-toxic oligomeric structure. At the same time these peptides interfere with formation and/or growth of larger oligomeric structures (*P2*), which may contribute to A $\beta$ 42 toxicity. In contrast, inhibition of fibril growth in the presence of A $\beta$ (29–42), A $\beta$ (30–42), or A $\beta$ (31–42) correlates roughly with inhibition of oligomerization but not with inhibition of toxicity.

The results demonstrate that up to a certain point, peptide length determines the properties of A $\beta$ 42 CTFs but beyond that point, the particular sequence is the predominant factor in determining the biophysical and inhibitory properties of the CTFs. Peptides up to 7–8 residues long have relatively high solubility and low propensity of self-aggregation and  $\beta$ -sheet formation. The two C-terminal amino acids I41–A42 are important for stabilizing  $\beta$ -sheet structure. Inhibition of A $\beta$ 42 oligomerization and fibril formation by CTFs correlates with low solubility, self-aggregation, and high propensity to form intramolecular  $\beta$ -hairpin [5]. In contrast, inhibition of A $\beta$ 42-induced neurotoxicity correlates with formation of a coil-turn structure [5], diminution and/or stabilization of *P1* particles, and concomitant inhibition of *P2* particle growth. Stabilization of particular oligomer populations as a mechanism for inhibition of A $\beta$ -induced toxicity is a common feature of A $\beta$ 42 CTFs and small molecule inhibitors. We propose that stabilization of non-toxic oligomers is a promising strategy for design of future inhibitors.

### **Acknowledgments**

The project is supported by grant AG027818 from NIH/NIA, grant 2005/2E from the Larry L. Hillblom Foundation, and by a generous gift from the Turken family.

### **References**

1. Monien, B.H., Apostolova, L.G., Bitan, G. *Expert Rev. Neurother.* **6**, 1293-1306 (2006).
2. Dahlgren, K.N., Manelli, A.M., Stine, W.B., Jr., Baker, L.K., Krafft, G.A., LaDu, M.J. *J. Biol. Chem.* **277**, 32046-32053 (2002).
3. Fradinger, E.A., Monien, B.H., Urbanc, B., Lomakin, A., Tan, M., Li, H., Spring, S.M., Condrón, M.M., Cruz, L., Xie, C.W., Benedek, G.B., Bitan, G. *Proc. Natl. Acad. Sci. U.S.A.* **105**, 14175-14180 (2008).
4. Bitan, G., Teplow, D.B. *Methods Mol. Biol.* **299**, 3-9 (2005).
5. Wu, C., Murray, M.M., Bernstein, S.L., Condrón, M.M., Bitan, G., Shea, J.E., Bowers, M.T. *J. Mol. Biol.* **387**, 492-501 (2009).

## SAR and Mechanistic Studies of Tetrapeptide Inhibitors of A $\beta$ 42-Induced Neurotoxicity

Huiyuan Li and Gal Bitan

Department of Neurology, David Geffen School of Medicine, University of California,  
Los Angeles, CA 90095, U.S.A.

### Introduction

Neurotoxic oligomers of amyloid  $\beta$ -protein (A $\beta$ ) are believed to be the main cause of Alzheimer's disease (AD) [1]. Recently, we identified the C-terminal tetrapeptide, A $\beta$ (39–42), as an inhibitor of A $\beta$ 42-induced neurotoxicity [2]. Here, we tested the mode of action of this peptide, investigated its binding sites on A $\beta$ 42, and performed structure–activity relationship (SAR) studies to test key structural features, including chirality, side chain identity, and functional groups at the N- and C-termini.

### Results and Discussion

A $\beta$ (39–42) was found to inhibit A $\beta$ 42-induced neurotoxicity in differentiated rat pheochromocytoma (PC-12) cells using the (3-(4,5-dimethylthiazol-2-yl)-2,5-diphenyltetrazolium bromide (MTT) ( $IC_{50}=16\pm5\ \mu\text{M}$ ) and lactate dehydrogenase (LDH) release ( $IC_{50}=47\pm14\ \mu\text{M}$ ) assays [2]. In addition, A $\beta$ (39–42) rescued mouse primary hippocampal neurons from A $\beta$ 42-induced inhibition of miniature excitatory postsynaptic current (mEPSC) frequency [2]. Taken together, the data suggest that A $\beta$ (39–42) inhibits A $\beta$ 42-induced toxicity in both of the early stage of synaptic activity and later stage of metabolism and cell death.

To test if A $\beta$ (39–42) inhibits A $\beta$ 42-induced neurotoxicity or acts as a general neuroprotective agent, we used the MTT and LDH assays to compare its effect on neurotoxicity induced by A $\beta$ 42 or staurosporine, a non-selective protein kinase inhibitor that induces apoptosis in multiple cell types [3]. The results showed that A $\beta$ (39–42) selectively inhibited toxicity induced by A $\beta$ 42 but not by staurosporine.

To determine the binding site of A $\beta$ (39–42), on A $\beta$ 42, we used A $\beta$ 42 analogues in which Tyr was introduced at positions 1, 20, 30, or 42, and the native Tyr10 was substituted by Phe [4,5]. We monitored changes in intrinsic fluorescence of Tyr in WT A $\beta$ 42 and each of these analogues as a function of A $\beta$ (39–42) binding [4]. When A $\beta$ (39–42) was added to these peptides, changes in Tyr fluorescence were observed with the analogues in which the Tyr residue was in positions 1 or 30, but not in positions 10, 20, or 42 (Figure 1). The results suggest that A $\beta$ (39–42) binds predominantly at two distinct sites on A $\beta$ 42 - one at the N-terminus and the other near position 30.

Systematic structural modifications were performed to study structure–activity relationships in A $\beta$ (39–42). To identify the side-chain function, chirality, and terminal group function, we substituted the Val and Ile residues in A $\beta$ (39–42) by Ala, changed the parent peptide to the inverse or retro sequences, and blocked the N- or C-termini by acetylation and amidation, respectively. We evaluated the inhibitory activity of each analogue on A $\beta$ 42-induced neurotoxicity in differentiated PC-12 cells using the MTT assay.

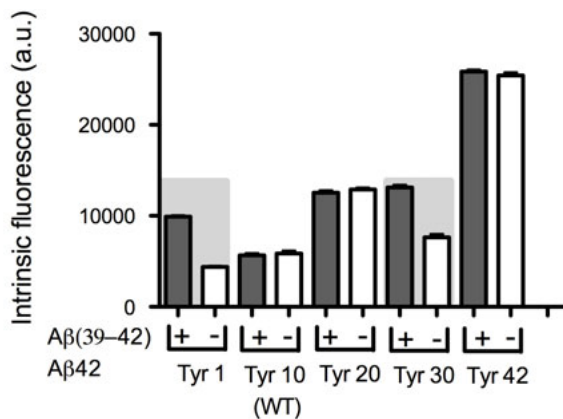


Fig. 1. Intrinsic fluorescence of A $\beta$ 42 derivatives in the absence (white) or presence (grey) of A $\beta$ (39–42).

The SAR data are presented in Figure 2. We found that:

1. Ala substitutions at positions 39 and 40 (full length A $\beta$  numbering) were tolerated, but not at position 41.

2. Inversion of configuration to the inversed (all D)-peptide leads to loss of activity, suggesting that chiral requirements exist for inhibitory activity.

3. A free -NH<sub>2</sub> group at the N-terminus is necessary for inhibitory activity. In contrast, the C-terminal carboxyl can be replaced by a carboxamide, providing protection from carboxypeptidases.

The results demonstrate that despite the small size of A $\beta$ (39–42) and the hydrophobic aliphatic nature of all four side chains, the interaction of A $\beta$ (39–42) and its derivatives with A $\beta$ 2 is based on specific interactions. The binding of A $\beta$ (39–42) at the N-terminus and position 30 of A $\beta$ 2 may relate to its inhibitory activity. Comparing the binding modes of active and inactive peptides will help deciphering the mechanism of action of A $\beta$ (39–42) and key regions of A $\beta$ 2 related to its toxicity. For example, the requirement for a free amino group for activity suggests that binding of A $\beta$ (39–42) at the N-terminus likely is mediated by interaction with negatively charged Asp or Glu side chains. The binding sites of A $\beta$ (39–42) analogues with acetylated N-terminus or amidated C-terminus currently are investigated. The data will serve as basis for design and testing of new peptidomimetics derivatives with improved activity and metabolic stability.

## Acknowledgments

The project is supported by grant AG027818 from NIH/NIA.

## References

1. Monien, B.H., Apostolova, L.G., Bitan, G. *Expert Rev. Neurother.* **6**, 1293-1306 (2006).
2. Fradinger, E.A., Monien, B.H., Urbanc, B., Lomakin, A., Tan, M., Li, H., Spring, S.M., Condrón, M.M., Cruz, L., Xie, C.W., Benedek, G.B., Bitan, G. *Proc. Natl. Acad. Sci. U.S.A.* **105**, 14175-14180 (2008).
3. Bertrand, R., Solary, E., O'Connor, P., Kohn, K.W., Pommier, Y. *Exp. Cell Res.* **211**, 314-321 (1994).
4. Maji, S.K., Amsden, J.J., Rothschild, K.J., Condrón, M.M., Teplow, D.B. *Biochemistry* **44**, 13365-13376 (2005).
5. Maji, S.K., Loo, R.R., Inayathullah, M., Spring, S.M., Vollers, S.S., Condrón, M.M., Bitan, G., Loo, J.A., Teplow, D.B. *J. Biol. Chem.*, *In press* (2009).

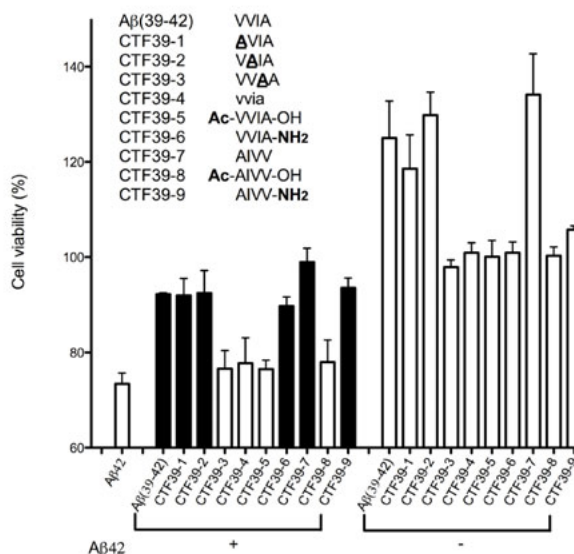


Fig. 2. A $\beta$ (39–42) derivatives were tested for inhibitory activity using the MTT assay in differentiated PC-12 cells. Ten-fold excess of each derivative was used with A $\beta$ 42 (10  $\mu$ M).

## Nuclear Localization of the Amyloid $\beta$ -peptide During Oxidative Stress in Neuronal Cells

Jason A. Bailey and Debomoy K. Lahiri

Department of Psychiatry, Indiana University School of Medicine, Indianapolis, IN 46202, U.S.A.

### Introduction

Alzheimer's disease (AD) is characterized principally by neuritic plaque deposition and hyperphosphorylated tau deposits in the brain. These pathological changes are thought to be the proximal cause of neuronal loss and, subsequently, memory dysfunction. The neuritic plaque is mostly composed of a 40–42 amino acid  $\beta$ -amyloid peptide ( $A\beta$ ), which is proteolytically cleaved from the much larger amyloid precursor protein (APP). The amyloid cascade theory proposes that overproduction or impaired clearance of  $A\beta$  is the root cause of AD, leading to a variety of pathogenic changes, including plaque deposition and microtubule associated protein tau hyperphosphorylation [1,2]. While  $A\beta$  is known to exhibit a variety of toxic effects, little is known about what, if any, physiological role it may play in the brain. Our goal is to understand the physiological and pathological functions of  $A\beta$  (both the short  $A\beta_{1-40}$  and long form  $A\beta_{1-42}$ ), including its sites of action and localization. Current research suggests that intracellular  $A\beta$  is more important than extracellular  $A\beta$ , since intraneuronal  $A\beta$  accumulation commonly precedes extracellular  $A\beta$  deposition in several transgenic mouse models of AD [3,4]. Furthermore, it has been demonstrated that over-expressed  $A\beta$  in the cytoplasm can translocate to the nucleus under conditions of oxidative DNA damage and can alter p53 levels [5]. We have tested the hypothesis that  $A\beta$  is taken up by neurons and localized to the nucleus and may participate in regulating expression of certain genes and other physiological functions, such as stress response. In this context, we have recently demonstrated sequence-specific DNA binding of  $A\beta$  peptides within the upstream regulatory regions of several genes involved in AD (Society for Neuroscience Meeting, 2008), suggesting a regulatory role for  $A\beta$  in gene transcription. Herein we present data that suggest cellular uptake and nuclear localization of  $A\beta$  during oxidative stress in neuronal cells.

### Results and Discussion

To investigate the possible uptake and nuclear localization of  $A\beta$ , human neuroblastoma (SK-N-SH) cells neuronally differentiated with retinoic acid were used. Cells were exposed to fluorescein isothiocyanate (FITC) tagged  $A\beta_{1-40}$  or  $A\beta_{1-42}$  in combination with Hoechst 33342 to label all nuclei, and ethidium homodimer (EthD-1) to label dead nuclei. Colocalization of FITC (green fluorescence) with Hoechst dye (blue fluorescence) was considered an  $A\beta$ -positive nucleus. Nuclei also stained with EthD-1 (red fluorescence) were considered dead and excluded, though nearly all dead nuclei were  $A\beta$ -positive.

Under the oxidative stress condition (with 50  $\mu$ M  $H_2O_2$  treatment), significantly more retinoic acid differentiated SK-N-SH cells transported detectable quantities of FITC- $A\beta_{1-40}$  to the nucleus, however there was much less  $A\beta$  uptake in the non- $H_2O_2$  treated or  $A\beta_{1-42}$  conditions. This suggests that  $A\beta$  uptake and nuclear localization is part of a stress response mechanism. This may be a more general response to cellular stress and not specific to oxidative conditions, as heat shock also produced  $A\beta$  translocation from the cytosol to the nucleus [5]. Furthermore, our results also suggest that the biologically active peptide is  $A\beta_{1-40}$  as uptake of  $A\beta_{1-42}$  was not stimulated by  $H_2O_2$  treatment (Figure 1).

To determine the effect of  $A\beta$  concentration on internalization, 1  $\mu$ M FITC- $A\beta_{1-40}$  was used for nuclear labeling, to which 5  $\mu$ M

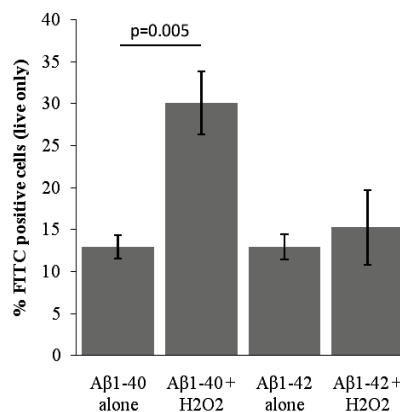


Fig. 1.  $H_2O_2$  treatment increased nuclear localization of  $A\beta_{1-40}$  but not  $A\beta_{1-42}$  in neuronally differentiated SK-N-SH cells.

unlabeled A $\beta$ <sub>1-40</sub> was added. It was expected that the unlabeled A $\beta$  would reduce nuclear labeling in the presence of H<sub>2</sub>O<sub>2</sub>, however it was observed that this treatment dramatically increased cell death as determined by nuclear counting. This effect was not observed when 5 $\mu$ M unlabeled A $\beta$ <sub>40-1</sub> (reverse sequence) peptide was used in combination with 1 $\mu$ M FITC-A $\beta$ <sub>1-40</sub>, indicating that this synergistic effect of A $\beta$ - and H<sub>2</sub>O<sub>2</sub>-mediated toxicity is not attributable to nonspecific peptide interactions in this cell culture system. We suspect this is the result of aggregation of the A $\beta$  peptides, which are known to bind to a number of cellular targets in their oligomeric forms. This observation of altered binding patterns could have important implications for the role of A $\beta$  in normal neuronal physiology and with respect to the pathogenesis of AD.

To test the functional significance of A $\beta$  binding to DNA, a 1.2kb fragment of the APP gene promoter region which is known to contain at least one A $\beta$  binding sequence was cloned into a reporter plasmid upstream of a firefly luciferase gene. This plasmid DNA was then incubated with A $\beta$ <sub>1-40</sub> under conditions found previously to induce specific A $\beta$ -DNA binding [7]. The A $\beta$ -DNA complexes were then transfected into PC12 cells along with a *renilla*

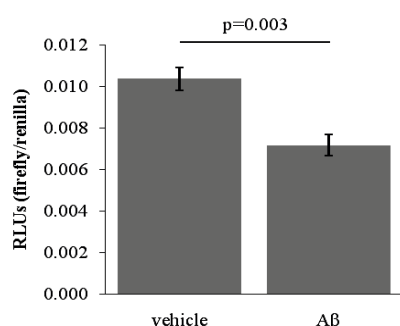


Fig. 2. A $\beta$  binding reduced APP gene promoter activity in PC12 cells.

luciferase control plasmid. A $\beta$  was observed to have an inhibitory effect on the APP gene promoter (Figure 2). This suggests that A $\beta$  may be involved in a negative feedback regulation mechanism that inhibits transcription of its own precursor, the APP gene.

Taken together, these findings suggest a novel physiological role for A $\beta$  and a mechanism for AD pathogenesis. Deposition of insoluble A $\beta$  aggregates is an invariable component of AD pathology, and our data using high A $\beta$  concentrations hint that aggregated A $\beta$  does not enter the nucleus, but rather binds to the cell elsewhere. If this is the case, high A $\beta$  levels leading to A $\beta$  aggregation could potentially exacerbate APP (and thereby A $\beta$ ) overproduction by removing the

inhibitory influence A $\beta$  exerts on the regulatory region of the APP gene. A $\beta$  is also known to bind metal ions and catalyze reactive oxygen species production [6], which leads to the hypothesis that under normal physiological conditions, A $\beta$  is taken up by neurons and localized to the nucleus as part of a stress response mechanism that results in reduced APP production. However, in AD, overproduction of A $\beta$  leads to aggregation, which prevents its participation in this stress response and allows continued overproduction of APP, which may then be processed to form even more A $\beta$ , continuing this cycle. Furthermore, as A $\beta$  is overproduced and transitions into its pathological aggregated state, it may produce oxidative damage or other toxic effects. Taken together, these results reinforce the idea that intracellular A $\beta$  could potentially be a novel therapeutic target for treating AD [3], and nuclear localization under pathological conditions and regulatory effects mediated by A $\beta$  need further attention.

## Acknowledgments

Supported by grants from the NIH and Alzheimer's Association Zenith Award to DKL.

## References

1. Lahiri, D.K. *Curr. Drug Targets* **4**, 97-112 (2003).
2. Aisen, P.S. *CNS Drugs* **19**, 989-996 (2005).
3. Ohnogi, Y. *Curr Alzheimer Res.* **5**, 555-561 (2008).
4. Oddo, S., et al. *Am. J. Pathol.* **168**, 184-194 (2006).
5. Ohnogi, Y., et al. *FASEB J.* **19**, 255-257 (2005).
6. Kontush, A. *Free Radic. Biol. Med.* **31**, 1120-1131 (2001).
7. Lahiri, D.K., Ge, Y.W., Maloney, B. *FASEB J.* **19**, 653-655 (2005).

## Total Chemical Synthesis of Islet Amyloid Polypeptide and its Precursors for Membrane Interaction Studies

Pieter Van de Vijver,<sup>1</sup> Lucie Khemtémourian,<sup>2</sup> Dennis Suylen,<sup>1</sup>  
 Liesbeth Scheer,<sup>1</sup> Gemma Lahoz Casarramona,<sup>3</sup> Hans J.D. Meeldijk,<sup>2</sup>  
 Ben de Kruijff,<sup>2</sup> J. Antoinette Killian,<sup>2</sup> Jo W.M. Höppener,<sup>3</sup>  
 and Tilman M. Hackeng<sup>1</sup>

<sup>1</sup>Cardiovascular Research Institute Maastricht (CARIM), Maastricht University, Maastricht, The Netherlands; <sup>2</sup>Research Group Biochemistry of Membranes, Bijvoet Institute, Institute of Biomembranes and Department of Cellular Architecture and Dynamics, Utrecht University, Utrecht, The Netherlands; <sup>3</sup>Department of Metabolic and Endocrine Diseases, University Medical Center Utrecht, and Netherlands Metabolomics Centre, location Utrecht, The Netherlands

### Introduction

The human islet amyloid polypeptide, also known as hIAPP or amylin, is a 37-residue peptide that is the major component of the amyloid deposits frequently found in patients suffering from diabetes mellitus type 2 [1].

Although it is not yet clear whether these amyloid deposits are a cause, consequence or side effect of the disease, it is hypothesized that the interaction between hIAPP and cellular membranes is a cause of IAPP cytotoxicity, leading to  $\beta$ -cell death [2].

To provide further insights in the interaction between cell membranes and IAPP, we chemically synthesized human (h) and murine (m) IAPP precursors (ProhIAPP, ProhIAPP<sub>1-48</sub>, PromIAPP and PromIAPP<sub>1-51</sub>) as well as mature IAPP (m/h) [3]. mIAPP differs at only 6 residues from hIAPP but is known not to aggregate into amyloid deposits. In addition, we also prepared fluorescently labeled derivatives of mature IAPP (m/h) (Figure 1).

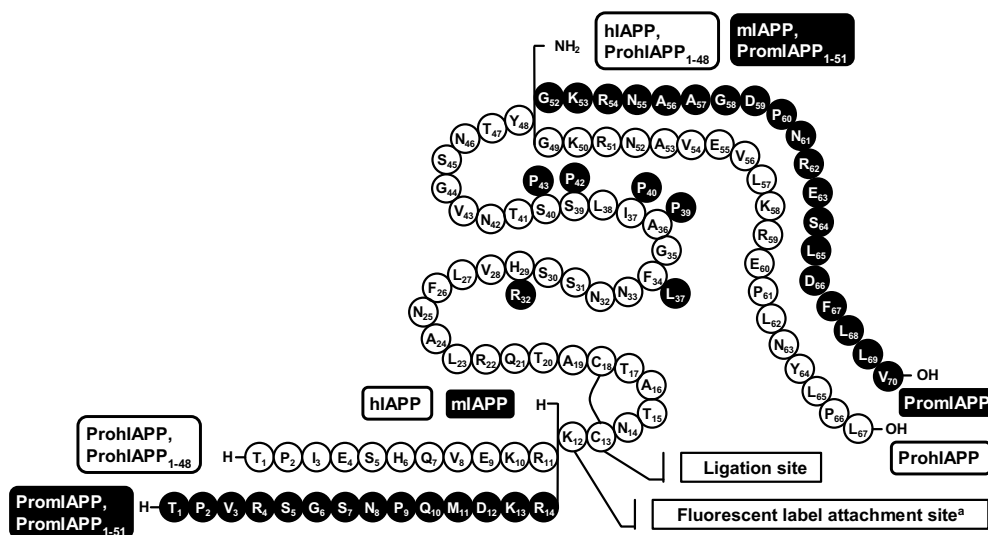


Fig. 1. Primary structures of murine/human IAPP and their precursors. Amino acids of the human proteins are shown in white, those of mouse proteins are shown in black. For the central part, only the amino acids at which the mouse proteins differ from their human counterparts are shown. <sup>a</sup>The fluorescent label used was 6-carboxytetramethylrhodamine (TMR).

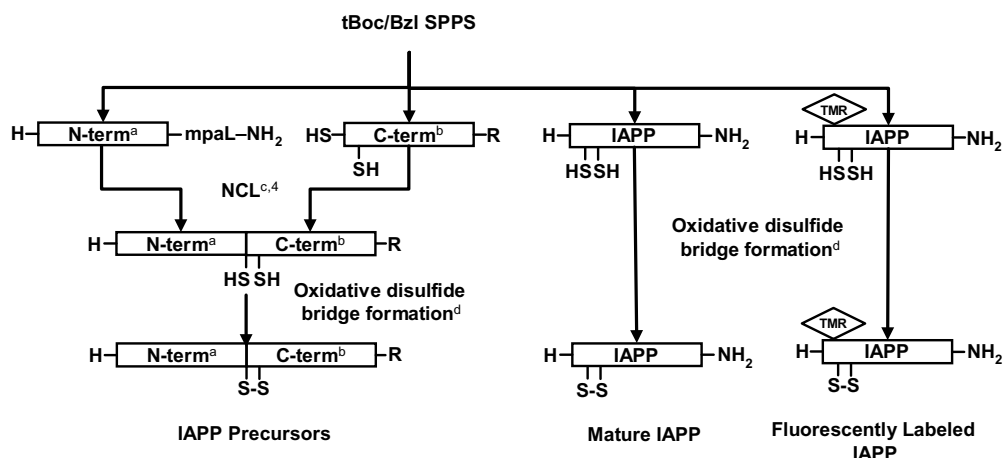
## Results and Discussion

Both murine and human mature IAPP were synthesized by standard Boc-SPPS, followed by disulfide bridge formation through air oxidation (Scheme 1). The latter procedure was carried out in 6 M guanidinium hydrochloride, to prevent peptide aggregation. Single disulfide formation was confirmed by HPLC and mass spectrometry. After each step, the peptides were purified using semi-preparative RP-HPLC (Vydac C18 column, 0.1% TFA in CH<sub>3</sub>CN/H<sub>2</sub>O gradient) and lyophilized.

The TMR-labeled mature IAPP derivatives were prepared by introducing the single lysine as its *N*<sub>ε</sub>-Fmoc derivative. Following Fmoc deprotection using piperidine/DMF, the peptides were reacted on-resin with 6-carboxytetramethylrhodamine *N*-hydroxysuccinimide ester and further processed as shown for native IAPP.

All IAPP precursors were prepared via a native chemical ligation strategy, using K<sub>12</sub>/C<sub>13</sub> (human) or K<sub>15</sub>/C<sub>16</sub> (mouse) as ligation sites [4]. Disulfide bridge formation and purification procedures were similar to those used for IAPP peptides.

The IAPP, ProhIAPP and ProhIAPP<sub>1-48</sub> peptides were used for studying the influence of IAPP precursors on IAPP fibril formation and IAPP-related membrane damage. A report on this work was submitted for publication [5]. Murine IAPP and its precursors, as well as the TMR-labeled IAPP (m/h) will be used for future biophysical studies.



*Scheme 1. Synthetic Strategies. a) N-term* = T<sub>1</sub>...K<sub>12</sub>-mpa-L-NH<sub>2</sub> (ProhIAPP<sub>1-48</sub>, ProhIAPP) or T<sub>1</sub>...K<sub>15</sub>-mpa-L-NH<sub>2</sub> (PromIAPP<sub>1-51</sub>, PromIAPP). *b) C-term* = C<sub>13</sub>...Y<sub>48</sub>-NH<sub>2</sub> (ProhIAPP<sub>1-48</sub>), C<sub>13</sub>...L<sub>67</sub>-OH (ProhIAPP), C<sub>16</sub>...Y<sub>51</sub>-NH<sub>2</sub> (PromIAPP<sub>1-51</sub>) or C<sub>16</sub>...V<sub>70</sub>-OH (PromIAPP). *c) Reaction conditions:* thiophenol 2%, guanidinium hydrochloride 6 M, pH 7.5-8, 37°C. *d) Reaction conditions:* guanidinium hydrochloride 6 M, pH 8, rt., overnight.

## References

- Höppener, J.W., Ahrén, B., Lips, C.J., *N. Eng. J. Med.* **343**, 411-419 (2000).
- Engel, M.F., Khemtémourian, L., Kleijer, C.C., Meeldijk, H.J., Jacobs, J., Verkleij, A.J., de Kruijff, B., Killian, J.A., Höppener, J.W., *Proc. Nat. Acad. Sci. U.S.A.* **105**, 6033-8 (2008).
- ProhIAPP<sub>1-48</sub>, synthesized via a similar SPPS/NCL procedure, has been reported before: Yonemoto, I.T., Kroon, G.J.A., Dyson, H.J., Balch, W.E., Kellym, J.W. *Biochemistry* **47**, 9900-9910 (2008). Multiple syntheses for mature m/h IAPP have been reported and these peptides are currently commercially available. To the best of our knowledge however, total chemical synthesis of the other precursors or TMR-labeled mature IAPP peptides has not been reported before.
- Dawson, P.E., Muir, T.W., Clark-Lewis, I., Kent, S.B. *Science* **266**, 776-779 (1994).
- Khemtémourian, L., Lahoz Casarramona, G., Suylen, D.P.L., Hackeng, T.M., Meeldijk, H.J.D., de Kruijff, B., Höppener, J.W.M., Killian, J.A. *submitted for publication* (2009).

## "Click Peptide" Based on "O-Acyl Isopeptide Method": *In Situ* Production of Monomer Amyloid $\beta$ Peptide from Water-Soluble Precursor Analogues

Atsuhiko Taniguchi,<sup>1</sup> Youhei Sohma,<sup>1,2</sup> Mariusz Skwarczynski,<sup>1,3</sup>  
 Yuta Hirayama,<sup>1</sup> Takuma Okada,<sup>4</sup> Keisuke Ikeda,<sup>4</sup> Halan Prakash,<sup>5</sup>  
 Hidehito Mukai,<sup>1</sup> Tooru Kimura,<sup>1</sup> Yoshio Hayashi,<sup>1,6</sup> Shun Hirota,<sup>5</sup>  
 Katsumi Matsuzaki,<sup>4</sup> and Yoshiaki Kiso<sup>1</sup>

<sup>1</sup>Department of Medicinal Chemistry, Center for Frontier Research in Medicinal Science, 21<sup>st</sup> Century COE Program, Kyoto Pharmaceutical University, Kyoto, 607-8412, Japan; <sup>2</sup>Department of Biochemistry and Molecular Biology, The University of Chicago, IL 60637, U.S.A.; <sup>3</sup>School of Molecular and Microbial Sciences, The University of Queensland, QLD, 4072, Australia; <sup>4</sup>Graduate School of Pharmaceutical Sciences, Kyoto University, Kyoto, 606-8501, Japan; <sup>5</sup>Graduate School of Materials Science, Nara Institute of Science and Technology, Ikoma, 630-0192, Japan; and <sup>6</sup>Department of Medicinal Chemistry, Tokyo University of Pharmacy and Life Science, Tokyo, 192-0392, Japan

### Introduction

Amyloid  $\beta$  peptides (A $\beta$ s) are the main proteinaceous components of amyloid plaques found in the brains of Alzheimer's disease (AD) patients. Although many studies support the notion that A $\beta$ s are crucial in the pathogenesis of AD [1], the details remain in controversies. To investigate its pathology, A $\beta$ s samples should be used in their monomeric random coil states, because the neurotoxicity of A $\beta$ s is directly related to their assembly states (monomer, oligomer and aggregate). However, it is difficult to prepare monomeric A $\beta$ s with random coil structures due to their low water-solubility and uncontrollable aggregation. These handling problems result in discrepant outcomes in A $\beta$  studies. Hence, we conceived the idea that an "*in situ*" production system that affords only monomeric A $\beta$ s from water-soluble and non-aggregative precursors would be a superb tool in understanding the pathological role of A $\beta$ s.

To achieve this system, we developed a water-soluble "click peptide" [2–6] of A $\beta$ 1–42 on the basis of an "O-acyl isopeptide method" [7] (Figure 1). The peptide has an O-acyl isopeptide structure at Gly<sup>25</sup>-Ser<sup>26</sup>, and converts to intact A $\beta$ 1–42 via an O-to-N intramolecular acyl migration upon a stimulus ("click"; e.g. pH-change or photo-irradiation). Here, we verified the useful features of pH-click peptide (**1**) for A $\beta$  studies.

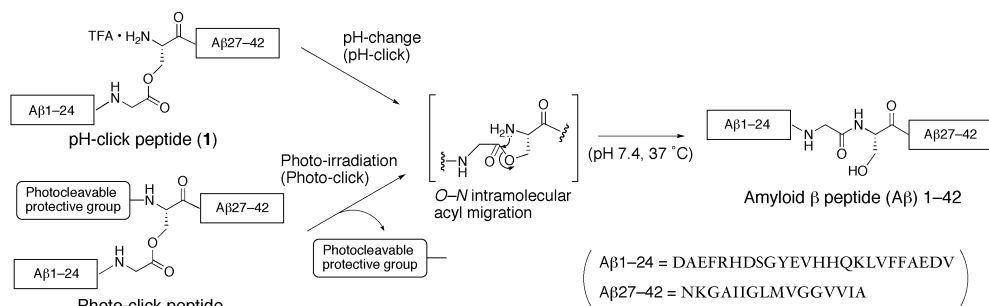


Fig. 1. Click peptide: Production of A $\beta$ 1–42 upon a stimulus ("click").

### Results and Discussion

pH-Click peptide **1** in 0.1% aqueous trifluoroacetic acid (TFA) was stable (>95%, 37 °C, 24 h). However, when the 0.1% aqueous TFA solution of **1** was neutralized by dilution with phosphate buffer (pH 7.4) and incubated at 37 °C ("pH-click"), **1** was converted to A $\beta$ 1–42 via the O-to-N acyl migration ( $t_{1/2}$ : ~10 s). The conversion mostly completed (>90%) after 2 min.

In size-exclusion chromatography (SEC) of pH-click peptide **1** (30  $\mu$ M) in 0.1% aqueous TFA at 37 °C ("before pH-click"), the monomeric form (elution time: 28 min) was



retained during 24 h incubation (Figure 2A). Moreover, circular dichroism (CD) spectrum of **1** showed a random coil structure after both ~1 min and 24 h incubations (Figure 2B).

pH-Click peptide **1** (140  $\mu\text{M}$ ) in 0.1% aqueous TFA was neutralized by dilution with phosphate buffer (pH 7.4) to obtain 30  $\mu\text{M}$  of **1** and incubated at 37  $^{\circ}\text{C}$  to produce A $\beta$ 1–42 ("after pH-click"). In the SEC profile of the A $\beta$ 1–42 right after pH-click (~2 min) (Figure 2C), the monomer was solely observed without any oligomer. An oligomer (>octamer, elution time: 17 min) appeared after 1 h incubation and increased with incubation time at the expense of the monomer. The CD spectrum of the A $\beta$ 1–42 showed a random coil structure right after pH-click (~1 min) (Figure 2D). A CD spectrum after 12 h incubation indicated a  $\beta$ -sheet structure.

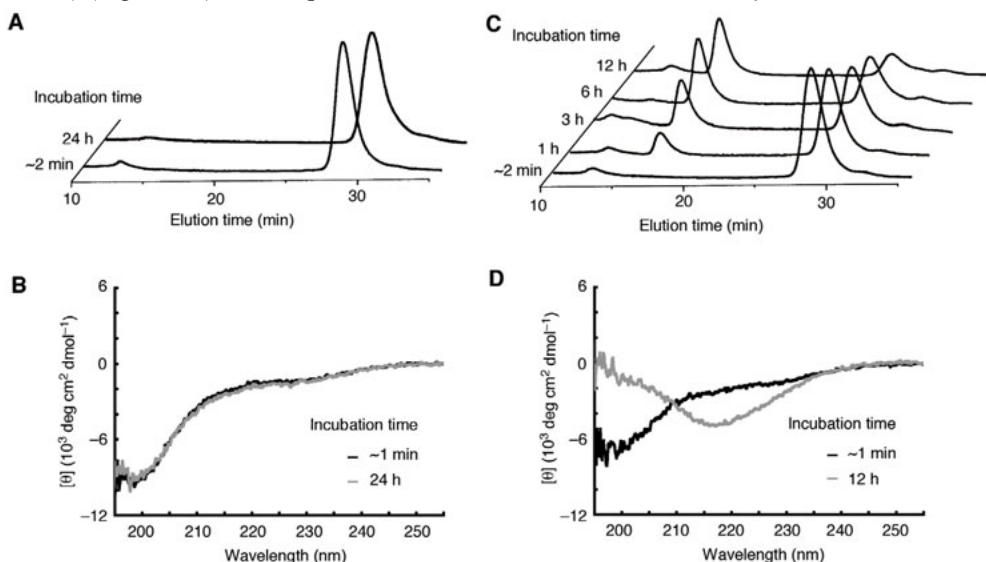


Fig. 2. Size-exclusion chromatography (SEC) (A,C) and circular dichroism (CD) spectroscopy (B,D) using pH-click peptide **1** in 0.1% TFA solution ("before pH-click") (A,B) or in pH 7.4 buffer ("after pH-click") (C,D).

We established an *in situ* system in which monomeric **1** quickly migrated to monomer A $\beta$ 1–42 with a random coil structure upon pH-change (pH-click) from acidic to neutral conditions, and the A $\beta$ 1–42 underwent both self-assembly and conformational changes. We also developed a photo-click peptide which produced A $\beta$ 1–42 upon photo-irradiation (photo-click) [2, 4]. These click peptides could provide a mean to recreate the A $\beta$  assembly events that originate from the monomeric random coil state. The study of these events is important in elucidating the pathological role of A $\beta$ 1–42 in AD. Thus, this click peptide strategy would provide a reliable experiment system in A $\beta$ -related AD research.

## Acknowledgments

A. T. and Y. S. are grateful for Research Fellowships of JSPS for Young Scientists.

## References

- Hardy, J., Selkoe, D.J. *Science* **297**, 353-356 (2002).
- Taniguchi, A., Sohma, Y., Kimura, M., Okada, T., Ikeda, K., Hayashi, Y., Kimura, T., Hirota, S., Matsuzaki, K., Kiso, Y. *J. Am. Chem. Soc.* **128**, 696-697 (2006).
- Sohma, Y., Kiso, Y. *ChemBioChem* **7**, 1549-1557 (2006).
- Taniguchi, A., Skwarczynski, M., Sohma, Y., Okada, T., Ikeda, K., Prakash, H., Mukai, H., Hayashi, Y., Kimura, T., Hirota, S., Matsuzaki, K., Kiso, Y. *ChemBioChem* **9**, 3055-3065 (2008).
- Taniguchi, A., Sohma, Y., Hirayama, Y., Mukai, H., Kimura, T., Hayashi, Y., Matsuzaki, K., Kiso, Y. *ChemBioChem* **10**, 710-715 (2009); spotlighted in *Angew. Chem. Int. Ed.* **48**, 2444 (2009).
- Kiso, Y., Taniguchi, A., Sohma, Y. *Wiley Encyclopedia of Chemical Biology, Vol. 1*, Wiley, Hoboken, 2009, pp. 379-383.
- Sohma, Y., Yoshiya, T., Taniguchi, A., Kimura, T., Hayashi, Y., Kiso, Y. *Biopolymers (Pept. Sci.)* **88**, 253-262 (2007).

## Aromatic Versus Hydrophobic Contributions to Amyloid Peptide Self-Assembly

Charles J. Bowerman, Todd M. Doran, Xianfeng Gu, Derek M. Ryan,  
 F. Timur Senguen, David A. Nissan, and Bradley L. Nilsson

Department of Chemistry, University of Rochester, Rochester, NY 14627-0216, U.S.A.

### Introduction

Peptide self-assembly processes are central to the etiology of amyloid diseases [1]. Much effort has been devoted to characterizing amyloid structure and the mechanisms of peptide self-assembly leading to amyloid. It has been proposed that aromatic  $\pi$ - $\pi$  interactions play a central role in early self-assembly recognition events [2], but this contention remains somewhat controversial [3]. Recent studies have indicated that in some amyloid peptides, including the islet amyloid polypeptide (IAPP), aromatic residues can be exchanged for other hydrophobic residues and these non-aromatic variant peptides still retain competency to form amyloid, although with attenuated kinetics [3]. In an effort to understand the relative contributions of aromatic versus generic hydrophobic interactions, studies to quantify the self-assembly properties of amyloid peptides as a function of increasing hydrophobicity and altered aromatic character have been undertaken. Model peptides have been chosen in which at least one aromatic side-chain is present; the focus of this abstract is the amphipathic (FKFE)<sub>2</sub> peptide [4]. The aromatic residues have been systematically replaced with natural and nonnatural residues with varying hydrophobicity and aromaticity and the self-assembly properties have been characterized [5]. These studies confirm that aromatic interactions are not strictly required for amyloid formation.

### Results and Discussion

Initial studies focused on a series of five (XKXE)<sub>2</sub> peptides (general sequence Ac-XKXEKXE-NH<sub>2</sub>, Table 1) with increasing hydrophobicity. (FKFE)<sub>2</sub>, peptide **1**, is the only member of the series with the potential for aromatic interactions. Peptides **2–4** (X = Ala, Val, Leu respectively) are less hydrophobic than peptide **1**, although Val, a  $\beta$ -branched amino acid, has a greater propensity to adopt the  $\beta$ -sheet secondary structure that is critical for self-assembly. In the context of self-assembly, it is impossible to separate hydrophobicity from the other biophysical characteristics of amino acids, and any effort to study this class of peptides must acknowledge that hydrophobicity alone does not drive self-assembly. The final peptide of the series, peptide **5**, contains cyclohexylalanine (Cha) in the X position. Cha is significantly more hydrophobic than Phe (Table 1) and lacks the ability to participate in aromatic interactions. Cha is sterically similar, but not identical to Phe, so it is possible that the intra- and interstrand packing modes will not be identical. Nonetheless, Cha to Phe is an intriguing mutation in the context of the hydrophobic/aromatic debate in peptide self-assembly. The Cha-containing peptide should display enhanced self-assembly rates if hydrophobicity is the most important determinant in molecular recognition events leading to nucleation and elongation in self-assembly.

Table 1. (XKXE)<sub>2</sub> peptide sequences, hydrophobicity, and secondary structure propensity

Peptide	Sequence	X	$\Pi^a$	$P_\beta^b$
1	Ac-(FKFE) <sub>2</sub> -NH <sub>2</sub>	Phe	1.79	1.33
2	Ac-(AKAE) <sub>2</sub> -NH <sub>2</sub>	Ala	0.31	0.75
3	Ac-(VKVE) <sub>2</sub> -NH <sub>2</sub>	Val	1.22	1.86
4	Ac-(LKLE) <sub>2</sub> -NH <sub>2</sub>	Leu	1.70	1.1
5	Ac-(ChaKChaE) <sub>2</sub> -NH <sub>2</sub>	Cha	2.72	–

<sup>a</sup> Amino acid hydrophobicity based on water/octanol partition coefficients relative to Gly [6]

<sup>b</sup> Propensity to occur in  $\beta$ -sheet secondary structures from the PDBselect dataset [7]

The self-assembly of these peptides was characterized by secondary structure analysis and microscopic analysis of the resulting aggregate structures. With the exception of (AKAE)<sub>2</sub>, peptide **2**, which failed to self-assemble at any of the concentrations studied (10  $\mu$ M to 4 mM), each of the other peptides self-assembled to form fibrillar structures (Figure 1). Peptides **3** and **4** formed morphologically similar fibrils 8–10 nm in diameter as observed using transmission electron microscopy (TEM) and atomic force microscopy (AFM). Both peptides displayed  $\beta$ -sheet secondary structures by CD and IR spectroscopy. Interestingly, the Phe-containing peptide **1** formed two morphologically distinct structures,  $\sim$ 8 nm diameter fibrils and left-handed helical ribbons having a diameter of  $\sim$ 8 nm with a helical pitch of  $\sim$ 19 nm. This polymorphism was only observed with the (FKFE)<sub>2</sub> sequence, implying an interesting potential role for aromatic  $\pi$ - $\pi$  interactions in the self-assembly of this peptide. The Cha-containing **5** displayed unique morphology. TEM images indicated a highly entangled fibril mesh containing fibrils that were significantly smaller than those observed for each of the other peptides (Figure 1D). Fibrils derived from **5** were  $\sim$ 3–4 nm in diameter in contrast to the  $\sim$ 7–9 nm fibrils observed in each of the other peptides. We hypothesize that the highly hydrophobic nature of the Cha-peptide results in very rapid nucleation and elongation, depleting the monomeric state at a rate that precludes the development of longer, wider fibrils. Unfortunately, the self-assembly of each of these variants was exceptionally rapid, even at concentrations as low as 10  $\mu$ M, precluding any quantitative kinetic analysis of self-assembly. This rapid assembly is likely due to the strong attractive ionic interactions that occur on the hydrophilic face of the bilayer architecture. Future studies will focus on peptide sequences that lack this strong ionic complementarity.

These studies confirm that aromatic  $\pi$ - $\pi$  interactions are not essential for peptide self-assembly. In addition, increasing the hydrophobicity appears to enhance and alter the self-assembly of (XKXE)<sub>2</sub> peptides even if X is not an aromatic amino acid. Future work will apply this strategy to other amyloid sequences in which the effects of increasing hydrophobicity can be more effectively quantified.

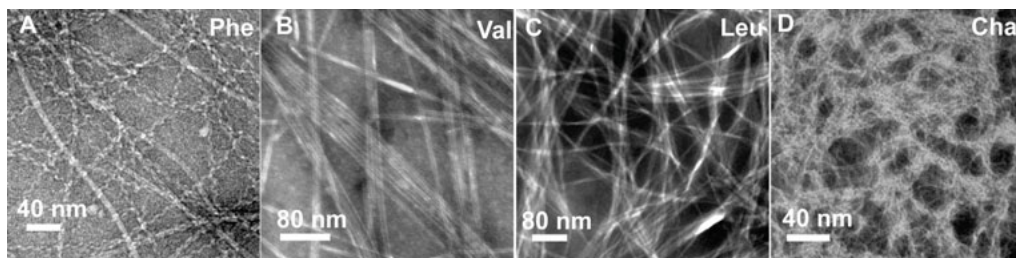


Fig. 1. TEM images of fibrils derived from peptides **1**, **2**–**5**. A. Peptide **1**; B. Peptide **3**; C. Peptide **4**; D. Peptide **5**.

## Acknowledgments

We are grateful to Professor Todd Krauss for assistance with AFM experiments and to Dr. Scott Kennedy for assistance with CD experiments. We also acknowledge Chris Willoughby and TA Instruments for the use of the AR-G2 Rheometer, and Karen Bentley of the URM Electron Microscope Research Core for assistance with TEM experiments. This work was supported in part by a DuPont Young Professor Award to BLN and by a grant from the Alzheimer's Association (NIRG-08-90797).

## References

1. Hamley, I.W. *Angew. Chem. Int. Ed.* **46**, 8128–8147 (2007).
2. Gazit, E. *FASEB J.* **16**, 77–83 (2002).
3. Marek, P., Abedini, A., Song, B., Kanungo, M., Johnson, M.E., Gupta, R., Zaman, W., Wong, S.S., Raleigh, D.P. *Biochemistry* **46**, 3255–3261 (2007).
4. Caplan, M.R., et al. *Biomacromolecules* **1**, 627–631 (2000).
5. Bowerman, C.J., et al. *Mol. BioSyst.* **5**, DOI: 10.1039/b904439f (2009).
6. Fauchère, J.L., et al. *Int. J. Peptide Protein Res.* **32**, 269–278 (1988).
7. Costantini, S., Colonna, G., Facchiano, A.M. *Biochem. Biophys. Res. Commun.* **342**, 441–451 (2006).

## Proteinous Microspheres Containing KLVFF Peptides Sequester Amyloid-Beta Protein and Inhibit its Aggregation

Michal Richman,<sup>1</sup> Sara Wilk,<sup>1</sup> Natalie Skirtenko,<sup>1</sup> Alex Perelman,<sup>2</sup>  
and Shai Rahimipour<sup>1</sup>

<sup>1</sup>Department of Chemistry and <sup>2</sup>Life Science, Bar-Ilan University, Ramat-Gan 52900, Israel

### Introduction

Alzheimer's disease (AD) is a progressive neurodegenerative disorder characterized clinically by progressive impairment in memory and cognition. The neuropathology of AD is characterized by extraneuronal deposition of amyloid- $\beta$  (A $\beta$ ) and neurofibrillary tangles. A $\beta$  is a short polypeptide (40 to 43 amino acids) that at sufficiently high concentration tend to self-assemble into soluble aggregates, which in turn accumulate as amyloids [1]. The aggregates are associated with pathological changes in the surrounding brain neurons that lead to neuronal death and synaptic loss. Therefore, interfering with A $\beta$  formation and aggregation or sequestering its accumulation in the brain are promising strategies for AD therapy. Lowe *et al.* have showed that compounds containing a recognition element KLVFF (residues 16-20 in A $\beta$ ) can bind to the homologous sequence in A $\beta$  through hydrophobic and  $\pi$ - $\pi$  interactions and disrupt its aggregation, thus protecting neurons from A $\beta$ -associated toxicity. Therefore, this fragment was served as a lead compound for the development of inhibitory agents that are aimed at preventing A $\beta$  aggregation *in vivo* [2]. Moreover, it was shown that dendrimeric analog of KLVFF display superior activity compared to the monomeric KLVFF [3]. The concept of multivalency to enhance the affinity and specificity of a ligand to its receptor is an important feature in biology. Here, we describe the design, preparation and characterization of novel proteinous microspheres (PM) decorated with KLVFF peptides at their surface, and demonstrate their efficacy to inhibit A $\beta$  aggregation by sequestering it from the solution. The preparation of these microspheres is based on sonochemical approach that uses high-intensity ultrasound to make aqueous suspensions filled with water-insoluble liquids [4]. The microspheres are spherical microcapsules that are generated from intermolecular disulfide bonds between protein's cysteines. We showed that the surface of such microspheres can be readily modified with different thiol containing substances through the exchange reaction with the disulphide groups of bovine serum albumin; and they can effectively encapsulate different substances such as drugs or contrasting agents.

### Results and Discussion

Amyloid- $\beta$  fragment, KLVFF, and its derivatives were synthesized by SPPS utilizing Fmoc-chemistry. A PEG-like spacer was used to separate the "recognition element" from the microsphere surface. The free SH group of the Cys at the C-terminal of the peptides was used to insert the KLVFF fragments to the proteinous shell of the microspheres by thiol exchange reaction, while the free  $\alpha$ -amine group of the terminal Lys was coupled to fluorescent tag (NBD) to follow its incorporation to the BSA shell. The peptides were mixed with different ratio of BSA (1:10 to 1:1000; BSA:Peptide molar ratio) in water, over-layered with soybean oil or dodecane and subjected to sonochemical reaction using an acoustic power of 150 W/cm<sup>2</sup> (20 kHz) for 3 min, while it was cooled in an ice-water bath. The microspheres were also loaded with Nile red as a fluorescent model for different drugs by dissolving different amounts of the dye in dodecane prior to the irradiation. Figure 1 shows the morphology, size distribution and encapsulation capability of KLVFF-conjugated microspheres, studied by electron microscopy (SEM), light scattering and fluorescent microscopy. The data revealed that the observed microspheres are core-shell structures with average size of 1.8  $\mu$ M and narrow size distribution ( $\pm$ 1.43  $\mu$ M), enabling them to be used for different therapeutic and diagnostic applications. The fluorescent studies demonstrated that the microspheres have a hydrophobic core that can encapsulate different molecules, such as Nile red (Figure 1E. and F.) or curcumin (not shown) as a fluorescent dye or an anti-amyloidogenic agent [5], while the shell of the microspheres is composed of BSA and KLVFF molecules (Figure 1D, F).

To evaluate the effect of the conjugated microspheres on A $\beta$ (1-40) aggregation, the thioflavin (ThT) assay was performed [6] and further confirmed by electron microscopy (TEM, Figure 2J. and K.).

The data revealed that KLVFF-conjugated PMs potentially inhibit the aggregation of A $\beta$  (1-40), while unconjugated microspheres have no effect (data not shown).

To unravel the mechanism by which conjugated microspheres inhibit the aggregation of A $\beta$ , they were incubated with soluble FITC-labeled A $\beta$  (1-40) for 4 days and studied by fluorescent and electron microscopy (Figure 2). The data demonstrated that KLVFF-conjugated microspheres selectively bind A $\beta$ (1-40) and thus sequester it from the solution, while the naked BSA microspheres did not interact with A $\beta$ (1-40) and thus had no effect on its aggregation.

In conclusion, we have demonstrated a facile and efficient sonochemical method for preparation of proteinous microspheres containing anti-amyloidogenic peptides, such as KLVFF analogs, on their outer surface. The microspheres were characterized by their particle size, surface morphology, stability and drug entrapment efficiency. We found that the conjugated microspheres effectively inhibit the aggregation of soluble A $\beta$ (1-40) and sequester it from the solution by adsorbing it on their surface.

## Acknowledgments

We thank the Bar-Ilan Presidential fellowship program for predoctoral and travel grant fellowship and American Peptide Society for the travel grant provided to M. Richman.

## References

1. Goedert, M., et al. *Science* **314**, 777- 781 (2006).
2. Lowe, T.L., et al. *Biochemistry* **40**, 7882-7889 (2001).
3. Chafekar, S.M., et al. *ChemBioChem* **8**, 1857 - 1864 (2007)
4. Suslick, K.S., et al. *J. Am. Chem. Soc.* **112**, 7807- 7809 (1990).
5. Yang, F., et al. *J. Biol. Chem.* **280**, 5892-5901 (2005).
6. Levine III, H. *Protein Sci.* **2**, 404- 410 (1993).

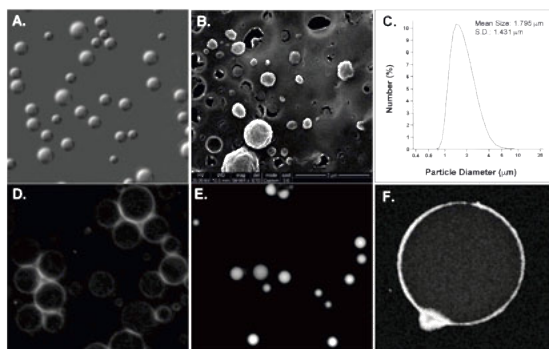


Fig. 1. The morphology (A. and B.), size distribution (C.) and encapsulating capability (E. and F.) of KLVFF-conjugated PMs prepared from sonochemical irradiation of aqueous solutions of BSA and KLVFF analogs.

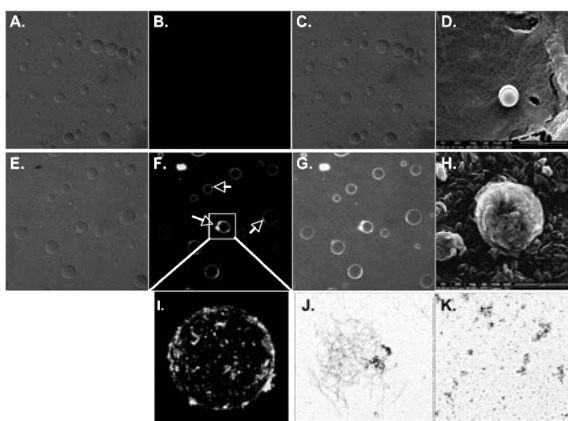


Fig. 2. KLVFF conjugated PMs (E-I) and native PMs (A-D) were incubated with FITC-labeled A $\beta$ (1-40) for 72 h. The microspheres were then washed with cold PBS and visualized by fluorescent microscope (A-C and E-G) and SEM (D. and H.). Pictures A. and E. represent the bright field micrographs of the native and conjugated PMs, respectively, while micrographs B. and F. demonstrate the fluorescent images. Pictures C. and G. show the merge of bright field and fluorescent images. The microspheres were also analyzed by SEM (D. and H.). The 3D images of KLVFF-conjugated PM's interacted with FITC-labeled A $\beta$  were analyzed by confocal microscopy (I.). Image J. and K. respectively show the TEM images of A $\beta$ (1-40) fibrils that were generated from incubation of soluble A $\beta$ (1-40) for 4 days, and the effect of the conjugated microspheres on the fibrilization process.

## The ApoE Mimetic Peptide, Ac-hE18A-NH<sub>2</sub> Recycles in THP-1 Monocyte-Derived Macrophages

Palgunachari Mayakonda, Manjula Chaddha, Gaurav Nayyar,  
Shaila P. Handattu, David W. Garber, Candyce E. Monroe,  
C. Roger White, G. M. Anantharamaiah, and Geeta Datta

Department of Medicine, University of Alabama Medical Center, Birmingham, AL 35294, U.S.A.

### Introduction

ApolipoproteinE (apoE) mimetic peptide Ac-hE18A-NH<sub>2</sub> was designed to test the hypothesis that covalently linking the arginine rich putative receptor binding region from residues 141-150 of apoE (LRKLRKRLLR) to a class A amphipathic helical peptide 18A (DWLKAFYDKVAEKLKEAF) would produce a peptide with cholesterol lowering properties as well as anti-inflammatory properties. We have already shown the ability of this peptide to bind to apolipoprotein-B (apo-B) containing lipoproteins and enhance their clearance both in vivo and in vitro [1]. We have also shown that injecting this peptide causes rapid clearance of plasma cholesterol in different dyslipidemic mouse models because of its ability to cause rapid uptake and degradation of apo-B containing lipoproteins [2]. Such an effect was not observed with Ac-18A-NH<sub>2</sub> (2F). Injection of this peptide into Watanabe Heritable Hyperlipidemic Rabbits caused a dramatic reduction in plasma cholesterol levels and also reduced plasma lipid hydroperoxide levels [3]. The objective of this study was to determine if the addition of LRKLRKRLLR to 18A alters the cellular function of 2F.

### Results and Discussion

Many differences were observed in the cellular properties of 2F and Ac-hE18A-NH<sub>2</sub>. Pulse chase studies using [<sup>125</sup>I]-Ac-hE18A-NH<sub>2</sub> in THP-1 derived macrophages and HepG2 cells showed greater amounts of intact peptide in the cells at later time points indicating recycling of the peptide. Such an effect was not observed with 2F. Ac-hE18A-NH<sub>2</sub>, unlike 2F, induced a 2.5 fold increase in pre $\beta$ -HDL in the conditioned media of HepG2 cells. Cells incubated with 2F for 20h were similar to control cells; 92% of secreted apoA-I was in the  $\alpha$ -HDL form and only 8% of apoA-I was in the pre $\beta$ -HDL form while the Ac-hE18A-NH<sub>2</sub> treated cells the conditioned medium contained 99% of apoA-I in the pre $\beta$ -HDL form. This effect persisted for three days after removal of the peptide from culture medium. Ac-hE18A-NH<sub>2</sub> also induced the secretion of cell-surface apoE from THP-1 macrophages. In addition, the peptide increased cholesterol efflux from THP-1 cells by an ABCA-1 independent mechanism. In contrast, 2F-mediated cholesterol efflux was ABC1 dependent.

Both 2F and Ac-hE18A-NH<sub>2</sub> inhibited LPS-induced vascular cell adhesion molecule-1 (VCAM-1) expression, and reduced monocyte adhesion in human umbilical vein endothelial

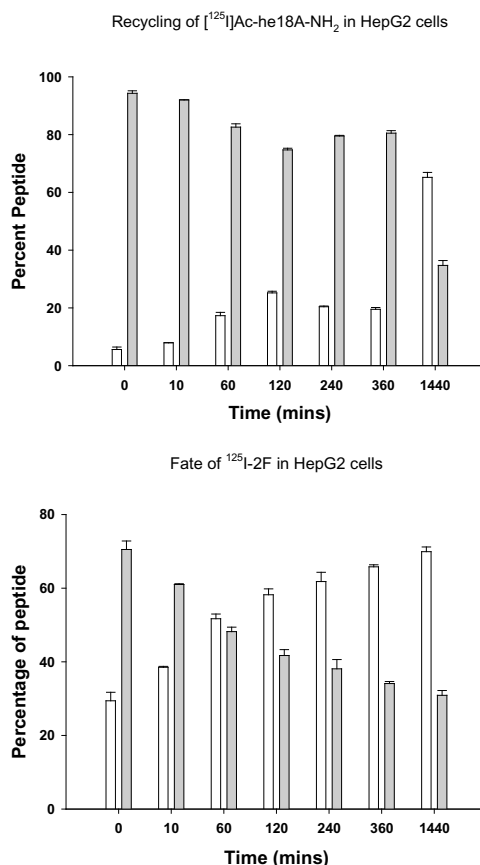


Fig. 1. Ac-hE18A-NH<sub>2</sub> recycles in HepG2 cells (top panel), unlike 2F (bottom panel). Black bar: medium, grey bar: cell.

cells (HUVECs). Both peptides reduced the secretion of LPS-induced secretion of interleukin-6 (IL-6) and monocyte chemoattractant protein-1 (MCP-1) from THP-1 macrophages when administered with LPS. However, only Ac-hE18A-NH<sub>2</sub> reduced the secretion of interleukin-6 (IL-6) and monocyte chemoattractant protein-1 (MCP-1) from THP-1 macrophages when administered post-LPS and pre-LPS treatment. Taken together, these results suggest that addition of the putative apoE receptor-domain to the Class A amphipathic peptide, 18A results in a peptide that, similar to apoE, recycles, thus enabling the potentiation and prolongation of its anti-atherogenic and anti-inflammatory effects. Such a peptide has great potential as a therapeutic agent in the management of atherosclerosis and other inflammatory diseases.

## Acknowledgments

This work was supported by NIH grants.

## References

1. Datta, G., Garber, D.W., Chung, B.H., Chaddha, M., Dashti, N., Bradley, W.A., Gianturco, S.H., Anantharamaiah, G.M. *J. Lipid Res.* **42**, 959–966 (2001).
2. Garber, D.W., Handattu, S., Aslan, I., Datta, G., Chaddha, M., Anantharamaiah, G.M. *Atherosclerosis* **168**, 229–237 (2003).
3. Gupta, H., White, C.R., Handattu, S., Garber, D.W., Datta, G., Chaddha, M., Dai, L., Gianturco, S.H., Bradley, W.A., Anantharamaiah, G.M. *Circulation* **111**, 3112–3118 (2005).



## Cryptides: Discovery of Functional Cryptic Peptides Hidden in Protein Structures and Identification of Their Signaling Mechanisms

Hidehito Mukai,<sup>1,2</sup> Tetsuo Seki,<sup>2</sup> Eisuke Munekata,<sup>2</sup> and Yoshiaki Kiso<sup>1</sup>

<sup>1</sup>21st Century COE Program, Kyoto Pharmaceutical University, Kyoto, 607-8412, Japan; and

<sup>2</sup>Institute of Applied Biochemistry, University of Tsukuba, Ibaraki 305-8572, Japan

### Introduction

Peptidergic hormones and neurotransmitters are produced from their inactive precursor proteins by specific proteolytic cleavages. Recently, we discovered mitocryptide-1, a novel neutrophil-activating peptide that was produced from mitochondrial cytochrome c oxidase subunit VIII [1,2]. We named these functional peptides that were hidden in protein structures as “cryptides” [2,3]. We also found that many cryptides activated other cells such as mast cells [4-6]. Here, we report the identification of mitocryptide-2 (MCT-2), another type of neutrophil-activating cryptide from porcine heart. MCT-2 activated not only HL-60 cells, which differentiated into neutrophilic/granulocytic cells, but also purified neutrophils from human peripheral blood. These results suggest the presence of novel regulatory mechanisms involving such cryptides.

### Results and Discussion

Several chemokines such as interleukin 8 have been implicated in the induction of neutrophil infiltration into damaged tissues of the heart and lungs after reperfusion injuries. However, the molecular mechanisms underlying the actions of neutrophils at their migrated sites are not well understood. Namely, neutrophil migration in tissues such as the heart and lungs after reperfusion injury appears to be very rapid, proposing that substances inducing such migration may exist even in healthy tissues. In fact, the presence of neutrophil-activating peptides in various healthy organ extracts including those from the heart has been observed in our preliminary experiments. Therefore, we tried to identify peptidergic neutrophil-activating factors by purifying them from porcine hearts.

Peptides that activate neutrophils were extracted and purified from porcine hearts as described previously [2] with several modifications (Figure 1). The activity of the purified fractions was monitored for the induction of  $\beta$ -hexosaminidase ( $\beta$ -HA) release from differentiated HL-60 cells into neutrophilic/granulocytic cells, because these cells share a number of common features with neutrophils. In addition, well-known neutrophil-activating factors such as C5a and fMLF are demonstrated to stimulate the release of  $\beta$ -HA from the differentiated HL-60 cells [2,3].

First, after inactivating proteases by boiling in distilled water, we extracted peptides from porcine hearts with 1M AcOH containing 20 mM HCl. Various proteins were then removed by precipitation with 60% acetone. Extracted peptides were separated into three fractions by cation-exchange chromatography using SP-Sephadex C25. Since the PA fraction eluted with 2 M pyridine-AcOH (pH 5.0) significantly induced  $\beta$ -HA release, this fraction was further purified by gel filtration chromatography using Sephadex G-25. The active

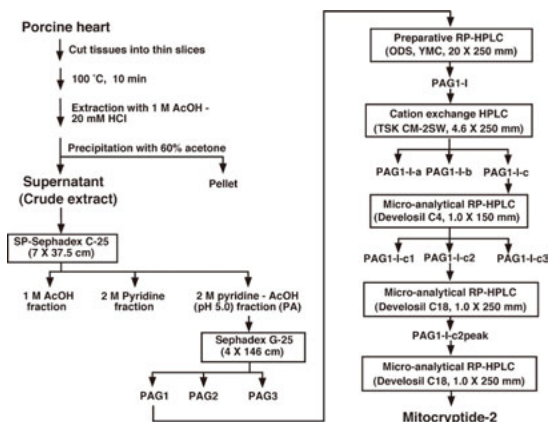


Fig. 1. Purification procedure of mitocryptide-2.

fractions containing peptides whose molecular weights were approximately 1,000 ~ 3,000 were combined as the PAG1 fraction. The fraction was concentrated and purified by preparative RP-



HPLC using ODS column (20 × 250 mm, YMC, Kyoto, Japan). The following purification by cation-exchange HPLC on a TSK-CM2SW column (4.6 × 250 mm, Tosoh, Tokyo, Japan) gave three major active fractions. Among these three major active fractions, the PAG1-I-c fraction was then purified by micro-RP-HPLC using a C4 column (Develosil C4, 1.0 × 150 mm, Nomura Chemicals, Aichi, Japan). This purification process yielded three active fractions: PAG1-I-c1, PAG1-I-c2, and PAG1-I-c3. The most active PAG1-I-c2 fraction was purified twice by micro-RP-HPLC using analytical ODS column (Develosil ODS-HG5, 1.0 × 250 mm, Nomura Chemicals), and ultimately yielded the active PAG1-I-c2 peak-peak fraction.

The substance in the PAG1-I-c2 peak-peak fraction was analyzed for its structural identification. Since a modification at the N-terminus of the peptide was suggested by MS/MS analysis, the fraction was treated with proteolytic enzyme Arg-C and the cleaved peptides were purified by micro-RP-HPLC. We collected four major peaks and investigated the amino acid sequences of the corresponding peptides by Edman degradation and MS/MS analysis using FAB-mass spectrometry. Taken together the analyses, the primary structure of the peptide is shown in Figure 2. We named the active peptide “mitocryptide-2” (MCT-2) because it is a cryptide hidden in mitochondrial cytochrome b, and because we purified and identified it as the second neutrophil-activating peptide derived from a mitochondrial protein [2].

#### **Mitocryptide-2 (MCT-2) (cytochrome b(1-15), N-terminal formylated)**

Porcine: fMet - Thr - Asn - Ile - Arg - Lys - Ser - His - Pro - Leu - Met - Lys - Ile - Ile - Asn

Human: fMet - Thr - Pro - Met - Arg - Lys - Ile - Asn - Pro - Leu - Met - Lys - Leu - Ile - Asn

*Fig. 2. Amino acid sequences of mitocryptide-2 and its human homologue.*

Because the primary structure of MCT-2 was identified, we next synthesized MCT-2 and its human homologue hMCT-2, and investigated their activities on not only differentiated HL-60 cells into neutrophilic/granulocytic cells but also human neutrophils isolated from peripheral blood. MCT-2 and hMCT-2 induced chemotaxis and the increase in intracellular  $\text{Ca}^{2+}$  concentration in the differentiated HL-60 cells. Moreover, both MCT-2 and hMCT-2 promoted  $\beta$ -HA release in the differentiated HL-60 cells and human neutrophils. These results demonstrate that both peptides are neutrophil-activating cryptides.

In conclusion, we purified and identified MCT-2, a novel neutrophil-activating cryptide from porcine hearts. These results suggest the presence of regulatory mechanisms involving such mitocryptides in innate immunity [7].

#### **Acknowledgments**

This study was supported by research grants from the Special Research Project on Circulation Biosystem, University of Tsukuba; the Naito Foundation; the Ministry of Education, Culture, Sports, Science and Technology, Japan (No. 06680605; 21603014; 40089107); JT, Inc.; and Mitsubishi Chemical Corporation.

#### **References**

1. Mukai, H., Hokari, Y., Seki, T., Nakano, H., Takao, T., Shimonishi, Y., Nishi, Y., Munekata, E. In Lebl, M., Houghten, R.A. (eds.) *Peptides, The Wave of the Future (Proceedings of the 2nd International and 17th American Peptide Symposium)*, American Peptide Society, San Diego, 2001; p. 1014-1015.
2. Mukai, H., Hokari, Y., Seki, T., Takao, T., Kubota, M., Matsuo, Y., Tsukagoshi, H., Kato, M., Kimura, H., Shimonishi, Y., Kiso, Y., Nishi, Y., Wakamatsu, K., Munekata, E. *J. Biol. Chem.* **283**, 30596-30605 (2008).
3. Ueki, N., Someya, K., Matsuo, Y., Wakamatsu, K., Mukai, H. *Biopolymers* **88**, 190-198 (2007).
4. Mukai, H., Kikuchi, M., Suzuki, Y., Munekata, E. *Biochem. Biophys. Res. Commun.* **362**, 51-55 (2007).
5. Mukai, H., Suzuki, Y., Kiso, Y., Munekata, E. *Protein Pept. Lett.* **15**, 931-937 (2008).
6. Mukai, H., Kikuchi, M., Fukuhara, S., Kiso, Y., Munekata, E. *Biochem. Biophys. Res. Commun.* **375**, 22-26 (2008).
7. Mukai, H., Seki, T., Nakano, H., Hokari, Y., Takao, T., Kawanami, M., Tsukagoshi, H., Kimura, H., Kiso, Y., Shimonishi, Y., Nishi, Y., Munekata, E. *J. Immunol.* **182**, 5072-5080 (2008).

## Highly Active and Selective Integrin Ligands for Imaging Purposes

S. Neubauer,<sup>1</sup> D. Heckmann,<sup>1</sup> J. Eckardt,<sup>1</sup> G. Zahn,<sup>2</sup> D. Vossmeier,<sup>2</sup>  
 R. Stragies,<sup>2</sup> H.-J. Wester,<sup>3</sup> and H. Kessler<sup>1</sup>

<sup>1</sup>Department of Chemistry, Institute for Advanced Study at the TU München, Garching, 85747, Germany;

<sup>2</sup>Jerini AG, Berlin, 10115, Germany; and <sup>3</sup>Nuklearmedizinische Klinik und Poliklinik,

Klinikum rechts der Isar, TU München, Munich, 81675, Germany

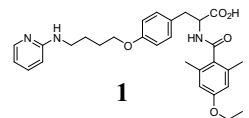
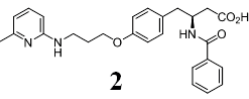
### Introduction

Integrins constitute a family of transmembrane cell surface receptors mediating various cell-cell and cell-extracellular matrix interactions. The pioneering observation that integrins - especially  $\alpha v\beta 3$  and  $\alpha 5\beta 1$  - are hallmarks of metastatic cancer and seriously involved in the process of tumor angiogenesis turned them into attractive targets for cancer therapy. Recent reevaluation pointed out the importance of the subtype  $\alpha 5\beta 1$  in the process of tumor angiogenesis in contrast to  $\alpha v\beta 3$  as assumed so far [1]. Hence, the imaging of cancer via integrin ligands is one of the major goals in personalized medicine. Potent ligands are currently developed but integrin subtype specific ligands have not yet been modified for application in Molecular Imaging.

### Results and Discussion

Starting from  $\alpha 5\beta 1$  (**1**) and  $\alpha v\beta 3$  (**2**) selective RGD-mimics based on a tyrosine scaffold (Table 1) [2,3] we succeeded in functionalizing these ligands with the 1,4,7,10-tetraazacyclodecane-1,4,7,10-tetraacetic acid (DOTA) derivative, suitable for radioisotope labeling [5]. By means of SAR-studies and docking experiments [4] we determined the linking position of the ligand.

Table 1. Highly active and selective nonpeptidic  $\alpha v\beta 3$  and  $\alpha 5\beta 1$  integrin ligands.

	$IC_{50} \alpha v\beta 3$ [nM]	$IC_{50} \alpha 5\beta 1$ [nM]	Selectivity
 <b>1</b>	1455	2.0	~700 fold
 <b>2</b>	13	3946	~300 fold

For the  $\alpha 5\beta 1$  ligand **9** we started with 4-bromo-3,5-dimethyl phenol (Figure 1). After introduction of the *tert*-butyl protected carboxylic group and the Mitsunobu-type alkylation we coupled with an aminooxy component.

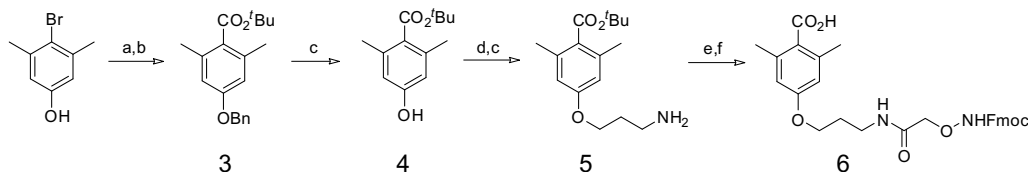


Fig. 1. Synthesis of the integrin ligand: a) NaH, 0°C, 30 min, BnBr, 2 h, DMF; b) BuLi, -78°C, 30 min, di-*tert*-butyl dicarbonate, 2 h, THF; c) Pd/C, H<sub>2</sub>, 1 atm, 12 h, MeOH; d) 3-(benzyloxy-carbonylamino)-propan-1-ol, PPh<sub>3</sub>, ADPP, 0°C, 18 h, THF; e) Fmoc-3-(aminooxy) acetic acid, TBUT, DIPEA, 24 h, DMF; f) 95% TFA, 2.5% TIPS, 2.5% H<sub>2</sub>O, 18 h.

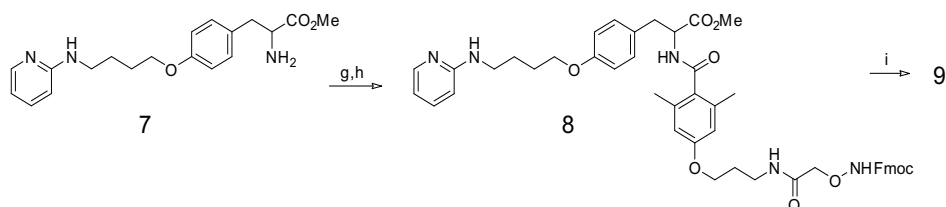
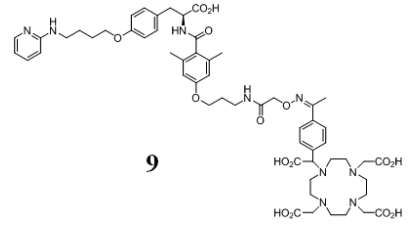
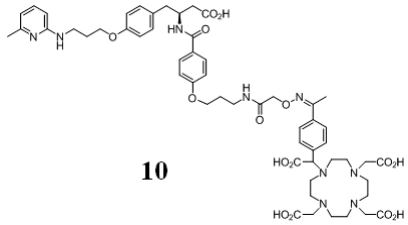


Fig. 2. Synthesis of the integrin ligand: g) **6**, HATU, DIPEA, 20 h, DMF; h) LiOH, 18 h, MeOH/H<sub>2</sub>O; i) 2-[1-(1,4,7,10-tetraazacyclodecane)-4,7,10-trisacetate]-(4-acetylphenyl) acetic acid, 20 h, TFA, ACN/H<sub>2</sub>O.

The resulting compound **6** reacted with the ligand precursor (precursor of **2**) and after deprotection the aminoxy-functionalized compound reacts under formation of an oxime bond via an oxime ligation with the 4-acetylphenyl-DOTA derivative [6] (Figure 2). The resulting ligand **9** was tested in a competitive enzyme-linked immunosorbent assay using the immobilized natural integrin ligands fibronectin and vitronectin and the soluble integrins respectively.

As can be seen in Table 2, the functionalisation of both the  $\alpha 5 \beta 1$  (**9**) and the  $\alpha v \beta 3$  (**10**) selective compounds by the oxime ligation with a DOTA-derivate results in new ligands that still show activity in the nanomolar range. To our knowledge, there is no nonpeptidic radiolabeled subtype selective  $\alpha 5 \beta 1$  ligand for imaging reported in literature until now.

Table 2. Highly active and selective integrin ligands for radioimaging

	$IC_{50} \alpha v \beta 3$ [nM]	$IC_{50} \alpha 5 \beta 1$ [nM]	Selectivity
 <p><b>9</b></p>	>1000	18.6	>50 fold
 <p><b>10</b></p>	4.4	1134	~250 fold

Furthermore, we succeeded in labeling the compounds with <sup>69</sup>Ga and <sup>68</sup>Ga (suitable for PET).

## Acknowledgments

SN thanks CompInt (Materials Science of Complex Interfaces) of the “Elitenetzwerk Bayern” for funding.

## References

- Hynes, R.O. *Nature Medicine* **8**, 918-921 (2002).
- Heckmann, D., Meyer, A., Marinelli, L., Zahn, G., Stragies, R., Kessler, H. *Angew. Chem. Int. Ed.* **46**, 3571-3574 (2007).
- Heckmann, D., Meyer, A., Laufer, B., Zahn, G., Stragies, R., Kessler, H. *ChemBioChem* **9**, 1397-1407 (2008).
- Marinelli, L., Meyer, A., Heckmann, D., Lavecchia, A., Novellino, E., Kessler, H. *J. Med. Chem.* **48**, 4204-4207 (2005).
- Schottelius, M., Laufer, B., Kessler, H., Wester, H.-J. *Accounts Chem. Res.* **42**, 969-980 (2009).
- Knör, S., Modlinger, A., Poethko, T., Schottelius, M., Wester, H.-J., Kessler, H. *Chem. Eur. J.* **13**, 6082-6090 (2007).

## ***iso*DGR: A New Sequence for Integrin Ligands**

**E. Otto,<sup>1</sup> D. Heckmann,<sup>1</sup> G. Zahn,<sup>2</sup> D. Vossmeier,<sup>2</sup>  
R. Stragies,<sup>2</sup> and H. Kessler<sup>1</sup>**

<sup>1</sup>Department of Chemistry TU Muenchen, Lichtenbergstr. 4, 85747 Garching, Germany; and

<sup>2</sup>Jerini AG, Invalidenstr. 130, 10115 Berlin, Germany

### **Introduction**

Integrins are heterodimeric transmembrane glycoproteins which are found in many animal species ranging from sponges to mammals. These cell adhesion receptors regulate cell-cell and cell-extracellular matrix interactions [1], thus mediate the physical anchoring and the bidirectional transmembrane signalling. Hence they are involved in fundamental cellular processes such as migration, proliferation, differentiation, and apoptosis. The peptide sequence Arg-Gly-Asp (RGD) is by far the most prominent ligand to promote specific cell adhesion through integrin stimulation. It is known to bind integrins, e.g.,  $\alpha 5 \beta 1$  (Fibronectin, Vitronectin, Fibrinogen),  $\alpha \nu \beta 3$  (Fibronectin, Vitronectin), and  $\alpha \text{IIb} \beta 3$  (Fibronectin, Vitronectin, Fibrinogen) among many others.

Fibronectin (Fn) is a large glycoprotein which is secreted as a disulfide-bonded dimer consisting primarily of three types of repeating modules. It is an ubiquitous and abundant ECM protein, which plays an important role in haemostasis, thrombosis, inflammation, wound repair, angiogenesis, and embryogenesis.

Recently, it was shown that a mutation of the RGD sequence in the Fn-III-10 domain to RGE still exhibits binding, although RGE binds no integrin. However, these fibrils have a slightly different phenotype than wild-type Fibronectin. *Takahashi et al.* observed that only a  $\alpha \nu \beta 3$ -selective compound is able to block the 'irregular' Fn assembly. This suggests that  $\alpha \nu \beta 3$  is, to some extent, able to bind to fibronectin at another binding site [2].

A hypothetical model for these unexpected results was proposed by *Curnis et al.* [3]. The NGR (Asn-Gly-Arg) sequence, present at four positions in the fibronectin molecule, is able to undergo a rearrangement into *iso*DGR (*iso*Asp-Gly-Arg), which shows activity on  $\alpha \nu \beta 3$  and - with much less potency - on  $\alpha 5 \beta 1$ .

The mechanism of Asn-deamidation has already been known for a long time and has widely been considered to be a process of degradation, acting as a biochemical clock that limits protein lifetimes in vivo [4]. This non-enzymatic *iso*Asp formation can be enzymatically repaired to RGD by the protein-L-*iso*Asp-O-methyltransferase [3].

However, *Curnis et al.* have shown that the asparagine deamidation occurs via hydrolysis of the succinimide intermediate which leads to the formation of DGR or *iso*DGR [3]. The deamidation reactions can take a few hours, days, or years to occur, depending on neighboring amino acid sequences, temperature, buffer composition, and ionic strength. Hence, *Curnis et al.* have shown for the first time that the deamidation process can also increase protein function and does not necessarily lead to functional degradation [3]. So the Asn in the retro-sequence NGR is used as a switching element in the ECM protein fibronectin by rearrangement into *iso*Asp.

This new sequence could be interpreted as a kind of retro sequence of RGD. Such a retro sequence approach had already been investigated by *Wermuth et al.* in 1996, but only a few compounds out of their synthesized library showed activity towards  $\alpha \nu \beta 3$  [5].

Cyclic peptides are well known to adopt stable conformations, which can be determined using NMR techniques. Biologically active peptides incorporating the *iso*DGR sequence can serve as model compounds for the various NGR-containing modules of Fn and may help to elucidate the structure-activity and the structure-selectivity relationships of the *iso*DGR sequence. Additionally, these compounds form a new class of peptidic integrin ligands, whose application potential in biology and medicine is under investigation.

### **Results and Discussion**

The findings of *Curnis et al.* stimulated us to create a library of cyclic peptides containing the *iso*DGR sequence. Biological evaluation of this library showed various new peptides with high activity and selectivity towards the integrin receptor  $\alpha 5 \beta 1$  or towards  $\alpha \nu \beta 3$ .

Table 1. *isoDGR* peptides as integrin ligands

Analogue	$\alpha 5 \beta 1$ (nM)	$\alpha \nu \beta 3$ (nM)
c(-G- <i>isoDGR</i> -G-)	147	106
c(- <b>phg</b> - <i>isoDGR</i> G-)	<b>3.3</b>	518
c(- <b>Phg</b> - <i>isoDGR</i> -G-)	<b>29</b>	>1000
c(-G- <i>isoDGR</i> - <b>Phg</b> -)	643	<b>16.4</b>
c(-G- <i>isoDGR</i> - <b>phg</b> -)	225	<b>6.7</b>

Our goal was to introduce an *isoDGR*-sequence into head-to-tail cyclized pentapeptides. First of all, the *isoDGR*-sequence was surrounded with two flanking glycines to create a structure similar to the GNGRG loops found in Fn [6]. Furthermore, we substituted one of the flanking glycines with phenylalanine (Phe), phenylglycine (Phg), and homophenyl alanine (homoPhe) (Table 1). Surprisingly, our new *isoDGR* peptides show either affinity for the integrin  $\alpha 5 \beta 1$  or no affinity at all. We observed the highest activity and selectivity towards the integrin receptor  $\alpha 5 \beta 1$  with 3.3 nM for the cyclic peptides with D-phenylglycin. But also the peptide with L-phenylglycin showed good activity. All cyclic peptides with a D-*isoAsp* in their sequence show very low affinity for both integrins. Moreover, the inverso peptides of the first library showed very low affinity for the integrins  $\alpha 5 \beta 1$  and  $\alpha \nu \beta 3$ .

After these results, we continued screening in two different directions: we changed the amino acid flanking the Arg and, additionally, synthesized some cyclic hexa-peptides. Surprisingly, both show activity for the  $\alpha \nu \beta 3$  integrin. The comparisons of the peptides with phenylglycine on different positions show different integrin affinity (as depicted in Table 1). The conformation of the active cyclic peptides by NMR spectroscopy is currently under investigation.

We were able to show that it is possible to address the  $\alpha \nu \beta 3$  and  $\alpha 5 \beta 1$  integrin ligands selectively using the recently found *isoDGR* sequence. Our library approach resulted in a series of highly active and already quite selective cyclic pentapeptides that could be used as a basis towards a new class of integrin ligands.

It is important to point out that it seems that nature uses the enzymatic or non-enzymatic rearrangement of Asn to *isoAsp* as a switch to regulate adhesion function.

## References

1. Hynes, R.O. *Nat. Med.* **8**, 918-921 (2002).
2. Takahashi, S., Leiss, M., Moser, M., Ohashi, T., Kitao, T., Heckmann, D., Pfeifer, A., Kessler, H., Takagi, J., Erickson, H.P., Fässler, R. *J. Cell Biol.* **178**, 167-178 (2007).
3. Curnis, F., Longhi, R., Crippa, L., Cattaneo, A., Dondossola, E. Bachi, A., Corti, A. *J. Biol. Chem.* **281**, 36466-36476 (2006).
4. Robinson, N.E., Robinson, A.B. *Proc. Natl. Acad. Sci. U.S.A.* **98**, 944-949 (2001).
5. Wermuth, J., Goodman, S.L., Jonczyk, A., Kessler, H. *J. Am. Chem. Soc.* **119**, 1328 – 1335 (1997).
6. Di Matteo, P., Curnis, F., Longhi, R., Colombo, G., Sacchi, A., Crippa, L., Protti, M.P., Ponzoni, M., Toma, S., Corti, A. *Mol. Immunol.* **43**, 1509-1518 (2006).

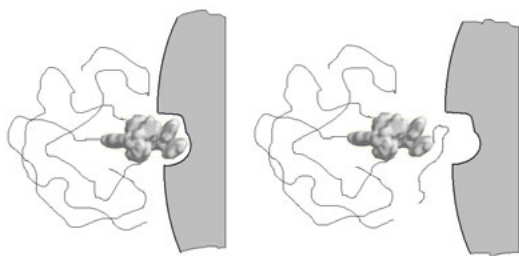
## **PEGylation – A Key Technology to Improve Solubility and Pharmacokinetic of Peptides, Proteins and Other Biopharmaceuticals for Superior Drug Delivery**

**Thomas Bruckdorfer**

*IRIS Biotech GmbH, Waldershof Str. 49-51, D-95615 Marktredwitz, Germany,  
thomas.bruckdorfer@iris-biotech.de*

### **Introduction**

In 2006, the market of modern biopharmaceuticals has reached a volume of over \$40.3 billion in USA and over \$45 billion world wide (IMS Health, Inc.). It is projected to grow to an annual value of some \$100 billion within the next 5 years. The big advantage of proteins, antibodies, siRNA, and other natural products in their usage as drugs is their high specificity in combination with their low side effects. They normally interact with the dedicated target only, and thus do not have activities at any other place in the body. A current focus is the study of modern drug carrier systems where polyethylene glycol linkers are connecting a recognition part with a drug-active part. Such conjugations can reach the size of a nanoparticle. The recognition part can be a peptide or hormone, which binds specifically to the surface of a certain cell. After



*Fig. 1. If the PEG part of the conjugate interferes physically and/or chemically with the receptor pocket, the pharmacological activity of the drug compound is drastically reduced.*

internalization of the whole nanoparticle the active part (DNA or siRNA, for example) is released. Inhibition or activation of certain enzymes or the nucleus follows with the consequence to repair the sick cell, to shut it down by initiating apoptosis or other mechanisms. In conjugation with hydrophobic compounds forming amphiphilic and biodegradable block-copolymers like PEG-PLA (polylactic acid) and PEG-PLGA (copolylactic acid-glycolic acid) sophisticated micelles are formed, where drug molecules can be masked and protected against attacks of the immune system. Modern biopharmaceuticals are ideal drugs; however, their significant

drawback is their low stability under physiological conditions. Due to the fact that they are similar to biological components, they are also easily attacked by the immune system of the body, i.e. by antibodies and proteolytic degradation enzymes. Many efforts have been made by highly sophisticated formulation techniques, special application methods (depots) and chemical modification to improve their pharmacokinetic properties. One recent approach, which shows much better results than other methods tried in the past, is PEGylation, i.e. attaching PolyEthylene Glycol chains (PEG) to the active component. The simplest possibility of PEGylation is attaching a monofunctional PEG chain to a protein, antibody or small drug molecule. Using bifunctional PEGs a link between two compounds can be formed, in order to build dimers or more complex conjugates. Many highly sophisticated compositions are under development and already published.

### **Advanced Applications of PEGs in Drug Carriers**

The simplest possibility of PEGylation is attaching a monofunctional PEG chain to a protein, antibody or small drug molecule. Using bifunctional PEGs with the same or different chemical functional groups enables the capabilities to bridge and link two compounds forming dimers or more complex conjugates. Many highly sophisticated compositions are under development and already published.

A current focus is the study of modern drug carrier systems, where polyethylene glycol linkers are connecting a recognition part with a drug-active part. Such conjugations can reach

the size of a nanoparticle. The recognition part can be a peptide or hormone, which binds specifically to the surface of a certain cell. After internalization of the whole nanoparticle the active part (DNA or siRNA, for example) is released. Inhibition or activation of certain enzymes or the nucleus follows with the consequence to repair the sick cell or shut it down by initiating apoptosis [1-5]. In conjugation with hydrophobic compounds forming amphiphilic and biodegradable block-copolymers like PEG-PLA (polylactic acid) and PEG-PLGA (co-poly(lactic acid-glycolic acid)) micelles are formed, where drug molecules can be masked and protected against attacks of the immune system.

In order to improve the pharmacokinetic properties and the drug performance in general of biopharmaceuticals PEGylation is an efficient tool. It has shown promising results as drug delivery technology and seems to have a bright future, as products are stabilized, which

tend to be degraded under physiological conditions rather quickly. Looking at lead compounds, which have failed in the past in toxicology or clinical studies, PEGylation might help to diminish the toxicologic property. Many more applications are expected in the future, which require tailor made PEG reagents protecting the drug compound properly against the immune system, but not against interactions with the target receptor. A renaissance of failed drugs substances is expected, as PEGylation technology can help to formulate these drugs into safe, stable and efficacious delivery systems.

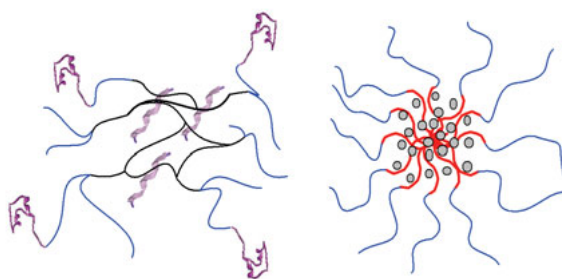


Fig. 2. Modern PEG applications in drug carrier systems conjugated with PEI (polyethyleneimine) forming a polymeric cationic network, which can uptake polyanionic DNA or RNA. Conjugated with hydrophobic parts micelles are formed, which can carry small drug molecules.

## References

1. Duncan, R. *Nature Reviews Drug Discovery* **2**, 347-360 (2003).
2. Veronese, F.M. *Drug Discovery Today* **10**(21) 1451-1457 (2005).
3. PEGylation; *Advanced Drug Delivery Reviews* **54**, 459-476 (2002).
4. Veronese, F.M., Harris, J.M. (Editors); *Peptide and protein PEGylation III: advances in chemistry and clinical applications; Advanced Drug Delivery Reviews* **60**, 1-97 (2008).
5. Morpurgo, M., Veronese, F.M., Kachensky, D., Harris, J.M. *Bioconjug. Chem.* **4**, 314-318 (1993).

## Pegylation of Intermediate Peptides: Thymosin $\alpha_1$ and Growth Hormone-Releasing Factor

Arthur M. Felix and Sandralynn Veech

Ramapo College of New Jersey, School of Theoretical and Applied Science,  
 Mahwah, NJ 07430, U.S.A.

### Introduction

Thymosin  $\alpha_1$  is a natural peptide hormone that circulates in the thymus gland, a gland that plays a critical role in the immune system where T-cells mature. Thymosin  $\alpha_1$  is being used for the treatment of hepatitis B and C in several countries, and is a potential cancer therapy [1]. It is being evaluated as a combination therapy with interferon alpha for the treatment of other immunomodulatory diseases including chronic hepatitis C [2]. Combination therapy of thymosin  $\alpha_1$  with PEG-interferon  $\alpha$ -2a plus Ribavirin is reported to be well tolerated [3]. These preliminary reports encouraged us to prepare pegylated thymosin  $\alpha_1$  for eventual biological studies with interferon or pegylated interferon.

Growth hormone-releasing factor (GRF) stimulates the pituitary gland to release growth hormone (GH), which causes an increase in lean body mass, bone density and skin thickness, and decreases adipose tissue mass [4]. GH is currently being used to treat several conditions, which include pediatric growth hormone deficiency, short stature, and adult growth hormone deficiency. Our goals in this study were to develop conditions for the pegylation of these intermediate-sized peptides, GRF(1-29)-NH<sub>2</sub> and GRF(1-44)-NH<sub>2</sub> as well as the pegylation of thymosin  $\alpha_1$ .

### Results and Discussion

Before modification of GRF(1-29)-NH<sub>2</sub>, GRF(1-44)-NH<sub>2</sub> or thymosin  $\alpha_1$ , a model pentapeptide, H-Leu-Lys(Boc)-Lys(Boc)-Gly-Thr(tBu)-NH<sub>2</sub> was used to optimize pegylation conditions. PEG<sub>2000</sub>-aldehyde was used followed by reduction with NaCNBH<sub>3</sub> in methanol. The crude PEG<sub>2000</sub>-Lys(Boc)-Lys(Boc)-Gly-Thr(tBu)-NH<sub>2</sub> was purified by dialysis, followed by lyophilization and characterized by hydrolysis and amino acid characterization using thin layer chromatography.

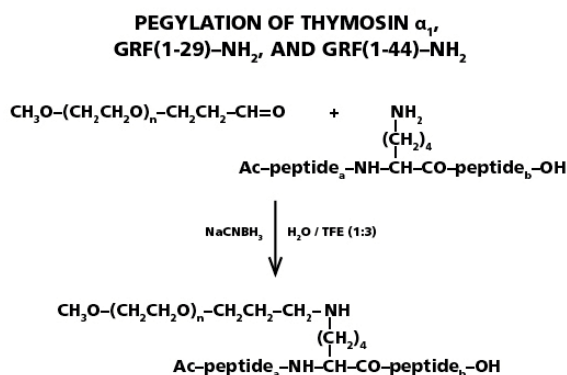


Fig. 1. Procedure for the pegylation of intermediate-sized peptides.

Thymosin  $\alpha_1$  was pegylated by a slightly modified aminoalkylation procedure with PEG<sub>2000</sub>-aldehyde (2.5 eq), followed by reduction with NaCNBH<sub>3</sub> using a novel H<sub>2</sub>O-TFE (1:3) solvent required to maintain complete solubility of the reaction mixture. Purification by dialysis was followed by lyophilization and characterization by hydrolysis and amino acid characterization using thin layer chromatography. This procedure was successfully repeated using various excesses (2.5 and 5.0 eq) of PEG<sub>5000</sub>-aldehyde.

These reaction conditions were extended to include the pegylation of GRF(1-29)-NH<sub>2</sub> and GRF(1-44)-NH<sub>2</sub> using PEG<sub>5000</sub>-aldehyde (Figure 1). It was determined that the optimum conditions for pegylation of these intermediate-sized peptides were achieved using a minimum of 2.5 equivalents of PEG<sub>5000</sub>-aldehyde. Confirmation of structure and successful pegylation were provided by hydrolysis of samples of GRF(1-29)-NH<sub>2</sub> and PEG-GRF(1-29)-NH<sub>2</sub>, followed by thin layer chromatography (Figure 2, left). Similar chromatographic procedures were used for GRF(1-44)-NH<sub>2</sub> and PEG-GRF(1-44)-NH<sub>2</sub> (Figure 2, center) and for thymosin  $\alpha_1$  and PEG-thymosin  $\alpha_1$  (Figure 2, right).



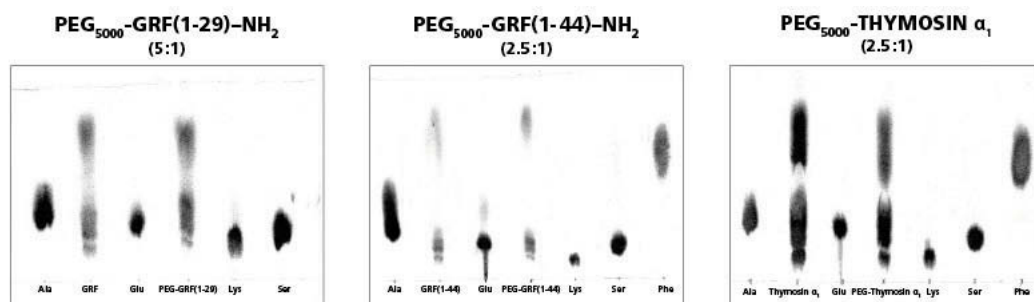


Fig. 2. Hydrolysis/tlc of peptides and pegylated peptides.

Using ESI-MS mass spectrometric methods we were able to confirm the consumption of GRF(1-29)-NH<sub>2</sub> during the pegylation step, but were unable to directly detect PEG-GRF(1-29)-NH<sub>2</sub> by this method.

In conclusion, reaction conditions for the pegylation of GRF(1-29)-NH<sub>2</sub>, GRF(1-44)-NH<sub>2</sub> and thymosin  $\alpha_1$  have been developed using PEG-aldehyde in H<sub>2</sub>O-TFE followed by reduction with NaCNBH<sub>3</sub>. Preliminary *in vitro* studies revealed that combination of thymosin  $\alpha_1$  or PEG-thymosin  $\alpha_1$ , with IFN- $\alpha_2a$  showed no synergistic effects on the virus over IFN- $\alpha_2a$  alone using an A549/EMCV CPE assay system [5]. Plans are being made to carry out additional biological studies to further delineate the advantages of PEG-thymosin  $\alpha_1$ . In addition, since GRF has been reported to be effective in the treatment of growth hormone deficiency in children, and because GH is being used for adult growth hormone deficiency, we anticipate that these PEG-GRF derivatives will be of importance as an alternative to GRF itself due to the many advantages of pegylation.

## Acknowledgments

We thank Dr. Sidney Pestka and his colleagues of Pestka Biochemical Laboratories for carrying out preliminary *in vitro* biochemical assays. We also thank Dr. Marshall Siegel of Wyeth Research for carrying out the ESI-MS mass spectrometric analyses.

## References

1. *Science, Newsfocus* **316**, 682-683 (2007).
2. Andreone, P., Gramenzi, A., Cursaro, C., Flline, F., Loggi, E., D'Erico, A., Spinosa, M., Lorenzini, S., Biselli, M., Bernardi, M. *J. Viral Hepat.* **11**, 69-73 (2004).
3. Camerini, R., Ciancio, A., De Rosa, A., Rizzetto, M. *Annals N.Y. Acad. Sci.* 368-374 (2007).
4. Felix, A.M. *Pharmaceutical Technology* **15**, 28 (1991).
5. Pestka, S., Vy, D., Jubin, R. (unpublished results).

## An Integrated Strategy for Improving Plasma Half-life of Therapeutic Peptides

Hongjian Li,<sup>1</sup> Yi Ma,<sup>1</sup> Tianhong Zhou,<sup>1</sup> Xuemei Huang,<sup>1</sup> Tao Zeng,<sup>1</sup>  
 Yanhong Ran,<sup>1</sup> Meilan Qiu,<sup>1</sup> Xi Zhou,<sup>2</sup> and Zhengding Su<sup>2,3</sup>

<sup>1</sup>Department of Biotechnology, Jinan University, Guangzhou, Guangdong 510632 China;

<sup>2</sup>Amersino Biodevelop Inc. Kitchener and <sup>3</sup>Department of Chemistry, University of Waterloo,  
 Waterloo, Ontario N2L 3G1, Canada

### Introduction

Peptides are viable biopharmaceutical agents because of their superior specificity and their smaller size [1]. The clinical application of peptides has been limited by their susceptibility to proteolysis. Of many strategies for improving their pharmacokinetics, coupling therapeutic peptides to serum albumin or a peptide (protein) domain that will allow association with albumin, represents a promising strategy for extending the circulation half-life ( $t_{1/2}$ ) of peptides [2-3]. In this work, we demonstrate the application of native plasma proteases to sustained release albumin-protected peptides in order to achieve the effective peptide concentration *in vivo*, using glucagon like peptide-1 (GLP-1), a potent therapeutic peptide for Type 2 diabetes [4], as model.

### Results and Discussion

A fusion polypeptide was designed in such a construction that it can associate with human serum albumin (HSA). The fusion polypeptide is composed of three functional segments: a therapeutic peptide (PEP), an albumin-binding peptide (ABP) and a protease-cleavable linker (LK). One simple constitution of the fusion polypeptide is ABP-LK-PEP. Human thrombin (TBN) is used as scissors to release the therapeutic peptide from the polypeptide, as TBN is a sequence-specific protease for the amino acid sequence of FNPR-GA/P/S.

We selected ABPs by biopanning a M13 phage-peptide library against HSA. One peptide exhibited high affinity binding to HSA and the sequence of the peptide is LPHSHRAHSLPP. Therefore, three ABP-LK-GLP fusion polypeptides were constructed based on selected ABP (Figure 1a), and prepared by recombinant peptide expression system [5]. These fusion polypeptides exhibited very similar binding affinities for HSA to their cognate ABP moieties alone measured by surface plasma resonance (SPR), as shown in Figure 1b for GP62 fusion polypeptide.

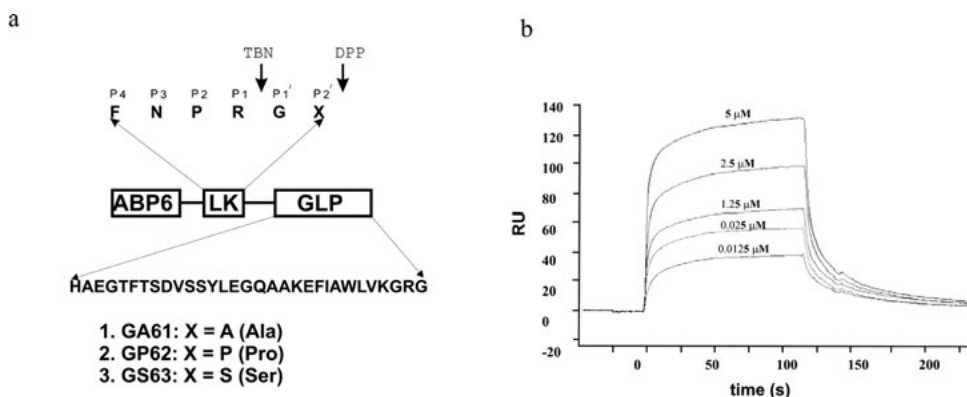


Fig. 1. The construction of albumin-associated GLP-1 fusion polypeptides is shown in detail with TBN-cleavable sequences and the GLP-1 peptide (a). The binding affinity of GP62 fusion polypeptide to HSA was assayed using SPR.

Table 1. The  $t_{1/2}$  (hours) of ABP-LK-GLP fusion polypeptides

Peptide (nM)	TBN	DPP IV	HSA ( $\mu$ M)	GLP-1	GA61	GP62	GS63
10	+	-	0	ND	$4.2 \pm 0.4$	$5.6 \pm 0.8$	$2.6 \pm 0.3$
10	+	-	600	ND	$8.7 \pm 0.8$	$8.9 \pm 0.7$	$6.8 \pm 0.7$
100	+	-	600	ND	$8.5 \pm 0.6$	$9.2 \pm 0.5$	$6.7 \pm 0.4$
10	+	+	0	0.063	$4.1 \pm 0.4$	$5.8 \pm 0.3$	$2.5 \pm 0.3$
10	+	+	600	0.077	$8.6 \pm 0.5$	$9.5 \pm 0.4$	$6.7 \pm 0.5$
100	+	+	600	0.068	$8.4 \pm 0.4$	$9.8 \pm 0.5$	$6.5 \pm 0.3$

Note that all errors are expressed as standard deviation ( $\pm$ s.d.). ND, not determined.

In *in-vitro* experiments, TBN can function as scissors to release GLP-1 from three ABP-LK-GLP fusion polypeptides in a simulated plasma environment. The half-life of these fusion polypeptides is summarized in Table 1. Fusion polypeptides containing FNPR-GA/P linker exhibited longer half-lives than those containing FNPR-GS linker. The presence of HSA in reactions significantly increased the half-life of polypeptide against TBN-cleavage. For instance, the half-life of GP62 polypeptide is increased two-fold when reaction mixture contains 600  $\mu$ M HSA. Furthermore, our data suggests that the presence of DPP IV does not affect the half-life of fusion polypeptides, regardless if reaction solutions contain HSA or not.

Through protease-mediated hydrolysis, ABP-LK-GLP polypeptides can generate active GLP-1 peptide as detected by HPLC (data not shown). The amount of GLP-1 released from polypeptides with FNPR-GA/P linkers reached a maximum within 4 hrs. Afterwards, the GLP-1 concentration in these reactions decreased because of the sensitivity of the two N-terminal residues (i.e., HA) of GLP-1 to DPP IV. On the other hand, we found that DPP IV can also recognize GS dipeptide but its turnover is slower than that of GA/P dipeptide.

In future work, we are planning to examine whether GP62 fusion polypeptides has the same biological activity *in vivo* as GLP-1 as well as exendin-4. Nevertheless, this work represents a new direction in the design of effective controlled delivery systems simply utilizing plasma environment. Sustained release of GLP-1 from albumin-associated fusion polypeptides is not only just one example of this strategy, but also provides a promising treatment for Type-2 diabetes. Moreover, our strategy could be applied to other therapeutic peptides as well as small molecules, providing an alternative approach to improving the pharmacokinetics of many medicinal compounds.

## Acknowledgments

This work was funded by China National Center of Biotechnology Development (2009ZX09103-606).

## References

1. Marx, V. *C&EN News* **83**, 17-24 (2005).
2. Pawar, R., Ben Ari, A., Domb, A.J. *Expert. Opin. Biol. Ther.* **4**, 1203-1212 (2004).
3. Dennis, M.S., et al. *J. Biol. Chem.* **277**, 35035-35043 (2002).
4. Baggio, L.L., Huang, Q., Brown, T.J., Drucker, D.J. *Diabetes* **53**, 2492-2500 (2004).
5. Su, Z., Vinogradova, A., Koutychenko, A., Tolatchev, D., Ni, F. *Protein Eng. Des. Sel.* **17**, 647-657 (2004).

## **PEGylation of the Anorexigenic Peptide Neuromedin U Yields a Promising Candidate for the Treatment of Obesity**

**Paolo Ingallinella,<sup>1</sup> Andrea Peier,<sup>2</sup> Karolina Zytko,<sup>1</sup> Annalise Di Marco,<sup>3</sup>  
Kunal Desai,<sup>2</sup> Ying Qian,<sup>2</sup> Edith Monteagudo,<sup>4</sup> Ralph Laufer,<sup>3</sup>  
Donald J. Marsh,<sup>2</sup> Elisabetta Bianchi,<sup>1</sup> and Antonello Pessi<sup>1</sup>**

*IRBM P. Angeletti, <sup>1</sup>MRL Peptide Center of Excellence, <sup>3</sup>Pharmacology, <sup>4</sup>DMPK, 00040 Pomezia (Rome) Italy, <sup>2</sup>Department of Metabolic Disorders, Merck Research Laboratories, P.O. Box 2000, RY80T-126, Rahway, NJ 07065, U.S.A.*

### **Introduction**

Neuromedin U (NMU) is a highly conserved peptide, widely distributed throughout the body with particular abundance in the central nervous systems (CNS), gastrointestinal and genitourinary tracts. NMU has two high affinity G-protein coupled receptors: NMUR1, which is widely expressed in the peripheral tissues, and NMUR2, which is mainly expressed in the CNS. Originally isolated for its ability to contract uterine smooth muscle, NMU has later been found implicated in many physiological processes, including stress, nociception, immunity, inflammation, blood pressure, feeding and energy homeostasis. The latter role in particular is supported by a wealth of pharmacologic and genetic data [1,2], including the report that acute and chronic central administration of NMU in mice inhibits food intake and increases energy expenditure, and that NMU-deficient mice are hyperphagic and obese, while transgenic mice overexpressing NMU are lean and hypophagic. In addition, an association has been found between NMU gene variants and obesity in humans [1,2].

While the above literature suggests the potential of NMU as an anti-obesity agent, the typical liabilities of native peptides (proteolytic degradation, rapid renal clearance) preclude its direct use as therapeutic. Derivatization with poly(ethylene)glycol ("PEGylation") has emerged as a promising method to extend circulatory half-life, decrease metabolism and immunogenicity of peptides and proteins [3]. These improvements are correlated with the size of the attached polymer, with larger sizes being more effective. PEGylation however typically reduces the biological activity of the attached molecule, because of steric hindrance preventing access to and/or recognition of the receptor, and this decrease is also correlated with increasing PEG size. In addition, the effect is dependent on the specific site of attachment of the polymer [3]. Overall therefore, development of a PEGylated peptide/protein requires multi-parameter optimization, which is molecule-specific. Here we describe the development of a PEGylated analog of NMU.

### **Results and Discussion**

The sequence of human NMU is shown in Table 1. The peptide hormone consists of 25 amino acids and has a carboxy-terminal amide, which is essential for biological activity. While the N-terminal region of the peptide differs in length and/or amino acid composition between species, the C-terminal region (aa 19-25) is remarkably conserved, and indeed has been shown to be the biologically active part of the molecule [1] (Table 1).

To determine the minimal size of a PEGylated NMUR agonist, we prepared four PEGylated analogs of increasing length, starting from the C-terminus: NMU<sub>19-25</sub>, NMU<sub>12-25</sub>, NMU<sub>7-25</sub> and full-length NMU. All were synthesized with an extra-Cys residue at the N-terminus, to enable chemoselective ligation with maleimido-activated PEG.

As expected, PEGylation dramatically reduced the *in vitro* potency of the shorter-length analog, and the effect of shielding was progressively attenuated in the analogs with PEG farthest from the C-terminus. Still, C(PEG40)NMU was 10-40-fold less potent than the naked peptide. The control peptide C(NEM)NMU showed that N-terminal addition of cysteine did not influence the activity.

Accordingly, we found that the conjugation chemistry did not significantly influence potency. Taking advantage of the absence of other amine groups in the sequence, we PEGylated full-length NMU by regioselective amide bond formation between the N-terminus and N-hydroxysuccinimide-PEG. PEG40-NMU and C(PEG40)NMU are comparably potent (Table 1).

Table 1. Activity of NMU and analogs on the human receptors NMUR1 and NMUR 2

Peptide	Sequence <sup>a</sup>	EC <sub>50</sub> (nM) <sup>b</sup>	
		hR1	hR2
NMU	FRVDEEFQSPFASQSRGYFLFRPRN	2.3	1.4
Ac-NMU	Ac-FRVDEEFQSPFASQSRGYFLFRPRN	4.8	2.6
Ac-NMU <sub>19-25</sub>	Ac-FLFRPRN	0.6	2.8
C(PEG40)NMU <sub>19-25</sub>	Ac-C (PEG40) -Tds-FLFRPRN	>1000	>1000
C(PEG40)NMU <sub>12-25</sub>	Ac-C (PEG40) -ASQSRGYFLFRPRN	434	>1000
C(PEG40)NMU <sub>7-25</sub>	Ac-C (PEG40) -FQSPFASQSRGYFLFRPRN	227	224
C(PEG40)NMU	Ac-C (PEG40) -FRVDEEFQSPFASQSRGYFLFRPRN	36	109
C(PEG20)NMU	Ac-C (PEG20) -FRVDEEFQSPFASQSRGYFLFRPRN	20	37
C(PEG5)NMU	Ac-C (PEG5) -FRVDEEFQSPFASQSRGYFLFRPRN	5.8	12
C(NEM)-NMU	Ac-C (NEM) -FRVDEEFQSPFASQSRGYFLFRPRN	8.9	5.2
PEG40-NMU	(PEG40) -FRVDEEFQSPFASQSRGYFLFRPRN	125	147

<sup>a</sup>All peptides C-terminal carboxyamide; NEM, N-ethyl-maleimide; Tds = 1-amino-4,7,10-trioxa-13-tridecamine succinimic acid; PEG40 is a branched PEG, PEG20 and PEG5 are linear PEGs of 40, 20 and 5 kDa average molecular weight, respectively. <sup>b</sup>Calcium mobilization assay using cell lines expressing the human NMU receptors

We then explored if reducing PEG size would mitigate the loss of activity, and produced C(PEG20)NMU and C(PEG5)NMU. While the in vitro potency of the derivative with 20 kDa PEG was comparable to that with 40 kDa PEG, the derivative with 5 kDa PEG was equipotent to the parent peptide (Table 1). However, this smaller PEG size was not sufficient to modulate the pharmacokinetic properties appropriately (see below).

Based on the above data, a number of PEGylated NMU analogs were profiled in vivo. We found that the significantly lower potency in vitro was more than compensated by the superior pharmacological properties, resulting in a performance in vivo considerably better than the native peptide.

First, unlike the parent peptide, which has a half-life of <5 min in mice, PEG40-NMU showed excellent pharmacokinetics in lean mice upon subcutaneous and intravenous administration (10 and 1 mg/kg respectively), with a half-life of 25 hours, a clearance of 0.03 ml/min/kg, and 47% bioavailability. Similar results were obtained for C(PEG40)-NMU.

Second and more important, in diet-induced obese (DIO) mice a single subcutaneous administration of 10 mg/kg of PEG40-NMU induced robust food intake suppression, accompanied by body weight loss, which lasted for three days (51% food intake reduction relative to vehicle on day 1, 57% on day 2, and 22% on day 3). At the same dose (which corresponds to approximately 10-fold higher molar dose), native NMU showed an effect only on the first day after administration (45% food intake reduction relative to vehicle). These data clearly indicate the benefit of the improved pharmacological profile brought by PEGylation. The derivatives with smaller-size PEG (20 and 5 kDa) both showed greater acute efficacy than PEG40-NMU at the same molar dose (99% and 79% food intake reduction relative to vehicle on day 1), but their duration of action was reduced to two and one day post-administration, respectively. Overall, N-terminal PEGylation with a 40 kDa polymer appears the best compromise to maximize the biological potency of the peptide.

In conclusion, PEGylation of human NMU yields analogs, able to induce robust and long-acting food intake and body weight reduction upon subcutaneous administration, which represent promising leads for an anti-obesity peptide therapeutic.

## Acknowledgments

We thank Fabrizio Fiore and Giuseppe Mesiti, Fabio Bonelli, Simone Bufali, and Simona Cianetti for help with the experiments, Gennaro Ciliberto and Nancy Thornberry for advice throughout this study.

## References

- Brighton, P.J., Szekeres, P.G., Willars, G.B. *Pharmacol. Rev.* **56**, 231–248 (2004).
- Peier, A., et al. *Endocrinol.* **150**, 3101–3109 (2009).
- Kang, J.S., DeLuca, P.P., Lee, K.C. *Expert Op. Emerging Drugs* **14**, 363–380 (2009).

## Structure-Property of PEGylated Peptides in Normal and Renal Insufficient Rat Models

Kevin Yin, Sarah Walter, Amos Baruch, Shawn Alexander, Eiketsu Sho,  
 Felix Karim, Steven Harrison, and Derek Maclean

KAI Pharmaceuticals, Inc., South San Francisco, CA 94080, U.S.A.

### Introduction

PEGylation is an important approach for prolonging the *in vivo* half-life of therapeutic peptides. PEGylation typically reduces renal clearance and proteolytic digestion of the peptide. However, these advantages are often accompanied by some loss in potency as a result of steric interference between the PEGylated peptide and its target.

We explored PEGylation as a technique to modify the pharmacokinetic profile of therapeutic peptides. We report the results of various PEGylation strategies investigated in normal rats and in a rat model of renal insufficiency.

### Results and Discussion

Aspects of PEGylation chemistry which have been explored include polymer length (5–40 kDa), site of attachment, linkage chemistry (disulfide, amide, alkane and thioether) and spacers of different length and rigidity. As expected, 40 kDa PEG conjugates presented the most attractive PK profile in rats, with an *in vivo* half life of >10 hours (Figure 1). In conjunction with the extended plasma exposure of these PEG adducts, losses in potency were observed correlating with polymer length, but independent of the structure of the PEGylated moiety (Figure 2).

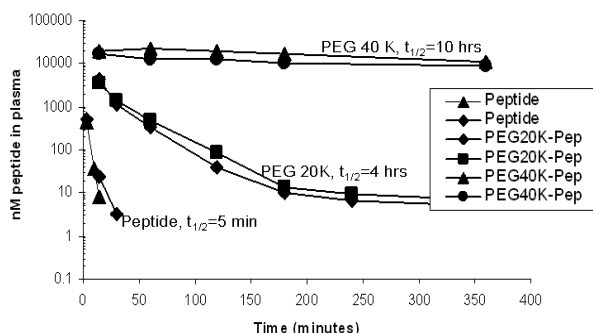


Fig. 1. PK of PEG conjugates in Normal Rats. In normal rats, addition of 20 kDa PEG extended  $t_{1/2}$  about 50 fold while addition of a 40 kDa PEG extended  $t_{1/2}$  more than 100 fold over non-PEGylated peptide.

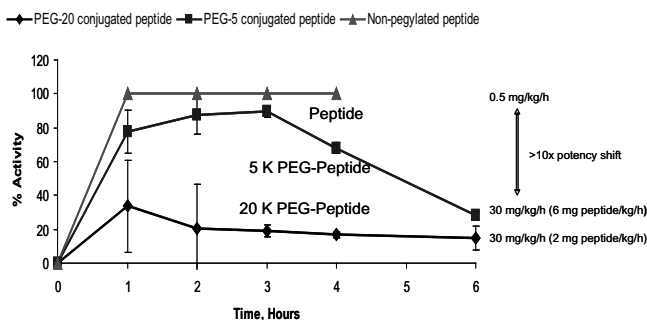


Fig. 2. Effect of 5K & 20K PEG on Potency in Normal Rats. In normal rats, loss of the potency upon PEGylation was correlated to the size of the PEG but independent of the PEGylation site in conjugate structure (data not shown).

In disease indications where patients have renal insufficiency, PEG adducts of smaller size may be sufficient to achieve prolonged drug exposure. In a rat model of renal insufficiency, 5 kDa and 20 kDa PEGylated analogs of selected peptides showed a similar *in vivo* half life of 6 hours (Figure 3), suggesting that low molecule weight PEG offers the same level of protection as high molecule weight PEG in the absence of renal clearance. Low molecule weight PEG (2 kDa and 5 kDa) may be expected to have minimal effect on the intrinsic potency of the peptide, but can potentially contribute to the stability of the peptide in the absence of renal clearance. These studies may help the design of PEGylated peptides for optimal application in disease indications in which different clearance pathways dominate.

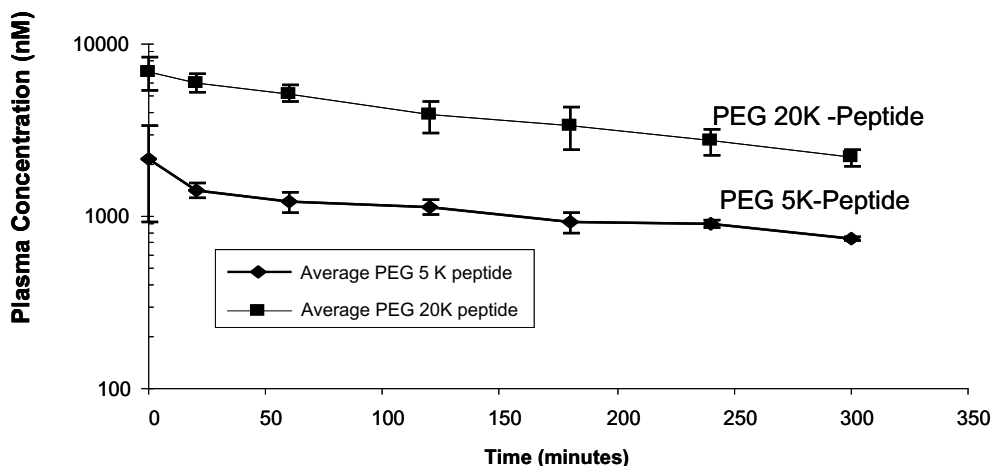


Fig. 3. **PK of 5K & 20K PEG-Peptide in Rat Model of Renal Insufficiency.** In a disease model of renal insufficiency, both the 5 kDa PEG and the 20 kDa PEG provided similarly prolonged drug exposure for a therapeutic peptide.

## Conclusions

PEGylation provided extended pharmacokinetic profile for a peptide therapeutic. The addition of a 40 kDa PEG extended the  $t_{1/2}$  about 100 fold compared to non-PEGylated peptide in normal rats. PEGylation was associated with loss of potency of a peptide therapeutic. In normal rats, the potency shift was correlated with the size of the PEG but was independent of the PEGylation site. In a rat model of renal insufficiency, 5 kDa and 20 kDa PEGylated peptides had similar *in vivo* half-lives, suggesting that, in the absence of renal clearance, drug exposure was independent of the size of the PEG which may allow PEGylation strategy to focus on minimizing loss of potency.

These studies may help the design of PEGylated peptides for optimal application in disease indications in which different clearance pathways dominate.

## References

1. Harris, J.M, Chess, R.B. *Nature Reviews Drug Discovery* **2**, 214-221 (2003).
2. Greenwald, R.B. *Critical Reviews in Therapeutic Drug Carrier Systems* **17**(2), 101-161 (2000).
3. Abuchowski, A., et al. *J. Biological Chem.* **252**, 3578-81 (1977).

## Development of Compstatin Derivative-Albumin Binding Peptide Chimeras for Prolonged Plasma Half-Life

Hongchang Qu, Paola Magotti, Daniel Ricklin, and John D. Lambris

Department of Pathology and Laboratory Medicine, University of Pennsylvania,  
 Philadelphia, PA 19104, U.S.A.

### Introduction

Complement is a powerful arm of the innate immune system and a bridge to adaptive immunity, which plays important roles in antimicrobial defense and apoptotic cell clearance [1]. Under normal conditions, complement activation is tightly controlled by various fluid-phase and cell-surface-bound regulatory proteins. However, inappropriate or excessive complement activation can overwhelm this delicate balance and cause host tissue damage as implicated in many pathological conditions including age-related macular degeneration (AMD), rheumatoid arthritis, sepsis, ischemia-reperfusion injuries and graft-rejection during transplantation etc. [2]. In 1996, our laboratory discovered a peptide named Compstatin (H-Ile-c[Cys-Val-Val-Gln-Asp-Trp-Gly-His-His-Arg-Cys]-Thr-NH<sub>2</sub>) that selectively binds to human and primate complement component 3 (C3) and its active fragment C3b, and effectively inhibits complement activation [3]. Many years of optimization have led to the development of a largely improved Compstatin analog (Figure 1, **1**, IC<sub>50</sub>=205 nM), which is 264-fold more potent than the original peptide [4]. Recently, a Compstatin derivative successfully completed a phase I clinical trial under the name POT-4 (Potentia Pharmaceuticals, Inc.) for the treatment of AMD and showed a highly beneficial safety and toxicity profile. Once injected intravitreally, it forms a gel-like deposit in the eye, which slowly releases active peptide over a prolonged period of time. The size of the deposit is depending on the amount of peptide injected [5]. In contrast to these advantageous properties for local injection in the eye, the relatively short in vivo half-life of Compstatin so far limited its potential for diseases requiring systemic administration. Conjugation of drugs to an albumin binding peptide (ABP: Ac-RLIEDICLPRWGCLWEDD-NH<sub>2</sub>, IC<sub>50, human</sub>=467 nM) has been described as a promising approach to significantly increase peptide half-life by taking advantage of the transporter/depot function of the highly abundant serum albumin [6]. Therefore, we have designed two chimeric peptides (**2** and **3**), in which ABP was conjugated to a Compstatin derivative (**1**) in either N-terminal or C-terminal position via a mini-PEG linker (Peptides International, Louisville, KY). Advanced peptide synthesis protocols were used since both Compstatin and ABP contain one disulfide bridge each that has to be formed sequentially. Their activities were investigated using ELISA and surface plasmon resonance (SPR).

### Results and Discussion

The conjugated linear peptide chimeras were synthesized manually on MBHA Rink amide resin via Fmoc chemistry. DIC and HOBt were used for all coupling reactions. To avoid shuffling of the two distinct disulfide bonds, the two pairs of cysteine were orthogonally protected with Trt and Ac<sub>m</sub> groups, respectively. After the peptides were cleaved from the resin with concurrent Trt group removal, they were subjected to air oxidation to form the first disulfide bond. The resulting products were purified by reverse-phase HPLC and lyophilized. They were then treated with AgOTf in TFA/anisole to remove the Ac<sub>m</sub> protecting group. The second disulfide bond was formed when the deprotected peptides were treated with a 1N HCl/DMSO (1:1)

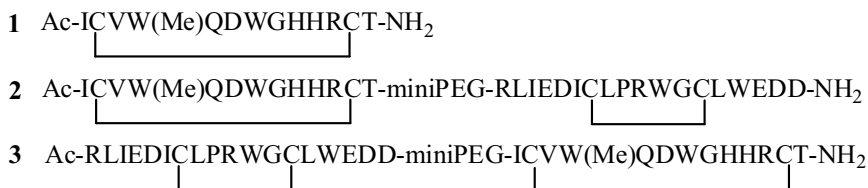


Fig. 1. Sequences of peptide **1** and chimeric peptides **2** and **3**.



Table 1. Results of ELISA and SPR studies of compstatin analogues

Peptide	$IC_{50}$ ( $\mu M$ , CP)	$IC_{50}$ ( $\mu M$ , AP)	$k_{on}$ ( $10^5 M^{-1} s^{-1}$ )	$k_{off}$ ( $10^{-3} s^{-1}$ )	$K_D$ (nM)
<b>1</b>	0.22	0.20	9.9	11.0	11.0
<b>2</b>	0.83	0.36	4.2	6.5	15.3
<b>3</b>	0.48	0.40	4.9	7.0	14.5

solution [7]. Reverse-phase HPLC purification provided the final products with >95% purity. The inhibitory activities of the purified chimeras were tested using ELISA in human serum and their kinetic profiles were assessed on immobilized C3b using a Biacore 2000 instrument [8]. The results are summarized in Table 1. Both chimeric peptides displayed an only slightly decreased inhibitory potency (2-4 fold) for both the classical pathway (CP) and alternative pathway (AP) of complement activation. According to the SPR analysis, the drop in binding affinity was even lower (1.3-1.4 fold), which can be primarily attributed to slower  $k_{on}$  rates because of the increased size of the peptides. Additional ELISA assays (data not shown) show that the chimeric peptides are able to bind both C3 and human serum albumin simultaneously. The collective data indicate that both chimeras are equally potent in serum. Considering the long half-life of human albumin (20 days), the compound is very likely to have significantly increased plasma half-life in human. To determine the plasma half-life of **3** in mice, the peptide was injected into the mouse tail vein. Plasma samples at different time points (up to 24 hour) were collected and analyzed using LC-MS. Our preliminary results indicate that the peptide is still detectable 24 hours after the initial injection. Thus, the chimeric peptides represent promising candidates for the treatment of a broader range of diseases associated with imbalanced complement activation.

In conclusion, chimeras containing a Compstatin derivative and ABP were successfully constructed using a combination of solid phase and solution phase peptide synthesis techniques. ELISA and SPR assays show that their ability to inhibit complement activation is mostly retained, and the position of peptide **1** in the chimeras does not affect their activity. Preliminary in vivo experiments in mice suggest that these chimeras feature a largely improved plasma half-life. Further in vivo investigations in primates are planned and data will be reported in due course.

## Acknowledgments

This work was supported by National Institutes of Health grants GM062134 and AI068730.

## References

1. Ricklin, D., Lambris, J.D. *Nat. Biotechnol.* **25**, 1265-1275 (2007).
2. Sjöberg, A.P., Trouw, L.A., Blom, A.M. *Trends Immunol.* **30**, 83-90 (2009).
3. Sahu, A., Kay, B.K., Lambris, J.D. *J. Immunol.* **157**, 884-891 (1996).
4. Katragadda, M., Magotti, P., Sfyroera, G., Lambris, J.D. *J. Med. Chem.* **49**, 4616-4622 (2006).
5. Patent WO 2009046198.
6. Dennis, M.S., Zhang, M., Meng, Y.G., Kadkhodayan, M., Kirchhofer, D., Combs, D., Damico, L.A. *J. Biol. Chem.* **277**, 35035-35043 (2002).
7. Tamamura, H., Otaka, A., Nakamura, J., Okubo, K., Koide, T., Ikeda, K., Ibuka, T., Fujii, N. *Int. J. Pept. Protein Res.* **45**, 312-319 (1995).
8. Magotti, P., Ricklin, D., Qu, H., Wu, Y., Lambris, J.D. *J. Mol. Recognit.* *In press*.

## Peptide Regulators of Protein-Protein Interactions with Selectivity for Specific Sub-Cellular Compartments

Nir Qvit, Marie-Helene Disatnik, and Daria Mochly-Rosen

Department of Chemical and Systems Biology, Stanford University School of Medicine,  
Stanford, CA 94305, U.S.A.

### Introduction

Protein kinase C (PKC) is a large family of 11 serine/threonine homologous isozyme kinases that are key enzymes in many signaling events as well as in disease states such as cancer [1], heart failure [2] and regulation of the immune response [3]. There are two major domains in PKC: (a) a conserved C-terminal catalytic domain, and (b) a N-terminal regulatory domain. Although the catalytic region in different PKC isozymes is highly conserved, each isozyme mediates unique cellular functions. There are no commercial isozyme-specific activators of PKC and the commercial inhibitors target the conserved catalytic domain of the enzyme and thus fail to be PKC isozymes-specific. The regulatory domain contains a C1 and C2 domains that play a critical role in PKC activation and translocation through interactions with second messengers, phospholipids, and inter- and intra-molecular protein-protein interactions [4]. Relevant to this study, we showed that peptides derived from the C2 domain regulate the activity of single PKC isozyme by regulating isozyme-specific protein-protein interactions [4].

PKC delta ( $\delta$ PKC) isozyme participates in a variety of signal transduction pathways such as apoptosis [5], cell proliferation [6] and tumor suppression [7], and plays a significant role in many diseases such as cancer [8], stroke [9] and cardiac ischemia [10]. We previously described the use of  $\delta$ V1-1 and  $\delta\psi$ RACK,  $\delta$ PKC-selective antagonist and agonist, respectively. They were rationally designed [4] and are referred to here as: "First generation peptide regulators".  $\delta\psi$ RACK induces translocation of  $\delta$ PKC to several sub-cellular sites where the enzyme phosphorylates select substrates.  $\delta$ V1-1 blocks  $\delta$ PKC translocation to all these sites and inhibits the interaction of PKC to its downstream signaling pathway [11] whereas  $\delta\psi$ RACK induces translocation to these sites.

Focusing on  $\delta$ PKC, we sought to identify new regulators that are selective in regulating the biological activity of  $\delta$ PKC related to a particular disease without affecting other house-keeping functions.

### Results and Discussion

Based on the structure of the  $\delta$ PKC C2 domain, a series of short peptides was developed using a rational approach designed to regulate  $\delta$ PKC interaction with selective substrate at each sub-cellular sites. Four second generation peptides,  $\delta$ -P4.5,  $\delta$ -P5,  $\delta$ -P7 and  $\delta$ -P11 (5-10 amino acids long) were generated. These peptides were conjugated to TAT<sub>47-57</sub> peptide for cell permeability.

PKC activation results in translocation of the enzyme from the cell soluble to the cell particulate fraction.  $\delta$ PKC translocation to different sub-cellular compartments was determined in *in vitro* and *in vivo* models. In the *in vitro* model cardiac-fibroblasts were treated with the C2 domain-derived peptides and Myristoylated Alanine-Rich C Kinase (MARCKS) phosphorylation was determined as a marker of PKC activation. In the *in vivo* model, mouse hearts were treated with the C2 domain-derived peptides and  $\delta$ PKC translocation was measured to determine the specificity of the respective peptides for  $\delta$ PKC. We previously showed that the 1<sup>st</sup> generation peptides,  $\delta\psi$ RACK, induces translocation of  $\delta$ PKC to the mitochondria and  $\delta$ V1-1 inhibits the translocation of  $\delta$ PKC to the mitochondria. We demonstrated that  $\delta$ -P4.5, a 2<sup>nd</sup> generation peptide, induces  $\delta$ PKC translocation to the mitochondria in *in vitro* and *in vivo* models (similar to the  $\delta$ PKC activator,  $\delta\psi$ RACK).

$\delta$ PKC translocation to sub-cellular compartments was then determined in rat hearts subjected to ischemia/reperfusion, which mimics myocardial infarction (MI), in the presence of various peptides. Infarct size and stress markers (e.g. level of JNK phosphorylation) were determined.  $\delta$ -P4.5 was found to be a selective  $\delta$ PKC translocation activator, inducing  $\delta$ PKC translocation to the mitochondria, yet mediating tissue protection from ischemia and reperfusion; the infarct size decreased by 50% in the presence of  $\delta$ -P4.5 and JNK1, JNK2

Table 1. Summary of biological results regarding the 1<sup>st</sup> and 2<sup>nd</sup> generation  $\delta$ PKC regulating peptides

	$\delta$ -P4.5 - 2 <sup>nd</sup> generation	$\delta$ -V1-1 - 1 <sup>st</sup> generation
Selective $\delta$ PKC translocation	Activator	Inhibitor
$\delta$ PKC translocation regulator	Inducing translocation specifically to the mitochondria	Inhibiting translocation to all sub-cellular sites
CPK (cytolysis)	Decrease	Decrease
TTC staining (live tissue)	Protection	Protection
Cell death	Decrease	Decrease
Cardiac ischemic damage	Protection	Protection

activation were inhibited by  $\sim 70\%$ . This cardiac protection was similar to that achieved by the translocation inhibitor  $\delta$ V1-1 [11]. Furthermore creatine phosphokinase (CPK) release, a tissue damage marker, was decrease by 50% when the hearts were subjected to  $\delta$ -P4.5, during ischemia/reperfusion.

We previously suggested that the C2 domain of PKC participates in critical protein-protein interactions [12]. We therefore extended the search for a new generation of peptides that may help to map the interaction sites on the surface of the  $\delta$ PKC C2 domain. A series of four 2<sup>nd</sup> generation peptides were developed using rational based design. These peptides were used to identify the role of  $\delta$ PKC in protection from cardiac ischemic damage. One peptide,  $\delta$ -P4.5, was found to: i) induce MARCKS phosphorylation in *in vitro* assay; ii) induce  $\delta$ PKC translocation to the mitochondria in *in vivo* and induces  $\delta$ PKC translocation in MI model and iii) mediate tissue protection from ischemia and reperfusion in that model. See Table 1 for comparison between  $\delta$ -P4.5, 2<sup>nd</sup> generation peptide and  $\delta$ -V1-1, 1<sup>st</sup> generation peptide.

*How do both the  $\delta$ PKC activator ( $\delta$ -P4.5) and inhibitor ( $\delta$ -V1-1) protect the heart from ischemic injury?*

We conclude that based on the present results we suggest that  $\delta$ -P4.5 inhibits access to only one substrate in the mitochondria, and thus lead to inhibition of  $\delta$ PKC function at that site. This sub-cellular-specific translocation inhibitor represents a 2<sup>nd</sup> generation peptide regulator, which may provide unique tools to regulate cell signaling.

## Acknowledgments

Supported by grant NIH HL52141 for DM-R.

## References

1. Kim, J., et al. *Cancer Res.* **68**, 6831-6839 (2008).
2. Murphy, S., Frishman, W.H. *Cardiol. Rev.* **13**, 3-12 (2005).
3. Tanaka, M., et al. *Circulation* **110**, II194-II199 (2004).
4. Churchill, E.N., Qvit, N., Mochly-Rosen, D. *Trends Endocrinol. Metab.* **20**, 25-33 (2008).
5. Murriel, C.L., et al. *J. Biol. Chem.* **279**, 47985-47991 (2004).
6. Braun, M.U., Mochly-Rosen, D. *J. Mol. Cell. Cardiol.* **35**, 895-903 (2003).
7. Lu, Z., et al. *Mol. Cell Biol.* **17**, 3418-3428 (1997).
8. Weinstein, I.B. *Princess Takamatsu Symp.* **22**, 277-283 (1991).
9. Inagaki, K., et al. *Circulation* **108**, 2304-2307 (2003).
10. Bright, R., et al. *J. Neurosci.* **24**, 6880-6888 (2004).
11. Inagaki, K., Mochly-Rosen, D. *J. Mol. Cell. Cardiol.* **39**, 203-211 (2005).
12. Brandman, R., et al. *J. Biol. Chem.* **282**, 4113-4123 (2007).

## Potent Inhibitors of PHEX Derived from Succinic Acid Hydroxamates

Elaref S. Ratemi,<sup>1</sup> Mostafa Hatam,<sup>1</sup> Denis Gravel,<sup>1</sup> Philippe Crine,<sup>2</sup>  
Guy Boileau,<sup>2</sup> and Isabelle Lemire<sup>2</sup>

<sup>1</sup>Departments of Medicinal Chemistry; and <sup>2</sup>Pharmacology, Enobia Pharma Inc.,  
2901 Rachel Street East, Montreal, Quebec, Canada

### Introduction

Osteogenesis is a complex biological process that includes proliferation and differentiation of bone-forming cells (osteoblasts), synthesis of an organic matrix composed mainly of type I collagen, and mineralization of the organic matrix by deposition of hydroxyapatite crystals. These physiologic processes are controlled by circulating hormones and local factors. Various technologies have been developed to stimulate osteogenesis for bone regeneration in osseous reconstructive surgery. These include the use of bone morphogenetic proteins (BMPs) as osteogenic agents, mostly in combination with a solid support such as metal meshes [1], atelopeptide type I collagen [2] or hydroxyapatite [3]. Mutations in the *PHEX* gene, a gene encoding a peptidase (formerly *PEX*; Phosphate regulating gene with homologies to endopeptidases on the X chromosome), are responsible for X-linked hypophosphatemic rickets. Numerous observations indicate that mineralization of the bone matrix could be under the control of still uncharacterized peptidergic systems, and establish PHEX as a putative target to regulate osteogenesis.

### Results and Discussion

Results presented in Figure 1 clearly indicate that sPHEX (a soluble form of PHEX) is capable of inhibiting <sup>45</sup>Ca incorporation [4] into the secreted bone matrix of rat osteoblast in culture; the extent of inhibition was dose dependent. These results suggest that PHEX peptidase activity is capable of inactivating a peptide involved in the stimulation of the mineralization of the bone matrix deposited by cultures of rat osteoblasts. This peptide, still to be identified, thus appears to be part of an autocrine loop acting on mineralizing osteoblasts. Decreasing PHEX peptidase activity with specific inhibitors might therefore provide a useful strategy for potentiating this putative mineralizing peptide.

We first investigated a series of simple aromatic hydroxamates as potential PHEX inhibitors. This series which lacks the omnipresent carboxylic acid side chain in P'1 of our previous series (mercaptoacyl dipeptide) was initiated with the aim of finding a new hydrophobic binding pocket in the vicinity of the chelated zinc atom at the active site of PHEX. Although the number of varied structures remains small, no relevant hits were found; all compounds showed IC<sub>50</sub> values in the low millimolar range. When an aspartic acid side chain equivalent to the P'1 position was introduced, low micromolar and submicromolar inhibitors were initially obtained (Table 1, compounds 1-4).

This result, obtained with a new series of inhibitors, therefore confirms our original notion of the importance of an aspartic acid pharmacophore at this position of the inhibitor for good biological activity. Table 1 shows that even though the S'2 of the enzyme tolerates aromatic moieties as was expected, it is rather specific in terms of the substitution on the

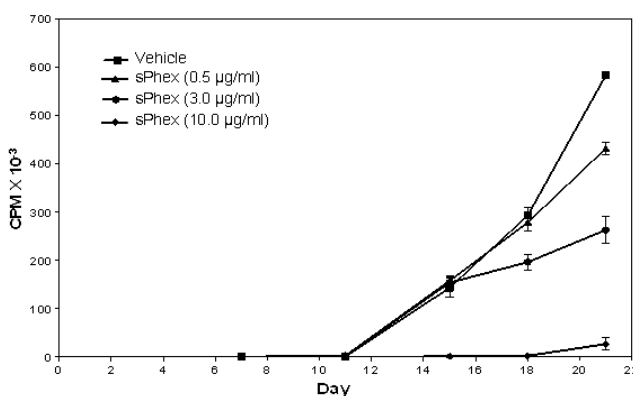


Fig. 1. Inhibition of mineralization by sPHEX.

Table 1. Influence of the P'2 pharmacophore on potency in the succinic hydroxamate series

Cpd#	R	IC50 (nM)	Cpd#	R	IC50 (nM)
1		860	6		190
2		560	7		360
3		1700	8		240
4		5000	9		270
<b>5</b>		<b>17</b>	10		54

aromatic rings. As indicated, the best hydroxamate inhibitor of this series, compound **5**, stands at 17 nM. The *S* enantiomer of **5**, which was prepared through a stereoselective synthesis using the Evan's auxiliary-based method, had an IC50 of 9 nM.

Compound **5** was chosen for study in an animal model (Rat mandibular defect [5]) and was shown to possess very encouraging osteogenic properties. Analysis (microcomputed tomography and scanning electron microscopy) of the defects treated with implant of porous hydroxyapatite in absence of PHEX inhibitor show bone formation after 14 days of healing. The addition of the PHEX inhibitor **5** to hydroxyapatite particles at a concentration of  $1 \times 10^{-5}$  M, a concentration that completely inhibits PHEX, reduced significantly bone formation compared to saline suggesting that the rate of healing has been negatively affected by high concentration of this compound. On the contrary, lower concentrations of PHEX inhibitor significantly stimulated bone formation. It is worth mentioning here that **5** is not an inhibitor of NEP. These results are consistent with the observation that PHEX inhibitors have a biphasic effect on mineralization by cultured cells, and also suggest that low doses of PHEX inhibitors could be used in vivo as osteogenic agents in order to stimulate the bone healing process.

## Acknowledgments

We thank the National Research Council (Canada) for an IRAP grant.

## References

1. Vehof, J.W., et al. *Plast. Reconstr. Surg.* **108**, 434-443 (2001).
2. Ikeuchi, M., et al. *J. Biomed. Mater. Res.* **60**, 61-69 (2002).
3. Yoshida, K., et al. *J. Dent. Res.* **78**, 1505-1510 (1999).
4. Ecarot, B., Desbarats, M. *Endocrinology* **140**, 1192-1199 (1999).
5. Bellows, C.G., Aubin, J.E., Heersche, J.N., Antosz, M.E. *Calcif. Tissue Int.* **38**, 143-154 (1986).

## Design and Synthesis of Mercaptoacyl Dipeptides as Potent and Selective PHEX Inhibitors

Elaref S. Ratemi,<sup>1</sup> Denis Gravel,<sup>1</sup> Philippe Crine,<sup>2</sup> Guy Boileau,<sup>2</sup> and Isabelle Lemire<sup>2</sup>

<sup>1</sup>Departments of Medicinal Chemistry; and <sup>2</sup>Pharmacology, Enobia Pharma Inc.,  
 2901 Rachel Street East, Montreal, Quebec, Canada

### Introduction

Osteogenesis is a complex biological process that includes proliferation and differentiation of bone-forming cells (osteoblasts), synthesis of an organic matrix composed mainly of type I collagen, and mineralization of the organic matrix by deposition of hydroxyapatite crystals. Mutations in the PHEX gene are responsible for X-linked hypophosphatemic rickets. This human genetic disease is characterized by undermineralization of the bone extracellular matrix amongst other clinical features. There have been many observations indicating the involvement of PHEX in mineralization/ undermineralization of the bone matrix which establish PHEX as a putative target to regulate osteogenesis.

### Results and Discussion

During our search [1] for a suitable substrate for PHEX, we discovered that unlike NEP, which shows a wide specificity for its S<sub>1</sub>' and S<sub>2</sub>' pockets, PHEX showed a very restricted specificity for the same sub-sites. Of all peptides tested as putative PHEX substrates (approximately 15 different peptides) only PTHrp<sub>107-139</sub> was cleaved. It was cleaved at three positions, all in amino-terminus of aspartate residues indicating a strong specificity of the S<sub>1</sub>' pocket for this residue (Figure 1). Support for this conclusion came later when libraries of short internally-quenched fluorogenic peptides [2] were screened against PHEX. We learned that the P'1 aspartic acid could also be flanked by a more hydrophobic residue at P'2 such as phenylalanine, tyrosine or tryptophan. Building on the above information, we initially prepared simple derivatives containing the P'1 aspartic acid side chain mimic, the thiol zinc-binding group, and an amino acid in P'2 (**HS-CH<sub>2</sub>-CH(CH<sub>2</sub>CO<sub>2</sub>H)CO-amino acid**). We examined a whole host of charged, uncharged, polar uncharged, non-polar and hydrophobic natural and non-natural amino acids at P'2. This effort yielded a dozen compounds or so where activities ranged from low micromolar to sub-micromolar. In an attempt to increase binding, we explored the mercaptoacyl moiety as the zinc-binding group. We also envisioned that additional binding could later be explored by installing an  $\alpha$ -substituent on the mercaptoacyl group (vide infra). The initial efforts in this series focused on optimizing the P'2 site. All the derivatives in this series have the mercaptoacyl group as the ligand with an aspartic acid residue in P'1 and different amino acids (AA) in P'2 (Figure 2). Unfortunately, this series also resulted in only sub-micromolar activity (Figure 2).

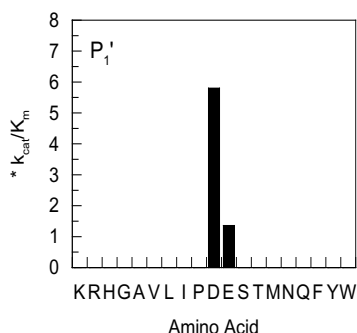


Fig. 1. Specificity of the S'1 pocket of PHEX.

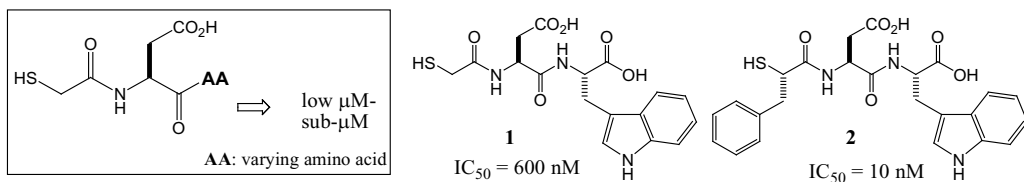
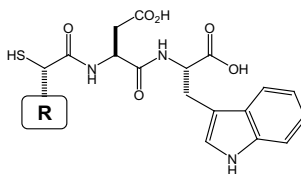


Fig. 2. Contribution of the P1 pharmacophore.

Table 1. Optimization of the P1 pharmacophore



Compound	R	IC <sub>50</sub> (nM)	Compound	R	IC <sub>50</sub> (nM)
2	Benzyl	10	10	Phenethyl	4
3	4-Methoxybenzyl	20	11	Hydroxymethyl	48
4	4-F-Benzyl	6	12	3-Hydroxy-3-methyl	4
5	Phenyl	2	13	Methyl	68
6	2-Naphthylmethyl	15	14	Isopropyl	6
7	2-Indolylmethyl	23	15	Isobutyl	94
8	Biphenylmethyl	8	16	<i>n</i> -Butyl	7
9	4-Benzoxylbenzyl	8	17	Cyclohexylmethyl	20

As exemplified in Figure 2, a major breakthrough in our endeavors came when we decided to explore the potential of gaining additional binding by seeking to introduce a ligand in the S1 pocket of the enzyme. In the event, introduction of a P1 benzyl group, derived from phenylalanine, gave an inhibitor, compound **2**, with an IC<sub>50</sub> of 10 nM, which constitutes a sixty fold increase in potency (**1** versus **2**, Figure 2). Another important observation is that changing the stereochemistry of the chiral center bearing the benzyl group from S to R leads to a complete loss of the advantage of a group in the S1 pocket. In an effort to draw maximum benefit from the P1 pharmacophore, we explored in greater detail binding in the S1 pocket. As can be seen by examination of Table 1, the S1 pocket of PHEX is very receptive to hydrophobic pharmacophores of various sizes and selective single-digit nanomolar PHEX inhibitors can be designed and synthesized.

Finally, it is noteworthy that although ACE and NEP are also metalloproteinase bearing a zinc atom at the active site, they differ in a very important way from PHEX in the sense that the S'1 pockets bind inhibitors [3] having a hydrophobic residue in P'1 which is in complete contrast to PHEX which binds inhibitors having an aspartic acid residue in that position. Replacing L-aspartic acid with its D enantiomer led to about a seven fold loss of potency. Substituting aspartic acid for glutamic acid resulted in a major drop in potency, and replacing L-Asp for L-Leu which has a hydrophobic side chain led to a complete loss of activity. A number of potent inhibitors of PHEX were tested against NEP and they were relatively inactive. These results augur well for the endeavor of developing selective inhibitors of PHEX.

## Acknowledgments

We thank the National Research Council (Canada) for an IRAP grant.

## References

1. Boileau, G., Tenenhouse, H.S., DesGroseillers, L., Crine, P. *Biochem J.* **355**, 707-713 (2001).
2. Carvalho, K.M., Boileau, G., Camargo, A.C., Juliano, L. *Anal Biochem.* **237**, 167-173 (1996).
3. Bertini, I., et al. *J. Med. Chem.* **48**, 7544-7559 (2005).

## Synthesis and Biological Activity of New Esters of Acyclovir

Ivanka G. Stankova,<sup>1</sup> Stoyan Shishkov,<sup>2</sup> Angel S. Galabov,<sup>3</sup>  
 and Tsenka S. Milkova<sup>1</sup>

<sup>1</sup>Department of Chemistry, South-West University "Neofit Rilski", 2700 Blagoevgrad, Bulgaria;

<sup>2</sup>St. Kl. Ohridski Sofia University, Faculty of Biology, Laboratory of Virology, Sofia 1164, Bulgaria; and

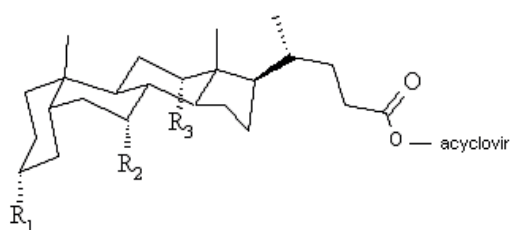
<sup>3</sup>The Stephan Angeloff Institute of Microbiology, Bulgarian Academy of Sciences, 1113 Sofia, Bulgaria

### Introduction

Acyclovir, 9-[(2-hydroxyethoxy)methyl] guanine (ACV), demonstrates high specificity against Herpes simplex virus (type I and type II) and varicella-zoster viruses. It is comparatively more active against the Herpes simplex virus. It has been applied successfully at viral infections. This therapeutic agent is not toxic, no resistance is observed at its application. One of the problems connected with its practical use is its poor bioavailability – 15% [1-3]. It causes a serious problem for medical treatment of AIDS suffering or transplantation undergoing patients. In order to improve the acyclovir bioavailability the drug valacyclovir (L-Val-acyclovir ester) was obtained in 1992. It is the famous and the most used acyclovir prodrug in practice today. In the living organisms it is rapidly transformed into acyclovir and valine. The advantage of this analogue is its higher bioavailability (nearly 60%). Possibility to make the acyclovir delivery across the cell membrane easier is its conjugation to amphiphilic transport molecules. Valacyclovir bioavailability improvement by bile acids modification was recently reported in literature. It was found that the valacyclovir connection to chenodeoxycholic acid increases two times its bioavailability. The aim of this study was to design and to synthesize new esters of acyclovir with bile acid and to explore their activity on the HSV-1, HSV-2.

### Results and Discussion

Acyclovir esters with bile acids (cholic, deoxycholic acid and chenodeoxycholic acid) were prepared by DDC mediated condensation. A mixture of bile acid and DDC in dimethylformamide (DMF) was stirred for 1 h at nitrogen atmosphere. A solution of acyclovir and 4-*N*, *N*-(dimethylamino)-pyridine (DMAP) was added to the reaction mixture and stirred for 24 h. Then DMF was evaporated *in vacuo* and the residue was chromatographed on silica gel, using 1:4 MeOH:CH<sub>2</sub>CH<sub>2</sub>. The <sup>1</sup>H and <sup>13</sup>C-NMR, mass-spectra were consistent with desired structure (Figure 1).



$R_1=OH$ ;  $R_2=OH$ ;  $R_3=OH$ - cholic acid

$R_1=OH$ ;  $R_2=H$ ;  $R_3=OH$ -deoxycholic acid

$R_1=OH$ ;  $R_2=OH$   $R_3=H$ -chenodeoxycholic acid

Fig. 1. Acyclovir esters.

acyclovir (Figure 2). The tested compounds significantly inhibited replication in dose-dependent manner without apparent cytotoxicity. They had markedly similar effect as the reference drug. IC<sub>50</sub> for the cholic acid-Acv was 2.9 μg/ml and for chenodeoxycholic-Acv it was 8.7 μg/ml in comparison with the value for acyclovir – 1.2 μg/ml. Deoxycholic-Acv did not suppress replication of HSV-1. The viral replication after addition of 20 μg/ml was suppressed completely with both substances.

### Biological activity

#### Cytotoxicity *in vitro*.

The compounds were applied in concentration range from 20 to 1 μg/ml. The data showed no effect on the morphology of the cell cultures. Therefore the value of MTC could not be determined. This is probably due to the natural components of the compound.

#### Inhibitory effect of the substances on the replications of HSV-1 and HSV-2.

The associations of the molecule of acyclovir with cholic acid (chlol-Acv) and chenodeoxycholine (Ksdeochlol-Acv) added in concentrations 1, 2, 5, 10 and 20 μg/ml preserved inhibitory activity of



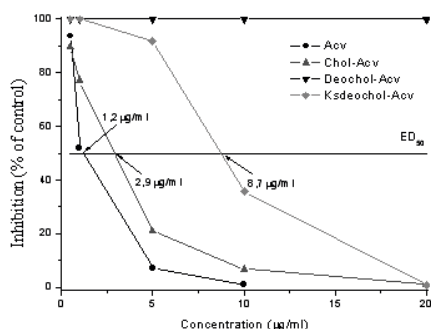


Fig. 2. Inhibitory activity on HSV-1.

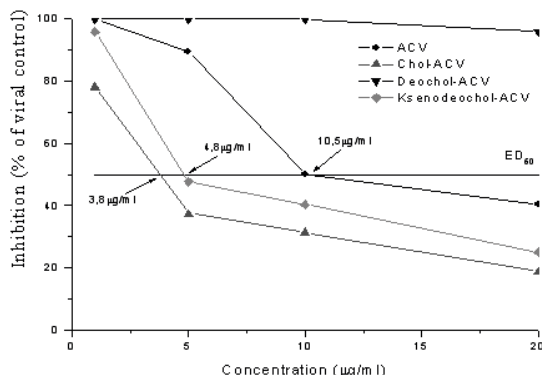


Fig. 3. Inhibitory activity on HSV-2.

The results of treatment of cells infected with HSV-2 with the tested substances are presented in Figure 2. The effects were similar to the effect on the replication of HSV-1. The difference in the values of  $ED_{50}$ , is relatively insignificant (4.8  $\mu\text{g/ml}$  and 10.5  $\mu\text{g/ml}$ ). Different results for inhibitory effect against HSV-1 and HSV-2 may be due to different thymidine kinase activity of the viruses.

Results of this study indicate that the investigated substances show strong antiviral effect against the replication of HSV type 1 and type 2 in cell line MDBK. Hence, our results can be considered as an early step in elucidating the possibility for application of the investigated derivatives against acyclovir-resistant strains of HSV-1 and HSV-2.

## Acknowledgments

We gratefully acknowledge financial support from the South-West University, Blagoevgrad.

## References

1. Anand, B.S., Mitra, A.K. *Pharm. Res.* 1194–1202 (2002).
2. Beauchamp, L.M., Orr G.F., de Miranda, P., Burnette, T.C., Krenitsky, T.A. *Antiviral Chem. Chemother.* **3**, 157–164 (1992).
3. Beauchamp, L.M., Krenitsky, T.A. *Drugs Future* **18**, 619–628 (1993).

## Engineering of Better HIV Entry Inhibitor Peptides through Chemical Modification

Junpeng Xiao<sup>1</sup> and Thomas J. Tolbert<sup>1,2</sup>

<sup>1</sup>Interdisciplinary Biochemistry Graduate Program; <sup>2</sup>Department of Chemistry,  
University of Indiana, Bloomington, IN 47405, U.S.A.

### Introduction

Entry inhibitor peptides are a new class of antiretroviral drugs for the treatment of HIV infection. T20 (also known as Fuzeon, Enfuvirtide, or DP-178) is the only one in this class approved by FDA [1]. Although T20 has been successfully used in the treatment of HIV infection, it still faces many challenges. For example, T20 is a synthetic peptide that requires 106 steps to synthesize, which is costly and time-consuming. It has low solubility at neutral pH, short half-life in human serum and HIV strains resistant to T20 have been reported recently [2]. Herein, we describe a successful method for the biosynthesis of the T20 and another HIV entry inhibitor peptide C37H6, and efforts to improve their solubility, biological activity and half-life through chemical modification of the expressed peptides.

### Results and Discussion

The HIV entry inhibitor peptides T20 and C37H6 were expressed in bacteria as fusion proteins containing a TEV protease cleavage sequence (Scheme 1). The SUMO-T20 fusion protein with a TEV protease cleavable sequence was expressed and purified from *E. coli*. The SUMO-T20 fusion protein was then cleaved by TEV protease to produce N-terminal cysteine containing T20 peptide (Scheme 1a) [3]. The GPRT-C37H6 fusion protein with a TEV protease cleavable sequence was also expressed and purified from *E. coli*. The GPRT-C37H6 fusion protein was then cleaved by TEV protease to produce N-terminal cysteine containing C37H6 peptide (Scheme 1b) [4].

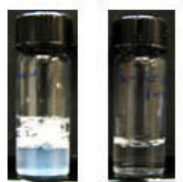
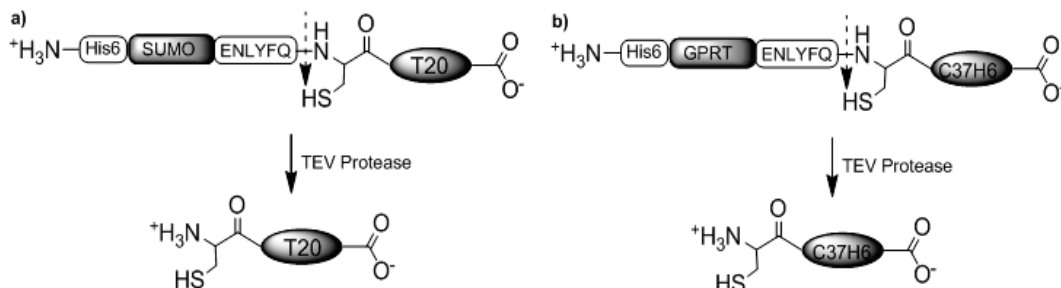


Fig. 1. Betaine modification increases the solubility of T20.

To increase the solubility of T20, the N-terminal cysteine of T20 was modified with a quaternary ammonium betaine group using native chemical ligation (NCL). The betaine modified T20 showed increased solubility and reduced aggregation propensity compared to the unmodified T20 (Figure 1). In addition, the betaine modified T20 can function as an aggregation inhibitor to prevent the aggregation of the unmodified T20 in a mixture of the two peptides. CD spectroscopy and HIV fusion inhibition assay indicate that the betaine modification of T20 does not significantly affect the structure and inhibition activity of the T20 peptide [3].

To increase the inhibition activity of C37H6, the N-terminal cysteine of C37H6 was modified with azide and alkyne moieties. The azide and alkyne modified C37H6 peptides were coupled together to produce a C37H6 homodimer. The alkyne modified C37H6 was also coupled to two diazide linkers with different linker lengths to form linker-conjugated



Scheme. 1. The strategies for the biosynthesis of N-terminal cysteine containing T20 and C37H6.

homodimers. The azide modified C37H6 was coupled to a trialkyne linker to form a linker-conjugated homotrimer. All the dimers showed slightly increased potency compared to the C37H6 monomer, and the long linker-conjugated dimer has the best inhibition activity (3-fold better). To further increase the activity, longer linkers might be used in the future. The C37H6 trimer showed slightly decreased inhibition activity, which might be due to the short space between the linker and the peptides.

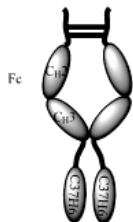


Fig. 2. Structure of IgG Fc-C37H6.

To increase the half-life of C37H6, a fusion protein of IgG Fc-C37H6 was expressed and purified from yeast (Figure 2), in which the C37H6 peptide was fused to the C-terminus of the antibody fragment immunoglobulin G fragment crystallizable (IgG Fc). Although the IgG Fc-C37H6 fusion proteins (different glycoforms) were less potent than the C37H6 peptide (18~33 fold worse), the serum half-life of the IgG Fc-C37H6 fusion protein should be increased because of the long serum half-life of IgG Fc. In conclusion, we have demonstrated approaches to improving the solubility, activity, and half-life of HIV entry inhibitor peptides through chemical modification of the expressed peptides.

## Acknowledgments

We thank Alex Burn for assistance in cloning of the SUMO-T20 fusion protein plasmid. We thank Jonathan A. Karty and Angela M. Hansen for assistance in mass spectrometry. We thank Brian S. Hamilton for assistance in the CD measurements. We gratefully acknowledge Indiana University Bloomington for financial support for this work. We thank Interdisciplinary Biochemistry Graduate Program at Indiana University Bloomington for the Peglow Travel Award.

## References

1. Krambovitis, E., Porichis, F., Spandidos, D.A. *Acta. Pharmacol. Sin.* **26**, 1165-1173 (2005).
2. Briz, V., Poveda, E., Soriano, V. *J. Antimicrob. Chemother.* **57**, 619-627 (2006).
3. Xiao, J., Burn, A., Tolbert, T.J. *Bioconjugate Chem.* **19**, 1113-1118 (2008).
4. Tolbert, T.J., Franke, D., Wong, C.H. *Bioorg. Med. Chem.* **13**, 909-915 (2005).

# Synthesis and Conformational Analysis of a Natural Peptide Inhibitor of HIV-1 Integrase

**Marta De Zotti,<sup>1</sup> Francesca Damato,<sup>1</sup> Fernando Formaggio,<sup>1</sup> Marco Crisma,<sup>1</sup> Elisabetta Schievano,<sup>1</sup> Stefano Mammi,<sup>1</sup> Bernard Kaptein,<sup>2</sup> Quirinus B. Broxterman,<sup>2</sup> Peter J. Felock,<sup>3</sup> Daria J. Hazuda,<sup>3</sup> Sheo B. Singh,<sup>3</sup> Jochem Kirschbaum,<sup>4</sup> Hans Brückner,<sup>4</sup> and Claudio Toniolo<sup>1</sup>**

<sup>1</sup>ICB, Padova Unit, CNR, Department of Chemistry, University of Padova, 35131 Padova, Italy; <sup>2</sup>DSM Pharmaceutical Products, Advanced Synthesis, Catalysis and Development, 6160 MD Geleen, The Netherlands; <sup>3</sup>Merck Research Laboratories, Rahway, NJ 07065 and West Point, PA 19486; U.S.A.

<sup>4</sup>Department of Food Sciences, University of Giessen, 35392 Giessen, Germany

## Introduction

Integramide A, an effective inhibitor of the coupled reaction of HIV-1 integrase, is a 16-mer linear peptide characterized by nine C<sup>α</sup>-methylated α-amino acids [five Iva, isovaline, and four Aib, α-aminoisobutyric acid, residues (Figure 1)] that was isolated from fungal extracts of *Dendrodochium* sp. The amino acid sequence was fully elucidated by the Merck group a few years ago [1]. On the other hand, the chiral sequence was only partially determined. In particular, the precise stereochemistry of the Iva<sup>14</sup>-Iva<sup>15</sup> dipeptide (known to contain one D- and one L-residue) near the C-terminus was not reported.

We solved this unsettled issue by performing *via* solution methods the total chemical independent syntheses of both L-D and D-L 16-mer diastereomers and compared their chromatographic and spectroscopic properties with those of the natural inhibitor [2].

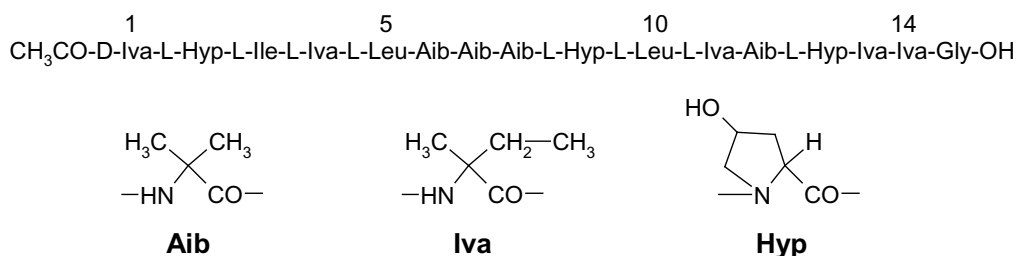


Fig. 1. Amino acid sequence of integramide A and chemical structures of Aib, Iva, and Hyp. Here, Hyp is (2*S*, 4*R*)-4-hydroxyproline.

## Results and Discussion

The occurrence in the sequence of integramide A of as many as nine poorly reactive residues (Aib and Iva), including di- and tripeptide stretches, precludes an efficient peptide synthesis by the solid-phase approach. Therefore, we decided to synthesize by solution methods the L-Iva<sup>14</sup>-D-Iva<sup>15</sup> and D-Iva<sup>14</sup>-L-Iva<sup>15</sup> 16-mer diastereoisomeric peptides. To speed up the preparation of the two peptides and allow, in the future, a relatively fast synthesis of additional analogues, we followed a segment-condensation strategy [2].

Taking into account (i) the racemization risks associated with segment couplings, (ii) the acid lability of the Aib-Pro(Hyp) amide bond, and (iii) the remarkable tendency of the H-Aib-Pro- N-terminal dipeptide sequence to cyclize to the Aib-Pro diketopiperazine, we designed and prepared 4 segments: **A** (CH<sub>3</sub>CO-D-Iva-OH), **B** (residues 2-8), **C** (residues 9-12), and **D** (residues 13-16). **B**, **C** and **D** were N- and C-protected with Z and OtBu, respectively, whereas the secondary alcoholic function of the three L-Hyp residues was left unprotected. After selective removal of the protecting groups, the four segments were covalently linked (from **D** to **A**) by means of the highly effective EDC/HOAt activation procedure. The yields of each individual coupling step were from moderate to good (50-85%).

The two 16-mer peptides and their synthetic intermediates were characterized by HPLC, NMR, mass spectrometry, and chiral chromatography (with Chirasil-L-Val) analysis on the total acid hydrolyzates.

For the unambiguous assignment of the Iva<sup>14</sup>-Iva<sup>15</sup> stereochemistry of the natural integramide A, we relied on HPLC and NMR techniques. In particular, we observed that the HPLC retention times and the NMR chemical shifts of a natural sample (obtained from a purified fungal extract) were perfectly matching those of the synthetic L-Iva<sup>14</sup>-D-Iva<sup>15</sup> diastereoisomer [2].

We also performed an in-depth conformational analysis of the two final synthetic compounds and selected intermediates, of different main-chain length, in the crystal state (by X-ray diffraction) and in solvents of different polarities (using CD, FT-IR absorption, and 2D NMR techniques). By a combination of HMBC, HMQC, NOESY, and TOCSY experiments we were able to assign all proton and carbon NMR resonances. These data, together with molecular dynamics calculations, were also extremely useful to elucidate the preferred 3D-structure (Figure 2) for integramide A: a helical conformation characterized by the alignment on one face of all three L-Hyp residues.

Overall, our 3D-structural results have provided useful information to shed light on the mechanism of inhibition of HIV-1-integrase, an important target for anti-HIV therapy.

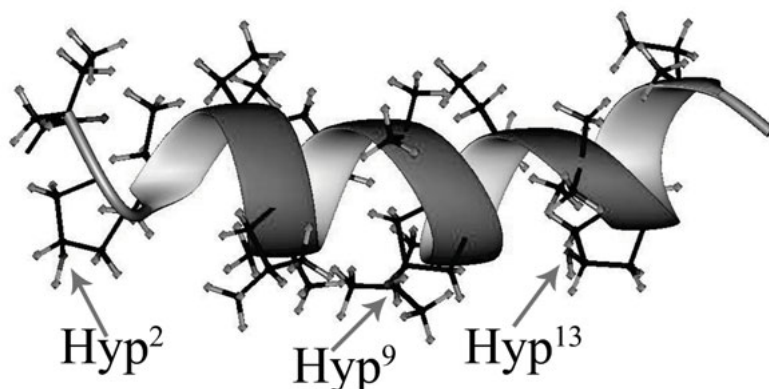


Fig. 2. Representation of the 3D-structure with the lowest energy obtained for integramide A from 2D-NMR experiments and molecular dynamics calculations. The three L-Hyp residues are located on the same face of the amphiphilic helical structure.

## References

1. Singh, S.B., Herath, K., Guan, Z., Zink, D.L., Dombrowski, A.W., Polishook, J.D., Silverman, K.C., Lingham, R.B., Felock, P.J., Hazuda, D.J. *Org. Lett.* **4**, 1431-1434 (2002).
2. De Zotti, M., Formaggio, F., Kaptein, B., Broxterman, Q.B., Felock, P.J., Hazuda, D.J., Singh, S.B., Brückner, H., Toniolo, C. *ChemBioChem* **10**, 87-90 (2009).

## Functional Reconstruction of Structurally Complex Protein Binding Sites Using CLIPS<sup>TM</sup> Technology

Peter Timmerman,<sup>1,2</sup> Wouter C. Puijk,<sup>1</sup> Jerry W. Slootstra,<sup>1</sup>  
 Peter van Dijken,<sup>1</sup> and Rob H. Melen<sup>1,3</sup>

<sup>1</sup>Pepscan Therapeutics B.V., Zuidersluisweg 2, 8243 RC Lelystad, the Netherlands; <sup>2</sup>Van 't Hoff Institute for Molecular Sciences, University of Amsterdam, the Netherlands; and  
<sup>3</sup>Academic Biomedical Centre, University of Utrecht, the Netherlands

### Introduction

Many proteins exert their biological activity through small regions of their folded surfaces, which could be replaced by small “designer” molecules retaining the local bioactive surface, while displaying improved pharmacodynamic and kinetic properties [1]. Such protein mimics could have enormous potential for the development of (therapeutic) antibodies [2], where an increasing number of protein targets is difficult to address with classical therapies (HIV, GPCR's). Occasionally, short linear peptides have been shown to adequately mimic the function of a whole protein, but this approach is largely limited to unstructured N- and C-termini [3]. For mimicry of conformational and/or discontinuous binding sites linear peptides generally fail, because they do not adopt the correct secondary and/or tertiary structure. For that purpose, more elaborate tools are needed to position correctly the important functionalities in space, which is an absolute prerequisite for activity.

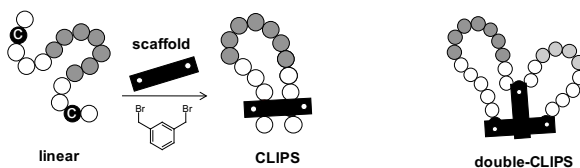


Fig. 1. Structural fixation of peptides via CLIPS technology.

We recently developed a novel and generic technology for structural fixation of linear peptides (Figure 1) [4-6]. This technology, termed **CLIPS<sup>TM</sup>** (Chemical **L**inkage of **P**eptides onto **S**caffolds, (<http://www.pepscan.com>), is applicable to peptides in solution as well as on microarrays used for epitope mapping (PEPSCAN method). This technology has proven to be an extremely valuable tool for 1) binding site mapping of therapeutically relevant mAbs, 2) generating hyperimmune sera via immunization with **CLIPS** peptides, and 3) the generation of monoclonal antibodies (mAbs) via the use of hybridoma technology. Currently, we have data available for more than 50 therapeutic drugs.

Here we describe the development of peptide-based **CLIPS** mimics of Follicle Stimulating Hormone (hFSH), a protein involved in fertility regulation [6]. The hormone is a heterodimer, consisting of a common  $\alpha$ -subunit and a unique, hormone-specific  $\beta$ -subunit. *In vivo* neutralization of hFSH has been considered a viable option for contraceptive therapy in men.

### Results and Discussion

Epitope mapping studies with an anti-FSH monoclonal antibody (6602) with high neutralizing activity for hFSH using overlapping libraries of 12- to 18-mer **CLIPS** peptides (1-12, 2-13, 3-14, etc.) showed that this mAb binds to a highly conformational binding site located mainly at the top of  $\beta$ 3-loop (core is R<sub>62</sub>-L<sub>73</sub>). It was found that for 12-mer peptides

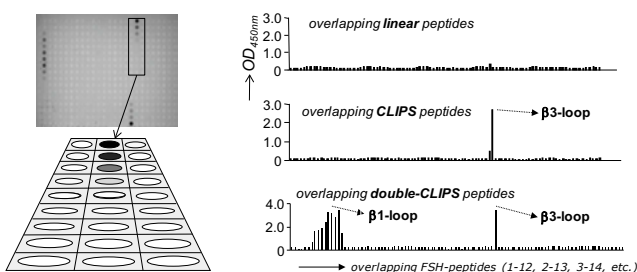


Fig. 2. Mapping of anti-FSH monoclonal antibody 6602 using **CLIPS** peptides derived from FSH.

the binding of **CLIPS** variants was far superior to linear peptides (Figure 2), while for longer peptides (18-mers) the difference in binding levelled off. Furthermore, libraries of overlapping double-loop **CLIPS** peptides (Figure 1) also showed strong binding for peptides derived from the top of the  $\beta$ 1-loop (residues E<sub>16</sub> and R<sub>18</sub>). This showed that the binding site for mAb 6602 on FSH- $\beta$  is also discontinuous in nature, covering residues on top of both the  $\beta$ 3- and  $\beta$ 1-loop region. These results illustrate nicely the use of **CLIPS** technology to aid in visualizing binding sites on proteins that were “invisible” using our standard PEPSCAN-method involving only linear peptides.

Immunization studies in rats demonstrated the potential of **CLIPS** peptides to elicit antibodies specific for hFSH. In cases where the linear peptide failed completely, we observed that double-constrained peptide C<sub>(S-)</sub>VYETC<sub>(CLIPS)</sub>RVPGNAHHADSLC<sub>(CLIPS)</sub>TYPVC<sub>(S-)</sub> (**CLIPS/SS**) derived from the  $\beta$ 3-loop of hFSH elicited reproducibly (4/4) antisera able to neutralize the bioactivity of hFSH in a Y1-cell assay [6]. This peptide comprises both a **CLIPS** module (connecting the two cysteines that replace V<sub>61</sub> and Y<sub>74</sub>) and an additional SS bond between the cysteines replacing L<sub>56</sub> and A<sub>79</sub>. The neutralizing activity of the most potent antisera was equivalent to that of a 50-100 mg/mL solution of the strongest neutralizing anti-FSH mAb (6602) available. The activity of double-constrained **CLIPS** peptides was at least an order of magnitude higher than that of the corresponding single-constrained (only **CLIPS** or only SS) analogues. Competition ELISA, CD and NMR spectroscopy measurements were performed in order to determine if differences in antigenicity of linear, single and double-constrained peptides can be related to structure of the peptides in solution. It was found that the increased antigenicity of double-constrained **CLIPS/SS**-peptide indeed correlates with improved binding to mAb 6602 (competition ELISA; data not shown) and with increased structural fixation (CD and NMR spectroscopy data; Figure 3).

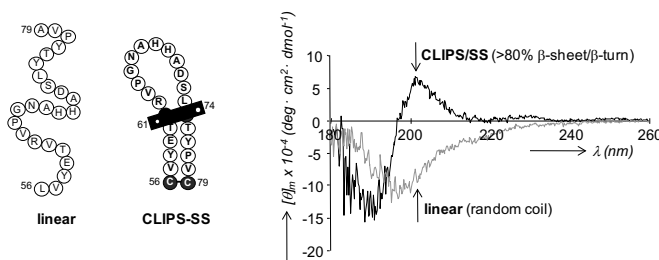


Fig. 3. CD spectroscopy data for linear and **CLIPS/SS** peptide derived from the top of the FSH  $\beta$ 3-loop.

In conclusion, **CLIPS**<sup>TM</sup> technology proves to be useful in protein binding site reconstruction, not only for epitope mapping purposes, but more importantly also to raise neutralizing antibodies. The technology is particularly attractive for its ease of application, the extremely fast and clean conversions of the peptides involved, and the mild reaction conditions combined with the chemical robustness of the cyclised peptides.

## Acknowledgments

We acknowledge financial support from the EU (EUREKA-BIT, project E1255811) and Senter/Novem (IS-052039).

## References

1. Fairlie, D.P. *Curr. Med. Chem.* **5**, 29-62 (1998).
2. Waldmann, T.A. *Nat. Med.* **9**, 267-277 (2003).
3. Langeveld, J.P.M., et.al. *J. Virol.* **68**, 4506-4513 (1994).
4. Timmerman, P., Beld, J., Puijk, W.C., Meloen, R.H. *Chembiochem.* **6**, 821-824 (2005).
5. Timmerman, P., et. al. *Open Vacc. J.* **2**, 56-67 (2009).
6. Timmerman, P., Puijk, W.C., Meloen, R.H. *J. Mol. Recognit.* **20**, 283-299 (2007).

## Fusion of Bioactive Peptides to Antibody Fragments

Junpeng Xiao,<sup>1</sup> Allison Kukuch,<sup>2</sup> Mark A. Pawlicki,<sup>1</sup> Brian S. Hamilton,<sup>1</sup>  
and Thomas J. Tolbert<sup>1,2</sup>

<sup>1</sup>Indiana University Interdisciplinary Biochemistry Program, Bloomington, IN 47405, U.S.A.;

<sup>2</sup>Department of Chemistry, Indiana University, Bloomington, IN 47405, U.S.A.

### Introduction

Our laboratory has been involved in fusing bioactive peptides to human immunoglobulin G Fragment crystallizable (IgG Fc) recombinantly produced in yeast. The attachment of bioactive peptides to immunoglobulin G fragment crystallizable (IgG Fc) can have several desirable effects which can aid biochemical studies or the development of therapeutics [1]. These effects include increasing the avidity of binding of bioactive peptides through dimeric presentation by the Fc region, linking antibody effector functions to binding of peptides to cellular targets, and increasing the *in vivo* circulatory half-life of small bioactive peptides. Investigations into the production and properties of bioactive peptide-Fc fusion proteins using recombinant methods have been carried out. In this research yeast expression systems have been utilized to produce antibody Fc regions with controlled glycosylation for study of antibody effector functions.

### Results and Discussion

IgG1 Fc is a homodimeric protein linked by interstrand disulfide bonds. It contains a single conserved N-linked glycosylation site at Asn297. We have produced yeast expression vectors for the recombinant expression of peptides fused to either the N- or C-terminus of IgG1 Fc (Figure 1). Secretory expression of the IgG1 Fc antibody fragment in the methylotrophic yeast *Pichia pastoris* results in the formation of the full-length IgG1 Fc glycoprotein. Single-step protein G affinity purification allows convenient recovery of IgG1 Fc and IgG1 Fc fusion proteins from yeast media. Protein yields range from 5 to 40 mg of IgG1 Fc and peptide-IgG1 Fc fusion proteins per liter from shake flask and spinner flask cultures.

We have utilized a combination of expression of IgG1 Fc in a glycosylation deficient strain of *Pichia pastoris* [2] and *in vitro* enzymatic synthesis to produce homogeneous, human-type glycoforms of IgG1 Fc. The use of purified glycosidases and glycosyltransferases *in vitro* allows a high degree of control of enzymatic glycosylation reactions. Using this approach it is possible to produce homogeneous high mannose, hybrid, and complex type glycoforms which do not contain the sugar fucose. Such nonfucosylated IgG1 Fc glycoforms have been shown to have increased antibody dependent cellular cytotoxicity activity [3].

As an example of a C-terminal fusion to IgG1 Fc we have attached the HIV entry inhibitor peptide C37H6 [4]. C37H6 contains a N-linked glycosylation site in its sequence, so expression of the IgG1 Fc-C37H6 fusion protein in yeast results in the formation of a dimeric glycoprotein with two N-linked glycosylation sites. Incomplete glycosylation of C37H6 results in a mixture of glycosylated forms. Treatment of the IgG1 Fc-C37H6 fusion protein with

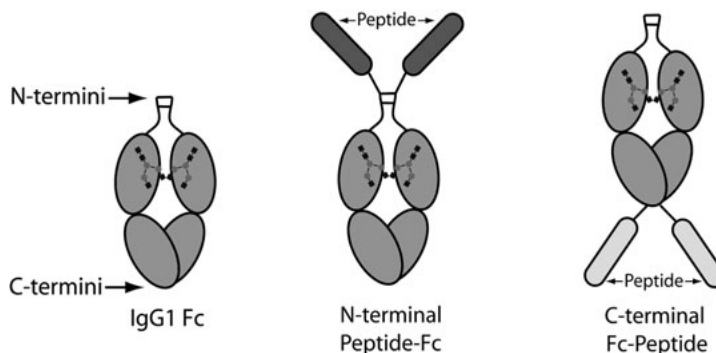


Fig. 1. N- and C-terminal IgG1 Fc peptide fusion proteins.



glycosidases such as Endo H or PNGase F to trim or remove the N-linked oligosaccharides simplifies the mixture of glycoforms obtained from yeast expression. HIV entry inhibition assays of differentially glycosylated forms of IgG1 Fc-C37H6 demonstrate that they are all active at inhibiting HIV entry. Even though fusion of C37H6 to IgG1 Fc reduces inhibitory activity compared to the parent HIV entry inhibitor peptide 18-33 fold, the potentially increased half-life of the fusion proteins relative to the free peptide may prove useful.

As an example of an N-terminal fusion to IgG1 Fc we have attached the diabetes related peptide exendin-4 [5]. Exendin-4 is an glucagon-like peptide-1 (GLP-1) mimic which helps to regulate blood glucose and insulin levels in the treatment of type 2 diabetes. Secretory expression of exendin-4 fused to IgG1 Fc in yeast results in a mixture of full-length fusion protein and proteolyzed forms, where approximately one third of the fusion protein is full length. Even though the fusion protein is partially proteolyzed it still retains significant biological activity, being only 2.2 fold less active than GLP-1 and 4.4 fold less active than the free exendin-4 peptide. The potential increase in *in vivo* half-life gained by fusing IgG1 Fc to exendin-4 may compensate for the lower observed activity of this IgG1 Fc peptide fusion.

Recombinant expression of bioactive peptides in yeast as described here has several advantages. Peptide-Fc constructs can be cloned rapidly and bioactive peptides can be fused to either the N- or C-terminus of IgG1 Fc. Expression in yeast allows production of sufficient material to conduct biochemical experiments from just 1L of growth. The use of glycosylation deficient yeast coupled with enzymatic synthesis allows for control of IgG1 Fc glycosylation and potentially modulation of antibody effector functions. Many bioactive peptides retain significant bioactivity when fused to IgG1 Fc's such as the HIV entry inhibitor peptide and GLP-1 agonist presented here.

## Acknowledgments

The GLP-1 related research is a collaboration with the DiMarchi Laboratory at IU and we gratefully acknowledge the DiMarchi Laboratory for helpful discussions and collaborative support with a special thanks to James Patterson for GLP-1 assays. This research was supported by Indiana University, Bloomington.

## References

1. Nelson, A.L., Reichert, J.M. *Nature Biotechnology* **27**, 331-337 (2009).
2. Nett, J.H., Gerngross, T.U. *Yeast* **20**, 1279-1290 (2003).
3. Shinkawa, T., et al. *J. Biol. Chem.* **278**, 3466-3473 (2003).
4. Tolbert, T.J., et al. *Bioorg. Med. Chem.* **13**, 909-915 (2005).
5. Aulinger, B., D'Alessio, D. *Curr. Opin. Endocrinol. Diabetes Obes.* **14**, 68-73 (2007).

## Exenatide Rescues Sirt1 Expression in Apoptotic RINm-5F Cells

Xueyun Wang, Jiayi Yu, Jing Wang, Shijie Yang, and Wei Li

College of Life Science, Jilin University, Changchun, 130021, P.R. China

Email: liweian@jlu.edu.cn

### Introduction

Exenatide is a 39 amino acid peptide which has been used to treat type 2 diabetes. Aside from its clinical application, detailed molecular mechanisms are not fully understood yet. Sirt1 is a class III histone protein deacetylase, which is essential in the aging process. It has been reported that Sirt1 is involved in glucose metabolism and can improve insulin sensitivity by repressing PTP1B [1]. Furthermore, it is suggested that Sirt1 can regulate insulin secretion by repressing UCP2 in pancreatic  $\beta$  cells [1]. We hypothesize that exenatide may regulate glucose metabolism through Sirt1. Here, we chose to use RINm-5F cells (an insulinoma cell line) as cell model, induced the cells into apoptosis state and treated the cells with exenatide. We found that sirt1 gene expression is decreased under the induction of apoptosis and exenatide is able to rescue the sirt1 expression in both gene and protein level.

### Results and Discussion

We have used the ELISA method to investigate whether exenatide could stimulate insulin secretion under high concentration glucose (16.7mM) and maintain the insulin content at low level under normal concentration glucose (4.0mM). RINm-5F Cells were cultured in 6-well plates with RPMI1640 medium. The medium was removed on the day of the experiment, and the cells were washed three times with warm KRB buffer before incubated with KRB containing glucose (16.7mM) and exenatide (50uM) for 1 h at 37 °C. The supernatant was collected and insulin level was measured by ELISA. Figure 1 shows that exenatide maintains basal insulin level in the presence of 4.0mM glucose. High glucose level (16.7mM) together with exenatide treatment additively induced insulin secretion by over 1.5 fold.

Sirt1 expression has been shown to be down-regulated during beta cell apoptosis. We hypothesized that exenatide protect pancreatic beta cell against apoptosis and this may function through regulating Sirt1 gene expression. The mRNA level of sirt1 has been measured by RT-PCR (Figure 2), and real-time PCR (Figure 3). Glucose +Palmitate (Pal) treatment repressed sirt1 gene expression to 20% in RINm-5F cells and 100  $\mu$ mol exenatide is able to partially reverse the repression.

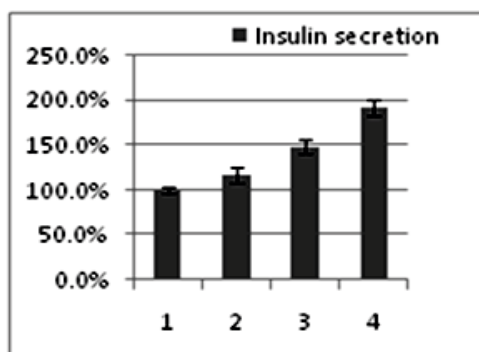


Fig. 1. Exenatide stimulate insulin secretion in RIN-5F cells. 1 – Blank, 2 – Exenatide, 3 – 16.7 mM Glucose, 4 – Exenatide + 16.7 mM Glucose.

We then investigate whether exenatide would also rescue sirt1 protein level in RINm-5F cells. Same treatments have been applied to the RINm-5F cells as described in the real-time PCR experiment, cell lysates were collected and protein level of Sir 1 were measured by western blot. Treatment of exenatide alone did not change Sirt1 protein level (Figure 4, lane1, 4). While high glucose significantly decreases Sirt1 protein level (Figure 4, lane3), add back in exenatide could partially rescue the level of Sirt1 (Figure 4, lane 2).

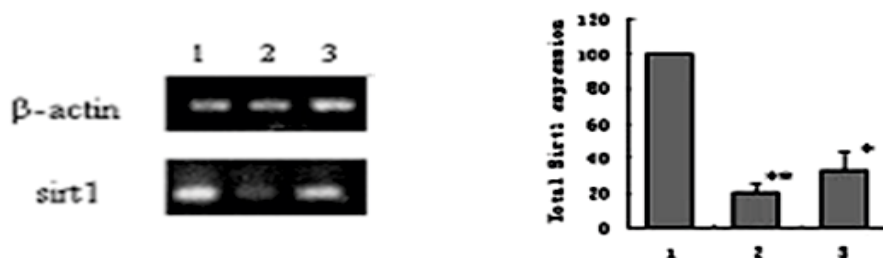


Fig. 2. RT-PCR of *Sirt1* in RINm-5F cells. 1 – Blank, 2 – 50 mM Glucose + 0.2 mM Pal, 3 – 100 μmol Exenatide + 50 mM Glucose + 0.2 mM Pal.

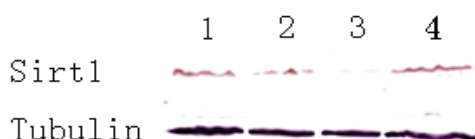


Fig. 4. *Sirt1* protein levels examined by western blot. 1 – 100 μmol Exenatide, 2 – 100 μmol Exenatide + 50 mM Glucose + 0.2 mM Pal, 3 – 50 mM Glucose + 0.2 mM Pal 4 – Blank.

Exenatide is a new drug for treating type 2 diabetes which has been approved by FDA. Although it is known to protect beta-cell against apoptosis [4], detail mechanism is not clear. Our results suggest that exenatide help to maintain normal *Sirt1* expression under apoptosis condition.

## References

1. Bordone, L., Motta, M.C., et al. *PLoS. Biol.* **4(2)**: e31 (2006).
2. Nelson, P., Poon, T., et al. *Diabetes Technol. Ther.* **9**, 317-326 (2007).
3. Sun, C., Zhang, F., et al. *Cell Metab.* **6**, 307-319 (2007).
4. Whitehill, D.S. *D. Med.* **60**, 197-199 (2007).

## Towards Peptide Vasodilators as Anticancer Drug Delivery Vehicles

Rachel J. White,<sup>1</sup> Paul G. Plieger,<sup>1</sup> Nadia G. Kandile,<sup>2</sup> and David R.K. Harding<sup>1</sup>

<sup>1</sup>Chemistry, Institute of Fundamental Sciences, Massey University, PN, 5301, New Zealand;

<sup>2</sup>Chemistry Department, Faculty of Girls, Ain Shams University, Cairo, Egypt

### Introduction

Controlled drug release has been studied in depth for many years aiming for the treatment of cancer. Although there are a number of methods that have been successful, they often come with unwanted side effects. Bradykinin (BK) offers potential as a targeting vehicle in the fight against cancer. Composites of BK with the carrier potential of cyclodextrin and the advantages of sulfonamide drugs have great potential for successful drug targeting [1,2]. Herein we report for the first time the *selective* derivatisation of beta-cyclodextrin ( $\beta$ -CD) with a series of model

peptides using solid phase peptide synthesis. This versatile and robust method enables the attachment of one or more peptides using SPPS (and solution synthesis if desired) by the selective removal of the Fmoc-protecting group. This versatility allows for the addition and growth of C- and/or N-terminal peptides with the same and/or different functional properties (Figure 1). Peptide attachment of resin in solution using stepwise or ligation synthetic protocols is also possible.

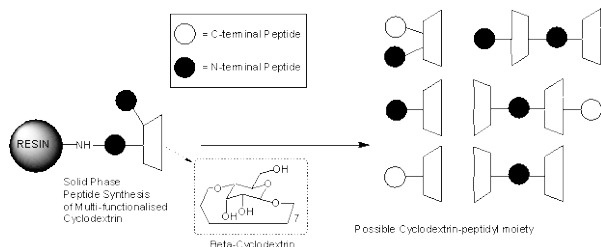


Fig. 1. Schematic diagram indicating the potential for this cyclodextrin-peptide sulfonamide carrier system.

### Results and Discussion

Figure 2 outlines a six-step process to multi-functionalise cyclodextrin **1** to allow for its use in Fmoc-SPPS for the attachment of one or more peptides on the resin. The end product **7**, an amino acid, is thus set up for peptide synthesis. The synthetic procedure was carried out by initial mono-tosylation of a primary hydroxyl group of  $\beta$ -cyclodextrin **1** to yield **2** (mono-6-(4-methylbenzenesulfonate)- $\beta$ -cyclodextrin) as per known procedures [3]. Conversion to the mono-6-amino- $\beta$ -cyclodextrin, **3** and Cbz protection leads to compound **4** (mono-6-carbobenzyloxyamino- $\beta$ -cyclodextrin). Addition of a succinyl group through an ester linkage (**5**, mono-6-carbobenzyloxyamino-succinyl- $\beta$ -cyclodextrin) on the CD gave the carboxy terminal suitable for SPPS. This ester linkage was found to be stable to standard Fmoc-SPPS reaction conditions. HPLC purification using a stepwise methanol gradient enabled separation of the isomers, but the racemic mixture was used for the continuation of the synthesis. Hydrogenation

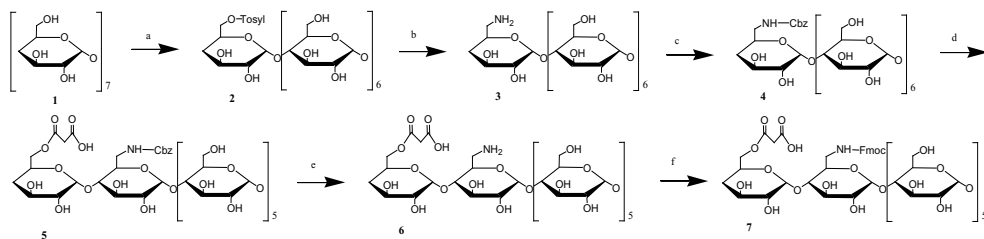


Fig. 2. Multi-functional synthesis of  $\beta$ -Cyclodextrin. a) tosyl chloride, water, 0-5 °C, 5 hours, 38%; b) 35% aqueous ammonia, 7 days, 90%; c) Cbz-OSu, NaHCO<sub>3</sub>, dioxane/water, RT, overnight, 51%; d) Succinic anhydride, pyridine, RT overnight, 40%; e) H<sub>2</sub>, Pd/C, DMF, RT, 90%; f) Fmoc-OSu, NaHCO<sub>3</sub>, dioxane/water, R.T, overnight, 40%.

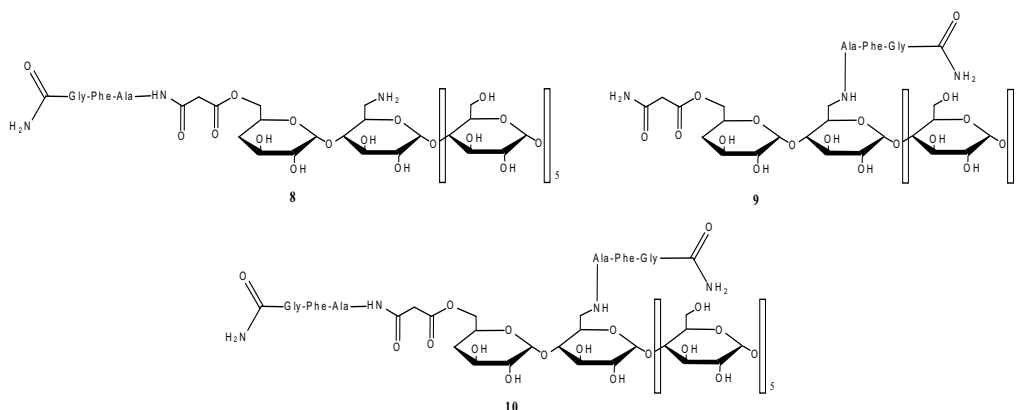


Fig. 3. Peptidyl growth on  $\beta$ -Cyclodextrin using Fmoc-SPPS on Rink resin. 8 Peptidyl growth at the C-terminus, 9 Peptidyl growth at the N-terminus, 10 Peptidyl growth at both the C and N-Terminus.

of the Cbz group (**6**) followed by Fmoc protection [4] of the free amino group gives the multi-functionalised CD species, **7** (mono-6-fluorenylmethyloxycarbonylamino-succinyl- $\beta$ -cyclodextrin) as a racemic mixture. Purification of each compound was achieved using HPLC with HR-MS and NMR characterisation.

The attachment of a short model peptide to **7** (Figure 3) at either the C- or N-terminus has been achieved using Fmoc-SPPS to give **8** and **9** respectively. The addition of a peptide to both the C- and N-terminus using Fmoc-SPPS gives compound **10**. The coupling of Fmoc-amino acids and compound **7** to Rink resin was achieved using standard Fmoc-coupling conditions [TBTU (O- (benzotriazol-1-yl)-N,N,N',N'-tetramethyluronium tetrafluoroborate) and DIPEA (diisopropylethylamine) in DMF in excess]. Each peptide product was purified using HPLC using a stepwise acetonitrile gradient resulting in pure 15%, 25%, and 12% yields for **8**, **9** and **10** respectively (Figure 3). The products were characterised by LR-MS (MALDI-TOF). The attachment of a model sulfonamide, 4-aminobenzenesulfonamide, to the C and/or N-terminus of the peptide in compounds **7**, **8**, and **9** has also been achieved using standard SPPS conditions. Bioactive testing by means of the carbonic anhydrase assay of these compounds is now under investigation to see whether the activity of sulfonamide is affected by the presence of the CD moiety.

We have demonstrated a versatile and robust method for the development of a model peptide derivatised cyclodextrin for the potential use in the transportation of drugs. The versatility of this approach allows for the selective attachment of one or more different peptides to the CD moiety. It also allows for the selective synthesis of a combination of molecules incorporating one or more peptides and/or CD molecules in varying combinations. Studies are continuing into the attachment and analysis of potential bioactive peptides (bradykinin) and sulfonamide drugs for their potential in drug transportation and delivery. Metal complexation may also be investigated.

## Acknowledgments

Massey University and The Royal Society of Chemistry is thanked for granting R.J. White a PhD scholarship and funds to attend this conference. D. Lun is thanked for his synthetic advice.

## References

1. Handbook of Biologically Active Peptides, Kastin, A.J. ed., Elsevier, (2006).
2. Ashton, P.R., Koeniger, R., Stoddart, J.F., Alker, D., Harding, V. D. *J. Org. Chem.* **61** 903-908 (1996).
3. Byun, H.-S., Zhong, N., Bittman, R. *Organic Syntheses* **77**, 225-230 (2000).
4. *Fmoc Solid Phase Peptide Synthesis. A Practical Approach*. Chan, W.C. and White, P.D. (Eds), Oxford University Press, (2000).

## Development of Selective, Exosite Binding Matrix Metalloproteinase (MMP) Inhibitors

Janelle L. Lauer-Fields and Gregg B. Fields

Department of Biochemistry, University of Texas Health Science Center, San Antonio, TX 78229, U.S.A.

### Introduction

Alterations in activities of the matrix metalloproteinase (MMP) family of proteases have been implicated in primary and metastatic tumor growth, angiogenesis, and pathological degradation of extracellular matrix (ECM) components, such as collagen and laminin. Since hydrolysis of the collagen triple-helix is one of the committed steps in ECM turnover, we envisioned modulation of collagenolytic activity as a strategy for creating selective MMP inhibitors. Specifically, we considered two strategies for inhibitor design that took advantage of triple-helix interactions with MMP secondary binding sites (exosites) [1]. The first strategy incorporated a phosphinate transition state analog within a triple-helical peptide template, while the second strategy developed a triple-helical construct from a known exosite binding sequence.

### Results and Discussion

The type V collagen-derived sequence Gly-Pro-Pro-Gly<sub>439</sub>~Val<sub>440</sub>-Val-Gly-Glu-Gln, when incorporated into a triple-helical structure, is hydrolyzed efficiently by MMP-2 and MMP-9 but not by MMP-1, MMP-3, MMP-13, or MT1-MMP [2]. The sequence was thus used as a template for the design of a potentially selective MMP inhibitor. The P<sub>1</sub>-P<sub>1</sub>' subsites of the triple-helical peptide, which are Gly~Val in the substrate, were substituted by a GlyΨ{PO<sub>2</sub>H-CH<sub>2</sub>}Val transition state analog to create C<sub>6</sub>-(Gly-Pro-Hyp)<sub>4</sub>-Gly-Pro-Pro-GlyΨ{PO<sub>2</sub>H-CH<sub>2</sub>}(S)Val-Val-Gly-Glu-Gln-Gly-Glu-Gln-Gly-Pro-Pro-(Gly-Pro-Hyp)<sub>4</sub>-NH<sub>2</sub> [3].

The GlyΨ{PO<sub>2</sub>H-CH<sub>2</sub>}Val triple-helical peptide (THP) was initially tested against MMP-2 and MMP-9 (Table 1). Due to the low melting temperature of the potential inhibitor (*T*<sub>m</sub> ~ 25°C), *K*<sub>i</sub> values were first determined at 10°C. GlyΨ{PO<sub>2</sub>H-CH<sub>2</sub>}Val THP was found to be a very effective inhibitor of MMP-2 and MMP-9, with *K*<sub>i</sub> values of 4 and 2 nM, respectively. When inhibition assays were repeated at 37°C, the *K*<sub>i</sub> value increased for MMP-2 but not for MMP-9 (Table 1). Thus, triple-helical structure modulated inhibition of MMP-2 but not MMP-9.

To determine if an increase in *K*<sub>i</sub> as a function of temperature was general trend for inhibition of MMP-2, inhibition of MMP-2 by MMP inhibitor III (a hydroxamic acid-Leu-homoPhe dipeptide) was examined. At 10°C, the *K*<sub>i</sub> value for MMP-2 inhibition was 3 nM (Table 1). Increasing the temperature to 37°C decreased the *K*<sub>i</sub> to 0.8 nM (Table 1). Thus, for a small molecule inhibitor, an increase in temperature slightly increased the affinity towards MMP-2, most likely due to enhanced hydrophobic interactions. This further suggested that the decreased inhibition of MMP-2 by the THP as a function of increasing temperature was due to unfolding of the inhibitor triple-helical structure.

MMP-1, MMP-3, MMP-8, MMP-13, and MT1-MMP were tested for inhibition by the GlyΨ{PO<sub>2</sub>H-CH<sub>2</sub>}Val THP. No inhibition of MMP-1, MMP-3, or MT1-MMP was observed up to a THP concentration of 25 μM. MMP-8 and MMP-13 were inhibited weakly, with IC<sub>50</sub> values in the range of ~50 and ~10 μM, respectively. Thus, the GlyΨ{PO<sub>2</sub>H-CH<sub>2</sub>}Val THP bound selectively at the S<sub>1</sub>-S<sub>1</sub>' site of MMP-2 and MMP-9. Selective inhibition of these MMPs is desirable, as MMP-2 has been validated as an anti-cancer drug target, while MMP-9 inhibition may be useful in treating early-stage cancers [4].

Our second inhibitor design was based on a THP substrate mimicking the interstitial collagen sequence α1(I-III)769-783 (Gly-Pro-Gln-Gly~Leu-Ala-Gly-Gln-Arg-Gly-Ile-Arg) which is hydrolyzed by MMP-1, MMP-2, MMP-8, MMP-9, MMP-13, MT1-MMP, and MT2-MMP [5-8]. The P<sub>1</sub>-P<sub>1</sub>' subsites of the triple-helical peptide, which are Gly~Leu in the substrate, were substituted by a GlyΨ{PO<sub>2</sub>H-CH<sub>2</sub>}Leu transition state analog. Because the *T*<sub>m</sub> value for GlyΨ{PO<sub>2</sub>H-CH<sub>2</sub>}Val THP was considerably lower than that for the analogous substrate [3], the GlyΨ{PO<sub>2</sub>H-CH<sub>2</sub>}Leu THP incorporated the non-natural amino acid (2*S*,4*R*)-4-fluoroproline (Flp) to enhance triple-helicity [9-11]. Thus, the sequence of this inhibitor was C<sub>6</sub>-Gly-Pro-Flp-(Gly-Pro-Hyp)<sub>4</sub>-Gly-Pro-Gln-GlyΨ{PO<sub>2</sub>H-CH<sub>2</sub>}(R,S)Leu-Ala-Gly-Gln-Arg-Gly-

Table 1. Inhibition of MMP-2, MMP-9, and MMP-1

Enzyme	Inhibitor	Temperature (°C)	$K_i^{(app)}$ (nM)
MMP-2	GlyΨ{PO <sub>2</sub> H-CH <sub>2</sub> }Val THP	10	4.14 ± 0.47
“	“	37	19.23 ± 0.6
“	MMP inhibitor III	10	3.17 ± 0.23
“	“	37	0.83 ± 0.03
“	GlyΨ{PO <sub>2</sub> H-CH <sub>2</sub> }Leu THP	10	0.18 ± 0.00
“	“	37	0.08 ± 0.01
MMP-9	GlyΨ{PO <sub>2</sub> H-CH <sub>2</sub> }Val THP	10	1.76 ± 0.05
“	“	37	1.29 ± 0.00
“	GlyΨ{PO <sub>2</sub> H-CH <sub>2</sub> }Leu THP	10	0.02 ± 0.01
“	“	37	0.09 ± 0.00
MMP-1	GlyΨ{PO <sub>2</sub> H-CH <sub>2</sub> }Leu THP	10	7.83 ± 1.03
“	“	37	26.70 ± 5.2
“	MMP inhibitor III	10	2.48 ± 0.35
“	“	37	4.72 ± 0.38

Ile-Arg-(Gly-Pro-Hyp)<sub>4</sub>-Gly-Pro-Flp-NH<sub>2</sub>, and it exhibited a  $T_m$  value of 30°C [12]. Low nM  $K_i$  values were observed for inhibition of MMP-1, MMP-2, and MMP-9 (Table 1). Our second transition state analog inhibitor appeared to be effective against a broader range of collagenolytic MMPs than the first inhibitor. Interestingly, MMP-1 was sensitive to the triple-helical structure of the inhibitor ( $K_i$  increased ~4 times when the inhibitor was thermally unwound), but neither MMP-2 nor MMP-9 was (Table 1). This contrasts with the sensitivity of MMP-2 to the triple-helical structure of GlyΨ{PO<sub>2</sub>H-CH<sub>2</sub>}Val THP (Table 1), and indicates that there is a *sequence-dependent sensitivity to triple-helical structure for some MMPs*.

Recently, a single-stranded peptide model of the α1(I)715-721 collagen sequence was identified as a ligand for the MMP-2 fibronectin type II (FN II) insert and inhibited MMP-2 gelatinolysis [13]. We assembled a triple-helical version of this ligand [α1(I)715-721 THP] which had a  $T_m$  value of 47 °C. α1(I)715-721 THP was evaluated for its ability to inhibit MMP-2 and MMP-9 triple-helical peptidase and gelatinase activities [12]. Dose-dependent inhibition of gelatinolysis was observed for both MMP-2 and MMP-9, with  $K_i$  values of 52 and 54 μM, respectively (Table 2). There was no inhibition of MMP-2 or MMP-9 hydrolysis of a single-stranded, short substrate [Mca-Lys-Pro-Leu-Gly-Leu-Lys(Dnp)-Ala-Arg-NH<sub>2</sub>] or a triple-helical substrate that modeled interstitial collagens (fTHP-15) by α1(I)715-721 THP (Table 2). However, MMP-2 and MMP-9 hydrolysis of a triple-helical substrate that modeled type V collagen [α1(V)436-447 fTHP] was inhibited by α1(I)715-721 THP, with  $K_i$  values of 144 and 123 μM, respectively (Table 2). Thus, α1(I)715-721 THP inhibited type V collagen-model triple-helical peptidase activity but not interstitial collagen-model triple-helical peptidase activity. To our knowledge, this demonstrated the first use of an exosite binder to selectively inhibit one collagen-based MMP activity but not another.

Most inhibitor design uses hydrophobicity to generate binding energy, which creates a favorable  $\Delta G$  but poor selectivity [14], and this is generally a feature of low molecular weight inhibitors (<800 Da) [15]. It may be possible to generate selective inhibitors that are more polar by incorporating interactions that are more specific for MMP sub-classes. Protein-protein recognition sites usually have larger contact areas (>1500Å<sup>2</sup>), and thus developing larger inhibitors might allow for greater specificity. One could design inhibitors that bind to regions that, in a family of enzymes, have similar structures but differing mobility [15] or where unique exosites exist within the family. The drawback of this approach has typically been the flexibility of larger inhibitors. However, triple-helical peptide inhibitor (THPI) design optimizes

Table 2. Inhibition of MMPs by  $\alpha 1(I)$ 715-721 THP at 37°C

Enzyme	Substrate	$K_i^{(app)}$ ( $\mu M$ )
MMP-2	DQ gelatin	52.3 $\pm$ 5.1
“	Mca-Lys-Pro-Leu-Gly-Leu-Lys(Dnp)-Ala-Arg-NH <sub>2</sub>	NI <sup>a</sup>
“	fTHP-15	NI <sup>a</sup>
“	$\alpha 1(V)$ 436-447 fTHP	143.5 $\pm$ 11.4
MMP-9	DQ gelatin	54.4 $\pm$ 7.6
“	Mca-Lys-Pro-Leu-Gly-Leu-Lys(Dnp)-Ala-Arg-NH <sub>2</sub>	NI <sup>a</sup>
“	fTHP-15	NI <sup>a</sup>
“	$\alpha 1(V)$ 436-447 fTHP	122.7 $\pm$ 5.83

<sup>a</sup> NI = no inhibition

conformational entropy due to imino acid restriction of peptide backbone mobility. Specificity can then be generated by inhibitor binding to multiple sites on the enzyme (active site and exosites). This can lead to inhibitors that are highly selective between members of an enzyme family or inhibitors that are selective between activities of specific enzymes.

## Acknowledgments

This work was supported by an NIH COSTAR Postdoctoral Fellowship (to JLL-F) and the NIH (CA98799), the Robert A. Welch Foundation, and the Texas Higher Education STAR Program (to GBF).

## References

1. Lauer-Fields, J.L., Chalmers, M.J., Busby, S.A., Minond, D., Griffin, P.R., Fields, G.B. *J. Biol. Chem.*, in press (2009).
2. Lauer-Fields, J.L., Sritharan, T., Stack, M.S., Nagase, H., Fields, G.B. *J. Biol. Chem.* **278**, 18140-18145 (2003).
3. Lauer-Fields, J.L., Brew, K., Whitehead, J.K., Li, S., Hammer, R.P., Fields, G.B. *J. Am. Chem. Soc.* **129**, 10408-10417 (2007).
4. Overall, C.M., Kleifeld, O. *Nat. Rev. Cancer* **6**, 227-239 (2006).
5. Lauer-Fields, J.L., Fields, G.B. *Biol. Chem.* **383**, 1095-1105 (2002).
6. Minond, D., Lauer-Fields, J.L., Nagase, H., Fields, G.B. *Biochemistry* **43**, 11474-11481 (2004).
7. Minond, D., Lauer-Fields, J.L., Cudic, M., Overall, C.M., Pei, D., Brew, K., Visse, R., Nagase, H., Fields, G.B. *J. Biol. Chem.* **281**, 38302-38313 (2006).
8. Minond, D., Lauer-Fields, J.L., Cudic, M., Overall, C.M., Pei, D., Brew, K., Moss, M.L., Fields, G.B. *Biochemistry* **46**, 3724-3733 (2007).
9. Holmgren, S.K., Taylor, K.M., Bretscher, L.E., Raines, R.T. *Nature* **392**, 666-667 (1998).
10. Holmgren, S.K., Bretscher, L.E., Taylor, K.M., Raines, R.T. *Chem. Biol.* **6**, 63-70 (1999).
11. Malkar, N.B., Lauer-Fields, J.L., Borgia, J.A., Fields, G.B. *Biochemistry* **41**, 6054-6064 (2002).
12. Lauer-Fields, J.L., Whitehead, J.K., Li, S., Hammer, R.P., Brew, K., Fields, G.B. *J. Biol. Chem.* **283**, 20087-20095 (2008).
13. Xu, X., Chen, Z., Wang, Y., Bonewald, L., Steffensen, B. *Biochem. J.* **406**, 147-155 (2007).
14. Rubin, A. J., Kiso, Y., Freire, E. *Chem. Biol. Drug Des.* **67**, 2-4 (2006).
15. Luque, I., Freire, E. *Proteins: Struct. Funct. Gen.* **4**, 63-71 (2000).



## Design of Structured gp41 N-heptad Repeat Peptides as HIV-1 Vaccine Candidates

Elisabetta Bianchi,<sup>1</sup> Joseph Joyce,<sup>2</sup> Michael D. Miller,<sup>3</sup> Xiaoping Liang,<sup>2</sup>  
 Marco Finotto,<sup>1</sup> Paolo Ingallinella,<sup>1</sup> Philip M. McKenna,<sup>3</sup> Michael Citron,<sup>2</sup>  
 Elizabeth Ottinger,<sup>2</sup> Robert Hepler,<sup>2</sup> Renee Hrin,<sup>3</sup> Debbie Nahas,<sup>2</sup>  
 Chengwei Wu,<sup>2</sup> John W. Shiver,<sup>2</sup> Peter S. Kim,<sup>4</sup> and Antonello Pessi<sup>1</sup>

<sup>1</sup>IRBM P. Angeletti, 00040 Pomezia (Rome) Italy, Departments of <sup>2</sup>Vaccine Basic Research,

<sup>3</sup>Antiviral Research, Merck Research Laboratories, West Point, PA 19486, U.S.A.

<sup>4</sup>President, Merck Research Laboratories, Upper Gwynedd, PA 19454, U.S.A.

### Introduction

Efforts to develop an HIV-1 vaccine have focused on conserved structural elements which are the target of broadly neutralizing monoclonal antibodies (mAb). In recent years we have validated the N-heptad repeat (NHR) region of gp41 as a potential vaccine target, based on the identification of mAb D5 which binds to a highly conserved hydrophobic pocket on the NHR coiled-coil [1].

To identify a candidate vaccine, able to elicit a D5-like antibody response, we designed a series of constructs in which the gp41 NHR is presented as highly structured trimeric coiled-coils. Here we review the evolution of our immunogen design, and report preliminary results on their immunological properties.

### Results and Discussion

The structure of the constructs that we prepared as candidate vaccines is schematically shown in Figure 1, while their sequence is given in Table 1. They all include a region of NHR fused to the trimerization domain, IZ, described by Eckert and Kim [2].

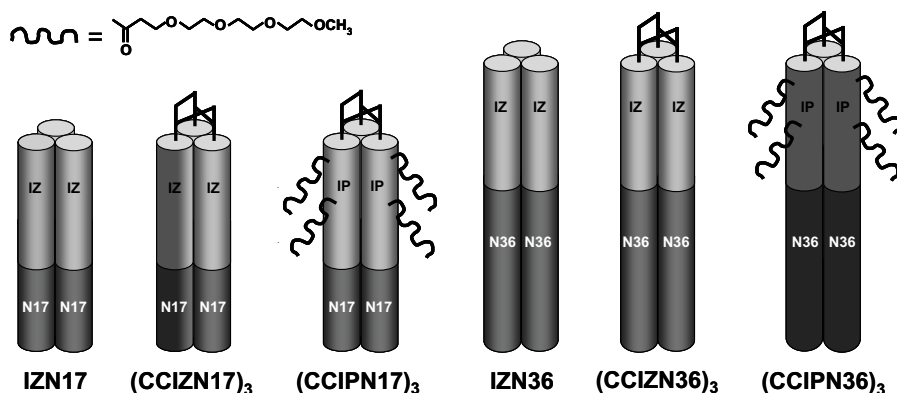


Fig. 1. Schematic representation of the NHR immunogens described in the text.

The first construct was based on the hypothesis that the structural stability of IZN17 was limited at low concentrations by the self-association equilibrium, and dissociation of the structure was expected at the highly diluted concentrations resulting from vaccination. In (CCIZN17)<sub>3</sub>, we used intramolecular disulfide bonds to form a covalent trimer, whose association state is independent of concentration [3]. Addition of the CysCysGlyGly- sequence N-terminally to the IZ scaffold allowed smooth disulfide pairing at neutral pH. Not only was (CCIZN17)<sub>3</sub> more stable to thermal denaturation, but it also showed enhanced antiviral potency [3].

Table 1. Sequence of the immunogens described in this study

Peptide	Sequence <sup>a</sup>
IZN17	IKKEIEAIKKEQEAIKKKIEAIEKLLQLTVWGIKQLQARIL
CCIZN17	CCGGIKKEIEAIKKEQEAIKKKIEAIEKLLQLTVWGIKQLQARIL
CCIPN17	CCGGIK*EIEAIK*EQEAIKKKIEAIEKLLQLTVWGIKQLQARIL
IZN36	IKKEIEAIKKEQEAIKKKIEAIEKEISGIVQQNNLLRAIEAQQHLLQLTVWGIKQLQARIL
CCIZN36	CCGGIKKEIEAIKKEQEAIKKKIEAIEKEISGIVQQNNLLRAIEAQQHLLQLTVWGIKQLQARIL
CCIPN36	CCGGIK*EIEAIK*EQEAIKKKIEAIEKEISGIVQQNNLLRAIEAQQHLLQLTVWGIKQLQARIL

<sup>a</sup>All peptides N-terminal acetyl, C-terminal amide; \*Lys[NH-CO-(CH<sub>2</sub>-CH<sub>2</sub>-O)<sub>3</sub>-CH<sub>2</sub>-CH<sub>2</sub>-OCH<sub>3</sub>]

Although (CCIZN17)<sub>3</sub> was highly immunogenic, we found that a substantial amount of the elicited antibodies were directed against the scaffold IZ. To circumvent this, we selectively "shielded" the IZ epitope by attachment of small molecular weight polyethylene glycol chains at suitable locations (indicated as an asterisk in Table 1) (Figure 1). Immunization with (CCIPN17)<sub>3</sub> elicited an intact antibody response against the gp41 region, equivalent to that obtained with (CCIZN17)<sub>3</sub>, while the response directed to the scaffold region, as measured by antibodies against (CCIZ)<sub>3</sub> and (CCIP)<sub>3</sub> in ELISA, was very low [4].

Our work leading to the selection of mAb D5 had shown that, when using the N36 region to select from a scFv phage library, the preferred binding region was the hydrophobic pocket comprised in the N17 region. This was the motivation to initially focus on N17-based peptides. However, the neutralization efficiency of the elicited humoral response might be improved by the presence of additional antibodies, recognizing NHR at sites outside the hydrophobic pocket. Therefore our next set of immunogens consisted of chimeric N-peptides, where IZ was fused to N36. These included IZN36, which had been previously employed for D5 selection [1], (CCIZN36)<sub>3</sub>, analogous to (CCIZN17)<sub>3</sub>, and (CCIPN36)<sub>3</sub>, analogous to (CCIPN17)<sub>3</sub> (Table1 and Figure 1). The three new constructs were fully helical at 10 μM, as determined by CD. Thermal denaturation experiments indicated a high degree of stability in HEPES buffer at 10 μM concentration, with no melting up to 90°C. In the presence of 2M guanidine hydrochloride, IZN36 had T<sub>m</sub> = 72°C, while both covalent constructs had T<sub>m</sub> > 90°C, which compares favorably with the data previously obtained for the corresponding N17-based constructs [3,4].

Comparative immunogenicity studies are in progress with the immunogens shown in Figure 1. The preliminary results obtained in guinea pigs and rabbits indicate that the chosen design strategy is indeed producing candidate vaccines with incrementally improved properties. First, a clear trend was observed towards greater neutralization potency in antisera elicited by immunization with covalently-stabilized trimers, relative to their non covalent counterparts, strongly suggesting that the former are more accurate mimetics of the NHR-trimeric coiled coil. Second, neutralization potency increased with increasing length of the gp41 sequence, with N36-based constructs being better than the N17-based ones. Third, unfractionated sera raised against the best vaccine candidates, (CCIZN36)<sub>3</sub> and (CCIPN36)<sub>3</sub> could neutralize the virus. To our knowledge, this is the first demonstration of a neutralizing response against a highly conserved gp41 NHR epitope.

## Acknowledgments

We thank Gennaro Ciliberto and Daria J. Hazuda for advice throughout this study.

## References

1. Miller, M.D., et al. *Proc. Natl. Acad. Sci. U.S.A.* **102**, 14759-14764 (2005).
2. Eckert, D.M., Kim, P.S. *Proc. Natl. Acad. Sci. U.S.A.* **98**, 11187-11192. (2001).
3. Bianchi, E., et al. *Proc. Natl. Acad. Sci. U.S.A.* **102**, 12903-12908 (2005).
4. Bianchi, E., et al. In Del Valle, S., Escher, E., Lubell, W.D. (Eds.) *Peptides for Youth (Proceedings of the 20<sup>th</sup> American Peptide Symposium)*, American Peptide Society, 2007, p. 359.

## TMZ-BioShuttle, an Exemplary Drug Reformulation by Inverse Diels Alder Click-Chemistry

R. Pipkorn, M. Wiessler, W. Waldeck, H. Fleischhacker,  
 P. Lorenz, and K. Braun

German Cancer Research Center, Im Neuenheimer Feld 280; D-69120 Heidelberg, Germany

### Introduction

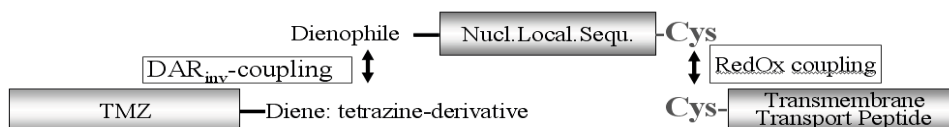
The role of solid phase peptide synthesis (SPPS) [1] and “Click chemistry” [2] continually became more and more important in the recombinant chemistry for development of modern drugs which in turn demand not solely the specificity and efficiency, but also a sufficient local concentration of the drug at the target site. Circumventing the drawbacks of new active substances, like poor diffusion across biological membranes and a restricted solubility in physiological solvents requires both transport facilitating-(CPP) and address-peptides (NLS) [3-5].

The nature’s treasure chest harbours excellent models for the development of pharmacological substances which allow a broad therapeutic index and simultaneously cause minimal adverse reactions of the transported active substances. Manifold multi-functional proteins like HIV-Tat and Homeo Box gene products which meet the demands are well identified.

### Results and Discussion

Our approach to this problem is schematically outlined and consists of coupling of TMZ to the nuclear localization sequence NLS(SV40-T), which is disulfide-bridged to the cell-penetrating peptide p<sup>Antp43-58</sup> resulting in an active nuclear targeting. Such a non-viral construct, named BioShuttle, was expected to facilitate the cellular entry and nuclear targeting of TMZ as previously observed in our laboratory for the delivery of PNAs [6]. Indeed, after the passage of the TMZ-BioShuttle across the cellular membrane into the cytoplasm, the peptide-module responsible for the transport across the cell membrane and discharges its TMZ-NLS(SV40-T)-Cys-OH module containing the cargo TMZ by cytoplasmic glutathione or disulfide reductases. Thereby the NLS sequence serves as a substrate for the import in/Ran mediated active transport into the cell nucleus. The TMZ connection to transporter molecules resulted in a near 10-fold higher pharmacological effect in glioma cell lines while using reduced TMZ-BioShuttle doses [7].

Fig. 1. Illustrates the modular composition of the TMZ-BioShuttle.

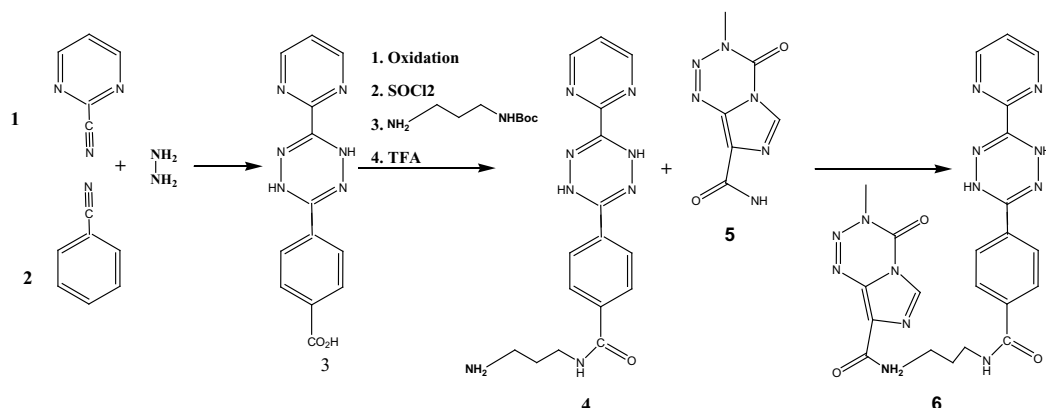


According to the nature’s example we demonstrate this complexity for new more efficient solutions of the proper synthesis of the TMZ-BioShuttle incorporating these different methods as follows; the SPPS and the Diels Alder Reaction with inverse electron demand as described in the following methods part [8].

## Methods

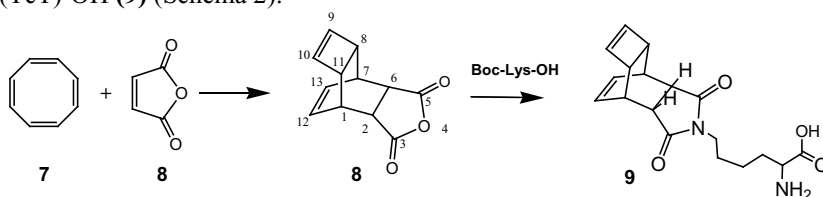
### Synthesis of the diene compound

Compound **4** (0.5 mmol) and the chloride **5** (0.5 mmol) were dissolved in 5 ml chloroform and 5 ml TEA at 0-5 °C. After 4 h at room temperature, the solution was washed with water, 1 N HCl and with water again. The organic layer was dried over Na<sub>2</sub>SO<sub>4</sub> and evaporated (Scheme 1).



Scheme 1. Synthesis of the dienophile compound.

The Reppe anhydride (**8**) was prepared from 42 mg of (1Z,3Z,5Z,7Z)-cyclo-octa-1,3,5,7-tetraene (**7**) and 44 mg maleic anhydride (**8**) in chloroform described by Reppe. The anhydride (10 mmol) was reacted with Boc-Lys-OH (10 mmol) in 50 ml methanol under reflux over 3h to Boc-Lys(TcT)-OH (**9**) (Scheme 2).



Scheme 2. Synthesis of modified lysine.

For solid phase syntheses of the NLS peptide as well as of the CPP peptide, we employed the Fmoc-strategy in a fully automated multiple synthesizer (Syrro II). The synthesis was carried out on a 0.05 mmol Fmoc-Lys(Boc)-polystyrene resin 1% crosslinked and on a 0.053 mmol Fmoc-Cys(Trt)-polystyrene resin (1% crosslinked). As coupling agent 2-(1H-Benzotriazole-1-yl)-1,1,3,3-tetramethyluronium hexafluorophosphate (HBTU) was used. The last amino acid of the NLS-peptide was incorporated as Boc-Lys(TcT)-OH. Cleavage and deprotection of the peptide resin were affected by treatment with 90% trifluoroacetic acid, 5% ethanedithiol, 2.5% thioanisole, 2.5% phenol (v/v/v/v) for 2.5 h at room temperature. The products were precipitated in ether. The crude material was purified by preparative HPLC on an Kromasil 300-5C18 reverse phase column (20 × 150 mm) using an eluent of 0.1% trifluoroacetic acid in water (A) and 60% acetonitrile in water (B). The peptides were eluted with a successive linear gradient of 25% B to 60% B in 40 min at a flow rate of 20 ml/min. The fractions corresponding to the purified peptides were lyophilized.

As last step the (TcT)-NLS-Cys and the transport peptide were oxidized in an aqueous solution of 2mg/ml in 20% DMSO for about five hours. The oxidation progress was monitored by analytical C18 reversed-phase HPLC. The peptide was purified as described above. The purified material was characterized with analytical HPLC and laser desorption mass spectrometry in a Bruker Reflex II.

Equimolar amounts of the TMZ-tetrazine conjugate (**6**) (1.03 mg; 2  $\mu$ mol) and H-Lys(Tct)-NLS(SV40-T)-Cys<sup>-S-S-</sup>Cys-pAntp43-58 (**9**) (7.3 mg, 2  $\mu$ mol)) were dissolved in aqueous solution and stored at room temperature for 24 h.



The work in this article was done in close collaboration with other members of our group. We cordially thank Dr. Christian Kliem and Dr. Jochen vom Brocke for critical reading the manuscript.

1. Merrieffield, R.B., *J. Americ. Chem Soc.* **85**, 2149-2154 (1963).
2. Kolb, H.C., Finn, M.G., et al. *Angew. Chem. Int. Ed Engl.* **40**, 2004-2021 (2001).
3. Duncan, R., *J. Drug Target.* **5**, 1-4 (1997).
4. Lindgren, M., Hallbrink, M., et al. *Trends. Pharmacol. Sci.* **21**, 99-103 (2000).
5. Kalderon, D., Roberts, B.L., et al. *Cell* **39**, 499-509 (1984).
6. Braun, K., Peschke, P., et al. *J. Mol. Biol.* **318**, 237-243 (2002).
7. Waldeck, W., Wiessler, M., et al. *Int. J. Med. Sci.* **5**, 273-284 (2008).
8. Pipkorn, R., Waldeck, W., et al. *J. Pept. Sci.* **15**, 235-241 (2009).

## **Dramatic Increase of Antiviral Potency of an HIV Peptide Fusion Inhibitor by Targeting to Lipid Rafts via Addition of a Cholesterol Group**

**Antonello Pessi,<sup>1</sup> Paolo Ingallinella,<sup>1</sup> Elisabetta Bianchi,<sup>1</sup> Ying-Jie Wang,<sup>2</sup>  
Renee Hrin,<sup>2</sup> Alessia Santoprete,<sup>1</sup> Annunziata Langella,<sup>1</sup>  
Maria Veneziano,<sup>3</sup> Fabio Bonelli,<sup>3</sup> Thomas J. Ketas,<sup>4</sup>  
John P. Moore,<sup>4</sup> and Michael D. Miller<sup>2</sup>**

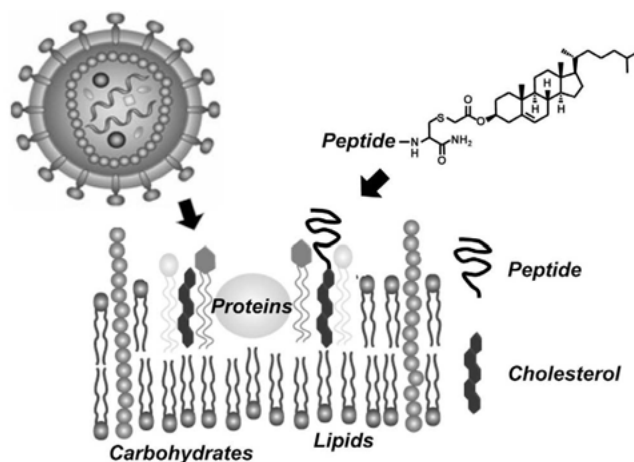
<sup>1</sup>IRBM-MRL Peptide Centre of Excellence, 00040 Pomezia, RM, Italy; <sup>2</sup>Department of Antiviral Research, Merck Research Laboratories, West Point, PA 19486, U.S.A.; <sup>3</sup>Department of Drug Metabolism, IRBM P. Angeletti, 0040 Pomezia, RM, Italy; <sup>4</sup>Department of Microbiology and Immunology, Weill Medical College of Cornell University, New York, NY 10021, U.S.A.

### **Introduction**

Despite considerable progress in the treatment of HIV-infected patients, the need for new antiviral agents remains a major medical need. Ideally, these agents should exploit alternative mechanisms to those targeted by the existing drugs, which are mostly directed to the viral enzymes, the reverse transcriptase, the protease, and most recently, the integrase. The only approved drug targeting viral fusion is the peptide enfuvirtide (T20, Fuzeon<sup>®</sup>) [1]. Enfuvirtide is safe and effective in patients resistant to other antiviral drugs, but requires a high dose and twice daily subcutaneous injections, thus making attractive the development of second-generation fusion inhibitors (FI) with improved pharmaceutical properties. In the following we describe the strategy that we used to develop such a peptide.

### **Results and Discussion**

The mechanism of action of enfuvirtide, and the other known peptide inhibitors derived from the fusogenic protein gp41, is to interfere with the key conformational change of the protein leading to fusion, through binding to a critical intermediate known as the "pre-hairpin" structure [2].

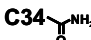
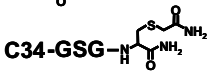
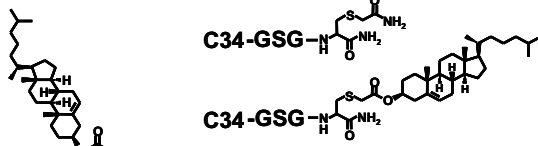

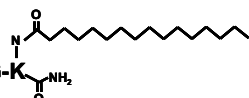


*Fig. 1. Cartoon showing the hypothesized mechanism through which cholesterol derivatization increases the antiviral potency of a peptide. HIV entry occurs in cholesterol-rich domains known as "lipid rafts", and a cholesterol-tagged peptide co-localizes in the same membrane microdomain, driven by cholesterol affinity for the raft. The increase in the effective concentration of the peptide at the fusion site results in increased inhibitory potency.*

A number of studies suggest that the pre-hairpin intermediate is formed in membrane microdomains ('lipid rafts') enriched in cholesterol and sphingolipids, where HIV entry takes place [3]. We reasoned that if local concentration of a fusion inhibitor could be selectively enriched into the same lipid domains targeted by the virus, its antiviral potency would be considerably increased. Further, we envisaged that this might be realized by attaching to the inhibitor cholesterol, which is naturally enriched in the rafts. Our hypothesis is illustrated in Figure 1.

We applied this concept to peptide C34, which is more potent than T20 in cell-based assays, but unlike T20 has a very short half-life in vivo. We found that indeed attachment of cholesterol to C34 to produce compound **3** (C34-chol) dramatically increased its antiviral potency: C34-chol is >50-fold more potent than C34 (**1**) and the control peptide **2**, where the cysteine is alkylated with iodoacetamide (Table 1). To confirm that the observed increase of activity is consistent with the expected mechanism of action, we prepared peptides **4** and **5**. Comparison between peptides **3** and **4** shows that the addition of cholesterol must be done at the C-terminus of the peptide, in line with the need for antiparallel orientation of the inhibitor in the pre-hairpin intermediate [2]. Comparison between peptide **3** and **5** shows that a different lipid group like palmitic acid, which is not enriched in rafts, cannot substitute for cholesterol.

Table 1. The SAR of C34-chol is in agreement with the hypothesized mechanism (see text).

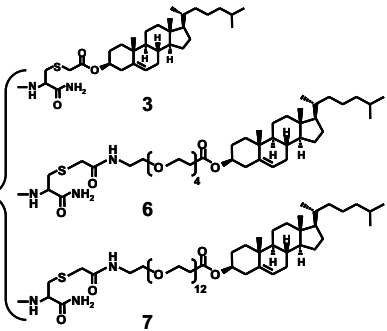
Peptide	#	IC <sub>50</sub> (nM)
<b>C34</b> 	<b>1</b>	0.21 ± 0.06
<b>C34-GSG</b> 	<b>2</b>	0.27 ± 0.09
<b>C34-GSG</b> 	<b>3</b>	0.004 ± 0.001
<b>C34-GSG</b> 	<b>4</b>	9.51 ± 3.17
<b>C34-GSG-K</b> 	<b>5</b>	0.71 ± 0.31

We next examined if the length of the spacer between cysteine and cholesterol had an effect on antiviral potency. The IC<sub>90</sub> of peptides **3**, **6**, **7** which differ only for the spacer length, and **C34** (**1**) against a panel of HIV strains, including primary isolates, are tabulated in Table 2. The results indicate that the spacer has no or minor influence, and that the GSG linker is sufficient to provide flexibility between C34 and the cholesterol group.

Table 2. Addition of a spacer between cholesterol and cysteine does not alter antiviral potency

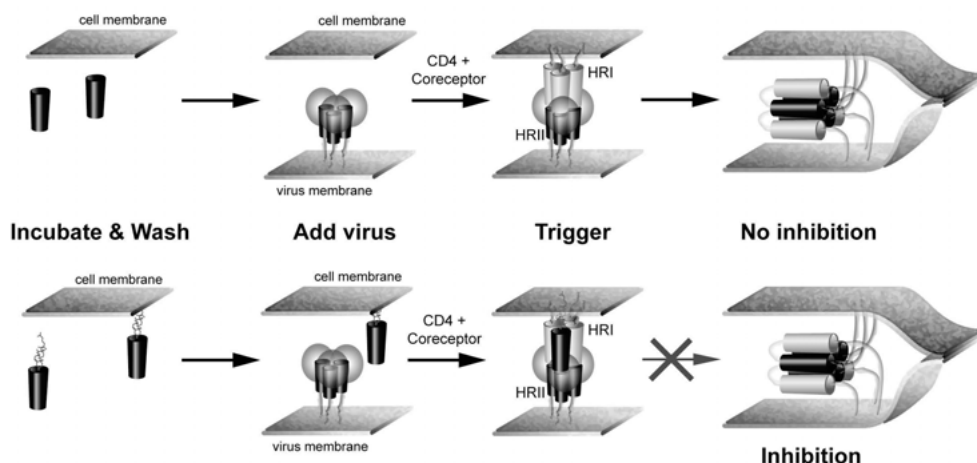
HIV Strain	IC <sub>90</sub> (nM)			
	C34	3	6	7
DJ258	4.6	0.20	0.08	0.09
JRFL	20	0.16	0.11	0.10
NL4-3	5.4	0.16	0.05	0.04
CC 7/86	22	1.0	0.14	0.21
94ZW103	5.3	0.41	0.13	0.18
UG270	51	1.5	0.54	0.39
CM235	20	1.8	0.60	0.71
BZ162	6.1	0.37	0.11	0.10

C34-GSG



The three cholesterol-tagged peptides **3**, **6**, **7** are 15-150-fold more potent than **C34**. Similarly, compound **3** is 15-300-fold more potent than enfuvirtide and the second-generation inhibitor **T1249** [4], making it the most potent HIV fusion inhibitor known to date [5].

Next, we investigated if C34-chol accumulates at the target cell membrane, as expected based on the mechanism of action. In a washout experiment, we incubated peptide **2** and **3** with P4-2/R4 cells for 1h, washed the cells to remove unbound peptide, and initiated infection by addition of the virus. While the antiviral activity of peptide **2** was dramatically reduced ( $IC_{50}$  194 pM and 109 nM without and with wash, respectively), that of cholesterol-tagged peptide **3** was nearly unchanged ( $IC_{50}$  7 pM and 50 pM). Our explanation is illustrated in Figure 2.



*Fig. 2. Cholesterol-tagged peptides retain their inhibitory potency after cell wash. The cartoon shows the hypothesized mechanism for retention of antiviral activity. The inhibitor needs to be present at the point along the reaction pathway where the "pre-hairpin" intermediate is formed. Incubation of the cells with the inhibitor and subsequent wash, prior to addition of the virus, results in loss of antiviral activity for C34 (Top) but not for C34-chol (Bottom) which binds to and remains localized in the membrane microdomain where the intermediate is formed.*

Finally, we investigated if cholesterol derivatization can improve the peptide half-life, as described for other lipids, by increasing the binding of the peptide to plasma proteins. A pharmacokinetic study in mice indeed showed that C34-chol had a considerably longer circulatory half-life than C34 (3 vs. 0.6h) and a 30-fold reduced clearance (0.2 vs. 5.7 mL/min/kg) [5]. Upon subcutaneous injection at the dose of 3.5 mg/kg, the plasma concentration of C34-chol after 24h was still >100-fold higher than the highest  $IC_{90}$  value against the panel of viruses in Table 2.

In conclusion, cholesterol derivatization is a viable strategy to improve the potency and pharmacological properties of peptide fusion inhibitors, one that goes beyond HIV and may be applied to many other enveloped viruses.

## Acknowledgments

We thank Gennaro Ciliberto and Daria J. Hazuda for continuous support and critical discussions, Marco Finotto for peptide synthesis, Simone Bufali for formulation studies, and Manuela Emili for the artwork. T.J.K. and J.P.M. were funded by National Institutes of Health Grants U19 AI65413 and U19 AI76982.

## References

1. Matthews, T., et al. *Nat. Rev. Drug. Discov.* **3**, 215-225 (2004).
2. Eckert, D.M., Kim, P.S. *Annu. Rev. Biochem.* **70**, 777-810 (2001).
3. Aloia, R., Tian, H., Jensen, F.C. *Proc. Natl. Acad. Sci. U.S.A.* **90**, 5181-5185 (1993).
4. Eron, J.J., et al. *J. Infect. Dis.* **189**, 1075-1083 (2004).
5. Ingallinella, P., et al. *Proc. Natl. Acad. Sci. U.S.A.* **106**, 5801-5806 (2009).



## Angiogenesis Inhibition using VEGF Receptor Blockade Approach

Sharad V. Rawale,<sup>1</sup> Daniele Vicari,<sup>2</sup> Kevin C. Foy,<sup>3</sup>  
and Pravin T. P. Kaumaya<sup>1,2,3</sup>

<sup>1</sup>Department of Obstetrics and Gynecology, Division of Reproductive Biology and Vaccine Research,

<sup>2</sup>Department of Microbiology, <sup>3</sup>The Comprehensive Cancer Center and Solove Research Institute, The  
Ohio State University, Columbus, OH 43210, U.S.A.

### Introduction

Angiogenesis is the process of new blood vessel formation from existent vascular network and it is tightly regulated by a balance between pro- and anti-angiogenic factors [1]. Physiologically, angiogenesis is activated in wound healing, ovulation and menstruation. However, it is also observed in pathologic conditions such as cancer, macular degeneration in the eyes and others. Angiogenesis has been highly explored as drug target in cancer therapy after observations that tumors can only grow beyond a few millimeters when well supplied by vascular vessels [2]. Anti-angiogenic therapies have been demonstrated as an alternative to adjuvant therapy in cancer treatment after the correlation between angiogenesis and cancer development [2] was established. Our laboratory has developed peptide-based cancer vaccines with emphasis on the conformational epitopes of HER-2 which is over-expressed in at least 25% of breast cancer [3,4]. Expression of VEGF induced by HER-2 positive tumors led us to target VEGF dependent angiogenesis as a combination therapy. Our long term goal is to develop angiogenic inhibitors that can be used in combination with breast cancer peptide vaccines [3,4]. In this work, we focus on the VEGF activated pathway and propose an approach to interrupt VEGF and VEGFR-2 receptor interaction using peptides designed to mimic the VEGF binding site. The interaction between VEGF and VEGFR-2 has been mapped by alanine scanning showing that the binding site is most localized at loop between  $\beta 5$ - $\beta 6$ . This loop corresponds to "hot spots" for VEGF binding, which includes monoclonal epitope binding (Avastin, G-6 and B20-4) and VEGF receptors binding sites. We selected the VEGF sequence surrounding residues 70-100 to design a VEGF peptide mimic.

### Results and Discussion

In order to understand the inhibition effect of VEGF mimic peptides, we performed number of *in-vitro* and *in-vivo* assays. The tube formation in Matrigel assay (Figure 1) indicates the peptide VEGF-P3(CYC) showing enhanced effect, while VEGF-RI-P4(CYC) with lower effect in tube formation in Matrigel. We performed HUVEC proliferation assay (data not shown), in which all VEGF peptide mimics showed inhibition of HUVEC proliferation in a dose dependent manner. The peptide VEGF-P3(CYC) inhibited proliferation of endothelial cell with higher efficiency compared with the tyrosine kinase inhibitor, while peptide mimics VEGF-RI-P4(NC) and VEGF-RI-(CYC) were not able to inhibit endothelial cell proliferation. The phosphorylation assay (data not shown) using VEGF mimic peptides demonstrated the peptide VEGF-P3(CYC) as the best inhibitor in VEGF-dependent pathways and affinity for VEGFR-2. VEGF-P3(CYC) was also efficient in delaying tumor growth in VEGF<sup>+/-</sup>/Neu2-5<sup>+/+</sup> mice. The retro-inverso cyclic peptide VEGF-RI-P4(CYC) showed no inhibition in tumor growth, while VEGF-RI-P4(NC) demonstrated 2-fold increase in inhibition on VEGF-R2 phosphorylation compared with irrelevant retro-inverso peptide. Combining *in vitro* and *in vivo* results, peptide mimic VEGF-P3(CYC) demonstrated to be the best candidate for development of peptide inhibitors. The conformational peptide mimic VEGF-P3(CYC) also demonstrated better affinity to the receptor and was efficient in delaying tumor burden in a VEGF over-expressing animal model. In order to further support these observations, we have synthesized two peptides; MVFVEGFP3(CYC) and MVFVEGF-RI-P4(CYC), comprising of T<sub>H</sub> epitope MVF as reported earlier [3,4] and raised antibodies against MVFVEGFP3(CYC) peptide in rabbits and mice. We are evaluating these antibodies *in-vivo* and *in-vitro* assays for VEGF inhibition. We are also raising antibodies against MVFVEGF-RI-P4(CYC) peptide in rabbits and mice to further evaluate VEGF inhibition using these antibodies.

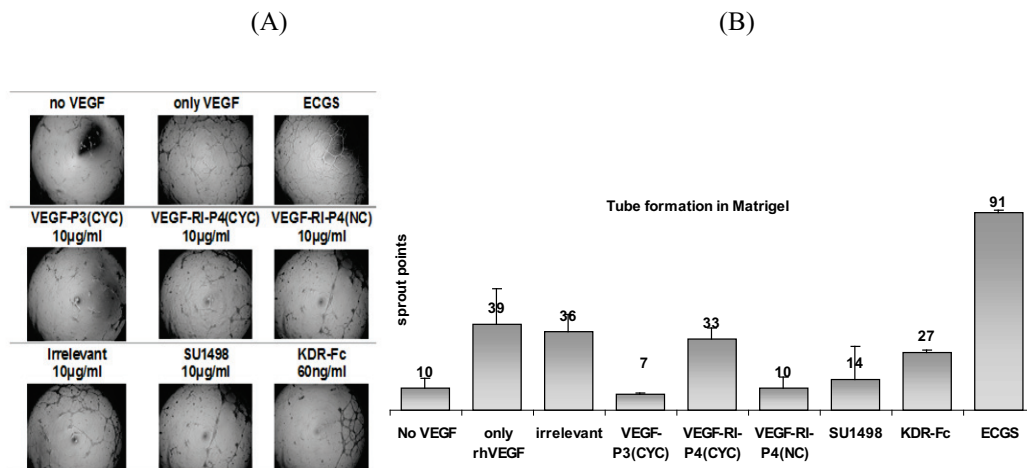


Fig. 1. (A) Pictures from magnification 40X from light microscopy. (B) Average sprout points counted using the software imageJ (NIH) from two different set of experiments carried in duplicates. Inhibitors were used at indicated concentration. KDR-Fc is an extracellular domain from VEGFR2 (R&D System, Minneapolis, MN) and SU1498 (Calbiochem) is a small molecule tyrosine kinase inhibitor. ECGS represent a positive control where growth condition was used - medium supplemented with 20%FBS and ECGS.

## Acknowledgments

This work was supported by NIH/NCI grant #84356 to P.T.P.K.

## References

1. Ferrara, N., et al. *Nature*. **380**, 439-442 (1996).
2. Meduri, G., Bausero, P., Perrot-Applanat, M. *Biol Reprod*, **62**(2), 439-447 (2000).
3. Dakappagari, N.K., Lute, K.D., Rawale, S., Steele, J.T., Allen, S.D., Gary Phillips, G., Reilly, R.T., Kaumaya, P.T.P. *J. Biol. Chem.* **280**, 54-63 (2005).
4. Garrett, J.T., Rawale, S., Allen, S.D., Phillips, G., Forni, G., Morris, J.C., Kaumaya, P.T.P. *J. Immunol.* **178**, 7120-7131 (2007).

## **Phase I Clinical Trial with Her-2 B-Cell Chimeric and Multi-Epitope Based Peptide Vaccines in Patients with Metastatic and/or Recurrent Solid Tumors**

**Pravin T.P. Kaumaya, Kevin Chu Foy, Joan Garrett, Sharad V. Rawale, Daniele Vicari, Tammy Lamb, Aruna Mani, Yahaira Kane, Catherine Balint, Donald Chalupa, Gregory Otterson, Charles Shapiro, Jeffrey Fowler, Michael Grever, Tanios Bekaii-Saab, and William E. Carson III**

*Department of Obstetrics and Gynecology, Division of Reproductive Biology and Vaccine Research, Division of Gynecology Oncology, Departments of Hematology/Oncology, Internal Medicine, Surgery, Comprehensive Cancer Center and Solove Research Institute, Ohio State University, Columbus, OH 43210, U.S.A.*

### **Introduction**

Trastuzumab and Pertuzumab are two humanized Abs that target two different regions of the extracellular domain of HER-2/neu. Although humanized Mabs have been approved by the FDA, a number of concerns still exist. They are expensive and require repeated administration due to their limited duration of action and produce side effects like cardiotoxicity. We have evaluated the safety, toxicity and immunogenicity of increasing doses of two chimeric HER-2 B-cell epitope vaccines derived from the extracellular domain (ECD) in patients with metastatic and/or recurrent solid tumors. Twenty four patients received three inoculations at the intended dose levels and the vaccine was well tolerated, with the maximum tolerable dose (MTD) being the highest dose level (1.5mg each of MVF-316-339 and MVF 628-647) (Table 1) [1] as no dose limiting toxicity was identified for any dose level. After vaccination, four patients were judged to stable disease, two patients had partial response and eleven patients had progressive disease. Anti-peptide abs recognized HER-2 and inhibited HER-2/neu –specific cellular proliferation and receptor phosphorylation. The antibodies were also able to cause antibody dependent cellular cytotoxicity (ADCC) of HER-2 positive cells. This study shows the safety and immunogenicity of the vaccine in a population of patients with metastatic disease.

*Table 1. Two HER-2 peptide sequences used for vaccinating patients*

<i>Peptide</i>	<i>Amino acid Sequence</i>
316-339	MVF-PLHNQEVTAE <del>DT</del> QRA EKCSKPCA
628-647	MVF-INGTHSCVDLDDKGC <del>PAE</del> QR

### **Results and Discussion**

Of 24 patients receiving 3 immunizations of the HER-2 peptide vaccines, 6 patients demonstrated clinical benefit after radiologic reassessment (Table 2). Only one patient (1B) was HER-2 positive whereas the others were all negative. IgG ab responses were performed using ELISA assays and there was an increase in response from dose level 1-4. Dose level 4 was determined to be the MTD. Importantly, these patients also elicited HER-2 specific recombinant Abs. These results confirm that one of the vaccines (316-339) elicited pertuzumab-like abs whereas Trastuzumab did not bind the rhHER-2 because the protein was truncated at sequence 419 lacking the Trastuzumab binding site.

Binding of the peptide Abs to intact HER-2 receptor was evaluated by immunofluorescence staining of single-cell suspension of BT-474. Differential binding was obtained at each dose level. In dose level 4, Abs elicited by each patient bound similarly or better to the HER-2 receptor as compared to the positive control Trastuzumab with pre-sera serving as negative control. The effects of the peptide Abs on both proliferation and phosphorylation were tested using BT-474 cells in the presence of HRG. The patient's sera were

*Table 1. Patient Characteristics. Patients with histologically confirmed metastatic and/or recurrent solid tumors were eligible for enrollment after having received standard therapy and were no longer responding. Patients were not required to have HER-2 over-expression for enrollment.*

<i>Patient ID &amp; Cohorts</i>	<i>Age/Gender</i>	<i>Malignancy</i>	<i>ECOG PS n=</i>	<i>Metastatic sites</i>	<i>Prior Chemo n=</i>	<i>Clinical Benefit</i>	<i>HER-2 status</i>
Cohort 1 :1A	73/F	Colon	0	Lung	2	+SD	-
1B	75/F	SCC	0	Thigh	2	+SD	FISH+
1C	65/F	Ovarian	1	Liver cyst	5	-	FISH+
1D	78/F	Endometrial	2	l. Peritoneum	2	+PR***	-
1E	74/F	Breast	1	Breast, bone	8	-	IHC 3+
1F	37/F	Breast	0	Lung	3	-	IHC 3+
Cohort 2 :2A	57/M	Adrenal	1	Lungs, liver	2	+SD	-
2B	55/M	Pancreas	0	Pancreas	3	-	-
2C	67/F	Ovarian	1	Liver	9	-	-
2D	59/M	Rectal	1	Lung, liver	3	-	-
2E	53/F	Leiomyosarcoma	0	Lung	4	-	-
2F	75/F	Endometrial	1	Lung	2	-	FISH +
Cohort 3 :3A	66/F	Breast	1	Liver	6	-	IHC 3+
3B	41/F	Breast	0-1	Liver	4	-	IHC 3+
3C	46/F	Rectal	2	Periaortic	2	-	-
3D	58/M	Colon	0	Liver, lung	3	-	-
3E	61/M	Colorectal	0	Liver, bone	6	-	-
3F	66/F	Breast	0	Lung, chest	3	-	IHC 2+
Cohort 4 :4A	65/F	Ovarian	0	Pelvis	1	-	IHC 2+
4B	35/F	GIST	-	Lung	1	-	-
4C	70/F	Cervical	1	s. intestine	3	-	-
4D	74/F	Ovarian	0	Abdomen	7	+PR	-
4E	71/F	Ovarian	0	Abdomen	3	+SD	-
4F	49/F	NSCLC	0	Abdomen	3	-	-

*Abbreviations: ECOG PS = Eastern Cooperative Oncology group performance status; SCC = squamous cell carcinoma; GIST = gastrointestinal stromal tumor; NSCLC = non-small-cell lung cancer; SD = stable disease; PR = partial response; PD = progressive disease \*\*\*Patient 1D: durable clinical benefit 4 years+. All patients received doses except 1A, 1D, 2A, 2D, 2E that received 4 doses and 5 for 1D.*

able to inhibit proliferation and phosphorylation of the HER-2 overexpressing cell line BT-474 (Figure 1). In most of the cases, the difference in inhibition between the Abs from the pre-sera and post 3y +3w: 3 weeks post 3<sup>rd</sup> immunization was significant at dose level 4 (Figure 1). 84% of patients in dose level 4 lowered the concentration of the phosphotyrosine on BT-474 cells by 40-50% as compared to the HER-2 phosphorylation inhibitor AG825 used as the positive control.

This first man/woman clinical trial described here consists of a vaccine strategy using two B-cell epitope peptides, MVF 316-339 and MVF 628-647, in combination with nor-MDP adjuvant in oil in water vehicle. The Disis group has vaccinated patients with HER-2 overexpressing breast, NSCLC and ovarian cancers with peptides derived from the Th epitopes of the HER-2 protein in combination with GM-CSF [2]. 92% of patients developed T-cell immunity to the HER-2 peptides. Several preclinical studies have demonstrated that the inductions of anti-HER-2/neu abs are both necessary and sufficient for protection of BALB-neuT mice [3, 4].

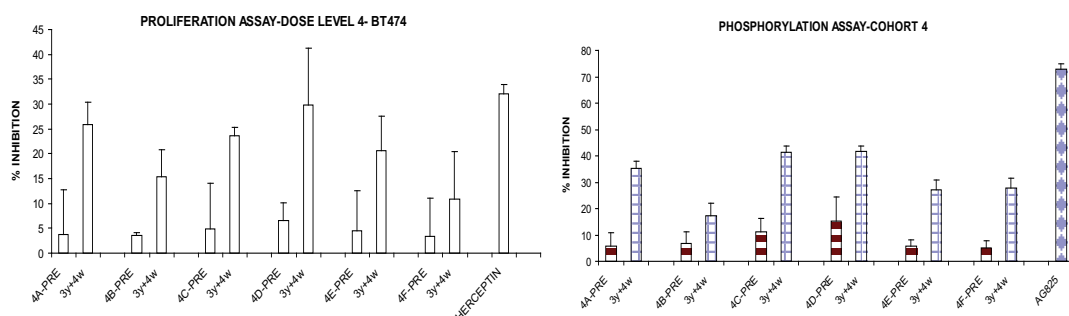


Fig. 1. Effects of purified anti-peptide antibodies on proliferation and phosphorylation of BT-474 cells. Cells were incubated with medium alone or treated with pre abs, peptide abs and Trastuzumab (100ug). The inhibition rate was calculated using the formula  $(OD_{\text{medium alone}} - OD_{\text{treated}}) / OD_{\text{medium alone}} \times 100$ . Error bars represent SD.

We demonstrate here that the peptide vaccine elicited IgG abs at all dose levels indicating peptide specific T cell activation was provided by the promiscuous MVF T-epitope. Dose level 4 was determined to be the MTD based on the lack of dose limiting toxicity and a significant dose dependent increase in IgG ab response in patients. It is important to underscore that our vaccine epitopes correspond to overlapping sequences of Trastuzumab and Pertuzumab binding sites that target different extracellular regions of HER-2 tyrosine kinase receptor. Trastuzumab binds domain IV, causes ADCC and inhibits proliferation whereas Pertuzumab binds domain II and blocks its ability to dimerize with other HER receptors. Although the intent of our study was to determine the efficacy, we did find evidence of preliminary activity in 6 patients who had either PR or SD. Interestingly, only one of these 6 patients was HER-2 positive as determined by FISH and with the remaining five not overexpressing HER-2. Given the nature of our combination vaccine, one could anticipate that several mechanisms could be operative between HER-2 negative and positive patients. However it is difficult to infer clinical benefit to any immune response given the small number of patients.

In conclusion, this Phase I study demonstrates the peptide vaccine is safe and it elicited IgG Abs in a population of patients with metastatic disease that have been heavily pre-treated. These abs recognized HER-2, specifically suppress its phosphorylation and inhibit cell proliferation. This study is the first to show that a combination B cell epitope vaccine can elicit abs that disrupt two different HER-2 signaling pathways. The design of HER-2 based peptides should offer safer alternatives given that clinicians are still facing many uncertainties concerning the optimal use of tyrosine kinase inhibitors. The clinical benefit of this vaccine remains to be investigated in a future Phase II clinical trial.

## Acknowledgments

This work was funded by a National Cancer Institute Grant CA 094555 to P.T.P Kaumaya.

## References

1. Dakappagari, N., Pyles, J., Kaumaya, P., *Journal of Immunology* **170**, 4242-4245 (2003).
2. Disis, M.L., Grabstein, K.H., Sleath, P.R., Cheever, M. *Clin. Cancer Res.* **5**, 1289-1297 (1999).
3. Allen, D., Garrett, J., Kaumaya, P. *Journal of Immunology* **179**, 472-482 (2007).
4. Garrett, J., Rawale, S., Allen, S., Kaumaya, P. *Journal of Immunology* **178**, 7120-7131 (2007).

## Combination Treatment with Her-2 and VEGF Peptide Mimics Induces Potent Anti-Tumor and Anti-Angiogenic Responses *In Vitro* and *In Vivo*

Kevin C. Foy,<sup>1</sup> Zhenzhen Liu,<sup>2</sup> Sharad Rawale,<sup>3</sup> Gary Phillips,<sup>4</sup> Megan Miller,<sup>1</sup> Aravind Menon,<sup>1</sup> Nina D. Osafo,<sup>1</sup> and Pravin T.P. Kaumaya<sup>1,2,3,4</sup>

<sup>1</sup>Department of Microbiology, <sup>2</sup>The Ohio State Biochemistry Program, <sup>3</sup>Department of Obstetrics and Gynecology, <sup>4</sup>Arthur G. James Comprehensive Cancer Center, Ohio State University, Columbus, OH 43210, U.S.A.

### Introduction

HER-2 is a member of the EGFR family and is overexpressed in 20-30% of breast cancers. HER-2 overexpression causes increased expression of VEGF at both the RNA and protein level [1]. These two proteins are therefore considered good targets for cancer treatment which have led to the development of two humanized monoclonal antibodies (mAb) Pertuzumab and Bevacizumab that target HER-2 and VEGF respectively. Exposure of HER-2 overexpressing cells to trastuzumab/herceptin another mAb that targets HER-2 significantly decreases VEGF expression [2]. Although passive immunotherapy with these Abs has been approved for treatment of advanced breast cancer, a number of concerns exist with passive immunotherapy. Treatment is expensive, and has a limited duration of action, necessitating repeated administrations of the mAb. Peptide therapy with conformational B-cell epitope mimics can be cheaper with a longer half-life. The goal of the present study was to show that combination treatment with HER-2 and VEGF peptide mimics provides greater efficacy than single treatment. We designed and synthesized peptides based on the binding of (i) HER-2 with Pertuzumab and (ii) VEGF with VEGFR2. We show that combination treatment with these peptides induces potent anti-tumor and anti-angiogenic responses *in vitro* and *in vivo*.

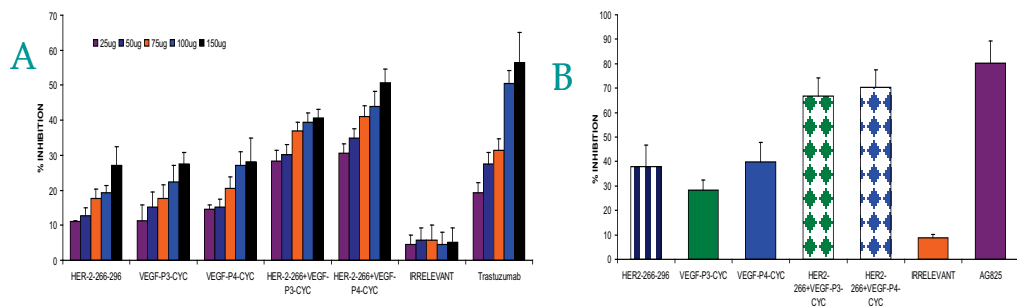
### Results and Discussion

B-cell epitopes from the HER-2 and VEGF (Table 1) proteins were synthesized using Fmoc chemistry on a Milligen/Bioscience 9600 peptide synthesizer (Bedford, MA). We synthesized the peptide VEGF-P3 cyclized (CYC), a conformational epitope, consisting of an anti-parallel  $\beta$ -sheet and it required two artificial cysteine residues to be introduced between Gln79 and Gly92, and between Ile80 and Glu93. After synthesis and purification of the VEGF-P3 non-cyclized (NC) peptide, the disulfide bond was formed using iodine oxidation reaction, enabling the formation of the twisted anti-parallel  $\beta$ -sheet structure. Following characterization by HPLC and MS, peptides were kept lyophilized and dissolved prior to use in subsequent assays. The retro-inverso (RI) peptide analog VEGF-RI-P4 is synthesized using D-amino acids with the amino acid sequence in reverse order. The HER-2 266 peptide was synthesized and disulphide pairing accomplished as described above.

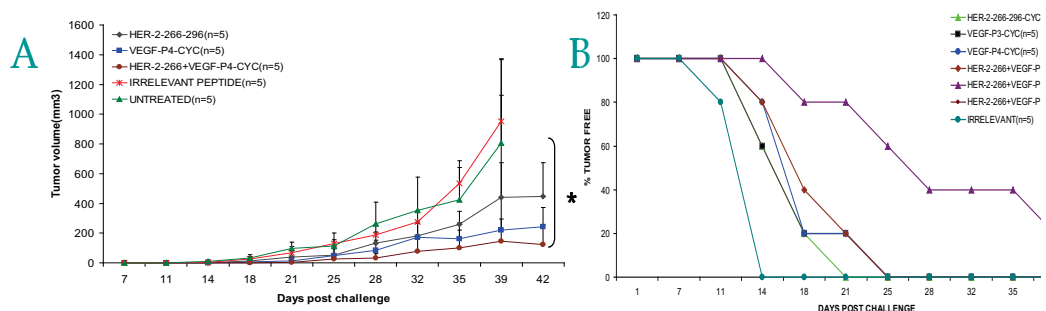
Table 1. HER-2 and VEGF mimic peptide sequences

HER-2-266-296(CYC)	LHCPA LVTYNTDTFESMPNPEGRYTFGASCV
VEGF-P3(CYC)	76-ITMQ-79-C-92-GIHQQGHPKIRMI-80-C-EMSF-96
VEGF-RI-P4(CYC)	(D)-96-FSME-80-C-92-IMRIKPHQGQHIG-79-C-QMTI-76

Combination treatment with HER-2 and VEGF peptide mimics were shown to cause a greater inhibition of cell proliferation using HER-2 positive cell lines (BT-474) (Figure 1A). HER-2 signaling mainly occurs via dimerization with other receptors and the prevention of this dimerization will prevent intracellular signaling and phosphorylation. The peptides were also able to inhibit HER-2 specific phosphorylation due inhibition of HER-2 dimerization with other HER- receptors and combination treatment showed the best response (Figure 1B). *In vivo*



**Fig. 1.** Effects of combination treatment with peptides on (A) cancer cell proliferation, (B) HER-2 specific phosphorylation using BT474 Cells (HER-2 overexpressors) incubated with HER-2 peptide, VEGF peptides or combination of both. Trastuzumab, AG825 (Calbiochem) a potent HER-2 phosphorylation inhibitor and irrelevant peptide were used as controls. The inhibition rate was calculated using the formula  $(OD \text{ normal Untreated} - OD \text{ peptides or Ab}) / (OD \text{ normal untreated} \times 100)$ . Error bars represent SD).



**Fig. 2.** Wild type BALB/c mice ( $n = 5$ ), at the age of 5-6 weeks was challenged with TUBO cells that were derived from BALB-neuT mice which are transgenic for the rat HER-2/neu oncogene, and were treated intravenously with HER-2 and VEGF peptide mimics, and scrambled irrelevant peptide, Tumor measurements were performed twice a week using calipers. The data are presented as the average tumor size per group and are reported as  $\text{mm}^3$  for combination treatment for HER-2 peptide with D-amino acid VEGF peptide (A) and percentage tumor free (B) as compared to the control groups. Error bars represent mean standard deviations.

studies using a transplantable mouse model showed that combination treatment with both peptide epitopes produced a greater delay in tumor growth and development as compared to single treatments (Figure 2B). In the case of combination treatment with both HER-2 and the retro- inverso peptide, there was an increase in % tumor free and one mouse remained tumor free at the end of the experiment (Figure 2A). Finally, combination treatment with the D-amino acid VEGF peptide mimic also produced a reduction in tumor weight with a statistically significant difference from the control (Figure 3). These results indicates that targeting both HER-2 and VEGF is a better strategy in treating HER-2 positive cancers since this will destroy two different targets of the same pathway

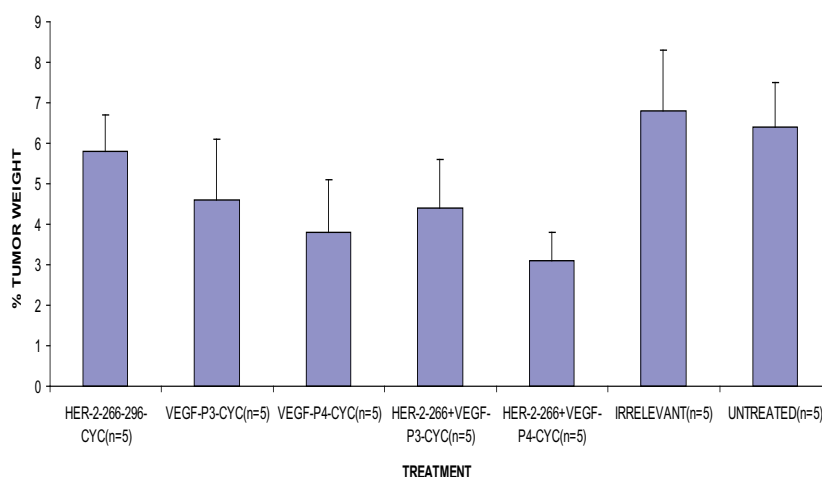


Fig. 3. Effects of combination treatment on tumor weight. Wild type BALB/c mice ( $n = 5$ ), at the age of 5-7 weeks was challenged with TUBO cells that were derived from BALB-neuT mice which are transgenic for the rat HER-2/neu oncogene, and were treated intravenously with HER-2 and VEGF peptide mimics, and scrambled irrelevant peptide. Tumors were removed at the end of treatment and % tumor weight was calculated using the formula tumor weight/ weight of mice with tumor  $\times 100$ . The group treated both HER-2 and D-amino acid VEGF peptide showed the lowest percentage tumor weight as compared to the control group with a  $p$  value of 0.05 (#) Error bars represent mean standard deviations.

## Acknowledgments

This work was funded by a National Cancer Institute grant to P.T.P Kaumaya.

## References

1. Liang, Y., Hyder, M. *Endocrinology* **146**, 3632 (2005).
2. Konecny, G.E., Meng, G., et al *Clin. Cancer Res.* **10**, 1706 (2004).



## Structure-Activity Relationship Study of New FK228 Analogues as Antitumor Agents

Salvatore Di Maro,<sup>1</sup> Rey-Chen Pong,<sup>2</sup> Jer-Tsong Hsieh,<sup>2</sup> and  
Jung-Mo Ahn<sup>1</sup>

<sup>1</sup>Department of Chemistry, University of Texas at Dallas, Richardson, TX 75080, U.S.A.; <sup>2</sup>Department of Urology, University of Texas Southwestern Medical Center at Dallas, Dallas, TX 75390, U.S.A.

### Introduction

Histone deacetylases (HDACs) are a family of enzymes that play a crucial role in regulating numerous vital functions by influencing on gene expression through the modification of chromosomal DNA conformation. They are typically grouped into four classes, and classes I, II and IV are characterized to have  $\text{Zn}^{2+}$  as a critical component at their active sites, whereas class III HDACs distinctly use a cofactor,  $\text{NAD}^+$  [1]. In the past two decades, many studies showed a correlation between an increased activity of  $\text{Zn}^{2+}$ -dependent HDACs and tumorigenesis processes, and this makes HDACs a new attractive therapeutic target for cancer treatment [2]. A number of small molecules have been identified or developed as HDAC inhibitors that trigger cell cycle arrest, differentiation, and apoptosis in cancer cells [3].

Isolated from *Chromobacterium violaceum*, FK228 (also known as FR901,228 or depsipeptide) is a highly potent inhibitor with selectivity toward class I HDACs that appears to be more relevant for intervention in oncology [4,5]. Despite its promising therapeutic profile, FK228 has a unique bicyclic structure and several synthetically challenging moieties. These synthetic difficulties prevented the synthesis of FK228 analogues that would promote the understanding of the molecular mechanism underling its anti-cancer activity.

### Results and Discussion

To investigate structural requirements of FK228 for its functions, we have recently developed novel analogues of FK228 that were designed by replacing the most synthetically challenging unit, (3*S*,4*E*)-3-hydroxy-7-mercapto-heptenoic acid with a structure that can be easily assembled with readily available chemicals [6] (Figure 1). And, an efficient solid-phase synthetic strategy was achieved to prepare a series of FK228 analogues.

As described in Scheme 1, the synthesis started from a reductive amination of a cysteamine to a solid support, and the subsequent coupling of an Asp produced a surrogate (**2**) for the synthetically challenging heptenoic acid in FK228. After the remaining four amino acids were sequentially coupled, a macrolactam (**5**) was created and oxidized with iodine on resin to produce FK228 analogues (**6-20**) in high yield (>75%) and purity (>80%).

The synthesized FK228 analogues (**6-20**) were evaluated for their inhibitory activity on human bladder cancer cell line, T24. Each compound was incubated with T24 cells at various concentrations over 3 days and cell proliferation was measured after treating with MTT for 4 h. As shown in Figure 2, a range of cell growth inhibition was observed by the FK228 analogues, and several compounds (**10**, **17**, and **19**) were identified as the most potent analogues showing 70-98% inhibition at 0.5  $\mu\text{M}$ . Then, selected leads (**10** and **19**) were examined on six human cancer cell lines derived from either prostate or bladder tumor, and also demonstrated effective growth inhibitions on all six cancer cells ( $\text{IC}_{50}$  = 0.18-1.8  $\mu\text{M}$  for **10**;  $\text{IC}_{50}$  = 0.03-0.22  $\mu\text{M}$  for **19**).

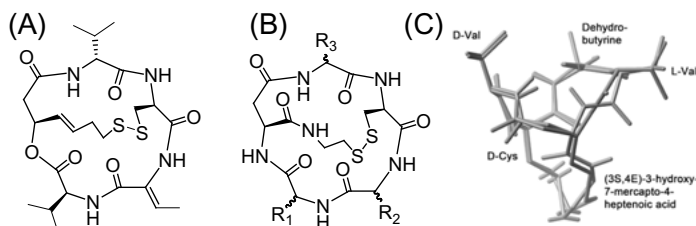
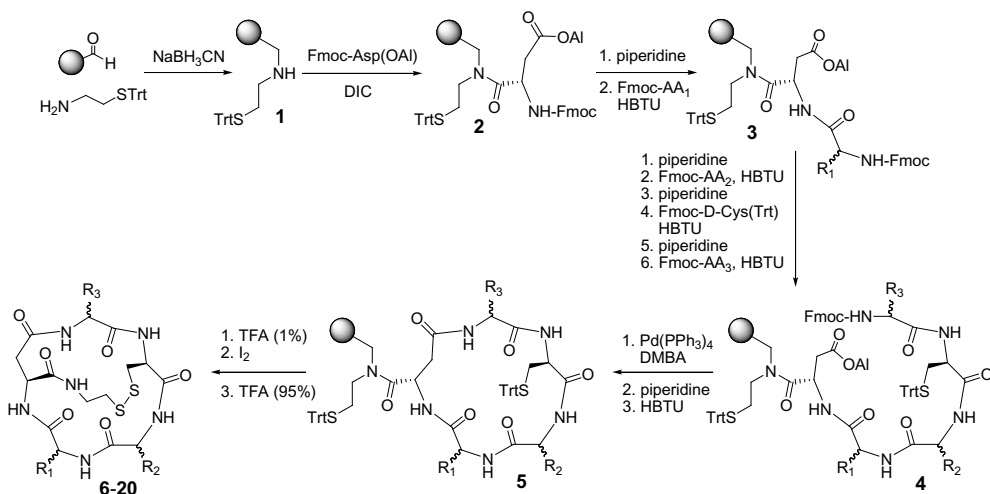


Fig. 1. Structures of (A) FK228 and (B) its analogues, and (C) superimposition of the two.



Scheme 1. Solid-phase synthesis of FK228 analogues.

From this limited structure-activity study, introduction of two aromatic amino acids (e.g., *L*-Phe, *L*-2-Nal) at the positions of *L*-Val and *Z*-Dhb in FK228 was found to improve potency, and a bulkier aromatic ring (e.g., 2-naphthyl group in **17** and **19**) appears to be more effective. In addition, a stereochemical preference at the position of the *Z*-Dhb was observed as *D*-Phe in **13** led to a significant loss in potency.

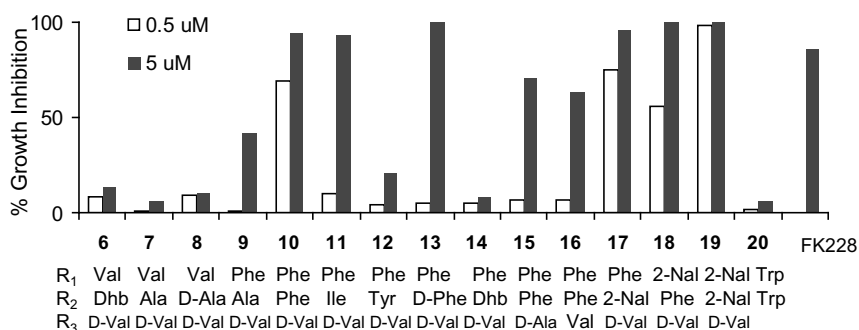


Fig. 2. Antitumor activity of FK228 analogues on human bladder cancer cells.

## Acknowledgments

Supported by start-up funds (University of Texas at Dallas, J.-M.A.), grant AT-1595 (Welch Foundation, J.-M.A.), CA95730 (NIH, J.-T.H.), and fellowship (University of Naples, "Federico II", S.D.M).

## References

- Pazin, M.J., Kadonaga, J.T. *Cell* **89**, 325-328 (1997).
- Johnstone, R.W. *Nat. Rev. Drug Discov.* **1**, 287-299 (2002).
- Monneret, C. *Eur. J. Med. Chem.* **40**, 1-13 (2005).
- Fujisawa Pharmaceutical Co., Ltd., Jpn. Kokai Tokkyo Koho JP, 03141296 (1991).
- Curtin, M., Glaser, K. *Curr. Med. Chem.* **10**, 2373-2392 (2003).
- Di Maro, S., Pong, R.-C., Hsieh, J.-T. Ahn, J.-M. *J. Med. Chem.* **51**, 6639-6641 (2008).

## DhHP-6 Extends *Caenorhabditis elegans* Lifespan in a SIR2.1-Dependent Manner

Shuwen Guan,<sup>1</sup> Pengfei Li,<sup>1</sup> Yuanyuan Li,<sup>2</sup> Shuhua Zhang,<sup>1</sup>  
 Xiaoguang Chen,<sup>1</sup> Liping Wang,<sup>1\*</sup> and Wei Li<sup>1</sup>

<sup>1</sup>College of life science, Jilin University, Changchun, 130021, P.R. China; <sup>2</sup>Jilin Province Product Quality Supervision Test Institute, Changchun, 130021, P.R. China

\* Corresponding author Tel: +86-431-88499505; Fax: +86-431-88921591; Email: wanglp@jlu.edu.cn

### Introduction

SIR2 (silent mating type information regulation-2) and its orthologs represent a conserved group of genes encoding NAD<sup>+</sup>-dependent protein deacetylases that play important roles in lifespan-extending effects [1]. Increased dosage of SIR2 orthologs from *S. cerevisiae*, *D. melanogaster*, and *C. elegans* extend their lifespan, suggesting that Sir2 genes are conserved regulators of the aging process [2]. In *C. elegans*, it has been identified that SIR-2.1 functions through 14-3-3 proteins and affect DAF-16 transcriptional activity [3]. DhHP-6 is a nonapeptide that contains deuterohaemin and histidine. It was designed as a mimetic of peroxidase. Our recent studies show that DhHP-6 extends the lifespan of wild type *C. elegans* by 20%. Here we found that DhHP-6 treatment up-regulates *sir-2.1* gene encoding SIR2 like protein in *C. elegans* and the lifespan extension by DhHP-6 is also dependent upon *sir-2.1*. We predict that DhHP-6's lifespan extension effect is mediated by *sir-2.1*/DAF-16 pathway.

### Results and Discussion

DhHP-6 increased both the mean and maximum lifespan and a nearly 20% increase in a *daf-16* dependent manner in mean lifespan was observed in wild type worms with 0.2mM DhHP-6. To further identify genetic components that may contribute to DhHP-6 mediated lifespan extension, we analyzed several *daf-16* upstream genes of worms grown in the presence and absence of DhHP-6 by real time RT-PCR. *Sir-2.1*, encoding SIR2 like protein in *C. elegans*, was upregulated ~6-fold in wild type (wt) worms after 4 days treatment (Figure 1A). This finding is in consistence with others' result that over-expressing SIR-2.1 lead to further extension of lifespan in WT worms [4]. Expression level of *daf-2* or *daf-16* gene does not change upon DhHP-6 treatment.

According to the former results that DhHP-6 extended worm's lifespan in a *daf-16* dependent manner, we hypothesized that DhHP-6 might be a positive transcriptional regulator of *sir-2.1* gene and thus result in nuclear localization of DAF-16. In *sir-2.1* (*ok434*)/IV mutant,

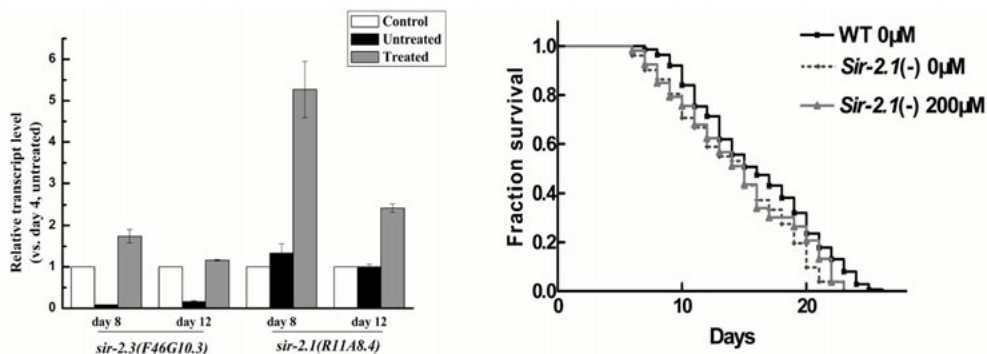


Fig. 1. Effect of DhHP-6 on gene expression and lifespan. A: Expression levels of *sir-2.1* and *sir-2.3* genes, relative to housekeeping gene *gpd-1*, were determined by real time RT-PCR. B: Lifespan extension was blocked in the *sir-2.1*(*ok434*) mutant. Data listed in Table 1.

Table 1. The effects of DhHP-6 on *Caenorhabditis elegans*

Strains	Treatment	Mean lifespan $\pm$ SE (n)	Max lifespan	P value*
Wt	<i>E.coli</i> (0)	16.12 $\pm$ 0.3 (275)	25	-
Wt	<i>E.coli</i> (50)	19.35 $\pm$ 0.38 (168)	27	<0.001
<i>daf-16(mgDf50)</i>	<i>E.coli</i> (0)	12.76 $\pm$ 0.38 (121)	21	-
<i>daf-16(mgDf50)</i>	<i>E.coli</i> (50)	11.06 $\pm$ 0.38 (93)	19	0.001
<i>sir-2.1 (ok434)</i>	<i>E.coli</i> (0)	14.35 $\pm$ 0.68 (51)	23	-
<i>sir-2.1 (ok434)</i>	<i>E.coli</i> (50)	14.7 $\pm$ 0.7 (53)	23	0.471

Wt=wild type; *E.coli*, *E.coli* OP50 to OD600=0.3 (about  $1 \times 10^8$ - $1 \times 10^9$  cells/ml); \*P value (log rank test) compared with untreated control

we found that this lifespan extension mediated by DhHP-6 was fully blocked (Table 1 and Figure 1B). This result suggests that SIR-2.1 protein is essential for DhHP-6's lifespan extension effects. Compared to other compounds that can also extend the lifespan of *C. elegans* [5], DhHP-6 has two major advantages. First, as a peptide-structured mimetic, DhHP-6 has higher activity, is easily synthesized, and has low toxicity even at a high dosage. Second, DhHP-6 has low molecular weight and high stability. As a stable peptide mimetic of low toxicity, DhHP-6 has the potential to be a useful clinical tool in delaying aging and ameliorating oxidation and age-related disease.

## Acknowledgments

We thank prof. Xueqi Fu of College of Life Science of Jilin University for assistance with the culture of wild type *C.elegans*. The *sir-2.1 (ok434)* and *daf-16(mgDf50)* mutant strains were provided by *Caenorhabditis* Genetics Center, which is funded by the National Institutes of Health (NIH) National Center for Research Resources.

## References

1. Van der Linden, A.M., Plasterk, R.H.A. *Genomics* **5**, 225-229 (2004).
2. Weijian, J. *B.B.R.C.* **373**, 341-344 (2008).
3. Ala, B., Mohan, V., Robert, H., Leonard, G. *Cell* **125**, 1165-1177 (2005).
4. Tissenbaum, H.A., Guarente, L. *Nature* **410**, 227-230 (2001).
5. Collins, J., Kornfeld, K. *Experimental Gerontology* **41**, 1032-1039 (2006).

## Solid Phase Synthesis of Lipidated Peptidotriazoles as Bisubstrate Inhibitors of Protein Geranylgeranyltransferase-I

Animesh V. Aditya and Richard A. Gibbs

Dept. of Med. Chem. and Mol. Pharm., Purdue University, West Lafayette, IN 47907, U.S.A.

### Introduction

Protein prenylation is an important post-translational modification that controls the subcellular localization and membrane trafficking of more than one hundred human proteins, particularly G-proteins belonging to the Ras and Rho families [1]. Prenylation is executed by prenyltransferases - Farnesyltransferase (FTase) and Geranylgeranyltransferases-I & II (GGTase-I and GGTase-II) that catalyze the transfer of a C<sub>15</sub> or C<sub>20</sub> isoprenoid to the cysteine thiol present close to the C-terminus of the protein. FTase and GGTase-I have been established as promising targets for the development of cancer therapeutics [2]. These bisubstrate enzymes couple their protein substrates (or peptides containing a C-terminal CaaX-motif) with the respective isoprenoid pyrophosphate co-substrate. The C-terminal CaaX motif of the substrates comprises a cysteine residue followed by two 'a' residues that are typically aliphatic, and the "X" residue that plays a major role in prenyltransferase recognition and specificity [3]. These substrate structural features have been utilized in developing GGTIs designed to be competitive with the peptide or the isoprenoid substrates [1]. This paper explores an alternative approach to inhibition of GGTase-I based on bisubstrate analog design.

### Results and Discussion

Bisubstrate inhibition of CaaX prenyltransferases offers a unique approach for structure-based inhibitor design. These analogues display the structural elements of the CaaX peptide as well as the isoprenoid substrate. This approach is particularly attractive because structural variations can be systematically carried out on two different platforms – the peptide motif and the isoprenoid motif – to fine-tune the potency and selectivity of inhibitors for a specific CaaX prenyltransferase. We investigated the feasibility of this approach by designing lipidated peptidotriazoles as readily prepared bisubstrate mimetics (Figure 1).

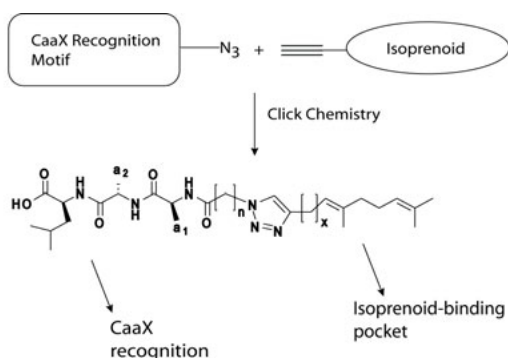


Fig. 1. Bisubstrate analog design for CaaX-Prenyltransferases.

generation of these analogs. We also envisioned that the triazole could serve as an alternative zinc-binding moiety, thereby eliminating the requirement for a free thiol in the peptide moiety.

These peptidotriazoles were assembled on chlorotriyl resin [5] in a C- to N-terminal manner. The peptide fragment was assembled by standard Fmoc solid phase peptide synthesis methodology. The azide functionality was subsequently introduced by on-resin diazo transfer [6] to the free amine at the N-terminal of the peptide followed by click chemistry with isoprenoid alkynes. This methodology was optimized by utilizing a combination of qualitative tests and ESI-MS for analysis. The peptidotriazoles were cleaved from the resin using mild acidic conditions and purified by reverse phase preparative-HPLC.

All peptidotriazoles were screened versus FTase and GGTase-I using a well-established continuous fluorescence assay [7]. Substrate turnover is measured through fluorescence enhancement caused by prenylation of the fluorescent CaaX-peptide. Initial

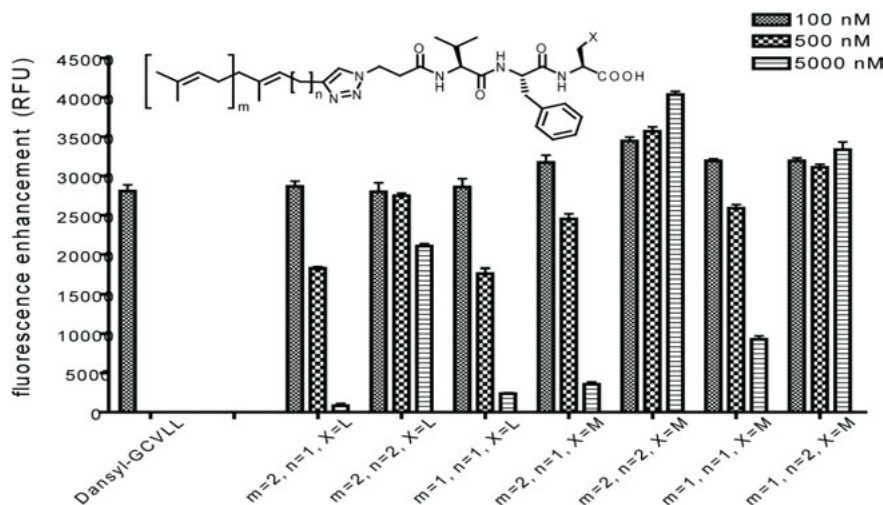


Fig. 2. Screening of prenylated peptidotriazoles versus GGTase-I in a fluorescence assay.

screening with lipidated peptidotriazoles demonstrated very poor inhibition of FTase, but more promising results were obtained with GGTase-I. The potency of bisubstrate peptidotriazoles was fine-tuned by systematically modifying the diversity elements such as the residues in “aaX” motif, the linker length between the peptide and triazole, and length of the isoprenoid chain. These SAR studies indicate the requirement for VFL as the peptide fragment for optimal potency. Additionally, the activity of these peptidotriazoles varied with the flexibility of the linker between the peptide fragment and the disubstituted triazole. As seen in Figure 2, the best bisubstrate analogs obtained exhibit nanomolar  $IC_{50}$  values for GGTase-I.

Selected peptidotriazoles that are potent GTIs were also screened versus FTase to determine the selectivity of these inhibitors. The most potent inhibitor of GGTase-I obtained by this methodology did not show any inhibition of FTase even at a concentration ten-fold higher than its  $IC_{50}$ , revealing a high selectivity for GGTase-I.

In conclusion, solid phase synthesis combined with Huisgen cycloaddition offers a unique strategy to develop non-thiol bisubstrate inhibitors of CaaX-prenyltransferases. The potency and selectivity of these inhibitors can be fine-tuned by appropriately modifying the peptide and isoprenoid fragments in these compounds.

## Acknowledgments

This work was supported by NIH grants R01 CA78819 (to RAG) and P30 CA21368 (to the Purdue Cancer Center), and a Purdue Research Foundation fellowship (to AVA).

## References

1. Lane, K.T., Beese, L.S. *J. Lipid Res.* **47**, 681-699 (2006).
2. Konstantinopoulos, P.A., Karamouzis, M.V., Papavassiliou, A.G. *Nat. Rev. Drug Discov.* **6**, 541-555 (2007).
3. Reid, T.S., Terry, K.L., Casey, P.J., Beese, L.S. *J. Mol. Biol.* **343**, 417-433 (2004).
4. Rostovtsev, V.V., Green, L.G., Fokin, V.V., Sharpless, K.B. *Angew. Chem. Int. Ed. Engl.* **41**, 2596-2599 (2002).
5. Barlos, K., Chatzi, O., Gatos, D., Stavropoulos, G. *Int. J. Pept. Protein Res.* **37**, 513-520 (1991).
6. Angelo, N.G., Arora, P.S. *J. Org. Chem.* **72**, 7963-7967 (2007).
7. Cassidy, P.B., Dolence, J.M., Poulter, C.D. *Methods Enzymol.* **250**, 30-43(1995).

# Effect of Net Positive Charge and Charge Distribution on the Polar Face of Amphipathic $\alpha$ -Helical Antimicrobial Peptides on their Biological and Biophysical Properties

Ziqing Jiang,<sup>1</sup> Adriana I. Vasil,<sup>2</sup> Michael L. Vasil,<sup>2</sup> and Robert S. Hodges<sup>1</sup>

<sup>1</sup>Department of Biochemistry & Molecular Genetics and <sup>2</sup>Department of Microbiology,  
University of Colorado Denver, School of Medicine, Aurora, CO 80045, U.S.A.

## Introduction

This is a systematic study of varying the number of positively charged residues on the polar face of our amphipathic  $\alpha$ -helical antimicrobial peptides, D1 and analogs D5 [1-5] and D17 to D22 (Table 1). The nonpolar face is identical in the six analogs D17 to D22. As shown in Table 1, the number of lysine residues increases systematically from 4 (D17), 5 (D18), 6 (D19), 7 (D20), 8 (D21) to 9 (D22) on the polar face. The net charge on the peptides concomitantly increases from +5 to +10 because of the specificity determinant on the nonpolar face, K13, in each analog.

Table 1. Peptides used in this study

Peptide	Substitution <sup>a</sup>	Sequence <sup>b</sup>			Hydrophobicity tr <sup>c</sup> (min)
		1	13	26	
D1	D-(V13K)	Ac-K-W-K-S-F-L-K-T-F-K-S-A-K-K-T-V-L-H-T-A-L-K-A-I-S-S-amide			76.75
D5	D-(V13K, V16K, A12L, A20L, A23L)	Ac-K-W-K-S-F-L-K-T-F-K-S-L-K-K-T-K-L-H-T-L-L-K-L-I-S-S-amide			80.44
D17	D-(V13K, V16A, A20L, K10S, S11K, T15K, H18K, K1S, K3S, K7S, K22S)	Ac-S-W-S-S-F-L-S-T-F-S-K-A-K-K-K-A-L-K-T-L-L-S-A-I-S-S-amide			98.81
D18	D-(V13K, V16A, A20L, K10S, S11K, T15K, H18K, K1S, K3S, K22S)	Ac-S-W-S-S-F-L-K-T-F-S-K-A-K-K-K-A-L-K-T-L-L-S-A-I-S-S-amide			97.87
D19	D-(V13K, V16A, A20L, K10S, S11K, T15K, H18K, K1S, K3S)	Ac-S-W-S-S-F-L-K-T-F-S-K-A-K-K-K-A-L-K-T-L-L-K-A-I-S-S-amide			97.94
D20	D-(V13K, V16A, A20L, K10S, S11K, T15K, H18K, K1S)	Ac-S-W-K-S-F-L-K-T-F-S-K-A-K-K-K-A-L-K-T-L-L-K-A-I-S-S-amide			95.90
D21	D-(V13K, V16A, A20L, S11K, K10S, T15K, H18K, K1S, S26K)	Ac-S-W-K-S-F-L-K-T-F-S-K-A-K-K-K-A-L-K-T-L-L-K-A-I-S-S-amide			93.77
D22	D-(V13K, V16A, A20L, K10S, S11K, T15K, H18K, S26K)	Ac-K-W-K-S-F-L-K-T-F-S-K-A-K-K-K-A-L-K-T-L-L-K-A-I-S-K-amide			90.67

<sup>a</sup>D- denotes that all amino acid residues in each peptide are in the D conformation. <sup>b</sup>Peptide sequences are shown using the one-letter code for amino acid residues; Ac- denotes N $\alpha$ -acetyl and -amide denotes C $\alpha$ -amide. <sup>c</sup>t<sub>R</sub> denotes retention time in RP-HPLC at pH 2 and room temperature, and is a measure of overall peptide hydrophobicity.

## Results and Discussion

**Hemolytic activity:** The hemolytic activities of the peptides against human erythrocytes were determined as a measure of peptide toxicity toward eukaryotic cells. The effect of peptide concentration on erythrocyte hemolysis (18 hours at 37°C) is shown in Figure 1. From these plots the peptide concentration that produced 50% hemolysis was determined (HC<sub>50</sub>, Table 2). Increasing the number of positively charged residues on the polar face decreases the hemolytic activity (D19 to D22, Table 2). Peptide D22 showed the weakest hemolytic activity among the

new analogs (HC<sub>50</sub>=249  $\mu$ g/mL), and compares favorably with D1 (HC<sub>50</sub>=421.5  $\mu$ g/mL).

### Antimicrobial activity:

*Pseudomonas* is a genus of gram-negative bacteria with high intrinsic resistance to traditional antibiotics and resistance levels have been steadily increasing in recent years. We have chosen a diverse group of six *Pseudomonas aeruginosa* clinical isolates. We determined the MIC values for our peptides in two different media: Muller Hinton medium (Table 2A) and Brain Heart Infusion medium (Table 2B). In Muller Hinton medium, all the tested peptides except D17 have similar activity: their geometric mean MIC values were all low

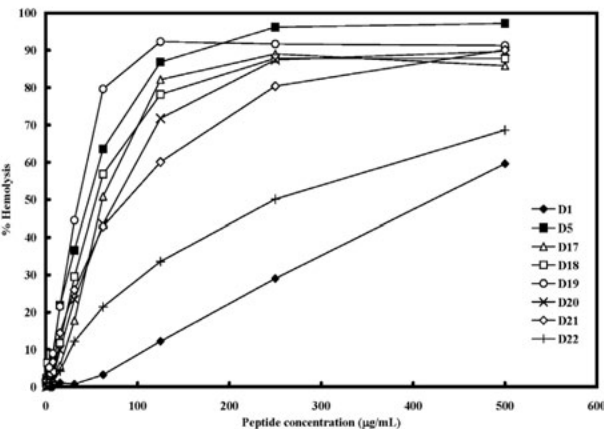


Fig. 1. The Hemolytic Activity of Peptide D1 (D-V13K) and analogs. The concentration-response curves of peptides for lysis of human red blood cells.

(varied from 6.2 µg/ml to 12.4 µg/ml or 2.1 µM to 4.1 µM) within a 2-fold difference (the geometric mean MIC value for D17 was 22.1 µg/ml). In Brain Heart Infusion medium, similar results were obtained for D17 to D22: their geometric mean MIC values were all low (varied from 6.2 µg/mL to 14.7 µg/mL or 2.1 µM to 5.1 µM) within a 2-fold difference except D17 which had a geometric mean MIC value of 35.1 µg/ml.

Table 2. Biological activity of D1 (D-V13K) analogs against six *Pseudomonas aeruginosa* strains in Muller Hinton medium (A) and Brain Heart Infusion medium (B)

A	Peptide Name	Net Charge	Hemolytic activity		Antimicrobial activity measured in Muller Hinton medium							Therapeutic index <sup>d</sup>	
			HC <sub>50</sub> (µg/mL) <sup>a</sup>		MIC(µg/mL) <sup>b</sup>							HC <sub>50</sub> /MIC	Fold <sup>e</sup>
					PAO 1	PAK	PA 14	CP 204	WR 5	M 2	GM <sup>c</sup>		
	D1	+7	421.5		7.8	15.6	15.6	15.6	15.6	7.8	12.4	34.0	1.00
	D5	+8	47.0		7.8	15.6	7.8	15.6	15.6	7.8	11.0	4.3	0.13
	D17	+5	62.0		15.6	15.6	15.6	31.3	31.3	31.3	22.1	2.8	0.08
	D18	+6	55.0		7.8	7.8	7.8	15.6	15.6	7.8	9.8	5.6	0.16
	D19	+7	36.0		3.9	3.9	3.9	15.6	15.6	15.6	7.8	4.6	0.14
	D20	+8	77.0		7.8	7.8	7.8	31.3	15.6	15.6	12.4	6.2	0.18
	D21	+9	88.5		7.8	3.9	0.5	15.6	15.6	15.6	6.2	14.2	0.42
	D22	+10	249.0		3.9	3.9	0.5	31.3	31.3	15.6	7.0	35.6	1.05
B	Peptide Name	Net Charge	Hemolytic activity		Antimicrobial activity measured in Brain Heart Infusion medium							Therapeutic index <sup>d</sup>	
			HC <sub>50</sub> (µg/mL) <sup>a</sup>		MIC(µg/mL) <sup>b</sup>							HC <sub>50</sub> /MIC	Fold <sup>e</sup>
					PAO 1	PAK	PA 14	CP 204	WR 5	M 2	GM <sup>c</sup>		
	D1	+7	421.5		31.3	31.3	15.6	62.5	15.6	62.5	31.2	13.5	1.00
	D5	+8	47.0		31.3	31.3	15.6	31.3	15.6	15.6	22.1	2.1	0.16
	D17	+5	62.0		31.3	31.3	15.6	62.5	31.3	35.1	35.1	1.8	0.13
	D18	+6	55.0		10.4	10.4	10.4	41.7	20.8	10.4	14.7	3.7	0.28
	D19	+7	36.0		7.8	15.6	3.9	15.6	15.6	7.8	9.8	3.7	0.27
	D20	+8	77.0		7.8	15.6	7.8	15.6	7.8	7.8	9.8	7.8	0.58
	D21	+9	88.5		15.6	3.9	3.9	15.6	3.9	3.9	6.2	14.3	1.06
	D22	+10	249.0		15.6	7.8	3.9	31.3	15.6	3.9	9.8	25.3	1.88

<sup>a</sup>HC<sub>50</sub> is the maximal peptide concentration that produces 50% hemolysis of human red blood cells after 18 h in the standard microtiter dilution method. <sup>b</sup>MIC is minimal inhibitory concentration that inhibited growth of different strains in Mueller-Hinton (MH) medium or Brain Heart Infusion (BHI) medium at 37°C after 24h. MIC is given based on three sets of determinations. <sup>c</sup>GM, geometric mean of the MIC values. <sup>d</sup>Therapeutic index is the ratio of the HC<sub>50</sub> value (mg/mL) over the geometric mean MIC value (µg/mL). Large values indicate greater antimicrobial specificity. <sup>e</sup>The fold improvement in therapeutic index compared to that of D1.

**Therapeutic Index:** In Muller Hinton medium (Table 2A), only one peptide, D22, had a therapeutic index (35.6) similar to peptide D1 (34.0). Interestingly, in Brain Heart Infusion medium, peptides D21 and D22 had therapeutic indices similar or better than peptide D1. The therapeutic index for D1 was 13.5 (Table 2B) compared to peptide D21 with a value of 14.3 and peptide D22 with a value of 25.3. These results show that the number of positively charged residues and their location on the polar face can be varied dramatically compared to peptide D1 to achieve a similar or higher therapeutic index, as shown for peptide D22.

It is important to note that peptide D22 has much higher overall hydrophobicity (90.7 min) than D1 (76.8 min) (Table 1). Thus, you can have a wide range of sequences varying in hydrophobicity on the non-polar face and varying in number and location of the positively charged residues on the polar face and still maintain the desired biological properties. However, the changes in sequence must be complementary, that is, if hydrophobicity is increased on the non-polar face you must simultaneously increase the number of positively charged residues on the polar face. Since different sequences may be optimal for a particular organism, the above understanding provides us with know-how to optimize a particular sequence for a particular organism, based on screening a reasonable number of peptide analogs that vary in positive charge on the polar face and hydrophobicity on the non-polar face.

## Acknowledgments

This research was supported by a NIH grant from the National Institute of Allergy and Infectious Diseases (NIAID) R01 AI067296 and the John Stewart Chair in Peptide Chemistry to R.S.H.

## References

1. Chen, Y., et al. *J. Biol. Chem.* **280**, 12316-29 (2005).
2. Chen, Y., et al. *Chem. Biol. Drug Des.* **67**, 162-73 (2006).
3. Chen, Y., et al. *Antimicrob. Agents Chemother.* **51**, 1398-406 (2007).
4. Jiang, Z., et al. *Biopolymer* **90**, 369-83 (2008).
5. Jiang, Z., et al. *Chem. Biol. Drug Des.* **72**, 483-495 (2008).



## Lysine Trimethylation, a Tool for Improving the Therapeutic Index of Antimicrobial Peptides

Beatriz G. de la Torre,<sup>1</sup> María Fernández-Reyes,<sup>2</sup> Dolores Díaz,<sup>2</sup>  
Ania Cabrales-Rico,<sup>1</sup> Mariona Vallès-Miret,<sup>1</sup> Jesús Jiménez-Barbero,<sup>2</sup>  
Luis Rivas,<sup>2</sup> and David Andreu<sup>1</sup>

<sup>1</sup>Department of Experimental and Health Sciences, Pompeu Fabra University, Barcelona 08003, Spain;

<sup>2</sup>Center for Biological Research-CSIC, Madrid 28006, Spain

### Introduction

Despite their interest as alternatives to conventional antibiotics in the face of an alarming worldwide antibiotic resistance crisis, antimicrobial peptides (AMPs) are still to gain a foothold in therapeutics, largely due to the limitations intrinsic to their peptide nature. A number of structural modifications tending to enhance AMP biological lifetimes have been proposed with various results. Lys trimethylation, despite its predicament in epigenetic studies [1], has surprisingly received little attention from peptide medicinal chemists. Among other effects, lysine trimethylation (i) preserves global charge but (ii) abrogates the hydrogen bond-forming ability of the amino group, and (iii) increases side chain bulkiness as well as hydrophobicity.

### Results and Discussion

We have examined the effect of Lys trimethylation using a well-known AMP platform, the cecropin A-melittin hybrid CA(1-7)M(2-9), KWKLFFKIGAVLKVL-amide [2]. Before Fmoc-Lys(Me<sub>3</sub>)-OH became commercially available, trimethylation of designated Lys residues in the CA(1-7)M(2-9) sequence was achieved by (i) protection of the selected residue(s) with either Fmoc or Mmt (Boc or Fmoc chemistry, respectively), (ii) selective removal of these groups (piperidine or 1% TFA, respectively), (iii) treatment of the peptide-resin with methyl iodide/DIEA (1:2) in DMF, (iv) full deprotection and cleavage. Ten analogues displaying different levels of Lys trimethylation have been made and tested for antimicrobial activity on *Leishmania* promastigotes and amastigotes, as well as for hemolysis as a gauge of cytotoxicity.

As shown in Table 1, trimethylation of all five Lys residues caused a significant decrease in antimicrobial potency but, interestingly, an even more marked reduction in cytotoxicity. The singly and doubly trimethylated analogues, on the other hand, provided more encouraging results: most were non-cytotoxic up to 60 µM yet retained antimicrobial activities in the µM range, thereby amounting to a sizable enhancement of their therapeutic indexes.

As expected, trimethylated derivatives had improved proteolytic stability profiles relative to the parent CA(1-7)M(2-9), and thus the permethylated K<sub>1,3,6,7,13</sub>(Me<sub>3</sub>)<sub>5</sub> analogue was basically inert to trypsin. On the other hand, derivatives with lower levels of trimethylation were protease-sensitive, albeit marginally more stable than CA(1-7)M(2-9). All in all, the proteolysis data do not appear to support the hypothesis that protease shielding plays a major role in the improved performance of the trimethylated analogues.

The secondary structures of the analogues were investigated in solution by 2D-NMR (DQF-COSY, TOCSY and NOESY) experiments. While only random structures were observed in aqueous solution, upon TFE addition cross peaks with well-resolved, well-dispersed resonances in the αH-NH and NH-NH regions were detected, indicative of stable conformers. Upfield-shifted αH and NH resonances in TFE relative to water were suggestive of helical structures. For the different derivatives in Table 1, a switch from random coil to partial helical structures as the number of trimethyl-Lys residues increased was found, with a good correlation between trimethylation level and global helical content.

The mechanism of antimicrobial action of the peptides was investigated by (i) analysis of plasma membrane permeabilization and (ii) electron microscopy. In the first approach, the influx of the vital dye SYTOX Green into *Leishmania* promastigotes following peptide addition was measured [3]. All peptides tested, except the K<sub>1,3,6,7,13</sub>(Me<sub>3</sub>)<sub>5</sub> were able to permeabilize the membrane to a substantial extent, regardless of the degree of trimethylation. Thus, membrane disruption appears to be the main mechanism responsible for the lethal activity of the peptides.

Table 1. Leishmanicidal and hemolytic activities of trimethylated CA(1-7)M(2-9) derivatives

Peptide <sup>a</sup>	Promastigotes <i>L. donovani</i>		Amastigotes <i>L. pifanoi</i>		Hemolysis <sup>b</sup> (%)	
	EC <sub>50</sub> ( $\mu$ M) <sup>b</sup>	LC <sub>50</sub> ( $\mu$ M) <sup>b</sup>	EC <sub>50</sub> ( $\mu$ M)	LC <sub>50</sub> ( $\mu$ M)	60 $\mu$ M	80 $\mu$ M
CA(1-7)M(2-9)	1.8 ( $\pm$ 0.0)	1.5 ( $\pm$ 0.1)	4.3 ( $\pm$ 0.2)	4.5 ( $\pm$ 0.2)	60	100
K <sub>1</sub> (Me <sub>3</sub> )	3.9 ( $\pm$ 0.3)	2.8 ( $\pm$ 0.0)	6 ( $\pm$ 0.8)	6.4 ( $\pm$ 1.2)	50	85
K <sub>3</sub> (Me <sub>3</sub> )	3.3 ( $\pm$ 0.0)	3.1 ( $\pm$ 0.6)	9.4 ( $\pm$ 0.8)	8.2 ( $\pm$ 1.0)	0	0
K <sub>6</sub> (Me <sub>3</sub> )	3.7 ( $\pm$ 0.0)	1.7 ( $\pm$ 0.0)	13.4 ( $\pm$ 0.1)	16.3 ( $\pm$ 1.3)	0	0
K <sub>7</sub> (Me <sub>3</sub> )	3.7 ( $\pm$ 0.2)	2.3 ( $\pm$ 0.0)	11.4 ( $\pm$ 0.8)	12.1 ( $\pm$ 1.2)	0	40
K <sub>13</sub> (Me <sub>3</sub> )	3.5 ( $\pm$ 0.1)	2.5 ( $\pm$ 0.0)	10.1 ( $\pm$ 0.6)	11.6 ( $\pm$ 0.5)	0	10
K <sub>1,3</sub> (Me <sub>3</sub> ) <sub>2</sub>	12.8 ( $\pm$ 0.4)	15.5 ( $\pm$ 0.6)	16.2 ( $\pm$ 0.1)	24.8 ( $\pm$ 1.2)	0	6
K <sub>3,6</sub> (Me <sub>3</sub> ) <sub>2</sub>	5.1 ( $\pm$ 0.2)	6.7 ( $\pm$ 0.2)	7.4 ( $\pm$ 0.3)	16.5 ( $\pm$ 1.6)	0	36
K <sub>6,7</sub> (Me <sub>3</sub> ) <sub>2</sub>	6.1 ( $\pm$ 0.1)	5.3 ( $\pm$ 0.6)	9.2 ( $\pm$ 2.0)	27 ( $\pm$ 1.2)	0	13
K <sub>1,13</sub> (Me <sub>3</sub> ) <sub>2</sub>	8.8 ( $\pm$ 0.3)	7.6 ( $\pm$ 0.1)	17 ( $\pm$ 3.0)	13.5 ( $\pm$ 1.4)	0	0
K <sub>1,3,6,7,13</sub> (Me <sub>3</sub> ) <sub>5</sub>	>30	>30	>30	>30	0	0

<sup>a</sup> CA(1-7)M(2-9) is KWKLFFKKIGAVLKVL-amide. Subscripts refer to the Lys positions undergoing trimethylation. <sup>b</sup> Parasite viability evaluated by MTT reduction; hemolysis as hemoglobin release.

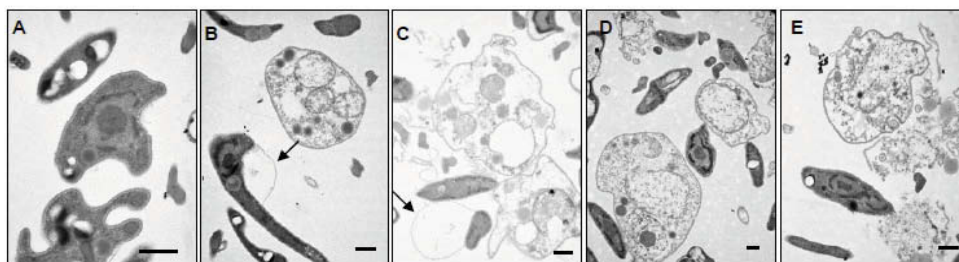


Fig. 1. Electron microscopy of *Leishmania* promastigotes incubated with CA(1-7)M(2-9) (panel A) and trimethylated derivatives (panels B-E) at an equipotent concentration causing 70% inhibition of proliferation. Membrane blebbing (indicated by arrows), breakage as well as depletion of electron-dense cytoplasmic material can be observed (bar: 0.5  $\mu$ m).

The electron microscopy data, on the other hand (Figure 1), suggest that the peptides act through an all-or-none mechanism.

In conclusion, trimethylation appears to be a useful tool for modulating the action of CA(1-7)M(2-9) and possibly other AMPs.

## References

1. Roman-Gomez, J., et al. *J. Clin. Oncol.* **27**, 1316-1322 (2009).
2. Andreu, D., et al. *FEBS Lett.* **296**, 190-194 (1992).
3. Chicharro, C., et al. *Antimicrob. Agents Chemother.* **45**, 2441-2449 (2001).

## Design and Synthesis of New Potent Melanocortin Peptides with Candidacidal Activity

Luigia Auriemma,<sup>1</sup> Stefania Malfi,<sup>1</sup> Salvatore Di Maro,<sup>1</sup> Pietro Campiglia,<sup>2</sup>  
 Ettore Novellino,<sup>1</sup> Anna Catania,<sup>3</sup> and Paolo Grieco<sup>1</sup>

<sup>1</sup>Department of Chimica Farmaceutica e Tossicologica, University of Naples "Federico II",  
 80131 Naples, Italy; <sup>2</sup>Department of Scienze Farmaceutiche, University of Salerno,  
 84084 Fisciano, Italy; <sup>3</sup>Divisions of Internal Medicine and Liver Transplantation,  
 Ospedale Maggiore di Milano IRCCS, 20122 Milano, Italy

### Introduction

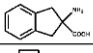
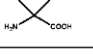
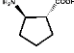
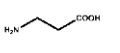
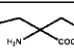
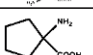
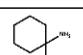
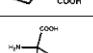
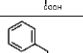
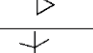
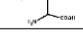
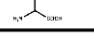
In the last two decades, the incidence of human fungal infections has increased dramatically. Pathogenic fungi, mainly *Candida* and *Aspergillus* species, determine opportunistic infection in immunocompromised patients, including those affected by AIDS, cancer patients treated with chemotherapy, transplant recipients on immunosuppressive drugs and patients with advanced diabetes. Additionally, the spread of antibiotic resistance among pathogens especially in hospital environments but also in the community has occurred at an alarming rate. Therefore the necessity of alternative antimicrobial agents has increased.

Antimicrobial peptides are promising candidates for treatment of resistant bacterial and fungal infections due primarily to their potency against pathogenic microbes that are resistant to conventional antibiotics, as well as their broad-spectrum activity. Antimicrobial peptides are ubiquitous, conserved in evolutionary scale and do not induce resistance.

$\alpha$ -Melanocyte stimulating hormone is an endogenous linear peptide originated from enzymatic cuts of proopiomelanocortin (POMC). It belongs to melanocortin peptide family and it has antipyretic, anti-inflammatory and pigmentary effects.

$\alpha$ -MSH and mainly C-terminal tripeptide Lys-Pro-Val have potent antimicrobial activity against two representative pathogens: *Staphylococcus aureus* and *Candida albicans*. Experimental evidence shows that  $\alpha$ -MSH exerts antimicrobial effect through a different mechanism, in fact the antifungal effect is linked to the cAMP-inducing activity of the peptide:  $\alpha$ -MSH increased cAMP production in *C. albicans* and the adenylyl cyclase inhibitor ddAdo partly reversed the candidacidal effect of peptide. It is remarkable that this mechanism of action in yeast mimics the influence of  $\alpha$ -MSH in mammalian cells where the peptide binds to melanocortins receptors linked to G-proteins and induces the increase of cAMP [1].

Table 1. Amino acids used

	AA		AA
1	Gly-Gly	8	
2		9	
3		10	
4		11	
5		12	
6		13	
7			

Previous studies allowed to obtain [D(2)Nal-7, Phe-12]- $\alpha$ -MSH(6-13), originated from changes into the sequence of  $\alpha$ -MSH(6-13) [1,2]. This  $\alpha$ -MSH analogue showed the most potent candidacidal activity and it became our lead compound.

### H-His-D(2)Nal-Arg-Trp-Gly-Lys-Phe-Val-NH<sub>2</sub>

To improve antifungal activity the residue of glycine of lead compound [3] was replaced with natural and unnatural aminoacids and we obtained 13 new  $\alpha$ -MSH analogues.

### H-His-D(2)Nal-Arg-Trp-AA-Lys-Phe-Val-NH<sub>2</sub>

The amino acids used for the replacement of glycine are reported in Table 1.

Table 2. Antimicrobial activity of compounds synthesized

<i>Candida</i> strain	Peptides												
	1	2	3	4	5	6	7	8	9	10	11	12	13
<i>C.albicans</i>													
ATCC 76615	no	no	no	61	117	no	no	31	no	no	no	60	122
ATCC 24433	no	no	no	31	59	no	no	31	no	no	no	60	122
995439	no	no	no	31	59	no	118	31	117	no	118	60	122
995147	no	no	no	31	117	no	no	31	no	no	no	60	122
000954	no	no	no	61	117	no	no	31	no	no	no	60	122
991185	no	no	no	61	59	no	no	31	117	no	no	60	61
994199	no	no	no	31	59	no	no	31	117	no	118	60	61
983201-R1	no	no	no	61	117	no	no	61	no	no	no	60	122
011587	no	115	no	31	117	no	no	61	117	no	118	60	122
<i>C.glabrata</i>													
18012	no	no	no	122	no	no	no	123	no	no	no	no	no
995667	no	no	no	122	no	-	no	123	no	no	no	no	no
995651	no	no	no	122	no	no	no	123	no	no	no	no	no
<i>C.krusei</i>													
995668	no	115	no	61	117	no	no	61	117	no	118	119	no
991388	no	115	no	31	117	no	118	61	117	no	118	119	122
004490	no	115	no	31	117	no	118	31	117	no	118	60	122

## Results and Discussion

Peptides were synthesized using the conventional Fmoc-based solid-phase strategy in a manual reaction vessel.

The purification of final products was achieved using a semipreparative RP-HPLC. Analytical HPLC indicated a purity greater than 97%, and molecular weights were confirmed by ESI-MS. Antifungal susceptibility testing was performed using the broth microdilution method according to the NCCLS M27-A guidelines (National Committee for Clinical Laboratory Standards. 1997).

The peptides were tested on three different common strains of *Candida* for evaluating their antimicrobial activities. The results of the assays are reported in Table 2 below showing the MIC 90 at 48 hours, denoted as µg/ml concentration, for the peptide compounds.

The replacement of glycine with β-cyclohexyl-(L)-alanine (Cha) and 2-aminointhane-2-carboxylic acid (Aic) allowed to obtain the compounds 4 and 8 with potent candidacidal activity on all *Candida* strains. Therefore, the position next to core sequence of melanocortin peptides is critical for candidacidal activity. Structural studies performed to understand the relationship structure-antimicrobial activity are ongoing. The results obtained are the starting point for the design of new α-MSH analogues.

## References

1. Grieco, P., et al. *J. Med. Chem.* **46**, 850-855 (2003).
2. Grieco, P., et al. *J. Med. Chem.* **48**, 1384-1388 (2005).
3. Carotenuto, A., et al. *Chem. Biol. Drug Des.* **69**, 68-74 (2007).

## Structure-Antibacterial Activity Relationship of Cyclic Lipodepsipeptide Antibiotic Fusaricidin A

Nina Bionda, Daniela Treitl, Maciej Stawikowski, and Predrag Cudic

Department of Chemistry and Biochemistry, Florida Atlantic University,  
 777 Glades Road, Boca Raton, FL 33431, U.S.A.

### Introduction

Fusaricidin A is a cyclic lipodepsipeptide originally isolated from *Bacillus polymyxa* KT-8 strain, and exhibits promising activity against various kinds of fungi and Gram-positive bacteria, including methicillin-resistant *S. aureus* [1]. Fusaricidin's relatively simple structure and potent antimicrobial activity make this natural product particularly interesting lead structure for the development of new and more potent antibiotics. In order to investigate structural basis for fusaricidin's antimicrobial activity, and to define its minimal bioactive pharmacophore, we have synthesized fusaricidin A's analogs that differ in the lipid tail part and alanine-scanning analogs. Defining the minimal structural requirements responsible for fusaricidin's antibiotic activity may facilitate chemical synthesis of the antibiotic by reducing structural complexity and promote judicious chemical modifications for modulation of its pharmacological or physiochemical properties.

### Results and Discussion

All analogs were synthesized using standard Fmoc-solid-phase chemistry and methods developed in our laboratory [2]. Figure 1 represents a schematic summary of all synthesized analogs and the corresponding sequences. In order to elucidate the role of the lipid tail in the biological activity of the peptide, analogs without the lipid tail were synthesized and tested against several Gram-positive bacterial strains, including methicillin- and vancomycin-resistant strains. No biological activity was observed for the analogs containing acetate group or 12-aminododecanoic acid as lipid tail, respectively. On another hand, analog containing 12-guanidinododecanoic acid, the closest commercially available compound to the 15-guanidino-3-hydroxypentanedecanoic acid found in the natural product, showed significant antimicrobial activity. All these results indicate importance of the lipid tail and guanidino functionality for the antimicrobial activity. To determine which of the amino acids present in the peptide ring are important for the biological activity, fusaricidin's alanine-scanning analogs were synthesized. Alanine-scanning technique is commonly used to determine relative importance of each amino acid residue by comparing the activity of analogs obtained in this manner with the activity of the natural product. Each amino acid in the sequence was replaced with alanine, alanine was replaced with glycine, and in analog 9 ester bond was replaced with lysine which accounted for the number of atoms in the ring and mimicked the ester bond.

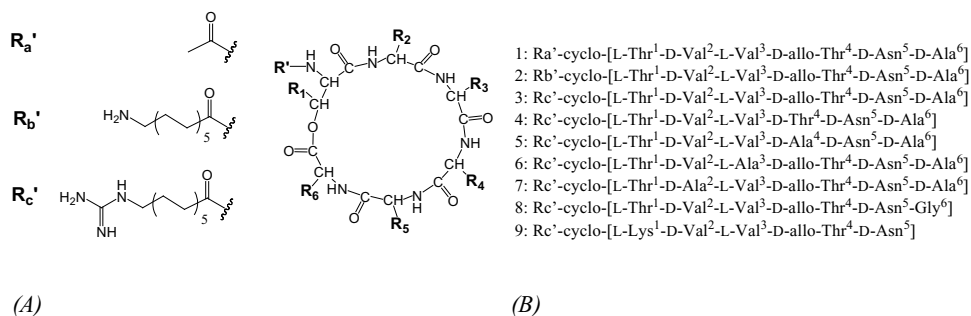


Fig. 1. (A) General structure of tested fusaricidin A's analogs. (B) Amino acid sequences of tested cyclic fusaricidin A analogs.

Table.1 Antimicrobial activity of fusaricidin A analogs

Microorganism	MIC values (µg/mL)*								
	1	2	3	4	5	6	7	8	9
<i>S. aureus</i> (MRSA)	>128	>128	32	32	>128	16	64	>128	128
<i>S. aureus</i> Mu50 (VRSA)	>128	>128	32	32	>128	32	128	>128	>128
<i>S. epidermidis</i>	ND	ND	ND	ND	64	16	32	>128	>128
<i>S. pyogenes</i>	ND	ND	ND	ND	128	32	128	>128	>128
<i>E. faecium</i> (VRE)	>128	>128	>32	ND	ND	ND	ND	ND	ND

\* MIC (µg/mL) - minimum inhibitory concentration. ND=not determined.

The assessment of antibacterial activity and determination of minimal inhibitory concentration (MIC) was done in sterilized 96-well flat-bottomed polystyrene microtiter plates using standard micro dilution broth method [3]. Controls on each plate were media without bacteria, bacterial inoculum without antimicrobials added, bacterial inoculum to which methicillin was added and bacterial inoculum to which vancomycin was added. Concentrations of these antibiotics were the same as of the tested peptides, in the range from 0.01 to 128 µg/mL. All samples were loaded in duplicates. Since the peptides were poorly soluble in water, they were dissolved in 5% or 10% of dimethylsulfoxide (DMSO) in water. After serial dilutions, the final concentration of DMSO in wells was 0.5% or 1%, depending on the synthetic peptide solubility. However, to eliminate possible effect of DMSO on bacterial growth all controls contained the same amount of DMSO. Plates were loaded with 90 µL of mid-logarithmic phase cells with initial 0.001 O.D. at 600 nm, and 10 µL aliquots of two-fold serial dilutions of the control antibiotics or fusaricidin analogs. Plates were incubated at 37 °C overnight with gentle shaking. The inhibition of the bacterial growth was determined by reading the O.D. at 600 nm. In the case of fungi, *Candida albicans*, the assays were done in RPMI 1640 media containing morpholinepropanesulfonic acid (MOPS) and glucose (final concentration of glucose was 2%) [4]. In this case commercially available antibiotics fluconazole and amphotericin B were used as controls. All tested microorganisms were purchased from the American Type Culture Collection (ATCC). Results of antimicrobial assays are shown in Table 1. Replacing either D-Ala<sup>6</sup> with Gly<sup>6</sup> (analog 8) or both L-Thr<sup>1</sup> and D-Ala<sup>6</sup> with L-Lys<sup>1</sup> (analog 9) causes complete loss of peptide's antimicrobial activity, indicating an important role of fusaricidin's ester bond for its antimicrobial activity. On the other hand, replacing D-Val<sup>2</sup> with D-Ala<sup>2</sup> (analog 7) or D-Val<sup>3</sup> with D-Ala<sup>3</sup> (analog 6) does not result in complete loss of peptide's antimicrobial activity. No significant antimicrobial activity loss was also observed in the case where D-*allo*-Thr<sup>4</sup> was replaced with D-Thr<sup>4</sup> (analog 4). In conclusion, this study revealed fusaricidin's minimal bioactive pharmacophore allowing further dissection of its structure and identification of new active compounds for combinatorial chemistry optimization.

## Acknowledgments

We wish to acknowledge support of this work by the NIH (1S06-GM073621-01) and AHA (0630175N) Grant to P.C.

## References

1. Kajimura, Y., Kaneda, M. *J. Antibiot.* **49**, 129-135 (1996).
2. Cudic, P., Stawikowski, M. *Tetrahedron Lett.* **47**, 8587-8590 (2006).
3. Otvos, L., Cudic, M. *Peptide Characterization and Application Protocols, Methods in Mol. Biol. (G.B. Fields Ed.)* 2007, p. 309.
4. Anaissie, E.J., et al. *Antimicrob. Agents Chemother.* **40**, 2387-2391 (1996).

## Probing the Effect of Gomesin and Its Linear Analogue on Giant Unilamellar Vesicles Via Optical Microscopy

Tatiana M. Domingues,<sup>1</sup> Sirlei Daffre,<sup>2</sup> Karin A. Riske,<sup>1</sup>  
and Antonio Miranda<sup>1</sup>

<sup>1</sup>Department of Biophysics, Federal University of São Paulo, São Paulo, 04044-020, Brazil; and

<sup>2</sup>Department of Parasitology, Institute of Biomedical Science, University of São Paulo,  
São Paulo, SP, 05509-800, Brazil

### Introduction

Gomesin (Gm) is a potent cationic antimicrobial peptide that was isolated and characterized from hemocytes of the Brazilian spider *Acanthoscurria gomesiana* [1]. The peptide contains eighteen amino acid residues, including four cysteines that form two disulfide bridges: Cys<sup>2-15</sup> and Cys<sup>6-11</sup>. The molecule adopts a  $\beta$ -hairpin-like structure, as determined by 2-D nuclear magnetic resonance and molecular dynamics studies [2] (Figure 1). The presence of two internal disulfide bridges plus a C-terminal amidation and a pyroglutamic acid in the N-terminus, certainly contributes to the stability of the peptide to human serum proteases. Due to its large range of antimicrobial and antifungal activities Gm seems to be an interesting lead peptide in the development of alternative new drug for human therapy [3-5].

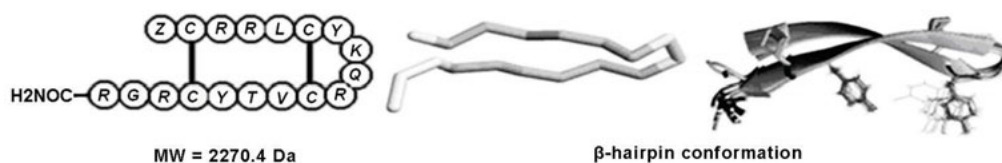


Fig. 1. Gomesin structure.

To further understand the mechanism of the interaction of this peptide with membranes, we studied here the lytic action of Gm and its poorly active linear analogue ([Ser<sup>2,6,11,15</sup>]-Gm) [6] on giant unilamellar vesicles (GUVs) [7], composed of mixtures of neutral [1-palmitoyl-2-oleoyl-phosphatidylcholine (POPC)] and anionic [1-palmitoyl-2-oleoyl-phosphatidylglycerol (POPG)] phospholipids by using optical and fluorescence microscopies.

### Results and Discussion

Two different experimental setups were used to study the interaction between the antimicrobial peptides and the GUVs with optical microscopy. First we observed the effect of injecting fluorescently labeled Gm (Gm with a rhodamine group attached to the N $\epsilon$ -amino group of the lysine residue; denoted Gm-Rh) by a micropipette placed at the vicinities of a GUV. Generally, we observed that, Gm-Rh first binds to the vesicle surface, then accumulates at certain points (small high-contrast regions). Afterwards, the vesicles suddenly burst through the opening of a large hole, and the membrane rearranges into an interconnected tubular structure. As control, in the absence of peptide, the GUVs were never spontaneously disrupted. A similar bursting behavior was observed previously with other antimicrobial peptide [8]. In the second setup, GUV solutions of different composition were mixed with increasing concentrations of Gm or [Ser<sup>2,6,11,15</sup>]-Gm. The number of GUVs as a function of time was used to quantify the lytic activity of the peptides. In the absence of the peptide, GUVs accumulate at the bottom of the cover slip, whereas in the presence of the peptide, the number of GUVs was considerably reduced. Figure 2A shows a typical set of data obtained with 25 mol% POPG, where the number of GUVs is shown as a function of time for different Gm concentrations.

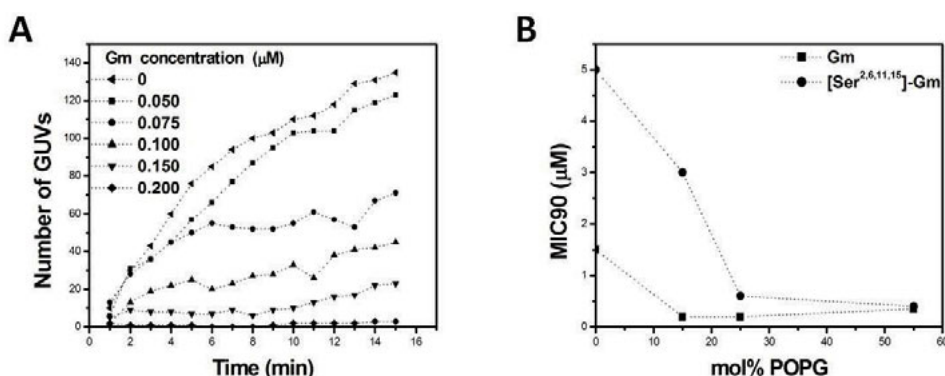


Fig. 2. Effect of antimicrobial peptides on GUVs permeability.

Such measurements as shown in Figure 2A were done for different compositions of GUVs and concentrations of Gm and [Ser<sup>2,6,11,15</sup>]-Gm. The lytic activity was measured employing the minimal peptide concentration that induced >90% vesicle bursting (MIC90). As it can be seen in Figure 2B, the lytic activity is enhanced when negatively charged GUVs (containing 15, 25 and 55 mol% POPG) were used. On the other hand, a higher concentration of both peptides had to be used to induce a similar lytic effect on pure POPC vesicles. For low POPG content, a higher concentration of [Ser<sup>2,6,11,15</sup>]-Gm in comparison to Gm was required to cause a similar lytic effect. We attribute this behavior to the particular lytic mechanism, i.e., the carpeting model. This partial insertion model is reasonable because short peptide sequences (18 residues) cannot cross the bilayer due to the mismatch between the bilayer thickness and the peptide length [9].

## Acknowledgements

This work was supported by FAPESP, CNPq and FADA/UNIFESP.

## References

1. Silva, Jr., P.I., et al. *J. Biol. Chem.* **275**, 33464-70 (2000).
2. Mandard, N., et al. *Eur. J. Biochem.* **269**, 1190-1198 (2002).
3. Moreira, C.K., et al. *Exp. Parasitol.* **116**, 346-353 (2007).
4. Barbosa, F.M., et al. *FEMS Microbiology Letters*, **274**, 279-286 (2007).
5. Rodrigues, E.G., et al. *Neoplasia* **10**, 61-68 (2008).
6. Fazio, M.A., et al. *Biopolymers* **88**, 386-400 (2006).
7. Dimova, R., et al. *R. J. Phys., Condens. Matter* **18**, 1151-1176 (2006).
8. Ambroggio, E.E., et al. *Biophys. J.* **89**, 1874-1881 (2005).
9. Tamba, Y., et al. *Biophys. J.* **92**, 3178-3194 (2007).



## Total Fmoc Solid-phase Synthesis of Naturally Occurring Depsipeptide Antibiotic Katanosin B

Nina Bionda, Diego Binetti, Predrag Cudic, and Mare Cudic

Florida Atlantic University, Department of Chemistry and Biochemistry, Boca Raton, FL 33431, U.S.A.

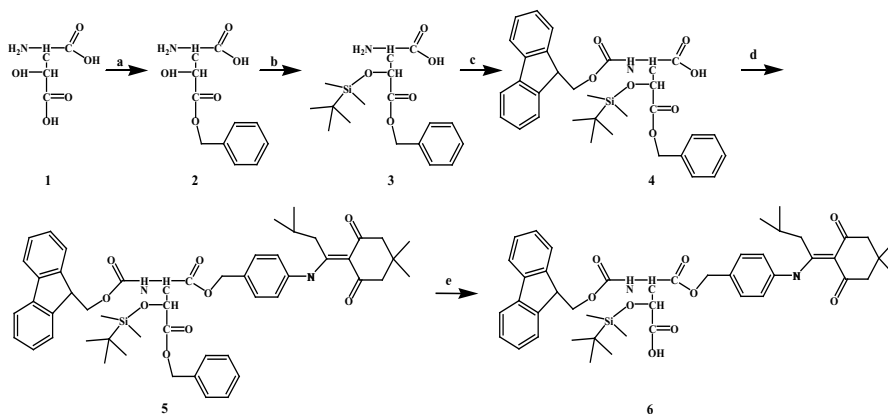
### Introduction

Katanosin B belongs to a large and diverse family of the non-ribosomally synthesized peptides, a family of microbial natural products that contain in addition to the known 20 proteinogenic amino acids, unusual residues that are not present in proteins. It was isolated in 1988 from *Cytophaga sp.* strain PBJ-5356 [1]. This natural product exhibits strong activity against methicillin-resistant *Staphylococcus aureus* (MRSA) and vancomycin-resistant *Enterococcus faecium* (VRE). However, lack of commercial sources of katanosin B producing organism and, particularly, unlimited access to its synthetic analogs hampered katanosin B utilization as a lead compound for the development of new antibiotics. Therefore, a total solid-phase synthesis of this natural product represents the first step toward complete exploitation of its antibacterial potential.

### Results and Discussion

A key building block in the synthesis of katanosin B is L-threo- $\beta$ -hydroxyaspartic acid (L-*t*HyAsp). We have successfully developed a method for the synthesis of suitably protected L-*t*HyAsp for use in Fmoc solid-phase peptide synthesis. Our method is based on the D,L-*t*HyAsp racemic mixture resolution by co-crystallization with L-Lys followed by the ion exchange chromatography [2]. RP-HPLC analysis of fractions obtained after ion-exchange chromatography and derivatization with Marfey's reagent [3] confirmed enantiomeric separation. The specific optical rotation ( $[\alpha]_D^{25} = +6.0^\circ$ ;  $c=1.0$ , 5N HCl) was also determined and is in a good agreement with the literature data [2].

First selected approach towards the synthesis of orthogonally protected HyAsp employed benzyl (Bzl) protection of the side chain carboxyl group, 9-fluorenylmethoxycarbonyl (Fmoc) protection of the  $\alpha$ -amino group, tetrahydropyranyl ether (THP) protection of the  $\beta$ -hydroxyl-group, and allyl protection of the  $\alpha$ -carboxyl group. Although it was previously reported that benzyl-protecting group can be selectively removed by mild basic hydrolysis, such as  $K_2CO_3$  in ethanol [4], we were not able to optimize this reaction in such a manner that the yields were satisfactory. The initial approach was then modified and alternative protecting groups were chosen (Scheme 1).



Scheme 1. a) Bzl-OH, HCl, 4 h (yield, 85 %); b) TBDMS-Cl (1.5 eq), DBU (1.5 eq), ACN, 3-8 h (yield, 82 %); c) Fmoc-OSu (1.1 eq),  $NaHCO_3$  (2 eq), acetone/ $H_2O$ , 2 h (yield, 95 %); d) Dmab-OH (1.1 eq), EDCI (1.5 eq), DMAP (1 eq), DCM, 10-18 h (yield, 65 %); e)  $H_2$ , 5% Pd/C, EtOAc, 50 min (yield, 75 %).

The THP and Allyl protecting groups were replaced with TBDMS and Dmab groups, respectively, in order to be in compliance with the orthogonal protection necessary for the synthesis of resin-bound cyclic peptides. Using this protection strategy HyAsp **1** was successfully converted into desired Fmoc-HyAsp(TBDMS)-ODmab **6** in 5 reaction steps and total yield of 32%. The final product was characterized by NMR and MALDI-MS (calculated:  $[M+H]^+ = 796.3$ , observed:  $[M+H]^+ = 795.6$ ). Fmoc solid-phase synthesis approach towards katanosin B was based on previously reported protocol by our group for the synthesis of cyclic lipodepsipeptides [5]. PEG-based resin, TentaGel S RAM, was chosen because of its best performance in on-resin ester bond formation. Our strategy for the katanosin B total SPPS included amide resin attachment of HyAsp *via* side chain, use of combination of four quasi-orthogonal removable protecting groups, stepwise Fmoc solid-phase synthesis of a linear precursor peptide, followed by the last amino acid coupling *via* ester bond formation and on-resin head-to-tail macrolactamization. Optically unresolved form of the HyAsp was used for the peptide assembly. Pentafluorophenyl activation was chosen for the HyAsp side-chain carboxyl group attachment to the resin. The efficiency of the coupling (90 %) was determined by a spectrophotometric Fmoc-quantitation assay. Linear precursor peptide (Boc-D-Leu-L-Leu-L-PhSer-L-HyLeu-L-Leu-D-Arg-L-Ile-L-*allo*-Thr-Gly-D,L-HyAsp) was assembled using standard Fmoc-chemistry. Ester bond formation between Fmoc-Ser-OH and hydroxyl group of the resin-bound PhSer was performed using *N,N'*-diisopropylcarbodiimide/4-dimethylaminopyridine (DIC/DMAP) in dichloromethane as previously described [5]. Dmab and the Fmoc protecting groups were removed by hydrazine treatment. Partial cleavage of the ester bond was observed during this step by MALDI-TOF MS and HPLC analyses. The linear peptide was cyclized using PyBOP coupling reagent. The peptide was cleaved from the resin using two cleavage cocktails: mixture of TFA, water, and thioanisol (90:5:5; v/v/v) and reagent K, respectively. The crude product was purified by HPLC. The significant amount of the side product was observed. The presence of HyAsp-Ser sequence and the results of the MALDI-TOF MS analysis (observed:  $[M+H]^+ = 1258.41$ ) suggest possible aspartimide formation. Further NMR studies are needed to confirm the true identity of the side product. The pure fraction of katanosin B was characterized by HPLC and MALDI-TOF MS analyses (calculated:  $[M+H]^+ = 1275.72$ ; observed:  $[M+H]^+ = 1274.47$ ). Circular dichroism (CD) spectroscopy of the katanosin B confirmed the random coil structure in water solution. Antimicrobial activity of katanosin B was determined against four representative strains (Table 1). Higher MIC values compared to the original katanosin B could be explained by the presence of the D,L-HyAsp that has been used in this first attempt to synthesize katanosin B on solid support by the Fmoc approach.

Table 1. Antimicrobial activity of katanosin B

Microorganism	MIC* ( $\mu\text{g/mL}$ )
<i>S. aureus</i> (MRSA)	8
<i>S. aureus</i> Mu50 (VRSA)	8
<i>S. epidermidis</i>	8
<i>S. aureus</i> 6538P	8

## Acknowledgments

We would like to thank American Heart Association for the financial support of this work through grant 0630175N awarded to P.C.

## References

- (a) Shoji, J., Hinoo, H., Matsumoto, K., Hattori, T., Yoshida, T., Matsura, S., Kondo, E. *J. Antibiot.* **41**, 713-718 (1988); (b) Kato, T., Hinoo, H., Terui, Y., Kikuchi, J., Shoji, J. *J. Antibiot.* **41**, 719-725 (1988).
- Okai, H., Imamura, N., Izumiya, N. *Bull. Chem. Soc. Jap.* **9**, 2154-2159 (1967).
- Bhushan, R., Brückner, H. *Amino Acids* **27**, 231-247 (2004).
- Verbeure, B., Lacey, C.J., Froeyen, M., Rozenski, J., Herdewijn, P. *Bioconjugate Chem.* **13**, 333-350 (2002).
- Stawikowski, M., Cudic, P. *Tetrahedron Lett.* **47**, 8587-8590 (2006).

## Efficient Total Synthesis of Dipeptidic Antibiotics (+)-Negamycin and Its Derivatives

Yoshio Hayashi,<sup>1,2</sup> Akihiko Taguchi,<sup>1</sup> Thomas Regnier,<sup>2</sup>  
Shigenobu Nishiguchi,<sup>2</sup> and Yoshiaki Kiso<sup>2</sup>

<sup>1</sup>Department of Medicinal Chemistry, School of Pharmacy, Tokyo University of Pharmacy and Life Sciences, Hachioji, Tokyo 192-0392, Japan; and <sup>2</sup>Department of Medicinal Chemistry, Kyoto Pharmaceutical University, Kyoto 607-8412, Japan

### Introduction

(+)-Negamycin **1** [1], a dipeptidic antibiotic containing a hydrazine peptide bond is recently thought to be a potential therapeutic agent for genetic diseases such as Duchenne muscular dystrophy (DMD) with a nonsense mutation in the dystrophin gene [2]. Negamycin has attracted a great deal of synthetic interest. Several syntheses of negamycin in both racemic and optically active forms have been accomplished over three decades after its discovery. However, an efficient shortened synthetic route of (+)-**1** and its derivatives appears significant to develop promising new therapeutic candidates for DMD and other diseases caused by nonsense mutations. In the previous study, we developed a new synthetic route to obtain (+)-**1** from (*R*)-ethyl-4-chloro-3-hydroxybutanoate in 26% overall yield over 13 steps [3]. Here, we report another attractive synthetic route for (+)-**1** from commercially available achiral Boc-glycinal **2** using modern organic chemistry techniques, including asymmetric allylboration, microwave-assisted ruthenium catalyzed cross-metathesis and asymmetric Michael addition to afford (+)-**1** with an overall yield 41% in 8 steps [4].

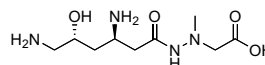


Fig. 1. Structure of (+)-negamycin ((+)-**1**).

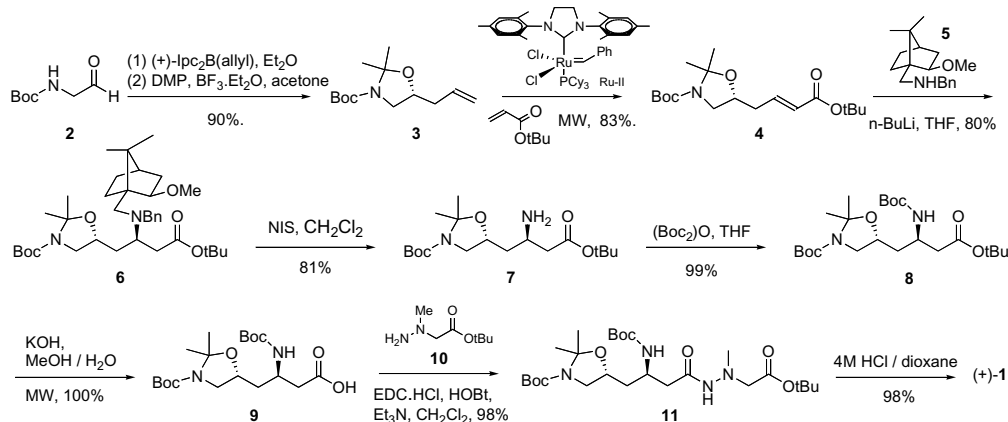
### Results and Discussion

Our efficient route consists first on an asymmetric allylboration of *N*-Boc-glycinal **2** using the established Brown's procedure for preparation of chiral allylic alcohols that led to a corresponding chiral intermediate (Scheme 1). This resulting chiral amino alcohol was directly used without further purification to form the target oxazoline **3** by treatment with 2,2-dimethoxypropane (DMP) in the presence of BF<sub>3</sub>·Et<sub>2</sub>O in acetone. As a result, oxazoline **3** was generated in high yield after purification by silica gel column chromatography (90%). To prepare the key intermediate **4**, a cross-metathesis (CM) reaction between oxazoline **3** and *tert*-butyl acrylate was investigated. As a result, intermediate **4** was efficiently synthesized with 83% yield in the presence of 5 mol% Grubbs 2nd generation catalysis under a microwave irradiation condition for 15 min. NOE experiments revealed that the stereochemistry of the olefin moiety in **4** was an *E* configuration ( $J_{\text{vinyllic protons}} = 15.7$  Hz). Thus, the desired chiral intermediate **4** was obtained with 75% yield after 2 steps from achiral starting material **2**.

With intermediate **4** in hands, our focus shifted toward the asymmetric Michael addition reaction. Recently, Node *et al.* reported a highly stereoselective asymmetric Michael addition toward *tert*-butyl  $\alpha,\beta$ -unsaturated carbonyl compounds using chiral amine **5** [5]. The chiral reagent **5** was reacted with **4** in the presence of *n*-BuLi in THF at -78°C to afford compound **6** as a single diastereomer (*de* >99%) with 80% yield after purification. Removal of both benzyl and 2-methoxyboryl protecting groups located on the same amine moiety could be achieved efficiently using 4 equiv of *N*-iodosuccinimide (NIS) in CH<sub>2</sub>Cl<sub>2</sub> to obtain free amino compound **7** with 81% yield. No epimerization was observed during this reaction.

The last part of the synthesis of (+)-**1** consisted of introducing a hydrazine unit, prior to a final deprotection. A Boc-protection of **7** using standard procedures was first quantitatively performed to afford *N*-protected *tert*-butyl ester **8**, that was then efficiently converted to acid **9** by a microwave-assisted saponification with 2M KOH in MeOH, and coupling with hydrazine unit **10** was then performed using the EDC-HOBt method. The synthesis of hydrazine **10** was achieved by reacting *N*-methylhydrazine with *t*-butyl bromoacetate with 40% yield after purification. Deprotection of compound **11** and purification by ion exchange chromatography on Amberlite CG50 (NH<sub>4</sub><sup>+</sup> form) afforded the target compound (+)-**1** with 98% yield,  $[\alpha]_{\text{D}}^{25.2} +2.4^\circ$

(c 0.36, H<sub>2</sub>O), lit.  $[\alpha]_D^{29.0} +2.5^\circ$  (c 2.00, H<sub>2</sub>O). The final compound was fully characterized and compared with the published data for the natural product to confirm the success of this new total synthesis of (+)-**1**. Furthermore, in vivo read-through activity of termination codons of synthesized (+)-**1** during protein biosynthesis in mice was similar to that of the native (+)-**1**.



Scheme 1. Total synthesis of (+)-negamycin ((+)-**1**).

For the purpose of preparing a sample of 5-*epi*-negamycin for biological testing, the opposite stereoisomer at the 5-position viz. a compound **3R,5S-6** was synthesized according to the same method, which begins with achiral *N*-Boc-glycinal **2**, followed by an asymmetric allylboration using (-)-*B*-allyldiisopinocampheylborane [(-)-*Ipc*<sub>2</sub>B(allyl)] with the opposite stereochemistry, cross-metathesis reaction using Grubbs second-generation [Ru-**II**] catalyst, and asymmetric Michael addition. The obtained compound **3R,5S-6** was then subjected to the same sequence of reactions as just described for (+)-negamycin to give 5-*epi*-negamycin in 41% yield from substrate **3R,5S-6**.

In conclusion, the proposed synthetic route for the total synthesis of optically active (+)-negamycin starting from *N*-Boc-glycinal **2**, led to the desired product with a total yield of 42% from only 8 steps. To our knowledge, this study represents the most efficient strategy to prepare (+)-**1**. Current efforts with this synthetic approach are expanding into Medicinal Chemistry to discover new drug candidates with potent read-through activity for chemotherapy of DMD.

## Acknowledgments

This research was supported by The Research Grant (20B-13) for Nervous and Mental Disorders from the Ministry of Health, Labour and Welfare, and Grant-in-Aid for Exploratory Research 20659017 from MEXT.

## References

- (a) Kondo, S., Shibahara, S., Takahashi, S., Maeda, K., Umezawa, H., Ohno, M. *J. Am. Chem. Soc.* **93**, 6305-6306 (1971). (b) Uehara, Y., Hori, M., Umezawa, H. *Biochim. Biophys. Acta* **374**, 82-95 (1974).
- Arakawa, M., Shiozuka, M., Matsuda, R., et al. *J. Biochem.* **34**, 751-758 (2003).
- Hayashi, Y., Nishiguchi, S., Hashimoto, D., Sydnes, M.O., Regnier, T., Hasegawa, J., Katoh, T., Kajimoto, T., Shiozuka, M., Matsuda, R., Node, M., Kiso, Y. *Peptide Science* 2007, pp 163-164.
- Hayashi, Y., Regnier, T., Nishiguchi, S., Sydnes, M.O., Hashimoto, D., Hasegawa, J., Katoh, T., Kajimoto, T., Shiozuka, M., Matsuda, R., Node, M., Kiso, Y. *Chem. Commun.* 2379-2381 (2008).
- (a) Katoh, T., Node, M., et al. *Tetrahedron Lett.* **49**, 598-600 (2008). (b) Node, M., Kajimoto, T., et al. *Org. Lett.* **10**, 2653-2656 (2008).

## Design, Synthesis and Conformational Studies of New Analogues of Temporins A and L

Stefania Malfi,<sup>1</sup> Maria Rosaria Saviello,<sup>1</sup> Ludovica Marcellini,  
 Hercolani Gaddi,<sup>2</sup> Cristina Marcozzi,<sup>1</sup> Alfonso Carotenuto,<sup>1</sup>  
 Maria Luisa Mangoni,<sup>2</sup> Luigia Auriemma,<sup>1</sup>  
 Isabel Gomez-Monterrey,<sup>1</sup> Pietro Campiglia,<sup>3</sup>  
 Ettore Novellino,<sup>1</sup> and Paolo Grieco<sup>1</sup>

<sup>1</sup>Department of Pharmaceutical Chemistry and Toxicological, University of Naples "Federico II" Naples, 80131, Italy; <sup>2</sup>II Facoltà di Medicina e Chirurgia, University of Rome "La Sapienza" Rome, 00185, Italy; <sup>3</sup>Department of Pharmaceutical Sciences, University of Salerno, Fisciano Salerno, 84084, Italy.

### Introduction

Temporins are short, linear 10-14 residues long peptides, with a net charge positive and an amidate C-terminal. To get insight into mechanism of action and biological activity of these compounds, we have investigated two members: temporin L (TL) (FVQWFSKFLGRIL-NH<sub>2</sub>) and temporin A (TA) (FLPLIGRVLSGIL-NH<sub>2</sub>). The first has the highest activity among all temporins but shows haemolytic activity too. TA active against Gram-positive bacterial strains, exerts the antimicrobial activity by its ability to form a transmembrane pore via a 'barrel-stave' mechanism or to form a 'carpet' on the membrane surface via the 'carpet-like' model [1, 2]. We have investigated the preferential conformation of TL and TA in SDS and DPC solutions. On the bases of the NMR results, we have designed and synthesized new TA and TL analogues, called Pro<sup>3</sup>TL (FVPWFSKFLGRIL-NH<sub>2</sub>), Gln<sup>3</sup>TA (FLQLIGRVLSGIL-NH<sub>2</sub>), D-isomers (fvqwfskflgril-NH<sub>2</sub>) and a Retro-TL (lirglfksfwqv-NH<sub>2</sub>) analogue.

### Results and Discussion

The difference observed between the TA and TL secondary structures both in SDS and DPC micelle solutions was the presence of a turn conformation in the N-terminal region of TA, likely induced by the Pro<sup>3</sup> residue, we have investigated this position both in TA and in TL. We have replaced the Gln<sup>3</sup> of TL with a Pro residue obtaining the Pro<sup>3</sup>-TL analogue, analogously we have replaced a Pro<sup>3</sup> residue in TA with a Gln<sup>3</sup> residue obtaining the Gln<sup>3</sup>-TA analogue. Furthermore on the bases of the CD data about Retro-TL and D-Isomer we have investigated the biological activity of all derivatives (Table 1). For D-isomer and the Retro-TL it is possible to highlight a decrease of the antimicrobial activity, respect to TL template, due to an absence of  $\alpha$ -helix structure. CD and NMR analysis [3] (Figure 1). The two analyzed peptides TA and TL, show in both SDS and DPC a stable amphipathic  $\alpha$ -helix (Figure 2). Moreover the CD in DPC results show an  $\alpha$ -helix structure for the template TL (a, Figure 1), and for the Retro-TL derivative there is a random coil structure (c, in Figure 1). Finally the D-isomer analogue (b, in Figure 1) shows neither the  $\alpha$ -helix nor random coil structure; in fact their

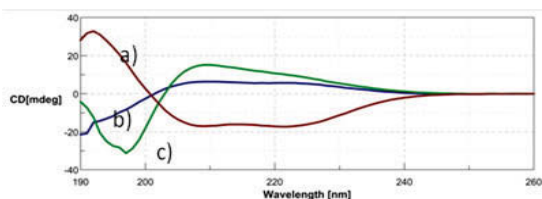


Fig. 1. a) TL template profile; b) D-isomer profile; c) Retro-TL profile.

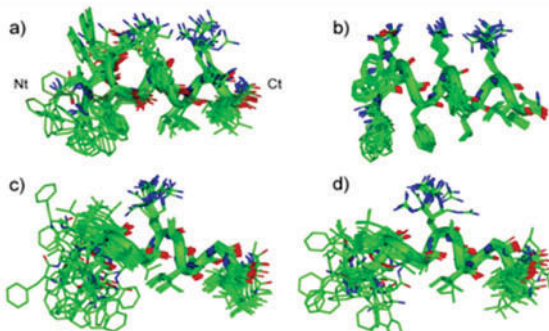


Fig. 2. Superposition of the 20 lowest energy conformers of TL in SDS (a), TL in DP (b), TA in SDS (c), TA in DPC (d). Structures were superimposed using the backbone heavy atoms of residues 3-11.

Table 1. Biological data

Strains	Peptides( $\mu$ M concentration)					
	TL	Pro <sup>3</sup> -TL	Retro-TL	D-Isomer	TA	Gln <sup>3</sup> -TA
<i>Gram negative</i>						
<i>E. Coli D21</i>	12	12	12.5	12.5	>24	>24
<i>E. Faecalis ATCC 29212</i>	6	6	3	12.5	12	6
<i>P. Aeruginosa ATCC 15692</i>	24	24	50	>100	>24	>24
<i>P. Syringae pv tobaci</i>	6	6	6	6	>24	>24
<i>Y.Pseudotuberculosis YPIII</i>	6	6	3	6	12	6
<i>Gram positive</i>						
<i>B. Megaterium Bm11</i>	1.5	1.5	1.6	1.6	1.5	0.75
<i>S. Aureus Cowan I</i>	3	1.5	3	3	1.5	1.5
<i>S. Aureus ATCC 25923</i>	3	3	3	12.5	3	1.5
<i>S. Capitis</i>	1.5	1.5	3	6	1.5	1.5
<i>S. Epidemidis ATCC12228</i>	3	1.5	3	6	3	1.5
<i>S. Pyogenes ATCC 21547</i>	6	6	6	6	12	6
<i>Yeast</i>						
<i>C. Albicans ATCC 10231</i>	12	6	6	12.5	12	6
<i>S. Cerevisae</i>	6	6	6	---	6	6
<i>S. Pombe</i>	6	3	6	---	3	3
<i>Peptides concentration (<math>\mu</math>M)</i>	<i>% Haemolysis</i>					
25	94	92	90	81	28	92
12.5	92	42	88	49	6	70
6.25	48	10	46	15	4.5	18
3.12	13	6	13	6	3	9

calculated value of the  $\alpha$ -helix content is about 14%.

Our results point to a different molecular mechanism underlying antimicrobial and haemolytic actions of TA and TL. The ‘carpet-like’ and the ‘barrel-stave’ models were employed to interpret the antimicrobial and haemolytic activities of temporins, respectively. Biological data show that the analogue Pro<sup>3</sup>-TL, with respect to the native TL, has an increased antimicrobial potency and a decreased haemolytic activity which make it an interesting molecule for further structure-function relationship studies.

## References

1. Shai, Y. *Biopolymers* **66**, 236–248 (2002).
2. Mangoni, M.L., et al. *J. Biochem.* **267**, 1447–1454 (2000).
3. Carotenuto, A., et al. *J. Med. Chem.* **51**, 2354–2362 (2008).

## Novel Antimicrobial Peptides from the Venom of Eusocial Bee *Halictus sexcinctus* (Hymenoptera: Halictidae)

Lenka Monincová,<sup>1</sup> Oldřich Hovorka,<sup>1</sup> Josef Cvačka,<sup>1</sup> Zdeněk Voburka,<sup>1</sup>  
Vladimír Fučík,<sup>1</sup> Lenka Borovičková,<sup>1</sup> Lucie Bednářová,<sup>1</sup> Miloš  
Buděšínský,<sup>1</sup> Jiřina Slaninová,<sup>1</sup> Jakub Straka,<sup>2</sup> and Václav Čerovský<sup>1</sup>

<sup>1</sup>Institute of Organic Chemistry and Biochemistry, Academy of Sciences of the Czech Republic,  
Flemingovo nám. 2, 166 10 Prague 6, Czech Republic <sup>2</sup>Department of Zoology, Faculty of  
Science, Charles University, Viničná 7, 120 00 Prague 2, Czech Republic

### Introduction

Antimicrobial peptides (AMPs) initially discovered as a part of innate immunity system of practically all-living organisms, ranging from prokaryotes to humans, are attracting target as potential antimicrobial agents with different mode of action than traditional antibiotics. The most studied group of AMPs represents those which can adopt  $\alpha$ -helical structure within the bacterial cell membrane. These peptides which exhibit significant activity against a wide range of Gram-positive and -negative bacteria are frequently found in the venom of hymenoptera. In our laboratory we are currently focusing on the identification of novel AMPs in the venom of wild bees. Here we describe structural features and biological activities of two novel peptides named halictines (HAL-1, HAL-2) isolated from the venom of wild bee *Halictus sexcinctus*. We also prepared several HAL-1 analogs to study the effect of enhanced cationicity on antimicrobial and hemolytic activity.

### Results and Discussion

Bee specimens were collected in the central part of the Czech Republic during June 2008 and kept frozen at -20 °C. The venom reservoirs of 6 individuals were removed by dissection and their contents extracted with a mixture (25  $\mu$ l) of acetonitrile/water (1:1) containing 0.1% TFA. The extract was fractionated by RP-HPLC (Figure 1). The components detected at 220 nm were collected, the solvent was evaporated and the material was analyzed by mass spectrometry. Two peptides of the peaks labeled as HAL-1 (1408.8 Da) and HAL-2 (1451.9 Da) were subjected to Edman degradation. Internally calibrated electrospray mass spectra of both peptides resulted in accurate masses which corresponded to calculated masses of the C-terminally amidated compounds (Table 1). For biological assays and CD and NMR study, the peptides were synthesized by the standard protocol of N<sup>α</sup>-Fmoc chemistry with DIPCI/HOBt as coupling reagents on a Rink Amide MBHA resin.

The secondary structures of HAL-1 and HAL-2 were studied by CD spectroscopy in water and in the various mixtures of water/trifluorethanol (0-50 % TFE) and water/SDS (0-16 mM). The peptides occurred as a random coil structure in water and in the low concentrations of

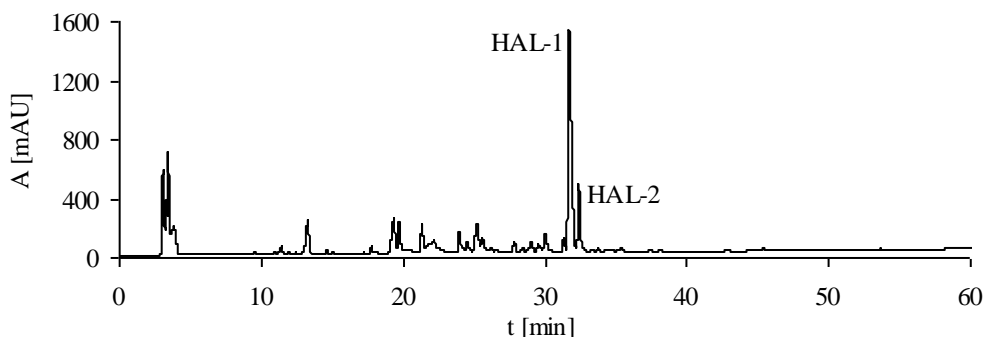


Fig. 1. RP-HPLC profile of *Halictus sexcinctus* venom extract at 220 nm on Vydac C-18, 250 x 4.6 mm column. An elution gradient of solvents from 5% to 70% of acetonitrile/water/0.1% TFA was applied for 60 min at 1ml/min flow rate.

Table 1. Antimicrobial and hemolytic activity of halictines and their analogs compared to other antimicrobial agents

Peptide <sup>a</sup>	Sequence <sup>b</sup>	<i>M<sub>w</sub></i> [Da]	Antimicrobial activities MIC [μM] <sup>c</sup>				Hemolytic activity LC <sub>50</sub> [μM]	Net charge
			<i>B.s.</i>	<i>E.c.</i>	<i>S.a.</i>	<i>P.a.</i>		
HAL-1	GMWSKILGHLIR-NH <sub>2</sub>	1408.8	0.8	3.8	7.7	45.0	82.0	+ 3
HAL-2	GKWMSLLKHILK-NH <sub>2</sub>	1451.9	1.0	2.5	8.1	42.1	78.1	+ 4
HAL-1/6	GMWSKILGHL <b>I</b> K-NH <sub>2</sub>	1380.8	1.3	7.2	15.8	65.0	132	+ 3
HAL-1/4	GMWSKILGHL <b>K</b> R-NH <sub>2</sub>	1423.8	2.2	28.3	100	93.0	>200	+ 4
HAL-1/9	GMWSKILG <b>K</b> LIR-NH <sub>2</sub>	1399.9	0.9	3.7	9.2	26.3	143	+ 4
HAL-1/18	GMWSKIL <b>K</b> HLIR-NH <sub>2</sub>	1479.9	0.9	2.3	3.7	13.5	45.0	+ 4
HAL-1/5	GMW <b>K</b> KILGHLIR-NH <sub>2</sub>	1449.9	0.9	1.8	8.4	16.3	92.9	+ 4
HAL-1/12	<b>G</b> KWSKILGHLIR-NH <sub>2</sub>	1405.9	3.0	3.7	23.3	71.7	>200	+ 4
HAL-1/17	<b>K</b> MWSKILGHLIR-NH <sub>2</sub>	1479.9	2.1	6.3	41.7	73.3	>200	+ 4
HAL-1/10	GMW <b>K</b> KIL <b>G</b> KLIR-NH <sub>2</sub>	1440.9	0.8	2.3	15.0	13.1	>200	+ 5
HAL-1/14	GMWS <b>K</b> <b>K</b> L <b>K</b> HLIR-NH <sub>2</sub>	1494.9	13.3	60.0	>100	>100	>>200	+ 5
Anoplin	GLLKRIKTLL-NH <sub>2</sub>	1152.8	5.0	20.0	>100	40.0	>200	+ 4
Indolicidin	ILPWKWPWPWRR-NH <sub>2</sub>	1906.3	1.0	>100	13.0	>100	>200	+ 4
Tetracycline	-	444.4	12.5	0.4	1.5	75.7	>200	-

<sup>a</sup> Working names <sup>b</sup> Amino acid replacement are in bold <sup>c</sup> *B.s.*, *Bacillus subtilis*; *S.a.*, *Staphylococcus aureus*; *E.c.*, *Escherichia coli*; *P.a.*, *Pseudomonas aeruginosa*

TFE or SDS. With increased TFE or SDS concentrations the peptides adopted  $\alpha$ -helical structures characterized by CD spectra with two typical minima at 207 and 221 nm. <sup>1</sup>H NMR spectroscopy also confirmed that halictines in water solution behave as random coil peptides while they form  $\alpha$ -helix in presence of 30% TFE. Halictines are rich in hydrophobic and positively charged amino acids (Lys and Arg). We assume that also in the anisotropic environment of the bacterial cell membrane halictines form amphipathic  $\alpha$ -helix with hydrophobic amino acid residues on one side of the helix and hydrophilic amino acids residues on the opposite side. The adaptation of such secondary structure is essential for their antimicrobial activity. Both structural investigations showed that HAL-2 has a better tendency to adopt  $\alpha$ -helical secondary structure in the anisotropic environment than HAL-1.

A quantitative antimicrobial activity determination, the minimal inhibitory concentrations (MICs), was established by observing bacteria growth in multi-well plates. Hemolytic (as a toxicity measure) activities were established with rat red blood cells. Halictines exhibit potent antimicrobial activity against both Gram-positive and -negative bacteria and moderate hemolytic activity against rat erythrocytes (Table 1). To study the effect of increasing cationicity on biological activity, we prepared HAL-1 analogs in which additional Lys was walked through the HAL-1 sequence replacing stepwise single or double residues (Table 1). Antimicrobial potency of HAL-1/9 and HAL-1/5, where His9 or Ser4 were replaced by Lys, respectively, and HAL-1/10, where both amino acids were replaced by Lys, was enhanced against Gram-negative bacteria, especially against *P.a.*. In the case of HAL-1/10 also the undesired hemolytic activity was reduced. Comparison of antimicrobial and hemolytic activities of halictines and their analogs to other AMPs of the similar size - amphipathic  $\alpha$ -helical peptide anoplin [1] and Trp rich indolicidin [2] shows, that under our testing conditions, halictines exhibit better antimicrobial properties than those AMPs and are comparable to tetracycline.

## Acknowledgments

The work was supported by the Czech Science Foundation, grant No. 203/08/0536 and by the research project No. Z40550506 of the Institute of Organic Chemistry and Biochemistry, Academy of Sciences of the Czech Republic.

## References

1. Konno, K., Hisada, M., Fontana, R., et. al. *Biochim. Biophys. Acta* **1550**, 70-80 (2001).
2. Selsted, M.E., Novotny, M.J., Morris, W.L., et. al. *J. Biol. Chem.* **267**, 4292-4295 (1992).



## Role of the Strongly Helicogenic Aib Residues on the Properties of the Lipopeptaibol Trichogin GA IV

Barbara Biondi, Marta De Zotti, Cristina Peggion, Fernando Formaggio, and Claudio Toniolo

ICB, Padova Unit, CNR, Department of Chemistry, University of Padova, 35131 Padova, Italy

### Introduction

Trichogin GA IV [1] (Figure 1) is a 10-mer member of the class of short lipopeptaibols [2] that are linear, membrane-active, peptide antibiotics of fungal origin, characterized by the presence of three strongly helicogenic Aib residues [3], a fatty acyl moiety at the N-terminus, and an 1,2-aminoalcohol at the C-terminus. Trichogin GA IV and some of its analogues exhibit a strong activity against Gram positive bacteria and methicillin-resistant *S. aureus* with low hemolytic effect and a remarkable resistance to proteolytic degradation [4].

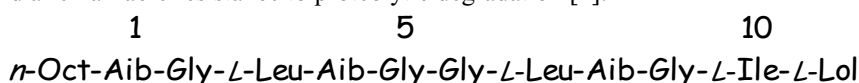


Fig. 1. Primary structure of trichogin GA IV (*n*-Oct, *n*-octanoyl; Aib,  $\alpha$ -aminoisobutyric acid; Lol, leucinol).

### Results and Discussion

We prepared by SPPS and fully characterized a novel set of trichogin GA IV analogs where the three Aib residues at positions 1, 4, and 8 are replaced by one or two L-Leu residues. Leu is still a helix-supporting amino acid, but less effective than the non-coded Aib. Also, the Aib lipophilicity is even enhanced in Leu.

To investigate the role of the Aib→L-Leu replacements, we carried out a conformational study using FT-IR absorption and CD (Figure 2) spectroscopies, and 2D-NMR accompanied by membrane leakage experiments. Interestingly, the results support the view that the L-Leu-based trichogin GA IV analogs do preserve the predominant  $3_{10}$ -helix [5] conformation and the membrane permeability properties of the parent lipopeptaibol despite the presence of only one or two Aib residues in the 10-mer sequence.

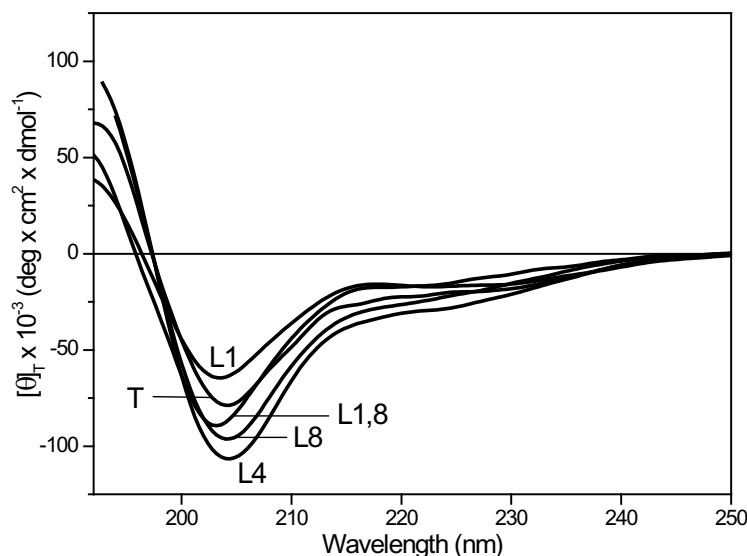


Fig. 2. Far-UV CD spectra of trichogin GA IV (**T**) and its [L-Leu<sup>1</sup>] (**L1**), [L-Leu<sup>4</sup>] (**L4**), [L-Leu<sup>8</sup>] (**L8**), and [L-Leu<sup>1,8</sup>] (**L1,8**) analogs in MeOH solution.

## References

1. Peggion, C., Formaggio, F., Crisma, M., Epand, R.F., Epand, R.M., Toniolo, C. *J. Pept. Sci.* **9**, 679-689 (2003).
2. Toniolo, C., Crisma, M., Formaggio, F., Peggion, C., Epand, R.F., Epand, R.M. *Cell. Mol. Life Sci.* **58**, 1179-1188 (2001).
3. Toniolo, C., Crisma, M., Formaggio, F., Peggion, C. *Biopolymers (Pept. Sci.)* **60**, 396-419 (2001).
4. De Zotti, M., Biondi, B., Formaggio, F., Toniolo, C., Stella, L., Park, Y., Hahm, K.S. *J. Pept. Sci.* (2009) in press.
5. Toniolo, C., Benedetti, E. *Trends Biochem. Sci.* **16**, 350-353 (1991).

# Solution and Solid-Phase Syntheses and Conformational Analysis of a Novel Medium-Length Peptaibiotic

**Marina Gobbo, Claudia Poloni, Marta De Zotti, Cristina Peggion,  
Barbara Biondi, Fernando Formaggio, and Claudio Toniolo**

ICB, Padova Unit, CNR, Department of Chemistry, University of Padova, 35131 Padova, Italy

## Introduction

A few years ago, a novel, medium-length (14-mer) peptaibol (tylopeptin B) was extracted from the fruiting body of the mushroom *Tylophilus neofelleus* and sequenced [1,2]. Its primary structure (Figure 1) is characterized by an N-terminal Trp (an excellent intrinsic chromophoric probe) and a central Ser (which can be easily functionalized in the side chain), both residues rarely occurring in peptaibiotics, and by two Gln (one in the center and one near the C-terminus) and five strongly heliogenic Aib residues. This peptaibiotic is an interesting target in that it is selectively active against Gram-positive bacteria, but it is inactive against pathogenic fungi and Gram-negative bacteria. It is also almost unique among medium-length (14-15 amino acid) peptaibiotics in that it does not contain any Aib-Pro(Hyp) sequence. We synthesized in solution and in the solid phase as well, and fully characterized, tylopeptin B. A conformational analysis was performed on the full-length peptaibiotic and selected, protected, synthetic segments thereof.



## Results and Discussion

For the synthesis in solution we used the segment (1-4, 5-8, and 9-14) condensation approach. The Gln residues were introduced as Glu(OMe) derivatives. For SPPS [3] we exploited a 2-chlorotrityl resin (which, upon treatment with HFIP, affords the 1,2-aminoalcohol peptide), the Fmoc/tBu, Trt, Boc strategy, and double coupling in the difficult Xxx-Aib peptide bond formation.

A conformational analysis was performed on the full-length (protected and deprotected) peptaibiotic and selected segments thereof using FT-IR absorption, CD (Figure 2) and fluorescence spectroscopies, and 2D-NMR spectrometry. The results indicate that tylopeptin B is largely helical in  $\text{CDCl}_3$ , MeOH, and TFE solutions and in aqueous SDS, a membrane-mimetic environment. In general, the  $\alpha$ -helix structure seems to prevail over the  $3_{10}$ -helix.

Both protected and unprotected tylopeptins B exhibit remarkable membrane-modifying properties as highlighted by measuring the induced leakage of carboxyfluorescein entrapped in egg phosphatidylcholine/cholesterol small unilamellar vesicles.

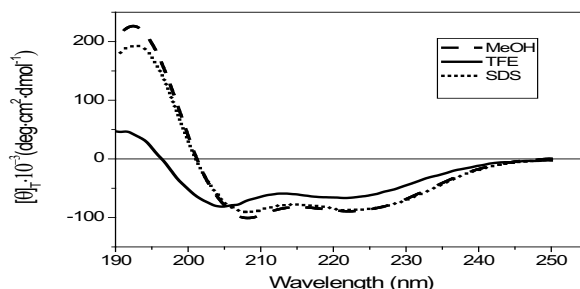


Fig. 2. Far-UV CD spectra of tylopeptin B in MeOH and TFE solutions, and in 300 mM SDS in water (peptide concentration: 0.1 mM).

## References

1. Lee, S.-J., Yun, B.S., Cho, D.-H., Yoo, I.-D. *J. Antib.* **52**, 998-1006 (1999).
2. Neuhof, T., Berg, A., Besl, H., Schwecke, T., Dieckmann, R., von Döhren, H. *Chem. Biodivers.* **4**, 1103-1115 (2007).
3. Hjørringgaard, C.U., Pedersen, J.M., Vosegaard, Th., Nielsen, N. Ch., Skrydstrup, T. *J. Org. Chem.* **74**, 1329-1332 (2009).

## Multivalent Antimicrobial Peptides with Enhanced Activity Against MDR Bacteria

Anne W. Young, Zhigang Liu, Chunhui Zhou, Po Hu, Yingkai Zhang, and Neville R. Kallenbach

Department of Chemistry, New York University, New York, NY 10003, U.S.A.

### Introduction

The lack of sequence or structural homology among antimicrobial peptides (AMPs) makes it difficult to predict the activity or target molecules to specific bacteria. Recently Strom et al reported that short R, W rich sequences are a pharmacophore for AMPs related to indolicin and tritypticin [1]. We have pursued this lead and shown that (RW)<sub>n</sub> peptides with n ranging from 1 to 5 are active against MDR Gram positive and negative bacterial strains [2]. Although longer chains are more effective antibacterial agents, they are cytotoxic. Next we explored the biological activity of dendrimeric displays of (RW)<sub>n</sub> sequences, seeking to enhance the intrinsic activity of these sequences by multivalency. We report here the antibacterial and hemolytic activity of the dendrimers as well as its stability against proteolytic degradation compared to the natural AMP indolicidin (ILPWKWPWWPWRR-NH<sub>2</sub>) with a sequence rich in R and W. The results show that dendrimeric displays of short RW sequences substantially reduce the MIC<sub>50</sub> value against bacterial strains as well as the hemolytic activity. (RW)<sub>4</sub>D is more stable and economical to synthesize than natural AMPs and offers a potentially practical topical or oral antimicrobial agent.

### Results and Discussion

The solid phase synthesis of the dendrimeric (RW)<sub>4</sub>D, (RW)<sub>4</sub>-Lys<sup>2</sup>-Lys-β-Ala-NH<sub>2</sub>, was carried out according to Tam [3]. Molecular weight of (RW)<sub>4</sub>D were verified by M/S using a Bruker MALDI-TOF spectrometer, which were in agreement with theoretical masses: M+H<sup>+</sup> calcd 1843.2, found 1843.5. Growth inhibition and hemolysis assays were carried out as previously described [2]. The minimum inhibitory concentrations (MIC<sub>50</sub>) of (RW)<sub>4</sub>D, indolicidin and two control antibiotics were determined under physiological conditions. Relative to indolicidin, (RW)<sub>4</sub>D is more active against ampicillin- and streptomycin-resistant *E. coli* (D31) and the MDR strain *S. aureus* (Table 1).

Table 1. Biological activity and selectivity of AMPs (μg/ml)

AMPs	MIC <sub>50</sub> , μg/ml		HD <sub>50</sub> , μg/ml
	<i>E.coli</i>	<i>S.aureus</i>	RBC
Indolicidin	48	29	293
Den (RW) <sub>4</sub> D	4.5	16	1410
Gentamicin	1.2	51	>2000
Ceftazidime	44	63	>2000

<sup>a</sup> The results are the mean of three independent experiments

<sup>b</sup> HD<sub>50</sub> determined from dose-response curve is peptide concentrations corresponding to 50% hemolysis

The use of peptides in vivo has largely been limited by their short half-lives, since peptides are susceptible to endogenous proteases and peptidases. The antimicrobial activity of (RW)<sub>4</sub>D was assayed out in the presence of protease. AMPs were incubated with trypsin, either at a constant enzyme concentration for various time intervals or with varied concentrations of the trypsin for 1hr, and the antibacterial activity was then determined using standard broth microdilution protocols with *E.coli* and *S.aureus* as target bacteria. The data from these experiments indicate that trypsin inactivates the antibacterial activity of indolicidin in a time- and concentration-

dependent manner (Figure 1). After indolicidin was treated with 100nM trypsin for 1 hr or 1  $\mu$ M trypsin for 2-5 min, its antibacterial activity decreased to 25–30% of the untreated control. By contrast, the antibacterial activity of (RW)4D was resistant to inactivation by the trypsin at high concentration, and over various time intervals.

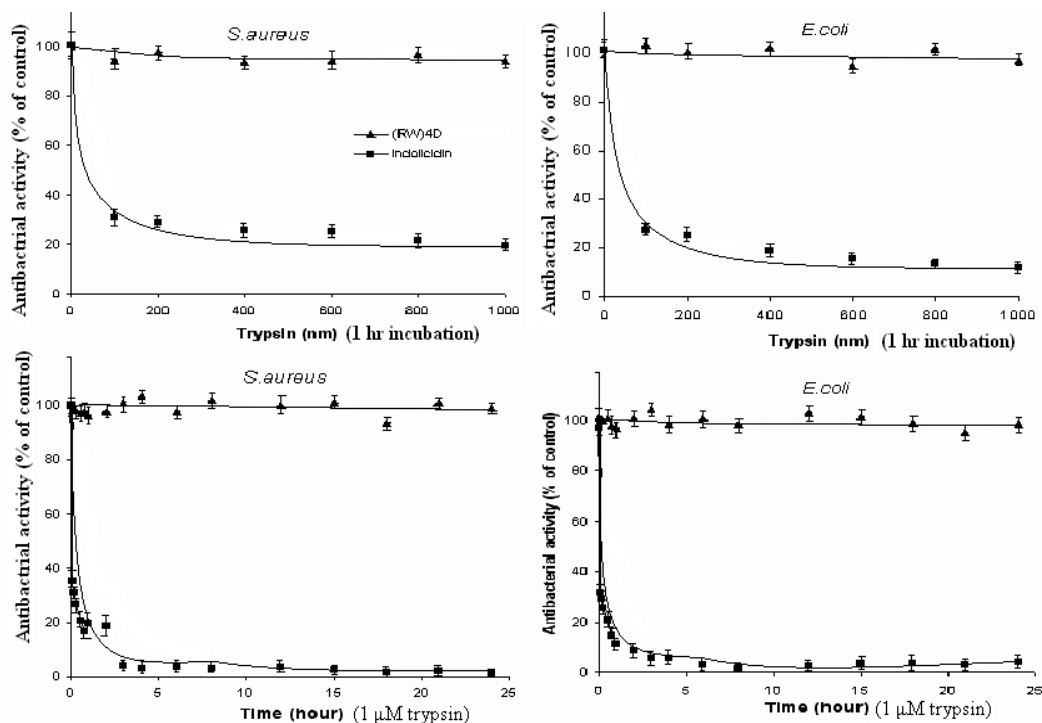


Fig. 1. Protease stability of AMPs.

## Acknowledgments

This work was funded by a grant from ONR (N00014-03-1-0129). We acknowledge the NCRR/NIH for a Research Facilities improvement Grant (C06 RR-16572) at NYU.

## References

1. Strom, M.B., Haug, B.E., Skar, M.L., Stensen, W., Stiberg, T., Svendsen, J.S. *J. Med. Chem.* **46**, 1567-1570 (2003).
2. Liu, Z., Brady, A., Young, A., Rasimick, B., Chen, K., Zhou, C., Kallenbach, N.R. *Antimicrob. Agents Chemother.* **51**, 597-603 (2007).
3. Tam, J.P. *Proc. Natl. Acad. Sci. U.S.A.* **85**, 5409-5413 (1988).

Note: This paper was presented at 20<sup>th</sup> APS in Montreal (2007) but was not included in the Proceedings of 20<sup>th</sup> APS.

## Novel Peptide-based Antimicrobial Agents for the Treatment of *Clostridium Difficile* Associated Disease

David A. Kennedy and Marc Devocelle

Centre for Synthesis and Chemical Biology, Department of Pharmaceutical & Medicinal Chemistry,  
123 St. Stephen's Green, Dublin 2, Ireland

### Introduction

*Clostridium difficile* is the main cause of nosocomial diarrhoea in developed countries. The incidence of disease due to this gram-positive bacterium has been increasing in recent years, with several outbreaks, including from strains such as 027 associated with increased severity and mortality [1]. The number of antibiotics for clinical treatment of *Clostridium difficile* infection is limited [2]. Antimicrobial peptides offer promise as novel anti-infective agents to which the development of resistance by microbes may be restricted [3]. We have developed a novel approach to combined delivery of antimicrobial peptides and agents that protect host epithelia from clostridial toxins for treatment of *Clostridium difficile* infection and disease and report here the synthesis and preliminary evaluation of the antimicrobial constituent of these multi-component delivery systems.

There is a lack of development of new classes of antibiotic drugs. Many of the existing classes operate by targeting a specific aspect of microbial biochemistry. Consequently, microbes may easily evolve resistance mechanisms.

Host defence peptides are molecular effectors of innate immunity in multicellular organisms. These cationic amphipathic peptides offer potential as novel therapeutic antimicrobial [3-5] and anticancer agents [6]. Their assets include potent and broad spectrum activity, low propensity to select resistant mutants and activity that does not rely upon bacterial division. However, to date, in clinical development host defence peptides have met a number of shortcomings, including lack of stability limiting their efficacy.

The mode of action of these evolutionarily conserved mediators of innate immunity involves non-specific targeting of microbial function and structure such as anionic components of the microbial membrane [5]. Antimicrobial peptides can also be active against anaerobic bacteria, such as *Clostridium* species.

Electrostatic properties, such as charge and hydrophobicity, and structural characteristics, such as alpha-helicity with segregation of polar and hydrophobic regions, of antimicrobial and host defence peptides impart selective action against membranes of pathogenic over host cells. Non-coded or uncommon amino acids such as occurring in fungal peptaibiotics [7] may be incorporated into synthetic antimicrobial peptide sequences to enhance hydrophobicity or promote alpha-helicity [8]. We have synthesized antimicrobial peptides bearing alpha-methylalanine or alpha-aminoisobutyric acid (Aib) at the amino terminal, with the strategy of improving antimicrobial activity and stability over the parent peptide against the representative gram-positive bacterium *Staphylococcus aureus*. This approach contributes to the conversion of linear alpha-helical host defence peptides into peptidomimetics and should improve pharmacodynamic properties of these candidates.

A method has been developed for combined delivery of antimicrobial peptides and anti-inflammatory agents for treatment of *Clostridium difficile* infection and associated colitis.

### Results

**Peptide synthesis:** The sequences were assembled by standard Solid Phase Peptide Synthesis on an automated synthesiser, according to the Fmoc/t-Bu protection strategy. The sequences were elongated from a Rink amide MBHA (4-methylbenzhydrylamine) or Sieber amide resin. Peptides were purified and analysed by reverse-phase HPLC and MALDI (Matrix Assisted Laser Desorption Ionisation) or ES<sup>+/−</sup> (ElectroSpray, positive/negative mode) mass spectrometry.

**Aib coupling:** Boc-Aib-OH (10 equiv.) was coupled manually to a resin-bound peptide (1 equiv.) by fluoro-*N,N,N',N'*-tetramethylformamidinium hexafluorophosphate (10 equiv.)

Table 1. Susceptibility of *Staphylococcus aureus* to antibiotics

Antibiotic	MIC <sup>a</sup> ( $\mu\text{g}\cdot\text{mL}^{-1}$ )	Absorbance range (OD <sub>570</sub> ) <sup>b</sup>
Aib-temporin	50	
Aib-temporin+BSA <sup>c</sup>	25	0.621±0.086
cephalothin	6.25	
Bac8c	100	
Bac8c+BSA <sup>c</sup>	>10	0.463±0.053
cephalothin	0.78	

<sup>a</sup>MIC: Minimum Inhibitory Concentration; <sup>b</sup>Absorbance range is the difference between the OD<sub>570</sub>, Optical Density at 570nm, of the positive (minus antibiotic) and negative (minus bacteria) controls. Errors shown are one standard deviation; <sup>c</sup>BSA: Bovine Serum Albumin.

coupling reagent in dimethylformamide (18ml·mmol<sup>-1</sup> peptide) with *N,N*-di-isopropyl-ethylamine (20 equiv.).

**Determination of Minimum Inhibitory Concentrations (MIC):** Bacterial broth suspension adjusted to  $5 \times 10^5$  cfu ml<sup>-1</sup> was incubated with antimicrobial agents in a 96 well microtitre plate for 18 hours at 37°C. Absorbance was measured in a plate reader with a 570nm filter.

**Peptide synthesis results:** The following peptides were synthesized: Temporin analogue L512TA[9], FLPLLGRVLSGLL-NH<sub>2</sub>; LPLLGRVLSGLL-NH<sub>2</sub>; Lactoferricin decapeptide[10], YRWWRWARRW-NH<sub>2</sub>; Lactoferricin decapeptide D-isomer, yrwwrwarw-NH<sub>2</sub>; Bac8c[11]: RIWVIWRR-NH<sub>2</sub>; CAMEL-24[12], KWKLFKHIGAVLKVL-NH<sub>2</sub>; Aib-lactoferricin, Aib-YRWWRWARRW-NH<sub>2</sub>; Aib-RWWWRWARRW-NH<sub>2</sub>; Aib-temporin, Aib-FLPLLGRVLSGLL-NH<sub>2</sub>; Aib-LPLLGRVLSGLL-NH<sub>2</sub>; *N*<sup>α</sup>-isobutyryl-temporin

**Antimicrobial testing:** The results of susceptibility testing are displayed in Table 1.

## Discussion

A series of antimicrobial peptides has been synthesized for susceptibility determination against bacterial pathogens causing nosocomial infection. Antimicrobial activity of Aib-terminal peptide against gram-positive bacterium *Staphylococcus aureus* has been demonstrated. These results indicate the potential of antimicrobial peptides for treatment of colonic infection due to bacterial pathogens. These peptides and other candidates synthesised are currently evaluated against *Clostridium difficile*, as single agents and as part of a multi-component delivery system.

## Acknowledgments

This publication has emanated from research conducted with the financial support of Science Foundation Ireland.

## References

- McFarland, L.V. *Nat. Clin. Pract. Gastroenterol. Hepatol.* **5**, 40-48, (2008).
- Bricker, E., et al. *Cochrane Database Syst. Rev.* CD004610, (2005).
- Hancock, R.E., Sahl, H.G., *Nat. Biotechnol.* **24**, 1551-1557, (2006).
- Zaslöff, M. *Nature* **415**, 389-395, (2002).
- Zhang, L., Falla, T.J. *Expert Opin. Pharmacother.* **7**, 653-663, (2006).
- Mader, J.S., Hoskin, D.W. *Expert Opin. Investig. Drugs* **15**, 933-946, (2006).
- Degenkolb, T., Kirschbaum, J., Bruckner, H. *Chem. Biodivers.* **4**, 1052-1067, (2007).
- Conlon, J.M., et al. *Peptides* **28**, 2075-2080, (2007).
- Wade, D., et al. *FEBS Lett.* **479**, 6-9, (2000).
- Strom, M.B., Rekdal, O., Svendsen, J.S. *J. Pept. Sci.* **8**, 431-437, (2002).
- Hilpert, K., et al. *Nat. Biotechnol.* **23**, 1008-1012, (2005).
- Oh, H., Hedberg, M., Wade, D., Edlund, C. *Antimicrob. Agents Chemother.* **44**, 68-72, (2000).



## Virtual Screening Targeting the PhoP Response Regulator to Inhibit Bacterial Virulence

Yat T. Tang,<sup>1</sup> Tammy Latifi,<sup>2</sup> Eduardo A. Groisman<sup>3</sup>, and  
Garland R. Marshall<sup>1</sup>

<sup>1</sup>Department of Biochemistry and Molecular Biophysics, Washington University School of Medicine,  
St. Louis, MO 63110, U.S.A.; <sup>2</sup>Howard Hughes Medical Institute, Department of Molecular Microbiology,  
Washington University School of Medicine, St. Louis, MO 63110, U.S.A.

### Introduction

Two-component signal transduction (TCST) is the predominant signaling system used in bacteria to sense and respond to environmental changes in order to survive and thrive under various conditions. During infection, pathogens regulate the expression of specific sets of genes to adapt to conditions within its host. The PhoP/PhoQ signaling pathway in *Salmonella enterica* serovar Typhimurium senses and responds to pH and external Mg<sup>2+</sup> levels to distinguish between the environment inside and outside of the host cell [1]. In this signaling scheme, PhoQ, the histidine kinase, senses low extracellular Mg<sup>2+</sup> levels, which leads to autophosphorylation on a conserved histidine. PhoQ then interacts with the inactive PhoP monomer, leading to phosphorylation by PhoQ at a conserved aspartate. Phosphorylation of PhoP mediates the transition from the inactive monomer state to the active PhoP dimer state, and allows it to bind to its DNA promoter and act as a transcription factor to modulate gene expression. PhoP regulates the transcription of key virulence genes essential for invasion of host cells and for growth and survival in macrophages of a number of gram-negative pathogens (e.g. *Shigella flexneri*, *Yersinia pestis*, *Neisseria meningitidis*).

PhoP is a member of the OmpR/PhoB family of response regulators, which accounts for about 30% of all TCST response regulators. Critical salt-bridges conserved at the interface govern PhoP dimerization and function [2]. Mutagenesis studies on other members of this family across various species suggest three sets of salt-bridge residues to be important in PhoP dimerization [3]. Mutating only one of the salt-bridge residues (Glu 107-Lys 87, Arg 111-Asp 97, Arg 118-Asp 96) to an alanine or a residue of opposite charge will disrupt PhoP dimer formation in addition to its function as a transcription factor [4]. The hypothesis is that inhibiting PhoP dimerization will modulate gene expression and regulation of bacterial virulence.

A computational approach using virtual screening combined with consensus scoring revealed drug-like compounds that inhibit the function of the PhoP TCST response regulator. Electrophoretic mobility shift assays were used to test the predictability of the computational approach. This study serves as a proof-of-principle for targeting the two-component signal transduction response regulator to inhibit its function as a transcription factor and modulate gene expression and regulation of bacterial virulence.

### Results and Discussion

**Virtual Screening and Consensus Scoring:** AutoDock 4 [5] was used to virtually screen a drug-like version of the NCI Diversity library with 1420 compounds [6] to generate possible ligand poses (30 poses for each ligand, 42600 poses total). All docked ligand poses were then evaluated in a consensus manner with three separate scoring functions: AutoDock 4, X-SCORE [7], and CSCORE [8]. Compounds that scored in the top 15% (6390 poses, 220 unique compounds) of all three scoring functions were experimentally tested. This computational strategy has proven to be effective in identifying hit compounds [9].

**Electrophoretic Mobility Shift Assay (EMSA):** PhoP-His<sub>6</sub> was activated by phosphorylation using acetyl phosphate, and then incubated with the predicted compounds. Radiolabeled  $\gamma$ -<sup>32</sup>P DNA containing PhoP boxes to represent the *phoP* promoter were incubated with the mix to test for the compounds' ability to disrupt DNA binding.

**EMSA Revealed 11 Hit Compounds From the NCI Diversity Library:** 11 compounds out of 220 tested disrupted formation of the PhoP-DNA complex. Compound **1** (NSC130183) was identified with an estimated  $IC_{50}$  of 49  $\mu$ M, and compound **2** (NSC311153) is estimated to have an  $IC_{50}$  of 29  $\mu$ M (Figures 1 and 2).

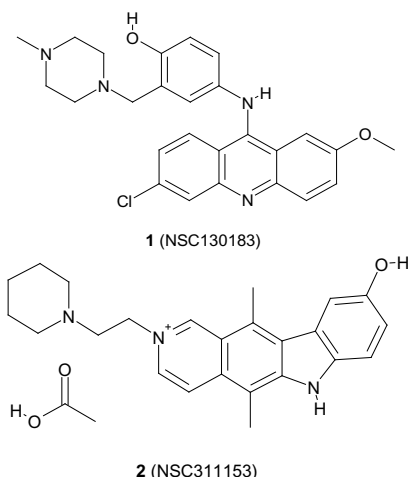


Fig. 1. Two of the 11 compounds predicted by virtual screening and consensus scoring. The predictions were validated by EMSA for inhibition activity on PhoP-DNA binding.

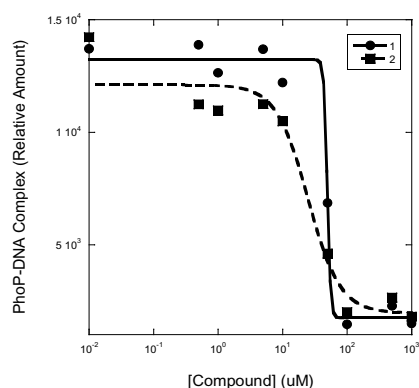


Fig. 2. Dose response studies of **1** (NSC130183) and **2** (NSC311153) reveal  $IC_{50}$  values of 49  $\mu$ M and 29  $\mu$ M, respectively. The intensity of the bands were quantified with ImageJ (NCI).

Future studies will include testing predicted compounds using size exclusion chromatography and multi-angle light scattering to confirm the mechanism of action. Compounds will also be tested with circular dichroism to confirm that they do not bind to the *phoP* promoter instead of PhoP. Similarity searches for confirmed hits will be performed and tested to identify second-generation hits with increased inhibition activity and selectivity to further characterize the PhoP dimerization interface. Binding constants and thermodynamic parameters will be determined by isothermal titration calorimetry. With the increasing resistance of pathogenic bacteria to current antibiotics, the success of this strategy suggests targeting two-component signal transduction systems as a promising potential approach for the development of novel antibiotics.

## Acknowledgments

The authors thank members of the Marshall Lab and the Groisman Lab for continued support and helpful discussions; C M. Taylor for intellectual and technical contributions; the National Cancer Institute Developmental Therapeutics Program for providing compounds for testing. This work was partially supported by the following: WUSM Cancer Biology Pathway and NIH Vision Sciences Training Grant EY13360 (Y.T.T.); NIH and HHMI (T.L., E.A.G.); E.A.G. is an investigator of the Howard Hughes Medical Institute; NIH GM 68460 (G.R.M.).

## References

- Groisman, E.A. *J. Bacteriol.* **6**, 1835-1842 (2001).
- Bachhawat, P., Stock, A.M. *J. Bacteriol.* **16**, 5987-5995 (2007).
- Mack, T.R., Gao, R., Stock, A.M. *J. Mol. Biol.* **389**, 349-364 (2009).
- Chen, Y., Birck, C., Samama, J.P., Hulett, F.M. *J. Bacteriol.* **185**, 262-273 (2003).
- Morris, G.M., Goodsell, D.S., Halliday, R.S., Huey, R., Hart, W.E., Belew, R.K., Olson, A.J. *J. Comput. Chem.* **19**, 1639-1662 (1998).
- Betzi, S., Suhre, K., Chetrit, B., Guerlesquin, F., Morelli, X. *J. Chem. Inf. Model.* **46**, 1704-1712 (2006).
- Wang, R., Lai, L., Wang, S. *J. Comput. Aided Mol. Des.* **16**, 11-26 (2002).
- CSCORE, Tripos, St. Louis, MO.
- Taylor, C.M., Barda, Y., Kisselev, O., Marshall, G.R. *J. Med. Chem.* **51**, 5297-5303 (2008).

## Pyrazinoylation and Benzoylation of Anoplin as a Plausible Approach of Preparing Novel Potent Antibacterial Drugs

Maxilmilien Alaric O. Tan,<sup>1</sup> Portia Mahal G. Sabido<sup>1,2</sup>

<sup>1</sup>Institute of Chemistry, University of the Philippines-Diliman, Quezon City, 1101, Philippines; <sup>2</sup>Natural Sciences Research Institute, University of the Philippines-Diliman, Quezon City, 1101, Philippines

### Introduction

Structure-activity studies of antimicrobial peptides reveal the complement between hydrophobicity and cationicity being responsible for the desired properties of target specificity and selective toxicity [1]. Over the previous years, literature reports the augmentation of antimicrobial peptide activity by N-terminal acylation with fatty acids of different lengths [2-5]. Aside from this, attaching cinnamic acid into the peptide can also be a viable strategy in enhancing its antimicrobial properties [6]. This has inspired our study to introduce other aromatic carboxylic acids into the model antimicrobial wasp venom peptide, anoplin (GLLKRIKTLL-NH<sub>2</sub>), thereby creating a conjugate that comprises both moieties of the antimicrobial peptide and a small molecule drug.

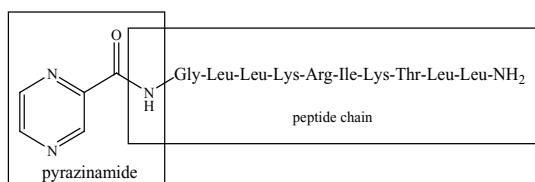


Fig. 1. Pyrazinoylated anoplin (PZ-Anoplin).

### Results and Discussion

Addition of a pyrazinoyl ring results in a hybrid product constituting anoplin and the anti-tuberculosis drug pyrazinamide (Figure 1). On the other hand, benzoylating the glycine residue would allow the product to structurally resemble the N-peptidyl substituted carboxamide derivative of hippuric acid, a common therapeutic for urinary tract infections (Figure 2).

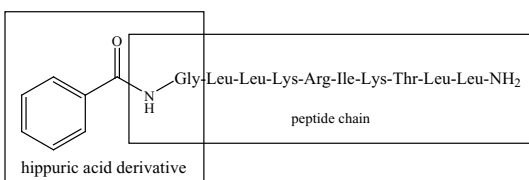


Fig. 2. Benzoylated anoplin (BZ-Anoplin).

The absence of conjugated  $\pi$ -electron ring systems in anoplin renders the peptide inactive towards UV-Vis absorption. With this parent peptide as the baseline profile, scanned BZ-Anoplin and PZ-Anoplin respectively show the presence of aromatic groups as these values are comparable to the maxima of hippuric acid ( $\lambda_{\text{max}} = 258 \text{ nm}$ ) and pyrazinamide ( $\lambda_{\text{max}} = 269 \text{ nm}$ ) (Figure 3). Further analysis by MALDI-TOF MS indicates that the observed MS peak signals of BZ-Anoplin and PZ-Anoplin match their respective calculated molecular weights (Table 1). This given information, clearly indicates the successful incorporation of benzoic acid and pyrazinoic acid into the peptide chain.

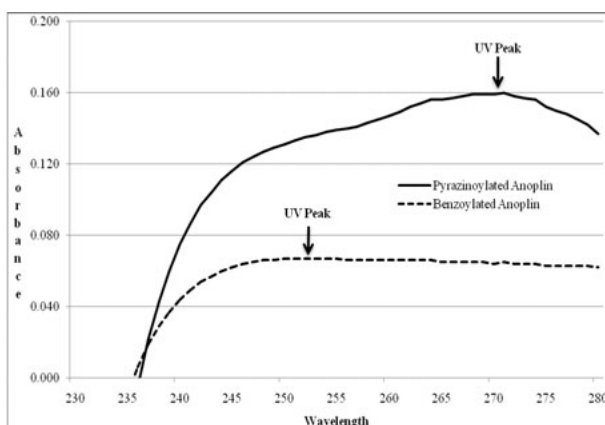


Fig. 3. UV Profile of BZ-Anoplin and PZ-Anoplin.

Table 1. Characterization (% area HPLC, MALDI-TOF MS analysis) of the synthesized compounds

Compound	Purity <sup>a</sup> (% area)	Molecular Weight (m/z)	
		Calculated	Observed
Anoplin	35.0%	1153.50	1139.22 <sup>b</sup>
BZ-Anoplin	30.5%	1257.61	1258.28
PZ-Anoplin	21.8%	1259.59	1260.28

<sup>a</sup> Crude peptides were profiled for 30 minutes by analytical HPLC using 250 mm X 4.6 mm 5  $\mu$  Hypersil C18 column with linear gradients of 0.1% aqueous TFA and 0.1% TFA in acetonitrile as the mobile phase.

<sup>b</sup> Signal of 1139.22 m/z might be a background signal as both MALDI-TOF MS analysis of BZ-Anoplin and PZ-Anoplin also detected a peak at 1139.2 m/z.

Screening 1mg/1mL of each crude peptide sample for antimicrobial activity shows that all compounds were tested negative against *E. coli*, *P. aeruginosa*, *C. albicans* (Table 2). Only PZ-Anoplin completely inhibited the growth of *M. phlei*, whereas the BZ-anoplin showed significant activity towards *S. aureus*. Peptide purification by preparative HPLC and optimization of antimicrobial peptide activity in terms of concentration will be evaluated in the future.

Table 2. Antimicrobial activity of the following samples against different microorganisms<sup>a</sup>

Sample	<i>S. aureus</i> UPCC 1143	<i>C. albicans</i> UPCC 2168	<i>P. aeruginosa</i> UPCC 1244	<i>E. coli</i> UPCC 1195	<i>M. phlei</i> UPCC 1365
Anoplin	#	#	#	#	#
Benzoic Acid	#	#	#	#	+
Pyrazinoic Acid	#	#	#	#	#
Pyrazinamide	#	#	#	#	#
BZ-Anoplin	20	#	#	#	+
PZ-Anoplin	#	+	#	+	*

<sup>a</sup> Antimicrobial activities are determined using the agar well method under acetate buffer at pH = 6. Values are expressed in terms of area of clearing zones. (# - no clearing zone; + - not tested; \* - no growth)

## Acknowledgments

We thank the Microbiological Research and Services Laboratory of the Natural Sciences Research Institute, University of the Philippines-Diliman for running the antimicrobial assay and Ms. Rofe-Amor Obena of the Institute of Chemistry, Academia Sinica for the MALDI-TOF MS analysis. This work was supported by the Natural Sciences Research Institute of the University of the Philippines-Diliman.

## References

- Yeaman, M.R., Yount, N.R. *Pharm. Rev.* **55**, 27-55 (2003).
- Avrahami, D., Shai, Y. *Biochemistry* **42**, 14946-14956 (2003).
- Chu-Kung, A.F., Bozzelli, K.N., Lockwood, N.A., Haseman, J.R., Mayo, K.H., Tirrell, M.V. *Bioconjug. Chem.* **15**, 530-535 (2004).
- Malina, A., Shai, Y. *Biochem. J.* **390**, 695-702 (2005).
- Makovitzki, A., Avrahami, D., Shai, Y. *Proc. Natl. Acad. Sci. U.S.A.* **103**, 15997-16002 (2006).
- Bisht, G.S., Rawat, D.S., Kumar A., Kumar, R., Pasha, S. *Bioorg. Med. Chem. Lett.* **17**, 4343-4346 (2007).

## Scale-up of an Antiviral Polyamide Comprising Pyrrole and Imidazole Amino Acids

Kam F. Fok,<sup>1</sup> Kevin J. Koeller,<sup>1</sup> Holly M. Pope,<sup>1</sup> Terri G. Edwards,<sup>2</sup>  
Christopher Fisher,<sup>2</sup> and James K. Bashkin<sup>1,2</sup>

<sup>1</sup>Department of Chemistry & Biochemistry, Center for Nanosciences, University of Missouri-St. Louis,  
One University Blvd, St. Louis, MO 63121, U.S.A.; <sup>2</sup>NanoVir, LLC, 4717 Campus Drive, Suite 1300,  
Kalamazoo, MI 49008, U.S.A.

### Introduction

Cervical cancer is caused by the human papillomavirus (HPV) [1,2]. The existence of traditional “druggable” targets for HPV is minimal at best because a very small number of proteins is encoded by the small HPV genome (see below). Our nontraditional approach to HPV16 antivirals is to target viral DNA sequences, including those at or near the viral origin of replication (*ori*), using DNA-binding drug candidates. The compounds we used are polyamides (PAs) derived from N-methylpyrrole (Py) and N-methylimidazole (Im); they are selective DNA binding agents that can physically block access to target DNA sequences by proteins or alter the DNA local structure to prevent protein binding. Previous studies from other labs [3] have shown that PAs cause physical changes in DNA structure, widening the minor groove, narrowing of the major groove, raising the *T<sub>m</sub>*, etc.

HPV16 and 18 are the most common cancer-causing strains [2]. Viral proteins E1 and E2 bind to HPV DNA, at the *ori* and recruit human DNA polymerase; they control viral replication and some viral gene expression. We proposed that HPV16 replication could be stopped by designing DNA-binding polyamide molecules to bind viral DNA sites with possible targets, including the E1 and E2 binding sites and other regions of the HPV16 genome. The polyamides we chose to work with have a hairpin structure [2,4]. Armed with the HPV16 sequence and the PA binding rules [3], polyamides can be synthesized [5,6] to selectively bind to specific regions of the HPV16 genome, which is a circular dsDNA molecule.

By testing in human keratinocyte monolayers, we discovered significant antiviral activity for certain polyamides; e.g. NV-HPV16-1 has an apparent IC<sub>50</sub> of  $0.10 \pm 0.02$   $\mu$ M in human cell culture. The sequence of NV-HPV16-1 is Im-Py-Py- $\beta$ -Py-Py-Py- $\gamma$ -Py-Py- $\beta$ -Py-Py-Py- $\beta$ -Ta in which  $\beta$ ,  $\gamma$  and Ta refer to  $\beta$ -alanine,  $\gamma$ -aminobutyric acid and N-N-((dimethylamio)propyl)amine respectively. To further advance candidate NV-HPV16-1, we needed to scale-up the synthesis using a solid-phase method.

### Results and Discussion

NV-HPV16-1 was successfully synthesized by the solid-phase method with 10g Boc- $\beta$ -alanine PAM resin. The reactions were monitored by LC/MS. (Figure 1A and B). Figure 1A shows two product peaks, which is evidence of aggregation under HPLC conditions, even at 40 °C: the peaks at 1.6 and 4.4 min both show desired compound by ESI+ ms. The isolated yield of the tris(TFA) salt following synthesis (16 cycles) and HPLC was 17%. Although standard peptide methodology is applicable to the general synthetic process, the nucleophilicity of the aromatic amines of the pyrrole and imidazole-based building blocks is poor. Prolonged coupling time and/or double coupling are often necessary when the synthesis is near completion. Fmoc reagents became unstable during long reactions in the presence of DIEA, making tBoc methods preferred in this case (Boc is also preferred for atom economy).

### Conclusions

The target antiviral polyamide has been synthesized by manual solid-phase methods on 10 g of Boc- $\beta$ -alanine PAM resin with a 17% isolated yield.

**Statement:** Drs. Fisher and Bashkin are co-founders and owners of NanoVir, LLC.

Data File C:\CHEM32\1\DATA\NV1028.RP1049\081-0201.D  
Sample Name: nv1028.kf1049

Acq. Operator : kan Seq. Line : 2  
Acq. Instrument : Instrument 1 Location : Vial 81  
Injection Date : 5/29/2009 11:50:03 AM Inj : 1  
Inj Volume : 10 µl  
Acq. Method : C:\CHEM32\1\METHODS\120\_60ACN\_10\_500-220  
Last changed : 5/26/2009 3:56:31 PM by kan  
Analysis Method : C:\CHEM32\1\METHODS\MS\AP1-ES\_Pos\_Scan\_Flag\_200.M  
Last changed : 3/25/2009 1:35:43 PM by kan  
Method Info : MS/MS report  
Sample Info : control, TBA only

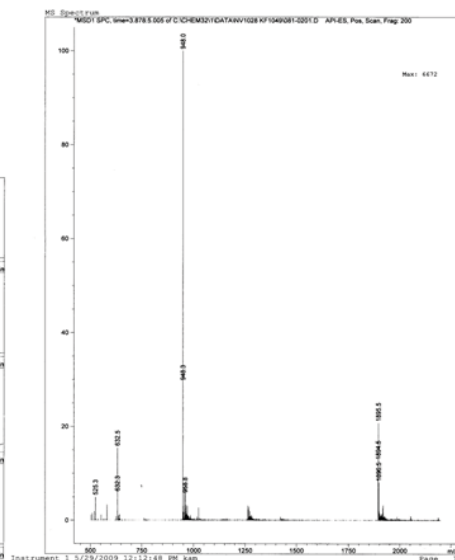
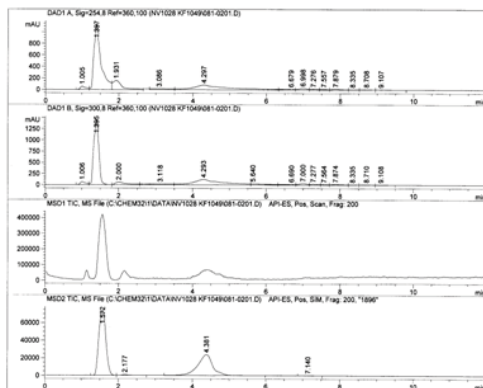


Fig. 1. A. RP HPLC, HPLC/MS of crude NV-HPV16-1. B. ESI mass spec of NV-HPV16-1 showing  $[M+H]^+$  and  $[M+2H]^+$  at  $m/z = 1894.5$  and  $948$ .

## Acknowledgments

This work has been supported by NIH grants R41AI062182 and R42AI062182. NanoVir, LLC has kindly loaned a mass spectrometer to the team at UMSL. The University of Missouri-St. Louis provided support for equipment in the form of an Institutional Research Grant.

## References

1. [www.cdc.gov/cancer/cervical/statistics/](http://www.cdc.gov/cancer/cervical/statistics/)
2. Hausen, H. *Nature Reviews: Cancer* **2**, 342-350 (2002).
3. Dervan, P.B., Burli, R.W. *Curr. Op. Chem. Biol.* **3**, 688-693 (1999).
4. Lai, Y.-M., Fukuda, N., Ueno, T., Matsuda, H., Saito, S., Matsumoto, K., Ayame, H., Bando, T., Sugiyama, H., Mugishima, H., Serie, K. *J. Pharm. Exper. Ther.* **315**, 571-575 (2005).
5. Dervan, P.B., Urbach, A.R. *Essays Contemp. Chem.* 327-339 (2001).
6. Krutzik, P.O., Chamberlin, A.R. *Bioorg. Med. Chem. Letters* **12**, 2129-2132 (2002).

## Synthetic Study of Voltage-Gated Proton Channel (VSOP/Hv)

Ken'ichiroh Nakamura,<sup>1</sup> Toshiaki Hara,<sup>1</sup> Hiroko Tamagaki,<sup>1</sup> Yuichi Akai,<sup>1</sup>  
 Takeshi Sato,<sup>1</sup> Toru Kawakami,<sup>1</sup> Tatsuki Kurokawa,<sup>2</sup> Yuichiro Fujiwara,<sup>2</sup>  
 Yasushi Okamura,<sup>2</sup> and Saburo Aimoto<sup>1</sup>

<sup>1</sup>Institute for Protein Research, Osaka University, Suita, Osaka, 565-0871, Japan; <sup>2</sup>Department of Integrative Physiology, Graduate School of Medicine, Osaka University, Suita, Osaka, 565-0871, Japan

### Introduction

The voltage-gated proton channel (VSOP/Hv) contains four transmembrane domains that are analogous to the voltage-sensor in voltage-gated cation ( $\text{Na}^+$ ,  $\text{K}^+$ , or  $\text{Ca}^{2+}$ ) channels. Although VSOP contains no pore region (ion pathway), it allows protons to permeate the cell membrane from the inside by the sensing membrane potential [1,2]. VSOP(78-222) has sufficient functions such that it is comparable with the full-length VSOP [3]. To elucidate structural changes that are involved in voltage-sensing, we carried out the synthesis of VSOP(78-222).

### Results and Discussion

The amino acid sequence of VSOP(78-222) (**1**) is shown in Figure 1(A). In our synthetic strategy for preparing VSOP(78-222) (**1**), three segments, VSOP(78-120), VSOP(121-157), and VSOP(158-222), were prepared and then sequentially ligated by the thioester method [4,5] as shown in Figure 1(B). Peptide thioesters containing a single transmembrane (TM) domain, Fmoc-VSOP(78-120)-SR (**2**, -SR = - $\text{SCH}_2\text{CH}_2\text{CO-Gly-Arg}_3\text{-Ala-OH}$ ) and Fmoc-VSOP(121-157)-SR' (**3**, -SR' = - $\text{SCH}_2\text{CH}_2\text{CO-Gly-Arg}_3\text{-Leu-OH}$ ), were prepared based on Boc solid-phase

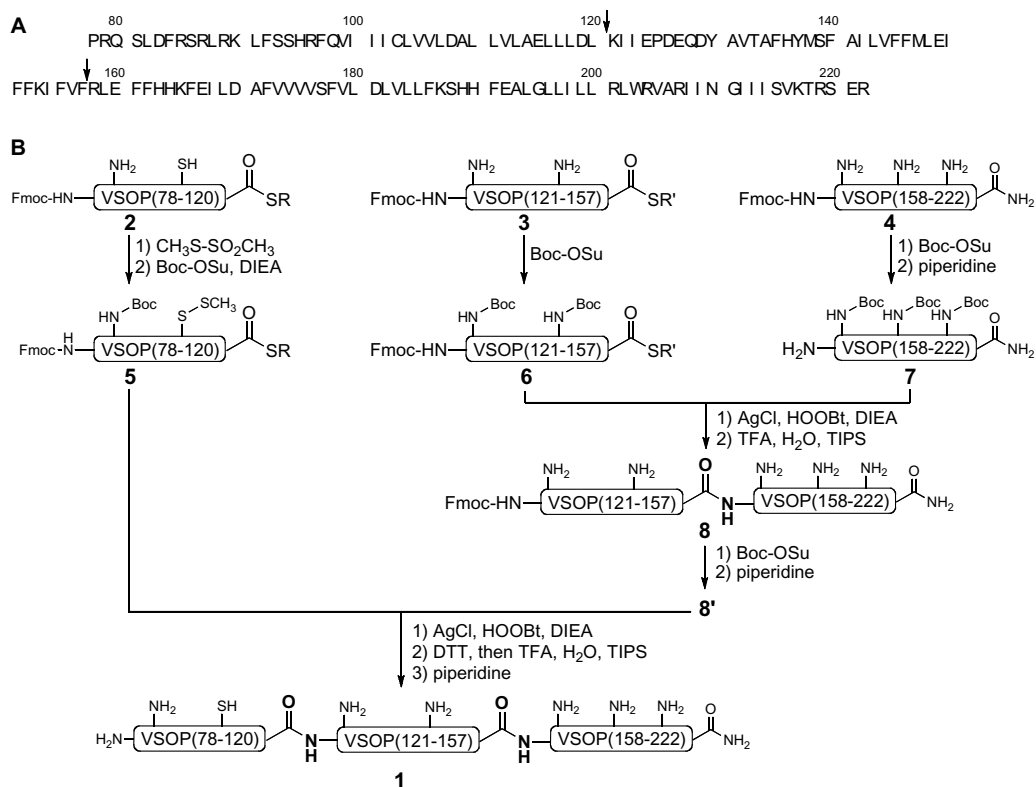


Fig. 1. (A) Amino acid sequence of VSOP(78-222) (**1**). Arrows indicate the ligation sites. Putative transmembrane regions are underlined. (B) Synthetic scheme for preparing VSOP(78-222) (**1**).

peptide synthesis (SPPS). In this synthesis, we used Arg tags to increase the solubility of peptide thioesters **2** and **3** [6,7]. Fmoc-VSOP(158-222)-NH<sub>2</sub> (**4**) containing two TM domains was prepared by Fmoc SPPS. All peptides were purified by RP-HPLC using a mixture of formic acid, 1-propanol, and water as the eluent [8]. Side chain amino groups and thiol groups of the purified peptides were protected by Boc and methylthio groups [9], respectively, to produce Fmoc-[Lys(Boc)<sup>91</sup>, Cys(SMe)<sup>103</sup>]VSOP(78-120)-SR (**5**), Fmoc-[Lys(Boc)<sup>121,153</sup>]VSOP(121-157)-SR' (**6**), and Fmoc-[Lys(Boc)<sup>165,187,217</sup>]VSOP(158-222)-NH<sub>2</sub> (**7'**). Peptide **7'** was continuously treated with piperidine to give H-[Lys(Boc)<sup>165,187,217</sup>]VSOP(158-222)-NH<sub>2</sub> (**7**). Peptide thioester **6** was condensed with peptide **7** by treatment with silver chloride, 3,4-dihydro-3-hydroxy-4-oxo-1,2,3-benzotriazine (HOObt), and *N,N*-diisopropylethylamine (DIEA) to give the ligation product, and Fmoc-VSOP(121-222)-NH<sub>2</sub> (**8**) was obtained after trifluoroacetic acid (TFA) treatment. The side chain amino groups of peptide **8** were protected with Boc groups and the *N*-terminal Fmoc group was removed by treatment with piperidine to provide H-[Lys(Boc)<sup>121,153,165,187,217</sup>]VSOP(121-222)-NH<sub>2</sub> (**8'**). Peptides **5** and **8'** were ligated following the same procedure as described above. After treating the ligated product with dithiothreitol (DTT), followed by a TFA solution, Fmoc-VSOP(78-222)-NH<sub>2</sub> (**1'**), which was subjected to MALDI-TOF MS (*m/z* 17410.2, calculated for [M+H]<sup>+</sup>, 17403.8) and SDS-PAGE. However, isolation of the product remains problematic. Experiments aimed at the purification and characterization, including an assay study are currently in progress.

In conclusion, it is feasible to prepare a peptide containing four transmembrane domains, namely, Fmoc-VSOP(78-222)-NH<sub>2</sub> (**1'**) using the thioester method.

## Acknowledgments

This work was supported, in part, by Grant-in-Aids for Scientific Research from the Ministry of Education, Culture, Sports, Science and Technology, Japan. The first author (K. N.) is supported by a research fellowship of Japan Society for the Promotion of Science (JSPS Research Fellow). K. N. also expresses his special thanks to the global COE (center of excellence) program "Global Education and Research Center for Bio-Environmental Chemistry" of Osaka University.

## References

1. Sasaki, M., Takagi, M., Okamura, Y. *Science* **312**, 589–592 (2006).
2. Ramsey, I.S., Moran, M.M., Chong, J.A., Clapham, D.E. *Nature* **440**, 1213–1216 (2006).
3. Koch, H.P., Kurokawa, T., Okochi, Y., Sasaki, M., Okamura, Y., Larsson, H.P. *Proc. Natl. Acad. Sci. U.S.A.* **105**, 9111–9116 (2008).
4. Hojo, H., Aimoto, S. *Bull. Chem. Soc. Jpn.* **64**, 111–117 (1991).
5. Aimoto, S. *Biopolymers (Pept. Sci.)* **51**, 247–265 (1999).
6. Sato, T., Saito, Y., Aimoto, S. *J. Pept. Sci.* **11**, 410–416 (2005).
7. Johnson, E.C.B., Kent, S.B.H. *Tetrahedron Lett.* **48**, 1795–1799 (2007).
8. Sato, T., Kawakami, T., Akaji, K., Konishi, H., Mochizuki, K., Fujiwara, T., Akutsu, H., Aimoto S. *J. Pept. Sci.* **8**, 172–180 (2002).
9. Akai, Y., Takemura, L., Aoki, Y., Waseda, M., Kawakami, T., Aimoto, S. (Ed. by Nomizu, M.) *Pept. Sci. 2008 (Proceeding of the 45<sup>th</sup> Japanese Peptide Symposium)*, The Japanese Peptide Society, Minoh, 2009, 201–202.



## **Functional Studies of AT1 Antagonist SII Analogues Reveal Selective Cell Signaling and Inhibition of Ang-II Mediated NHE3 Activation**

**Minying Cai,<sup>1</sup> Hua Xu,<sup>2</sup> Zhihua Liu,<sup>1</sup> Hongchang Qu,<sup>1</sup> Jing Li,<sup>2</sup>  
Fayez K. Ghishan,<sup>2</sup> and Victor J. Hruby<sup>1</sup>**

<sup>1</sup>*Department of Chemistry, University of Arizona, Tucson, AZ 85721, U.S.A.* <sup>2</sup>*Departments of Pediatrics and Physiology, University of Arizona, Tucson, AZ 85719, U.S.A.*

### **Introduction**

The angiotensin II (Ang-II) is widely implicated in the development of hypertension and several progressive renal diseases by causing salt and fluid retention and inducing growth and proinflammatory responses. Ang-II has been shown to induce expression of the epithelial sodium channel, the sodium and hydrogen exchanger-3 (NHE3) [1] etc. Ang-II regulates NaCl reabsorption through both directly acting on the proximal tubule, and indirectly acting on aldosterone secretion. In isolated proximal tubule cells and also brush-border membrane vesicle preps, Ang-II stimulates Na<sup>+</sup> absorption by increasing the activity of NHE3. Previous studies have shown that increased NHE3 function contributes to hypertension observed in rat models induced by Ang-II, and Ang-II stimulates NHE3 activity through increasing NHE3 gene expression levels [2]. These observations suggest the possible role of NHE3 in the pathophysiology of hypertension. The current studies revealed a group of newly designed and synthesized peptides which are selective antagonists of AT1, but are able to recruit  $\beta$ -arrestins, and can block the effect of A-II on NHE3 expression.

### **Results and Discussion**

Earlier work from Holloway et al. [3] demonstrated that side-chain substitution within angiotensin II revealed different requirement for signaling, internalization, and phosphorylation of type 1A angiotensin receptors. Studies by Lefkowitz et al. [4] established two major components for AT1 receptor signaling: G protein-dependent and -independent signaling, which will lead to selective physiological functions. In order to develop specific ligands with selective physiological functions of the AT1 receptor, a series of peptide has been designed and synthesized (Table 1). All of these peptides have unique lowest energy conformations which are similar to Ang II share a  $\beta$ -turn binding domain (data not shown). It is interesting to note that these peptides are antagonists of AT1, but they are still able to recruit  $\beta$ -arrestins (data not shown). Furthermore, they can specifically block the effect of Ang-II on NHE3 expression. In OPK cells, Ang-II homologue peptides **1**, **2** and **11** had no effect on stimulating NHE3 promoter activity. Other Ang-II homologue peptides retained the A-II function of activating NHE3 promoter activity. In OK cells, A-II analogue peptides **1**, **2**, **11** significantly inhibited NHE3 promoter activity induced by Ang-II.

The cellular signaling of the AT1 receptor has been studied extensively. It involves multiple signaling molecules including heterotrimeric G Proteins, kinases and scaffold proteins. According to the classical paradigm, Ang II first binds on the receptor and causes the conformation change of the receptor. The conformation change caused by agonist will lead to the activation of the heterotrimeric G protein initiating downstream cell signaling, which includes G-protein Coupled Receptor Kinases (GRKs) or a second messenger system (PKA, PKC, Ca<sup>2+</sup> IP3, DRG etc), and finally promoting  $\beta$ -arrestins recruitment, whereas the antagonist will not have these responses. The binding of  $\beta$ -arrestins sterically hinders further G protein interaction. Finally,  $\beta$ -arrestins binding terminates the G-protein signaling.  $\beta$ -Arrestins also work as scaffold proteins to mediate receptor internalization through clathrin coated pits. The novel paradigm of GPCR signaling expands our vision of cell signaling. The typical example is Ang II analogue SII, an antagonist of AT1. SII is able to induce  $\beta$ -arrestin 2-dependent signaling that includes receptor internalization and activation of extracellular signal regulated kinases (ERK 1/2) without generation of inositol phosphate second messengers by the AT1 receptor. Peptides **1**, **2**, **11** are analogues of SII, the inhibition of NHE3 promoter activity induced by SII could be via ERK-dependent pathway (data not shown).

The AT1 receptor's selective activation of G protein independent signaling has proven relevant in OK and OKP cells in this work and many other primary cells, isolated organs and *in vivo* [5]. Similar observations from an increasing number of GPCRs have led to the development of concepts such as functional selectivity and change the fundamental pharmacological paradigms to allow description of multiple discrete states of receptor activation and ligands with different collateral degrees of efficacy for individual responses. Thus, developing G protein dependent and independent drugs will be promising for the future drug discovery in this area.

Table 1. SII Alanine scan and D-amino acid scan

Code	Sequence	Formula	Ave. Mass	Ave.M+TFA
<b>1</b>	H-Sar-Ala-Val-Ile-Val-His-Pro-Ile-OH	C <sub>39</sub> H <sub>66</sub> N <sub>10</sub> O <sub>9</sub>	819.0029	933.0263
<b>2</b>	H-Sar-Arg-Ala-Ile-Val-His-Pro-Ile-OH	C <sub>40</sub> H <sub>69</sub> N <sub>13</sub> O <sub>9</sub>	876.0576	990.0810
<b>11</b>	H-Sar-Arg-Val-Ile-Val-D-His-Pro-Ile-OH	C <sub>42</sub> H <sub>73</sub> N <sub>13</sub> O <sub>9</sub>	904.1107	1018.1341
<b>Ang II</b>	NH <sub>2</sub> -Asp-Arg-Val-Tyr-Val-His-Pro-Phe-COOH	C <sub>49</sub> H <sub>69</sub> N <sub>13</sub> O <sub>12</sub>	1031.52	1145.52

## Acknowledgments

We thank Dr. R. J. Lefkowitz (Departments of Medicine and Biochemistry, and Howard Hughes Medical Institute of Chemistry) for guiding the project and performing the binding, second messenger, and  $\beta$ -arrestins recruitment assays for the entire group of Ang II analogues. This research was supported by grants from the U.S. Public Health Service, National Institutes of Health DK-17420 (V.J. Hruby), DA-06284 (V.J. Hruby), DK-073638 (Ghishan).

## References

1. Saccomani, G., Mitchell, K.D., Navar, L.G. *Am. J. Physiol.* **258** F 1188-1195 (1990).
2. Xu, L., Dixit, M.P., Nullmeyer, K.D., Xu, H., Kiela, P.R., Lynch, R.M., Ghishan, F.K. *Biochim. Biophys. Acta, Biomembrane* **1758**, 519-526 (2006).
3. Holloway, A.C., Qian, Hongwei, Pipolo, L., Ziogas, J., Miura, S., Karnik, S., Southwell, B.R., Lew, M.J., Thomas, W.G. *Mol. Pharmacol.* **61**, 768-77 (2002).
4. Shukla, A.K., Violin, J.D., Whalen, E.J., Gesty-Palmer, D., Shenoy, S.K., Lefkowitz, R.J. *Proc. Natl. Acad. Sci. U.S.A.* Early Edition, (July 11 2008), 1-6 (2008).
5. Aplin, M., Bonde, M.M., Hansen, J.L. *J. Mol. Cell. Cardiology* **46**, 15–24 (2009).

## NMR Studies on a Double Transmembrane-Containing Fragment of a G Protein-Coupled Receptor

Leah S. Cohen,<sup>1,2</sup> Alexey Neumoin,<sup>3</sup> Boris Arshava,<sup>1</sup> Melinda Hauser,<sup>4</sup>  
Jeffrey M. Becker,<sup>4</sup> Oliver Zerbe,<sup>3</sup> and Fred Naider<sup>1,2</sup>

<sup>1</sup>Department of Chemistry, The College of Staten Island, City University of New York (CUNY), Staten Island, NY 10314, U.S.A.; <sup>2</sup>Department of Biochemistry, The Graduate Center of CUNY, New York, NY 10016, U.S.A.; <sup>3</sup>Institute of Organic Chemistry, University of Zurich, Zürich, CH-8057, Switzerland; and <sup>4</sup>Department of Microbiology, University of Tennessee, Knoxville, TN 37996, U.S.A.

### Introduction

Integral membrane proteins (IMPs) are essential for cell signaling, cell proliferation, and cell death. These membrane proteins propagate extracellular signals to the intracellular matrix, generally starting a cascade of events to trigger a response. Unfortunately, structural analysis of IMPs, in particular of G protein-coupled receptors (GPCRs), is hindered by difficulties in crystallization and by size limitations in NMR spectroscopy. GPCRs contain 7 transmembrane domain regions (TM) regions as well as connecting loops and N- and C-terminal regions and these large hydrophobic proteins need a membrane-like environment for proper structure formation. Studying smaller fragments of these GPCRs may be a useful tool in the determination of overall receptor folding and structure.

The yeast GPCR, Ste2p, has been studied extensively using biological and biochemical analyses. Biophysical analysis using NMR has helped to elucidate the structural tendencies of each of its individual seven TM domains [1]. The analysis of larger double TM fragments of Ste2p required biosynthesis due to the need to incorporate stable isotopes for NMR analysis [2,3]. Recently, we solved the NMR structure of a double TM domain fragment of Ste2p(G31-T110, TM1-TM2) in lyso-palmitoylphosphatidylglycerol (LPPG) micelles [4]. The observation of long range connectivities between the two TM helices in this high resolution structure was only possible when we used a selective methyl group labeling technique that resulted in one protonated methyl group on each Ile, Leu, Val in an otherwise perdeuterated background and high field magnets [4,5].

Structure determination of peptide fragments of IMPs in organic aqueous membrane mimetic media has been used in the past [6,7]. To this point, no systematic study comparing structures of multi-TM fragments of a GPCR in detergent micelles and organic aqueous membrane mimetics has been performed. Therefore, comparison of the structure of Ste2p(G31-T110) in LPPG micelles to that obtained in TFE:water (1:1, v:v) would be useful to determine whether the protein would fold into a similar conformation. Here, data comparing the NMR structures of Ste2p(G31-T110) in LPPG micelles and trifluoroethanol (TFE):water (1:1,v:v) is presented.

### Results and Discussion

The protein fragment Ste2p(G31-T110) was cloned into an *E. coli* expression vector containing an upstream TrpALE and expression was optimized in BL21-AI cells [3]. Cleavage using CNBr to removed the TrpALE and purification were also different growth conditions. Circular dichroism (CD) was used as a screening technique to determine the conditions under which NMR could be performed. Only solvent mixtures found to optimized resulting in yields ranging from 8 to 20 mg/L depending on the labeling schemes and support helical structures were analyzed using NMR. Using this technique, the NMR structure was analyzed in LPPG micelles [4].

Based on CD analysis we concluded that TFE:water (1:1, v:v) would also be useful in the study of this protein fragment. [<sup>15</sup>N,<sup>1</sup>H]-HSQC analysis resulted in sharp well-resolved peaks that were assigned. Chemical shift perturbation analysis was performed comparing the [<sup>15</sup>N,<sup>1</sup>H]-

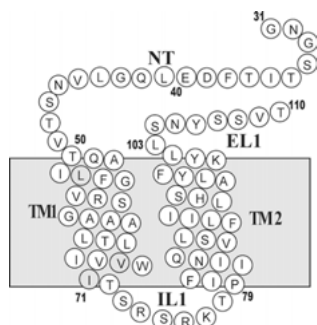


Fig. 1. Schematic of Ste2p(G31-T110).

HSQC peaks from Ste2p(G31-T110) in LPPG micelles to those from TFE:water (1:1,v:v). Chemical shift differences between spectra measured in TFE:water at 25°C and 45°C were generally small, whereas larger differences were observed when comparing spectra in TFE:water and LPPG at 45°C. For the two membrane mimetic solvents, chemical shift differences in the two TM regions were less than those in the loops and N-terminus. C $\alpha$ -C $\beta$  chemical shift indexing data for TM1-TM2 in TFE and LPPG was used as an indicator of secondary structure. In all cases evidence for strong  $\alpha$ -helical tendencies were observed. Finally H-D exchange rate analysis was performed on the LPPG micelles and TFE:water at 25°C. The exchange in LPPG was determined using a water presaturation experiment. The exchange in TFE:water was determined by following [ $^{15}\text{N}$ , $^1\text{H}$ ]-HSQC peak intensity after dissolving the peptide in TFE-d $_3$ :D $_2$ O. The relative exchange rates were very similar when comparing the two conditions. This may indicate that they are folding into similar structures even in the different membrane mimetics.

Initial calculations of the structure of the Ste2p(G31-T110) protein fragment in TFE:water (1:1,v:v) at 25°C show similarities to the bundles obtained in LPPG micelles (Figure 2). These similarities indicate that TFE:water may, under certain conditions, be used to determine the secondary and even the tertiary structure of large domains of GPCRs. We are currently obtaining additional constraints to improve the quality of the TFE:water (1:1, v:v) structure. Application of this methodology may aid in the future structure characterization of larger IMP proteins or protein fragments.

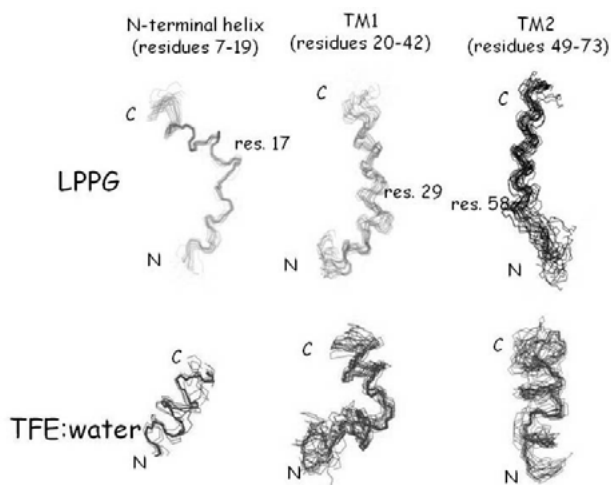


Fig. 2. Preliminary structural analysis. Bundles of minimized conformers generated from NOEs for TM1-TM2 in LPPG micelles (top) and TFE:water (1:1, v:v, bottom).

## Acknowledgments

This work was supported by the National Institute of General Medical Sciences, Grants:GM22086 and GM22087 and the CUNY Doctoral Research Grant Program, Competition #4.

## References

1. Arshava, B., et al. *Biopolymers* **64**, 161-176 (2002).
2. Englander, J., et al. *Biopolymers* **84**, 508-518 (2006).
3. Cohen, L.S., et al. *Biopolymers* **90**, 117-30 (2008).
4. Neumoin, A., et al. *Biophys. J.* **96**, 3187-96 (2009).
5. Tugarinov, V., Kay, L.E. *J. Am. Chem. Soc.* **125**, 13868-13878 (2003).
6. Ma, D., et al. *Biochemistry* **44**, 8790-8800 (2005).
7. Estephan, R., et al. *Biochemistry* **44**, 11795-11810 (2005).

## Photoactive Isoprenoid-containing Peptides

Kelly Kyro,<sup>1</sup> Daniel Mullen,<sup>1</sup> Surya Manandhar,<sup>2</sup> Walter K. Schmidt,<sup>2</sup> and Mark Distefano<sup>1</sup>

<sup>1</sup>Department of Chemistry, University of Minnesota, Minneapolis, MN 55455, U.S.A.; <sup>2</sup>Department of Biochemistry and Molecular Biology, University of Georgia, Athens, GA 30602, U.S.A.

### Introduction

Prenylation is an essential post-translational modification that increases protein hydrophobicity and targets them to membranes. The 3-step process consists of initial addition of a C15 or C20 isoprenoid to proteins followed by the proteolytic removal of the -a<sub>1</sub>a<sub>2</sub>X tripeptide by *ras* converting enzyme 1 (RCE1), and methylation of the C-terminal prenylcysteine by the enzyme isoprenylcysteine carboxyl methyltransferase (Icmt). Many proteins involved in signal transduction pathways are farnesyl or geranylgeranylated, including the Ras family of oncoproteins. Because mutations in the *ras* oncogene are responsible for ~15-20% of human cancers, inhibitors of enzymes in the prenylation pathway hold potential as anticancer agents [1,2].

### Results and Discussion

We are synthesizing RCE1 peptide substrates that incorporate photoactive isoprenoids in order to perform photaffinity-labeling experiments and map the active site of RCE1. Lipidated photoprobes containing the C-terminal Ca<sub>1</sub>a<sub>2</sub>X sequence were developed for photaffinity-labeling of catalytic residues in the RCE1 active site. Peptides were synthesized by standard Fmoc methods and subsequently alkylated with the requisite allylic bromides to yield the corresponding peptides.

A peptide substrate (**1**, Figure 1), derived from the C-terminal sequence of mammalian K-Ras (CVIM) was synthesized as a natural substrate analogue. The dinitrophenyl (Dnp) group at the V position acts as a quencher of the 2-aminobenzoyl (Abz) fluorophore [3]. Following proteolysis, there is a linear increase in fluorescence at 420 nm. Peptide analogs **3** and **5** incorporating the C5BP or C10BP photoactive isoprenoid [4, 5, 6] were designed to imitate the naturally-occurring, prenylated protein and were shown in this fluorogenic Ca<sub>1</sub>a<sub>2</sub>X proteolysis assay to be substrates for RCE1.

Comparative analysis of substrate cleavage by yRCE1p indicated that the photoactive peptides **3** and **5** are processed by the enzyme at rates 10-20 times less than the natural, farnesylated substrate, **1**. Nonetheless, RCE1 is capable of accepting these non-natural Ca<sub>1</sub>a<sub>2</sub>X peptides as alternative substrates. The kinetic data was further supported by MS/MS sequencing of the products of RCE1 cleavage (peptides **4** and **6**). The structures of the processed probes and

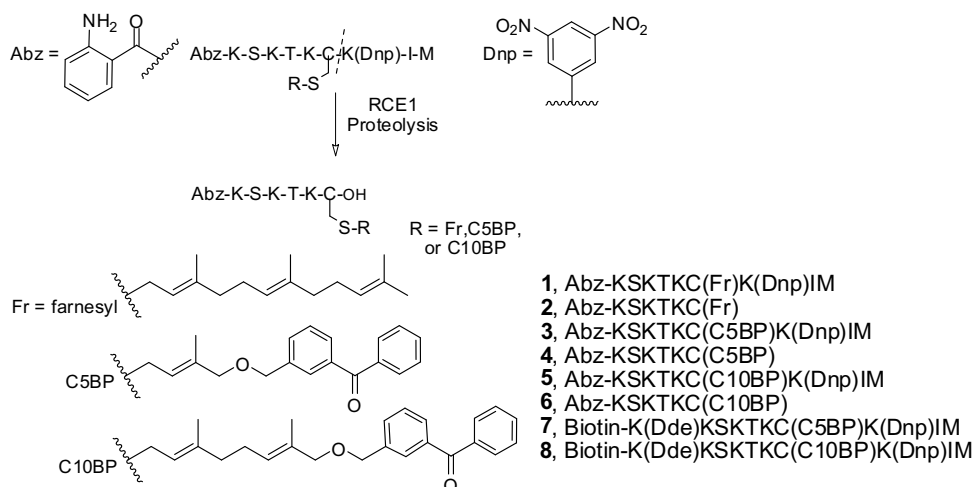


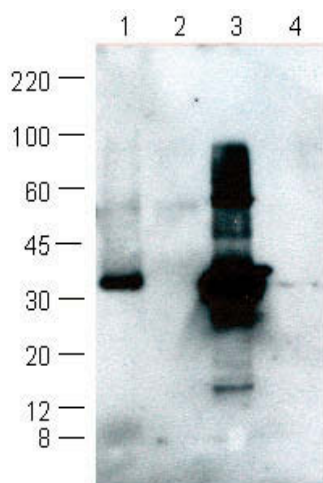
Fig. 2. RCE1 processing of prenylated substrates.

the site of cleavage as the C-terminal side of the modified cysteine were confirmed.

Membrane protein containing hemagglutinin (HA)-epitope-tagged RCE1 was photolyzed in the presence of biotinylated substrate (peptides **7** and **8**). Streptavidin (SA) pull-down was done to isolate protein cross-linked to the biotinylated probe, followed by Western blot analysis to detect  $\gamma$ RCE1-HA. Probing for HA using anti-HA antibodies gave Western analysis that visualized only protein containing the HA tag (RCE1 construct).

Lane 1 (Figure 2) shows a band at 35kDa which corresponds to RCE1 photolabeled by substrate **7**, not present in the control (lane 2, membranes lacking RCE1). Lane 3 visualizes crude RCE1 membrane protein not subjected to SA pull-down. Lane 4 indicates competition between substrates **1** and **7** when photolyzed in the presence of RCE1.

The results presented here demonstrate that peptides that incorporate photoactive benzophenone groups in place of isoprenoids can be effectively processed by RCE1. Photolysis of RCE1 in the presence of probes **7** and **8** results in crosslinking with the protein. Efforts to isolate the crosslinked protein and determine the site of crosslinking are in progress.



*Fig. 2. Western Blot Analysis of Photolysis Reactions after SA Pull-down and HA Detection.*

*Lane 1:  $\gamma$ RCE1-HA, **7**, 30 min. photolysis*

*Lane 2: control membranes, **7**, 30 min. photolysis*

*Lane 3:  $\gamma$ RCE1-HA (no SA pull-down or photolysis)*

*Lane 4:  $\gamma$ RCE1-HA, **1**, and **7**, 30 min. photolysis*

## Acknowledgments

Bruce Witthuhn, Univ. of MN Center for Mass Spectrometry and Proteomics; Schering Plough. Supported by NIH (GM58442) and ECBC.

## References

1. Zhang, F.L., Casey, P.J. *Ann. Rev. Biochem.* **65**, 241-269 (1996).
2. Ohkanda, J., et al. *Curr. Top. Med. Chem.* **2**, 303-323 (2002).
3. Hollander, I., et al. *Biochimica et Biophysica Acta* **1649**, 24-29 (2003).
4. Turek, T., et al. *J. Org. Chem.* **66**, 3253-3264 (2001).
5. Gaon, I., Turek, T.C., Distefano, M.D. *Tetrahedron Letters* **37**, 8833-8836 (1996).
6. Kale, T.A., et al. *J. Am. Chem. Soc.* **123**, 4373-4381 (2001).

## Chemical Synthesis, Isolation and Assembly of c-Subunits of Human F<sub>0</sub>F<sub>1</sub>-ATP Synthase

Toshiaki Hara, Akira Tainosho, Takeshi Sato, Ken'ichiroh Nakamura,  
Toru Kawakami, Hideo Akutsu, and Saburo Aimoto

*Institute for Protein Research, Osaka University, 3-2 Yamadaoka, Suita, Osaka, 565-0871, Japan*

### Introduction

The human c-subunit of F<sub>1</sub>F<sub>0</sub>-ATP synthase is comprised of 75 amino acid residues (DIDTAAKFIG AGAATVGVAG SGAGIGTVFG SLIIGYARNP SLKQQLFSYA ILGFALSEAM GLFCLMVAFL ILFAM, MW 7608) and contains two transmembrane helices. The multimeric c-subunits assemble into ring-like architecture in membranes that functions as a rotary proton-channel for F<sub>0</sub>-proton motor. We previously reported on the synthesis of a c-subunit of *E. coli* F<sub>1</sub>F<sub>0</sub>-ATP synthase, which was accomplished by means of the thioester method [1]. However, little is known concerning the structural details of c-subunit of human F<sub>1</sub>F<sub>0</sub>-ATP synthase (Sub.c) due to the inherent difficulties in producing, handling and purifying the protein. Large scale methods for the isolation and purification of human Sub.c by molecular biology techniques have not yet been achieved. Here we report on the status of our studies on the chemical synthesis of human Sub.c. The study largely involved elucidating the structure-function relationships of ATP synthase using solution and solid-state NMR techniques.

### Results and Discussion

Sub.c(1–75) was synthesized using an Fmoc-solid phase strategy involving stepwise chain elongation on a Wang-ChemMatrix resin. Our initial attempts at a conventional workup using reagent K (TFA/thioanisole/water/phenol/EDT = 82.5:5:5:5:2.5) cleavage/deprotection, ether precipitation and RP-HPLC analysis were not successful and the desired peptide was not detected by RP-HPLC (Figure 1A) and MALDI-MS analysis. We hypothesized that this was due to the low solubility and high tendency of Sub.c(1–75) to undergo aggregation. RP-HPLC is widely used for the analysis and purification of chemically synthesized peptides, but difficulties are frequently encountered during the RP-HPLC analysis and purification of peptides that contain a transmembrane region(s) due to their insolubility in the mobile phases, and the fact that they have a tendency to absorb irreversibly to the column.

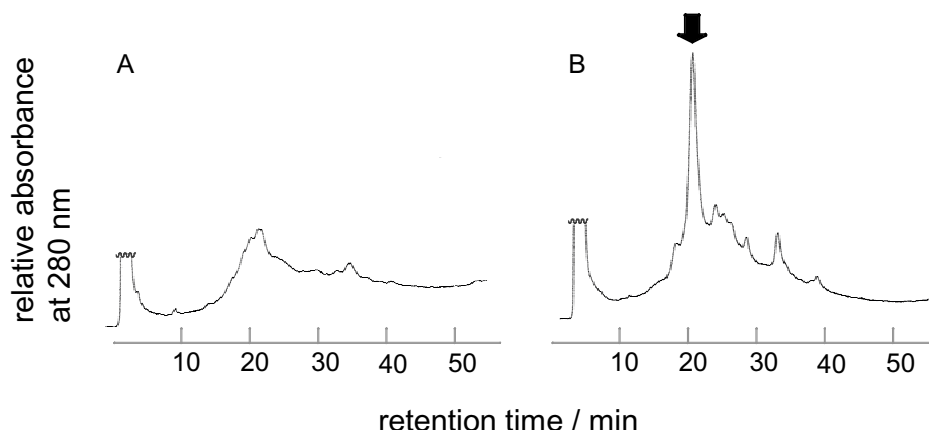


Fig. 1. RP-HPLC traces of crude Sub.c(1–75). (A) Sub.c(1–75) without tag, and (B) (Arg)<sub>5</sub>-photocleavable-tag incorporated-Sub.c(1–75). The arrow indicates the position of elution of the peptide. Conditions, Column: Nacalai 5C<sub>4</sub>-AR-300, 4.6 x 150 mm, Eluent A: formic acid/water = 2 : 3, B: formic acid/propanol = 4 : 1, Gradient: B: 60–90% / 50min.

To overcome this issue, we developed a new strategy in which penta-arginine, which serves to enhance the solubility of the protein, is conjugated to the N-terminus of the target peptide via a photocleavable-linker, a 5-(3-aminopropoxy)-2-nitrobenzyl oxycarbonyl group [2] (Figure 2). The addition of 5-6 arginine residues as “solubility enhancement peptide tags” to either the N or C terminus of low solubility proteins/peptides was successfully applied [3]. In contrast to the absence of a tagged peptide, (Arg)<sub>5</sub>-photocleavable incorporated Sub.c(1–75), which was obtained from the same peptidyl resin, was clearly detected by PR-HPLC/MALDI-TOFMS or ESI-MS analysis (Figure 1B). By taking advantage of the solubility enhanced penta-arginine and the chromophoric nature of the photocleavable linker, it became possible to purify tagged Sub.c(1–75) as a soluble peptide by RP-HPLC.

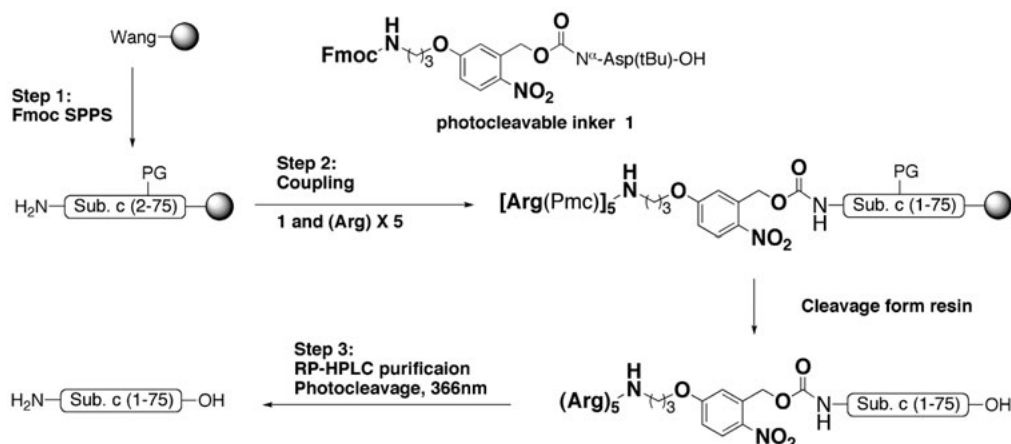


Fig. 2. Schematic representation for Sub.c(1–75) preparation by utilizing (Arg)<sub>5</sub>-tag and the photocleavable linker. PG: protecting groups.

Thus, the combination of a solubility enhancement tag and the photocleavable-linker strategy described herein may prove to be a useful method for minimizing aggregation and solubility problems that are associated with the isolation of transmembrane peptides. Studies related to the simultaneous photoremoval of the tag and linker, and the folding and assembly of Sub.c(1–75) are currently in progress.

## Acknowledgments

This work was supported, in part, by Grant-in-Aid for “Scientific Research on Priority Areas” and “Targeted Proteins Research Program” from the Ministry of Education, Culture, Sports, Science and Technology of Japan. This work was also partly supported by a Grant-in-Aid for “Research for Promoting Technological Seeds” from the Japanese Science and Technology Agency.

## References

1. Sato, T., Kawakami, T., Akaji, K., Konishi, H., Mochizuki, K., Fujiwara, T., Akutsu, H., Aimoto, S. *J. Pept. Sci.* **8**, 172–180 (2002).
2. A synthesis of the linker, see: Hara, T., Tainosho, A., Kawakami, T., and Aimoto, S., In Nomizu, M. (Ed.) *Peptide Science 2008*, 2009, p.199-200.
3. (a) Sato, T., Saito, Y., Aimoto, S. *J. Pept. Sci.* **11**, 410–416 (2005). (b) Johnson, E.C.B., Kent, S.B.H. *Tetrahedron Letters*, **48**, 1795–1799 (2007). (c) Kato, A., Maki, K., Ebina, T., Kuwajima, K., Soda, K., Kuroda, Y. *Biopolymers* **85**, 12–18 (2007).



## Antiparallel $\beta$ -Hairpin/ $\beta^{5,6}$ -Helical Structures

John L. Kulp III and Thomas D. Clark

Chemistry Division, Naval Research Laboratory, Washington, D.C. 20375-5342, U.S.A.

### Introduction

$\beta$  helices are helical peptide structures formed by sequences of alternating D- and L- $\alpha$ -amino acids (D,L peptides) and stabilized by  $\beta$ -sheet hydrogen bonding. Designing new foldamers based on D,L-peptides in general - and  $\beta$  helices in particular - is challenging due to the unpredictable folding of these peptides in solution. For example, linear D,L peptides can adopt multiple structures and/or aggregation states that depend strongly on the solvent and the identity of dissolved cations. This conformational polymorphism is undesirable for a functional foldamer; therefore, in earlier work we designed the cyclic 22-residue peptides **1** and **2** to limit

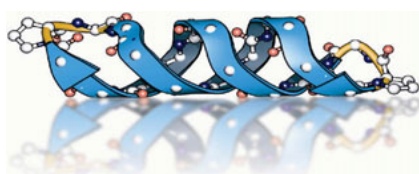


Fig. 1. Peptide backbone structure of a  $\beta$ -hairpin/ $\beta$ -helical supersecondary structure.

the conformation to a singular antiparallel ( $\downarrow\uparrow$ )  $\beta$ -hairpin/ $\beta$ -helical state [1,2]. Peptides **1** and **2** are hydrophobic and adopt unique conformations in nonpolar organic solvents, where folding is dominated by hydrogen bonding. We note that water is the most desirable medium for peptide model studies because biological interactions take place in this solvent. In comparison with organic solvents, however, water is known to reduce the propensity of peptides to form stable secondary structures. Nevertheless, our initial work on peptides **1** and **2** furnished synthetic and structural insights that led to the development of

peptide **3** [3], which folds stably in polar media such as methanol - a solvent that is often used as a surrogate for water in studies of new foldamers. Building on these results structural studies in methanol, we are currently working to achieve stable  $\beta$ -helical structures in water.

### Results and Discussion

Peptides **1**, **2**, and **3** consist of two 9-residue  $\beta$ -strand segments of alternating D-,L- $\alpha$ -amino acids (residues 1–9 and 12–20, Figure 2). We constrained the molecules by joining the two D,L-peptide strands with two copies of the enantiomeric  $\beta$ -turn segment L-Pro-Gly (**1** and **3**) and D-Pro-Gly (**2**). The chirality of the residues flanking the  $\beta$ -turn are opposite to the proline, and, as a result, we expected that peptides **1** and **3** would form a left handed  $\downarrow\uparrow\beta$  helix, and peptide **2** would form a right-handed  $\downarrow\uparrow\beta$  helix. The joining of the two D,L-peptide strands with  $\beta$ -turns effectively constrains the resulting peptide so that it can form only a single  $\downarrow\uparrow\beta$ -helical conformation [1,2], and prevents the formation of alternative double- or single-stranded species. We designed peptide **3** to be hydrophilic by distributing eight polar residues uniformly throughout the strands to increase water solubility. Four charged residues L-Glu(2), L-Lys(15), L-Arg(4), and L-Glu(13), form two salt bridges in the correctly folded  $\beta$ -hairpin/ $\downarrow\uparrow\beta$  helix. The salt bridges were designed to fold into an antiparallel double-stranded  $\beta$ -helix having ca. 5.6 residues per turn (a  $\downarrow\uparrow\beta^{5,6}$  helix) and prevent the folding of a  $\beta$ -helix having ca. 7.2 residues per turn (a  $\downarrow\uparrow\beta^{7,2}$  helix). Within the two  $\beta$ -stands, seven  $\beta$ -branched amino acids help restrict the backbone conformation and promote  $\beta$ -sheet  $\phi, \psi$  angles.

After synthesis and purification, we characterized the  $\beta$  helices using CD and NMR spectroscopies. The CD spectra of **1** and **2** displayed large bands at 220 nm which is consistent with D,L-peptides that form  $\beta$ -helical structures. Peptide **3** in methanol (**3-m**) revealed CD features that we previously established as arising from a left-handed  $\beta$ -hairpin/ $\downarrow\uparrow\beta^{5,6}$ -helical structure. Titration with water (**3-w**) triggered a transition to a shallow negative band at 204 nm, suggesting a  $\beta$ -hairpin-like conformation. We examined the structures in greater detail using NMR; the  $^3J$  coupling constants and C $\alpha$ H  $\Delta\delta$  chemical shifts indicate  $\beta$ -sheet-like character for peptides **1**, **2**, and **3-m**. The NOESY spectra for these peptides revealed many cross-peaks characteristic of an antiparallel  $\beta$  helix. The spectrum for **3-w** showed cross-strand NOEs but not helical NOEs, suggesting this structure is more akin to that of a simple  $\beta$  hairpin.

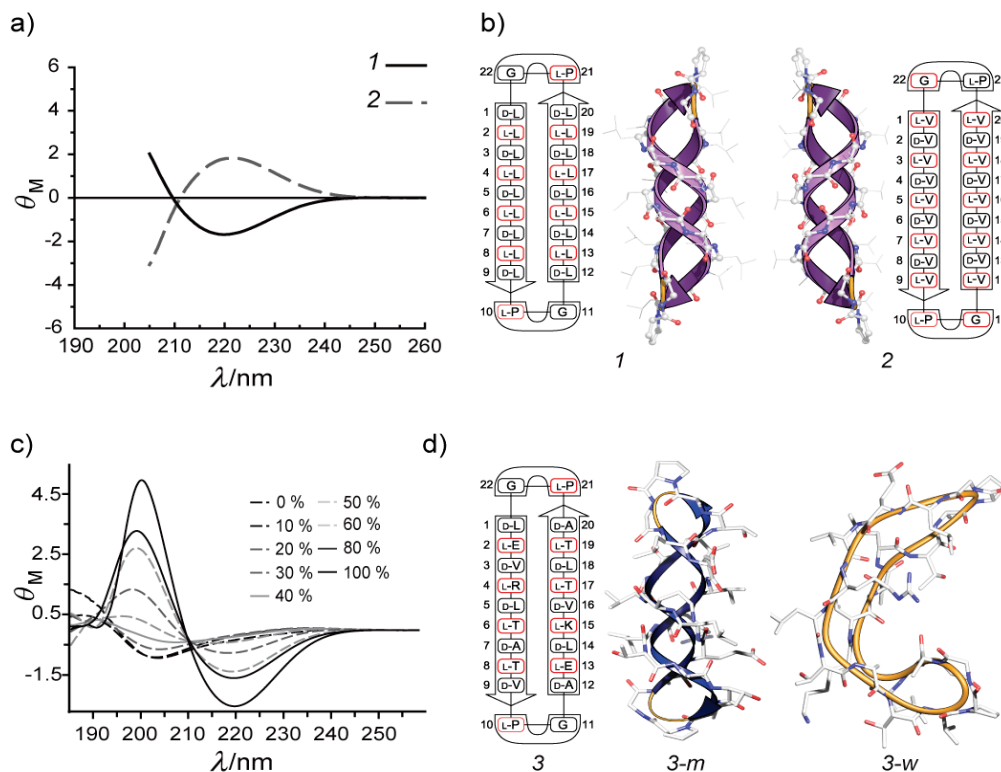


Fig. 2. (a) CD spectra of 1 and 2 are mirror images. (b) Sequence and numbering schemes for peptide 1 and 2, shown in a flat  $\beta$ -hairpin representation; L residues are boxed in red, while D residues are boxed in black (in CD color book version). Peptide 1 folds into a left-handed  $\beta$ -hairpin /  $\downarrow\uparrow\beta^{5,6}$ -helical structure and peptide 2 folds into a right-handed  $\beta$ -hairpin /  $\downarrow\uparrow\beta^{5,6}$ -helical structure. (c) CD spectra showing 3 in methanol containing varying percentages of PBS. (d) Illustration depicts sequence and numbering scheme with NMR derived structures of 3-m and 3-w.

## Conclusion

Our work demonstrated that addition of  $\beta$  turns and the corresponding cyclization of two D-, L-strands not only traps the structures into a discrete conformation, but also allows control over left- versus right-handed helicity. By judiciously choosing the sequence of **3**, we achieved a left-handed  $\beta$ -hairpin/ $\downarrow\uparrow\beta^{5,6}$ -helical structure in the polar solvent methanol. In current work, we are examining longer peptides and peptides having optimized electrostatic interactions with the goal of obtaining more stable structures.

## Acknowledgments

This work was supported by the Office of Naval Research. We thank Dr. Mallika Sastry, Dr. Dmitri Petrovykh, and Dr. John Russell, Jr. for helpful discussions, and Prof. John S. Evans for access to NMR instrumentation. J.L.K. acknowledges the American Society of Engineering Education (ASEE) for a Postdoctoral Fellowship.

## References

1. Sastry, M., Brown, C., Wagner G., Clark, T.D. *J. Am. Chem. Soc.* **128**, 10650–10651 (2006).
2. Clark, T.D., Sastry, M., Brown, C., Wagner, G. *Tetrahedron* **62**, 9533–9540 (2006).
3. Kulp III, J.L., Clark, T.D. *Chem. Eur. J.* 2009, in press.

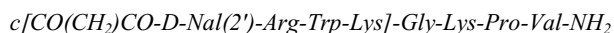
## Studies of Energy Balance and Cancer

**Joel Nyberg, Alexander Mayorov, Min Ying Cai,  
 Morgan Zingsheim, and Victor J. Hruby**

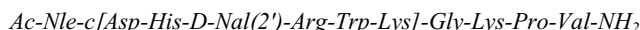
*Department of Chemistry, University of Arizona, Tucson, AZ 85721, U.S.A.*

### Introduction

The anti-inflammatory activities of the neuroimmunomodulator  $\alpha$ -melanocyte stimulating hormone ( $\alpha$ -MSH) has been traced to a 'message sequence' contained in the C-terminal: the tripeptide amino acid Lys-Pro-Val (KPV;  $\alpha$ -MSH 11-13) [1]. Inflammatory processes, in particular the induction of NF- $\kappa$ B by tumor necrosis factor (TNF- $\alpha$ ) have been shown to be inhibited by  $\alpha$ -MSH through inhibition of TNF- $\alpha$  [2]. NF- $\kappa$ B resides in the cytosol bound to an inhibitor called I $\kappa$ B. Binding of TNF- $\alpha$  to its receptor triggers phosphorylation of I $\kappa$ B. I $\kappa$ B then becomes ubiquitinated and destroyed by proteasomes, which liberates NF- $\kappa$ B to the nucleus. [3] NF- $\kappa$ B controls the synthesis of a number of genes required for an acute inflammatory response [4]. Cachexia is a clinical syndrome of wasting that accompanies many chronic diseases a condition found associated with diseases such as some cancers, infectious diseases, and cardiovascular disease [5]. Evidence from animal models suggests a compelling link between cachexia and inflammation, and a variety of pro-inflammatory cytokines such as TNF- $\alpha$  play an integral role in wasting syndrome [6]. This condition is marked by an increase in energy expenditure and preferential loss of lean body mass, creating a striking catabolic state. Few treatments have proved to be of significant benefit to patients suffering from cachexia. One new treatment that shows promise is pharmacological blockade of the central melanocortin system. The importance of this system is in maintaining normal body weight. In humans it is highlighted by the finding that disordered melanocortin signaling results in early-onset morbid obesity and dramatic increases in lean body mass in humans. Emerging evidence suggests that blocking this system via pharmacological antagonists of the type 4 melanocortin receptor (MC4R) may restore appetite and lean body mass in subjects with cachexia caused by a variety of underlying disorders [7]. Using the correlation between the anti-inflammatory effects of the KPV sequence found in  $\alpha$ -MSH [4] and the hMC4 antagonistic functions of SHU9119 and MBP10 [8], bi-functional peptides have been designed using various linkers such as Gly, Ala, or  $\beta$ -Ala.



*Fig. 1. Bifunctional ligand containing MBP10 as an hMC4 antagonist*



*Fig. 2. Bifunctional ligand containing SHU9119 as an hMC4 antagonist*

Table 1 Binding data for melanotropins

Code	Structure	hMC1R nM	hMC3R nM	hMC4R nM	hMC5R nM
1	Ac-Nle-c[Asp-His-D-Phe-Arg-Trp-Lys]-NH <sub>2</sub>	3.1	1.1	0.02	1.6
2	Ac-Nle-c[Asp-His-D-Nal(2')-Arg-Trp-Lys]-NH <sub>2</sub>		0.23	0.06	0.09
3	c[CO(CH <sub>2</sub> )CO-D-Nal(2')-Arg-Trp-Lys]-NH <sub>2</sub>		150	0.5	540
4	Ac-Nle-c[Asp-His-DNal(2')-Arg-Trp-Lys]-Ala-Lys-Pro-Val-NH <sub>2</sub>	1.2	1.5	0.4	2.7
5	Ac-Nle-c[Asp-His-DNal(2')-Arg-Trp-Lys]-Ala-Gly-Lys-Pro-Val-NH <sub>2</sub>	0.36	0.9	0.3	2.3

## Results and Discussion

There has been no significant difference in binding ability in regards to the various linkers used. Compound **1** is the melanocortin superagonist MTH. Compounds **2** and **3** are the known melanocortin 4 antagonists SHU9119 and MBP10 respectively. Compounds **4** and **5** are two of the bifunctional peptides synthesized combining the anti-inflammatory sequence KPV and the hMC4 antagonist SHU9119. It was found that compounds **4** and **5** show some selectivity towards the melanocortin 4 receptor. Based on experiments we have seen some TNF- $\alpha$  inhibition with these compounds (data not shown). Cachexia (wasting) is a serious issue for many patients suffering from states of chronic inflammation. Melanocortins and TNF- $\alpha$  are believed to be intimately involved in the process of inflammation and feeding behavior. Although it is not known for certain at this time if the anti-inflammatory effects of melanocortin (MSH) act directly on melanocortin receptors (MC-R) or via another substrate among the inflammation mediators, these studies can not only lead to the development of effective drugs against cachexia but also allow the elucidation of the exact processes involved in inflammation. Considerable effort has been made toward the development of highly potent hMC4R-selective agonists and antagonist due to the involvement of this receptor in the regulation of feeding and sexual behavior. The area of melanocortin research is vast and promises many exciting possibilities in modulating a large number of physiological processes in the human body.

## Acknowledgments

Supported by Grants from the U.S. Public Health Service, National Institutes of Health, DK 17420 and DA 06284.

## References

1. Lipton, J.M., et al. *Immunology Today* **18**, 140-145 (1997).
2. Yoon, S-W., et al. *J. Biological Chemistry* **278**, 32914-32920 (2003).
3. Palombella, V.J., et al. *Proc. Natl. Acad. Sci.* **95**, 15671-15676 (1998).
4. Kelly, J., et al. *Peptides* **27**, 431-43 (2006).
5. Cone, R.D. *Endocrine Reviews* **27**(7), 736-749 (2006).
6. Deans, C., et al. *Current Opinion in Clinical Nutrition and Metabolic Care* **8**, 265-269 (2005).
7. *The Role of Central Melanocortins in Cachexia, Energy Metabolism and Obesity*, Humana Press, 2008, 59-68
8. Joppa, M.A., et al. *Peptides* **26**, 2294-2301 (2005).

## Modulation of Function in Heme Binding Membrane Protein

Sandip Shinde, Jeanine Cordova, and Giovanna Ghirlanda

Department of Chemistry and Biochemistry, Arizona State University,  
 Tempe, AZ 85287-1604, U.S.A.

### Introduction

We previously reported the successful design and classification of a functional membrane protein, ME1, by engineering a bis-histidine binding site into a natural membrane protein, Glycophorin A. ME1 binds Fe (III) Protoporphyrin IX with submicromolar affinity, has a redox potential of -128 mV, and displays nascent peroxidase activity [1, 2]. Here we present a single-point mutant, G25F, which modulates the redox potential of the cofactor by 150 mV. To our knowledge, this is the largest effect observed for a single point mutant in a peptide model system. G25F was designed to test whether aromatic-porphyrin interactions can modulate the properties of the heme complex in the context of a membrane protein.

### Results and Discussion

**CD Spectroscopy:** Similar to the parent peptide ME1, the CD spectrum of G25F in DPC micelles shows minima at 208 and 222 nm, indicative of high helical content (Figure 1); no changes to the CD signal were observed upon addition of heme besides a weak induced dichroic signal at wavelengths corresponding the Soret band, suggesting that the peptide structure is preorganized independently from complex formation [1,2].

**Binding of hemin:** Binding affinity of G25F was assessed by spectrophotometric titrations, monitoring the appearance of a Soret band with maximum at 414 nm. The intensity of the band reached a maximum at the expected 2:1 peptide:hemin stoichiometry. A binding isotherm determined by titrating peptide into a low micromolar solution of hemin in DPC micelles was analyzed using a mutually depleting model [1,2], obtaining apparent dissociation constant,  $k_{dapp}$ , of

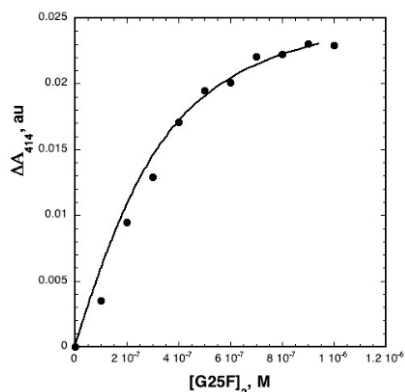


Fig. 2. The change in absorbance observed at the Soret maximum, 414 nm, was plotted against the increasing peptide concentration to obtain a binding isotherm.

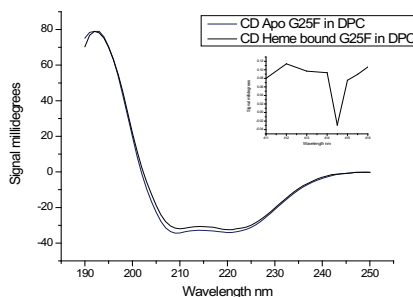


Fig. 1. CD spectroscopy of G25F in the apo form (black) and in the presence of stoichiometric amounts of heme (blue). The insert located in the left spectra is indicative of an induced Soret and demonstrates the heme is located in a chiral environment.

6.49  $\times 10^{-8}$  M (Figure 2). Thus, introducing a single aromatic residue (G25F) results in tighter binding compared to ME1 ( $5.3 \times 10^{-7}$  M). This change is consistent with effects observed in de novo designed water soluble systems, such as four helix maquettes, sandwiched two helix systems, and cyclic peptide models.

**Redox Potential:** The electrochemical reduction midpoint potential ( $E_{1/2}$ ) of G25F-Hemin complex determined by UV-vis monitored potentiometric titration is -280 mV vs. SHE [1,2]. This value is a dramatic shift of -152 mV compared to ME1 which has an  $E_{1/2}$  of -128 mV vs. SHE (Figure 3, Table 1).

G25F modulates the redox potential of ME1 to a larger extent than any other single-point mutant previously reported. The shift to more negative potentials is counterintuitive, given that one would expect a stabilization of the neutral  $Fe^{2+}$  form of the porphyrin in a more hydrophobic environment.

**Peroxidase activity:** The peroxidase activity of ME1 and G25F was assessed using ABTS, a standard compound for peroxidase studies that undergoes a single-electron oxidation as reducing agent (Figure 4). The kinetic parameters are similar to those obtained for water-soluble model heme proteins [1,2]. The most efficient catalyst is ME1, with a  $k_{\text{cat}}/K_M$  of  $5.05 \times 10^4 \text{ M}^{-1} \text{ s}^{-1}$ , compared to  $1.1 \times 10^4 \text{ M}^{-1} \text{ s}^{-1}$  for G25F. The trend appears to be inversely correlated to the affinity of each mutant for heme: the mutant with tighter binding to the cofactor is the least active.

## Conclusion

The results presented here show that the properties of bound cofactors in a minimalist membrane hemeprotein model, ME1, can be modulated by single-point mutation close to the binding site. The large shift to negative potential suggests that the G25F mutation has a much higher effect on the affinity for the ferric heme than the ferrous.

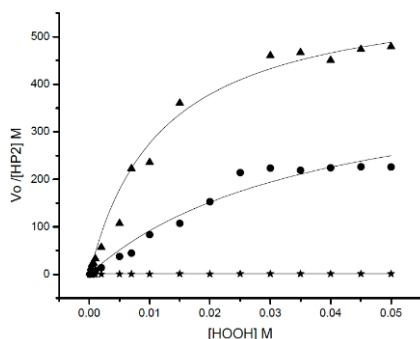


Fig. 4 Peroxidase activity of ME1 (triangles) and G25F (circles) at increasing hydrogen peroxide concentrations; Fe-PIX is reported as control. Conditions: peptide 4 mM, heme 2 mM, 50 mM PBS, pH 7.2.

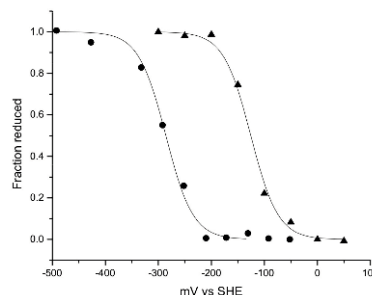


Fig. 3. Potentiometric titration of ME1/G25F-hemin: ME1 (triangles) and G25F (circles).

The difference in redox potential between ME1 and G25F can be linked to difference in binding affinity for the two states of the cofactor. With experimentally determined  $K_d^{\text{Fe(III)}}$  for ME1 approximately an order of magnitude larger than for G25F, we used the Nernst equation to conclude that the ratio of  $K_d^{\text{Fe(II)}}$ s must be close to 1.

Our studies show that bound heme in membrane proteins is more sensitive to factors such as aromatic stacking than in water soluble counterparts. While the binding constant shows a similar trend to what is observed in water soluble model hemoprotein, the shift in redox potential is unexpectedly higher. These results present a cautionary tale on the use of water soluble systems as models for membrane embedded hemoproteins, and point to the need for systematic, quantitative analysis of the factors affecting properties of cofactors in minimalistic membrane systems. Once fully investigated, these factors will be explicitly designed in artificial functional membrane proteins.

Table 1. Redox potential for ME1 and G25F. For comparison the redox potential of bis-imidazole coordinated Fe-Protoporphyrin IX in water and DPC micelles are reported.

Peptide	$E'_{1/2}$ mV
ME1	-128
G25F	-280
P-Im2 in water	-285
P-Im2 in DPC	-125

## Acknowledgments

We thank Prof. F. Ann Walker for help with collection and interpretation of EPR data, and Prof. David R. Benson for helpful discussions. This work was supported by NSF CAREER Award 0449842 to G.G. and by an NSF IGERT fellowship to J.M.C.

## References

1. Cordova, J.M. *J. Am. Chem. Soc.* **129**, 512-518 (2007).
2. Cordova, J.M., PhD thesis Arizona State Univ., Tempe, AZ, U.S.A. (2008).

## Temporal Analysis of Phosphopeptide Induced by Nocodazole Treatment

Kohji Nagano,<sup>1</sup> Takashi Shinkawa,<sup>1</sup> Hironori Mutoh,<sup>1</sup> Osamu Kondoh,<sup>2</sup>  
 Sayuri Morimoto,<sup>2</sup> Noriyuki Inomata,<sup>1</sup> Motooki Ashihara,<sup>1</sup> Nobuya Ishii,<sup>2</sup>  
 Yuko Aoki,<sup>2</sup> and Masayuki Haramura<sup>1</sup>

<sup>1</sup>Pharmaceutical Technology Department, <sup>2</sup>Pharmaceutical Research Department 2,  
 Chugai Pharmaceutical Company Limited, Kamakura, 247-8530 Japan

### Introduction

Protein and peptide phosphorylation is thought to play important roles in the biological aspects of drug activities. Different phosphorylation status in the pathway potentially distinguishes the biological output. However, detailed molecular understanding of protein phosphorylation is limited. Previously, we performed phosphoproteomic analysis using LC-MS/MS in the presence or absence of nocodazole, a known microtubule-interacting agent, in three distinct tumor cell lines (HeLa, HCT-116, and NCI-H460) (Figure 1) and found that 14 proteins were phosphorylated in all 3 tumor cell lines only as a result of treatment with nocodazole [1]. To gain more insight into the phosphorylation, we here performed phosphoproteomic analysis of HCT-116 cells in a time course of nocodazole treatment.

### Results and Discussion

Protein and peptide phosphorylation has been shown to affect mitotic events such as mitotic checkpoints, spindle formation, and the anaphase-promoting complex. We performed temporal phosphoproteomic analysis of HCT-116 cells treated with nocodazole, which induces the activation of stress response pathways, M-phase cell cycle arrest, and the induction of apoptosis.

Subconfluent HCT-116 cells were treated with nocodazole for 0, 6, 10, 14, or 24 h containing <10%, ~30%, ~50%, ~80%, or >90% of M-phase cells, respectively, and washed with PBS. The cells were then lysed by sonication and the proteins digested with N (alpha)-L-tosyl-L-phenylalanylchloromethyl ketone-treated porcine trypsin (Promega, Madison, WI). The phosphopeptides were affinity-purified using MassPREP<sup>TM</sup> (Waters, MA) according to the manufacturer's protocol, desalted, and concentrated using a C18 column (Oasis, Waters, MA). LC-MS analysis was carried out using an LTQ Orbitrap XL linear ITMS system (Thermo Fisher Scientific, CA) with a Paradigm MS4 dual solvent delivery nanoLC system

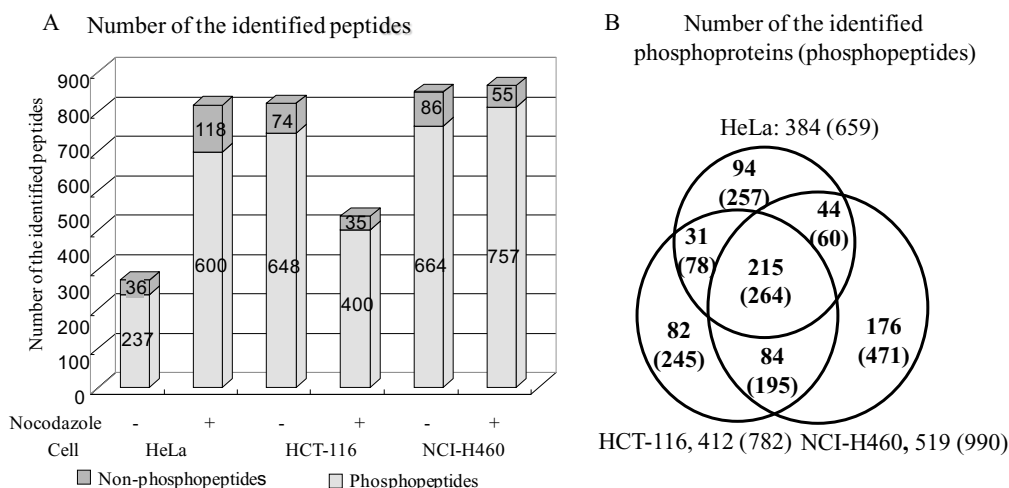


Fig. 1. Phosphopeptide analysis of HeLa, HCT-116, and NCI-H460 cells with or without nocodazole treatment.

Table 1. Time course analysis of nocodazole-induced phosphorylation of HCT-116

Molecule	Sequence*	Site	0hr	6hr	10hr	14hr	24hr
NPM1	MQASIEKGGS LPK	S254	0	<b>1</b>	<b>4</b>	3	3
COPA	NLSPGAVESDVR	S173	0	0	0	0	<b>2</b>
PSMA5	GVNTFSPEGR	S16	0	<b>2</b>	<b>1</b>	2	2
ILF3	LFPDTPLALDANK	T592	0	<b>2</b>	<b>2</b>	1	2
PCBP1	VMTIPYQMPASSPVICAGGQDR	S189	2	1	3	3	1
IF2A	SDKSPDLAPTAPQSTPR	S506	1	0	2	0	2
MYO1C	DVESPSWR	S389	0	0	1	0	0
RPL12	IGPLGLSPK	S38	0	0	0	0	0
TK1	KLFAPQQILQCSPAN	S231	1	1	1	<b>4</b>	<b>2</b>
TMPO	FQETEF LSPPR	S424	0	1	1	2	1
SFN	DNLT LWTADNAGEEGEAPQEPQS	S248	0	0	0	2	0
RBM4	LHVGNISPTCTNK	S86	0	1	1	1	0
RIC8A	VIQPMGMSPR	S508	0	1	1	2	2
IARS	APLKPYPVSPSDK	S1047	0	0	1	1	0

Values are the sum of the number of sequenced MS/MS spectra assigned to the phosphopeptide in 2 independent analyses.

\*Identified phosphorylation sites are shown in boldface type. **Bold number**: early phosphorylation, *Italic number*: late phosphorylation.

(Microm BioResources, CA). A database search for protein identification was performed with Mascot Ver.2.2.02 (Matrix Science, London, UK) against Refseq human database (NCBI), and the data were processed by in-house software STEM [2] to generate a list of identified proteins.

Temporal changes of phosphorylation induced by nocodazole varied among the molecules (Table 1). Phosphorylations of NPM1 S254, PSMA5 S16, ILF3 T592, and TMPO S424 were induced by nocodazole after 6 h and sustained until 24 h. This result implies that phosphorylation of NPM1 S254 may be the early indicator of nocodazole treatment and may also be functionally involved in the induction of M-phase arrest by nocodazole. Phosphorylations of COPA S173, TK1 S231, and RIC8A S508 were observed after 14 h or more when the majority of the cells were arrested in M-phase. Especially, phosphorylation of COPA S173 was observed from 14 h of nocodazole treatment when ~80% of cells were in M-phase, suggesting that COPA S173 may be phosphorylated as a result of M-phase arrest and may also be a candidate for an M-phase-specific biomarker. Phosphorylations of MYO1C S389 and SFN S248, which were identified only from cells treated with nocodazole for 10 h and 14 h, respectively, seemed to be induced transiently in the course of the nocodazole treatment. These results imply that phosphorylation may be involved in the induction of M-phase arrest by nocodazole and may be induced as a result of M-phase arrest, also suggest that phosphorylation of NPM1 S254 and COPA S173 may serve as biomarkers to monitor the efficacy of microtubule-interfering agents for cancer chemotherapy.

## Acknowledgments

We thank Mr. Hiroshi Ohmori, and Ms. Nami Yabuki (Chugai Pharmaceutical) for their useful advice. We also thank Dr. Masahiro Aoki (Chugai Pharmaceutical) for his special support for this work.

## References

1. Nagano, K., et al. *Proteomics* **9**, 2861-2874 (2009).
2. Shinkawa, T., et al. *J. Proteome Res.* **4**, 1826-1831 (2005).



## Regulation of Protein Binding by Photoswitchable Peptides

Christian Hoppmann,<sup>1,2</sup> Sabine Seedorff,<sup>1,2</sup> Anja Richter,<sup>2</sup> Heinz Fabian,<sup>3</sup>  
Peter Schmieder,<sup>1</sup> Karola Rück-Braun,<sup>2</sup> and Michael Beyermann<sup>1</sup>

<sup>1</sup>Leibniz Institut für Molekulare Pharmakologie, Robert-Rössle Straße 10, Berlin, 13125, Germany;

<sup>2</sup>Institut für Chemie, Technische Universität Berlin, Straße des 17. Juni 135, Berlin, 10623 Germany;

<sup>3</sup>Robert-Koch-Institut, Nordufer 20, 13353, Berlin, Germany

### Introduction

$\beta$ -Hairpin structures are frequently occurring structural elements in proteins involved in protein-protein interaction. The modeling of such structural elements is particularly difficult because of the complexity of  $\beta$ -hairpin structures given by access, stability and solubility. In the cell the extended PDZ domain of the neuronal nitric oxide synthase (nNOS) heterodimerizes with the  $\alpha$ -1-syntrophin PDZ domain [1]. The formation of this heterodimer requires the  $\beta$ -finger peptide [2] of the extended PDZ domain to bind into the binding pocket of the syntrophin. This association allows the integration of nNOS in signaling pathways in muscle cells inducing the production of the second messenger NO to muscle contraction. The control of such protein-protein interactions by means of light-controlled switch units would result in an elegant tool to manipulate biological functions by external stimuli. Photoswitchable  $\omega$ -amino acids based on either azobenzene [3] or hemithioindigo [4] are good candidates for the modulation of peptide conformations [5]. We synthesized cyclic peptides that mimic the  $\beta$ -finger peptide of nNOS containing either **1** the -Val-D-Pro-Gly-His- motif for the non switchable form or **2** the 3,4'-AMPB as photoswitch [6].

### Results and Discussion

The azobenzene- $\omega$ -amino acid 3-((4'-aminomethyl)phenylazo) benzoic acid (3, 4'-AMPB) was embedded into the cyclic peptide **1** (Figure 1) replacing the -Val-D-Pro-Gly-His- motif. The extended geometry of the azobenzene in the *trans*-form compared to this of the *cis*-form was expected to disturb the binding site in the peptide ligand **2** [6].

High isomerization yields in the pss of the *cis*-form of **2** (90% *cis*-content) were achieved after irradiation of the thermodynamically stable *trans*-form at 330 nm in buffer solution at pH 7.5. The thermal *cis*-to-*trans* isomerization of **2** in aqueous solution was found to

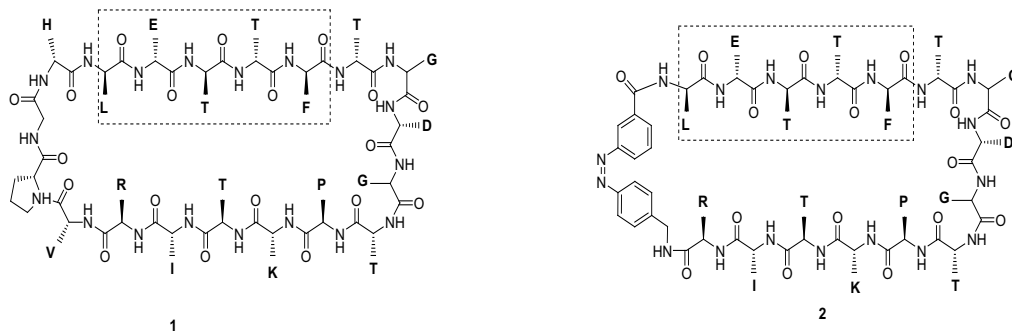


Fig. 1. Cyclic peptide ligands based on the sequence of the  $\beta$ -hairpin peptide of the neuronal NO synthase. The recognition motif is depicted in the dashed box.

be slow (half-life time 25 days). The repeated photochemical interconversion of the two states was achieved without occurrence of association, precipitation or photobleaching. The ligand was immobilized via the lysine side chain on a CM5 sensor chip to perform surface plasmon resonance spectroscopic measurements (SPR). The pure *trans*-form of peptide **2** showed almost no binding. After photoisomerization to the *cis*-form, a remarkable binding of the syntrophin PDZ domain was found which is comparable to that of the model peptide **1**.

Table 1. Photochromic properties of **2**

$\lambda_{\max}$ [ <i>trans</i> ] (nm)	$\lambda_{\max}$ [ <i>cis</i> ] (nm)	$\epsilon_{\text{trans}}$ (dm <sup>3</sup> M <sup>-1</sup> cm <sup>-1</sup> )	Isosb. points (nm)	$t_{1/2}$ (h)	<i>trans:cis</i> ( <i>cis</i> -pss)
327 / 424	297 / 424	11500	390 / 276	597.5	10 : 90

In solution the model peptide **1** adopts an antiparallel  $\beta$ -sheet structure [7]. The correlation between the binding affinities of either **2** in the *cis*-pss or **1** let us assume similar structural features of the binding site. FTIR spectroscopy reveals that the *trans*-form of **2** adopts an unordered peptide structure while photoisomerization to the *cis*-azobenzene induced the formation of a  $\beta$ -sheet secondary structure (Table 1). The protein binding affinity of a biologically relevant  $\beta$ -sheet has been controlled by a light-induced conformational change in a designed cyclic hairpin peptide. The *trans*-form (unordered peptide conformation) showed no binding while the *cis*-form exhibits increased  $\beta$ -sheet content along with a remarkable binding affinity to its target protein domain (Figure 2).

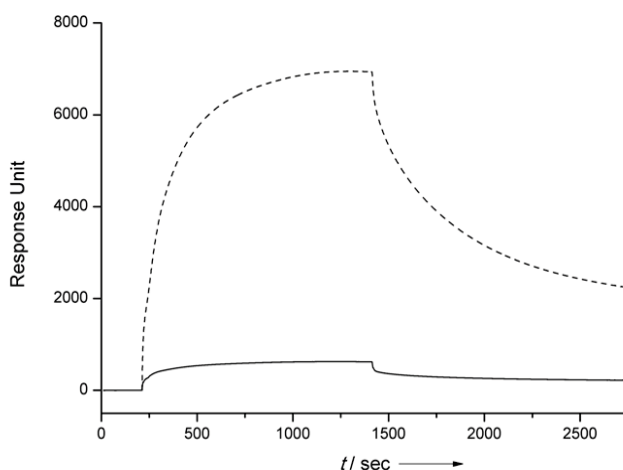


Fig. 2. SPR sensorgram of the interaction of **2** as *trans*-form (black) and *cis*-form (dashed) with syntrophin PDZ.

## Acknowledgments

The project was supported by the Volkswagen Stiftung.

## References

- Hillier, B.J., Christopherson, K.S., Prehoda, K.E., Bredt, D.S., Limm, W.A *Science* **284**, 812-815 (1999).
- Wang, P., Zhang, Q., Tochio, H., Fan, J.-S., Zhang, M. *FEBS J.* **267**, 3116-3122 (2000).
- Priewisch, B., Steinle, W., Rück-Braun, K. in *Peptides 2004*, edited by Flegel, M., Fridkin, M., Gilon, C., Slaninova, J. Kenes International, Genf, 2005, p. 756-757.
- Schadendorf, T., Hoppmann, C., Rück-Braun, K. *Tetrahedron Lett.* **48**, 9044-9047 (2007); b) Steinle, W., Rück-Braun, K. *Org. Lett.* **5**, 141-144 (2003); c) Cordes, T., Weinrich, D., Kempa, S., Riesselmann, K., Herre, S., Hoppmann, C., Rück-Braun, K., Zinth, W. *Chem. Phys. Lett.* **428**, 167-173 (2006).
- Ulysse, L., Cubillos, J., Chmielewski, J. *J. Am. Chem. Soc.* **117**, 8466-8467 (1995); b) Behrendt, R., Renner, C., Schenk, M., Wang, F., Wachtveitl, J., Oesterheld, D., Moroder, L. *Angew. Chem.* **111**, 2941-2943 (1999); *Angew. Chem. Int. Ed.* **38**, 2771-2777 (1999).
- Hoppmann, C., Seedorff, S., Richter, A., Fabian, H., Schmieder, P., Rück-Braun, K., Beyermann, M. *Angew. Chem.* 2009 accepted.
- Seedorff, S., Appelt, C., Beyermann, M., Schmieder, P. manuscript in preparation.

## Utilization of Hydrophobic Modification to Promote Internalization of a CAAX Box-containing Peptide

James W. Wollack,<sup>1</sup> Joseph Katzenmeyer,<sup>2</sup> Joshua D. Ochocki,<sup>2</sup>  
 Nicholette A. Zeliadt,<sup>3</sup> Daniel G. Mullen,<sup>2</sup> Edgar A. Arriaga,<sup>2</sup>  
 Elizabeth V. Wattenberg,<sup>3</sup> and Mark D. Distefano<sup>2</sup>

<sup>1</sup>Department of Chemistry, Hamline University, Saint Paul, MN 55104, U.S.A.; <sup>2</sup>Department of Chemistry, University of Minnesota, Minneapolis, MN 55455, U.S.A.; <sup>3</sup>The Division of Environmental Health Sciences, University of Minnesota, Minneapolis, MN 55455, U.S.A.

### Introduction

Addition of a hydrophobic moiety to a peptide increases a peptide's ability to penetrate plasma membranes. Hydrophobic moieties that increase peptide uptake include fifteen or twenty carbon isoprenoids, [1] fourteen carbon myristoyl groups, [2] and alkyl chains consisting of 10 or more carbons [3]. It is useful to attach these hydrophobic groups to a peptide via a disulfide linkage, since this linkage is reduced upon cellular entry [4]. This allows the peptide to localize in a manner that is not altered by hydrophobic modification. In this work, incorporation of a Cys(Acm) amino acid is utilized to produce a decyl-linked peptide attached by a disulfide bond. Attaching a decyl group to the sole Cys of the fluorescent peptide Flu-KKSRRCVLL via a disulfide linkage allowed the peptide to gain cellular entry via an energy independent pathway. After entry, the decyl group was reduced from the peptide leaving a C-terminus ending in CVLL. Proteins and peptides ending in the four amino acid sequence CVLL are natural substrates for subsequent processing by cellular enzymes; including geranylgeranylation of cysteine by GGTase, [5] proteolysis of VLL by RCE1, [6] and methylation of the resulting C-terminal acid by ICMT [7]. Since the peptide used was fluorescent, the processing of this peptide can be analyzed using micellar electrokinetic chromatography with laser induced fluorescence detection by comparing migration times of the fluorescent products found in cell lysates to migration times of synthetic standards of suspected products (peptides 2-5).

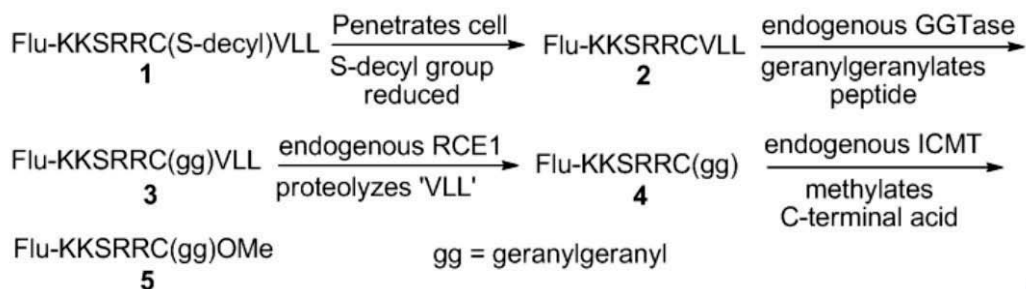


Fig. 1 Intracellular enzymatic reactions of the peptide KKSRRCVLL. After the peptide Flu-KKSRRRC(S-decyl)VLL internalizes the disulfide bond connecting the parent peptide to the decyl group is reduced resulting in peptide 2. Peptide 2 is then prenylated by endogenous GGTase, proteolyzed by endogenous RCE1, and methylated by endogenous ICMT.

### Results and Discussion

Linear peptides were synthesized by Fmoc-based SPPS on an Applied Biosystems 433A automated peptide synthesizer according to manufacturer protocols using Rink acid with the N-terminus set to be deprotected after the final coupling step. After automated synthesis, the peptide resin was dried in vacuo and the N-terminus was attached to 5-carboxyfluorescein (5-Fam) using HOBt, and DIPCDI as coupling reagents. Peptides were then cleaved from the resin and purified. Peptides 3 and 4 were then alkylated using geranylgeranyl bromide and ZnOAc<sub>2</sub> [8]. Peptide 5 was first methylated using methods developed by Waldmann and Peters [9] and subsequently alkylated using the acidic ZnOAc<sub>2</sub> conditions noted above. For peptide 1 the

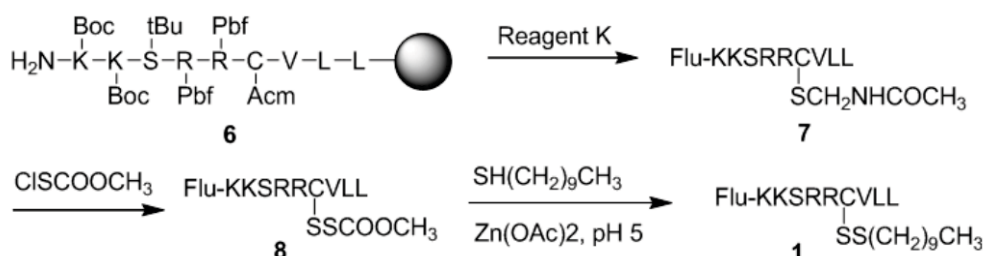


Fig. 2. Synthesis of fluorescent decyl-linked peptides.

sequence Fam-KKSRR(CAc)VLL was prepared and the Acm protecting group was converted to a Scm group by treatment with  $\text{CH}_3\text{O}(\text{CO})\text{SCl}$  [10]. The more reactive Scm group then underwent disulfide exchange when treated with decane thiol under acidic conditions to produce peptide **1**.

The cell-penetrating ability of decyl-linked peptide **1** was examined by incubating the peptide ( $1.0 \mu\text{M}$ ) with HeLa cells at  $37^\circ\text{C}$  ( $+5\% \text{CO}_2$ ) for 1 h. After this period of incubation, the plasma membranes were stained red with wheat germ agglutinin-Alexa Fluor 488 and the cells were fixed before confocal fluorescence microscopy imaging (Figure 3). Comparing the left and right panel of Figure 2 shows that the peptide has entered the cells and is not adhering to the outer plasma membrane. This result is similar to results obtained for prenylated peptides [1]. After it was confirmed that **1** was able to enter cells at  $37^\circ\text{C}$ , mechanistic studies were completed to determine if the uptake of the peptide was ATP-independent. HeLa cells that were ATP-depleted through treatment with rotenone and 2-deoxyglucose [11] before treatment with **1** and HeLa cells treated at lower temperatures ( $4^\circ\text{C}$ ) both showed similar localization to cells treated at  $37^\circ\text{C}$ . This indicates that decyl-linked peptide **1** internalized via an ATP-independent mechanism which allows the peptide to interact with enzymes without having to first escape endosomal entrapment. The efficiency of peptide uptake along with its localization to the cytosol and membrane bound organelles make **1** a good candidate to use for the study of enzymatic processing of prenylated biomolecules. Preliminary experiments using micellar electrokinetic chromatographic analysis with laser induced fluorescence detection suggest that the internalized peptides can be detected (Data not shown). Efforts to follow their subsequent processing are in progress. This should allow for the analysis of the *in vivo* rates of protein prenylation, RCE1-catalyzed proteolysis and ICMT-promoted methylation.

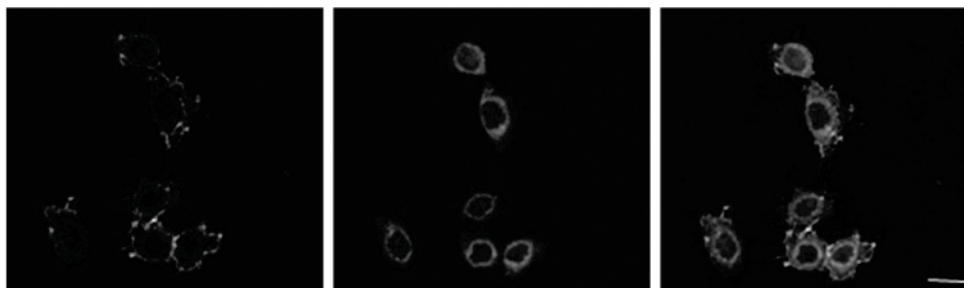


Fig. 3. Microscope images of HeLa cells that were treated with peptide **1** ( $1.0 \mu\text{M}$ ) for 1 h. The cells were washed, fixed, treated with ProLong Gold to limit fluorescence fading, and imaged. Left Panel: Red channel image showing the plasma membrane of the cells by staining with wheat germ agglutinin-Alexa Fluor 488. Middle Panel: Green channel image of the same cells showing that peptide **1** localizes to the cytoplasm and membrane bound organelles around the nucleus. Right Panel: Merged image of left and center panels. The bar in the lower right corner represent a distance of  $20 \mu\text{m}$ .

## Acknowledgments

The authors thank Mr. Jerry Sedgewick, Mr. Gregg Amundson, and Mr. John Oja of the University of Minnesota Biomedical Image Processing Lab for technical assistance regarding cell imaging and Dr. George Barany for use of his peptide synthesizer. This work was supported by the National Institutes of Health (Grant No GM058842, CA104609 and T32GM008347).

## References

1. Wollack, J.W., Zeliadt, N.A., Mullen, D.G., Amundson, G., Geier, S., Falkum, S., Wattenberg, E.V., Barany, G., Distefano, M.D. *J. Am. Chem. Soc.* **131**, 7293-7303 (2009).
2. Nelson, A.R., Borland, L., Allbritton, N.L., Sims, C.E. *Biochemistry* **46**, 14771-14781 (2007).
3. Carrigan, C.N., Imperiali, B. *Anal. Biochem.* **341**, 290-298 (2005).
4. Saito, G., Swanson, J.A., Lee, K.-D. *Adv. Drug Deliv. Rev.* **55**, 199-215 (2003).
5. Schafer, W.R., Rine, J. *Annu. Rev. Genet.* **26**, 209-237 (1992).
6. Boyartchuk, V.L., Ashby, M.N., Rine, J. *Science* **275**, 1796-1800 (1997).
7. Hancock, J.F.C., Paterson, K., Marshall, H.C.J. *EMBO J.* **10**, 4033-4039 (1991).
8. Xu, J., DeGraw, A.J., Duckworth, B.P., Lenevich, S., Tann, C.-M., Jenson, E.C., Gruber, S.J., Barany, G., Distefano, M.D. *Chem. Biol. Drug Des.* **68**, 85-96 (2006).
9. Peters, C., Waldmann, H. *J. Org. Chem.* **68**, 6053-6055 (2003).
10. Hiskey, R.G., Muthukumaraswamy, N., Vunnam, R.R. *J. Org. Chem.* **40**, 950-953 (1975).
11. Meriin, A.B., Yaglom, J.A., Gabai, V.L., Zon, L., Ganiatsas, S., Mosser, D.D., Sherman, M.Y. *Mol. Cell Biol.* **19**, 2547-2555 (1999).

## **Assessment of a Tat-Derived Peptide as a Vector for Hormonal Transport**

**Brian P. Finan,<sup>1</sup> Vasily M. Gelfanov,<sup>1</sup> and Richard D. DiMarchi<sup>1</sup>**

<sup>1</sup>*Department of Chemistry, Indiana University, Bloomington, IN 47405, U.S.A.*

### **Introduction**

Glucagon-like Peptide 1 (GLP-1) is a 30 amino acid gastrointestinal peptide hormone that is secreted in response to an oral glucose load to contribute to the normalization of plasma glucose levels by stimulating postprandial insulin secretion from pancreatic  $\beta$  cells while inhibiting glucagon secretion from pancreatic  $\alpha$  cells. Furthermore, GLP-1 regulates glucose homeostasis through extra-pancreatic effects, including promoting feelings of satiety and delaying gastric emptying [1]. The reptilian-derived analog of GLP-1, exendin-4 (Byetta), is an FDA-approved medicine for treatment of type 2 diabetes. Because exendin-4 and GLP-1 are peptides, they are inherently impermeable to cellular membranes and are not passively taken up by cells, meaning they are not transported across a cell monolayer and are not absorbed through the small intestine. Therefore, GLP-1 and exendin-4 must be administered through a subcutaneous injection. Conversion of exendin-4 or GLP-1 to a more orally bio-available form could improve the therapeutic quality, patient compliance, and appeal of the drug.

Extracellular HIV-1 Tat is a 101 amino acid protein that is taken up by cells to activate the transcription of the HIV-1 genome, and it has been shown that the cationic cluster that is derived from amino acids 47-57 of the HIV-1 Tat protein can be covalently fused to a wide degree of cargo molecules to stimulate delivery into cells [2]. Not only is this cationic cluster responsible for stimulating cellular uptake, but this same sequence is responsible for the secretion of expressed proteins from cells [3]. We hypothesize that this Tat-derived cationic peptide could function as a vector to improve the transduction efficiency of GLP-1 across the human epithelial cell layer of the small intestine.

### **Results and Discussion**

The cationic Tat-derived peptide, with the sequence of YGRKKRRQRRR, was covalently attached to the C-terminus of the GLP-1 sequence with an intermediate lysine residue at position 32. The intermediate lysine residue serves as the site of fluorescein attachment for cellular transport studies. The C-terminus of GLP-1 was chosen for the site of covalent attachment because structure-function studies performed in our lab as well as alanine scan mutagenesis [5] suggest that modifications to the C-terminus do not significantly alter activity at the GLP-1 receptor. The fusion of the Tat-derived cationic peptide to GLP-1 reduced the activity at the GLP-1 receptor ~3-fold, but was still extremely potent (30pM for GLP-1 relative to 100pM for Tat-extended GLP-1). Substitution of native amino acids at positions 22 and 25 with alanine yielded Tat-extended analogs with 7.2nM and 320pM potency, as similarly assessed relative to GLP-1 (EC<sub>50</sub>) in a GLP-1 receptor transformed cell. A GLP-1 scrambled sequence with a similar Tat-extension demonstrated a reduced potency in the same assay of 6.2nM.

The fusion of the Tat-derived sequence to native GLP-1 and to the scrambled GLP-1 sequence confers significant cellular uptake at micromolar concentrations whereas fusion to the two GLP-1 analogs (A<sup>22</sup> and A<sup>25</sup>) did not result in cellular uptake (Figure 1). This suggests that that cellular uptake is dependent on the physiochemical and biological properties of the cargo molecule. However, the degree of cellular uptake may be cell-type specific as well, as it is suggested that CaCo-2 cells may be resistant to Tat-derived peptides [6]. Of particular importance, permeability assays show the Tat-derived cationic peptide did not increase the transport of the GLP-1 cargo peptide from the apical domain to the basolateral domain of differentiated CaCo-2 cells. However, incubation with the GLP-1 Tat analogs that displayed a high degree of cellular internalization caused a severe disruption of the cell monolayer, as shown in a significant decrease in the trans-epithelial electrical resistance (TEER) values. When observed morphometrically, the CaCo-2 cells appeared to lyse when incubated with GLP-1 Tat analogs at concentrations that display a high degree of cellular uptake.

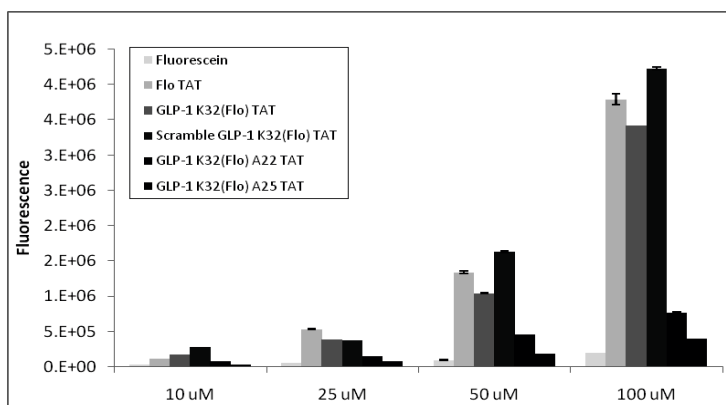


Fig. 1. Internalization into CaCo-2 cells.

Cytotoxicity studies suggest that internalization of the cargo molecule is required for Tat-mediated toxicity. The two GLP-1 Tat analogs that did not exhibit a high degree of cellular uptake ( $A^{22}$  &  $A^{25}$ ) did not induce cytotoxicity, whereas the two analogs that show a high degree of uptake (GLP-1 & Scramble) exhibit cytotoxicity at concentrations that confer cellular internalization (Table 2). However, cellular uptake without a GLP-ligand is not sufficient for

Table 2. Tat-Induced Cytotoxicity in CaCo-2 Cells

Peptide	GLP-1 Receptor $IC_{50}$ , $\mu M$	$n^*$
GLP-1	N/A	2
GLP-1 K32 Tat	$50.0 \pm 4.71$	3
GLP-1 K32(Flo) Tat	$39.50 \pm 3.96$	3
Scramble GLP-1 Tat	$35.45 \pm 3.51$	3
GLP-1 A22 K32 Tat	N/A	2
GLP-1 A25 K32 Tat	N/A	2
Flo-Tat	N/A	2

cytotoxicity because the Tat-derived sequence alone shows a high degree of cellular internalization (Figure 1) yet did not induce cytotoxicity in CaCo-2 cells (Table 2). Additionally, GLP-1 activity is not a requirement for cytotoxicity as the scrambled GLP-Tat peptide was transported and cytotoxic. These transported GLP-1 Tat analogs may be causing toxicity by micropinocytosis [7]. However, the molecular basis of this observation requires additional study. Most importantly, the Tat peptide does not seem suitable for peptide delivery since there was no apparent transcellular transport after internalization.

## References

1. Combettes, M.J. *Current Opinion in Pharmacology* **6**, 598-605 (2006).
2. Zhao, M., Weissleder, R. *Medicinal Research Reviews* **24**, 1-12 (2004).
3. Chang, H.C., et al. *AIDS* 1421-1431 (1997).
4. Schnolzer, M., Kent, S.B.H., et al. *Int. J. Peptide Protein Res.* **40**, 180-193 (1992).
5. Adelhorst, K., et al. *Journal of Biological Chemistry* **269**, 6275-6278 (1993).
6. Violini, S., et al. *Biochemistry* **41**, 12652-12661 (2005).
7. Gump, J.M., Dowdy, S.F. *TRENDS in Molecular Medicine* **13**, 443-448 (2007).

## Molecular Imaging of Angiogenesis: Cancer and Beyond

Weibo Cai<sup>1,2</sup>

<sup>1</sup>Departments of Radiology and Medical Physics, School of Medicine and Public Health,  
 University of Wisconsin - Madison, Madison, WI 53705, U.S.A.; <sup>2</sup>University of Wisconsin  
 Carbone Cancer Center, Madison, WI 53705, U.S.A.

### Introduction

Angiogenesis, the formation of new blood vessels, is a critical process in both physiological development and pathological processes such as tumor progression, wound healing, cardiovascular, inflammatory, ischemic, and infectious diseases [1]. One of the most extensively studied angiogenesis-related signaling pathways is the vascular endothelial growth factor (VEGF)/VEGF receptor (VEGFR) interactions [2]. Non-invasive imaging of VEGFR expression could serve as a new paradigm for the assessment of angiogenic/anti-angiogenic therapeutics and for better understanding the role and expression profile of VEGF/VEGFR in many angiogenesis-related diseases. In this presentation, we show that a <sup>64</sup>Cu (t<sub>1/2</sub> = 12.7 h; β<sup>+</sup>% = 17%) -labeled VEGF<sub>121</sub> can be used for positron emission tomography (PET) imaging of many angiogenesis-related diseases such as cancer, myocardial infarction (MI), peripheral artery disease (PAD), and stroke (Figure 1).

### Results and Discussion

We reported the first PET imaging of VEGFR expression with <sup>64</sup>Cu-DOTA-VEGF<sub>121</sub> (DOTA denotes 1,4,7,10-tetraazacyclododecane-1,4,7,10-tetraacetic acid) [3]. DOTA-VEGF<sub>121</sub> exhibited nano-molar receptor binding affinity (comparable to VEGF<sub>121</sub>) in vitro. MicroPET imaging revealed rapid, specific, and prominent uptake of <sup>64</sup>Cu-DOTA-VEGF<sub>121</sub> (~ 15%ID/g) in highly vascularized small U87MG human glioblastoma tumor with high VEGFR-2 expression but significantly lower and sporadic uptake (~ 3%ID/g) in large U87MG tumor with low VEGFR-2 expression. Western blotting of tumor tissue lysate, immunofluorescence staining, and blocking studies with unlabeled VEGF<sub>121</sub> confirmed that the tumor uptake is VEGFR specific. This study demonstrated the dynamic nature of VEGFR expression during tumor development in that even for the same tumor model, VEGFR expression level can be dramatically different at different stages.

Quantitative PET imaging of VEGFR will facilitate the planning of whether, and when, to start anti-angiogenic treatment and enable more robust and effective monitoring of such treatment. In a follow-up study, PET imaging of mice bearing different-sized U87MG tumors were performed and Western blotting and immunofluorescence staining of tumor tissue was carried out to correlate with/validate the imaging results [4]. The uptake of <sup>64</sup>Cu-DOTA-VEGF<sub>121</sub> in the tumor peaked when the tumor size was about 100–250 mm<sup>3</sup>. All tumors had similarly low VEGFR-1 expression. Most importantly, the tumor uptake value obtained from PET imaging had good linear correlation with the relative tumor tissue VEGFR-2 expression as measured by Western blot, where r<sup>2</sup> equals 0.68 based on the PET uptake at 4 h post-

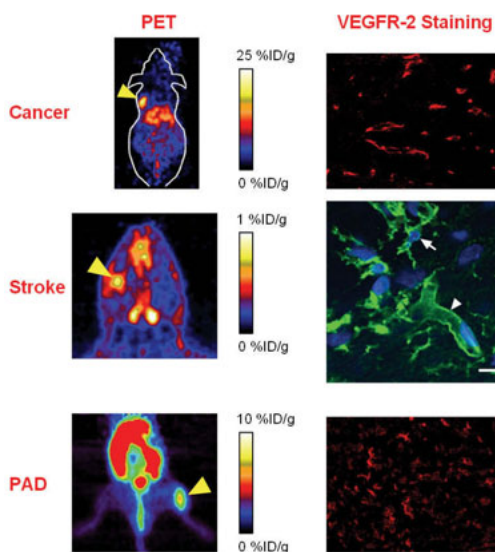


Fig. 1. PET imaging of VEGFR in various disease models with <sup>64</sup>Cu-DOTA-VEGF<sub>121</sub>. The in vivo imaging data are validated with ex vivo VEGFR-2 staining of the targeted tissue.



injection. Such correlation laid the foundation for the following studies where  $^{64}\text{Cu}$ -DOTA-VEGF<sub>121</sub> PET was utilized to non-invasively evaluate the kinetics of VEGFR-2 expression in various diseases (e.g. MI and stroke) as well as the biological response of PAD to therapeutic intervention. These studies are described below.

In a rat MI model, we performed serial  $^{64}\text{Cu}$ -DOTA-VEGF<sub>121</sub> PET imaging to evaluate the kinetics of post-MI VEGFR-2 expression non-invasively [5]. In Sprague-Dawley rats, MI was induced by ligation of the left coronary artery and confirmed by ultrasound. Weekly PET scans revealed that baseline myocardial uptake of  $^{64}\text{Cu}$ -DOTA-VEGF<sub>121</sub> was minimal. The uptake increased significantly after MI and remained elevated for about 2 weeks. VEGFR specificity of  $^{64}\text{Cu}$ -DOTA-VEGF<sub>121</sub> was confirmed by the use of a  $^{64}\text{Cu}$ -DOTA-VEGF<sub>mutant</sub> as the control. Studies like this may play a major role when studying pathophysiology and assessing therapies in different animal models of diseases and, potentially, in patients.

In another study, weekly  $^{64}\text{Cu}$ -DOTA-VEGF<sub>121</sub> PET scans were carried out for non-invasive spatial, temporal, and quantitative monitoring of VEGFR-2 expression in a murine model of hindlimb ischemia with and without treadmill exercise training [6]. Mice underwent unilateral ligation of the femoral artery and longitudinal VEGFR-2 expression in exercised and non-exercised mice was quantified weekly with  $^{64}\text{Cu}$ -DOTA-VEGF<sub>121</sub> PET and post-mortem  $\gamma$ -counting.  $^{64}\text{Cu}$ -DOTA-VEGF<sub>121</sub> uptake in ischemic hindlimbs increased significantly from the baseline level and peaked at post-operative day 8, then gradually decreased over the following 3 weeks. Compared with non-exercised mice,  $^{64}\text{Cu}$ -DOTA-VEGF<sub>121</sub> uptake was increased significantly in exercised mice (at day 15, 22, and 29) and correlated with VEGFR-2 levels as measured by Western blotting. Further, in exercised mice, microvessel density was also significantly higher than the non-exercised mice.

VEGF and VEGFRs also play important roles during neurovascular repair after stroke. In a recent study, we imaged VEGFR expression with PET to non-invasively analyze post-stroke angiogenesis [7]. Female Sprague-Dawley rats after distal middle cerebral artery occlusion surgery were subjected to weekly MRI,  $^{18}\text{F}$ -FDG PET, and  $^{64}\text{Cu}$ -DOTA-VEGF<sub>121</sub> PET scans. T2-weighted MRI correlated with the “cold spot” on  $^{18}\text{F}$ -FDG PET for rats undergoing surgery. The  $^{64}\text{Cu}$ -DOTA-VEGF<sub>121</sub> uptake in the stroke border zone peaked at 10 days after surgery, indicating neovascularization as confirmed by histology (VEGFR-2, BrdU, and lectin staining). VEGFR specificity of  $^{64}\text{Cu}$ -DOTA-VEGF<sub>121</sub> uptake was confirmed by significantly lower uptake of  $^{64}\text{Cu}$ -DOTA-VEGF<sub>mutant</sub> in vivo and intense  $^{125}\text{I}$ -VEGF<sub>165</sub> uptake ex vivo in the stroke border zone. This study suggested that in vivo imaging of VEGFR expression could become a significant clinical tool to plan and monitor therapies aimed at improving post-stroke angiogenesis.

In summary, we have imaged VEGFR expression in many angiogenesis-related diseases (cancer, MI, PAD, and stroke). These studies demonstrated the power of molecular imaging, which is molecular specific rather than disease specific, and the same tracer could be useful in a wide variety of diseases that involve the imaging target. We have also shown that VEGFR imaging can be used for both lesion detection and treatment monitoring, the two major goals of molecular imaging [8]. In the clinical setting, the right timing is critical for VEGFR-targeted therapy and imaging of VEGFR can help determine whether, and when, to start the treatment. Further, quantitative and non-invasive imaging of VEGFR expression in patients may allow for more accurate monitoring of therapeutic intervention.

## Acknowledgments

The author thanks all his colleagues at the Molecular Imaging Program at Stanford (MIPS), as well as all other collaborators, who participated in the studies described in this proceeding.

## References

1. Cai, W., Chen, X. *Front. Biosci.* **12**, 4267-4279 (2007).
2. Cai, W., Chen, X. *J. Nucl. Med.* **49 Suppl 2**, 113S-128S (2008).
3. Cai, W., Chen, K., Mohamedali, K.A., Cao, Q., Gambhir, S.S., Rosenblum, M.G., Chen, X. *J. Nucl. Med.* **47**, 2048-2056 (2006).
4. Chen, K., Cai, W., Li, Z.B., Wang, H., Chen, X. *Mol. Imaging Biol.* **11**, 15-22 (2009).
5. Rodriguez-Porcel, M., Cai, W., et al. *J. Nucl. Med.* **49**, 667-673 (2008).
6. Willmann, J.K., Chen, K., et al. *Circulation* **117**, 915-922 (2008).
7. Cai, W., Guzman, R., et al. *Stroke* **40**, 270-277 (2009).
8. Cai, W., Rao, J., Gambhir, S.S., Chen, X. *Mol. Cancer Ther.* **5**, 2624-2633 (2006).

## Development of an Europium(III) DOTA-based Luminescence Assay for Detection of Ligand-Receptor Interactions

Channa R. De Silva,<sup>1</sup> Josef Vagner,<sup>2</sup> Ronald Lynch,<sup>2,3</sup>  
Robert J. Gillies,<sup>4</sup> and Victor J. Hruby<sup>1</sup>

<sup>1</sup>The Dept. of Chemistry, The University of Arizona, Tucson, AZ 85721, U.S.A.; <sup>2</sup>Bio5, The University of Arizona, Tucson, AZ 85721, U.S.A.; <sup>3</sup>The Dept. of Physiology, The University of Arizona, Tucson, AZ 85721, U.S.A.; and <sup>4</sup>H. Lee Moffitt Center & Research Institute, Tampa, FL 33612, U.S.A.

### Introduction

Lanthanide-based luminescent ligand binding assays are superior to traditional radiolabel assays due to improved sensitivity and affordability in high throughput screening while eliminating the use of radioactivity [1]. Accordingly, dissociation enhanced lanthanide fluoroimmunoassay (DELFA) technology is rapidly emerging as a bioanalytical tool using Eu(III)-coordinated chelators such as DTPA (diethylenetriaminepentaacetic acid) and DTTA (diethylenetriaminetetraacetic acid) linked to peptides targeted towards a specific cell surface receptor. In DELFA assays, a ligand is labeled with a lanthanide(III) ion [such as Eu(III) or Tb(III)] that is competed off with screened ligand or directly used in saturation binding assays [2,3]. The amount of specifically bound lanthanide-labeled ligand is then analyzed by adding an "enhancement solution" which is capable of completely releasing Eu(III) ions from their non-photoactive chelator and rearranging them into highly luminescent coordination complexes. This process enhances the lanthanide-based luminescence by up to 10<sup>7</sup>-fold [4]. Despite the widespread usage, DOTA (1,4,7,10-tetraaza-1,4,7,10-tetrakis(carboxymethyl)-cyclododecane) and its derivatives offer the highest thermodynamic and kinetic stability with a selection of metal ions, and therefore have potential for implementation with a wide range of *in vivo* imaging applications. However, their application for these purposes has been limited due to the incomplete release of lanthanide(III) ions under standard DELFA. Here we report our preliminary results towards developing an improved DELFA assay for whole cell ligand-receptor binding studies, using lanthanide(III)-DOTA labeled ligands coupled with an acid treatment protocol.

### Results and Discussion

The requirement of an acid treatment procedure for the complete release of lanthanide(III) ions from DOTA-labeled ligands is shown in Figure 1. Release of Eu(III) ions depends on the acid strength of HCl as evidenced by Figure 1A. Without the acid treatment, we were only able to detect ~ 4 % of the total Eu(III) ions. In contrast, a complete release of Eu(III) ions from the DOTA chelate was observed using HCl acid (2M) treatment (Figure 1B). Complementary experiments performed with or without acid treatment detected the same number of Eu(III) ions in DTPA-labeled ligands. The modified DELFA protocol consists of additional acidification and neutralization steps prior to the addition of the enhancement solution. The conditions (concentrations, time, and temperature) were optimized for the complete release of Eu(III) ions. The optimized assay conditions, namely the volume of 2.0 M HCl and the incubation time with the acid are 50  $\mu$ L and 2 hours, respectively.

We evaluated the binding of NDP- $\alpha$ -MSH ([Nle<sup>4</sup>, D-Phe<sup>7</sup>]- $\alpha$ -melanocyte stimulating hormone) to Hek293 cells overexpressing the hMC4R (human melanocortin-4 receptors) as a model system using Eu(III)-DOTA labeled ligands [2]. DTPA labeled compounds were used for comparison with the traditional DELFA. The ligands were synthesized manually as previously described using N<sup>α</sup>-Fmoc/tBu solid-phase peptide synthesis strategy and standard DIC/HOBt or DIEA/HBTU activations on Rink amide Tentagel resin (0.23 mmol/g). A semi-rigid linker (PEG9, 8-amino-3,6-dioxaoctanoic acid) was introduced to the amino terminal of the NDP- $\alpha$ -MSH before the attachment of lanthanide(III) chelators (DOTA and DTPA) as shown in Figure 2. Attachment of the PEG9 linker to the  $\alpha$ -amino terminal of serine was carried out using DIEA/HBTU activation. A previously reported procedure was adapted for the attachment of DTPA to PEG9-NDP- $\alpha$ -MSH wherein an *in situ* di-HOBt ester of DTPA was formed before the coupling with the free amino group of the resin-bound ligands [2]. Activated DOTA-NHS

(DOTA mono N-hydroxysuccinimide ester) ester was used for the coupling of DOTA chelator to the PEG9-NDP- $\alpha$ -MSH. Chelator-attached ligands were cleaved off the resin, purified by HPLC, and characterized by high-resolution mass spectroscopy. Eu(III) labeling was performed under pH=8 buffer conditions in the solution phase [2].

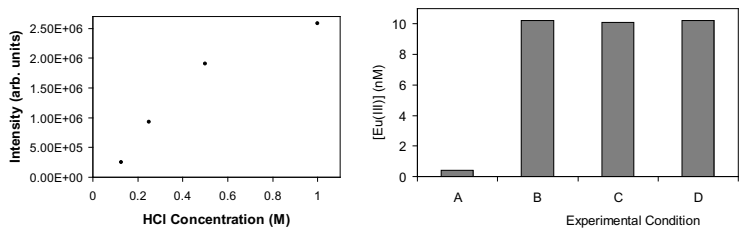


Fig. 1. (A) Eu(III) ion release kinetics of Eu(III)-DOTA-PEG9-NDP- $\alpha$ -MSH (HCl acid strength dependency) (B) Measured Eu(III) ion concentrations of Eu(III)-DOTA labeled NDP- $\alpha$ -MSH with no HCl (A) and with 2.0 M HCl (B) and Eu(III)-DTPA labeled NDP- $\alpha$ -MSH with no HCl (C) and with 2.0 M HCl (D) 10 nM ligand solutions predetermined using tryptophan assay were used for the analysis.

Table 1. Ligand-receptor saturation binding data

Compound	$K_d$ (nM)
Eu(III)-DOTA-PEG9- NDP- $\alpha$ -MSH	49
Eu(III)-DTPA-PEG9- NDP- $\alpha$ -MSH	38

DOTA chelator with NDP- $\alpha$ -MSH did not significantly alter its binding affinity to Hek293 cells overexpressing the hMC4R compared to that of Eu(III)-DTPA (Table 1). The use of time resolved luminescent measurements of Eu(III) improves the signal-to-noise ratio allowing the detection of amoles of Eu(III). In summary, we have optimized the conditions for the detection of total Eu(III) ions coordinated to a highly stable DOTA chelator linked to NDP- $\alpha$ -MSH using an acid treatment protocol. The developed functional DELFIA can be used in a whole cell binding assay using 96-well plates and provides a platform to explore novel ligands labeled with highly stable lanthanide chelators such as DOTA for evaluating ligand-receptor interactions.

The saturation binding experiments were carried out using Eu(III)-DTPA-PEG9-NDP- $\alpha$ -MSH and Eu(III)-DOTA-PEG9-NDP- $\alpha$ -MSH ligands. Non-specific binding was determined in the presence of 100  $\mu$ M NDP- $\alpha$ -MSH.  $K_d$  values of both Eu(III)-DTPA and Eu(III)-DOTA-labeled ligands were similar verifying that the presence of the Eu(III)-

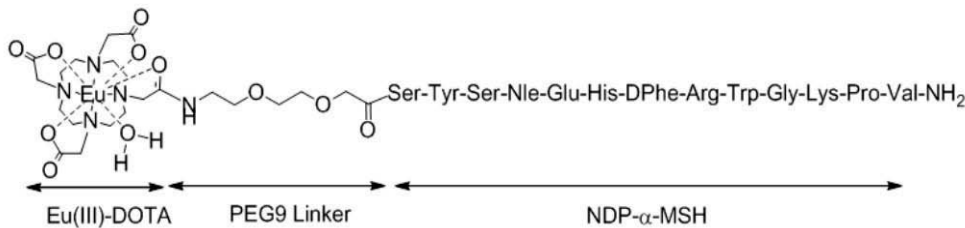


Fig. 2. Structures of the Eu(III)-DOTA labeled ligands used in this study.

Acknowledgments

This research was supported by grants from the U. S. Public Health Service, NIH/National Cancer Institute (RO1-CA123547 and RO1-CA97360) and the Arizona Biomedical Research Commission (# 0707).

References

1. Handl, H.L., Gillies, R.J. *Life Sciences* **77**, 361-371 (2005).  
2. Handl, H.L., Vagner, J., Yamamura, H.I., Hruby, V.J., Gillies, R.J. *Anal. Biochem.* **330**, 242-250 (2004).  
3. Hemmila, I., Dakubu, S., Mikkala, V.M., Siitari, H., Lovgren, T. *Anal. Biochem.* **137**, 335-343 (1984).  
4. Nishioka, T., Fukui, K., Matsumoto, K. *Handbook on the Physics and Chemistry of Rare Earths* **37**, 171-216 (2007).

## Specific Targeting of Cells by Heteromultivalent Ligands and its Implications in Cancer

Jatinder S. Josan,<sup>1</sup> Heather L. Handl,<sup>2</sup> Ronald M. Lynch,<sup>4</sup> Josef Vagner,<sup>1,4</sup>  
 Robert J. Gillies,<sup>2,3,4</sup> and Victor J. Hruby<sup>1,2,4</sup>

<sup>1</sup>Departments of Chemistry, <sup>2</sup>Biochemistry & Molecular Biophysics, <sup>3</sup>Radiology, and <sup>4</sup>BIO5 Institute, University of Arizona, Tucson, AZ 85721, U.S.A.

### Introduction

Current cancer therapies involve targeting either differential metabolism, especially nucleic acid biosynthesis pathways, or overexpressed specific gene products. We propose an alternative approach – to specifically target combinations of cell-surface receptors using heteromultivalent ligands (htMVLs). We envision that a combination of cell-surface proteins, which is expressed on a cancer cell but not on a normal cell, could be targeted with htMVLs displaying cognate binding motifs of moderate to weak affinities. These constructs should bind with high avidity and specificity to cancer populations *in vivo* [1,2]. As a proof-of-concept, we have synthesized series of heterobivalent ligands (htBVLs) composed of human melanocortin-4 receptor (hMC4R) and cholecystokinin-2 receptor (CCK-2R) ligand motifs (Figure 1). These motifs were connected *via* semi-rigid poly(Pro-Gly) linkers flanked by flexible polyethylene glycol based PEGO chains.

### Results and Discussion

Heterobivalent ligands were synthesized using Fmoc/*t*Bu chemistry on Tentagel Rink amide resin using parallel solid-phase peptide synthesis (SPPS) approach (Fig. 2) [3]. The residues for the first ligand (i.e., CCK-6) were coupled on the resin, followed by coupling of a PEGO linker as described previously [3,4]. Subsequently, proline and glycine residues were added, as many as were needed, to build the poly(Pro-Gly) linker, followed by a second PEGO assembly. Finally, the residues for the second ligand (i.e., MSH-7) were coupled, and the N-terminal capped. Following the completion of synthesis, compounds were cleaved from the resin with TFA-scavengers (82.5% CF<sub>3</sub>COOH, 5% H<sub>2</sub>O, 5% *i*Pr<sub>3</sub>SiH, 5% CH<sub>3</sub>-S-C<sub>6</sub>H<sub>5</sub>, 2.5% C<sub>2</sub>H<sub>5</sub>-S-S-C<sub>2</sub>H<sub>5</sub>), purified by C<sub>18</sub> RP-HPLC, and characterized by ESI-MS and/or MALDI-TOF and/or FT-ICR.

For labeling of heterobivalent ligands with fluorescent and other tags, Fmoc-Lys(Mtt)-OH (Mtt: methyltrityl) was introduced in the linker region of **1**. The tag was introduced in between the poly(Pro-Gly) and the PEGO linker region in order to provide adequate spacing between the labels and ligands. The choice of Mtt allows on-resin coupling of tags (following Mtt deprotection with 5% TFA, 5% *i*Pr<sub>3</sub>Si in CH<sub>2</sub>Cl<sub>2</sub>), or in-solution coupling following peptide cleavage from the resin. Thus, Cy5 was coupled in solution to the purified peptide (bearing a

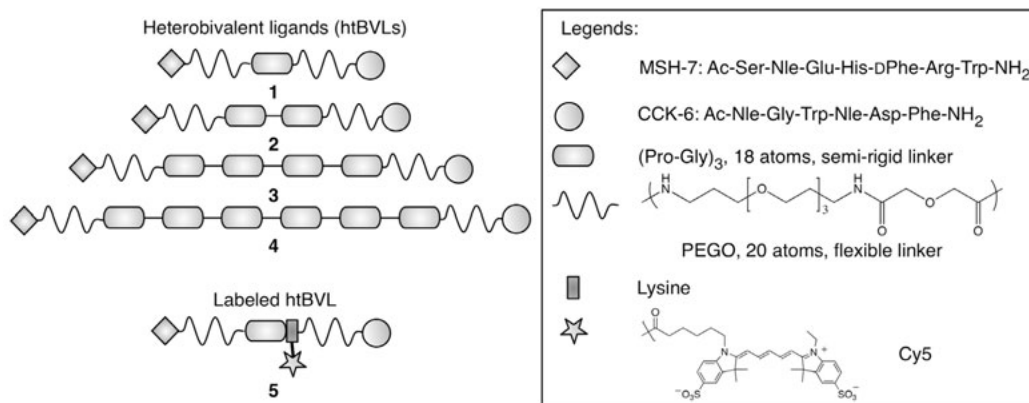


Fig. 1. Heterobivalent ligands (htBVLs) of melanocortin receptor (hMC4R) and cholecystokinin receptor (CCK-2R). The Cy5 label was introduced in the linker region of **1** between PEGO and Pro-Gly region.

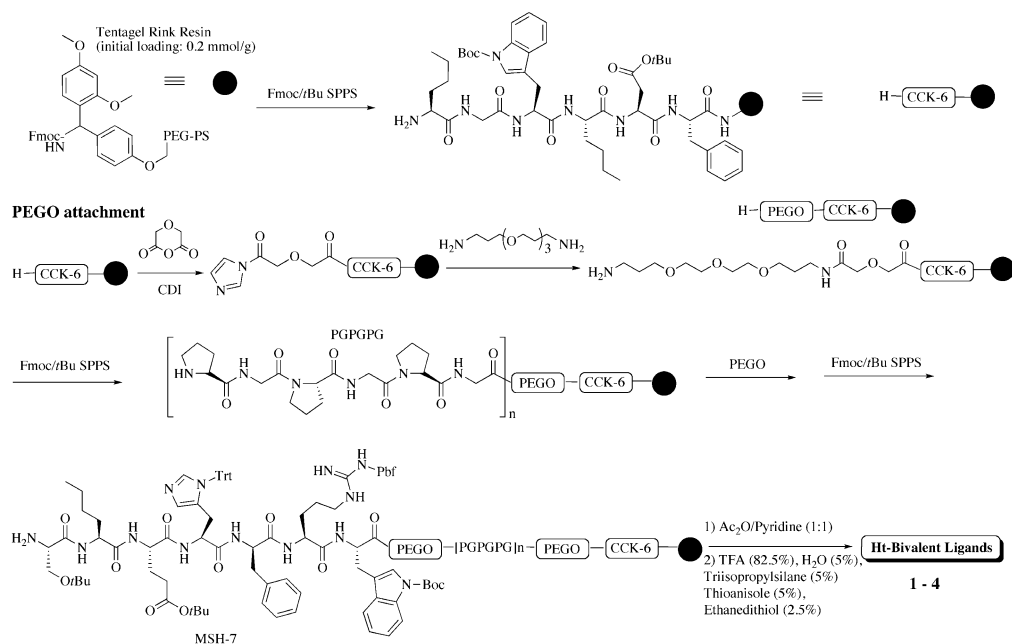


Fig. 2. Synthesis of MSH-CCK heterobivalent ligands. Fmoc/tBu SPPS procedure: 3 eq. each of Fmoc-amino acid, *Cl*-HOBt, DIC for amino acid couplings; and 20% Piperidine/DMF for Fmoc deprotection. The PEGO linker can be introduced by reacting the free amino groups with diglycolic anhydride (10 eq.) in DMF, followed by activation with carbonyldiimidazole (CDI, 20 eq.) in DMF for 30 min and substitution with diamine 4,7,10-trioxo-1,13-tridecanediamine (20eq) in DMF for 30 min. *n* is 1, 2, 4 or 6.

free amine side chain on lysine) with 1.1 eq. of Cy5-N-hydroxysuccinimide ester (Amersham Biosciences, Piscataway, NJ) in DMSO. The coupling was monitored with analytical HPLC and additional aliquots were added until reaction completion. The final product was isolated with solid-phase extraction (with  $\text{C}_{18}$  Sep-Pak<sup>TM</sup> Vac RC cartridges, Waters, Milford, MA).

The heterobivalent constructs were evaluated for bivalent binding in HEK293 cells lines that co-expressed hMC4R and CCK-2R. Monovalent binding was tested on cells lines that expressed only one of these receptors [5]. These compounds were shown to have enhanced bivalent binding affinities against cells expressing both receptors when compared to cells expressing only one of these receptors. For example, compound **1** exhibited a monovalent  $\text{IC}_{50}$  of 150 nM and a bivalent  $\text{IC}_{50}$  of 6.3 nM for CCK-6 binding. Thus, the construct exhibited a roughly 25-fold enhancement in binding affinity when targeted to a two-receptor combination. Clearly, this level of enhancement results from crosslinking of heterologous receptors. It is our contention that a high degree of specificity could be achieved in the context of this heterovalent affinity

Table 1. Binding data of htBVLs tested for crosslinking in HEK293/hMC4R/CCK-2R

No.	Ac-MSH(7)-Linker-CCK(6)-NH <sub>2</sub>	IC <sub>50</sub> (nM) of CCK-6 <sup>a</sup>		$\beta^*$	IC <sub>50</sub> (nM) of MSH-7 <sup>a</sup>		$\beta^*$
		CCK-2R <sup>b</sup>	Dual expression <sup>d</sup>		hMC4R <sup>c</sup>	Dual expression <sup>d</sup>	
1	-PEGO-[PG] <sub>3</sub> -PEGO-	150 (120-180)	6.3 (5.0-7.9)	24	390 (89-1700)	1600 (560-4700)	0.2
2	-PEGO-[PG] <sub>6</sub> -PEGO-	72 (56-94)	20 (15-26)	4	230 (160-340)	21 (17-27)	11
3	-PEGO-[PG] <sub>12</sub> -PEGO-	130 (110-150)	38 (29-50)	3	10 (6.7-16)	32 (25-39)	0.3
4	-PEGO-[PG] <sub>18</sub> -PEGO-	160 (130-200)	93 (78-110)	2	35 (26-47)	28 (21-40)	1.3

<sup>a</sup>IC<sub>50</sub> concentration in nM from at least 4 independent experiments reported. Values in parentheses represent the 95% confidence intervals of the IC<sub>50</sub> values; Binding data from competition with <sup>b</sup>Eu-DTPA-CCK-8 (unsulfated) against CCK-2R expressing cells, <sup>c</sup>Eu-DTPA-NDP- $\alpha$ -MSH against hMC4R expressing cells, and with either <sup>d</sup>Eu-DTPA-CCK-8 (unsulfated) or Eu-DTPA-NDP- $\alpha$ -MSH against cells expressing both CCK-2R and hMC4R. IC<sub>50</sub>'s of Ac-MSH(7)-NH<sub>2</sub> and Ac-CCK(6)-NH<sub>2</sub> are 39  $\pm$  4 nM and 26  $\pm$  4 nM, respectively.  $\beta^*$  (fold increase) is ratio of IC<sub>50</sub>'s of single- and dual-expressing cell lines.

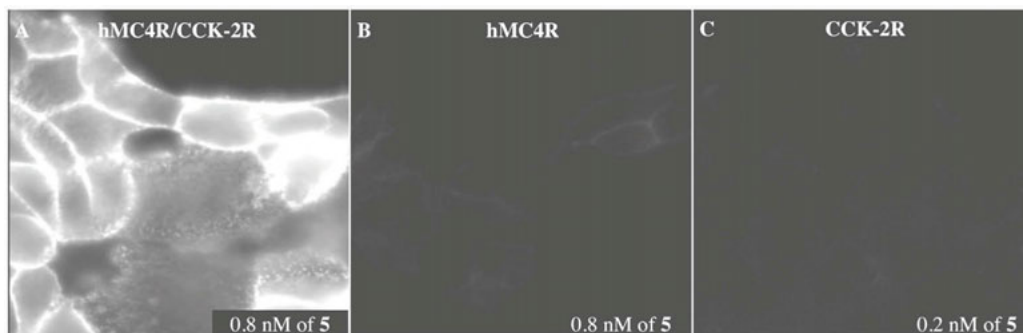


Fig. 3. *In vitro* imaging of cells expressing single or both complementary receptors as a proof-of-hypothesis of heteromultivalency-based enhanced targeting specificity. (A) Surface labeling of cells expressing both hMC4R and CCK-2R with Cy5 labeled htBVL **5** at a conc. of 0.8 nM each. (B&C) Surface labeling of cells expressing either hMC4R or CCK-2R only with Cy5 labeled htBVL **5** at a conc. of 0.8 nM and 0.2 nM, respectively. The images were acquired after 3 minutes of incubation with htBVL **5**, followed by washing the cells.

enhancement. This was validated with *in vitro* imaging of htBVL **5** tested for its binding avidity to cells expressing either one (i.e., hMC4R or CCK-2R only), or both receptors (Figure 3). High fluorescence intensity even at low nanomolar concentrations was achieved when the Cy5-htBVL was allowed to bind to both receptors simultaneously, highlighting its high binding avidity. Only a faint outline of monovalent binding to singly-expressing cells was observed at this ligand concentration and fluorescence detection settings (Figure 3B and C). Further, the data illustrates the remarkable gain in specificity in differentiating cell-surfaces with two-receptor combination *vs* single receptor target. Thus, this approach provides a venue for enhanced targeting specificity even when one of the receptors is expressed in normal tissues as well.

We envision that in the near future when a patient tissue expression profile would be easily identifiable, it will become feasible to tailor heteromultivalent ligands to different cancer populations (with defined receptor combinations). Further, good receptor combinations could become available when good individual targets are not (e.g., ~ 2.9 million two-receptor combinations from ~ 2408 known cell-surface proteins). Thus, a high degree of specificity in multivalent targeting coupled with the ability to identify unique receptor combinations will provide a novel and revolutionary platform technology for targeted diagnostics and therapeutics. The work presented here is a step towards this goal of personal medicine in cancer.

## Acknowledgments

The work was supported by grants R33 CA95944 and R01 CA97360 from the National Cancer Institute.

## References

1. Gillies, R.J., Hruby, V.J. *Expert Opin. Ther. Targets* **7**, 137-139 (2003).
2. Handl, H.L., Sankaranarayanan, R., Josan, J.S., Vagner, J., Mash, E.A., Gillies, R.J., Hruby, V.J. *Bioconjugate Chem.* **18**, 1101-1109 (2007).
3. Josan, J.S., Vagner, J., Handl, H.L., Sankaranarayanan, R., Gillies, R.J., Hruby, V.J. *Int. J. Pept. Res. Ther.* **14**, 293-300 (2008).
4. Vagner, J., Handl, H.L., Gillies, R.J., Hruby, V.J. *Bioorg. Med. Chem. Lett.* **14**, 211-215 (2004).
5. Vagner, J., Xu, L., Handl, H.L., Josan, J.S., Morse, D.L., Mash, E.A., Gillies, R.J., Hruby, V.J. *Angew. Chem. Int. Ed. Engl.* **47**, 1685-1688 (2008).

## LHRH-II Analog Design: Structure-Function Studies Toward the Development of a LHRH-II Based Radiotherapeutic Agent

Palaniappa Nanjappan, Sudha Khurana, Karen E. Linder,  
Natarajan Raju, Adrian D. Nunn, Edmund R. Marinelli,  
Bitha Narayanan, and Rolf E. Swenson

Bracco Research U.S.A., 305 College Road East, Princeton, NJ 08540, U.S.A.

### Introduction

The success of treating neuroendocrine tumors with somatostatin binding peptides linked to a  $^{177}\text{Lu}$ -chelate, such as [ $^{177}\text{Lu}$ -DOTA<sup>0</sup>,Tyr<sup>3</sup>]Octreotate [1] has stimulated the search for other G-coupled receptors appropriate for radiotherapy [2]. The observation of extrapituitary LHRH receptors on cancer cells has led to the investigation of this receptor. There is evidence that cancer cells may have abundant low affinity LHRH binding-sites as well as much fewer high affinity binding-sites [3]. LHRH-I and its analogs have been studied more extensively than LHRH-II. Not surprisingly, LHRH-I analogs have been conjugated to cytotoxic drugs (e.g. Doxorubicin) particularly at position-6 for targeted chemotherapy of cancer. In a recent report [4], the *in vitro* binding of LHRH-I analogs derivatized on Dlys<sup>6</sup> with [ $^{68}\text{Ga}$ ]DO3A10CM or  $\beta$ -Ala-[ $^{18}\text{F}$ ]FBOA to several tumor lines, including ovarian cancer (EFO-27) cells, were reported. High non-specific binding, low levels of LHRH-I receptor expression *in vitro* and poor uptake in tumors *in vivo* were observed. As the binding affinity and activity of LHRH-II analogs for peripheral sites is reported to be similar or superior to LHRH-I and the anti-proliferative effects of LHRH-II on ovarian cancer cells at various doses (1 nM to 10 mM) are similar to that of LHRH-I, [5] we attempted to prepare radiometal derivatized LHRH-II derivatives, for which little has been reported.

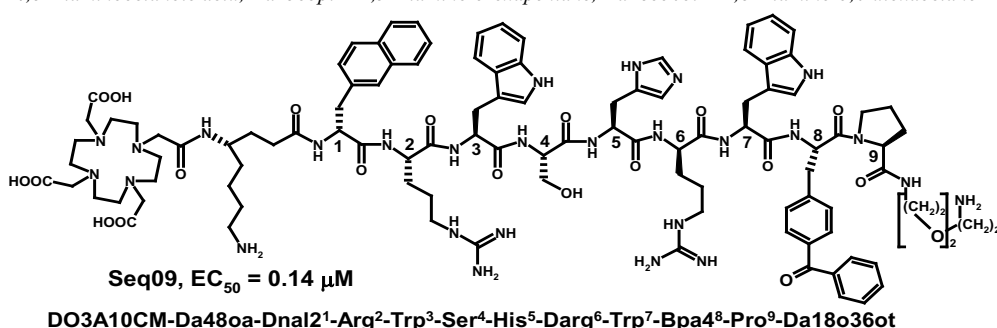
### Results and Discussion

As was found by Schottelius [5] for LHRH-I derivatives, we observed that substitution of the chelate DO3A10CM onto the Dlys<sup>6</sup> of LHRH-II analogs also produced lower affinity binding ligands. As a result, our initial studies focused on the attachment of the chelating agent to the N-terminus of the LHRH-II sequence. We found that the replacement of amino acids such as pyroglutamic acid (pGlu) with sarcosine (Sar) and Tyr with Bpa4 (L-4-Benzoylphenylalanine) yielded surprisingly an analog of LHRH-II, Seq04, with much improved *in vitro* binding affinity,  $\text{EC}_{50} = 0.95 \mu\text{M}$ . Sequences and cell binding results of these constructs in competition with the radioiodinated LHRH, [Darg<sup>6</sup>,  $^{125}\text{I}$ -Tyr<sup>8</sup>,azaGly<sup>10</sup>-LHRH-II] on human ovarian cancer (EFO-27) cells are shown in Table 1. The binding effect was presumably influenced by the known potency enhancing effect of the D-arginine (r, Darg) at the 6 position and an azaglycine (azaG) amide at position 10. These results prompted us to prepare LHRH-II analogs with DO3A10CM on the N-terminus and with various lipophilic and hydrophilic amino acids in the sequence, and molecules that were derivatized at the C-terminus with various alkylamines or oxyalkylamines.  $\text{EC}_{50}$  data were determined and structure-function analysis was performed; the results of the selective best binders ( $\text{EC}_{50} = \sim 0.20 \mu\text{M}$ ) are shown in Table 1. The increase in binding of Seq04 due to the lipophilicity of Bpa4 led us to make a series of LHRH-II analogs with modifications at position 8, using amino acids such as L-Trp, L-Tyrosine, D/L-1/2-Naphthylalanine, L-Diphenylalanine and L-Biphenylalanine with varied lipophilicity and in some cases bearing basic groups. Among them, sequences with Bpa4 at position 8 showed better binding potency (usually 10X better), indicating the important role played by the linear aromatic hydrophobic moiety and the positive influence of a group like C=O. In our initial studies, a peptide with D-2-naphthylalanine (Dnal2) and L-Arginine (R) at position 1 and 2 respectively (Seq05) showed  $\text{EC}_{50} = 0.33 \mu\text{M}$ . That led us to synthesize several LHRH derivatives incorporating amino acids with varied lipophilicity at position 1 in combination with hydrophilic amino acids at position 2. This study provided LHRH analogs, Seq05-Seq08 with increased binding potency  $\text{EC}_{50} = \sim 0.25 \mu\text{M}$ . These observations led us to the conclusion that basic lipophilic amino acids at positions 1 and 2, would yield LHRH-II good binders with increased biological potency. From the binding data of compounds, Seq07-Seq09, it appears

Table 1. LHRH-II Analogs with increased in vitro binding potency

Seq #	Chelating Group	Linker	Sequence (AA <sup>1</sup> to AA <sup>9</sup> )	AA <sup>10</sup>	EC <sub>50</sub> $\mu$ M
LHRH-I			pGlu <sup>1</sup> -H <sup>2</sup> -W <sup>3</sup> -S <sup>4</sup> -Y <sup>5</sup> -G <sup>6</sup> -L <sup>7</sup> -R <sup>8</sup> -P <sup>9</sup>	G-NH <sub>2</sub>	-
LHRH-II			pGlu <sup>1</sup> -H <sup>2</sup> -W <sup>3</sup> -S <sup>4</sup> -H <sup>5</sup> -G <sup>6</sup> -W <sup>7</sup> -Y <sup>8</sup> -P <sup>9</sup>	G-NH <sub>2</sub>	-
Seq01	-		pGlu <sup>1</sup> -H <sup>2</sup> -W <sup>3</sup> -S <sup>4</sup> -H <sup>5</sup> -Darg <sup>6</sup> -W <sup>7</sup> -Y <sup>8</sup> -P <sup>9</sup>	azaG-NH <sub>2</sub>	0.74
Seq02	-		Sar <sup>1</sup> -H <sup>2</sup> -W <sup>3</sup> -S <sup>4</sup> -H <sup>5</sup> -Darg <sup>6</sup> -W <sup>7</sup> -Y <sup>8</sup> -P <sup>9</sup>	azaG-NH <sub>2</sub>	0.25
Seq03	DO3A10CM		Sar <sup>1</sup> -H <sup>2</sup> -W <sup>3</sup> -S <sup>4</sup> -H <sup>5</sup> -Darg <sup>6</sup> -W <sup>7</sup> -Y <sup>8</sup> -P <sup>9</sup>	azaG-NH <sub>2</sub>	10.00
Seq04	DO3A10CM		Sar <sup>1</sup> -H <sup>2</sup> -W <sup>3</sup> -S <sup>4</sup> -H <sup>5</sup> -Darg <sup>6</sup> -W <sup>7</sup> -Bpa4 <sup>8</sup> -P <sup>9</sup>	azaG-NH <sub>2</sub>	0.95
Seq05	DO3A10CM		Dnal2 <sup>1</sup> -R <sup>2</sup> -W <sup>3</sup> -S <sup>4</sup> -H <sup>5</sup> -Darg <sup>6</sup> -W <sup>7</sup> -Bpa4 <sup>8</sup> -P <sup>9</sup>	azaG-NH <sub>2</sub>	0.33
Seq06	DO3A10CM	-	Bip <sup>1</sup> -R <sup>2</sup> -W <sup>3</sup> -S <sup>4</sup> -H <sup>5</sup> -Darg <sup>6</sup> -W <sup>7</sup> -Bpa4 <sup>8</sup> -P <sup>9</sup>	azaG-NH <sub>2</sub>	0.28
Seq07	DO3A10CM		Dnal2 <sup>1</sup> -R <sup>2</sup> -W <sup>3</sup> -S <sup>4</sup> -H <sup>5</sup> -Darg <sup>6</sup> -W <sup>7</sup> -Bpa4 <sup>8</sup> -P <sup>9</sup>	G-R-NH <sub>2</sub>	0.24
Seq08	DO3A10CM	-	Dnal2 <sup>1</sup> -R <sup>2</sup> -W <sup>3</sup> -S <sup>4</sup> -H <sup>5</sup> -Darg <sup>6</sup> -W <sup>7</sup> -Bpa4 <sup>8</sup> -P <sup>9</sup>	Da15o3pt	0.24
Seq09	DO3A10CM	Da48oa	Dnal2 <sup>1</sup> -R <sup>2</sup> -W <sup>3</sup> -S <sup>4</sup> -H <sup>5</sup> -Darg <sup>6</sup> -W <sup>7</sup> -Bpa4 <sup>8</sup> -P <sup>9</sup>	Da18o36ot	0.14

Darg = D-Arginine, DNa12 = D-2-Naphthylalanine, Bip = L-Biphenylalanine, Bpa4 = L-4-Benzoylphenylalanine, Da48oa = L-4,8-Diaminooctanoic acid, Da15o3pt = 1,5-Diamino-3-oxapentane, Da18o36ot = 1,8-Diamino-3,6-dioxaoctane



that the terminal azaglycine amide is not essential for high potency and the total chain length and the basic character of the substitution on the amide of Pro<sup>9</sup> play an important role in the binding affinity. Based on this observation, the introduction of L-4,8-diaminooctanoic acid (Da48oa) as a linker between AA<sup>1</sup> and DO3A10CM and 1,8-diamino-3,6-dioxaoctane (Da18o36ot) at the C-terminus resulted in Seq09, an agonist with higher *in vitro* potency, EC<sub>50</sub> = 0.14  $\mu$ M.

We have generated N-terminal DO3A10CM analogs of LHRH-II that exhibit enhanced binding affinity towards human ovarian tumor cells as a result of various amino acid substitutions, specifically oxyalkylamine as a C-terminus amide of Pro at position 9, Darg at position 6, Bpa4 at position 8 and a lipophilic amino acid with or without a basic moiety like guanidine at N-terminal positions. Though our results further highlight the general low affinity nature of the cancer cell LHRH binding sites, this structure-function relationship study opens a new route to LHRH analogs suggesting that fine tuning of the functional and conformational properties of new peptides bearing unusual amino acids at key positions could lead to analogs bearing not only enhanced binding affinity towards LHRH receptors but also improved inhibitory effects on cancer cell proliferation.

## References

1. Kwekkeboom, D.J., de Herder W., Kam, B.L., van Eijck, C.H., van Essen, M., Kooij, P.P., Feelders, R.A., van Aken, M.O., Krenning, E.P. *J. Clin. Oncol.* **26**, 2124-2128 (2008).
2. Reubi, J.C. *Endocrine Rev.* **24**, 389-427 (2003).
3. a) Ravenna, L., Salvatori, L., Morrone, S., Lubrano, C., Cardillo, M.R., Sciarra, F., Frati, L., Di Silverio, F., Petrangeli, E.J. *Androl.* **21**, 549-554 (2000). b) Volker, P., Gründker, C., Schmidt, O., Schulz, K.D., Emons, G. *Am. J. Obstet. Gynecol.* **186**, 171-179 (2002).
4. Schottelius, M., Berger, S., Poethko, T., Schwaiger, M., Wester, H-J. *Bioconjugate Chem.* **19**, 1256-1268 (2008).
5. Fister, S., Günthert, A.R., Emons, G., Gründker, C. *Cancer Res.* **67**, 1750-1756 (2007).



## Heterobivalent Ligands Crosslink Multiple Receptors for Targeting of Pancreatic $\beta$ -cell to Monitor $\beta$ -cell Mass

Josef Vagner,<sup>1</sup> Woo Jin Chung,<sup>1</sup> Craig S. Weber,<sup>2</sup> Sean W. Limesand,<sup>3</sup>  
 Channa R. De Silva,<sup>4</sup> and Ronald Lynch<sup>2</sup>

<sup>1</sup>Bio5, The University of Arizona, Tucson, AZ 85721, U.S.A.; <sup>2</sup>The Dept. of Physiology, The University of Arizona, Tucson, AZ 85721, U.S.A.; <sup>3</sup>Dept. of Animal Sciences, The University of Arizona, Tucson, AZ 85721, U.S.A.; and <sup>4</sup>The Dept. of Chemistry, The University of Arizona, Tucson, AZ 85721, U.S.A.

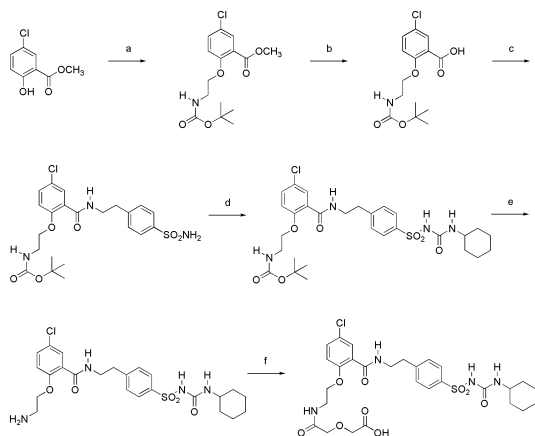
### Introduction

Dysfunction and loss of pancreatic  $\beta$ -cells is the primary cause of Diabetes, and is observed during the immunological destruction of  $\beta$ -cells in insulin dependent (Type 1) Diabetes Mellitus. The ability to monitor changes in  $\beta$ -cell mass (BCM) and function is critical to analyzing the developing pathology, as well as the efficacy of treatments. Specific ligands targeting single-receptors have been limited by poor discrimination between  $\beta$ -cells and other cell types within the imaging field such as non-endocrine pancreatic cells and hepatocytes. Development of approaches to improve specificity for  $\beta$ -cells is required to facilitate these in vivo analyses.

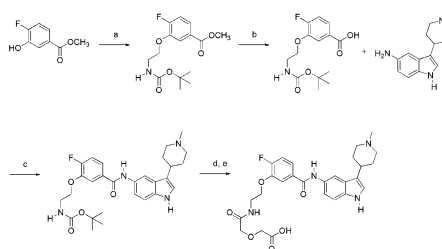
### Results and Discussion

Recently, we demonstrated that multiple surface receptors can be cross-linked using a synthetic heterobivalent ligand against the hMC4R, CCK2R and  $\delta$ -opioid receptors expressed at high levels ( $> 10^6$  copies per cell) in model systems. Multivalent interactions were characterized by enhanced affinities (avidities) and enhanced specificities 48-80 fold when binding was compared to cells with only one of the targeted receptors [1,2]. The relevance of multivalent ligands as well as theoretical definitions of interactions (avidity, cooperativity, etc.) is well documented [3] By combining multiple specific ligands into a single molecule, using suitable linkers, it is possible to create compounds which will selectively bind to cells expressing only the complementary set of receptors. The structure of the linker plays an important role in the orientation of the pharmacophores and must be chosen with care. The ideal linker should not interfere with the binding affinities of the ligand to the receptor, and preferably should be both

hydrophilic and small. Our previous studies indicated that short flexible ethylene glycol (PEGO) spacers in combination with semirigid Pro-Gly (PG) repeats were optimal as linkers for bivalent ligands [3,4]. In addition, modeling of GPCR (G-protein coupled receptor) dimers estimated the distance



**Scheme 1.** Synthesis of Glibenclamide carboxy analog. (a) Boc-glycinol,  $PPh_3$ , DEAD, 0 °C; (b) 2N NaOH; (c) (i) EtOCOCl, NMM, 0 °C, (ii) 4-(2-aminoethyl) benzenesulfonamide; (d) cyclohexylisocyanate, CuI; (e) TFA (f) diglycolic anhydride.



**Scheme 2.** Synthesis of 5-HT<sub>1F</sub> ligand. (a) Boc-glycinol,  $PPh_3$ , DEAD, 0 °C to rt; (b) 2N NaOH; (c) (i) EtOCOCl, NMM, 0 °C, (ii) aminoindole, DMF, 0 °C to rt; (d) TFA; (e) diglycolic anhydride.

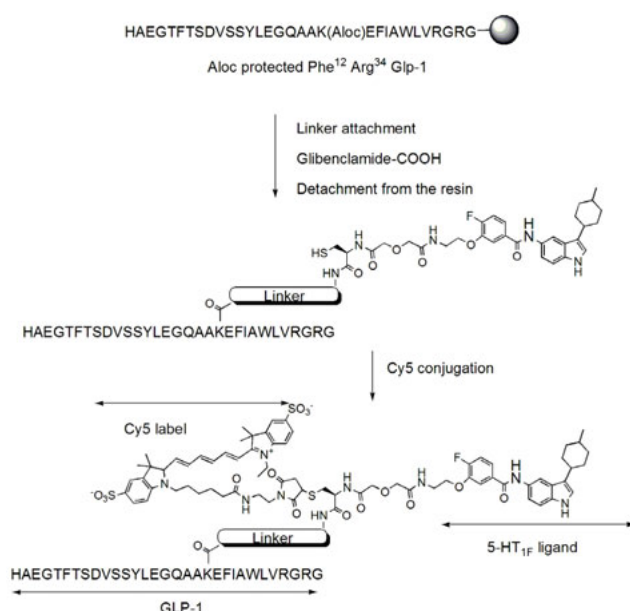


Fig. 1. Synthesis of GLP-1/ 5-HT<sub>1F</sub> heterovalent ligand.

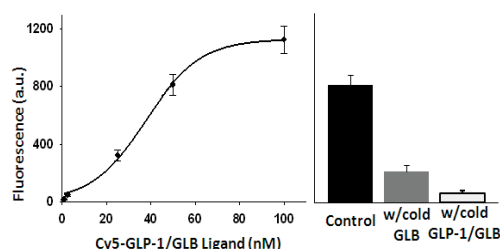


Fig. 2. Evaluation of GLP-1/GLB divalent binding to BTC3 cells. A. Saturation binding curve for the divalent GLP-1/GLB: 3 min. after the addition of ligand, cells were washed to decrease signal from the media. Binding measured at 7 min indicates  $K_m$  of ~30 nM. B. Cells were incubated in the presence of 50 nM Cy5-labeled ligand alone or in the presence of either saturating cold ligand (no Cy5 label) dimer or Glb alone (highest affinity monomer). Although the cold dimer was completely effective in blocking binding, saturating monomer had only partial inhibitory effect.

## Acknowledgments

This research was supported by grants from the NIH/National Cancer Institute (CA 123547 and CA97360), The Juvenile Diabetes Research Foundation and Arizona Biomedical Research Commission.

## References

1. Handl, H.L., et al. *Analytical Biochemistry* **330**, 242-250 (2004).
2. Handl, H.L., Gillies, R.J. *Life Sciences* **77**, 361-371 (2005).
3. Josan, J.S., et al. *Int. J. Pept. Res. Ther.* **14**, 293-300 (2008).
4. Vagner J., Xu L., Handl H.L., Josan J.S., Morse D.L., Mash E.A., Gillies R.J., Hruby V.J. *Angewandte Chemie Intl. Ed.* **47**, 1685-1688 (2008).

between two adjacent binding sites to be in the range of 25–50 Å and possibly longer up to 100 Å. Based on our initial findings, we designed multivalent ligand against specific receptors that are expressed on the surface of β-cells; the glucagon like peptide 1 receptor (GLP-1R) the sulfonylurea receptor 1 (SUR1), and the 5-Hydroxytryptamine 1F Receptor (5-HT<sub>1F</sub>R).

For bivalent ligands a semi-rigid linker [poly(Pro-Gly)] which was designed and optimized for this purpose, was used to tether the ligands. Briefly, derivatives of the SUR1 ligand glibenclamide and the 5-HT<sub>1F</sub>R ligand 5-aminoindole suitable for attachment to the bivalent linker were designed so that their binding affinity to their cognate receptors was retained. The synthesis of these analogs is depicted in Scheme 1 and 2. Glibenclamide carboxy-derivative was conjugated to the GLP-1 on solid support via lysine side chain as shown in Figure 1. Similarly, the 5-HT<sub>1F</sub>R ligand 5-aminoindole was attached to the Glp1-resin. Heterovalent dimers GLP-1/Glb and GLP-1/5-HT<sub>1F</sub> were cleaved off the resin, purified by HPLC, and characterized by high-resolution Mass Spec. The linker was modified with orthogonally protected cysteine or lysine for conjugation of Eu<sup>3+</sup>-DOTA or Cy5. Both labeled heterovalent ligands were prepared in high yield and purity.

Saturation binding of a Cy5-labeled heterobivalent GLP-1/SUR1 ligand to βTC3 cells which expresses normal levels of both receptors is shown in Figure 2. Single cell imaging demonstrates that within 10 minutes of incubation, the ligand is capped, and taken from the cell surface (not shown). Our findings indicate that heterovalent ligands may provide an approach for specific targeting, and analysis of β-cells in vivo.

## The Novel Cell Penetrating Peptide NrTP Exquisitely Targets the Nucleolus of Tumor Cells

Gandhi Rádis-Baptista,<sup>1,2</sup> Beatriz G. de la Torre,<sup>1</sup> and David Andreu<sup>1</sup>

<sup>1</sup>Department of Experimental and Health Sciences, Pompeu Fabra University, Barcelona, 08003, Spain;

<sup>2</sup>Institute for Marine Sciences, Federal University of Ceará, Fortaleza, Brazil

### Introduction

Localization sequences are specific signals that sort proteins to precise cellular compartments. Among those, cell-penetrating peptides (CPPs) are natural or synthetic sequences, cationic and amphipathic, capable of translocating eukaryotic membranes, occasionally localizing to the nucleus. Animal venoms, for their part, are a rich source of bioactive peptides that on occasion can be turned into useful drugs. Snakes, scorpions or spiders produce and secrete a valuable diversity of toxins capable of interacting with distinct molecular targets. A limited number of animal toxins is known to translocate the cytoplasmic membrane and localize into distinct cell compartments. One example is crostamine [1], a rattlesnake toxin of 42 amino acids that selectively translocates into cells at specific phases of cell cycle, and localizes to the nucleus. In solution, crostamine adopts an  $\alpha\beta\beta$  fold, stabilized by three disulfide bonds [2], similar to  $\beta$ -defensin 2 and Na<sup>+</sup>-channel scorpion toxin.

### Results and Discussion

Our laboratory has previously used structure-based deconstruction of complex, highly folded peptides to identify minimal traits essential for activity [3] and to design therapeutically useful, size-reduced versions. When applied to crostamine, with the goal of defining minimal motifs for translocation, one particularly interesting result of this type of minimalistic analysis was a peptide where the N-terminal (residues 1-9) and C-terminal (residues 38-42) regions were spliced together [4], with or without an Ahx spacer [YKQCHKKGXKKKGSG, X=Ahx (NrTP1) or nil (NrTP2)]. To explore peptide uptake and targeting, peptides were labeled with rhodamine B and analyzed by time-lapsed confocal microscopy on live HeLa cells (Figure 1). At 15  $\mu$ M, and as early as 15 min, both peptides translocated the membrane and localized to the nucleus, specifically to the nucleolus (Figure 1A), where they bound various stages of nucleolar organization, including pre-mitotic re-associating, self-organizing and cytokinetic nucleoli, as well metaphasic chromosomes. Given this ability to target the nucleolus, NrTP (nucleolar targeting peptides) was chosen as an appropriate acronym for this new family of CPPs.

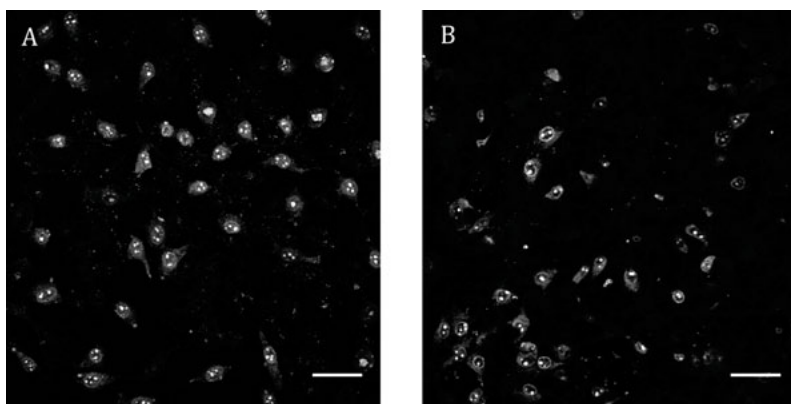


Fig. 1. Penetration and nucleolar localization of NrTP1 (panel A) and its retro isomer, NrTP3 (panel B), into HeLa cells.

The relative chemical similarity between the spliced N- and C-terminal segments, each displaying a KKG triad, prompted us to investigate an inverted version of NrTP1 (GSGKKXGGKKHCQKY, rNrTP1), which was found equally able to translocate into HeLa cells, albeit at concentrations  $>50\text{ }\mu\text{M}$ . Interestingly, an His $\rightarrow$ Ile replacement in this retro sequence resulted in an analogue (GSGKKXGGKKICQKY, NrTP3, Figure 1B) with uptake and localization properties similar to NrTP1 and NrTP2, suggesting that all three peptides share an intrinsic nucleolar homing trait. In all cases, the peptides were found by an MTT assay to be non-toxic to HeLa cells up to  $100\text{ }\mu\text{M}$ . To gain further insight on the process of cell penetration and nucleolar compartmentalization, the all-D version (ykqchkkGGXkkGsG, enantio-NrTP1) was made. When tested on HeLa cells, it failed to translocate, localizing instead on the plasma membrane (images not shown) and thus suggesting that internalization of the all-L peptides NrTP1-3 is mediated by some receptor capable of chiral discrimination. The translocating properties and nucleolar localization of NrTP1-3 in HeLa cells also applied to several other tumor cell lines such as human pancreatic adenocarcinoma (BxPC-3), human ductal mammary gland carcinoma (BT-474 or human colorectal adenocarcinoma (Caco2). Both NrTP1 and its retro version were also shown to penetrate mouse neuroblastoma (N2a) and mouse embryonic fibroblasts (NIH 3T3) cells.

Since nucleolar assembly/disassembly is known to depend on the dynamic traffic of cell cycle-dependent proteins, which in turn might affect the uptake efficiency of CPPs, we used multi-parametric flow cytometry (FC) analysis to investigate the extent, cell preference and cell-cycle dependency of NrTP uptake. NrTP1 was quite efficiently uptaken by HeLa cells at concentrations in the  $6\text{--}50\text{ }\mu\text{M}$  range (Figure 2a-b), and a clear-cut, quantitative distinction between cell populations uptaking (or not) the peptide could be established (Figure 2c-d). In addition, it was found that, of the total of HeLa cells uptaking fluorescently-labeled NrTP1, the fraction of those not alive, i.e., incorporating propidium iodide, was rather small, (Figure 2e-f), in agreement with the MTT assay data. Finally, FC analysis of NrTP1 uptake under conditions where HeLa cells were arrested to defined phases of their cycle confirmed that peptide uptake

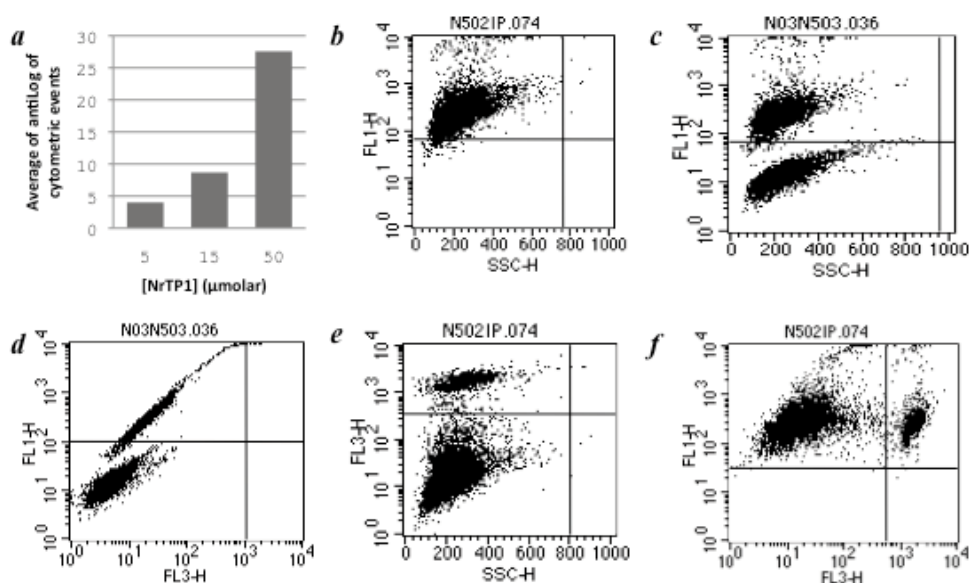


Fig. 2. Flow cytometry analysis of fluorescein (FL)-labeled NrTP1 uptake by HeLa cells. (a): concentration dependence of uptake. In panels (b)-(f), channels FL1-H, FL3-H and SSC-H detect green (FL) and red (propidium iodide, PI) fluorescence, and light scattering, respectively; (b): cells uptaking FL-NrTP1; (c): artificial 1:1 mixture of cells treated-untreated with FL-NrTP1 (upper and lower left, respectively); (d): as (c), with green vs. red detection; (e) PI-uptaking dead cells (upper left) vs. live cells (lower left) (f) live cells uptaking FL-NrTP1 (upper left) vs. dead cells uptaking PI (upper right).

and nucleolar localization were independent of the cell cycle phase (results to be published elsewhere).

Taken together, the above results appear to define a novel CPP family with fairly simple structural features (e.g., allowing sequence reversion) that nonetheless translate into precise nucleolar localization. A detailed biophysical elucidation of the structural features underlying the penetrating mechanism of these new CPPs is under way. Meanwhile, it is worth noting that the nucleolus is one of the most prominent structural and functional elements of the nucleus, with a role conventionally associated to ribosome biogenesis. Recently, additional biological functions mediated by nucleoli have been unveiled, including roles in viral infection, regulation of tumor suppression and oncogenic activities, stress sensing, aging control, and modulation of telomerase activity [5]. We expect that our new NrTPs will find use as probes for investigating protein traffic at the nucleolar level, and/or as carriers of drugs and other cargos into this important subnuclear organelle.

## Acknowledgments

G.R-B. thanks Fundación Carolina (Madrid, Spain) for a visiting scholarship and the Federal University of Pernambuco, Brazil, for a temporary leave from teaching duties. Research supported by the Spanish Ministry of Education and Science (grant BIO2005-07592-CO2-02 to D.A.)

## References

1. Kerkis, A., Kerkis, I., Rádis-Baptista, G., Oliveira, E.B., Vianna-Morgante, A.M., Pereira, L.V., Yamane, T. *FASEB J.* **18**, 1407-1409 (2004).
2. Nicastro, G., Franzoni, L., Chiara, C., Mancin, A.C., Giglio, J.R., Spisni, A. *Eur. J. Biochem.* **270**, 1969-1979 (2003).
3. Vila-Perelló, M., Tognon, S., Sánchez-Vallet, A., García-Olmedo, F., Molina, A., Andreu, D. *J. Med. Chem.* **49**, 448-451 (2006).
4. Rádis-Baptista, G., De la Torre, B.G., Andreu, D. *J. Med. Chem.* **51**, 7041-7044 (2008).
5. Olson, M.O., Dundr, M. *Histochem. Cell Biol.* **123**, 203-216 (2005).

## Quantum Dot-Based Dual-Modality Imaging of Integrin $\alpha_v\beta_3$ Expression on Tumor Vasculature

Weibo Cai<sup>1,2</sup>

<sup>1</sup>*Departments of Radiology and Medical Physics, School of Medicine and Public Health,  
University of Wisconsin - Madison, Madison, WI 53705, U.S.A.;* <sup>2</sup>*University of Wisconsin  
Carbone Cancer Center, Madison, WI 53705, U.S.A.*

### Introduction

Angiogenesis, the formation of new blood vessels from pre-existing blood vessels, is a fundamental process during tumor progression [1]. Molecules regulating angiogenesis include, but are not limited to, growth factor receptors, tyrosine kinase receptors, G-protein-coupled receptors for angiogenesis-modulating proteins, integrins, and matrix metalloproteinases. The focus of this presentation is on one of the most intensively studied angiogenesis-related molecular targets: integrin  $\alpha_v\beta_3$ . All the studies described here use the same tumor model: U87MG human glioblastoma xenograft in athymic nude mice. The tumor cells express high level of human integrin  $\alpha_v\beta_3$ . Further, immunofluorescence staining of the tumor tissue revealed that CD31 and mouse  $\beta_3$  staining co-localizes very well, indicating that the tumor vasculature expresses high level of mouse integrin  $\alpha_v\beta_3$ .

### Results and Discussion

In one early study, near-infrared (NIR) fluorochrome Cy7-labeled RGD peptides were tested for tumor integrin  $\alpha_v\beta_3$  targeting [2]. Mono-, di-, and tetrameric RGD peptides were synthesized and conjugated with Cy7. The tetrameric RGD peptide probe with the highest integrin affinity showed the highest tumor activity accumulation and strongest tumor-to-normal tissue contrast. Since the probes used in this study is quite small ( $< 5$  kDa), they were able to target both human (the tumor cells) and mouse (the tumor vasculature) integrin  $\alpha_v\beta_3$ .

In a subsequent report, Abegrin (MEDI-522 or Vitaxin), a humanized monoclonal antibody against human integrin  $\alpha_v\beta_3$ , was labeled with  $^{64}\text{Cu}$  for positron emission tomography (PET) imaging of integrin  $\alpha_v\beta_3$  [3]. Abegrin was conjugated with a macrocyclic chelating agent, 1,4,7,10-tetraazacyclododecane-1,4,7,10-tetraacetic acid (DOTA), for  $^{64}\text{Cu}$ -labeling. This radiolabeled antibody targeted exclusively the tumor cells and very high tumor uptake was observed at 24 h post-injection of the probe.

Many nanoparticles have been explored for tumor targeting and imaging [4]. One type of the most well-studied nanoparticles for biomedical applications is quantum dots (QDs) [5]. QDs are inorganic fluorescent semiconductor nanoparticles with many desirable optical properties for imaging applications, such as high quantum yields and narrow emission spectra. Specific targeting can be achieved by attaching targeting ligands to the QD surface. However, in vivo targeting and imaging is very challenging because of the relatively large overall size (typically  $> 20$  nm in hydrodynamic diameter) and short circulation half-life of most QD conjugates. One key question for such QD-based probes is whether they are targeting the tumor cells, the tumor vasculature, or both.

We reported the first NIR fluorescence (NIRF) imaging of integrin  $\alpha_v\beta_3$  on tumor vasculature with RGD peptide-conjugated QDs [6]. The QD705-RGD conjugates exhibited high-affinity integrin  $\alpha_v\beta_3$ -specific binding in cell culture and ex vivo. Tumor contrast was observed as early as 20 minutes after QD705-RGD conjugate injection, and the fluorescence intensity in subcutaneous U87MG tumors reached a maximum at 6 h after injection. As with most nanoparticles, the large size of the QD705-RGD conjugates ( $\sim 20$  nm in diameter) prevented efficient extravasation; therefore, the QD705-RGD conjugates mainly targeted integrin  $\alpha_v\beta_3$  on the tumor vasculature instead of the tumor cells, as confirmed by ex vivo immunofluorescence staining.

Among all molecular imaging modalities, no single modality is perfect and sufficient to obtain all of the necessary information for a particular question. For example, it is difficult to accurately quantify fluorescence signal in living subjects with fluorescence imaging alone, particularly in deep tissues; radionuclide-based imaging techniques are very sensitive but have relatively poor spatial resolution. Combination of multiple molecular imaging modalities can

offer synergistic advantages over any modality alone. Multimodality imaging with a small-molecule-based probe is very challenging, sometimes impossible, because of the limited number of conjugation sites and potential interference with its receptor-binding affinity. On the other hand, nanoparticles have large surface areas to which multiple functional moieties can be attached for multimodality molecular imaging [7].

We have developed a QD-based probe for both NIRF and PET imaging of integrin  $\alpha_v\beta_3$  (Figure 1) [8]. QD surface modification with RGD peptides allowed for integrin  $\alpha_v\beta_3$  targeting, and DOTA conjugation enabled PET after  $^{64}\text{Cu}$  labeling (Figure 2). With this dual-modality probe, we quantitatively evaluated its tumor-targeting efficacy, an evaluation that was not possible with NIRF imaging alone [6]. Ex vivo PET and NIRF imaging were also performed on harvested tissues (Figure 3). The trends for signal intensity were similar with both imaging modalities; the liver, spleen, and bone marrow all had very strong signals, and the U87MG tumor had significantly higher uptake than the heart, kidneys, and muscle.

With the quantitative data for in vivo/ex vivo PET imaging, ex vivo NIRF imaging, and tissue homogenate fluorescence, all obtained at 5 h after injection of DOTA-QD-RGD, the tissue-to-muscle ratios were plotted to correlate the quantification results obtained by different measurement methods. Excellent linear correlation was found between the ratios measured by in vivo PET imaging and ex vivo NIRF imaging as well as between the in vivo PET and tissue homogenate fluorescence data (Figure 3). Thus, in vivo PET of the QD-based probe can allow for accurate quantification of the probe distribution. As in the previous study [6], it was also found that the majority of the probe in the tumor was within the vasculature, as evidenced by excellent overlay of the QD fluorescence signal and vasculature integrin  $\alpha_v\beta_3$  staining. This dual-modality (PET/NIRF) probe can confer sufficient tumor contrast at a concentration much lower than that required for in vivo NIRF imaging, thus significantly reducing the potential toxicity of cadmium-based QDs, and may facilitate the future translation of QD-based imaging agents for clinical and biomedical applications.

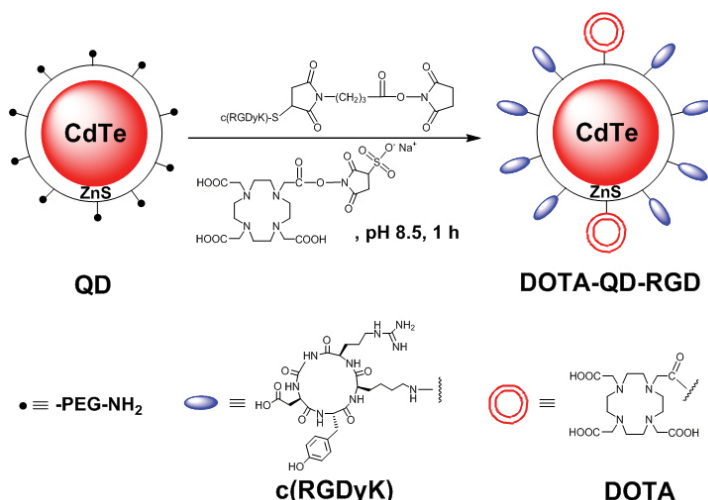


Fig. 2. Synthesis of the PET/NIRF probe DOTA-QD-RGD.

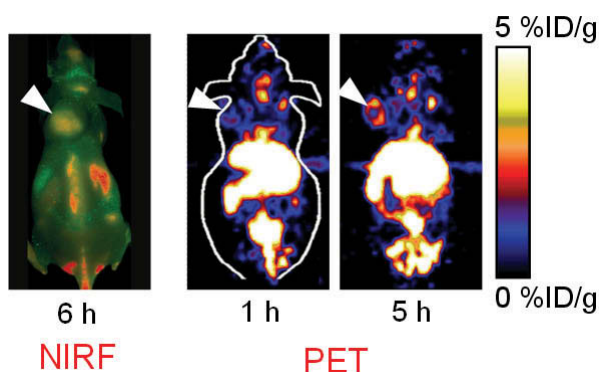


Fig. 1. NIRF (after injection of QD-RGD) and coronal PET (after injection of  $^{64}\text{Cu}$ -DOTA-QD-RGD) images of a U87MG tumor-bearing mice. Arrowheads indicate tumors.



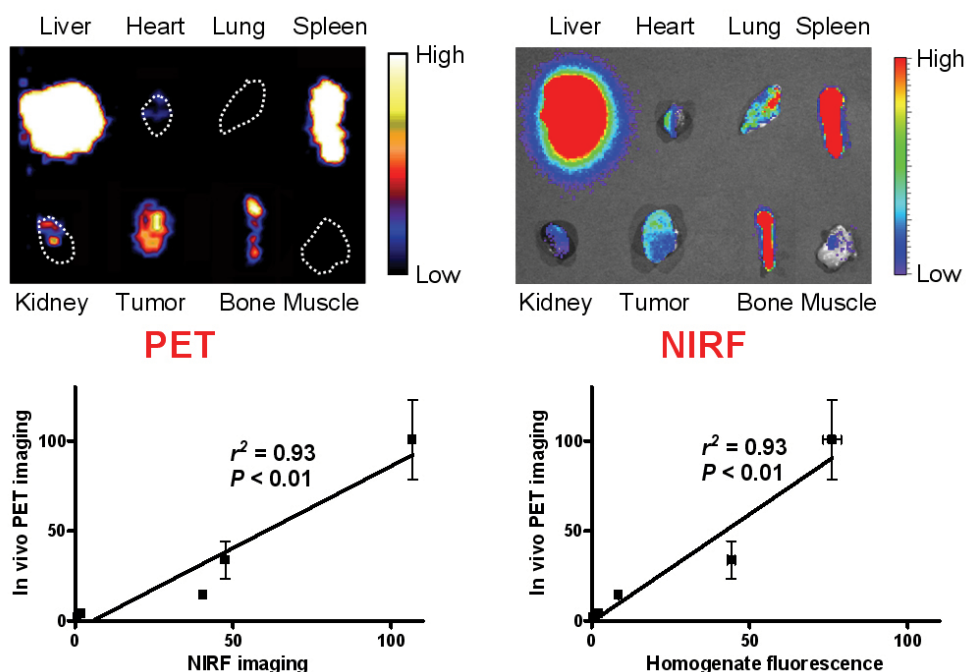


Fig. 3. Top: PET and NIRF image of harvested tissues at 5 h after injection of  $^{64}\text{Cu}$ -labeled DOTA-QD-RGD. Bottom left: Correlation among kidney-, U87MG-, bone-, spleen-, and liver-to-muscle ratios measured by in vivo PET and ex vivo NIRF imaging. Bottom right: Correlation among kidney-, U87MG-, bone-, spleen-, and liver-to-muscle ratios measured by in vivo PET and tissue homogenate fluorescence.

In summary, we have quantitatively evaluated the tumor-targeting efficacy of dual-modality QD-based probes using both PET and NIRF imaging. PET/NIRF imaging overcomes the tissue penetration limitation of optical imaging, thereby allowing quantitative imaging in deep tissue and can facilitate future biomedical applications of QDs. Multifunctional nanoplatform is the future for multimodality molecular imaging and cancer nanomedicine, and tumor vasculature targeting is more likely to succeed than tumor cell targeting.

## Acknowledgments

The author thanks all his colleagues at the Molecular Imaging Program at Stanford (MIPS), as well as all other collaborators, who participated in the studies described in this proceeding.

## References

1. Cai, W., Chen, X. *J. Nucl. Med.* **49 Suppl 2**, 113S-128S (2008).
2. Wu, Y., Cai, W., Chen, X. *Mol. Imaging Biol.* **8**, 226-236 (2006).
3. Cai, W., Wu, Y., Chen, K., Cao, Q., Tice, D.A., Chen, X. *Cancer Res.* **66**, 9673-9681 (2006).
4. Cai, W., Chen, X. *Small* **3**, 1840-1854 (2007).
5. Cai, W., Hsu, A.R., Li, Z.B., Chen, X. *Nanoscale Res. Lett.* **2**, 265-281 (2007).
6. Cai, W., Shin, D.W., Chen, K., Gheysens, O., Cao, Q., Wang, S.X., Gambhir, S.S., Chen, X. *Nano Lett.* **6**, 669-676 (2006).
7. Cai, W., Niu, G., Chen, X. *Curr. Pharm. Des.* **14**, 2943-2973 (2008).
8. Cai, W., Chen, K., Li, Z.B., Gambhir, S.S., Chen, X. *J. Nucl. Med.* **48**, 1862-1870 (2007).





**Biophysical Chemistry**  
**Folding, Recognition, and Catalysis**  
**Peptides in Materials Science**  
**Peptides as Research Tools**



## Conformation and Stability of the Helix-Loop-Helix Domain of the Id Protein Family

Sebastian D. Kiewitz,<sup>1,2</sup> Yoshiaki Kiso,<sup>2</sup> and Chiara Cabrele<sup>1,3</sup>

<sup>1</sup>Faculty of Chemistry and Pharmacy, University of Regensburg, Regensburg, 93053, Germany;

<sup>2</sup>Department of Medicinal Chemistry, Center for Frontier Research in Medicinal Science,

Kyoto Pharmaceutical University, Kyoto, 607-8412, Japan; and <sup>3</sup>Faculty of Chemistry and Biochemistry, Ruhr-University Bochum, Bochum, 44801, Germany

### Introduction

The Id proteins (inhibitors of DNA binding and cell differentiation Id1-Id4) are negative regulators of gene expression and key players in many biological processes, including angio-, neuro- and organogenesis. Moreover, they are crucial in the development of vascular diseases and cancer [1]. These small proteins (13-18 kDa) share a highly conserved HLH (helix-loop-helix) structural domain that is flanked by non-conserved *N*- and *C*-terminal regions. The HLH motif is required for protein-protein interaction. The *N*-terminus contains a phosphorylation site at Ser-5. A so-called destruction box (D-box) is present within the *C*-terminus of Id2, which is recognized by the anaphase promoting complex and triggers Id2 degradation [2]. Additionally, a nuclear export signal has been identified within the *C*-terminus of Id2, which is important for a nuclear receptor-dependent transport of the protein from the nucleus to the cytoplasm [3]. A proline-rich region *C*-terminal to the HLH motif is unique for Id3.

Contrarily to the parent bHLH transcription factors [4], the Id proteins lack the DNA-binding basic region *N*-terminal to the HLH domain. Consequently, unlike the homo-/heterodimers of two bHLH proteins, bHLH-Id-protein dimers are unable to form a ternary complex with the DNA: therefore, the Id proteins not only sequester positive bHLH factors, like the ubiquitous E proteins, into inactive (non-DNA binding) dimers, but also prevent their association with tissue-specific bHLH factors, like MyoD, which would lead to activation of DNA transcription. As the highly conserved Id HLH motif is essential for protein sequestration, we are interested in the characterization and modulation of its folding and dimerization.

### Results and Discussion

The conserved HLH region consists of two putative amphipathic helices (16 residues each) connected by a nine-residue-long loop (Figure 1). We have investigated the conformational properties of synthetic peptides reproducing the amino acid sequences of each putative helix by CD spectroscopy: the results indicate that the *C*-terminal segment has superior intrinsic helix propensity, whereas the *N*-terminal segment maintains alone a flexible conformation [5]. Instead, synthetic peptides representing the entire HLH domain of the Id proteins self-associate into dimeric and tetrameric structures characterized by high helix content and high conformational stability [6, 7].

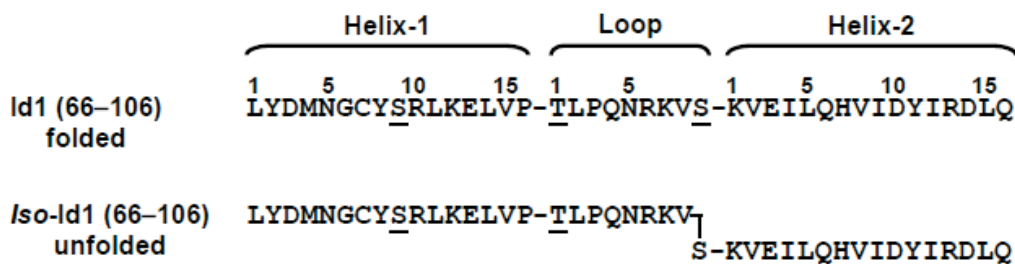


Fig. 1. Amino acid sequence of the human Id1 HLH domain (residues 66–106). The three Ser/Thr residues suitable for *O*-acyl-isodi-peptide replacement are underlined. The iso-Id1 HLH analog is shown, in which Ser at position nine of the loop has been used to incorporate the *O*-acyl-isodi-peptide.

The synthetic peptide reproducing the 41-residue long HLH domain of the Id2 protein has been further studied by 2D-NMR spectroscopy. However, to increase peptide solubility and reduce peptide aggregation, a water/TFE mixture has been used to prepare the NMR sample (40% alcohol). The chemical shift index of the  $\alpha$ -CH protons suggests the presence of two helical regions connected by a short flexible fragment in the middle of the sequence (positions 14-19). Moreover, the C-terminal helix appears to be longer and much better defined than the N-terminal one, thus confirming the CD results.

The Id HLH domains contain two conserved serine residues at positions nine of helix-1 and the loop, respectively, and, with the exception of Id3, a serine/threonine residue at position one of the loop (Figure 1). These positions are suitable for the replacement of the dipeptide units Xaa-Ser/Thr with the corresponding *O*-acyl-isodipeptide ones [8-10]. The resulting analogs – referred to as *iso*-Id-HLH analogs in this work – can be converted into the native domains by triggering the *O*→*N*-intramolecular acyl-migration at neutral pH values. Incorporation of the *O*-acyl-isodipeptide unit at the junction between the loop and helix-2 leads to complete loss of ordered structure [11]. However, after restoring the native amide bond the characteristic HLH fold is fully recovered. These results suggest that the residues at the loop-helix-2 junction are structurally important.

Two other *iso*-Id1-HLH analogs have been prepared, in which an *O*-acyl-isodipeptide unit has been incorporated in the middle of helix-1 or at the junction between helix-1 and the loop. In the latter case, it has been necessary to optimize the synthetic procedure to reduce diketopiperazine formation. The conformational properties of these *iso*-Id1 HLH analogs are currently investigated.

## Acknowledgments

This work was supported by the DFG Emmy-Noether grant CA296 to C.C.. S.D.K. is grateful to the Japanese Society for the Promotion of Science for a fellowship.

## References

1. Perk, J., Iavarone, A., Benezra, R. *Nat. Rev. Cancer* **5**, 603-614 (2005).
2. Lasorella, A., et al. *Nature* **442**, 471-474 (2006).
3. Kurooka, H., Yokota, Y. *J. Biol. Chem.* **280**, 4313-4320 (2005).
4. Massari, M.E., Murre, C. *Mol. Cell. Biol.* **20**, 429-440 (2000).
5. Colombo, N., Cabrele, C. *J. Peptide Sci.* **12**, 550-558 (2006).
6. Fairman, R., et al. *Proc. Natl. Acad. Sci. U.S.A.* **90**, 10429-10433 (1993).
7. Kiewitz, S.D., Cabrele, C. *Biopolymers (Peptide Sci.)* **80**, 762-774 (2005).
8. Carpino, L.A., et al. *Tetrahedron Lett.* **45**, 7519-7523 (2004).
9. Mutter, M., et al. *Angew. Chem. Int. Ed.* **43**, 4172-4178 (2004).
10. Sohma, Y., et al. *Chem. Commun.* 124-125 (2004).
11. Kiewitz, S.D., et al. *J. Peptide Sci.* **14**, 1209-1215 (2008).

## NMR Solution Structure Analysis of the C-terminal Linear and Cyclic Peptides of Pheromone Biosynthesis-Activating Neuropeptide (PBAN) from the Silkmoth *Bombyx mori*

Koji Nagata,<sup>1</sup> Akitoshi Okada,<sup>1</sup> Takeshi Kawai,<sup>1</sup> Jun Ohtsuka,<sup>1</sup>  
J. Joe Hull,<sup>2</sup> Ken-ichi Moto,<sup>2</sup> Shogo Matsumoto,<sup>2</sup>  
Hiromichi Nagasawa,<sup>1</sup> and Masaru Tanokura<sup>1</sup>

<sup>1</sup>The University of Tokyo, Tokyo, 113-8657, Japan; and

<sup>2</sup>The Institute of Physical and Chemical Research (RIKEN), Saitama, 351-0198, Japan

### Introduction

In most moths, the sex pheromone production is regulated by pheromone biosynthesis-activating neuropeptide (PBAN), a 33-34 amino acid neuropeptide [1]. PBAN exerts its pheromonotropic effects by binding to PBANR, a member of G protein-coupled receptors (GPCR), predominantly expressed in the pheromone-producing cells of the female pheromone gland [2]. The shortest peptide with the pheromonotropic activity is the C-terminal pentapeptide-amide, PBAN(29-33)-NH<sub>2</sub> (FSPRL-NH<sub>2</sub>), and the C-terminal amide group is required for the activity of PBAN [3]. In this study, we have analyzed the solution structures of the C-terminal decapeptides of PBAN with an amidated and a free C-termini (active and inactive, respectively), and an active cyclic octapeptide by two-dimensional NMR, and compared their structures to reveal the structural requirements for the PBAN activity.

### Results and Discussion

The decapeptides, SRTRYFSPRL-NH<sub>2</sub> and -OH, referred to as PBAN(24-33)-NH<sub>2</sub> and -OH, respectively, were synthesized by Fmoc-based solid-phase synthesis. The cyclic octapeptide, cyclo(NTSFTPRL) [4,5], referred to as cyclic PBAN, was synthesized by Fmoc-based solid-phase synthesis followed by cyclization by amide bond formation. Each sample for NMR measurements contained 10 mM PBAN(24-33)-NH<sub>2</sub>, -OH or cyclic PBAN dissolved in (1) 50 mM sodium phosphate buffer (pH 6.0)/100 mM NaCl/0.02% NaN<sub>3</sub> in 90%(v/v) H<sub>2</sub>O/10%(v/v) D<sub>2</sub>O (buffer A), (2) 500 mM dodecyl phosphocholine (DPC)-*d*<sub>38</sub> in buffer A, or (3) 30%(v/v) 2,2,2-trifluoroethanol (TFE)-*d*<sub>3</sub> in buffer A. DQF-COSY, TOCSY (mixing time, 50 ms) and NOESY (mixing time, 100, 200, 300, 400, or 500 ms) spectra were recorded at 25°C on a Unity Inova 500-MHz spectrometer (Varian). All the observed proton resonances were assigned by the conventional sequential assignment procedure. In buffer A, very few NOE cross-peaks were observed for all the peptides used even with a long mixing time (500 ms). Thus, all these peptides including cycloPBAN do not take a specific conformation in aqueous solution at pH 6.0. However, in the presence of DPC-*d*<sub>38</sub> micelles or 30%(v/v) TFE-*d*<sub>3</sub> in buffer A, many NOE cross-peaks were observed for all the peptides used. Thus, all these peptides adopt specific conformations under these solvent conditions. Solution structures of these peptides were calculated using interproton distance restraints derived from cross-peak intensities in their NOESY spectra (mixing time, 200 ms). Solution structures were calculated with ca. 100 NOE-derived distance restraints by torsion angle dynamics using the program CYANA. Twenty conformers with the lowest CYANA target functions were used to represent the solution conformation of these peptides. The RMS deviations of atomic coordinates of the 20 structures range 0.01-0.38 Å for the backbone atoms and 0.38-1.27 Å for all the non-hydrogen atoms. PBAN(24-33)-NH<sub>2</sub> and -OH take a similar β-turn structure at the active core region in the C-terminus, <sup>30</sup>SPRL<sup>33</sup>, in the presence of DPC micelles. On the other hand, the two linear peptides take different conformations in 30%(v/v) TFE. PBAN(24-33)-NH<sub>2</sub> adopts a type-I β-turn at the active core region in the C-terminus, whereas PBAN(24-33)-OH does not adopt a β-turn, but instead adopts an extended conformation. In other words, the β-turn structure is abolished in 30%(v/v) TFE when the amide group is lost. Several reports already show that the C-terminal active core region of PBAN can adopt a β-turn structure [4-8]. Our comparative NMR structural analyses of PBAN(24-33)-NH<sub>2</sub> and PBAN(24-33)-OH (preliminarily reported in [9]) have demonstrated for the first time that the C-terminal amide group of PBAN contributes to the stabilization of the β-turn. In addition, we have shown that cyclic PBAN, whose PBAN activity

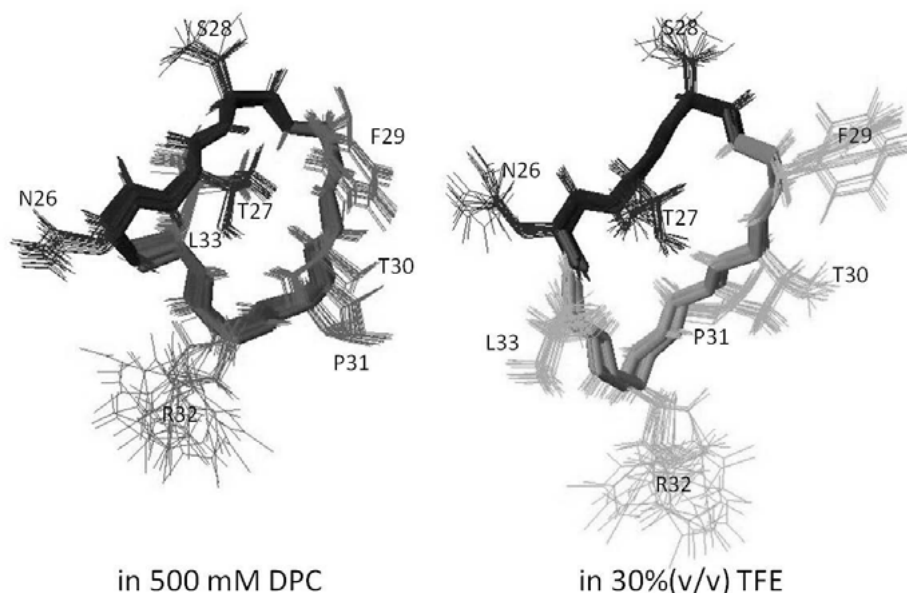


Fig. 1. Solution conformations of cycloPBAN, cyclo(<sup>26</sup>NTSFTPRL<sup>33</sup>), at pH 6.0 and 25°C in the presence of DPC micelles or 30%(v/v) TFE. The residue numbers are derived from the amino acid sequence alignment with *Bombyx mori* PBAN.

is comparable to PBAN(24-33)-NH<sub>2</sub>, also adopts a  $\beta$ -turn at the active core region, TPRL, in the presence of DPC micelles or 30%(v/v) TFE (Figure 1). In summary, our results support the proposition that the  $\beta$ -turn structure at the C-terminus of PBAN would be important for exerting the PBAN activity [4-8] and indicate the C-terminal amide group of PBAN would contribute to the stabilization of the  $\beta$ -turn.

## Acknowledgments

This research was supported by Targeted Proteins Research Program (TPRP) from the Ministry of Education, Culture, Sports, Science and Technology of Japan.

## References

1. Kitamura, A., Nagasawa, H., Kataoka, H., Inoue, T., Matsumoto, S., Ando, T., Suzuki, A. *Biochem. Biophys. Res. Commun.* **163**, 520-526 (1989).
2. Hull, J.J., Ohnishi, A., Moto, K., Kawasaki, Y., Kurata, R., Suzuki, M.G., Matsumoto, S. *J. Biol. Chem.* **279**, 51500-51507 (2004).
3. Nagasawa, H., Kuniyoshi, H., Arima, R., Kawano, T., Ando, T., Suzuki, A. *Arch. Insect Biochem. Physiol.* **25**, 261-270 (1994).
4. Nachman, R.J., Roberts, V.A., Dyson, H.J., Holman, G.M., Tainer, J.A. *Proc. Natl. Acad. Sci. U.S.A.* **88**, 4518-4522 (1991).
5. Nachman, R.J., Kuniyoshi, H., Roberts, V.A., Holman, G.M., Suzuki, A. *Biochem. Biophys. Res. Commun.* **193**, 661-666 (1993).
6. Wang, Y.S., Kempe, T.G., Raina, A.K., Mazzocchi, P.H. *Int. J. Peptide Protein Res.* **43**, 277-283 (1994).
7. Nachman, R.J., Roberts, V.A., Holman, G.M., Beier, R.C. *Reg. Peptides* **57**, 359-370 (1995).
8. Clark, B.A., Prestwich, G.D. *Int. J. Peptide Protein Res.* **47**, 361-368 (1996).
9. Nagata, K., Okada, A., Ohtsuka, J., Takahashi, M., Kawai, T., Sugisaka, A., Hull, J.J., Moto, K., Matsumoto, S., Nagasawa, H., Tanokura, M. In Lankinen, H. (ed.) *Peptides 2008*, The Finnish Peptide Society, Helsinki, 2008, pp. 578-579.

## A Donor–Acceptor Perspective on Carbonyl–Carbonyl Interactions in Proteins

Amit Choudhary<sup>1</sup> and Ronald T. Raines<sup>2</sup>

<sup>1</sup>Graduate Program in Biophysics, University of Wisconsin–Madison, Madison, WI 53706, U.S.A.,

<sup>2</sup>Department of Biochemistry and Chemistry, 433 Babcock Drive, University of Wisconsin–Madison, Madison, WI 53706, U.S.A.

### Introduction

Electronic delocalization, a central concept in organic chemistry, is being invoked increasingly in biological contexts [1–3]. We have discovered a non-covalent interaction in proteins, termed the  $n \rightarrow \pi^*$  interaction, in which the lone pair ( $n$ ) of the oxygen ( $O_{i-1}$ ) of a peptide bond overlaps with the antibonding orbital ( $\pi^*$ ) of the carbonyl group ( $C'_i=O_i$ ) of the subsequent peptide bond (Figure 1A, B) [1]. The  $n \rightarrow \pi^*$  interaction is reminiscent of the renowned Bürgi–Dunitz trajectory [1c] and analogous to a hydrogen bond, which likewise involves the delocalization of a lone pair of an acceptor atom over the antibonding orbital ( $\sigma^*$ ) of a donor [2]. The stereochemical constraints required for an energetically meaningful  $n \rightarrow \pi^*$  interaction are met in several fundamental structural elements in proteins, including  $\alpha$ -helices,  $3_{10}$  helices, and polyproline II type helices, as well as within the backbone of peptoids. A signature of the  $n \rightarrow \pi^*$  interaction is a short  $O_{i-1} \cdots C'_i$  contact [3]. Others have argued that the attractive  $C=O \cdots C=O$  interaction is primarily a dipole–dipole (Figure 1C) [4] or a charge–charge interaction (Figure 1D) [5]. We used a peptidic model system (Figure 2) to explore the origin of this interaction. Regardless of the nature of the interaction between the adjacent carbonyl groups, the interaction stabilizes the *trans* conformation preferentially over the *cis* conformation. Thus, the value of  $K_{trans/cis}$  reports on the strength of the  $C=X \cdots C=O$  interaction.

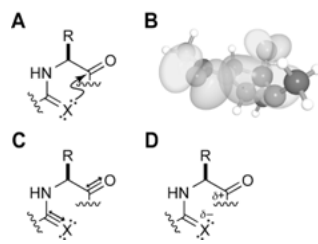


Fig. 1. Possible  $C=X \cdots C=O$  interactions.

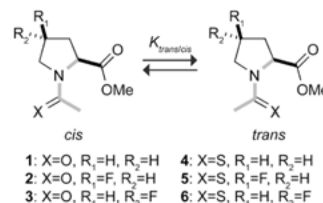


Fig. 2. Compounds used to examine the  $C=X \cdots C=O$  interaction.

### Results and Discussion

To distinguish between a charge–charge interaction and an  $n \rightarrow \pi^*$  interaction, we envisaged the replacement of  $O_{i-1}$  with sulfur,  $S_{i-1}$ , in this model system. A charge–charge interaction would be attenuated because sulfur is less negatively polarized than oxygen, whereas the  $n \rightarrow \pi^*$  interaction would be strengthened because sulfur is a softer base than oxygen. An increase in  $K_{trans/cis}$  is observed from this isosteric substitution. Hence, the stabilization of the *trans* conformation cannot be due to a charge–charge interaction. Another signature of the  $n \rightarrow \pi^*$  interaction is the pyramidalization of the acceptor carbonyl group. Such pyramidalization should appear in the computationally optimized, gas-phase geometries and the crystal structures. Additionally, the degree of pyramidalization should increase as the distance between the donor and the acceptor atoms is decreased. We employed a subtle means to alter the distance between the donor and acceptor atoms [6]. In accord with a potent  $n \rightarrow \pi^*$  interaction, a positive correlation is indeed observed between the  $C'_i$  pyramidalization and the  $K_{trans/cis}$  value in both the computational and experimental data (Figure 3).

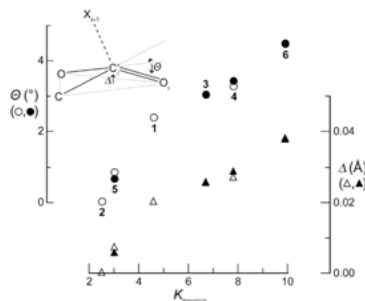


Fig. 3. Relationship between the degree of  $C'_i$  pyramidalization and the value of  $K_{trans/cis}$ . Open symbols, computational; filled symbols, experimental.



Next, we reasoned that the replacement of the C=O acceptor with a C–F bond would retain the dipole–dipole interaction but attenuate the  $n \rightarrow \pi^*$  interaction [7]. This isosteric substitution leads to reversal of the conformational preference from *trans* to *cis*. Again, the observed value of  $K_{trans/cis}$  again cannot be explained by classical electrostatic models.

A recent Protein Data Bank search has revealed that more than 81% of  $\alpha$ -helical residues exhibit a short contact ( $d < r_C + r_O$ ) between neighboring carbonyl groups [8]. Employing an AcAla<sub>4</sub>NHMe peptidic model system, we scanned the allowed regions of the Ramachandran map for  $n \rightarrow \pi^*$  interactions. We found a widespread prevalence of  $n \rightarrow \pi^*$  interaction in the allowed regions [9]. Common protein secondary structures, such as  $\alpha$ -helices and  $3_{10}$  helices, show significant stabilization by  $n \rightarrow \pi^*$  interactions. As the adjacent carbonyl dipoles repel each other in an  $\alpha$ -helix, the  $n \rightarrow \pi^*$  interaction likely plays an important role in helix nucleation. Considerable carbonyl bond lengthening [10], polarization of the  $\pi$ -electron cloud [10], and pyramidalization of the carbonyl carbon [9] have been observed in the  $\alpha$ -helices of high-resolution protein structures. Our computational analyses also predict significant  $n \rightarrow \pi^*$  interactions in the twisted  $\beta$ -sheet region. The conformational stability of the collagen triple helix has already been attributed, in part, to  $n \rightarrow \pi^*$  interactions [11].

The resonance character between adjacent carbonyl groups in proteins has important implications. The distorted conformation of a fluoroalkene isostere emphasizes the stabilization afforded by an  $n \rightarrow \pi^*$  interaction, which is absent in that system [7]. Short  $O_{i-1} \cdots C_i=O_i$  contacts are widespread in common protein folds [8]. Yet, closed shell repulsion between the lone-pair of  $O_{i-1}$  and the  $\pi$ -orbital of  $C_i=O_i$  tends to increase the  $O_{i-1} \cdots C_i=O_i$  distance and thereby compromise the structural integrity of proteins. We propose that the availability of a low-lying  $\pi^*$ -orbital effectively counters the closed shell repulsion and enables polypeptide chains to adopt  $\alpha$ -helices,  $3_{10}$  helices, and polyproline II type helices.

Finally, we note that  $n \rightarrow \pi^*$  electronic delocalization likely plays a role in many protein–ligand interactions and catalytic processes. Our data suggest that an isosteric substitution of an amide donor with a thioamide could be used to increase the ligand affinity and stabilize unstable intermediates in a catalytic cycle.

## Acknowledgments

This work was supported by grant AR044276 (NIH). We thank G. R. Krow, G. J. Bartlett, D. N. Woolfson, C. E. Jackobsche, and S. J. Miller for collaborative interactions, and F. W. Kotch, I. A. Guzei, L. C. Spencer, M. D. Shoulders, M. J. Palte, and C. N. Bradford for contributive discussions.

## References

1. (a) DeRider, M.L., et al. *J. Am. Chem. Soc.* **124**, 2497-2505 (2002). (b) Hinderaker, M.P., Raines, R.T. *Protein Sci.* **12**, 1188-1194 (2003). (c) Hodges, J.A., Raines, R.T. *Org. Lett.* **8**, 4695-4697 (2006).
2. (a) Isaacs, E.D., et al. *Phys. Rev. Lett.* **82**, 600-603 (1999). (b) Weinhold, F. *Adv. Protein Chem.* **72**, 121-155 (2005). (c) Head-Gordon, M., et al. *J. Phys. Chem. A.* **111**, 8753-8765 (2007).
3. Choudhary, A., et al. *J. Am. Chem. Soc.* **131**, 7244-7246 (2009).
4. (a) Diederich, F., et al. *Angew. Chem. Int. Ed.* **44**, 1788-1805 (2005). (b) Diederich, F., et al. *Proc. Natl. Acad. Sci. U.S.A.* **105**, 17290-17294 (2008).
5. (a) Milner-White, E.J., et al. *J. Mol. Biol.* **248**, 361-373 (1995). (b) Milner-White, E.J., et al. *J. Mol. Biol.* **248**, 374-384 (1995).
6. A 4*R* electron-withdrawing group (EWG) brings the  $O_{i-1}$  or  $S_{i-1}$  donor and  $C_i=O_i$  acceptor closer; a 4*S* EWG increases the distance between the donor and acceptor.
7. Jackobsche, C.E., Miller, S.J., unpublished results.
8. Bartlett, G.J., Raines, R.T., Woolfson, D.N., unpublished results.
9. Choudhary, A., Raines, R.T. unpublished results.
10. Lario, P.I., Vrielink, A. *J. Am. Chem. Soc.* **125**, 12787-12794 (2003).
11. Shoudlers, M.D., Raines, R.T. *Annu. Rev. Biochem.* **78**, 929-958 (2009) and references therein.

## Spectroscopic Analysis of a $\beta$ -hairpin Forming Miniprotein

Marcus P. D. Hatfield, Richard F. Murphy, and Sándor Lovas

Department of Biomedical Sciences, Creighton University Medical Center, Omaha, NE 68178, U.S.A.

### Introduction

$\beta$ -Hairpins, the simplest form of antiparallel  $\beta$ -sheet, are stabilized by cross-strand hydrogen bonds and sidechain-sidechain interactions, which include aromatic-aromatic, cation- $\pi$  and CH- $\pi$  interactions [1]. Recently designed  $\beta$ -hairpins show high melting temperatures ( $T_m$ ) and two-state folding [2].

The decapeptide Tyr-Tyr-Asp-Pro-Glu-Thr-Gly-Thr-Trp-Tyr (CLN025; Figure 1) forms a stable  $\beta$ -hairpin with a  $T_m$  of 70 °C [2]. It is a variant of chignolin with the terminal Gly residues replaced by Tyr. The central 8 residues were selected by statistical analysis using a position-specific scoring matrix with a peptide having a classical  $\beta$ -hairpin structure as the target [3]. CLN025 is stabilized by hydrogen bonds between Asp3 and Thr6, Gly7 and Thr8 and an aromatic-aromatic interaction between Tyr2 and Trp9 [2].

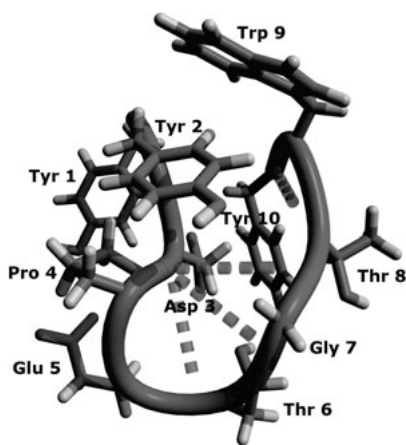


Fig. 1. The crystal structure of CLN025. H-bonds are represented by dotted lines [2].

The vibrational circular dichroism (VCD) spectroscopic properties of polypeptide structures including  $\alpha$ -helices, turns, poly Pro II helices and  $\beta$ -sheets have been studied extensively, but the properties of the  $\beta$ -hairpin have not. The previous studies of the VCD spectroscopic properties of  $\beta$ -hairpins were of those formed either by <sup>15</sup>Pro-Xxx turns or head-to-tail cyclization to form a stable structure [4-6]. In this study, the VCD spectroscopic properties of CLN025, which has been shown to form a stable  $\beta$ -hairpin in aqueous solution, with only naturally occurring amino acids [2], were determined.

CLN025 was synthesized by microwave SPPS with N<sup>α</sup>-Fmoc amino acids. The structure of the HPLC-purified CLN025 was confirmed by electro-spray mass spectrometry. VCD spectra were recorded in 5% (v/v) DMSO-d<sub>6</sub> in 20 mM deuterated potassium phosphate buffer (pD 7.4) by performing 8 block measurements obtained from 4500 scans for VCD and 225 scans for IR absorption at 8 cm<sup>-1</sup> resolution. The spectra were averaged and background spectra of the solvent and water vapor were subtracted. Spectra were set to 0 at 1800 cm<sup>-1</sup> and normalized by dividing each data point by the maximum IR absorbance in the amide I' region. Deconvolution and peak fitting of the IR spectra were performed with the PROTA software package.

### Results and Discussion

The VCD spectrum of CLN025 (Figure 2) shows a (-, +, -) pattern with bands at 1640 cm<sup>-1</sup>, 1667 cm<sup>-1</sup> and 1679 cm<sup>-1</sup>, respectively. The first couplet, centered at 1654 cm<sup>-1</sup>, is indicative of random meander structure and the second, centered at 1673 cm<sup>-1</sup>, is indicative of turn structure. The signal from the  $\beta$ -sheet component of the  $\beta$ -hairpin is not apparent, due to its lower intensity and the overlap of its negative band with the negative band of the first couplet, which might explain the larger width of the negative band at 1640 cm<sup>-1</sup>.

The IR absorption spectrum of CLN025 (Figure 2) has a maximum absorbance at 1647 cm<sup>-1</sup>. Shoulders at 1612 cm<sup>-1</sup>, 1630 cm<sup>-1</sup>, 1658 cm<sup>-1</sup>, 1675 cm<sup>-1</sup> and 1696 cm<sup>-1</sup> are seen in the deconvoluted spectrum. The band at 1612 cm<sup>-1</sup> is due to the tertiary amide of the Pro residue. The band at 1630 cm<sup>-1</sup> is due to  $\beta$ -sheet, while the bands at 1647 cm<sup>-1</sup> and 1658 cm<sup>-1</sup> are due to random meander structure and the bands at 1675 cm<sup>-1</sup> and 1696 cm<sup>-1</sup> are due to turn-like structure. The band at 1515 cm<sup>-1</sup> is caused by the ring vibration of the tyrosyl sidechain. Peak

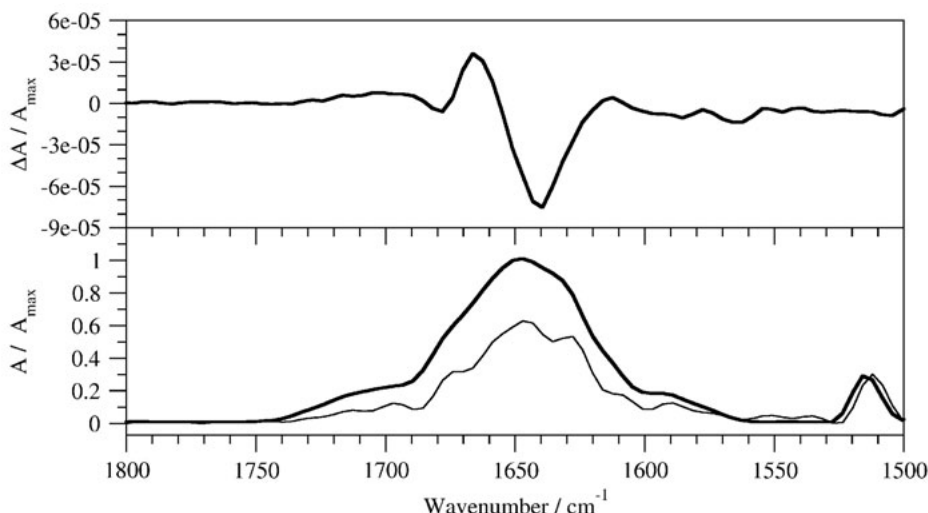


Fig. 2. Normalized VCD (top) and IR absorption (bottom) spectra of 20 mg/mL CLN025 in deuterated potassium phosphate buffer. The deconvoluted absorbance spectrum is shown by the thin curve.

Table 1. The areas of the component peaks in the deconvoluted FT-IR spectrum at the amide I' region of CLN025

Wavenumber / cm <sup>-1</sup>	1612	1630	1646	1658	1675	1696
Area (%)	4	16	40	27	5	2
Assignment	Pro	β-sheet	Random meander	Random meander	Turn	Turn

analysis of the IR absorption spectrum (Table 1) indicates that the peptide is approximately 10% turn, 20% β-sheet and 70% random meander.

The VCD spectral properties of CLN025 are comparable to those of less stable β-hairpins formed by <sup>D</sup>Pro residues. Zhao and colleagues [4] found a (-,+,+,-) pattern with bands at 1643 to 1659 cm<sup>-1</sup>, 1655 to 1670 cm<sup>-1</sup>, 1670 to 1678 cm<sup>-1</sup> and 1690 to 1697 cm<sup>-1</sup>, respectively, while Hilario and colleagues [5, 6] found a negative couplet with a negative band at 1635 to 1645 cm<sup>-1</sup> and positive band at 1660 to 1680 cm<sup>-1</sup>. The present results suggest that the negative couplet with bands at 1635 to 1659 cm<sup>-1</sup> and 1655 to 1680 cm<sup>-1</sup> is typical of β-hairpins.

## Acknowledgments

This work was supported by NIH-INBRE grant (1 P20 RR16469) and the Carpenter Endowed Chair in Biochemistry, Creighton University.

## References

1. Eidenschink, L., Kier, B.L., Huggins, K.N.L., Andersen, N.H. *Proteins* **75**, 308-322 (2009).
2. Honda, S., Akiba, T., Kato, Y.S., Sawada, Y., Sekijima, M., Ishimura, M., Ooishi, A., Watanabe, H., Odahara, T., Harata, K. *J. Am. Chem. Soc.* **130**, 15327-15331 (2008).
3. Honda, S., Yamasaki, K., Sawada, Y., Morli, H. *Structure* **12**, 1507-1518 (2004).
4. Zhao, C., Polavarapu, P.L., Das, C., Balaram, P. *J. Am. Chem. Soc.* **122**, 8228-8231 (2000).
5. Hilario, J., Kubelka, J., Syud, F.A., Gellman, S.H., Keiderling, T.A. *Biopolymers* **67**, 233-236 (2002).
6. Hilario, J., Kubelka, J., Keiderling, T.A. *J. Am. Chem. Soc.* **125**, 7562-7574 (2003).

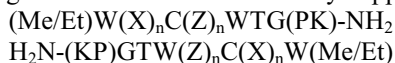
## Hyperstable $\beta$ Sheets Without Turns

Brandon L. Kier and Niels H. Andersen

Department of Chemistry, University of Washington, Seattle, WA 98195, U.S.A.

### Introduction

Recent investigations into the nature of  $\beta$ -sheet formation have involved simple  $\beta$ -hairpin structures: two antiparallel sheets connected by a turn or short reversing loop [1,2].  $\beta$ -Hairpins have proven to be useful model systems, and are considered to be the smallest unit of natural  $\beta$  structure available. However, despite their usefulness,  $\beta$  hairpins are not the universal  $\beta$  archetype. In proteins,  $\beta$  sheets may have very high contact order, exist at the interface of two proteins, or be arranged in parallel. Any investigation carried out on  $\beta$  hairpins is, by necessity, a study of both antiparallel  $\beta$  strands and reversing turns. Previous examples of cystine-linked turnless  $\beta$  structures have been very poorly folded in water, [3,4] but we hypothesized that well-folded cystine-linked  $\beta$  sheet homodimers could be achieved with the use of two highly fold-stabilizing  $\beta$  caps [5]. The general formula for this doubly-capped design would be:



where the central Cys functioned as the dimerizing unit, X and Z could be any residue(s), and sheet length could be modulated by varying  $n$ .

### Results and Discussion

#### Turnless Model Systems

Peptides with  $n=1$  and  $n=3$  were investigated. Peptide (Pr-WVCKWTGPK-NH<sub>2</sub>)<sub>2</sub> incorporated a single lysine at position Z for solubility, and a single valine at X; the optimal residue to precede a disulfide according to Cochran et al [6]. The expected  $\beta$ -sheet and  $\beta$ -cap characteristics were observed by NMR: Gly H<sub>N</sub> CSD (Chemical Shift Deviation) > 3ppm, W5 H $\epsilon$ 3>1.8ppm (cap) and alternating downfield H<sub>N</sub> and H $\alpha$  CSDs (strand association). Circular dichroism was used to determine a  $T_m$  of ~60 °C. Peptide (Pr-WTTCIRKWTGPK-NH<sub>2</sub>)<sub>2</sub> (X=TTV, Z=IRK) displayed analogous diagnostic strand and capping shifts, was highly soluble, melted at ~70 °C, and exhibited remarkably sharp lineshape in NMR, indicative of a fast folding process. The fold population was determined via an amide exchange study. The protection factors determined in this manner for the H-bonded amides are comparable to those we have determined for capped hairpin peptides, indicating a fold population of 96.4-99.4%

#### Capping Energies

Though the twin  $\beta$ -cap motifs [5] were considered essential for  $\beta$ -sheet formation, the longer sheet retained some fold population even after removal of the N-terminal propionyl abolished cap formation. The core 280K  $\beta$ -sheet fold population of (WTTVCIRKW-TGPK-NH<sub>2</sub>)<sub>2</sub> was reduced to <72% ( $\Delta\Delta G_u$ = -8.2 kJ/mol versus its capped counterpart) and showed severe terminal fraying. The capping energy in the turnless sheet context for the smaller system was hard to gauge due to near-complete loss of  $\beta$ -sheet fold, but was greater than 10 kJ/mol. After halving to account for dual  $\beta$ -cap content, these results imply a 4.1-5+ kJ/mol folding increment per capping unit.

Table 1. All observable protection factors (H-bonded amides in bold; estimates due to overlap in italics.)

	<i>Prot. Fact.</i> $k_{RC}/k_{exp}$	%fold	$\Delta G_u$ kJ/mol
Trp1	13.66	93.2	6.07
<b>Thr2</b>	<b>26.92</b>	<b>96.4</b>	<b>7.67</b>
<b>Val4</b>	<b>90.47</b>	<b>98.9</b>	<b>10.49</b>
<b>Ile6</b>	<b>153.57</b>	<b>99.4</b>	<b>11.72</b>
Arg7	5.77	85.2	4.08
<b>Lys8</b>	<b>156.02</b>	<b>99.4</b>	<b>11.76</b>
Thr10	3.53	77.9	2.94

Table 2. Diagnostic chemical shift deviations (CSDs) and core fold % calculated for turnless  $\beta$ -sheet dimers. Data at 280K. *italics: estimates.*

	Cys H $\alpha$ CSD	Edge W H $\epsilon$ 3	Fold%
(KKT <b>C</b> TTT) <sub>2</sub> pH 6.5	0.626		42%
(KKV <b>C</b> ITT) <sub>2</sub> pH 2.5	0.536		43%
(KKV <b>C</b> ITT) <sub>2</sub> pH 6.5	0.857		65%
(WV <b>C</b> K <b>W</b> TGPK-NH <sub>2</sub> ) <sub>2</sub>	0.199	-0.151	13%
(Pr-WV <b>C</b> K <b>W</b> TGPK-NH <sub>2</sub> ) <sub>2</sub>	1.301	-1.993	97%
WTTVC <b>I</b> RK <b>W</b> TGPK-NH <sub>2</sub>	-0.082	0.054	0%
(WTTVC <b>I</b> RK <b>W</b> TGPK-NH <sub>2</sub> ) <sub>2</sub>	0.884	-0.465	72%
(Pr-WTTVC <b>I</b> RK <b>W</b> TGPK-NH <sub>2</sub> ) <sub>2</sub>	1.15	-2.011	99%

### Minimalist Turnless Models

The partly viable uncapped  $\beta$ -sheets inspired the design of simpler sheets with terminal ion pairs. Peptide (KKTCTTT)<sub>2</sub> was 42% folded at 280K, suggesting that even short disulfide-linked sequences devoid of hydrophobic residues could exhibit some  $\beta$  structure. (This value was calculated from the alternating downfield H<sub>N</sub> and H $\alpha$  protons analogous to those in peptide (Pr-WTTVCIRKWTGPK-NH<sub>2</sub>)<sub>2</sub>). Introducing a hydrophobic cluster resulted in the 65% folded (280K) (KKVCITT)<sub>2</sub>. The importance of the twin ion pairings was deduced from the 22% reduction in fold population at pH 2.5 ( $\Delta\Delta G_u=1.1$  kJ per ion pair.)

### Implications

Turnless, hyperstable  $\beta$  sheets are viable replacements for  $\beta$  hairpins as models for dynamics studies, MD simulations, and biologically relevant  $\beta$ -sheet agonists; they enable the investigation of  $\beta$  sheets without potential interference from turns or loops. The very existence of well-folded  $\beta$  sheets lacking turns may finally dispel the notion that  $\beta$  hairpin folding invariably proceeds via a “zipper” mechanism, whereby turn formation acts as a nucleator for interstrand H-bond formation. Though all sheets were homodimeric (for ease of synthesis and assignment) a diverse array of mixed-strand systems should prove viable if ~50% yield reduction is not an issue. Capped  $\beta$  strands may also be linked by biologically relevant loop sequences that would not otherwise fold into a hairpin turn, thus forming minimal scaffolds for stabilizing loops that may not adopt the proper conformation with a disulfide alone.

### Acknowledgements

This research was supported by a grant from the NIH (GM059658).

### References

1. Andersen, N.H., et al. *J. Am. Chem. Soc.* **128**, 6101-6110 (2006).
2. Hughes, R.M., Waters, M.L. *Curr. Opin. Struct. Biol.* **16**, 514-524 (2006).
3. Cashman, T.J., Linton, B.R. *Org. Lett.* **9**, 5457-5460 (2007).
4. Aberle, A.M., Redy, H.K., Heeb, N.V., Nambiar, K.P. *Biochem. & Biophys. Res. Comm.* **200**, 102-107 (1994).
5. Kier, B.L., Andersen, N.H. *J. Am. Chem. Soc.* **130**, 14675-14683 (2008).
6. Russell, S.J., Blandl, T., Skelton, N.J., Cochran, A.G. *J. Am. Chem. Soc.* **125**, 388-395 (2003).

## Structural Studies of Mucin Glycoprotein Motifs

David Live,<sup>1</sup> Andrew Borgert,<sup>2</sup> George Barany,<sup>3</sup> and Mian Liu<sup>1</sup>

<sup>1</sup>Complex Carbohydrate Research Center, Univ. of Georgia, Athens, GA 30602, U.S.A.; <sup>2</sup>Biophysical Sciences and Medical Physics, and <sup>3</sup>Chemistry Dept., Univ. of Minnesota, Minneapolis, MN 55455, U.S.A.

### Introduction

Protein glycosylation is the most prevalent and complex form of protein post-translational processing. The variety and dynamic aspects of these modifications add an additional dimension to the diversity of protein properties and function. Mucin glycoproteins comprise a major subset of the universe of glycoproteins. This class is characterized by a high density of S and T residues, often in clusters, whose sidechains serve as loci of glycosylation, either throughout the length of the protein or in subdomains. A number of prominent examples are found as domains in cell surface proteins. The distribution of glycosylation is determined through the initial attachment of an  $\alpha$ -O-GalNAc residue to S or T residues as mediated by the particular member(s) of the repertoire of polypeptide GalNAc transferase enzymes that the cell is expressing at the time. Thus, the patterns and glycan structures reflect the condition of the cell in a time dependent way and can serve as biomarkers. These changes play an important role in modulating normal cellular interactions. Aberrant glycosylation of cell surface molecules often is a manifestation of diseases including cancer, [1] raising the prospect of using these unusual structures in targeted therapies. An understanding of the molecular recognition events of the normal and unusual forms of these molecules requires knowledge of their conformational properties at atomic resolution. Unfortunately, both the natural microheterogeneity of glycosylation on native glycoproteins, as well as their high molecular weight, has seriously limited this effort. Chemical synthesis, however, can provide homogeneous and well defined material that circumvents these problems, and solid phase synthesis has proven invaluable in preparing mucin glycopeptide motifs for our efforts to address the conformation of mucins by NMR [2]. Since glycosylated mucins naturally show extended structures, interactions with sequentially remote portion of the molecule are unlikely, and the short synthetic segments are expected to be subject to the same local forces that dominate the structure of the native glycoprotein. In this work we have characterized the conformations of a mucin glycoprotein motif derived from MUC2, systematically varying the distribution and density of  $\alpha$ -O-GalNAc glycosylation. Several members of this series have also previously been examined as substrates for polypeptide GalNAc transferase enzymes, allowing, as well, for potential insights into the structure/function relationships of the enzymatic reactions [3].

### Results and Discussion

A set of glycopeptides based on the MUC2 related sequence PTTTPLK were synthesized using solid-phase peptide synthesis techniques, [2] incorporating all permutations of  $\alpha$ -O-GalNAc substitutions on the sidechain hydroxyl groups of the T residues (Figure 1).

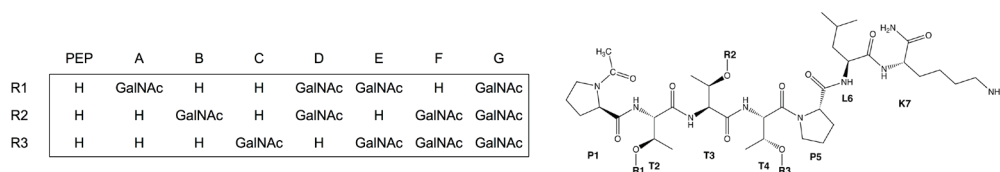


Fig. 1. MUC2 derived glycopeptides.

The variations in location and density of glycosylation provide an opportunity to assess the impact of glycosylation at the individual sites, and the incremental effect of neighboring modifications on the overall organization. A variety of 1D and 2D NMR experiments were carried out on these constructs in aqueous solution, from which we were able to extract J-coupling and NOE parameters, that were used in computing sets of structures consistent with the restraints for each of the members of the group. While the average structure for the peptide

backbone in the central core of each of the constructs were well-defined, and similar across the set, as the level of glycosylation was increased in the series, the distribution of the cluster of acceptable structures narrowed, suggesting an increase in rigidity. Interestingly, neither the local conformation at individual isolated glycosylated T residues nor the orientation of the sugar residue are significantly perturbed by the addition of neighboring GalNAcs as is illustrated in Figure 2 below where the three singly glycosylated constructs and the triglycosylated form are compared. The structure found for the fully glycosylated tri-T glycopeptide scaffold superimposes quite closely on that which we determined for the glycosylated STTAV sequence reported earlier, suggesting that this geometry may be more widely representative of a motif [4].

To begin relating the structures we have observed to biomolecular recognition, we have collaborated with Profs. David Smith and Richard Cummings at Emory University to immobilize these and some additional S/T-  $\alpha$ -O-GalNAc (Tn antigen) bearing glycopeptides on a microarray slide and investigate their binding to anti-Tn antibodies raised earlier in mice from immunization with Tn bearing cellular fractions. In these experiments, given antibodies show distinct selective binding to some members of the MUC2 structure group but not to others. Clearly these are recognizing more than just the presence of the sugar residue. The cross reactivities between antibodies raised to natural material and our constructs provide strong support for our contention that biologically relevant epitopes are captured in our synthetic motifs. Further, being able to define the epitope geometry from our conformational studies can be of considerable value in the design of immunotherapy directed against these targets. Pursuing this further will allow us to unravel the role of glycosylation patterns in contributing to the diversity of the glycoprotein interactions.

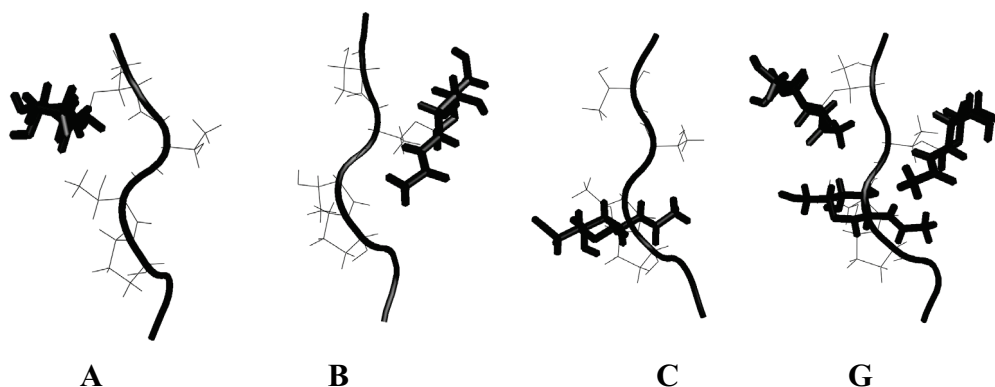


Fig. 2. The closest to the average of the NMR structures for constructs A, B, C, and G with the GalNAc residues highlighted.

## Acknowledgments

This work was supported by grants from NIH, GM 66148, and the Georgia Research Alliance, GRA.VAC09.1

## References

1. Hollingsworth, M.A., Swanson, B.J. *Nature Reviews Cancer* **4**, 45-60 (2004).
2. Liu, M., Barany, G., Live, D. *Carbohydrate Research* **340**, 2111-2122 (2005).
3. Takeuchi, H., Kato, K., Hassan, H., Clausen, H., Irimura, T. *Eur. J. Biochem.* **269**, 6173-6183 (2002).
4. Coltart, D.M., et al. *J. Amer. Chem. Soc.* **124**, 9833-9844 (2002).

## Replacement of Ala by Aib Improves Structuration and Biological Stability in Thymine-Based Nucleopeptides

Piero Geotti-Bianchini,<sup>1,2</sup> Alessandro Moretto,<sup>1</sup> Cristina Peggion,<sup>1</sup>  
Julien Beyrath,<sup>2</sup> Alberto Bianco,<sup>2</sup> and Fernando Formaggio<sup>1</sup>

<sup>1</sup>Department of Chemistry, University of Padova, 35131 Padova, Italy; and <sup>2</sup>CNRS, Institut de Biologie Moléculaire et Cellulaire, UPR 9021 Immunologie et Chimie Thérapeutiques, 67000 Strasbourg, France

### Introduction

Nucleopeptides containing alanyl-nucleoamino acids, carrying nucleobases at their side-chains, are a recently developed class of nucleic acid analogs displaying promising biological properties [1]. We have recently used  $\alpha$ -aminoisobutyric acid (Aib, Figure 1), a sterically hindered C $^{\alpha}$ -tetrasubstituted  $\alpha$ -amino acid promoting the adoption of helical structures [2], to freeze the conformational freedom of nucleopeptides [3]. In this communication we report the effects of the presence of Aib residues on the conformation and the biological properties of thymine-based nucleopeptides. Three water-soluble nucleo-heptapeptides have been synthesized (Figure 1): **T2A**, carrying two AlaT, one Lys and four Ala residues; **T2U**, in which the central Ala residue is replaced by an Aib residue, and **6TTK**, in which all Ala residues are replaced by Aib residues.

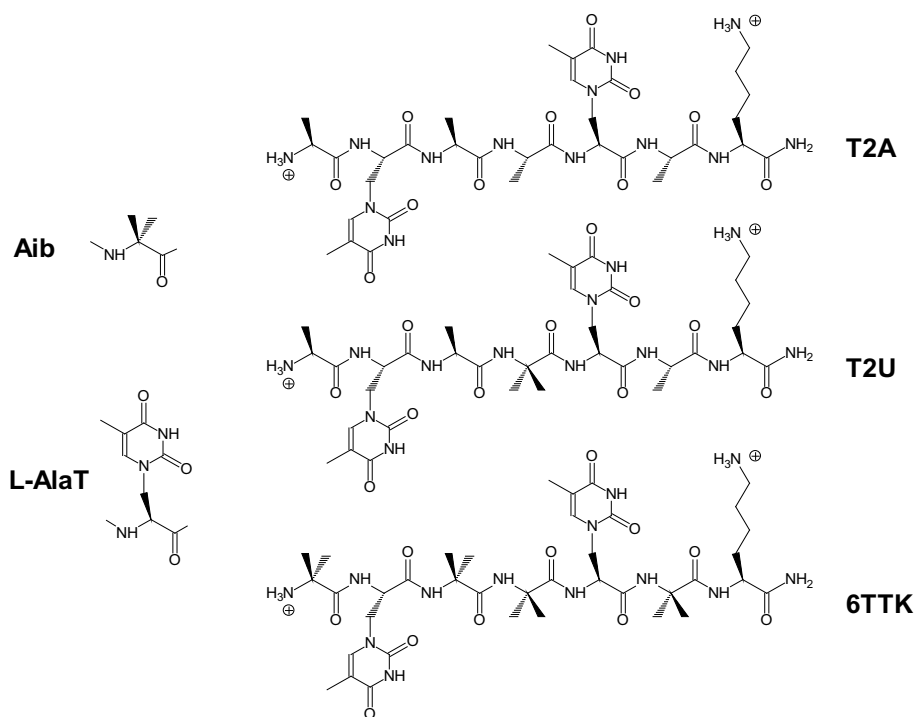


Fig. 1. Chemical structures of Aib, L-AlaT and the nucleo-heptapeptides **T2A**, **T2U**, and **6TTK**.

### Results and Discussion

AlaT was synthesized by nucleophilic ring opening of the N-protected (Boc or Z) serine  $\beta$ -lactone with thymine in the presence of NaH at low temperature [4]. The synthesis of the nucleo-heptapeptides **T2A** and **T2U** was accomplished on solid phase using the Boc/Bzl strategy on a MBHA resin. The Aib-rich nucleopeptide **6TTK** was synthesized in solution, by a segment condensation approach, because of the reduced reactivity of Aib in peptide bond formation.



The conformational preferences of the three nucleo-heptapeptide amides were investigated by means of 2D-NMR and CD techniques. Both in DMSO solution (NMR) and phosphate buffer (CD) nucleopeptide **6TTK** appears to be folded into a helical conformation, most likely of the  $3_{10}$  type, to a much higher extent as compared to **T2A** and **T2U**. In addition, **6TTK** appears to be structurally very stable, as its CD pattern is almost unaffected by a temperature variation of 60 °C (Figure 2A).

Stability tests in mouse serum reveal that **T2U**, in which a single Ala residue is replaced by Aib, is significantly more stable towards enzymatic degradation than **T2A** (Figure 2B). However, the replacement of all Ala with Aib residues in **6TTK** affords a nucleopeptide which is stable even after 8 hour incubation. Interestingly enough, nucleopeptide **6TTK** displays no cytotoxic effects on human lymphoid tumor Raji cells, after 24 hour incubation with peptide concentrations up to 100  $\mu$ M. Therefore, **6TTK** can be potentially exploited as a new carrier for drug delivery and for gene therapy applications. Indeed, its nucleobases might influence the cell biological functions by interacting with RNA or DNA chains in the cell cytoplasm or nucleus.

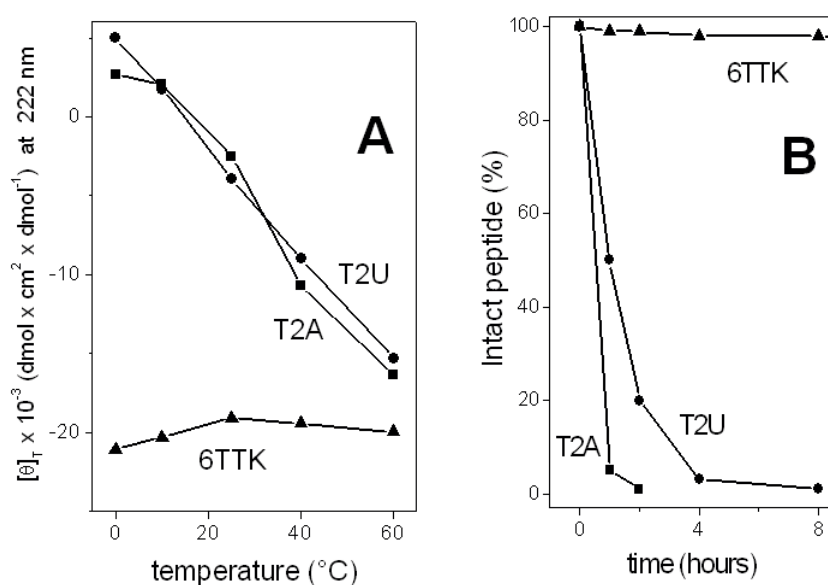


Fig. 2. **A**: Molar ellipticity values at 222 nm for the three nucleopeptides as a function of temperature. **B**: Fraction of intact nucleopeptide after different incubation times in 50% murine serum evaluated by analytical HPLC.

## Acknowledgments

The French-Italian University (UFI-UIF, VINCI Program) is gratefully acknowledged for its support through a Ph.D. scholarship and a travel grant to Piero Geotti-Bianchini.

## References

- Geotti-Bianchini, P., et al. *Org. Biomol. Chem.* **6**, 3661-3663 (2008).
- Toniolo, C., Crisma, M., Formaggio, F., Peggion, C. *Biopolymers (Pept. Sci.)* **60**, 396-419 (2001).
- Geotti-Bianchini, P., et al. *Chem. Commun.*, 3178-3180 (2009).
- Chaltin, P., Lescrinier, E., Lescrinier, T., Rozanski, J., Hendrix, C., Rosemeyer, H., Busson, R., Van Aershot, A., Herdewijn, T. *Helv. Chim. Acta.* **85**, 2258-2283 (2002).

## Do Gt<sub>α</sub>(340-350) Analogs Bind Opsin Similar to its X-ray Crystal Structure?

Christina M. Taylor,<sup>1</sup> Jiawen A. Feng,<sup>1</sup> and Garland R. Marshall<sup>1,2</sup>

<sup>1</sup>Departments of Biochemistry and Molecular Biophysics and of <sup>2</sup>Biomedical Engineering, Washington University School of Medicine, St. Louis, MO 63110, U.S.A.

### Introduction

The interaction between the GPCR, rhodopsin, and its G-protein, transducin is a widely studied interaction. Involved in the vision cascade, rhodopsin is comprised of the apoprotein opsin and 11-*cis* retinal. In its inactive form, rhodopsin is connected to 11-*cis* retinal via a protonated Schiff base. Rhodopsin is activated via a single photon, which leads to *cis-trans* isomerization of 11-*cis* retinal, deprotonation of the Schiff base, and a conformational change to the Metarhodopsin II (MII) state that can bind to transducin. MII decays via hydrolysis of the unprotonated Schiff base, leaving all-*trans* retinal and opsin. Recently, knowledge of the interaction between opsin and transducin has been enhanced by the X-ray crystal structure of opsin [1] bound to Gt<sub>α</sub>(340-350)K341L. The X-ray crystal structure of Gt<sub>α</sub>(340-350)K341L bound to opsin [1] was nearly identical to the TrNOE structure of Gt<sub>α</sub>(340-350) bound to MII-state of rhodopsin [2] solved nearly a decade prior to the crystal structure. However, it remained unclear if the X-ray crystal structure of opsin bound to Gt<sub>α</sub> 340-350)K341L was relevant to the MII state. In the present study, the TrNOE structures of Gt<sub>α</sub>(340-350) and several constrained analogs bound to the MII state were docked to opsin to determine if the MII-binding modes of these analogs were similar to the X-ray crystal structure of Gt<sub>α</sub>(340-350)K341L bound to opsin.

### Results and Discussion

The TrNOE structures of Gt<sub>α</sub>(340-350) and several analogs bound to photoactivated rhodopsin have been solved that have binding affinities similar to Gt<sub>α</sub>(340-350) [2-4]. In a previous study [5], we assumed that these very similar analogs (sequences shown in Table 1) stabilize the MII state by binding R\* (activated rhodopsin) in a manner similar to Gt<sub>α</sub>(340-350). A model of the intracellular (IC) loops in the MII state bound to Gt<sub>α</sub>(340-350) was generated by docking Gt<sub>α</sub>(340-350) and its analogs to an ensemble of low-energy IC loop models generated previously. Distance filters that required Gt<sub>α</sub>(340-350) and its analogs to bind near sites known to be important from experiments were applied to top poses from a low-resolution docking program and then these poses were optimized and scored using a higher-resolution scoring function. The study found that Gt<sub>α</sub>(340-350) and its analogs only bound to the “most open” set of IC loop conformations. A common binding mode for Gt<sub>α</sub>(340-350) and its analogs emerged from the study, revealing important residue-residue interaction necessary for complex formation with the C-terminal recognition motif of Gt<sub>α</sub>. Using these important residue-residue interactions as constraints, the model of the MII state bound to Gt<sub>α</sub>(340-350) was used with virtual screening to identify structurally diverse compounds that stabilized the MII state and also inhibited the

interaction between R\* and transducin [6]. Therefore, the assumption that Gt<sub>α</sub>(340-350) and its analogs bound in a similar manner to the IC loops yielded a model used successfully in virtual screening, indicating some validity of the model.

To determine if the binding site on opsin site is relevant to the MII state of rhodopsin, the same assumption that Gt<sub>α</sub>(340-350) and its analogs should bind opsin in a similar manner was made. Two different docking programs, SKATE (Feng and Marshall, unpublished) and RosettaLigand [7], were used to dock the set of peptides. SKATE performed an exhaustive systematic search anchored by hydrogen bonding where all poses were generated and later scored using a scoring function. There was no receptor side-chain flexibility. The set of TrNOE structures from each peptide were run

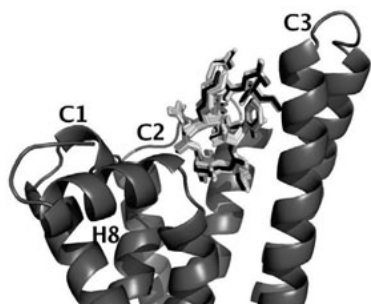


Fig. 1. Gt<sub>α</sub>(340-350)K341L redocked onto opsin.

Table 1. RMSD values for SKATE and RosettaLigand; X indicates a phenylethylamine derivative

Peptide Sequence	RMSD SKATE	RMSD RosettaLigand
Native - IKENLKDCGLF-OH	3.51 Å	7.60 Å
1LVZ - IRENLKDSGLF-OH	4.68 Å	----
GTA14 - IKENLKDCGLF-NH <sub>2</sub>	4.34 Å	6.79 Å
GTA13 - IKENLKDCGL(2-Nal)-NH <sub>2</sub>	----	7.50 Å
GTA19 - IKENLKDCGLX*	----	4.06 Å

separately and then the poses were combined and scored using FRED [8] with rigid-body optimization and minimization. A volume 9 Å in all directions from the binding site of Gt<sub>α</sub>(340-350)K341L in the crystal structure was sampled. The top 10 poses based on the FRED score were analyzed in detail. RosettaLigand was used in a separate docking calculation. The sampling with RosettaLigand was stochastic with receptor side-chain flexibility and some backbone flexibility during docking. RosettaLigand sampled poses within a 10 Å x 10 Å x 10 Å box with its center at the center of mass of Gt<sub>α</sub>(340-350)K341L from the X-ray crystal structure. The program sampled the sets of TrNOE structures and created 10,000 poses per analog. For both SKATE and RosettaLigand, the top 10 poses based on their respective scoring functions were analyzed and the pose closest to Gt<sub>α</sub>(340-350) is reported in Table 1. Those that dock horizontally along the receptor loops or upside down do not have RMSDs reported. A reference structure was generated by superimposing C<sub>α</sub> atoms of each analog onto the X-ray crystal structure of Gt<sub>α</sub>(340-350)K341L to calculate the RMSD.

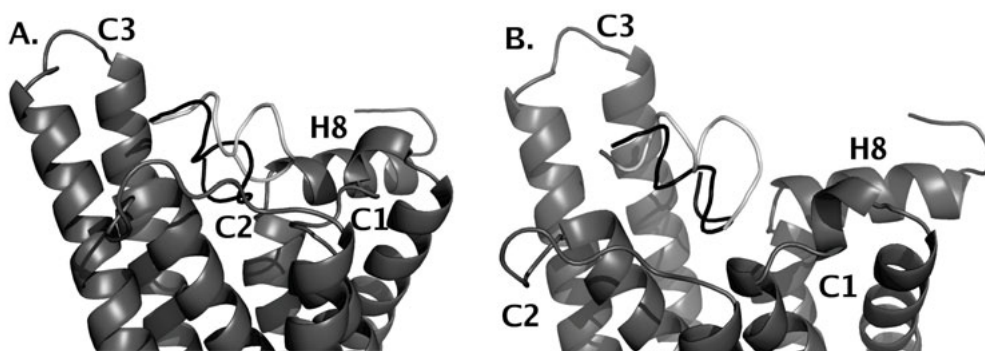


Fig. 2. Docked pose is shown in light grey and pose from the X-ray crystal structure is shown in black. Pose closest to Gt<sub>α</sub>(340-350)K341L from top 10 solutions using A. SKATE and B. RosettaLigand.

To test the methodology, RosettaLigand was used to dock the X-ray crystal structure of Gt<sub>α</sub>(340-350)K341L back onto a structure of opsin with its side chains repacked. The results are shown in Figure 1. All of the top 10 poses of Gt<sub>α</sub>(340-350) docked within 0.44 to 0.61 Å of the X-ray crystal structure as shown in light grey, and Gt<sub>α</sub>(340-350)K341L from the X-ray crystal structure is shown in black. RosettaLigand was able to recapitulate the binding pose of Gt<sub>α</sub>(340-350)K341L onto opsin.

The TrNOE structures of Gt<sub>α</sub>(340-350) were docked onto the opsin crystal structure using SKATE and RosettaLigand. Out of the top 10 solutions based on the respective scoring functions, the best docked pose is shown in Figure 2 along with the X-ray crystal structure of Gt<sub>α</sub>(340-350)K341L. The TrNOE structure from Gt<sub>α</sub>(340-350) docked in the same general area as the X-ray crystal structure of Gt<sub>α</sub>(340-350)K341, but the C-terminal region was tilted upwards more. The RMSD values, when compared to the reference structure, differ by a significant amount more than when the X-ray crystal structure itself is redocked onto opsin. The TrNOE structure gives the conformation of Gt<sub>α</sub>(340-350) and its analogs when bound to the MII state. These structures should dock well to opsin if the binding of Gt<sub>α</sub>(340-350)K341L to opsin is truly indicative of the binding of Gt<sub>α</sub>(340-350) to MII.

The TrNOE structures of Gt<sub>α</sub>(340-350) analogs were also docked onto the opsin crystal structure using SKATE and RosettaLigand. The RMSD of the pose closest to the Gt<sub>α</sub>(340-350)K341L X-ray crystal structure out of the top 10 best scoring poses is shown in Table 1. Some of the analogs docked with RMSD values similar to the TrNOE structure of Gt<sub>α</sub>(340-350), whereas other analogs docked horizontally along the receptor (those RMSD values are not shown in Table 1). Despite the difference in RMSD values between the docked pose and the reference structure, Gt<sub>α</sub>(340-350) and its analogs have a binding site on opsin similar to the X-ray crystal structure binding site. However, precise residue-residue interactions between Gt<sub>α</sub>(340-350) and its analogs are different in the X-ray crystal structure and the docked structures.

In conclusion, the TrNOE structures of Gt<sub>α</sub>(340-350) and its analogs bind to a similar region of opsin as Gt<sub>α</sub>(340-350)K341 in the crystal structure, making interactions with many of the same residues. However, the residue-residue interactions differ and the RMSD between the reference structure and the docked poses are significantly different. The inability to recapitulate the exact binding pose of native Gt<sub>α</sub>(340-350) via docking the TrNOE structures is concerning. Although there are potential inaccuracies in both docking calculations due to sampling and scoring, these docking results may indicate that the structure of opsin bound to Gt<sub>α</sub>(340-350)K341L is irrelevant to studies of MII bound to Gt<sub>α</sub>(340-350) for several reasons. First, opsin can be stabilized by the C-terminus of the α-subunit of transducin, Gt<sub>α</sub>(340-350), but activates at only 4000 to 2,000,000 of the rate MII exhibits. Secondly, transducin could not be built onto Gt<sub>α</sub>(340-350)K341L without transducin clashing with the membrane. To avoid the clash, the main body of transducin had to be tilted by 40° [1]. Recently, an intermediate conformation of Gt<sub>α</sub>(340-350)K341L has been suggested based on docking calculations using an extended model of Gt<sub>α</sub>(340-350)K341L and opsin [9]. The intermediate pose is similar to the pose seen in this study when the TrNOE structures of the native peptide and its analogs are docked onto opsin. In this study, the authors propose a switch between the R\*-G<sub>i</sub>-GDP complex and R\*-G<sub>i</sub>[empty] complex. In addition, another docking study also has suggested there may be multiple binding modes for Gt<sub>α</sub>(340-350) [10]. Further, the peptide in the X-ray crystal structure also has a mutation from Lys to Leu at 341, causing it to bind with a much higher affinity than the native peptide, too tight to be an object for TrNOE studies. Therefore, this analog, and the other analogs, may not have the same binding mode as native Gt<sub>α</sub>(340-350). In addition, the crystal structure itself may not be accurate enough to elucidate precise residue-residue interactions, as the X-ray crystal structure of opsin bound to Gt<sub>α</sub>(340-350)K341L has very high B-factors in the intracellular loop region and particularly on the Gt<sub>α</sub>(340-350)K341L peptide and also a resolution of only 3.2 Å. More research needs to be done to confirm the validity of Gt<sub>α</sub>(340-350)K341L bound to opsin before this structure is assumed to represent the interaction between rhodopsin and transducin in the MII state.

## Acknowledgments

This work was supported by a NIH NRSA Postdoctoral Fellowship F32GM082200 (C.M.T.) and National Institutes of Health grants GM68460, GM53630, and EY1211301 (G.R.M.).

## References

1. Scheerer, P., Park, J.H., Hildebrand, P.W., Kim, Y.J., Krauss, N., Choe, H.W., Hofmann, K.P., Ernst, O.P. *Nature* **455**, 497-502 (2008).
2. Kisselev, O.G., Kao, J., Ponder, J.W., Fann, Y.C., Gautam, N., Marshall, G.R. *Proc. Natl. Acad. Sci. U.S.A.* **95**, 4270-5 (1998).
3. Anderson, M.A., Ogbay, B., Arimoto, R., Sha, W., Kisselev, O.G., Cistola, D.P., Marshall, G.R. *J. Am. Chem. Soc.* **128**, 7531-41 (2006).
4. Anderson, M.A., Ogbay, B., Kisselev, O.G., Cistola, D.P., Marshall, G.R. *Chem. Biol. Drug. Des.* **68**, 295-307 (2006).
5. Taylor, C.M., Nikiforovich, G.V., Marshall, G.R. *Biophys. J.* **92**, 4325-34 (2007).
6. Taylor, C.M., Barda, Y., Kisselev, O.G., Marshall, G.R. *J. Med. Chem.* **51**, 5297-303 (2008).
7. Davis, I.W., Baker, D. *J. Mol. Biol.* **385**, 381-92 (2009).
8. *OE Chem*, version 1.3.4; OpenEye Scientific Software, Inc.: Santa Fe, NM, U.S.A. [www.eyesopen.com](http://www.eyesopen.com), 2005.
9. Scheerer, P., Heck, M., Goede, A., Park, J.H., Choe, H.W., Ernst, O.P., Hofmann, K.P., Hildebrand, P.W. *Proc. Natl. Acad. Sci. U.S.A.* (2009).
10. Nikiforovich, G.V., Taylor, C.M., Marshall, G.R. *Biochemistry* **46**, 4734-44 (2007).

## The Use of Paramagnetic and Fluorescent Quenching Amino Acid TOAC for Evaluating Angiotensin I-Converting Enzyme

Luis G. D. Teixeira,<sup>1</sup> Patricia A. Bersanetti,<sup>1</sup> Shirley Schreier<sup>2</sup>,  
Adriana K. Carmona,<sup>1</sup> and Clovis R. Nakaie<sup>1\*</sup>

<sup>1</sup>Department of Biophysics - Federal University of Sao Paulo, Sao Paulo, CEP 04044-020, Brazil;

<sup>2</sup>Department of Biochemistry, Institute of Chemistry, Sao Paulo University, CEP 05513-870, Brazil.

### Introduction

Advantageously to other fluorescent quenching probes known so far, the TOAC (2,2,6,6-tetramethylpiperidine-1-oxyl-4-amino-4-carboxylic acid) spin label, introduced earlier by us in the chemistry of peptides [1,2], can be inserted at any position of an enzyme substrate. Taking into account this characteristic, the present work examined the specificity of angiotensin I-converting enzyme (ACE) that cleaves the vasoactive angiotensin I (AI, DRVYIHPFHL) to produce the angiotensin II and on the other hand, inactivates the hypotensor bradykinin (BK, RPPGFSPFR) [3,4]. For this evaluation, TOAC-attaching AI (at positions 0, 1, 3, 5, 8, 9 and 10) and BK (at positions 0, 3, 7 and 9) were synthesized and evaluated towards their properties as ACE substrates. Moreover, EPR and fluorescence investigations were also initiated with these labeled analogues aiming at further investigating the structure-function relationship and also the possibility of monitoring kinetics of ACE activity.

### Results and Discussion

Following a previously described method [2,5], all TOAC-bearing AI and BK analogues were synthesized manually in 0.2 mmol scale and purified by preparative HPLC to > 97% purity. The peptides were assayed for ACE activity, taking either AI or BK as the control substrates. The progress of hydrolysis reaction was monitored through LC/ESI-MS of the components at different times (up to 120 min). TOAC-attaching AI analogues at positions 0, 1, 3, 5, 8, 9 and 10 indicated that only the first four analogues are substrates for ACE with *k*<sub>cat</sub>/*k*<sub>m</sub> values of 11.9; 9.2; 3.2 and 2.0 respectively, in comparison with 15.4  $\mu\text{M}^{-1}\cdot\text{min}^{-1}$  of the native AI. These results confirm that greater the proximity of the unnatural probe to the cleavage site, the smaller is the substrate specificity of analogues. Comparatively, a greater decrease in the substrate activity was observed with BK derivatives, where TOAC<sup>0</sup>-BK and TOAC<sup>3</sup>-BK presented *k*<sub>cat</sub>/*k*<sub>m</sub> of 20.9 and 38.9 respectively (against 202  $\mu\text{M}^{-1}\cdot\text{min}^{-1}$  for BK). Other two analogues (TOAC<sup>7</sup>-BK and TOAC<sup>9</sup>-BK) were devoid of substrate activity.

EPR spectra that the rotational correlation time ( $\tau_c$ ) at neutral pH, for AI derivatives attaching TOAC probe at positions 0, 1, 3, 5, 8, 9 and 10 were about 2.3; 2.0; 7.4; 8.4; 7.4; 3.3 and  $5.1 \times 10^{-10}$  s, respectively. In the case of BK derivatives labeled at positions 0, 3, 7 and 9, the calculated  $\tau_c$  values were about 2.2; 4.8; 5.4 and  $3.5 \times 10^{-10}$  s, respectively. These results indicated higher mobility for AI and BK analogues containing the paramagnetic probe at either N- or C-terminal positions.

Fluorescence studies clearly demonstrated the quenching property of the nitroxide function present in the TOAC structure, affecting mainly the Tyr<sup>4</sup> residue in AI and Phe<sup>5</sup> and Phe<sup>8</sup> in BK, respectively. In general, the fluorescence intensity of paramagnetically labeled substrates decreased with increasing proximity between TOAC and fluorescent residue, thus suggesting extended structures for most of these peptides. According to preliminary fluorescence results previously observed with TOAC-attaching AI derivatives [5], rather similar effect was also observed for BK analogues. Figure 1 displays the fluorescence spectra of BK and its four labeled derivatives.

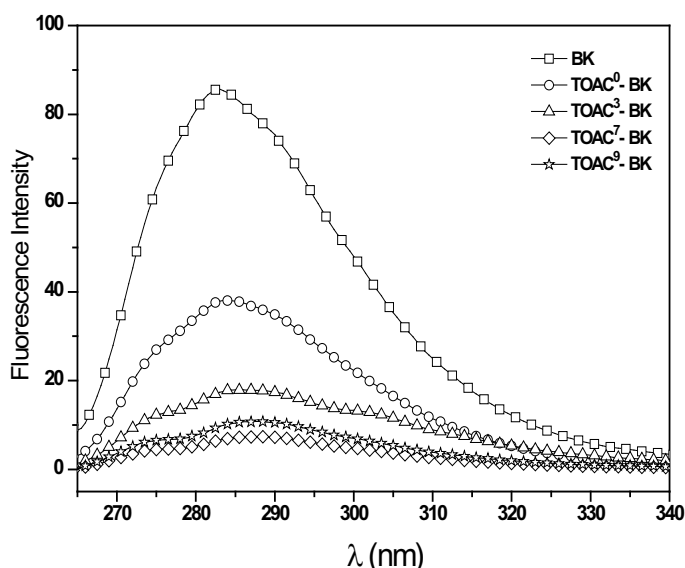


Fig. 1. Fluorescence spectra of BK and its TOAC-labeled analogues in water, pH 7.0.

A significant degree of quenching phenomenon is clearly observed when all the fluorescence curves of BK analogues are compared with the native peptide. Due to the greater proximity between TOAC probe and the two Phe residues located at positions 5 and 8 of the sequence, the TOAC<sup>3</sup>-BK, TOAC<sup>7</sup>-BK and TOAC<sup>9</sup>-BK induced greater quenching effect than the N-terminally labeled TOAC<sup>0</sup>-BK.

In conclusion, due to the feasibility of monitoring on the dynamics and conformation of TOAC-bearing peptides, the application of this paramagnetically substrate labeling strategy would be of great potential also for better understanding of enzyme-catalyzed peptide reactions.

## Acknowledgments

We thank CNPq and FAPESP for financial support.

## References

1. Nakaie, C.R., Goissis, G., Schreier, S., Paiva, A.C.M. *Braz. J. Med. Biol. Res.* **14**, 173-180 (1981).
2. Marchetto, R., Schreier, S., Nakaie, C.R. *J. Am. Chem. Soc.* **115**, 11042-11043 (1993).
3. Paul, M., Mehr, A. P., Kreutz, R. *Physiol. Rev.* **86**, 747-803 (2006)
4. Oliveira, L., Costa-Neto, C.M., Nakaie, C.R., Schreier, S., Shimuta, S., Paiva, A.C.M. *Physiol. Rev.* **87**, 565-592 (2007).
5. Teixeira, L.G.D., Bersanetti, P.A., Schreier, S., Carmona, A.K., Nakaie, C.R. *FEBS Lett.* **581**, 2411-2415 (2007).

## A Photolabile Thiol Protecting Group for Cellular Studies

Daniel Abate-Pella,<sup>1</sup> Nicholette Zeliadt,<sup>2</sup> Daniel Mullen,<sup>1</sup>  
Patrick McDonald,<sup>3</sup> Priyanka Pathak,<sup>1</sup> Timothy Dore,<sup>4</sup>  
Joachim Mueller,<sup>3</sup> Elizabeth Wattenberg,<sup>2</sup> and Mark D. Distefano<sup>1</sup>

<sup>1</sup>Department of Chemistry, University of Minnesota, Minneapolis, MN 55455, U.S.A.;

<sup>2</sup>Department of Public Health, University of Minnesota, Minneapolis, MN 55455, U.S.A.;

<sup>3</sup>Department of Physics, University Of Minnesota, Minneapolis, MN 55455, U.S.A.;

<sup>4</sup>Department of Chemistry, University of Georgia, Athens, GA 30602, U.S.A.

### Introduction

Caging groups that allow thiol groups to be revealed upon photolysis have significant utility in studying a plethora of biological processes [1,2]. Here we describe the preparation of peptides and peptidomimetics that include cysteine residues that have been masked with a photoremovable BHQ (brominated hydroxyquinoline) group. The protecting group can be installed in peptides either by post- synthetic modification or via standard Fmoc SPPS. Kinetic analysis reveals that BHQ uncaging of thiols is significantly more rapid compared to nitrobenzyl-based groups although BHQ photolysis results in other nonproductive photoproducts that decreases the overall efficiency. A peptidomimetic farnesyltransferase inhibitor (FTI) has been prepared that contains a BHQ-protected cysteine residue that attenuates its activity in inhibiting ras protein prenylation. Photolysis of that FTI-BHQ conjugate in the presence of living cells results in farnesyltransferase inhibition and a concomitant decrease in ras processing as evidenced by confocal microscopy.

### Results and Discussion

In order to examine the ability of BHQ to serve as a caging group for thiols, we synthesized the peptide dansyl-GC(BHQ)VLS (**1**) and peptidomimetic FTI BHQ-L-744,823 (**2**) (see Figure 1). Peptide **1** was irradiated with 365-nm light for varying amounts of time and the extent of the photochemical reaction was monitored by HPLC. From the HPLC data, an exponential decay time course was plotted (see Figure 2), and according to this data decay rate  $k = 0.028\text{ s}^{-1}$  and peptide half-life  $t_{1/2} = 25.2\text{ s}$ . This rate is faster than the uncaging of thiols containing nitrobenzyl protecting groups available in the literature [3,4]. LC-MS analysis of the uncaging

reaction was also performed in order to confirm the presence of free peptide (**3**) upon irradiation. However, in addition to detecting free thiol, a nonproductive photoproduct also appeared which seems to correspond to the loss of HBr from the caged peptide based on MS results. Though the formation of this byproduct decreases the overall efficiency of the reaction, its presence is not problematic since it remains caged and does not behave as the uncaged peptide.

We synthesize caged FTI **2** by coupling the commercially available FTI L-744,832 (**4**) with our BHQ protecting group. Irradiation with 365-nm light and subsequent HPLC analysis resulted in decay rate  $k = 0.056\text{ s}^{-1}$  and half life  $t_{1/2} 12.4\text{ s}$ . Additionally, LC-MS analysis revealed the presence of free thiol after uncaging as well as a byproduct that corresponds to the loss of HBr from the caged FTI. In order to study the photolysis reaction in cells, we utilized GFP-ras producing MDCK cells. Untreated cells have ras protein prenylated and fully processed and it localizes to the cell membrane (Figure 3, top left), whereas in FTI treated cells ras is unprenylated and localizes evenly throughout the cytoplasm (Figure 3, bottom left). Cells were treated with caged FTI **2**, irradiated for 4 min and allowed to grow for

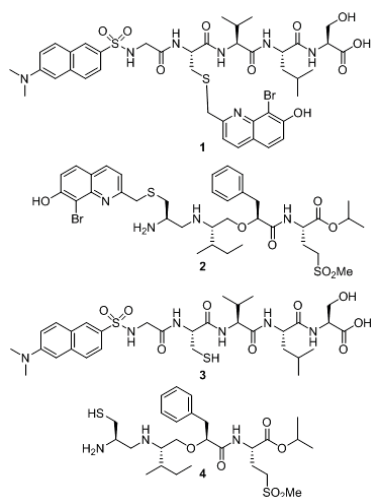


Fig. 1. BHQ-caged peptide and peptidomimetic and their respective uncaged products.



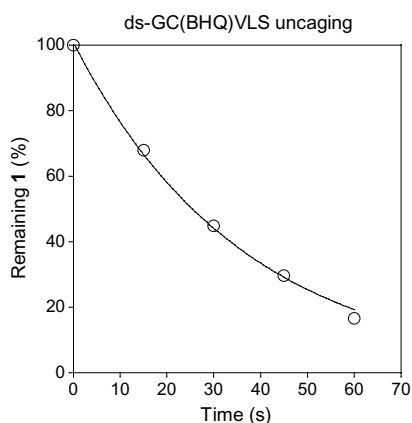


Fig. 2. Photolysis time course of peptide 1.

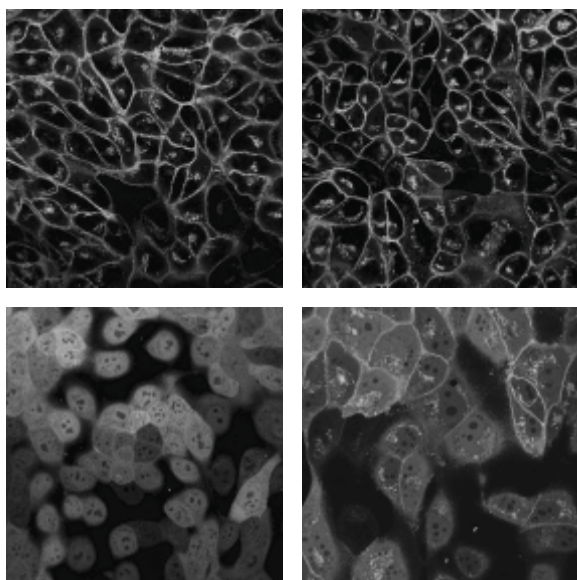


Fig. 3. MDCK cells localize Ras protein differently depending on its prenylation status. Top left: untreated cells. Top right: cells treated with 2, no UV. Bottom left: FTI treated cells. Bottom right: cells treated with 2 and UV light.

## Acknowledgments

This work was supported by the National Institutes of Health (GM58442).

## References

1. Furuta, T., Takeuchi, H., Isozaki, M., Takahashi, Y., Kanehara, M., Sugimoto, M., Watanabe, T., Noguchi, K., Dore, T., Kurahashi, T., Iwamura, M., Tsien, R. *Chem. BioChem.* **5**, 1119-1128 (2004).
2. Zhu, Y., Pavlos, C., Toscano, J., Dore, T. *JACS* **128**, 4267-4276 (2006).
3. Pan, P., Bayley, H. *FEBS Lett.* **405**, 81-85 (1997).
4. Specht, A., Ludwig, S., Peng, L., Goeldner, M. *Tet. Lett.* **43**, 8947-8950 (2002).



## Development of Imaginable Toxin A Peptide for Cellular Imaging Study

**Wei Wang, Zhi-Dong Jiang, Arlin G. Cameron, Michel E. Mawad,  
Herbert L. DuPont, and Shi Ke**

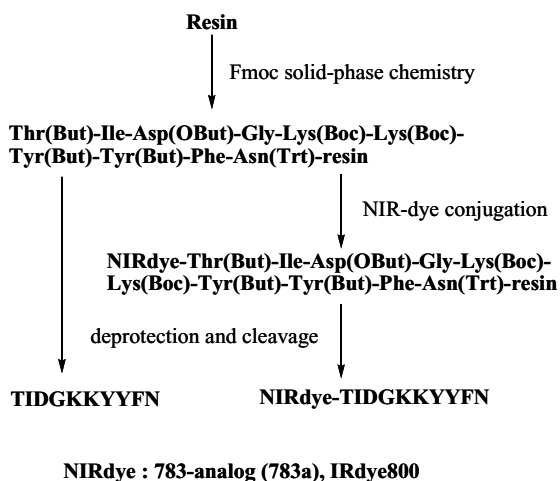
*Baylor College of Medicine, Houston, TX 77030, U.S.A.*

## Introduction

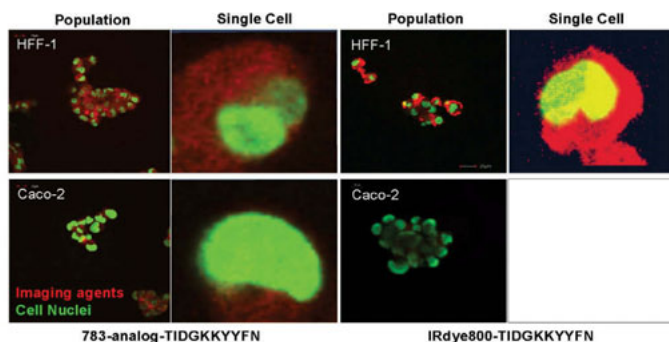
*C. difficile* is a gram-positive, strictly anaerobic, spore-forming bacillus which can cause pseudomembranous colitis requiring colectomy and resulting in death in hospitalized patients. Currently the treatment of *C. difficile* colitis is inadequate and relapse rates are close to 50%. Pathogenic strains of *C. difficile* produce toxins. The toxins can cause severe inflammatory changes of colonic mucosa, leading to formation of an inflammatory pseudomembrane. However, the mechanism of the pathogenesis of the toxins to cause the disease is not clear. Development of imaginable toxin peptides will allow us to better understand the interactions between the toxins and human cells.

## Results and Discussion

A toxin A peptide with 10 amino acids (TIDGKKYYFN) was synthesized and conjugated with near-infrared (NIR) dyes, either 783-analog dye generated in-house or commercial available IRdye 800CW (Figure 1). The cellular imaging study of both imaging agents was carried out on two cell lines, HFF-1 (normal human foreskin cell line) and .Caco-2 (human colorectal adenocarcinoma cell line) using a custom modified NIR Olympus confocal system (Figure 2). The cellular toxicity assay of toxin A, TIDGKKYYFN, and 783a-TIDGKKYYFN was performed on HFF-1, Caco-2 cell lines (Figure 3) and HT29 (human colorectal adeno-carcinoma cell line) (Figure 4).



*Fig. 1. Synthesis procedure for optical imaging toxin A peptides, 738a-TIDGKKYYFN and IRdye800-TIDGKKYYFN.*



**Fig. 2. Confocal images of 783a-TIDGKKYYFN (left) and IRDye800-TIDGKKYYFN (right) interactions with human cells HFF-1(top) and Caco-2 (bottom) respectively. Images demonstrate that imaging agent 783a-TIDGKKYYF binds to both cell lines while the IRDye800-TIDGKKYYFN only shows binding signal with HFF-1.**

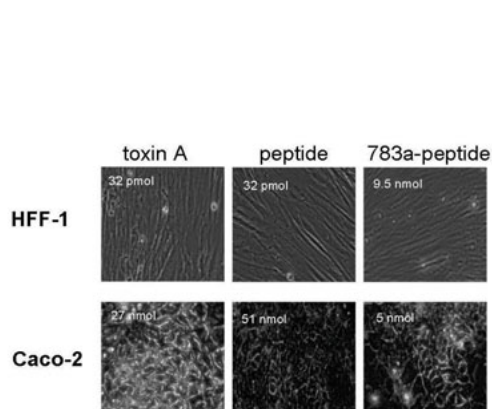


Fig. 3. Microscopic images of toxin A, peptide and 783a-peptide on HFF-1 and Caco-2 cell lines respectively. The results reveals that 783a-peptide possesses similar properties as Toxin A and unlabeled peptide.

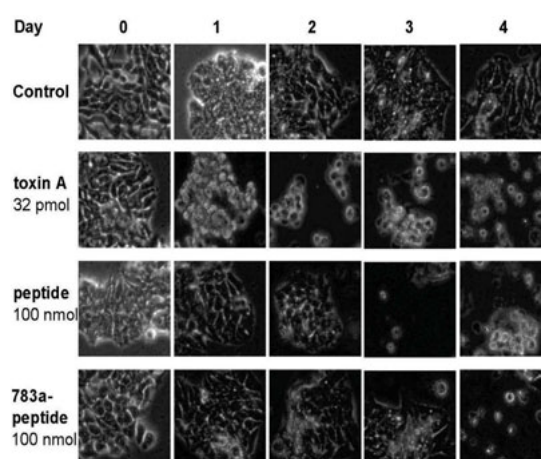


Fig. 4. Cellular toxicity assay. Microscope visualizes intoxicated rounding cells. Cell rounding effect stated at 1, 3, and 4 days for toxin A peptide and 783a-peptide respectively. The results demonstrate that peptide and peptide conjugated with NIR dye are less toxic than toxin A.

## Conclusions

Confocal images reveals that IRdye 800-TIDGKKYYF does not bind to the cell line Caco-2. It indicates that the conjugation of a fluorophore to a peptide can interfere with its binding affinity to the desired target.

The toxicity assay confirms that 783-analog-TIDGKKYYFN maintains same properties as the unlabeled toxin A peptide and commercial toxin protein. Furthermore, peptide and imaginable peptide are less toxic than toxin A.

The imaginable toxin A peptide (783a-TIDGKKYYFN) can be used as tool to study the toxin mechanisms as well as to develop inhibitors, blocking agents and therapeutic agents. Confocal images demonstrate that 783-analog-TIDGKKYYF internalizes into both tested cell lines (HFF-1 and Caco-2).

## Design of a Receptor Labeling Angiotensin II Analogue Containing a 3'-hydroxy-Tyrosine in Position 4

H. Jarine, J. Arsenault, M.-R. Lefebvre, D. Fillion, G. Guillemette,  
R. Leduc, and E. Escher

Université de Sherbrooke, Faculté de Médecine et des Sciences de la Santé, Département de pharmacologie, Sherbrooke, Québec, J1H 5N4, Canada

### Introduction

Biologically active G Protein Coupled Receptor (GPCR) structures are not yet accessible to analytical methods. The human angiotensin II type 1 receptor (hAT<sub>1</sub>) has been investigated with photoaffinity labeling approaches using Angiotensin II (DRVYIHPF, AngII) analogues with biologically acceptable photolabile moieties. The radio iodinated photolabile ligand would bind with high affinity to the hAT<sub>1</sub> receptor and UV irradiation would covalently link the ligand to the receptor. Following chemical and enzymatic digestions direct ligand receptor interactions could be elucidated. Many ligand-receptor contact points were found for most ligand residues; nevertheless, the central amino acid of AngII, the Tyrosine 4 residue could never be addressed due to inadequate SAR results with all attempted photolabile substitutions. For labeling experiments to succeed we needed an analogue with high specific affinity to its cognate receptor, a labeling moiety inserted in the analogue and a revealing moiety to identify the labeled receptor. To remediate this difficulty a DOPA (3', 4'-dihydroxyphenylalanine or 3'-hydroxy-tyrosine) was introduced into position 4 of AngII, maintaining low nM receptor affinity (Table 1). Once oxidized with NaIO<sub>4</sub>, the DOPA moiety may form a covalent bond to a Cysteine residue of the target receptor through a Michael addition of the free thiol group (Figure 1). The

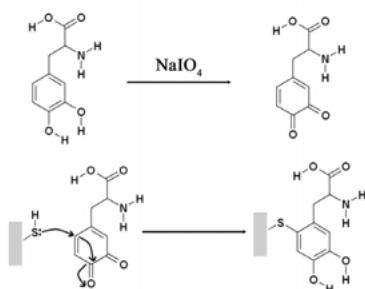


Fig. 1. Oxidation and Michael addition mechanism.

oxidized DOPA forms an electrophilic ortho-quinone that reacts with nearby nucleophiles such as Cysteine or Histidine and through a Schiff base formation with Lysine [1,2]. This analogue can thus maintain native like binding and permit the oxidative labeling of hAT<sub>1</sub>.

### Results and Discussion

Position 4 of AngII is refractive to modification and all photolabile amino acid substitution of this residue resulted in a great loss of affinity and efficacy. Previous unpublished experiment had shown when AngII was modified to incorporate a traditional photoprobe in position 4, such as Bpa and Tdf, the ligand's affinity dropped a thousand fold (Table 1). The electronegativity of Tyrosine's aromatic ring had been shown to be of importance for ligand binding [3,4]. The AngII analogue first prepared was the [Sar<sup>1</sup>, Dopa<sup>4</sup>] AngII on solid phase peptide synthesis. The DOPA structure maintains the para orientation of the hydroxy on the aromatic ring, like tyrosine, which is important for SAR [4]. This peptide had sub nM affinity, slightly better than native AngII to displace <sup>125</sup>I-[Sar<sup>1</sup>, Ile<sup>8</sup>] AngII (Table 1). Also the binding affinity was tested on the constitutively active (CAM) hAT<sub>1</sub> mutant: N111G hAT<sub>1</sub>. This CAM has been shown to be more permissive to ligand modification than WT hAT<sub>1</sub>. The N111G hAT<sub>1</sub> mutant also showed sub nM affinity towards [Sar<sup>1</sup>, Dopa<sup>4</sup>] AngII.

To assure thiol linking capabilities, this peptide was incubated in 1 mM H-Cys-OH, oxidized with 1mM of NaIO<sub>4</sub> for 10 min and the reaction was quenched with 0.1M DTT. Samples were submitted to MALDI-TOF mass spectrometry. Free Cysteine addition to the analogue was confirmed. The peptide was also iodinated as previously described [5] to permit subsequent radiolabeling and autoradiographic identification of the ligand hAT<sub>1</sub> receptor complex. Mass spectrometry also confirmed peptide iodination but the iodinated peptide could not be confirmed to link free Cysteine. This is due to the Iodine's electrophilic addition within

Table 1. AngII analogue affinities on WT hAT<sub>1</sub> and N111G hAT<sub>1</sub>.

Ligand	<i>K<sub>d</sub></i> (nM)	<i>K<sub>d</sub></i> (nM)
	WT hAT <sub>1</sub>	N111G hAT <sub>1</sub>
AngII	1.7±0.1	0.7±0.1
[Sar <sup>1</sup> , Ile <sup>8</sup> ] AngII	0.8±0.2	0.6±0.2
[Sar <sup>1</sup> , Bpa <sup>4</sup> , Tyr <sup>8</sup> ] Ang II	>1000	>500
[Sar <sup>1</sup> , Tdf <sup>4</sup> , Tyr <sup>8</sup> ] Ang II	>1000	>500
[Sar <sup>1</sup> , Dopa <sup>4</sup> ] Ang II	0.5±0.4	0.8±0.4
[Iminobiotin-ACA <sup>0</sup> , Gly <sup>1</sup> , Dopa <sup>4</sup> ] AngII	5±2	0.4±0.2
[Sar <sup>1</sup> , Dopa <sup>4</sup> , Tyr <sup>8</sup> ] AngII	0.2±0.1	0.3±0.2

the aromatic ring of the DOPA residue. Such a modification either sterically hindered the reaction or modified the electronic density on the aromatic ring to inhibit normal quinone formation and subsequent Cysteine addition.

In order to reveal ligand labeled receptors two distinct modifications were undertaken. The first consisted of an iminobiotin addition with an aminocaproic acid (ACA) linker on the N-terminal part of the ligand. This would enable ligand identification through western blotting using a Streptavidin-HRP chemiluminescence reaction. Ligand affinity with the iminobiotinated analogue was assessed with a concentration-dependent displacement of the <sup>125</sup>I-[Sar<sup>1</sup>, Ile<sup>8</sup>] AngII radiotracer. This [Iminobiotin-ACA<sup>0</sup>, Gly<sup>1</sup>, DOPA<sup>4</sup>] AngII analogue shows a 10 fold loss of K<sub>d</sub> to WT hAT<sub>1</sub> receptors compared to the [Sar<sup>1</sup>, DOPA<sup>4</sup>] AngII analogue but a K<sub>d</sub> of 5nM should be sufficient for labeling attempts. Nevertheless, the same analogue maintained sub nM affinity towards the more SAR-tolerant N111G hAT<sub>1</sub> (Table 1).

The second approach, allowing the hitherto utilized autoradiography approach, was made possible with the addition of a Tyrosine in position 8 of AngII. This peptide demonstrated even higher affinity than the previous analogues on WT hAT<sub>1</sub> and N111G hAT<sub>1</sub> receptors with an almost 10 fold increase compared to AngII affinity. The 3',4'-dihydroxyphenyl moiety can be protected prior to synthesis with the semi-permanent acetonide group during peptide synthesis, cleavage, purification and radio iodination on the Tyrosine residue in position 8. Subsequent treatment with 95% TFA removed the acetonide group and thus protected DOPA during radiiodination.

These labeling analogues will be tested on the hundreds of Cysteine hAT<sub>1</sub> mutants previously prepared and characterized for the Substituted Cysteine Accessibility Method (SCAM) on AT<sub>1</sub> and on N111G-hAT<sub>1</sub> [6]. Reactive Cysteine mutants should then give exact ligand to receptor contact points as opposed to the variable binding affinities obtained from SCAM studies. These results would enhance our understanding of ligand receptor interactions and of receptor activation mechanisms.

## Acknowledgments

We would like to thank the Heart and Stroke Foundation of Canada and the Canadian Institutes of Health Research for funding. We would also like to thank the American Peptide Society and the 21<sup>st</sup> American Peptide Symposium organisation team for travel grant issued to Mr. Jason Arsenault.

## References

1. Umanah, G.K.E., et al. *Biochemistry* **48**, 2033-2044 (2009).
2. Liu, B., et al. *J. Am. Chem. Soc.* **127**, 15228-15235 (2006).
3. Guillemette, G., et al. *J. Med. Chem.* **27**, 315-320 (1982).
4. De Gasparo, M., et al. *Pharmacol. Rev.* **52**, 415-472 (2000).
5. Bosse, R., et al. *Regul. Pept.* **44**, 215-223 (1993).
6. Domazet, I., et al. *J. Biol. Chem.* **18**, 11922-11929 (2009).

## Synthesis and Biological Characterization of Novel Fluorescent Analogs of Vasopressin

Sylvia Chen,<sup>1</sup> Richard Bouley,<sup>2</sup> Jean-Pierre Vilardaga,<sup>1,2,3</sup>  
 Dennis A. Ausiello,<sup>2</sup> and Ashok Khatri<sup>1</sup>

<sup>1</sup>Endocrine Unit, <sup>2</sup>Center for Systems Biology, Program in Membrane Biology & Nephrology Division, Massachusetts General Hospital and Harvard Medical School, Boston, MA 02114, U.S.A. and  
<sup>3</sup>Dept. of Pharmacology and Chemical Biology, School of Medicine, University of Pittsburgh, Pittsburgh, PA 15261, U.S.A.

### Introduction

Since the original synthesis of vasopressin, hundreds of its analogs have been synthesized and studied. However, only a few fluorescent vasopressin analogs are available [1-4]. The need for suitable fluorescent tools to study intracellular trafficking of G protein-coupled receptors has resulted in the search of novel fluorescent vasopressin (VP) analogs for receptor-ligand interactions. We base our study on previous studies that show the feasibility of using cyclic fluorescent VP analogs to observe intracellular binding studies between ligand and VP receptor type 2 (V<sub>2</sub>R). The aim of this study was to develop a cyclic fluorescent vasopressin analog with high affinity, and containing a fluorophore with a good quantum yield and low pH-sensitivity. Thus, our studies involve the synthesis and biological activities of analogs with Lys<sup>8</sup> modifications. In these analogs, Lys<sup>8</sup> was coupled to spacers of different lengths on the ε-amine, followed by coupling of fluorophores, 5 or 6-carboxytetramethylrhodamine (TAMRA) at amino groups of these spacers. The N-terminus of some analogs were also altered to incorporate (2-mercapto)propionic acid which formed a disulfide linkage with Cys<sup>6</sup>. The biological activities of these analogs were measured using receptor affinity binding assays and cAMP production in LLC-PK1 cells.

### Results and Discussion

We studied the intracellular trafficking of V<sub>2</sub>R by using seven analogs, which include **1512-5 (VP<sup>TMR</sup>)**, synthesized by Fmoc solid-phase chemistry. Vasopressin analogs were purified and their structures were confirmed by Matrix-assisted Laser Desorption Ionization Time of Flight mass spectrometry (MALDI-TOF/MS). Of all the analogs tested, the analogue 1512-5 (VP<sup>TMR</sup>) as illustrated in Figure 1, with molecular mass of 1698.92 Da, exhibited a binding affinity (K<sub>d</sub>) (157 ± 52 nM) close to that of the native LVP (35 ± 18 nM). Affinity of ligands for the V<sub>2</sub>R were investigated by radioligand binding assays conducted in LLC-PK1a cells stably transfected with human Flag tagged V<sub>2</sub>R (LLC-FLAG-V<sub>2</sub>R cells) [5]. LLC-PK1a cells, a subtype of LLC-

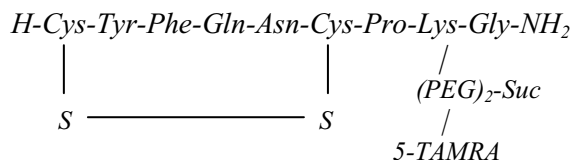
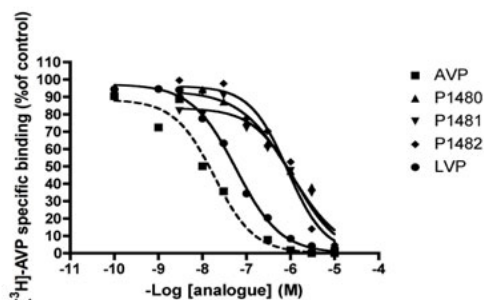


Fig. 1. Sequence of analog 1512-5 (VP<sup>TMR</sup>).

PK1 that expresses only few endogenous V<sub>2</sub>R [5]. Figures 2A and B show the concentration-dependent inhibition of [<sup>3</sup>H]-AVP binding to LLC-FLAG-V<sub>2</sub>R cells with [Mpa<sup>1</sup>]-VP-Tamra or [Cys<sup>1</sup>]-VP-Tamra analogs. Figure 2B suggested that the inhibition of [<sup>3</sup>H]-AVP binding to V<sub>2</sub>R by 1512-5 and 1512-6 is close to that of the native ligand LVP. cAMP assays conducted to measure and compare the intracellular levels of cAMP led to a comparable cAMP accumulation amount in cells in the presence of analogs 1512-5 and 1512-6 or if not better than that by native AVP and LVP (data not shown). We showed that fluorescent analogs coupled to a spacer at Lys<sup>8</sup> can be successfully synthesized by Fmoc chemistry, and the presence of an amino group at the N-terminus of analogs increased the affinity for VP receptor type 2 (V<sub>2</sub>R). Interestingly, our studies suggest the importance of linker-length and hydrophobicity. PEG based linkers were found to be more potent than hydrophobic linker. The analog (1512-5) containing (PEG)<sub>2</sub>-Suc linker [6] of 12 atoms in length exhibited a lower K<sub>d</sub> value than the analog (1505) that contained PEG<sub>2</sub>-COOH linker which was 20 atoms long (data not shown).

Panel A



Panel B

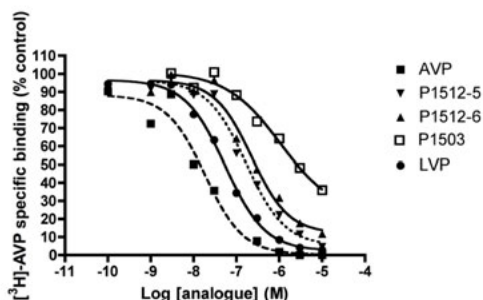


Fig. 2A and B. Concentration-dependent inhibition of  $[^3\text{H}]\text{-AVP}$  binding to LLC-FLAG- $\text{V}_2\text{R}$  cells by  $[\text{Mpa}^1]\text{-VP-Tamra}$  analogs (A) or  $[\text{Cys}^1]\text{-VP-Tamra}$  (B). LLC-FLAG- $\text{V}_2\text{R}$  cells were grown to confluence. In panel A, cells were incubated 3 h at  $4^\circ\text{C}$  with  $[^3\text{H}]\text{-AVP}$  (3nM) with an increasing amount of AVP ( $[\text{Cys}^1, \text{Arg}^8]\text{VP}$ ,  $\blacksquare$ ), LVP ( $[\text{Cys}^1, \text{Lys}^8]\text{VP}$ ,  $\bullet$ ), P1480 ( $[\text{Mpa}^1, \text{Lys-Tamra}^8]\text{VP}$ ,  $\blacktriangle$ ), P1481 ( $[\text{Mpa}^1, \text{Lys-(ahex)-Tamra}^8]\text{VP}$ ,  $\nabla$ ), P1482 ( $[\text{Mpa}^1, \text{Lys-(PEG}_2\text{)-Tamra}^8]\text{VP}$ ,  $\blacklozenge$ ). In Panel B, cells were incubated with an increasing amount of AVP ( $\blacksquare$ ), LVP ( $\bullet$ ), P1512-5 ( $[\text{Cys}^1, \text{Lys-(PEG}_2\text{)-5-Tamra}^8]\text{VP}$ ,  $\nabla$ ), P1512-6 ( $[\text{Cys}^1, \text{Lys-(PEG}_2\text{)-6-Tamra}^8]\text{VP}$ ,  $\blacktriangle$ ), P1503 ( $[\text{Cys}^1, \text{Lys-Tamra}^8]\text{VP}$ ,  $\square$ ). Each point represents the mean of triplicate determinations. The data are expressed as values relative to the total binding observed in the absence of unlabeled ligand and are corrected for nonspecific binding. This experiment is representative of at least three separate experiments. (ahex): aminohexanoic acid; (PEG<sub>2</sub>): Polyethyleneglycol; (Mpa): 1-(2-Mercapto)propionic acid].

Confocal immunofluorescent microscopy studies showed the internalization of  $\text{VP}^{\text{TMR}}$  analogs in LLC-PK1a, whereas more significant amount of  $\text{VP}^{\text{TMR}}$  ligands were found to be internalized in LLC-FLAG- $\text{V}_2\text{R}$  cells. The level of  $\text{VP}^{\text{TMR}}$  internalization seems to be proportional to the level of cell surface  $\text{V}_2\text{R}$ . Interestingly, internalized  $\text{VP}^{\text{TMR}}$  was observed as being co-localized with  $\text{V}_2\text{R}$  in LLC-PK1a stably transfected with the green fluorescence protein (GFP) tagged  $\text{V}_2\text{R}$  (LLC- $\text{V}_2\text{R-GFP}$ ) cells ( $n = 3$ , data not shown). Overall, these results confirm both the specificity of  $\text{VP}^{\text{TMR}}$  to interact with  $\text{V}_2\text{R}$  and its ability to induce  $\text{V}_2\text{R}$  activation and internalization. Thus,  $\text{VP}^{\text{TMR}}$  is a functional new tool to study  $\text{V}_2\text{R}$  intracellular trafficking.

We conclude that fluorescent analogs such as **VP-Lys<sup>8</sup>-(PEG)<sub>2</sub>-Suc-TAMRA (1512-5)** or **VP<sup>TMR</sup>** can be used to study  $\text{V}_2\text{R}$  trafficking in live cells as well as be applied to other G protein-coupled receptors' intracellular trafficking studies.

## Acknowledgments

This work was supported by NIH grants PO1DK38452 (DB and DAA). R. Bouley received an investigator award from the National Kidney Foundation. The Microscopy Core facility of the MGH Program in Membrane Biology receives additional support from the Boston Area Diabetes and Endocrinology Research Center (DK57521) and the Center for the Study of Inflammatory Bowel Disease (DK43341).

## References

1. Lutz, W., Londowski, J.M., Kumar, R. *J. Biol. Chem.* **265**, 4657-4663 (1990).
2. Guillon, G., Barbeau, D., Neugebauer, W., Guay, S., Bilodeau, L., Balestre, M.N., Gallo-Payet, N., Escher, E. *Peptides* **13**, 7-11 (1992).
3. Terrillon, S., Chen, L.L., Stoev, S., Mouillac, B., Barberis, C., Manning, M., Durroux, T. *J Med Chem.* **45**, 2579-2588 (2002).
4. Mouillac, B., Manning, M., Durroux, T. *Mini Reviews in Med. Chem.* **8**(10):996-1005 (2008).
5. Bouley, R., Sun, T.X., Chenard, M., McLaughlin, M., McKee, M., Lin, H.Y., Brown, D., Ausiello, D.A. *Am. J. Physiol. Cell Physiol.* **285**, C750-762 (2003).
6. Song, A., Wang, X., Zhang, J., Marik, J., Lebrilla, C.B. *J. Am. Chem. Soc.* **125**, 6180 (2003).

## ( $\alpha$ Me)Pro Versus Pro $\beta$ -Turn Formation Propensity

Matteo De Poli,<sup>1</sup> Alessandro Moretto,<sup>1</sup> Marco Crisma,<sup>1</sup> Cristina Peggion,<sup>1</sup>  
Fernando Formaggio,<sup>1</sup> Bernard Kaptein,<sup>2</sup> Quirinus B. Broxterman,<sup>2</sup>  
and Claudio Toniolo<sup>1</sup>

<sup>1</sup>ICB, Padova Unit, CNR, Department of Chemistry, University of Padova, 35131 Padova, Italy;

<sup>2</sup>DSM Pharmaceutical Products, Advanced Synthesis, Catalysis and Development,  
6160 MD Geleen, The Netherlands

### Introduction

L-Proline (Figure 1) is conformationally unique among coded amino acids in that its  $\phi$  torsion angle is blocked ( $-65 \pm 10^\circ$ ) by its characteristic five-membered pyrrolidine ring structure and the preceding  $\omega$  torsion angle (tertiary amide) can undergo *cis* ( $0^\circ$ )  $\rightleftharpoons$  *trans* ( $180^\circ$ ) isomerization much easier than the secondary amides of the usual peptide bonds. In addition, its  $\psi$  torsion angle is commonly found either in the *right*-handed,  $3_{10}$ -/ $\alpha$ - helical, region ( $-40 \pm 10^\circ$ , or *cis'* conformation) or in the *left*-handed, *semi*-extended, region [ $-150 \pm 10^\circ$ , or *trans'*, or poly-(L-Pro)<sub>n</sub> conformation].

Methylation at the C $^\alpha$ -position of an L-Pro residue was suggested to block the preceding tertiary amide ( $\omega$ ) torsion angle of the resulting L-( $\alpha$ Me)Pro (Figure 1) to the *trans* disposition and to restrict the  $\phi$ ,  $\psi$  surface to a *single* region, that where the types I and III  $\beta$ -turns and the  $3_{10}$ / $\alpha$ -helices are found [1].

We have synthesized a large set of N $^\alpha$ -blocked, ( $\alpha$ Me)Pro-containing, dipeptide N'-alkylamides having the general formulas P-D-( $\alpha$ Me)Pro-Xxx-NH*i*Pr and P-Xxx-D-( $\alpha$ Me)Pro-NH*i*Pr, where P is Ac, *i*Bu, Z, or Boc and Xxx is D-Ala, L-Ala, Aib, Gly, D-( $\alpha$ Me)Pro, or L-( $\alpha$ Me)Pro, long enough to fold into intramolecularly H-bonded  $\beta$ -turns. The corresponding Pro-based peptides have been also prepared.

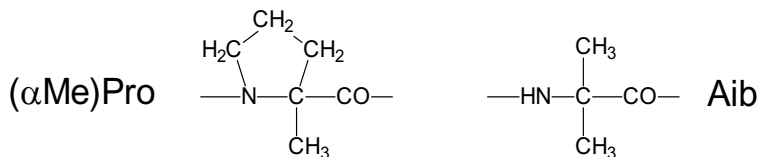


Fig. 1. Chemical structures of C $^\alpha$ -methyl proline [( $\alpha$ Me)Pro] and  $\alpha$ -aminoisobutyric acid (Aib).

### Results and Discussion

For the crystal state 3D-structural analysis we exploited X-ray diffraction, while our solution conformational study was heavily based on the FT-IR absorption and  $^1\text{H}$  (Figure 2) and  $^{13}\text{C}$  NMR techniques.

From the results of our investigation we conclude that ( $\alpha$ Me)Pro is able to explore both *trans'* and *cis'*  $\psi$  areas of the conformational space, but the latter, typical of type I and III  $\beta$ -turns, and the  $3_{10}$ / $\alpha$ -helices, is overwhelmingly more populated, in marked contrast to the Pro preference for type II  $\beta$ -turn and type II poly(Pro)<sub>n</sub> conformations. This finding is a clear indication that in ( $\alpha$ Me)Pro the major 3D-structural determinant is the C $^\alpha$ -methyl group.

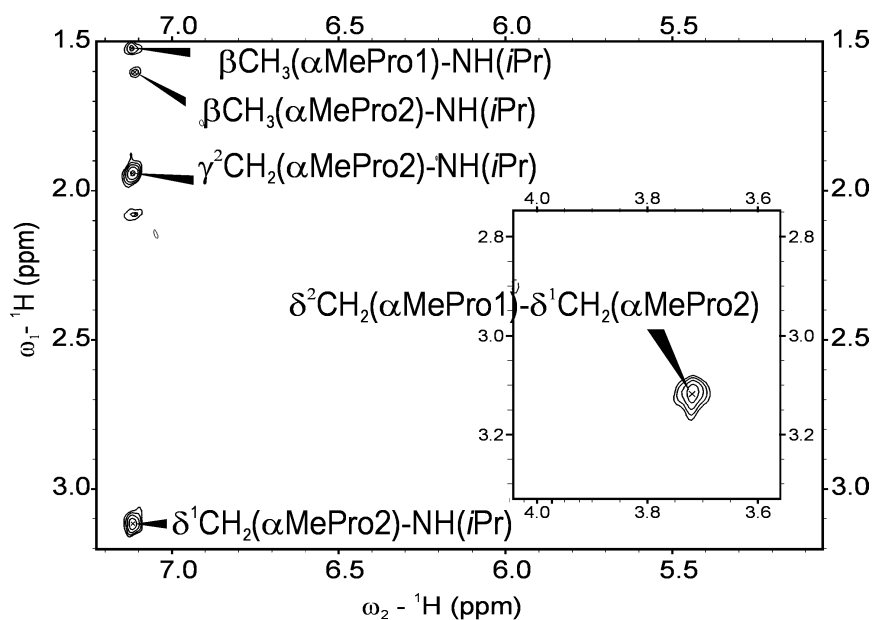


Fig. 2. Section of the ROESY spectrum of *Ac-D-(αMe)Pro-D-(αMe)Pro-NHiPr* in  $\text{CDCl}_3$  solution. The sequential and medium-range connectivities are indicated.

## References

1. Burgess, A., Paterson, Y., Leach, S.J. in Blout, E.R., Bovey, F.A., Goodman, M., Lotan, N., (Eds.) *Peptides, Polypeptides, and Proteins*, Wiley, New York, 1974, pp. 79-87.
2. De Poli, M., Moretto, A., Crisma, M., Peggion, C., Formaggio, F., Kaptein, B., Broxterman, Q.B., Toniolo, C. *Chem. Eur. J.* (2009) in press.



## Anti-angiogenic Properties of a Rhegnylogically-organised Cell Penetrating Peptide Derived from Endothelial Nitric Oxide Synthase

John Howl and Sarah Jones

Research Institute in Healthcare Science, School of Applied Sciences, University of Wolverhampton,  
Wolverhampton, WV1 1LY, UK

### Introduction

Cell penetrating peptides (CPP) are now widely utilised as biologically inert vectors to affect the highly efficient intracellular delivery of bioactive cargoes. Commonly, delivery is achieved by employing a sychnologically-organised tandem combination of a CPP and an additional bioactive moiety. More recently, a QSAR-based algorithm has been developed to identify cryptic CPP motifs within the primary sequences of proteins [1]. Our studies have, therefore, focussed upon the identification of rhegnylogic CPPs in which the multiple pharmacophores for cellular penetration and other biological activities are discontinuously organised within a single peptide [2]. As an example of this approach, we have studied a cryptic CPP derived from nitric oxide synthase, eNOS<sup>492-507</sup>, located within a helical domain known to tightly bind calmodulin.

### Results and Discussion

In accordance with the prediction algorithm, eNOS<sup>492-507</sup> demonstrated a strong propensity for cellular penetration (Figure 1). Most strikingly, eNOS<sup>492-507</sup> modulated biological features of *in vitro* angiogenesis and inhibited, in the nanomolar range, the proliferation, migration and tube-forming capacity of primary endothelial cells (Figure 2). Specifically, eNOS<sup>492-507</sup> inhibited, fibroblast growth factor (FGF-2, 25 ng/ml) induced proliferation of bovine aortic endothelial cells (BAEC) with an IC<sub>50</sub> of 83.7 nM, FGF-2-induced migration of BAEC with an IC<sub>50</sub> of 38.2 nM and FGF-induced tube formation of BAEC with an IC<sub>50</sub> of 509 nM. Furthermore, eNOS<sup>492-507</sup> displayed potent anti-angiogenic properties in an *in vivo* model of angiogenesis. Using the chick chorioallantoic membrane (CAM) assay, application of eNOS<sup>492-507</sup> to the egg abrogated neovascularisation induced by FGF-2 (200 µg). A feature that was evident even at an application dosage of 100 ng eNOS<sup>492-507</sup>.

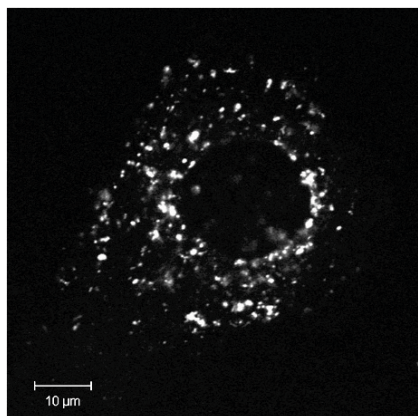


Fig. 1. Rho-eNOS<sup>492-507</sup> translocates plasma membranes of ECV304 cells. Live confocal cell imaging was captured 45 minutes after the addition of 5 µM rhodamine-labeled peptide.

Additional studies using eNOS<sup>492-507</sup> have also demonstrated an absence of non-specific cardiovascular and cytotoxic effects. *In vivo* pressor assays carried out in rats have shown that eNOS<sup>492-507</sup> has no effect upon resting blood pressure or elevated pressure induced by vasopressin. Similarly, we have performed viability assays on numerous cell lines and data from our laboratory indicate that eNOS<sup>492-507</sup> is not cytotoxic.

Clearly, eNOS<sup>492-507</sup> holds important pharmaceutical potential for the prevention of tumour angiogenesis. As a highly efficient CPP, eNOS<sup>492-507</sup> inhibits the proliferation, migration and tube-forming capacity of primary endothelial cells and displays potent anti-angiogenic properties *in vivo*. Further characterisation studies shall consolidate this peptide as a viable therapeutic. Therefore, synthesis and evaluation of structural analogues and analysis of the peptide's stability by high performance liquid chromatography shall be performed. We are also currently focussing upon the molecular mechanisms employed by this novel CPP and hope to shortly identify intracellular binding partners alongside any alterations in gene expression.

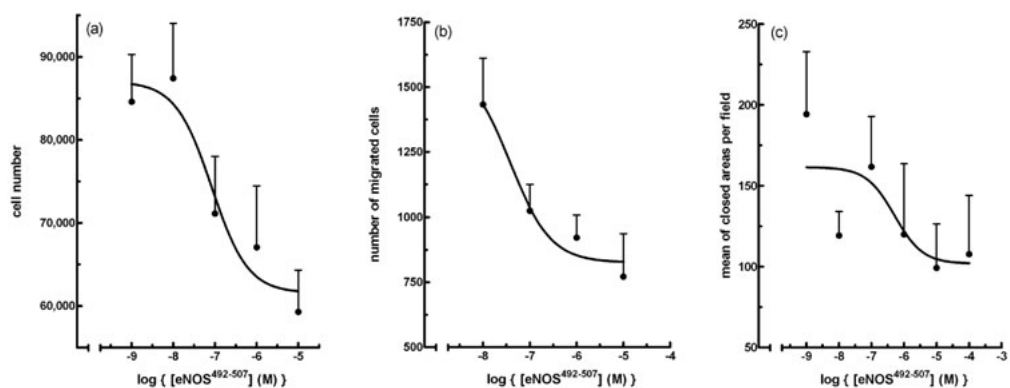


Fig. 2.  $eNOS^{492-507}$  is a potent inhibitor of FGF-2 (25 ng/ml)-induced proliferation (a), migration (b) and tube formation (c) of primary endothelial cells.

## Acknowledgments

The authors would like to thank Shant Kumar at the School of Medicine, the University of Manchester, UK and Jirina Slaninova at the Group of Peptide Biochemistry, Department of Biological Chemistry, Institute of Organic Chemistry and Biochemistry, Prague, Czech Republic.

## References

1. Howl, J., Jones, S. *Int. J. Pept. Res. Ther.* **14**, 359-366 (2008).
2. Hallbrink, M., et al. *Int. J. Pept. Res. Ther.* **11**, 249-259 (2005).

## Targeting the Nuclear Pore Complex with Cell Penetrating Peptides: A Novel Therapeutic Strategy

Sarah Jones and John Howl

Research Institute in Healthcare Science, School of Applied Sciences, University of Wolverhampton,  
Wolverhampton, WV1 1LY, UK

### Introduction

The past decade has witnessed an escalating interest in the therapeutic applications of cell penetrating peptides (CPP). We have employed a strategy for the modulation of intracellular biology using CPP that possess signal transduction modulatory properties. These novel constructs of rhegnylogic organization are proteomimetic CPP [1]. Such advances were pursued following the development of a prediction algorithm which identifies key cell penetrant peptide fragments within key intracellular signalling proteins [2]. Proteomimetic CPP, therefore possess the dual function of modulating intracellular events whilst being intrinsically cell penetrant, thus circumventing difficult conjugation steps. One such peptide, Cyt  $c^{77-101}$  (H-GTKMIFVGIIKKK-EERADLIAYLKKA-NH<sub>2</sub>) that is derived from the apoptogen cytochrome *c*, demonstrates a strong propensity for cellular penetration and moderate apoptotic activity when exogenously applied to U373MG astrocytoma [1].

Given our recent success with the mitochondriotoxic CPP mitP and its target-selective analogues [3], we evaluated a range of chimeric constructs combining apoptogenic CPP and peptidyl *address* motifs. The overriding objective of these studies was to enhance cytotoxicity and/or develop target-selective drug delivery vectors. One *address* motif, Nup153<sup>980-987</sup> (NFKFGLSS) was designed to target the nuclear pore complex as a novel therapeutic strategy and is a target mimetic of FG nucleoporins (Nups). FG Nups are components of the nuclear pore that control import and export between the cytoplasm and the nucleus and are characterized by multiple FXFG repeat sequences. This repeat sequence, NFKFGLSS residues 980-988 (Nup153<sup>980-987</sup>) was derived from the C-terminal of human Nup153. For the design of our target mimetic, Nup153 was the protein of choice and was based on the following lines of evidence; Nup153 is one of the most characterized of the Nups and assumes roles in nuclear import and the regulation of pore selectivity, nuclear basket formation, nuclear pore complex anchoring and nuclear envelope breakdown [4, 5]. Sequence design was based on there being 15 FXFG repeat sequences throughout the protein, 4 of which are FKFG. In addition numerous viscinal serines appear throughout the protein.

### Results and Discussion

The apoptogenic potency of the moderately apoptogenic CPP Cyt  $c^{77-101}$  was significantly enhanced by chimeric N-terminal extension with Nup153<sup>980-987</sup>. Thus, the chimeric construct *Ac*-Nup153<sup>980-987</sup>(Ahx)Cyt  $c^{77-101}$  induced apoptosis of U373MG astrocytoma with an LD<sub>50</sub> of 0.73  $\mu$ M, a concentration readily achieved *in vivo* (Figure 1). Apoptosis was confirmed as the mechanism of cell death and was demonstrated by the peptide's ability to activate caspase-3, as was measured by cleavage of the caspase-3 specific substrate DEVD, and induce inter-nucleosomal DNA fragmentation, as was measured by *in situ* TUNEL assay.

Interestingly, when translocated into cells by the inert CPP M918, as a fluorescein-conjugated disulphide-linked cargo (Fluo-Nup153<sup>980-987</sup>Cys-CysM918), Fluo-Nup153<sup>980-987</sup> accumulated around the nuclear envelope. Given the subcellular localization of Fluo-Nup153<sup>980-987</sup>, additional studies were carried out to establish whether *Ac*-Nup153<sup>980-987</sup>(Ahx)Cyt  $c^{77-101}$  was modulating the functional utility of the nuclear pore complex. Indirect immuno-fluorescence analysis demonstrated that *Ac*-Nup153<sup>980-987</sup>(Ahx)Cyt  $c^{77-101}$  facilitates the dramatic redistribution of Nup153 from the nuclear periphery to the nucleoplasm and cytoplasm (Figure 2). Interestingly, the intracellular delivery of Nup153<sup>980-987</sup> using either the inert CPP penetratin, or M918, induces only moderate reductions in cellular viability indicating that the chimeric peptide *Ac*-Nup153<sup>980-987</sup>(Ahx)Cyt  $c^{77-101}$  may target multiple intracellular sites, in addition to the nuclear pore complex, to induce apoptosis.

We conclude that *Ac*-Nup153<sup>980-987</sup>(Ahx)Cyt  $c^{77-101}$  demonstrates potential as a potent inducer of apoptosis and propounds the nuclear pore complex as a target for the therapeutic

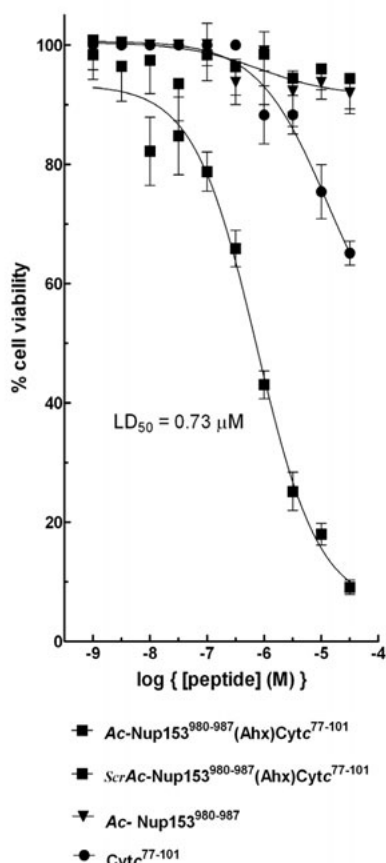


Fig. 1. Characterization of Ac-Nup153<sup>980-987</sup>(Ahx)Cyt c<sup>77-101</sup> as a potent apoptogenic chimera. N-terminal extension of Cyt c<sup>77-101</sup> with Nup153<sup>980-987</sup> significantly enhances the cytotoxic potency of Cyt c<sup>77-101</sup>, whilst Nup153<sup>980-987</sup> and the scrambled sequence chimera ScrAc- Nup153<sup>980-987</sup>(Ahx)Cyt c<sup>77-101</sup> (Ac-GFSNSFKLN(Ahx)Cyt c<sup>77-101</sup>) are inactive. U373MG were exposed to increasing concentrations of peptides for 24 hours. Cell viability was measured by MTT conversion and expressed as a percentage of those cells treated with medium alone. Data points are mean  $\pm$  S.E.M. from 3 experiments.

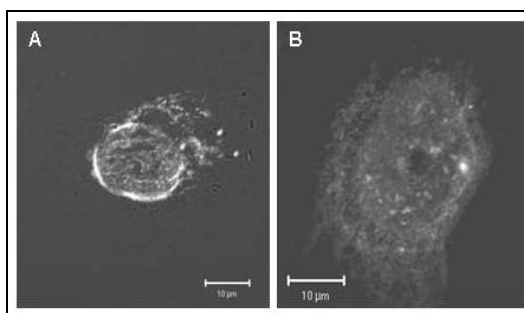


Fig. 2. Ac-Nup153<sup>980-987</sup>(Ahx)Cyt c<sup>77-101</sup> elicits redistribution of Nup153 in U373MG cells. Under control conditions, Nup153 resides in the nuclear periphery to face the nucleoplasm and can be visualised by predominant staining of the nuclear periphery (A). Following treatment with Ac-Nup153<sup>980-987</sup>(Ahx)Cyt c<sup>77-101</sup>, Nup153 assumes a more diffuse pattern and redistributes to the nucleoplasm and cytoplasm (B). Cells were treated for 4 hours with Ac-Nup153<sup>980-987</sup>(Ahx)Cyt c<sup>77-101</sup> (3  $\mu$ M) or vehicle (medium alone). Fixed cells were probed with primary (sheep polyclonal Anti-Nup153) and secondary (Anti-sheep IgG conjugated to FITC) antibodies and visualized by confocal microscopy.

induction of apoptosis. Future work shall be focussed upon assessing the impact of Ac-Nup153<sup>980-987</sup>(Ahx)Cyt c<sup>77-101</sup> on nuclear import and export, whilst we shortly anticipate the production of a protease resistant analogue with improved pharmacokinetic and pharmacodynamic parameters.

## Acknowledgments

We would like to thank the Samantha Dickson Brain Tumour Trust for their financial support.

## References

1. Howl, J., Jones, S. *Int. J. Pept. Res. Ther.* **14**, 359-366 (2008).
2. Hallbrink, M., et al. *Int. J. Pept. Res. Ther.* **11**, 249-259 (2005).
3. Jones, S., et al. *Biochim. Biophys. Acta* **1783**, 849-863 (2008).
4. Walter, T.C., et al. *EMBO J.* **20**, 5703-5747 (2001).
5. Prunuske, A.J., et al. *Mol. Biol. Cell* **2**, 760-769 (2006).

## A Conformationally Constrained, Benzophenone Containing, $\alpha$ -Amino Acid Photophore

Karen Wright,<sup>1</sup> Alessandro Moretto,<sup>2</sup> Marco Crisma,<sup>2</sup>  
Michel Wakselman,<sup>1</sup> Jean-Paul Mazayerat,<sup>1</sup> Fernando Formaggio,<sup>2</sup>  
and Claudio Toniolo<sup>2</sup>

<sup>1</sup>ILV, UMR CNRS 8180, University of Versailles, 78035 Versailles, France; <sup>2</sup>ICB, Padova Unit, CNR,  
Department of Chemistry, University of Padova, 35131 Padova, Italy

### Introduction

The para-benzoylphenylalanyl (Bpa) residue (Figure 1) [1] is extensively used as a photoaffinity label, particularly for studies of *intermolecular* (peptide)ligand-receptor(protein) interactions, where it is believed to most frequently remove a hydrogen atom from the side chain of a Met residue followed by covalent C-C bond formation of the resulting radical pair. We have recently investigated the chemical and 3D-structures of the products resulting from the *intramolecular* excited state Paternò-Yang photocyclization in Bpa-spacer-Met  $3_{10}$ -helical hexapeptides [2]. However, the remarkable flexibility of the Bpa side chain [3] may question the extrapolation of results of photocross-linking experiments and photophysical data to protein mapping and intramolecular distances. To overcome this problem, we designed and synthesized a new "constrained Bpa" amino acid, BpAib (Figure 1), belonging to the sub-class of C $^{\alpha}$ -tetrasubstituted  $\alpha$ -amino acids (strong  $\beta$ -turn and  $3_{10}$ -/ $\alpha$ -helix supporters in peptides), the prototype of which is Aib ( $\alpha$ -aminoisobutyric acid) (Figure 1).

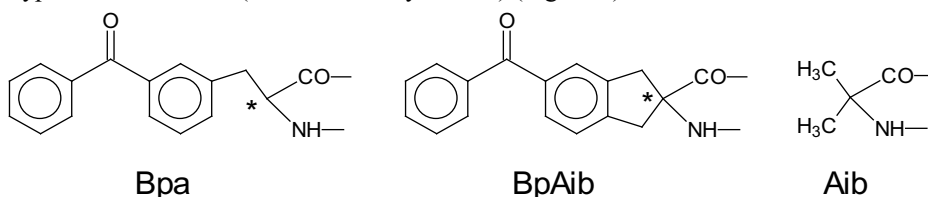


Fig. 1. Chemical structures of Bpa, BpAib, and Aib.

### Results and Discussion

In our synthetic approach both enantiomers of H-BpAib-OMe were obtained. The absolute configuration of the amino acid was determined by an X-ray diffraction study of the Z-(R)-BpAib-(S)-Phe-NHChx (Chx, cyclohexyl) dipeptide derivative.

Photochemical experiments indicate that the benzophenone moiety of BpAib does preserve its reactivity, which resembles that of Bpa mentioned above [2]. The HPLC profile of the photoreaction between Boc-(S)-BpAib-OMe and Boc-(S)-Met-Aib-OMe shows two newly formed, roughly equivalent peaks (Figure 2).

Mass spectrometry and NMR data favor the conclusion that the two products are diastereomeric adducts originated from the regioselective cross-linking of the BpAib derivative to the Met S-methyl function of the dipeptide substrate with formation of an additional chiral center at the reactive, former BpAib side-chain carbonyl carbon.

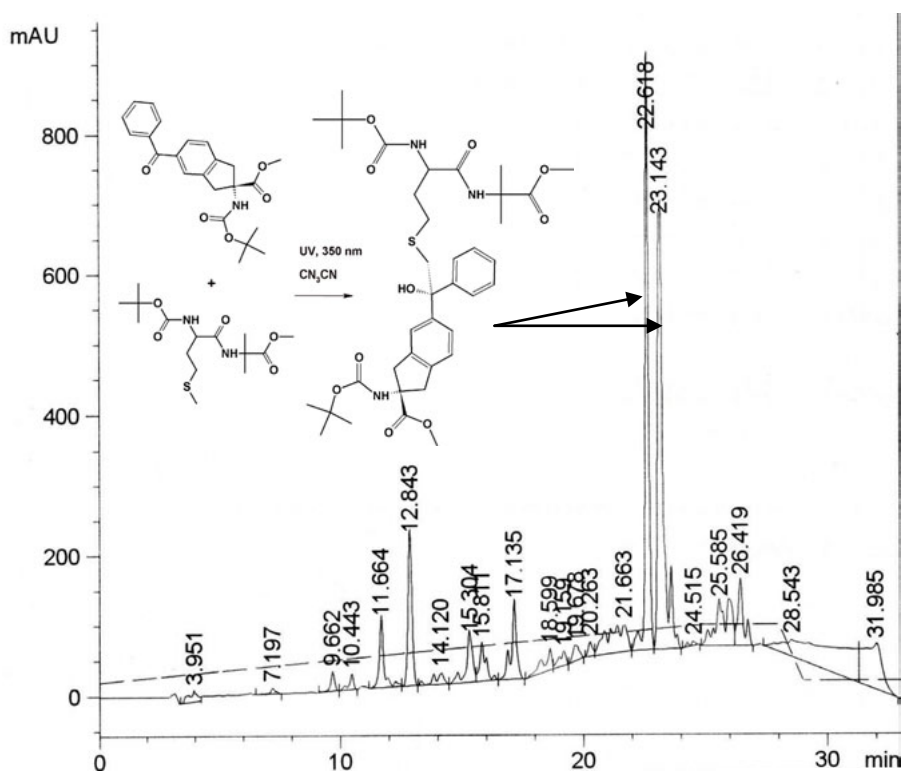


Fig. 2. Reverse-phase HPLC profile of the products of the photoreaction between Boc-(S)-BpAib-OMe and Boc-(S)-Met-Aib-OMe.

## References

1. Kauer, J.C., Erickson-Viitanen, S., Wolf, H.R. Jr., DeGrado, W.F. *J. Biol. Chem.* **261**, 10695-10700 (1986).
2. Moretto, A., Crisma, M., Formaggio, F., Huck, L.A., Mangion, D., Leigh, W.J., Toniolo, C. *Chem. Eur. J.* **15**, 67-70 (2009).
3. Saviano, M., Improta, R., Benedetti, E., Carrozzini, B., Cascarano, G.L., Didierjan, C., Toniolo, C., Crisma, M. *ChemBioChem* **5**, 541-544 (2004).

## A Peptido[2]rotaxane Molecular Machine

Alessandro Moretto, Ileana Menegazzo, Marco Crisma, Stefano Mammi,  
and Claudio Toniolo

ICB, Padova Unit, CNR, Department of Chemistry, University of Padova, 35131 Padova, Italy

### Introduction

Peptido[2]rotaxanes based on an achiral, aromatic, tetrabenzamido macrocycle locked onto various chiral Gly-L-Xxx dipeptide axles were first characterized by Leigh and coworkers [1]. We are currently expanding this field by synthesizing and studying the properties of a new set of peptido[2]rotaxanes. In this work we describe our results on non-symmetrical compounds involving a reversible peptido[2]rotaxane molecular shuttle (powered by light and heat), based on a rigid, helical peptide axle (Figure 1) and the Leigh's macrocyclic wheel.

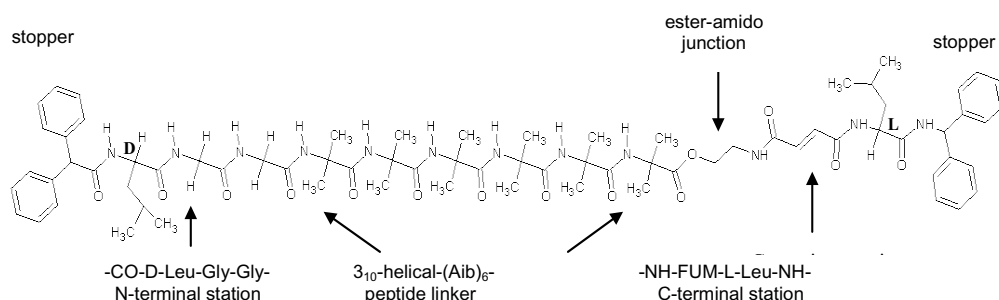


Fig. 1. The axle of this peptido[2]rotaxane is based on a D-Leu-(Gly)<sub>2</sub> tripeptide N-terminal station, a 3<sub>10</sub>-helical-(Aib)<sub>6</sub>-peptide spacer, and an ester-amido junction followed by a fumaramide (FUM)/L-Leu C-terminal station. The two stoppers are characterized by benzhydryl moieties.

### Results and Discussion

A significant part of the initial stabilization energy of this peptido[2]rotaxane stems from two sets of intermolecular N-H...O=C H-bonds originated from the four isophthalamide NH groups of the macrocycle and the two fumaramide carbonyls.

By use of NMR we were able to identify all of the stations of this novel class of peptido[2]rotaxanes and to switch the wheel by irradiation [fumaramide (*trans*) → maleamide (*cis*)] and heating from one station to the next. This is the first example of a [2]rotaxane where the wheel makes a journey [from compound (II) to compound (III) and vice versa] by wrapping up around a helical peptide axle (Figure 2).

Interestingly, we also characterized by X-ray diffraction a simplified, symmetrical, peptido[2]rotaxane with a [Fmoc-(Aib)<sub>4</sub>-O-(CH<sub>2</sub>)<sub>2</sub>-NH-FUM]<sub>2</sub> axle and the Leigh's tetrabenzamido wheel.

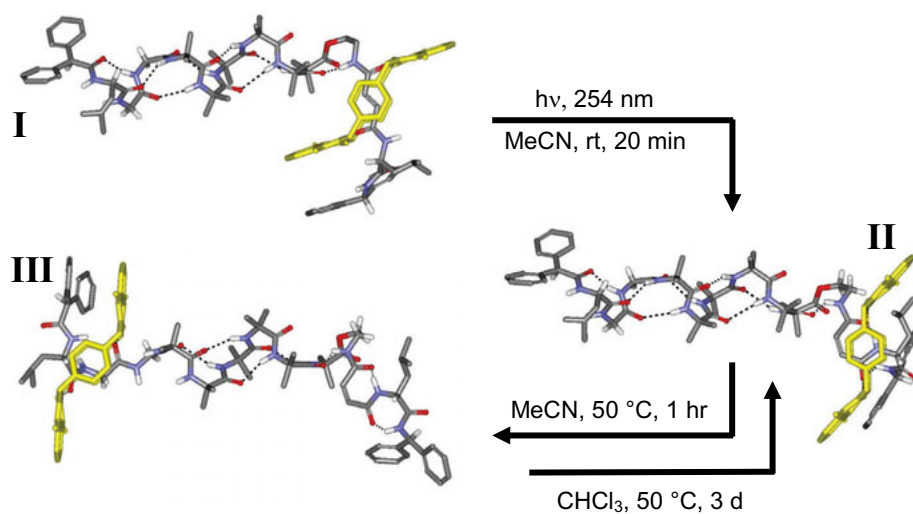


Fig. 2. Motions of this stimuli-responsive peptido[2]rotaxane molecular shuttle: (I) initial wheel position; (II) wheel position after UV light stimulus in MeCN solution at room temperature; (III) wheel position after heating in MeCN solution at 50 °C; again wheel position (II) after heating in CHCl<sub>3</sub> solution at 50 °C.

## References

1. Asakawa, M., Brancato, G., Fanti M., Leigh, D. A., Shimizu, T., Slawin, A. M. Z., Wong, J.K.Y., Zerbetto, F., Zhang, S. *J. Am. Chem. Soc.* **124**, 2939-2950 (2002), and references cited therein.



## Effects of Controlled Gamma Irradiation upon Structures of Bradykinin and Angiotensin II

Daniela T. Nardi,<sup>1</sup> Jose C. Rosa,<sup>2</sup> Guita N. Jubilut,<sup>1</sup> Murilo C. Silva,<sup>3</sup>  
Nanci Nascimento,<sup>3</sup> and Clovis R. Nakaie<sup>1\*</sup>

<sup>1</sup>Department of Biophysics –Federal University of Sao Paulo, Sao Paulo, CEP 04044-020, Brazil;

<sup>2</sup>Protein Chemistry Center and Department of Molecular and Cell Biology, School of Medicine, Sao Paulo University, Ribeirao Preto, CEP 14049-900, Brazil; and <sup>3</sup>Institute for Energy Research and Nuclear Science (IPEN)-SaoPaulo University, Sao Paulo, CEP 05508-000, Brazil

### Introduction

The reaction products and mechanisms involved in the radiolysis of macromolecules of biological relevance are object of several studies and they are known to be involved in many pathological diseases [1]. In order to evaluate the modifications that gamma radiation may cause upon structure of peptides - mainly the oxidation induced by free radicals produced in solution - the present report selected the vasoactive peptides angiotensin II (AngII) and bradykinin (BK) as models for investigation. Purified BK and AngII were submitted to 1 to 15 kGy gamma irradiation doses as preliminarily reported [2] and the most abundant components of the each irradiated peptide solutions were purified and characterized for further structure-function studies.

### Results and Discussion

All experiments were done using a Gammacell 220 irradiator (Atomic Energy of Canada Ltd., Ottawa, Canada), in the presence of oxygen, at room temperature and dose rate of 3.32 kGy/h. Solutions of 1mg/mL of AngII and BK - both synthesized manually according to early reported protocol [3] - were irradiated with 1, 2, 4, 6, 8, 10 and 15 kGy. By comparing the HPLC chromatogram of each irradiated solution and the corresponding peak absorbance values, it was possible to detect significant degradation occurring in parallel with increases in the radiation dose. Non-linear profiles for the degradation processes of both peptides were observed as the gamma radiation doses increased (Figure 1). The variation in the quantities of remaining AngII and BK present in irradiated solutions were determined by measuring the peak area of each peptide in solution. Noteworthy, AngII seems to be more stable to radiation than BK as the degradation values reached about 50% with 4 kGy and 2 kGy, respectively (Figure 1a and 1b).

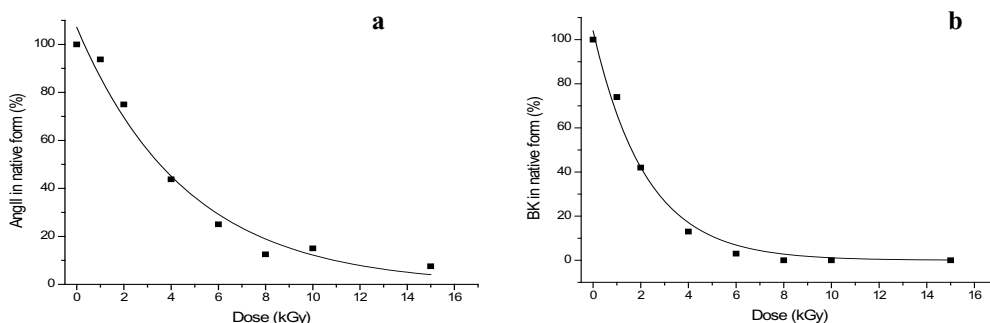


Fig. 1. Remaining AngII (a) and BK (b) quantities (in percentage) as a function of the gamma irradiation dose.

For initiating the evaluation of the radiation effect in the structures of AngII and BK molecules, 50 mg of both peptides were irradiated with 4 kGy and 2 kGy doses, respectively and the main components of solutions were fractionated in semi-preparative HPLC column. A combination of amino acid analysis (Biochrom 20 Plus Amino Acid analyzer - Biochrom Ltd., Cambridge, UK) and LC-ESI/MS (Waters) mass spectrometry were applied for characterization of fractionated

components of AngII and BK. Preliminary findings revealed that the former peptide (DRVYIHPF) generated the Tyr<sup>8</sup>-AngII and *m*-Tyr<sup>8</sup>-AngII as a consequence of the Phe<sup>8</sup> residue oxidation, inducing 16 Da increase in the molecular weight in these two derivatives. In complement, a small amount of Lys<sup>6</sup>-AngII was also isolated but the mechanism of His to Lys structural modification in this octapeptide induced by radiation is still unclear.

In the case of BK (RPPGFSPFR), initial results depicted that only one Phe residue of its sequence was affected by the radiation, generating two BK analogues bearing Tyr or *m*-Tyr residues in their sequences. To elucidate which Phe residue (positions 5 or 8) was modified, an electrospray triple-quadrupole Quattro II (Micromass, Manchester, UK) tandem mass spectrometry was next used for peptide sequencing, using the daughter ion scanning by collision induced dissociation (CID-MS/MS) strategy. Interestingly, the findings demonstrated that only the Phe residue at position 8 was affected, generating the Tyr<sup>8</sup>-BK and *m*-Tyr<sup>8</sup>-BK derivatives thus depicting a clear residue and sequence-dependent effect in the gamma irradiation process. Interestingly, the Phe<sup>8</sup> residue was also sensitive to radiation in the AngII sequence. By taking into account the sequences of both peptides, one can conclude that the Phe to Tyr or *m*-Tyr transformation is facilitated by the presence of a Pro residue at its N-terminal position. Our group has investigated both vasoactive peptides with different approaches for decades [4-6] and the present results strongly suggested that this gamma radiation approach seems to be of great potential for generating analogues, some of them, of uncommon structure. Other physiologically relevant peptides are currently been examined with this strategy.

## Acknowledgments

We thank CNPq and FAPESP for financial support.

## References

1. Garrison, W.M. *Chem. Rev.* **87**, 381-398 (1987).
2. Nardi D.T., Casare M.S., Teixeira L.G.D., Nascimento N., Nakaie C.R. *Int. J. Radiat. Biol.* **84**, 937-944 (2008).
3. Taborda, C.P., Nakaie, C.R., Cilli, E M., Rodrigues, E.G., Silva, L.S., Franco, M.F., Travassos, L.R. *Scand. J. Immunol.* **59**, 58-65 (2004).
4. Nakaie, C.R., Oliveira, M.C.F., Juliano, L., Paiva, A.C.M. *Biochem. J.* **205**, 43-47 (1982).
5. Pertinhez, T.A., Nakaie, C.R., Paiva, A.C.M., Schreier, S. *Biopolymers* **42**, 821-829 (1997).
6. Schreier, S., Barbosa, S.R., Casallanovo, F., Vieira, R.F.F., Cilli, E.M., Paiva, A.C.M., Nakaie, C.R. *Biopolymers* **74**, 389-402 (2004).

## Design of a Novel FRET Substrate with a Long Wavelength Fluorophore for Detection of Matrix Metalloproteinases

Vera Rakhmanova, Siu-Kei Lui, Fengying Li, Xiaofen Zhong,  
Jianjun He, Anita Hong, and Xiaohe Tong

AnaSpec Inc., 34801 Campus Dr., Fremont, CA 94555, U.S.A.

### Introduction

Matrix metalloproteinases (MMPs) belong to a family of secreted or membrane-associated zinc endopeptidases involved in both normal and disease related tissue remodeling. They are capable of degrading extracellular matrix (ECM) proteins and processing a number of bioactive molecules [1,2]. MMPs are key players in normal and pathological processes, including embryogenesis, wound healing, inflammation, arthritis, and cancer [3-5]. The use of FRET technology has facilitated MMP assay development. Previously described FRET substrates include Mca/Dnp, EDANS/DABCYL donor acceptor pairs. The introduction of the longer wavelength 5-FAM/QXL<sup>TM</sup> 520 FRET based MMP substrates increased assay sensitivity and signal/background ratio. To further improve MMP FRET assays, i.e. minimize autofluorescence from reaction components, we developed a new series of MMP substrates containing the 5-TAMRA/QXL<sup>TM</sup> 570 FRET pair. In these FRET peptides, the fluorescence of 5-TAMRA is quenched by QXL<sup>TM</sup> 570 and recovered upon cleavage of the peptide by active MMP enzyme. The resulting fluorescence is monitored at excitation/emission wavelengths = 540 nm/575 nm. After screening several 5-TAMRA/QXL<sup>TM</sup> 570 substrates, one sequence was identified to be cleaved by most of the MMPs. This substrate was chosen for the development of the SensoLyte<sup>®</sup> 570 Generic MMP Assay Kit. This kit provides high sensitivity and accuracy and can detect human MMP-1, 2, 7, 8, 9, 12, 13, and 14. It is ideal for detecting of enzyme activity in the samples containing multiple MMPs or for high throughput screening of MMP inhibitors using purified enzymes.

### Results and Discussion

MMP generic 5-TAMRA/QXL<sup>TM</sup> 570 FRET substrates were synthesized by Fmoc solid phase synthesis method. 5-TAMRA and QXL<sup>TM</sup> 570 is a new donor - acceptor pair for FRET peptides. The absorption spectrum of QXL<sup>TM</sup> 570 overlaps with the emission spectrum of 5-TAMRA. QXL<sup>TM</sup> 570 is an excellent quencher for 5-TAMRA.

One of the MMP peptide substrates containing the novel FRET pair 5-TAMRA/QXL<sup>®</sup> 570 was chosen for the development the SensoLyte<sup>®</sup> 570 Generic MMP Assay Kit. This substrate can detect most of human MMPs tested. MMP assay was performed as recommended by the protocol found in SensoLyte<sup>®</sup> 570 Generic MMP Assay Kit. The reaction volumes for this kit are 40  $\mu$ l of enzyme, 10  $\mu$ l of test compound/buffer, 50  $\mu$ l of substrate. Assays are performed in 96-well black opaque plates. Fluorescence was measured using FlexStation 384II

(Molecular Devices, Sunnyvale, CA).

MMP generic 5-TAMRA/QXL<sup>TM</sup> 570 FRET substrate is hydrolyzed by human MMP-1, 2, 9, and 13 and at less degree by MMP-7, 8, 12 and 14. SensoLyte<sup>®</sup> 570 Generic MMP Kit is very amenable for kinetic measurements due to its homogeneous assay format and continuous nature of the assay.

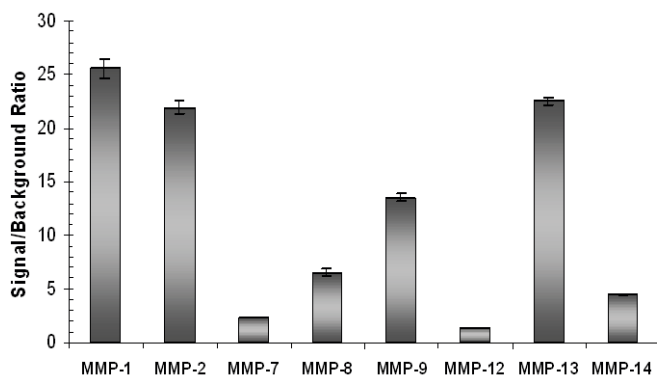


Fig. 1. Comparison of signal/background ratio for various MMPs.

To compare signal/background ratio for various MMPs APMA-activated MMPs, 30 ng each, were mixed with 5-TAMRA/QXL™ 570 FRET peptide substrate and fluorescence was monitored for 1 hr. Endpoint signals were compared to background (FRET substrate without enzyme) to demonstrate MMP activities (Figure 1).

The new 5-TAMRA /QXL™ 570 FRET substrate is highly sensitive and can detect at least nanogram range of MMPs tested. To evaluate sensitivity of assay for MMP-9, the activated enzyme was titrated with 5-TAMRA/QXL™ 570 FRET substrate. Sensitivity of assay at 1 hour incubation was 0.78 ng/mL of MMP-9 enzyme (Figure 2)

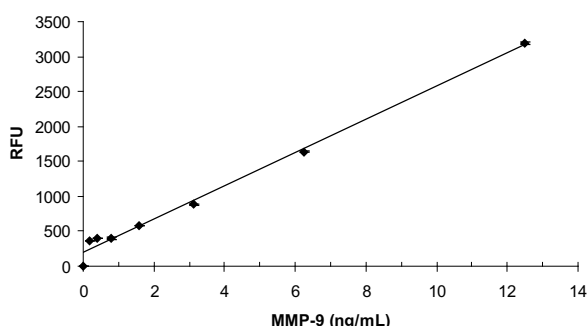


Fig. 2. MMP-9 titration with 5-TAMRA/QXL® 570 FRET substrate. Detection of low MMP-9 concentrations.

The SensoLyte® 570 Generic MMP Assay Kit was validated for inhibitor screening using a broad-spectrum matrix metalloproteinases inhibitor. 5-TAMRA/QXL® 570 substrate was incubated with 10 ng of each of human MMP-9 and MMP-13 enzymes in the presence of a broad-spectrum matrix metalloproteinases inhibitor, Galardin [6]. The calculated IC<sub>50</sub> were 0.27 nM and 0.77 nM for MMP-9 and MMP-13, respectively (Figure 3). The red-shifted excitation and emission wavelengths of 5-TAMRA show minimal interference from the autofluorescence of test compounds.

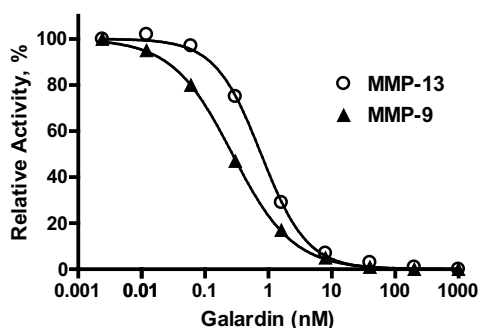


Fig. 3. Inhibitor studies.

## References

1. Woessner, J.F., et al. *J. Biol. Chem.* **263**, 16918-16925 (1988).
2. Woessner, J.F., et al. *FASEB J.* **5**, 2145-2154 (1991).
3. Goldberg, G.I., et al. *Ann. N.Y. Acad. Sci.* **580**, 375-384 (1990).
4. Stetler-Stevenson, W.G., et al. Liotta, *Annu. Rev. Cell Biol.* **9**, 541-573 (1993).
5. Gravalles, E.M., et al. *Arthritis Rheum.* **34**, 1076-1084 (1991).
6. Galardy, R.E., et al. *Cancer Res.* **54**, 4715-4718 (1994).

## Conformations of End-Capped Melanocortin Agonists RCO-X-Z-Arg-Trp-NH<sub>2</sub> by 2D-NMR, CD and Computations

Seetharama D. Satyanarayanajois,<sup>1</sup> Leonid Koikov,<sup>2</sup> Matt Wortman,<sup>3</sup>  
 Zalfa Abdel-Malek,<sup>2</sup> Renny Kavanagh,<sup>2</sup> and James J. Knittel<sup>4</sup>

<sup>1</sup>University of Louisiana at Monroe, College of Pharmacy, Monroe, LA 71201, U.S.A.;

<sup>2</sup>University of Cincinnati, College of Medicine, Cincinnati, OH 45267, U.S.A.; <sup>3</sup>University of Cincinnati, College of Medicine, Genome Research Institute, Cincinnati, OH 45237, U.S.A.; and <sup>4</sup>University of Cincinnati, James L. Winkle College of Pharmacy, Cincinnati, OH 45267, U.S.A.

### Introduction

Natural agonists of melanocortin receptors (MCR)  $\alpha$ -,  $\beta$ - and  $\gamma$ -melanocyte stimulating hormones (MSH) share the common melanocortin core sequence His<sup>6</sup>-Phe<sup>7</sup>-Arg<sup>8</sup>-Trp<sup>9</sup> (HFRW) existing in a  $\beta$ -turn conformation [1]. Stabilization of the  $\beta$ -turn conformation in MSH synthetic analogs (NDP-MSH, MT-II) with the His<sup>6</sup>-D-Phe<sup>7</sup>-Arg<sup>8</sup>-Trp<sup>9</sup> (HfRW) core is believed to be responsible for their increased potency [1,2]. Despite high potency, these peptide agonists are non-selective at MC1, MC3, MC4 and MC5Rs. Recently, we have reported [3] a superpotent hMC1R selective agonist LK-184 Ph(CH<sub>2</sub>)<sub>3</sub>CO-HfRW-NH<sub>2</sub> (**1**) with an EC<sub>50</sub> of 0.01 nM and *ca.* 500-fold selectivity for hMC1R compared to hMC3 and hMC4Rs and LK-394 Ph(CH<sub>2</sub>)<sub>3</sub>CO-HfRW-NH<sub>2</sub> (**2**) - a full hMC1 agonist with an EC<sub>50</sub> of 5 nM and weak partial agonism at hMC3/4Rs. In order to understand the origin of melanocortin activity of short linear peptides, conformations of **1**, **2**, the core tetrapeptide Ac-HfRW-NH<sub>2</sub> (**3**), and analogs of **1** with  $\beta$ -turn stabilizing AAs (**4-8**) were studied by 2D-NMR in CD<sub>3</sub>OH, circular dichroism (CD), NMR constrained MD (Insight II, CVFF force field) and conformational analysis (Macromodel, OPLS\_2005 in water, MCMM).

### Results and Discussion

The NMR data (Figure 1) show that in contrast to unstructured tripeptide **2** all tetrapeptides possess secondary structures in solution (well resolved peaks in Figure 1A vs. unresolved in 1B). The core melanocortin tetrapeptide **3** demonstrates a classic  $\beta$ -turn with three NH<sub>*i*+1</sub> contacts and one *i*+2 between His and Arg. Presence of the phenylbutyric tail in **1** leads to disruption of the  $\beta$ -turn and “hydrophobic collapse”:  $\beta$ -CH<sub>2</sub> of the tail interacts with NH of His (the tail folds inside),  $\alpha$ -CH of Arg interacts with  $\gamma$ - and  $\delta$ -CH<sub>2</sub> (side chain folds inside) and

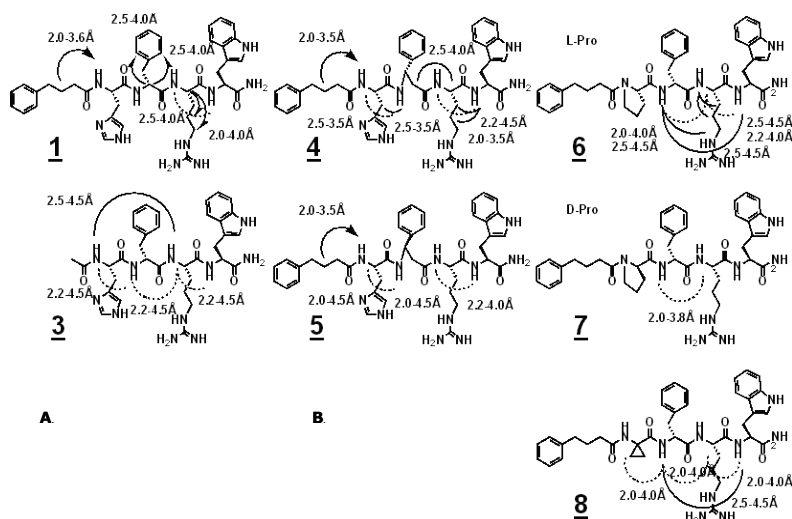


Fig. 1. <sup>1</sup>H NMR of amide region of **1** (A) and **2** (B) and NOE/ROE distances for tetrapeptides **1**, **3-8**.

Table 1. CD data for RCO-X-Z-Arg-(Trp)<sub>n</sub>-NH<sub>2</sub> ( $\beta$ -turn qualitative analysis)<sup>a</sup>

No.	R	X	Z	n	Methanol	Water
1	Ph(CH <sub>2</sub> ) <sub>3</sub>	His	D-Phe	1	Type I	Small % of Type I
2	Ph(CH <sub>2</sub> ) <sub>3</sub>	His	D-Phe	0	Type I (max. %)	Type I (max. %)
3	Ac	His	D-Phe	1	Type I (max. %)	Type I (max. %)
4	Ph(CH <sub>2</sub> ) <sub>3</sub>	His	D- $\beta$ -Phe	1	Type I	Type I
5	Ph(CH <sub>2</sub> ) <sub>3</sub>	His	L- $\beta$ -Phe	1	Small % of Type I	Small % of Type I
6	Ph(CH <sub>2</sub> ) <sub>3</sub>	L-Pro	D-Phe	1	Small % of Type I	Type I
7	Ph(CH <sub>2</sub> ) <sub>3</sub>	D-Pro	D-Phe	1	Small % of Type I	Not clear
8	Ph(CH <sub>2</sub> ) <sub>3</sub>	ACPC	D-Phe	1	Not clear	Type I

<sup>a</sup> Average of 4 scans at 50nm/min, *c* = 0.6 mg/mL

rotation of Ph in D-Phe becomes restricted (close contacts of *o*-CH<sub>Ar</sub> and  $\alpha$ -CH of D-Phe absent in **2**). The only contact that survives the transition from **3** to **1** is the most distal *i*+1 between Arg and Trp.

Since existing in the  $\beta$ -turn conformation **3** has low potency at MCRs [4,5] and existing in the totally different conformation **1** is superpotent, it appears that, contrary to the general belief, the  $\beta$ -turn conformation of the **HfRW** fragment is not crucial for melanocortin activity of short peptides. This is supported by the fact that **4** (D- $\beta$ -Phe analog of **1**) retaining the folded-in conformations of the tail and Arg similar to **1** with addition of rigidified backbone similar to **3** is practically inactive in human MC1R (determined as in [5]). Rigidifying different parts of the peptide backbone by introduction of  $\beta$ -turn inducing amino acids made compounds **5-8** inactive. NMR data are supported by MD simulations.

Conformational analysis [6] confirms that **2** lacks any structure [7], **3** exists exclusively in a  $\beta$ -turn conformation due to hydrogen bonding (only 5 conformations within 10 kcal/mol!) and **1** is much more flexible (122 conformations within 5 kcal/mol) but well aligned due to synergetic combination of hydrophobic and polar interactions.

CD data (Table 1) support the above results. The maximum percentage of the  $\beta$ -I turn (negative bands at 230 and 210 nm) were observed for the core melanocortin peptide **3**, D- $\beta$ -Phe derivative **4** and, rather unexpectedly, for the truncated peptide **2** both in MeOH and water. The latter finding can be explained by a slower time scale of NMR compared to CD and further support our conclusion that  $\beta$ -turn *per se* is not required for melanocortin activity.

Thus, we have shown that presumably flexible tetrapeptides RCO-X-Z-Arg-Trp-NH<sub>2</sub> in methanol and water solutions have clear conformational preferences that affect their biological activity. This information is useful for design of novel melanocortin ligands.

## Acknowledgments

Supported by a Skin Cancer Foundation Henry W. Menn Memorial Award for J.J.K. and grant RO1CA114095 (NIH) for Z.A.-M.

## References

1. Cone, R.D. (Ed.) *The Melanocortin Receptors Humana*, Totowa, 2000.
2. Sugg, E.E., et al. *Biopolymers* **25**, 2029-2042 (1986); Sugg, E.E., et al. *Biochem.* **27**, 8181-8188 (1988); Sun, H., et al. *Bioorg. Med. Chem.* **12**, 2671-2677 (2004); Fotsch, C., et al. *Bioorg. Med. Chem. Lett.* **13**, 2337-2340 (2003).
3. Koikov, L.N., et al. *Bioorg. Med. Chem. Lett.* **13**, 2647-2650 (2003); *ibid.*, 3997-4000 (2004).
4. Yang, Y., et al. *J. Biol. Chem.* **272**, 23000-10 (1997); Haskell-Luevano, C., et al. *J. Med. Chem.* **40**, 2133-2139 (1997).
5. Abdel-Malek, Z., et al. *Pigment Cell & Melanoma Res.* **22**, in print (2009).
6. Schrodinger Suite 2008 (Schrodinger LLC, New York, NY, 2008).
7. Ruwe, A.R., et al. *Bioorg. Med. Chem. Lett.* **19**, in print (2009).

## <sup>13</sup>C Shifts Reveal a Clear Pattern along Strands in $\beta$ Hairpins

Irene Shu, James M. Stewart, Brandon L. Kier, Michele Scian,  
 and Niels H. Andersen

Department of Chemistry, University of Washington, Seattle, WA 98195, U.S.A.

### Introduction

It has long been recognized that <sup>13</sup>C', <sup>13</sup>C <sub>$\alpha$</sub>  and <sup>13</sup>C <sub>$\beta$</sub>  chemical shift deviations (CSDs) from random coil values strongly correlate with protein backbone conformations [1,2]. <sup>13</sup>C', <sup>13</sup>C <sub>$\alpha$</sub>  CSDs are generally positive (more downfield relative to random coil shifts) in  $\alpha$ -helices and negative (more upfield) in  $\beta$ -sheets, while <sup>13</sup>C <sub>$\beta$</sub>  have opposite trend in the two types of secondary structures. Although the range of <sup>13</sup>C CSDs occurring in  $\beta$ -sheets slightly overlaps with the narrower range for  $\alpha$ -helices, <sup>13</sup>C chemical shifts are very useful for assigning secondary structure and thereby determining the 3D structure of a protein [3].

Since both backbone H <sub>$\alpha$</sub>  and amide protons H<sub>N</sub> of  $\beta$ -strands display an *i*/*i*+2 periodicity of downfield shifts in a  $\beta$ -hairpin or at the edge of a  $\beta$ -sheet, only the more positive CSDs are used for estimating hairpin fold population [4,5]. On the other hand, <sup>13</sup>C <sub>$\alpha$</sub>  and <sup>13</sup>C <sub>$\beta$</sub>  CSDs were also found to be a potential means to quantify  $\beta$ -hairpin fold population [6,7]. The CSDs of <sup>13</sup>C <sub>$\alpha$</sub>  and <sup>13</sup>C <sub>$\beta$</sub>  were separately averaged for all the strand residues in the considered peptide, excluding the non-protected N- and C-terminal residues, to estimate hairpin fold population. This implies that detailed pattern for <sup>13</sup>C CSDs along the  $\beta$ -strands do not appear to have been recognized in literature yet, unlike the case of <sup>1</sup>H <sub>$\alpha$</sub>  and <sup>1</sup>H<sub>N</sub> shifts.

In our aromatic-free hairpin model, we observed the diagnostic <sup>13</sup>C', <sup>13</sup>C <sub>$\alpha$</sub>  and <sup>13</sup>C <sub>$\beta$</sub>  shifts for  $\beta$ -structuring are, almost exclusively, associated with the cross-strand hydrogen-bonded residues. Their CSD magnitudes correlate qualitatively well with hairpin fold population based on measurements under different temperatures and incorporating different turn sequences into the hairpin model. HFIP (hexafluoroisopropanol) is shown to greatly influence <sup>13</sup>C shifts, and the random coil values applied to derive the  $\beta$ -strand CSD pattern should be adjusted when this co-solvent is present.

### Results and Discussion

**<sup>13</sup>C Random Coil Shifts Adjustment:** We measured the <sup>13</sup>C chemical shifts of Val residues within random coil control sequences that is Ala-rich or analogous to a single  $\beta$ -strand sequence. The sequential effect on the <sup>13</sup>C shifts under aqueous condition was revealed: <sup>13</sup>C' is 0.2 ppm more downfield being in a higher  $\beta$ -propensity environment, and <sup>13</sup>C <sub>$\alpha/\beta$</sub>  are about 0.1 ppm shifted. On the other hand, any <sup>13</sup>C nuclei in the random coil peptides are consistently downfield shifted by HFIP, suggesting that the solvent effect has significant influence on chemical shifts. Therefore the random coil shifts should be different when being applied to  $\beta$  hairpins under various solvent conditions.

**<sup>13</sup>C <sub>$\alpha$</sub>  and <sup>13</sup>C <sub>$\beta$</sub>  Patterns along Strands:** The CSD histograms show the clear *i*  $\rightarrow$  *i*+2 periodic pattern along  $\beta$  strands, and the diagnostic <sup>13</sup>C <sub>$\alpha$</sub>  and <sup>13</sup>C <sub>$\beta$</sub>  CSDs are strongly associated with the hydrogen bonded residues (Figure 1). The CSD magnitudes were compared under different turn propensities (pG > NG), temperatures, and solution conditions to see if they are consistent with the peptide stabilities. Indeed, the diagnostic shifts are all structurally induced. Such a pattern is also observed in other hairpin

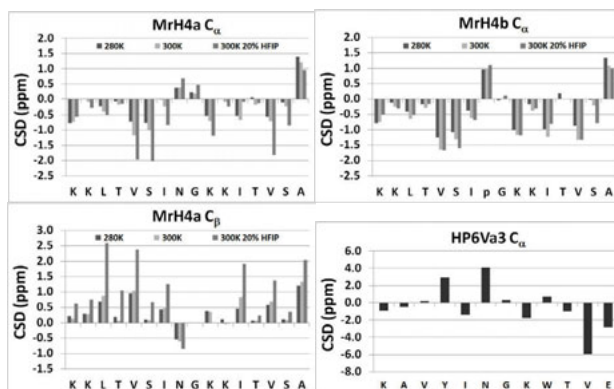


Fig. 1. The alternating magnitude pattern of <sup>13</sup>C <sub>$\alpha/\beta$</sub>  CSDs along  $\beta$  strands in hairpins MrH4a (left), MrH4b (top right); HP6Va3 (bottom right) peptide shows the aromatic residue effect.

Table 1. Averaged 100% CSDs in various hairpins

(ppm)	HB	HB turn	non-HB
$C_\alpha$	$-1.9 \pm 0.6$	$-1.2 \pm 0.6$	$-0.7 \pm 0.2$
$C_\beta$	$2.9 \pm 0.4$	$1.4 \pm 0.9$	$0.5 \pm 0.3$

models, including an antiparallel three-stranded  $\beta$  sheet. However, aromatic residues can, in some cases, have quite large effects on the pattern of backbone atom  $^{13}\text{C}_{\alpha/\beta}$  CSDs. In the case of HP6Va3 peptide, a non-hydrogen bonded residue **V11**  $C_\alpha$  has the largest CSD observed in the sequence, and the  $^{13}\text{C}_{\alpha/\beta}$  CSDs of the two aromatic residues (**Y4**, **W9**) have signs opposite to those observed in the hairpin lacking aryl functions.

**$^{13}\text{C}_{\alpha/\beta}$  CSDs vs. Percentage Fold (% fold):** In each studied hairpin, the  $^{13}\text{C}_{\alpha/\beta}$  CSDs values corresponding to fully folded (100%) state were extrapolated based on the hairpin fold population measured by  $H_\alpha$  CSDs of the non-HB residues [5]. The resulting 100% CSD values were averaged separately for hydrogen bonded (HB), turn flanking hydrogen bonded (HB turn), and non-hydrogen bonded (non-HB) residues from all systems examined (Table 1). It reveals that the nuclei of the hydrogen bonded residues, including that of the turn flanking sites, have larger structuring shifts than those of the non-hydrogen bonded residues. Therefore, the  $^{13}\text{C}$  results presented indicate that the structuring probes should be specifically chosen, mostly at hydrogen bonded sites, for evaluating the hairpin formation, instead of averaging the CSDs from all the strand residues [6,7]. Notice that the CSD difference between the hydrogen bonded and non-hydrogen bonded residues is even larger in  $^{13}\text{C}_\beta$  than that in  $^{13}\text{C}_\alpha$ .

**Cross-stranded Hydrogen Bonded  $^{13}\text{C}'$  CSDs Correlate with Hairpin Stability:**  $^{13}\text{C}'$  labeled residues were selectively placed at certain sites in  $\beta$  strands of hairpins with varied stabilities. The  $^{13}\text{C}'$  CSDs are strongly negative and weakly positive at hydrogen bonded and non-hydrogen bonded positions, respectively. The linear relationship of hydrogen bonded  $^{13}\text{C}'$  CSDs and hairpin fold population also suggests their direct correlation (Figure 2).

**Protein  $\beta$  Sheets:**  $^{13}\text{C}$  CSDs of natural protein  $\beta$  sheets are also examined, taken from biological magnetic resonance bank (BMRB) database. The examined residues are classified into three groups: residues on the edge-strand hydrogen-bonded with one neighboring  $\beta$ -strand (Inny), those on the strand hydrogen-bonded with two neighboring  $\beta$ -strands (Central), and those on the edge-strand that is not hydrogen-bonded with any other motifs (Outy). The observed CSDs are very similar to the pattern found in our hairpin models: the backbone-backbone hydrogen-bonding property strongly influences  $^{13}\text{C}$  CSDs, the trend is clearer for  $^{13}\text{C}_\beta$  and  $^{13}\text{C}'$  than for the  $^{13}\text{C}_\alpha$  CSDs.

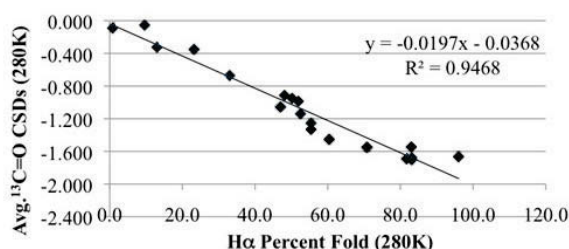


Fig. 2. Correlation of  $^{13}\text{C}'$  with fold population determined by  $H_\alpha$  CSD.

## Acknowledgments

This research was supported by a grant from the NSF (CHE-0650318).

## References

1. Spera, S., Bax, A. *J. Am. Chem. Soc.* **113**, 5490-5492 (1991).
2. Wishart, D.S., Sykes, B.D., Richards, F.M. *J. Mol. Biol.* **222**, 311-333 (1991).
3. Avbelj, F., Kocjan, D., Baldwin, R.L. *Proc. Natl. Acad. Sci. U.S.A.* **101**, 17394-17397 (2004).
4. Griffiths-Jones, S.R., Maynard, A.J., Searle, M.S. *J. Mol. Biol.* **292**, 1051-1069 (1999).
5. Fesinmeyer, R.M., et al. *J. Biomol. NMR* **33**, 213-231 (2005).
6. Santiveri, C.M., et al. *J. Biomol. NMR*, **19**, 331-345 (2001).
7. Santiveri, C.M., Pantoja-Uceda, D., Rico, M., Jimenez, M.A. *Biopolymers* **79**, 150-162 (2005).



## Characterization of Octapeptide GAP as a Precise Carrier for an Imaging or Cancer Therapeutic Agent

Chumpol Theeraladanon,<sup>1</sup> Keisuke Hamada,<sup>2</sup> Nobukazu Takahashi,<sup>1</sup>  
Ukihide Tateishi,<sup>1</sup> Kazuhiro Ogata,<sup>2</sup> and Tomio Inoue<sup>1</sup>

<sup>1</sup>Department of Radiology, Graduate School of Medicine, Yokohama City University, Yokohama, 236-0004, Japan; and <sup>2</sup>Department of Biochemistry, Graduate School of Medicine, Yokohama City University, Yokohama, 236-0004, Japan

### Introduction

The excitatory glutamic acid is a potent neurotransmitter in central nervous system. Glutamic Acid Peptide (GAP) exerts its action via binding to glutamate receptors (GluRs). GAP has been employed as a targeted carrier, which conjugate to an anticancer agent, a chemotherapeutic agent by peptide or ester linkage. Moreover, its acid residue could chelate to radiometallic isotopes such as <sup>68</sup>Ga, <sup>99m</sup>Tc for imaging or radiotherapeutic application. Previous study reported that a polyglutamate (MW. 20-50k) is not suitable for imaging needs due to high molecular weight. Thus, commercially available poly-L-glutamic acid (MW. 750-5,000) containing 5-33 glutamic acid moieties is an advantage for better quality of imaging. A wide variety of imaging or radiotherapeutic agents could be developed using this technology for example GAP-estradiol [1,2]. However, various ranges of peptide chain in commercially available GAP lead to occasionally difficult explanation of experiment results. Herein, we rationally designed GAP(YCU)-EDL, a model of conjugated GAP-anticancer, to avoid complicated debates by limiting peptide size to eight glutamic acid moieties. The octapeptide GAP-EDL was synthesized and well characterized to serve for an assessment of precise carrier.

### Results and Discussion

GAP(YCU)-EDL was synthesized by conjugation of 3-aminoethyl estradiol (EDL) to the first and fifth glutamic acid prior to sequence synthesis of octapeptide GAP prepared by solid phase peptide synthesis according to Fmoc/tBu strategy, and the remaining acid moieties were designed for chelating to <sup>68</sup>Ga (Figure 1).

Cocktail cleavage was performed to remove resin, Fmoc and tBu protecting groups by mixture of TFA:thioanisole:EDT (90:5: 5). The crude product was analyzed and purified by

HPLC using Wakopak C18-55 column, gradually eluted with eluent A (0.1% AcOH in CH<sub>3</sub>CN) and eluent B (0.1% AcOH in H<sub>2</sub>O) in 40 min at flow rate 3.0 mL/min. The sample was dissolved in eluent A and the peaks were detected at 210 nm. Subsequently, mass spectroscopy analysis resulted in the molecular weight for each of purified 7 peaks as in Table 1. Surprisingly, the 2<sup>nd</sup> and 6<sup>th</sup> peaks showed same molecular weight with different retention time.

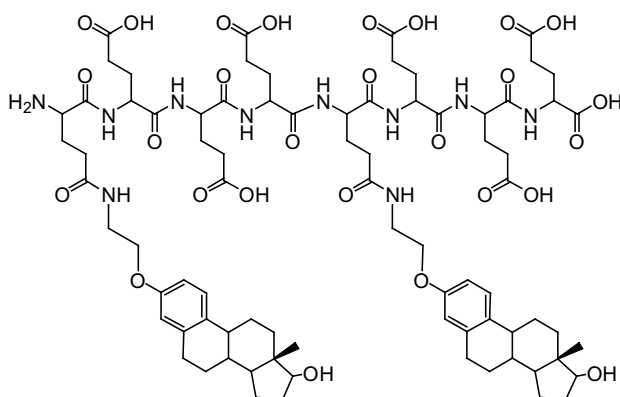


Fig. 1. GAP(YCU)-EDL.

We hypothesized that trace amount of metal cation in the solvent might chelate to the remaining acid residue to provide different configuration of same molecule. EDTA is mainly sequestering metal ions in solutions. Therefore, exploiting the same HPLC analysis system with adding 0.1 mM EDTA to eluents was performed. We first examine sample of 6<sup>th</sup> peak alone, an addition of EDTA resulted in shifting retention time of 6<sup>th</sup> peak from 26.5 min to 19.0 min, which could be identified as the 2<sup>nd</sup> peak whilst sample of 2<sup>nd</sup> peak and 6<sup>th</sup> peak mixture in presence of 0.1 mM EDTA was examined, only the 2<sup>nd</sup> peak was observed. These results suggested that the compound of 6<sup>th</sup> peak should be the same compound as 2<sup>nd</sup> peak with weakly chelating to metal cation by the acid residue of octapeptide GAP.

*Table 1. Mass spectroscopy analysis results*

<i>Peak</i>	<i>Retention Time (min)</i>	<i>Molecular Weight</i>
1	15.6	1218.5
2	19.0	1644.7
3	20.4	1314.4
4	22.0	927.3
5	24.2	1218.5
6	26.5	1644.7
7	32.0	1410.5

In summary, this methodology could be applied to the synthesis of conjugated anticancer agent or imaging agent to octapeptide GAP as precise carrier for radiotherapeutic or imaging application.

## Acknowledgments

This work was partially supported by grant for 2008 Strategic Research Project (Fund Number K19016) of Yokohama City University, Japan.

## References

1. Takahashi, N., Yang, D.J., Kohanim, S., Oh, C., Yu, D., Azhdarinia, A., Kurihara, H., Zhang, X., Chang, J.Y., Kim, E.E. *Eur. J. Nucl. Med. Mol. Imaging* **34**, 354-362 (2007).
2. Takahashi, N., Yang, D.J., Kurihara, H., Borne, A., Kohanim, S., Oh, C., Mawlawi, O., Kim, E.E. *Acad. Radio.* **14**, 1050-1057 (2007).

## Effect of Side-Chain Chirality on Peptide Helix Type and Screw Sense

Ivan Guryanov,<sup>1</sup> Cristina Peggion,<sup>1</sup> Fernando Formaggio,<sup>1</sup>  
 Ahmed Lakhani,<sup>2</sup> Timothy A. Keiderling,<sup>2</sup> and Claudio Toniolo<sup>1</sup>

<sup>1</sup>ICB, Padova Unit, CNR, Department of Chemistry, University of Padova, 35131 Padova, Italy;

<sup>2</sup>Department of Chemistry, University of Illinois at Chicago, Chicago, IL 60607-7061, U.S.A.

### Introduction

The conformational control of poly( $\alpha$ -olefin) exerted by the combined configurations of the main-chain and side-chain asymmetric carbon atoms of the monomeric unit was carefully investigated as early as in the 1960's. Conversely, for oligo- and polypeptides this potentially relevant influence has been only scarcely studied [1,2]. In this work, we made efforts to address this issue by investigating the conformational properties of the two diastereomeric *n*-But-Xxx-Aib-(Xxx)<sub>2</sub>-Aib-Xxx-NH<sub>2</sub> hexapeptides, where *n*-But is *n*-butanoyl and Xxx is L-Ile in one peptide and L-*allo*Ile (Figure 1) in the other.

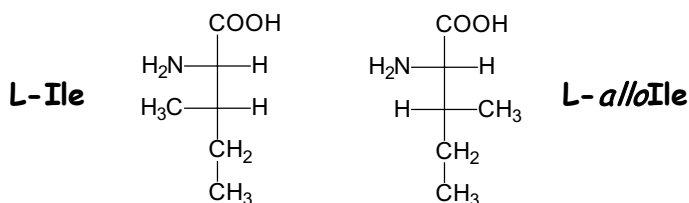


Fig. 1. Fischer's projections of the diastereomeric  $\alpha$ -amino acids L-Ile and L-*allo*Ile.

### Results and Discussion

Terminally-blocked hexapeptide amides containing two well-spaced, strongly helicogenic, achiral Aib ( $\alpha$ -aminoisobutyric acid) residues are known to be highly folded [3]. For the assignment of the preferred conformation(s) adopted by these peptides in structure-supporting solvents we heavily relied on FT-IR absorption, 2D-NMR, and electronic and vibrational circular dichroism (ECD and VCD, respectively) techniques.

The two peptides are largely helical (Figure 2) despite the presence of 66% of the  $\beta$ -sheet former (Ile, *allo*Ile) residues [4,5]. In these peptides based on  $\alpha$ -amino acids characterized by asymmetric  $\alpha$ - and  $\beta$ -carbons, the right-handed helical screw sense is largely dictated by the chirality (L) at the  $\alpha$ -position. The nature (mostly 3<sub>10</sub>) of the helix formed seems to be poorly influenced by the side-chain chirality.

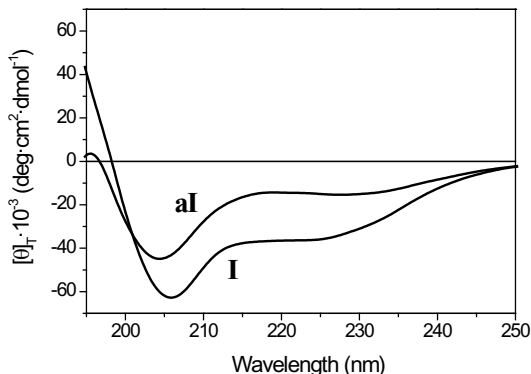


Fig. 2. Far-UV ECD spectra in MeOH solution for the *n*-But-Xxx-Aib-(Xxx)<sub>2</sub>-Aib-Xxx-NH<sub>2</sub> hexapeptides, in which **I** is the Xxx = L-Ile peptide and **al** is its L-*allo*Ile diastereomer (peptide conc.: 0.1 mM).

## References

1. Andreetto, E., Peggion, C., Crisma, M., Toniolo, C. *Biopolymers (Pept. Sci.)* **84**, 490-501 (2006).
2. Nagano, M., Tanaka, M., Doi, M., Demizu, Y., Kurihara, M., Suemune, H. *Org. Lett.* **11**, 1135-1137 (2009), and references cited therein.
3. Toniolo, C., Crisma, M., Formaggio, F., Peggion, C. *Biopolymers (Pept. Sci.)* **60**, 396-419 (2001).
4. Goodman, M., Naider, F., Toniolo, C. *Biopolymers* **10**, 1719-1730 (1971).
5. Toniolo, C., Bonora, G. M., Salardi, S. *Int. J. Biol. Macromol.* **3**, 377-384 (1981).

## Peptide-assisted Assembly and Patterning of Carbon Nanotubes

Zhengding Su and John F. Honek

Department of Chemistry, University of Waterloo, Waterloo, ON N2L 3G1, Canada

### Introduction

Carbon nanotubes are promising nanoscale building blocks for molecular devices ranging from molecular electronics to ultra-sensitive biosensors, thanks to their unique electrical and structural features. Creating intricate nanodevices requires the precise patterning of carbon nanotube arrays. However, creating such complex and carefully aligned structures at nanometer scales is a challenge for researchers, especially in large-scale fabrication [1].

Inspired by peptide self-assembly processes [2] and by the interaction of carbon nanotubes with aromatic amino acids [3-4], we have developed a simple protocol to assemble peptide-attached carbon nanotubes on a substrate surface, on which patterns were created by peptide functionalization. This strategy appears promising in the fabrication of carbon nanotube circuits with single-nanotube precision, and may enable nanotube-based devices, such as nano-biosensors, to be produced industrially.

### Results and Discussion

Single-walled carbon nanotubes (SWNTs) were functionalized through carboxylation to increase their solubility in aqueous solution (Figure 1). The dipeptide, L-phenylalanyl-L-phenylalanine (i.e., Phe-Phe), can form peptide nanotubes in aqueous solution through a process of self-assembly. When the dipeptide is dissolved in organic solvents, such as 1,1,1,3,3,3-hexafluoro-2-propanol [2] and acetonitrile [5] at concentrations greater than 100 mg/ml and then diluted with water to a final concentration of 2 mg/ml, hollow nanotubes are instantly formed. A schematic description of peptide nanotube formation through self-assembly (SAM) is shown in Figure 1. Hollow peptide nanotubes exhibited uniform size as visualized by scanning electron microscopy (SEM).

In this work, it is our interest to employ this SAM process to deposit dipeptides on the surfaces of SWNTs so that individual SWNTs as well as small bundles of SWNTs can be wrapped and separated from large aggregates. To achieve this purpose, the dipeptide is initially dissolved in organic solvents and then diluted with an aqueous solution containing oxidized SWNTs. Dipeptides were deposited and coated the SWNTs through peptide-SWNT interactions

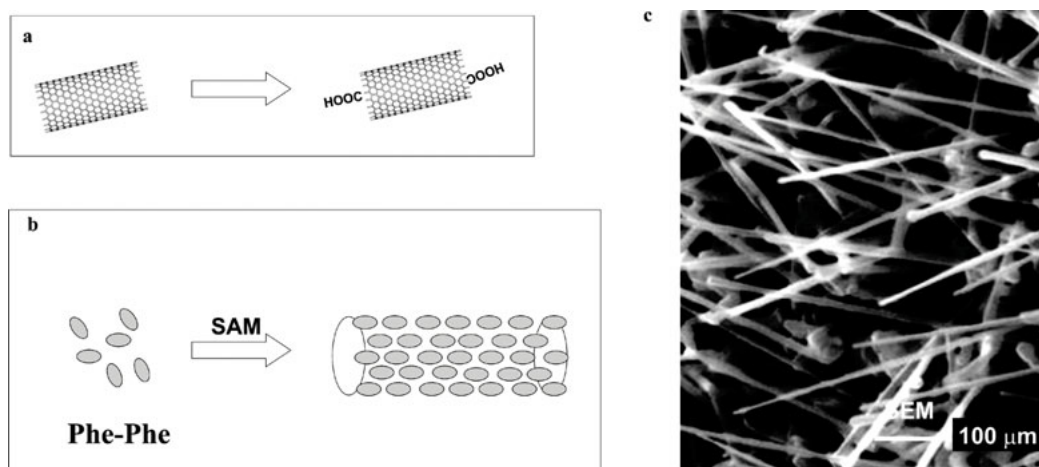


Fig. 1. Solubilization of SWNTs and Self-assembly of dipeptides. **a.** SWNTs were functionalized by strong acids. Only one carboxyl group is shown at each end of the SWNT for simplicity **b.** Dipeptide, i.e., L-phenylalanyl-L-phenylalanine which is represented as oval, can self-assemble into peptide nanotubes (PNTs) in aqueous solution. SAM: self-assembly. **c.** PNTs are visualized by scanning electron microscopy (SEM).

[4] and peptide-peptide interaction. Figure 2 represents a schematic configuration of the dipeptide/SWNT complex, in which dipeptides coat the surface of SWNTs. The complex was characterized by SEM, as shown in Figure 2, indicating that SWNTs are well separated. These wrapped SWNTs were further confirmed to have specific diameters, as indicated by the lineshapes of the radial breathing mode (RBM) in the Raman spectra.

Now we are interested in utilizing the dipeptide self-assembly process to guide the alignment of peptide-bound SWNTs on silica substrate surfaces. Dipeptide blocks (i.e., Phe-Phe) were directly deposited on silica substrate surfaces by use of dip-pen nanolithography [6]. This approach enabled us to functionalize any substrate without resorting to intermediate chemical steps, thereby minimizing surface contamination. When the substrate is placed in contact with a suspension of dipeptide-bound SWNTs, the dipeptide-bound SWNTs are attracted to areas on the silica substrate surface which contain pre-marked dipeptide blocks, and self-assembled to rapidly form pre-designed patterns (Figure 2). Unbound nanotubes could be washed away with H<sub>2</sub>O. Alternatively, conjugation of dipeptide at both ends of SWNT has been also used for guiding the template-oriented assembly of SWNTs on silica substrate with pre-marked dipeptides (data not shown).

In the future work, we are planning to incorporate this process into conventional microfabrication methods to synthesize SWNT-based field-effect transistors (FET) biosensors. In this case, we will focus on bridging nanotubes (preferably single nanotubes) between electrodes.

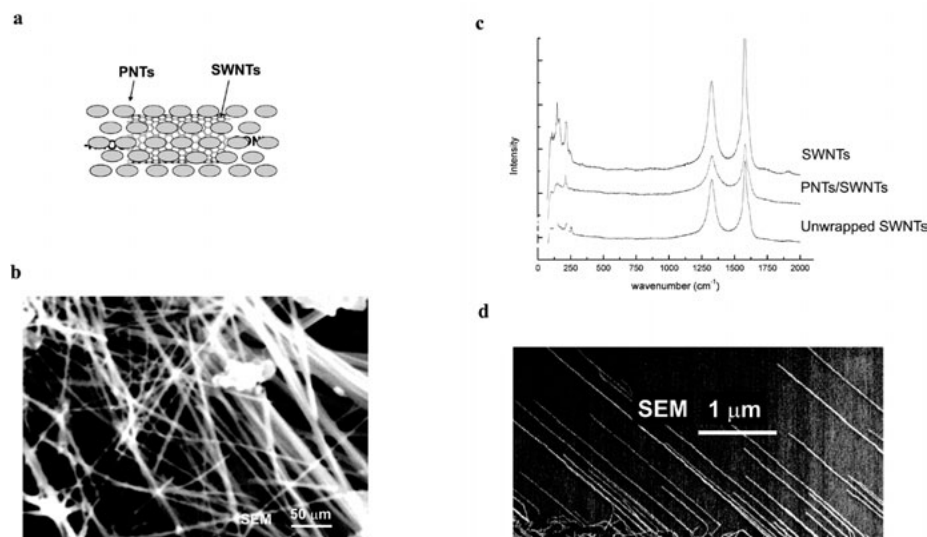


Fig. 2. Peptide-mediated alignment of SWNTs on silica substrate with pre-designed template. **a.** A schematic graphic which shows a possible structure for the peptide-bound SWNTs. **b.** Peptide-bound SWNTs are characterized by SEM. **c.** Peptide-bound SWNTs are assayed by Raman spectroscopy. **d.** Peptide-bound SWNTs are able to carry out self-assembly with dipeptides marked on silica substrate. The SEM image indicates aligned peptide-bound SWNTs.

## Acknowledgments

We would like to thank Dr. Zhen He for technical assistance in the scanning electron and atom force microscopy experiments. We thank NSERC and the University of Waterloo for financial resources.

## References

1. Heremans, P. *Nature* **444**, 828-831 (2006).
2. Reches, M., Gazit, E. *Science* **300**, 625-627 (2003).
3. Su, Z., Mui, K., Daub, E., Leung, T., Honek, J. *J. Phys. Chem. B* **111**, 14411-14417 (2007).
4. Su, Z., Leung, T., Honek, J. *J. Phys. Chem. B* **110**, 23623-23627 (2006).
5. Lu, K., et al. *Am. Soc. Chem.* **125**, (21), 6391-6393 (2003).
6. Demers, L.M., et al. *Science* **296**, 1836-1838 (2002).

## Manipulating Solvent Exposed Residues for the Formation of a pH-Dependent Coiled Coil Peptide

Dawn Ernenwein and Jean Chmielewski

Department of Chemistry, Purdue University, West Lafayette, IN 47907, U.S.A.

### Introduction

The coiled coil motif plays a prominent role in the structure and function of a range of proteins. The heptad repeat of coiled coil peptides (Figure 1) is a unique pattern of seven residues in which positions *a* and *d* are typically hydrophobic and positions *b*, *c*, *e*, *f*, and *g* are polar. **GCN4-p1** is a widely studied leucine zipper domain of the yeast transcription factor GCN4 [1], which is stabilized as a parallel homodimer. It has been established that different oligomerization states exist depending on the amino acid composition of the hydrophobic core at the *a* and *d* positions [2]. With regards to electrostatic interactions between peptides within the coiled coil, studies have focused on manipulating the residues at the *e* and *g* positions to control coiled coil formation [3]. In this case, however, we wished to investigate the effects on peptide conformation of modifying the solvent exposed position *f*. Through the incorporation of glutamic acid residues, it was proposed that pH could be used to manipulate the formation of a coiled coil. At neutral pH, electrostatic repulsion between the side chains would result in a random coil conformation, however, upon lowering the pH, the native coiled coil structure would be regained.

### Results and Discussion

**GCN4-p1** was used as the starting point for the design. The four solvent-exposed residues at the *f* positions of the coiled coil were altered to glutamic acids. Two residues at the *c* positions were also modified to alanine resulting in **GCN4-E** (Figure 1). This cofacial arrangement of glutamic acid residues should allow the conformation of **GCN4-E** to be controlled by pH. An anionic control peptide lacking the hydrophobic interface and grouping of Glu residues was also designed by scrambling residues of **GCN4-E** to produce **GCN4-X**. This peptide would allow us to determine if helicity was dependent solely on charge neutralization or by the placement of the negative charges.

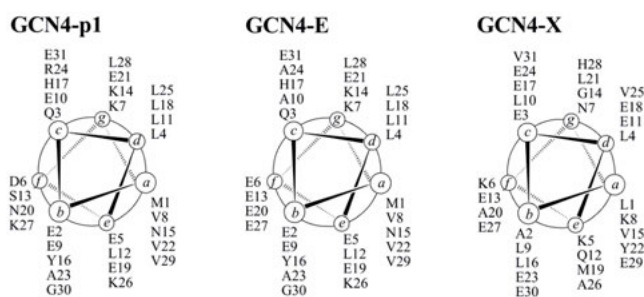


Fig. 1. Helical wheels of **GCN4-p1**, **GCN4-E**, and **GCN4-X**.

The peptides were synthesized by standard Fmoc solid phase peptide synthesis on Rink ChemMatrix resin, purified to homogeneity by reverse phase HPLC, and characterized by MALDI-TOF mass spectrometry. Circular dichroism (CD) was used to determine the helical content of **GCN4-E** and **GCN4-X** at neutral and acidic pH, to determine if a helical switch was obtained upon charge neutralization. At pH 7.4, both **GCN4-E** and **GCN4-X** resulted in mainly a random coil conformation with 17% and 10% helical content, respectively (Figure 2a). However, when the pH was lowered to 3.4, **GCN4-E** was found to mainly adopt an  $\alpha$ -helical conformation (90%), whereas **GCN4-X** was still mostly random coil with additional features of  $\alpha$ -helix and  $\beta$ -sheet in evidence. These data suggest that neutralization of the negative charge on

the glutamate residues can result in a helical conformation, and potentially a dimeric coiled coil, when the residues are arranged to promote amphiphilicity [4]. To determine the amount of coiled coil character, the ratio at  $\theta_{222}/\theta_{208}$  can be utilized. If this value is greater than 1.0, the peptide is considered to adopt a coiled coil conformation [5]. Under acidic conditions for **GCN4-E**, this ratio was found to be 1.05, whereas at neutral conditions the value was 0.45. These data indicate that **GCN4-E** does adopt a coiled coil helical conformation at acidic pH.

Further experiments were performed to determine the formation of the **GCN4-E** coiled coil with increasing salt concentrations at neutral pH (Figure 2b). Sodium sulfate is a known kosmotropic salt that disrupts hydrogen bonding with water, and has been shown to stabilize peptide conformation, such as the  $\alpha$ -helix, in aqueous solution at high concentrations [6-7]. Additions of increasing amounts of sodium sulfate were found to result in a corresponding increase in helicity of **GCN4-E**; addition of 500 mM of sodium sulfate was found to increase the helicity to 82%.

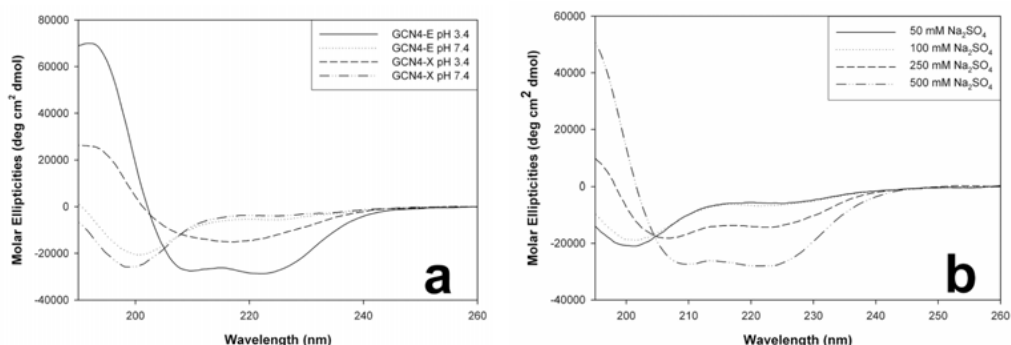


Fig. 2. CD spectra of **GCN4-E** and **GCN4-X** (15  $\mu$ M) at a) 10 mM acetate buffer pH 3.4 and phosphate buffer pH 7.4. b) CD spectra of **GCN4-E** (15  $\mu$ M) with increasing amounts of  $\text{Na}_2\text{SO}_4$ .

Next, to determine the oligomerization state of the coiled coil of **GCN4-E** under acidic conditions, analytical ultracentrifugation (AUC) was performed. At low concentration (<100  $\mu$ M), 90% of **GCN4-E** was found in the dimeric form (exp. MW 7949, calc. MW 7306). At higher concentrations increases in the tetrameric form of the peptide were observed.

In conclusion, solvent exposed residues of the coiled coil motif were replaced with glutamic acid residues without disrupting the overall secondary structure. A switch between random-coil to an  $\alpha$ -helix was observed by decreasing the pH from 7.4 to 3.4, or by increasing the kosmotropic salt content. The coiled coil at acidic pH was identified by AUC experiments to be a dimeric structure. It will be interesting to determine if cationic scaffolds may be also used to assembly **GCN4-E** into a coiled coil via charge complementation.

## Acknowledgments

We would like to acknowledge John Burgner for assistance with the AUC experiments. This work was supported by NSF and the Purdue Research Foundation.

## References

1. O'Shea, E.K., Klemm, J.D., Kim, P.S., Alber, T. *Science* **254**, 539-544 (1991).
2. Harbury, P.B., Zhang, T., Kim, P.S., Alber, T. *Science* **262**, 1401-1407 (1993).
3. Zeng, X., Zhu, H., Lashuel, H.A., Hu, J.C. *Protein Science* **6**, 2218-2226 (1997).
4. Zhou, N.E., Kay, C.M., Hodges, R.S. *J. Mol. Biol.* **237**, 500-512 (1994).
5. Lau, S.Y.M., Taneja, A.K., Hodges, R.S. *J. Bio Chem* **259**, 13253-13261 (1984).
6. Collins, K.D. *Biophys. J.* **72**, 65-76 (1997).
7. Hofmeister, F. *Arch. Exp. Pathol. Pharmacol.* **24**, 247 (1888).



## Collagen Peptide Fiber Formation Triggered by Metal Ions

David E. Przybyla and Jean Chmielewski

Department of Chemistry, Purdue University, West Lafayette, IN 47906, U.S.A.

### Introduction

Self-assembling peptides provide a bottom up approach for generating macro-scale materials from smaller peptide fragments [1,2]. These systems are of particular interest in the fields of drug delivery, cell adhesion, and regenerative medicine where self-assembling peptides have successfully been used as scaffolds for cellular proliferation and differentiation [3,4]. Because of collagen's ubiquitous involvement in the extracellular matrix and current widespread clinical applications in regenerative medicine, self-assembling collagen peptides have become an attractive alternative. To date, several groups have developed self-assembling collagen peptides by incorporating a variety of N- and C-terminal sticky ends that propagate through a linear mechanism [4-8]. As an alternative assembly strategy, we hypothesized that the placement of metal binding ligands within the collagen triple helix could facilitate assembly through a radial mechanism.

Our previously designed metal-triggered self-assembling peptide **H-bpy** utilized a bipyridine ligand to achieve radial-assembly, and was capable of assembling into collagen fibers in the presence of Fe(II) [9]. To expand the radial assembly strategy we have functionalized a collagen triple helical peptide with an iminodiacetate (IDA) ligand at the central trimer position (**H-IDA**) (Figure 1). Specifically, the tridentate coordination geometry of **H-IDA** allows for two collagen triple helices to join around one metal ion followed by further radial-assembly. This is in contrast to the bidentate coordination geometry of **H-bpy** that required three triple helices to assemble around each metal ion. We hypothesized that the different coordination geometry of the IDA ligand would still facilitate radial-assembly, but wished to evaluate how the different binding geometry would alter its structure as compared to the bipyridine ligand. This information may provide further insight into how radially-assembled collagen peptide structures can be controlled by altering the ligands.

### Results and Discussion

**H-IDA** was synthesized by standard Fmoc based chemistry on the ChemMatrix resin using Lys(Mtt) in the central position. After the deprotection of Lys(Mtt) (1.8% TFA:DCM) the resin-bound peptide was treated with tert-butyl bromoacetate (3 eq). The peptide was subsequently cleaved from the resin with TFA/TIPS/H<sub>2</sub>O (95:2.5:2.5), purified to homogeneity and characterized by MALDI-TOF mass spectrometry. To confirm that **H-IDA** formed a stable triple helix and to investigate how the addition of Ni(II) would alter its stability, circular dichroism (CD) in conjunction with thermal denaturation studies were implemented (Figure 2A). The CD spectrum of **H-IDA** (250  $\mu$ M in HEPES 10mM pH 7.0) revealed a characteristic type-II polyproline helix profile with and without the addition of Ni(II) (250  $\mu$ M). However, the addition of Ni(II) did enhance the thermal stability ( $T_m$ ) of the triple helix. Specifically, the  $T_m$  of **H-IDA** was observed to be 48 °C and 54 °C respectively in the absence and presence of Ni(II). The increase in the thermal stability was consistent with our previously reported bipyridine ligand, [9] and is presumably due to the metal binding of multiple triple helices.

The self-assembly resulting from the addition of Ni(II) was initially confirmed using dynamic light scattering (DLS). **H-IDA** (1 mM, HEPES 10 mM pH 7.0) was incubated in the presence of Ni(II) (1 mM) for 48 h at 20 °C. The hydrodynamic radius of a single **H-IDA** triple

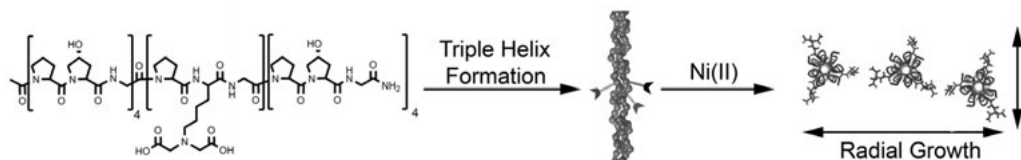


Fig. 1. **H-IDA** polypeptide chain. Triple helix formation leading to further assembly after the addition of Ni(II) to **H-IDA**.

helix was found to be approximately 4 nm indicated the absence of assembly, while the coordination of Ni(II) resulted in an increase to approximately 215 nm, a clear indication of metal-promoted assembly of the radius (Figure 2B). To further confirm that the assembly was a result of metal-ligand binding, EDTA (5 mM) was added to the assembly to chelate the Ni(II) from the IDA ligands. It was found that the addition of EDTA resulted in the loss of the assembled species and a return of the radius to that of the pre-metal state.

Visualization of assembly was performed by transmission electron microscopy (TEM). **H-IDA** (1 mM, HEPES 10 mM pH 7.0) and Ni(II) (500  $\mu$ M) were incubated for 48 h at 4  $^{\circ}$ C and visualized by TEM after staining with 1% phosphotungstic acid pH 7.2 on a carbon grid (Figure 2C). The TEM images revealed that the metal-promoted assembly of **H-IDA** resulted in fiber formation. Interestingly, these fibers differ from those previously reported [9] in that they appear to be flatter. This difference in structure is presumably a result of the tridentate IDA coordination geometry that does not allow three triple collagen peptide fragments to assemble around one Ni(II) ion, as compared to the bidentate coordination geometry of **H-byp** [9]. We hypothesized that fibers formed via the radial assembly of **H-IDA** as a result of a staggering between multiple metal-bound collagen segments, leading to sticky-ends and the subsequent fiber formation.

We have successfully shown that the **H-IDA** peptide can assemble in the presence of Ni(II) through a radial growth mechanism into collagen fibers. This data suggests that the placement of different ligands along the collagen triple helix may be a versatile approach for gaining control over specific collagen assemblies, leading to unique biological properties.

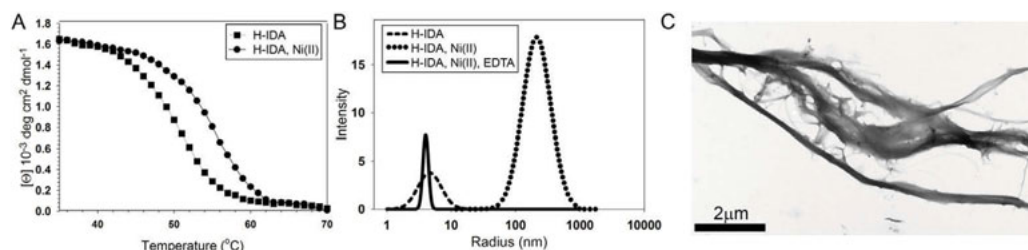


Fig. 2. (A) Thermal denaturing curve of **H-IDA** (250  $\mu$ M) and Ni(II) (250  $\mu$ M). (B) Dynamic light scattering of **H-IDA** (1 mM), with Ni(II) 1 mM, and EDTA (5 mM). (C) Transmission electron microscopy of **H-IDA** (1 mM) with Ni(II) 500  $\mu$ M in HEPES (10 mM, pH 7.0).

## Acknowledgments

We would like to thank Debby Sherman for her assistance with the TEM images. Supported by the NSF (Grant 0078923-CHE).

## References

1. Gunasekar, S.K., Haghpahan, J.S., Montclare, J.K. *Polym. Adv. Technol.* **19**, 454-468 (2008).
2. Woolfson, D.N., Ryadnov, M.G. *Curr. Opin. Chem. Biol.* **10**, 559-567 (2006).
3. Gelain, F., Horii, A., Zhang, S. *Macromol. Biosci.* **7**, 544-551 (2007).
4. Silva, G.A., et al. *Science* **303**, 1352-1355 (2004).
5. Cejas, M., et al. *J. Am. Chem. Soc.* **129**, 2202-2203 (2007).
6. Rele, S., et al. *J. Am. Chem. Soc.* **129**, 14780-14787 (2007).
7. Pires, M.M., Chmielewski, J. *J. Am. Chem. Soc.* **131**, 2706-2712 (2009).
8. Kotch, F.W., Raines, R. T. *Proc. Nat. Acad. Sci. U.S.A.* **103**, 3028-3033 (2006).
9. Przybyla, D.E., Chmielewski, J. *J. Am. Chem. Soc.* **130**, 12610-12611 (2008).

## Strand Exchange of Charged Collagen-Based Peptides

Jeeyeon Lee and Jean Chmielewski

Department of Chemistry, Purdue University, West Lafayette, IN 47907, U.S.A.

### Introduction

Collagen is the main structural component of animal connective tissues, and has a wide variety of medical applications in tissue engineering and drug delivery [1,2]. The tertiary structure of numerous types of collagen is composed of a common structural motif - the collagen triple helix (CTH). Repeating units of GlyXaaYaa are common within the different collagens, with a propensity for X being proline and Y being hydroxyproline (Hyp). Thermally unstable domains of collagen proteins, based on regions deficient in Hyp, have been reported to facilitate the unraveling of CTH structures [3]. Collagen-mimetic peptides have also been shown interact with collagen films and intact collagen fibers presumably through a strand invasion mechanism [4,5]. Herein, we demonstrate that charged-complemented collagen peptides can show strand exchange facilitated via electrostatic interaction.

### Results and Discussion

Previously we reported that O-alkylation of hydroxyproline may be used to introduce a carboxylic acid functionality (**P<sub>E</sub>**) or an amino group (**P<sub>K</sub>**) into functionalized proline residues. These modified amino acids were used to functionalize collagen peptides and cell penetrating peptides without disrupting the CTH or polyproline type II helical structure [6,7]. We hypothesized that a combination of negatively and positively charged collagen triple helical peptides may facilitate strand exchange due to charge compensation. With this in mind, we designed two peptides with complementary charges; **PP<sub>E</sub>G-5E** containing five negatively charged residues placed at both the N- and C- termini of the peptide, and **PP<sub>K</sub>G-3** with three positive residues located in the center of the peptide.

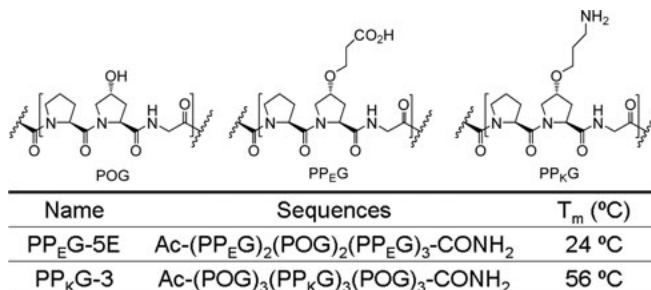


Fig. 1. Peptides sequences of this study, and melting temperatures (*T<sub>m</sub>*) for their triple helical structures.

The modified hydroxyproline residues with charged moieties, **P<sub>E</sub>** and **P<sub>K</sub>**, were synthesized by previously reported methods [6,7]. The collagen-based peptides were synthesized on the Chem matrix resin using Fmoc based chemistry and HBTU as a coupling agent. The peptides were cleaved from the resin using TFA/anisole (95:5), purified to homogeneity by reverse-phase HPLC and characterized by MALDI-TOF mass spectrometry. The formation of a polyproline type II helix and CTH thermal stability was confirmed by circular dichroism (CD) studies. The peptide **PP<sub>E</sub>G-5E** (200 μM, 10 mM phosphate buffer, pH 7.0) was found to form a triple helix with a *T<sub>m</sub>* of 24 °C, while **PP<sub>K</sub>G-3** under the same conditions displayed a more stable triple helix with a *T<sub>m</sub>* of 56 °C (Figure 1).

Strand invasion of the two peptides was investigated as a function of time by CD (Figure 2). Equimolar concentrations of **PP<sub>E</sub>G-5E** and **PP<sub>K</sub>G-3** (200 μM) were mixed in phosphate buffer (pH 7.0) at 4 °C and the thermal stability of the mixture was evaluated. Immediately upon mixing the peptides two distinct melting transitions were observed, corresponding to *T<sub>m</sub>* values of 40 °C and 23 °C (Figure 2A). The former melting temperature is significantly lower than the *T<sub>m</sub>* of **PP<sub>K</sub>G-3**, suggesting that there may be a rapid interaction

between the two peptides. After incubating the peptide mixture for 24 hr at 4 °C, evaluation of the melting curve revealed a new  $T_m$  value at approximately 32 °C, along with the two previous values (Figure 2B). This trend continued after 3 days of incubation at 4 °C as mainly one unfolding transition was observed corresponding to a  $T_m$  of 39 °C (Figure 2C). After 14 days of incubation, the mixture of **PP<sub>E</sub>G-5E** and **PP<sub>K</sub>G-3** also showed mainly one transition with a slightly lower melting temperature of 35 °C (Figure 2D). These data suggest that each homotrimeric helix of the two peptides is re-assembling at 4 °C to form new heterotrimeric helices. As a control experiment, we facilitated heterotrimer formation between **PP<sub>E</sub>G-5E** and **PP<sub>K</sub>G-3** by thermal denaturation and re-annealing [8]. An equimolar mixture of each peptide (200  $\mu$ M) was heated to 95 °C for 15 min followed by incubation at 4 °C for 24 hrs. The thermal denaturation profile of the heated peptide mixture was found to be identical to the profile of the unheated sample after 14 days: mainly one transition with a  $T_m$  value of 35 °C (Figure 2D-dashed line). These results support the occurrence of strand exchange at 4 °C between the trimers of the **PP<sub>E</sub>G-5E** and **PP<sub>K</sub>G-3** peptides leading to heterotrimeric helices.

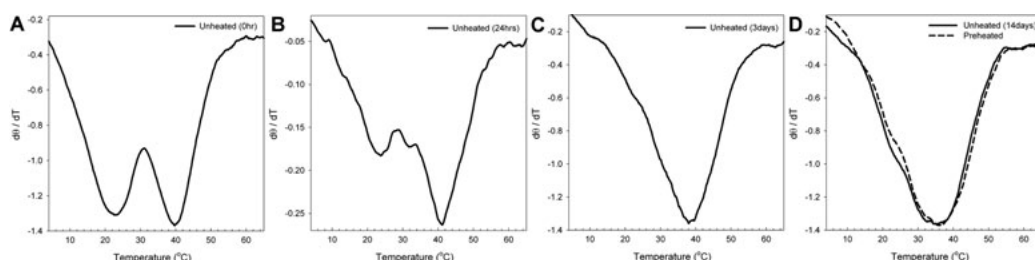


Fig. 2. The time course of strand invasion of **PP<sub>E</sub>G-5E** and **PP<sub>K</sub>G-3** (1:1 ratio, 200  $\mu$ M each) as monitored by CD spectroscopy at 4 °C in phosphate buffer, pH 7.0. Each graph represents the first derivative of unfolding versus temperature from thermal unfolding studies. (A) melting transitions observed immediately upon mixing the peptides, (B) after 24 hr incubation of the peptide mixture, (C) after 3 day incubation, (D) solid line - after 14 day incubation, and dashed line - the same peptide mixture after thermal annealing.

In conclusion, we have successfully demonstrated that charged collagen-based peptides can participate in strand exchange to form new heterotrimeric assemblies, an event that is presumably promoted by electrostatic interactions. Charged collagen-based peptides of this type may be helpful in understanding the behavior of fibril-associated collagens with interrupted triple helices [9] and may also play an interesting role in the modification of natural collagens.

## References

1. Lee, C.H., Singla, A., Lee, Y. *Int. J. Pharm.* **221**, 1–22 (2001).
2. Reddi, A.H. *Tissue. Eng.* **6**, 351–359 (2000).
3. Miles, C.A., Bailey, A. *J. Micron.* **32**, 325–332 (2001).
4. Wang, A.Y., Mo, X., Chen, C.S., Yu, S.M. *J. Am. Chem. Soc.* **127**, 4130–4131 (2005).
5. Mo, X., An, Y., Yun, C.S., Yu, S.M. *Angew. Chem. Int. Ed. Engl.* **45**, 2267–2270 (2006).
6. Lee, S.G., Lee, J.Y., Chmielewski, J. *Angew. Chem. Int. Ed. Engl.* **47**, 8429–8432 (2008).
7. Fillon, Y.A., Anderson, J.P., Chmielewski, J. *J. Am. Chem. Soc.* **127**, 11798–11803 (2005).
8. Gauba, V., Hartgerink, J.D. *J. Am. Chem. Soc.* **129**, 2683–2690 (2007).
9. Shaw, L.M., Olsen, B.R. *Trends Biochem. Sci.* **16**, 191–194 (1991).

## Site-Specific Delivery of BMP-2 Protein *via* Click Chemistry Derived Bifunctional Peptides

Shrikumar A. Nair, Krzysztof Krajewski, Guy Orgambide,  
and Paul T. Hamilton

Affinergy, Inc., 617 Davis Drive, RTP, Durham, NC 27713, U.S.A.

### Introduction

Growth factors are potent signaling molecules initiating essential cellular programs for differentiation, proliferation and survival. Recently these macromolecules have been deployed on medical devices to enhance the efficacy and specificity of medical therapies. Affinergy has developed bifunctional peptides that help promote biology at the critical interface between a biomaterial (collagen) or synthetic device materials (polymer, metals) and a biological material (growth factors, cells). Conjugating a peptide designed to bind a growth factor to another peptide designed to bind a medical device offer a simple and target-specific therapeutic strategy. Click chemistry was attempted as one such modular approach towards linking peptides in order to produce a combinatorial array of potential bifunctional peptides.

### Results and Discussion

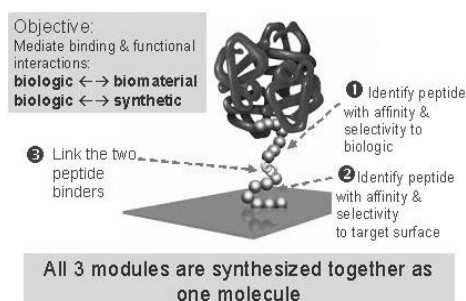


Fig. 1. Affinergy peptide bifunctional linker system.

Affinergy's bifunctional peptide linker system as outlined in Figure 1 is involved in mediating the interaction between a biologic and a biomaterial or a synthetic surface. All modules of the bifunctional peptides can be synthesized as one piece or the two peptide components can be synthesized separately and tethered together with a variety of linkers. Click chemistry as an example of later approach provides a rapid tool to build bifunctional peptides. In the present study, we demonstrate that bifunctional peptides synthesized using click chemistry improved the retention of BMP-2 onto a collagen matrix. We designed, synthesized and tested a panel of "collagen: BMP" peptides synthesized using this

[3+2] cycloaddition reaction. We optimized the reaction conditions and developed methods to facilitate the coupling of large (>15 mer) peptides in aqueous solution in a selective manner without altering the properties of the individual peptides and their resulting biological effects.

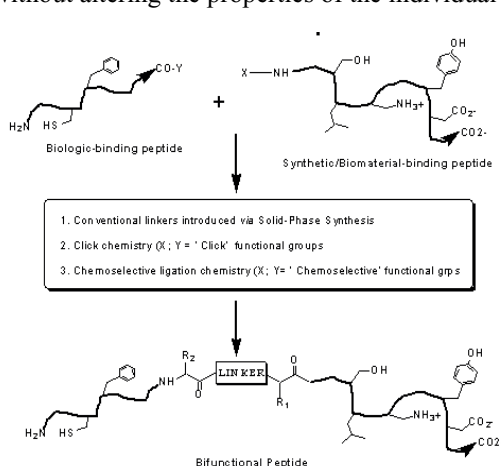


Fig. 2. Synthetic strategies for bifunctional peptides.

The synthesis strategies for bifunctional peptides is summarized in Figure 2. Click chemistry allows flexibility in the orientation of individual peptides within the bifunctional peptide framework. We developed click chemistry conditions that could be effectively used for the ligation of long, fully deprotected peptides in water or water/organic solvent mixtures. After evaluating several sets of click chemistry conditions such as sources of Cu(I), solvents, pH, temperatures, mixing/sonication, with/without stabilizer (TBTA), we determined that the published conditions [1,2] need several modifications in order to be compatible with our fully deprotected peptides.

The collagen peptide (AFF-0016) and BMP-2 binding peptide incorporating a linker was synthesized as one contiguous molecule using conventional peptide synthesis (AFF-7010). For click chemistry, the collagen-binding peptides and the BMP-2 peptides were derivatized using the click groups *via* alkyne and azide moieties at both peptide termini and then ligated using the modified click conditions to obtain products (AFF-7079) shown in Figure 3.

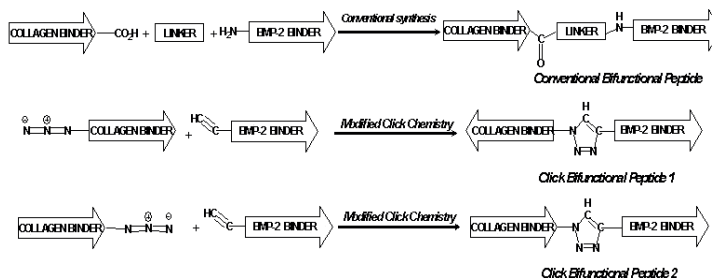


Fig. 3. Bifunctional peptides.

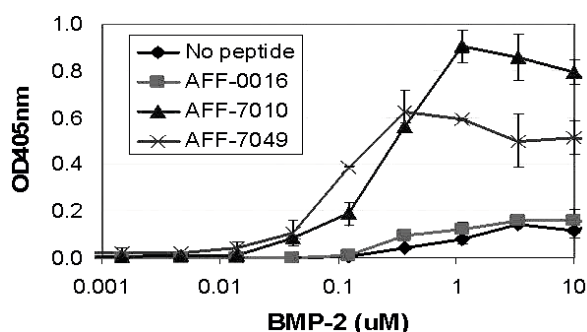


Fig. 4. Bifunctional peptides retain BMP-2 on collagen sponge.

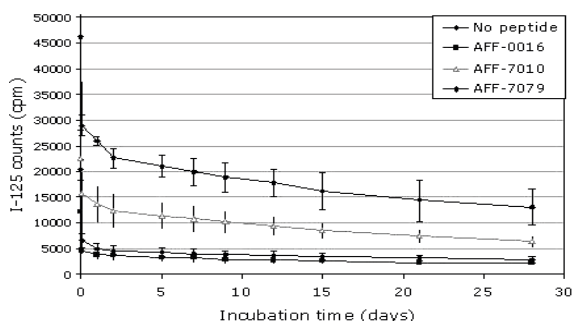


Fig. 5. Release of BMP-2 from peptide-coated collagen sponge.

## Acknowledgments

We thank Drs. Bruce Lamb, Hanne Gron, Nick Trotta, Laura Kiefer and Quinn Wickham for their support. Supported by National Institute of General Medical Sciences for partial support through SBIR Grant 1R43GM077753-01A1

## References

1. Tornøe, C.W., Christensen, C., Meldal, M. *J. Org. Chem.* **67**, 3057-3064 (2002).
2. Rostovtsev V.V., Green L.G., Fokin V.V., Sharpless K.B. *Angew. Chem. Int. Ed.* **41**, 2596-2599 (2002).

## Fabrication of Efficient Dye-Sensitized Solar Cells by Using Bulky Peptides

Mizuki Kitamatsu,<sup>1</sup> Yousuke Ooyama,<sup>2</sup> Yutaka Harima,<sup>2</sup>  
and Masahiko Sisido<sup>1</sup>

<sup>1</sup>Department of Medical and Bioengineering, Graduate School of Natural Science and Technology,  
Okayama University, 3-1-1 Tsushimanaka, Okayama 700-0082, Japan; and <sup>2</sup>Department of Applied  
Chemistry, Graduate School of Engineering, Hiroshima University, Higashi-hiroshima 739-8527, Japan

### Introduction

There has been an increasing interest in recent years in the issue of energy resources and CO<sub>2</sub> reduction. Therefore dye-sensitized solar cells (DSSCs) [1] that can be fabricated with low material and production costs have been receiving much attention as a means of resolving these issues. DSSCs have generally been prepared by adsorption of dyes (Ru complexes and metal-free organic compounds) on a TiO<sub>2</sub> substrate [2]. However, in many cases, adsorption of dyes causes aggregation of the dye molecules on the substrate. Therefore, DSSCs have an essential problem that the electronic injection through dyes decreases because the aggregation of dye molecules occasionally causes a self-quenching of the dye molecules. In this study, we report a new method that prevents aggregation of dye molecules on substrates and enables effective electronic injection through the dyes. For the new method, we used a dye modified with bulky peptide consisting of oligo(ethylene glycol)s. It was expected that the dye molecules would be adsorbed on the electrode without aggregation because of steric hindrance between the peptides.

### Results and Discussion

We synthesized peptides comprised of oligo(ethylene glycol)s, a tetramethyl rhodamine (TMR) modified on the N-terminus and two glutamic acids modified on the C-terminus by Fmoc-based solid-phase peptide synthesis. The structures of the peptides are shown in Figure 1. These peptides were identified by MALDI-TOF Mass. The N-terminus of these peptides is protected with an acetyl group and the C-terminus is a primary amide. The Lys(TMR) is utilized as a dye to transduce from photons to electrons. Two glutamic acids on the C-terminus play a role in adsorbance of the dyes on a TiO<sub>2</sub> substrate. We investigated the incident photons-to-current conversion efficiency (IPCE) spectra for dye-modified peptides on electrodes. Of the dye-modified peptides, maximum IPCE of TMR-G was the highest value (11.9%) as shown in Table 1.

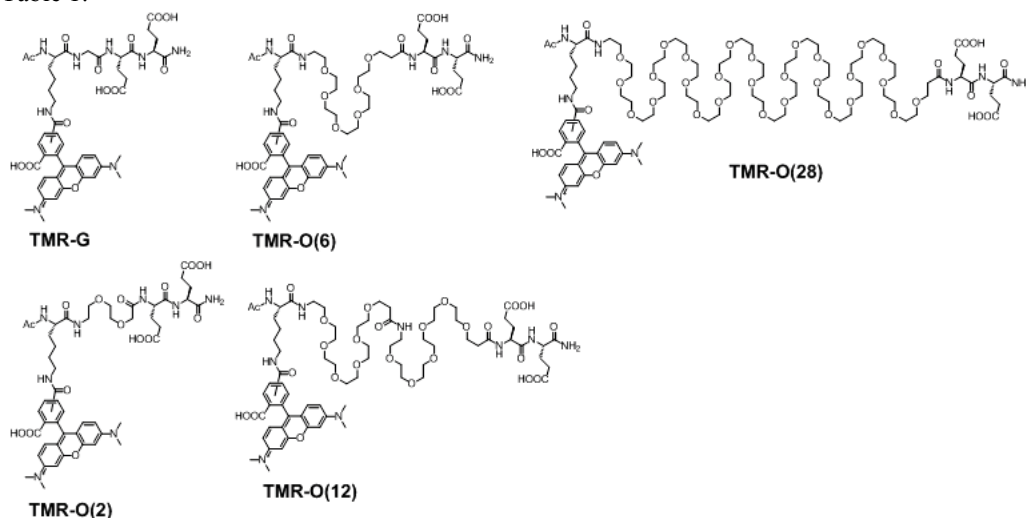


Fig. 1. Molecular structures of dye-modified oligo(ethylene glycol)s.

Table 1. Maximum IPCE, maximum wavelength, molecular area and maximum IPCE per molecule for DSSCs using oligo(ethylene glycol)-modified dyes

Sample	IPCE <sub>max</sub> (%)	Molecular area (nm <sup>2</sup> )	IPCE <sub>max</sub> /Molecules
5(6)-TMR	8.0	4.3	*1.0
TMR-G	11.9	18.5	6.1
TMR-O(2)	9.2	24.0	6.4
TMR-O(6)	9.4	34.3	7.5
TMR-O(12)	4.8	23.6	3.5
TMR-O(28)	4.5	49.2	5.9

Values of TMR-G, TMR-O(2) and TMR-O(6) were higher than that of 5(6)-TMR (8.0%). The dyes containing longer oligo(ethylene glycol) tended to show lower values of maximum IPCE.

We redissolved the dye-modified peptides adsorbed on electrodes in THF/DMSO/1 M NaOH aq and the dyes were measured by UV spectroscopy, which was used to determine the amount of dye-modified peptides adsorbed on the electrodes. We estimated molecular areas of the dye-modified peptides from the amounts and real surface area (1470 cm<sup>2</sup> for 1 cm<sup>2</sup> geometric area of the electrode). The molecular areas are listed in Table 1. The results indicate that the molecular area depends on chain length of oligo(ethylene glycol)s modified with the dyes. The molecular area tended to be larger when the chain length of oligo(ethylene glycol) was longer. For example, the molecular area of TMR-O(28) was approximately ten-times larger than that of 5(6)-TMR. This result indicates that the dyes are long away from the other dyes because of steric hindrance between peptides. This result also suggests that dye-modified peptides successfully control space between the dye molecules. Finally, we compared intensity of IPCE per dye molecule (IPCE max/Molecules) in Table 1. All dye-modified peptides have higher values than the value of 5(6)-TMR. The value of TMR-O(6) is highest in these peptides and the value of TMR-O(6) is 7.5-times higher than that of 5(6)-TMR.

In summary, we clarified that the performance of DSSCs was improved when dyes were adsorbed on electrodes through bulky peptides. First, we prepared DSSCs using dyes connected to oligo(ethylene glycol)s of various chain lengths by conventional SPPS. When the oligo(ethylene glycol)s in the peptides were longer, the density of the dye-modified peptide adsorbed on electrodes was lower due to steric hindrance between peptides. However, aggregation of the dye molecules can be prevented because of its steric hindrance. Also, the efficiency of conversion of photons to electrons per a dye molecule was ascended by virtue of elusion of the aggregation. Improvement in the performance of DSSCs using dyes connected to oligo(ethylene glycol)s depends on the density of dyes and the aggregation of dye molecules on electrodes.

## Acknowledgments

The authors gratefully acknowledge the financial contribution from DOWA Holdings CO., Ltd., Tokyo, Japan.

## References

- (a) O'Regan, B., Grätzel, M. *Nature* **353**, 737-740 (1991); (b) Nazeeruddin, M. K., Kay, A., Rodicio, I., Humphry-Baker, R., Muller, E., Liska, P., Vlachopoulos, N., Grätzel, M. *J. Am. Chem. Soc.* **115**, 6382-6390 (1993); (c) Grätzel, M. *Nature* **414**, 338-344 (2001).
- (a) Planells, M., Céspedes-Guirao, F.J., Forneli, A., Sastre-Santos, Á., Fernández-Lázaro, F., Palomares, E. *J. Mat. Chem.* **18**, 5802-5808 (2008); (b) Huang, S.-T., Hsu, Y.-C., Yen, Y.-S., Chou, H.H., Lin, J.T., Chang, C.-W., Hsu, C.-P., Tsai, C., Yin, D. J. *J. Phys. Chem. C* **112**, 19739-19747 (2008); (c) Erten-Ela, S., Yilmaz, M.D., Icli, B., Dede, Y., Icli S., Akkaya, E.U. *Org. Lett.* **10**, 3299-3302 (2008); (d) Wang, Z.-S., Koumura, N., Cui, Y., Takahashi, M., Sekiguchi, H., Mori, A., Kubo, T., Furube, A., Hara, K. *Chem. Mater.* **20**, 3993-4003 (2008).





**Author Index**  
**Subject Index**



- A**bate-Pella, Daniel 362  
 Abdel-Malek, Zalfa 126, 384  
 Acosta, Gerardo 48  
 Aditya, Animesh V. 264  
 Ahn, Jung-Mo 66, 70, 72, 74, 144, 260  
 Aimez, Vincent 35  
 Aimoto, Saburo 29, 298, 306  
 Akai, Yuichi 298  
 Akutsu, Hideo 306  
 Albericio, Fernando 48  
 Alexander, Shawn 217  
 Alvarez-Manilla, Gerardo 40  
 Andersen, Niels H. 386  
 Andrade, Iracema S. 128  
 Andreasen, Amy 119  
 Andreu, David 268, 334  
 Angel, Yvonne 164  
 Aoki, Yuko 314  
 Arriaga, Edgar A. 318  
 Arsenaault, J. 366  
 Arshava, Boris 64, 302  
 Ashihara, Motooki 314  
 Auriemma, Luigia 270, 280  
 Auriemma, Sara 48  
 Ausiello, Dennis A. 368  
**B**abinska, Anna 137  
 Bahekar, R.H. 68  
 Bailey, Jason 185, 191  
 Balint, Catherine 254  
 Bandyopadhyay, D. 68  
 Barany, George 353  
 Baruch, Amos 217  
 Bashkin, James K. 296  
 Becker, Jeffrey M. 64, 302  
 Bednárová, Lucie 282  
 Bekaii-Saab, Tanios 254  
 Belgi, Alessia 139  
 Bell, Robert G. 114  
 Benedek, George B. 187  
 Berezowska, Irena 183  
 Bersanetti, Patricia A. 360  
 Beyermann, Michael 316  
 Beyrath, Julien 355  
 Bhandari, Ashok 162, 164  
 Bhimani, Kajal 72  
 Bianchi, Elisabetta 215, 244, 249  
 Bianco, Alberto 355  
 Bindu, Lakshman 175  
 Binetti, Diego 276  
 Bionda, Nina 272, 276  
 Biondi, Barbara 284, 286  
 Bisello, Alessandro 144  
 Bitan, Gal 187, 189  
 Blanco-Canosa, Juan B. 33  
 Boeriu, Carmen 46  
 Boileau, Guy 223, 225  
 Bonelli, Fabio 249  
 Borgert, Andrew 353  
 Borovičková, Lenka 282  
 Bottaro, Donald P. 175  
 Bouley, Richard 368  
 Bourguet, Carine B. 76  
 Bours, Gilbert 46  
 Boutard, Nicolas 78  
 Bowerman, Charles J. 197  
 Brabez, Nabila 52  
 Braun, K. 246  
 Brothers, Franchesca 40  
 Broxterman, Quirinus B. 231, 370  
 Bruckdorfer, Thomas 44, 209  
 Bruckner, Hans 231  
 Buděšínský, Miloš 282  
 Burke, Terrence R. 102, 104, 175  
 Butler., Andrew A. 130  
 Byk, Gerardo 60  
**C**abralles-Rico, Ania 268  
 Cabrele, Chiara 343  
 Cai, Min Ying 300, 310  
 Cai, Weibo 323, 337  
 Cameron, Arlin G. 366  
 Campiglia, Pietro 270, 280  
 Caporale, Andrea 167  
 Carmona, Adriana K. 360  
 Caroccia, Katrina E. 64  
 Carotenuto, Alfonso 117, 280  
 Carroll, F. Ivy 42  
 Casarramona, Gemma Lahoz 193  
 Casciola, Allan 19  
 Catania, Anna 270  
 Čeřovský, Václav 282  
 Chabot, Vincent 35  
 Chaddha, Manjula 201  
 Chakraborti, G. 68  
 Chalupa, Donald 254  
 Chan, Linda 139  
 Charette, Paul G. 35  
 Chassaing, Gérard 52  
 Chatenet, David 133  
 Cheemala, Murthy N. 66, 70  
 Chen, Chao-Yu 93  
 Chen, Hang 135  
 Chen, Rui 39  
 Chen, Sylvia 368  
 Chen, Tianbao 135  
 Chen, Xiaoguang 82, 262  
 Cheng, Holland 88  
 Chmielewski, Jean 394, 396, 398  
 Choi, Won Jun 175  
 Choudhary, Amit 347  
 Chung, Nga N. 183  
 Chung, Woo Jin 332  
 Clark, Thomas D. 308  
 Clegg, Daniel J. 171  
 Clement, Cristina C. 137  
 Cohen, Leah S. 64, 302  
 Cooperman, Barry S. 80  
 Coppola, Teresa 52  
 Cordova, Jeanine 312  
 Crine, Philippe 223, 225  
 Crisma, Marco 231, 370, 376, 378  
 Cudic, Mare 276  
 Cudic, Predrag 272, 276  
 Cvačka, Josef 282  
**D**affre, Sirlei 274  
 Dagon, Djemile 84  
 Damato, Francesca 231  
 Darlak, Krzysztof 15  
 Davis, Matt 21, 23  
 Dawson, Philip E. 33  
 Day, Jonathan 146  
 Day, Jonathan W. 142  
 De, Arnab 160  
 Dealwis, Chris 80  
 Desai, Kunal 215  
 Devocelle, Marc 290  
 Diaz, Dolores 268  
 Dick, Fritz 25  
 Diego, Brancaccio 117  
 Dijken, Peter van 233  
 DiMarchi, Richard 146  
 DiMarchi, Richard D. 142, 153, 160, 177, 321  
 Dirain, Marvin 122  
 Dirain, Marvin L. 124, 126  
 Disatnik, Marie-Helene 221  
 Distefano, Mark 304  
 Distefano, Mark D. 318, 362  
 Do, Andrew 100  
 Domingues, Tatiana M. 274

- Dong, Jesse Z. 148  
Dong, Y. Sarah 162, 164, 169  
Doran, Todd M. 197  
Dore, Timothy 362  
Doti, Nunzianna 98  
Douglas, Alicia D. 17  
DuPont, Herbert L. 366  
**E**ckardt, J. 205  
Edison, Arthur S. 122  
Edwards, Terri G. 296  
Eggen, Ivo 46  
Ehrlich, Yigal H. 137  
Ernenwein, Dawn 394  
Escher, E. 366  
Escher, Emanuel 35  
Estephan, Racha 64  
**F**abian, Heinz 316  
Falciani, Chiara 48  
Fan, Qing 164  
Felix, Arthur M. 211  
Felock, Peter J. 231  
Feng, Jiawen A. 357  
Fernandez-Reyes, Maria 268  
Ferrari, Stefano 25  
Fields, Gregg B. 241  
Fillion, D. 366  
Finan, Brian P. 153, 321  
Finn, Thomas M. 27  
Fisher, Christopher 296  
Fisher, Robert J. 102, 175  
Fivash, Matthew J. 175  
Fleischhacker, H. 246  
Fok, Kam F. 296  
Formaggio, Fernando 231, 284, 286, 355, 370, 376, 390  
Fournier, Alain 133  
Fowler, Jeffrey 254  
Fowler, Wiley 88  
Foy, Kevin C. 252, 257  
Foy, Kevin Chu 254  
Fradinger, Erica A. 187  
Freed, Eric O. 102  
Frissen, Guus 46  
Fučík, Vladimír 282  
Fujiwara, Yuichiro 298  
**G**addi, Ludovica Marcellini  
Hercolani 280  
Galabov, Angel S. 227  
Galyean, Robert 155  
Gao, Guangzu 144  
Garber, David W. 201  
Gardella, Thomas J. 50  
Garrett, Joan 254  
Ge, Yuan-Wen 185  
Geho, W. Blair 150  
Gelfanov, Vasily M. 142, 146, 153, 321  
Geotti-Bianchini, Piero 355  
Ghirlanda, Giovanna 312  
Ghishan, Fayez K. 300  
Gibbs, Richard A. 264  
Gillies, Robert J. 325, 327  
Gini, Francesca 46  
Giubellino, Alessio 175  
Giulianotti, Marc 97  
Gobbo, Marina 286  
Gomez-Monterrey, Isabel 280  
Gordon, Thomas 19  
Grandbois, Michel 35  
Gravel, Denis 223, 225  
Green, Jennifer M. 164, 169  
Grever, Michael 254  
Grieco, Paolo 98, 117, 270, 280  
Groisman, Eduardo A. 292  
Grossman, Bryan 11  
Gu, Xianfeng 197  
Gu, Xuyuan 11  
Guan, Shuwen 62, 82, 262  
Guillemette, G. 366  
Guryanov, Ivan 390  
**H**ackeng, Tilman M. 193  
Hamada, Keisuke 388  
Hamel, Raymond Jr 35  
Hamilton, Brian S. 235  
Hamilton, Paul T. 400  
Handattu, Shaila P. 201  
Handl, Heather L. 327  
Hara, Toshiaki 298, 306  
Haramura, Masayuki 314  
Harding, David R. K. 239  
Harima, Yutaka 402  
Harrison, Steven 217  
Haskell-Luevano, Carrie 119, 122, 124, 126  
Haslach, Erica M. 124  
Hatam, Mostafa 223  
Hatfield, Marcus P. D. 349  
Hauser, Melinda 302  
Hawthorne, Susan 135  
Hayashi, Yoshio 54, 195, 278  
Hazuda, Daria J. 231  
He, Jianjun 382  
Heckmann, D. 205, 207  
Henklein, Petra 44  
Heusser, Andrew 97  
Heyl, Deborah L. 158, 171, 173  
Hirata, A. 106  
Hirayama, Yuta 195  
Hirota, Shun 195  
Hodges, Robert S. 266  
Hojo, Hironobu 37  
Holder, Jerry R. 122  
Holmes, Christopher P. 162, 164, 169  
Honek, John 392  
Hong, Anita 382  
Hopkins, Thomas E. 15  
Höppener, Jo W.M. 193  
Hoppmann, Christian 316  
Hossain, M. Akhter 139  
Houghten, Richard A. 97  
Hovorka, Oldrich 282  
Howl, John 372, 374  
Hrin, Renee 249  
Hruby, Victor 181  
Hruby, Victor J. 11, 111, 117, 179, 300, 310, 325, 327  
Hsieh, Jer-Tsong 72, 260  
Hu, Po 288  
Huang, Lei 82  
Huang, Xuemei 213  
Hull, J. Joe 345  
**I**keda, Keisuke 195  
Ingale, Sampat 33  
Ingallinella, Paolo 215, 249  
Inomata, Noriyuki 314  
Inoue, Tomio 388  
Ishii, Nobuya 314  
Ivanova, Galya 84  
Izzo, Irene 48  
**J**ain, M.R. 68  
Jamieson, Andrew G. 78  
Jarine, H. 366  
Jayaprakash, Anitha 173  
Jha, Shalini 80  
Jiang, Guangcheng 155  
Jiang, Zhi-Dong 366  
Jiang, Ziqing 266  
Jimenez-Barbero, Jesus 268  
Joharapurkar, A.A. 68  
Jones, Sarah 372, 374  
Josan, Jatinder S. 327  
Joyce, Joseph 244

- Jubilut, Guita N. 380  
**K**allenbach, Neville R. 288  
 Kandile, Nadia G. 239  
 Kane, Yahaira 254  
 Kaptein, Bernard 231, 370  
 Karim, Felix 217  
 Katayama, Hidekazu 37  
 Katzenmeyer, Joseph 318  
 Kaumaya, Pravin T.P. 252, 254, 257  
 Kaur, Jaskiran 80  
 Kavanagh, Renny 384  
 Kawai, Takeshi 345  
 Kawakami, Toru 29, 298, 306  
 Kawasaki, T. 106  
 Kawashima, Hiroyuki 13  
 Ke, Shi 366  
 Keiderling, Timothy A. 390  
 Kennedy, David A. 290  
 Kent, Michael 88  
 Kessler, H. 205, 207  
 Ketas, Thomas J. 249  
 Khatri, Ashok 50, 368  
 Khemtémourian, Lucie 193  
 Khurana, Sudha 330  
 Kier, Brandon L. 351, 386  
 Kiewitz, Sebastian D. 343  
 Killian, J. Antoinette 193  
 Kim, Myoung H. 72  
 Kim, Sung-Eun 175  
 Kimura, Tooru 13, 195  
 Kirschbaum, Jochem 231  
 Kiso, Yoshiaki 13, 54, 195, 203, 278, 343  
 Kitamatsu, Mizuki 402  
 Knight, Martha 27  
 Knittel, James J. 126, 384  
 Koeller, Kevin J. 296  
 Koerper, Lorraine M. 119  
 Koikov, Leonid 126, 384  
 Konda, Srikanth Reddy 173  
 Kondoh, Osamu 314  
 Kornecki, Elizabeth 137  
 Krajewski, Krzysztof 400  
 Kruijff, Ben de 193  
 Kukuch, Allison 177, 235  
 Kulp, John L. III 308  
 Kumar, K. Ganesh 130  
 Kumarasinghe, Isuru R. 179  
 Kumaresan, Pappanaicken R. 91  
 Kumirov, Vlad K. 11  
 Kung, Hsing-Jien 93  
 Kurokawa, Tatsuki 298  
 Kyro, Kelly 304  
**L**ahiri, Debomoy K. 185, 191  
 Lai, Josephine 179, 181  
 Lakhani, Ahmed 390  
 Lam, Kit S. 88, 91, 93, 100  
 Lamb, Tammy 254  
 Lambris, John D. 219  
 Langella, Annunziata 249  
 Latifi, Tammy 292  
 Lau, John R. 150  
 Lauer-Fields, Janelle L. 241  
 Laufer, Ralph 215  
 Lavielle, Solange 52  
 Leduc, R. 366  
 Lee, Jeeyeon 398  
 Lee, Joyce 88  
 Lee, Kwang-Soo 11  
 Lee, Kyung S. 104  
 Lee, Tae-Kyung 74  
 Lefebvre, M.-R. 366  
 Lehman, Alan 100  
 Lemieux, Carole 183  
 Lemire, Isabelle 223, 225  
 Létourneau, Myriam 133  
 Leu, Karen 162, 164  
 Lewin, Anita H. 42  
 Li, Fengying 382  
 Li, Fu-Peng 31  
 Li, Hongjian 213  
 Li, Huiyuan 187, 189  
 Li, Jing 300  
 Li, Pengfei 262  
 Li, Wei 62, 82, 237, 262  
 Li, Yuan-pei 88  
 Li, Yuanyuan 62, 262  
 Limesand, Sean W. 332  
 Lin, Feng 139  
 Linder, Karen E. 330  
 Liu, Chuan-Fa 31  
 Liu, Fa 102, 104, 175  
 Liu, Mian 40, 353  
 Liu, Zhenzhen 257  
 Liu, Zhigang 288  
 Liu, Zhihua 11, 300  
 Live, David 40, 353  
 Lomakin, Aleksey 187  
 Lorenz, P. 246  
 Lovas, Sandor 349  
 Lubell, William D. 56, 58, 76, 78, 86  
 Lui, Siu-Kei 382  
 Luo, Juntao 88  
 Lynch, Ronald 325, 332  
 Lynch, Ronald M. 327  
**M**a, Shou-Wu 179  
 Ma, Tao 146  
 Ma, Yi 213  
 Maclean, Derek 217  
 Maeda, Yoshiko 91  
 Magotti, Paola 219  
 Malfi, Stefania 270, 280  
 Maloney, Bryan 185  
 Mammi, Stefano 167, 231, 378  
 Manandhar, Surya 304  
 Mangoni, Maria Luisa 280  
 Mani, Aruna 254  
 Marasco, Daniela 98  
 Marco, Annalise Di 215  
 Marcozzi, Cristina 280  
 Marcucci, Eleonora 48  
 Marimganti, Srinivasa 66  
 Marinelli, Edmund R. 330  
 Maro, Salvatore Di 260, 270  
 Marsh, Donald J. 215  
 Marshall, Garland R. 292, 357  
 Martin, T. John 50  
 Martins, Marta N. C. 128  
 Matsumoto, Shogo 345  
 Matsuzaki, Katsumi 195  
 Mawad, Michel E. 366  
 Mayakonda, Palgunachari 201  
 Mayorov, Alexander 310  
 Mazaylerat, Jean-Paul 376  
 McDonald, Patrick 362  
 McElhinny, Charles J. 42  
 McElroy, K. Timothy 42  
 McLaughlin, Jay P. 97  
 McMahon, James B. 104  
 Meeldijk, Hans J.D. 193  
 Meloen, Rob H. 233  
 Menegazzo, Ileana 378  
 Menon, Aravind 257  
 Mierke, Dale F. 148  
 Milkova, Tsenka 84  
 Milkova, Tsenka S. 227  
 Miller, Megan 257  
 Miller, Michael D. 244, 249  
 Miranda, Antonio 128, 274  
 Mochly-Rosen, Daria 221  
 Monien, Bernhard H. 187

- Monincová, Lenka 282  
 Monroe, Candyce E. 201  
 Monteagudo, Edith 215  
 Moore, John P. 249  
 Moretto, Alessandro 355, 370, 376, 378  
 Mori, Yuki 54  
 Morimoto, Sayuri 314  
 Mortensen, Bruce 164  
 Moto, Ken-ichi 345  
 Mueller, Joachim 362  
 Mukai, Hidehito 195, 203  
 Mullen, Daniel 304, 318, 362  
 Munekata, Eisuke 203  
 Murage, Eunice N. 144  
 Murphy, Richard F. 349  
 Mutoh, Hironori 314  
 Mynatt, Randall L. 130  
**N**agano, Kohji 314  
 Nagasawa, Hiromichi 345  
 Nagata, Koji 345  
 Naider, Fred 64, 302  
 Nair, Shrikumar A. 400  
 Nakahara, Yoshiaki 37  
 Nakahara, Yuko 37  
 Nakaie, Clovis R. 360, 380  
 Nakamura, Ken'ichiroh 298, 306  
 Nanjappan, Palaniappa 330  
 Narayanan, Bitha 330  
 Nardi, Daniela T. 380  
 Nascimento, Nanci 380  
 Nayyar, Gaurav 201  
 Neubauer, S. 205  
 Neumoin, Alexey 302  
 Nicklaus, Marc C. 175  
 Nilsson, Bradley L. 197  
 Nishiguchi, Shigenobu 278  
 Nissan, David A. 197  
 Nokihara, K. 106  
 Novellino, Ettore 117, 270, 280  
 Nunn, Adrian D. 330  
 Nyberg, Joel 310  
**O**chocki, Joshua D. 318  
 Oda, Akiko 54  
 Ogata, Kazuhiro 388  
 Ohira, Tsuyoshi 37  
 Ohtsuka, Jun 345  
 Ohyama, T. 106  
 Oka, Y. 106  
 Okada, Akitoshi 345  
 Okada, Takuma 195  
 Okamura, Yasushi 298  
 Ooyama, Yousuke 402  
 Orgambide, Guy 400  
 Osafo, Nina D. 257  
 Osborne, Joshua M. 171  
 Osiek, Todd 19  
 Otterson, Gregory 254  
 Otto, E. 207  
**P**aisley, Brianna 181  
 Pan, Yijun 164  
 Park, Jung-Eun 104  
 Patel, H. 68  
 Patel, P.R. 68  
 Pathak, Priyanka 362  
 Patterson, James T. 142, 177  
 Pawar, V.D. 68  
 Pawlicki, Mark A. 235  
 Peddi, Durgaprasad 158  
 Pedone, Carlo 98  
 Peggion, Cristina 284, 286, 355, 370, 390  
 Peggion, Evaristo 167  
 Peier, Andrea 215  
 Penta, Kalyani 162, 164  
 Pereira, Jádson M. 128  
 Perelman, Alex 199  
 Pesaru, Ranadheer Reddy 158  
 Pessi, Antonello 215, 249  
 Philipp, Manfred 137  
 Phillips, Gary 257  
 Pilon, Aprile 27  
 Pipkorn, R. 246  
 Piserchio, Andrea 148  
 Plieger, Paul G. 239  
 Poli, Matteo De 370  
 Poloni, Claudia 286  
 Pong, Rey-Chen 260  
 Pope, Holly M. 296  
 Porecca, Frank 179  
 Portillo, Federico 126  
 Potts, John T. 50  
 Prakash, Halan 195  
 Proulx, Caroline 56  
 Przybyla, David E. 396  
 Puijk, Wouter C. 233  
**Q**ian, Ying 215  
 Qiu, Meilan 213  
 Qu, Hongchang 11, 219, 300  
 Qvit, Nir 221  
**R**ádis-Baptista, Gandhi 334  
 Rahimpour, Shai 199  
 Raines, Ronald T. 347  
 Raju, Natarajan 330  
 Rakhmanova, Vera 382  
 Ran, Yanhong 213  
 Ratemi, Elaref S. 223, 225  
 Rawale, Sharad 257  
 Rawale, Sharad V. 252, 254  
 Reddy, P. Anantha 42  
 Regnier, Thomas 278  
 Reilley, Kate J. 97  
 Rentsch, Daniel 25  
 Ribeiro, Eliane B. 128  
 Richman, Michal 199  
 Richter, Anja 316  
 Ricklin, Daniel 219  
 Ricq, Emily 52  
 Riske, Karin A. 274  
 Rivas, Luis 268  
 Rivier, Jean 155  
 Ronga, Luisa 86  
 Rosa, Jose C. 380  
 Rück-Braun, Karola 316  
 Ruvo, Menotti 98  
 Ruwe, Andrew R. 126  
 Ryan, Derek M. 197  
**S**abatella, Marco 98  
 Sabatino, David 58  
 Sabido, Portia Mahal G. 294  
 Sanii, Babak 100  
 Santoprete, Alessia 249  
 Sato, Takashi 306  
 Sato, Takeshi 298  
 Satyanarayanajois, Seetharama D. 384  
 Saviello, Maria Rosaria 280  
 Schatz, Peter J. 162, 164, 169  
 Schaub, Jay W. 119  
 Scheer, Liesbeth 193  
 Schievano, Elisabetta 167, 231  
 Schiller, Peter W. 183  
 Schmidt, Walter K. 304  
 Schmieder, Peter 316  
 Schreier, Shirley 360  
 Schteingart, Claudio 155  
 Schwach, Gregoire 155  
 Scian, Michele 386  
 Scognamiglio, Pasqualina L. 98  
 Seedorff, Sabine 316  
 Seki, Tetsuo 203  
 Senguen, F. Timur 197  
 Shabanpoor, Fazel 139

- Shapiro, Charles 254  
Shaw, Chris 135  
Shenoy, Shilpa R. 104  
Shinde, Sandip 312  
Shinkawa, Takashi 314  
Shishkov, Stoyan 227  
Sho, Eiketsu 217  
Shu, Irene 386  
Silva, Channa R. De 325, 332  
Silva, Murilo C. 380  
Singh, Anamika 122  
Singh, Sandeep K. 17  
Singh, Sheo B. 231  
Sisido, Masahiko 402  
Skirtenko, Natalie 199  
Skwarczynski, Mariusz 195  
Slaninová, Jiřina 282  
Slootstra, Jerry W. 233  
Sohma, Youhei 13, 195  
Soung, Nak-Kyun 104  
Spasova, Maya 84  
Spring, Sean M. 187  
Srivastava, Kripa 21, 23  
Stachelin, Christian 25  
Stalewski, Jacek 155  
Stankova, Ivanka G. 227  
Stawikowski, Maciej 272  
Steele, Miranda 19  
Stephen, Andrew G. 102, 175  
Stewart, James M. 386  
Stragies, R. 205, 207  
Straka, Jakub 282  
Su, Zhengding 213, 392  
Sunder, R. 68  
Suylen, Dennis 193  
Swenson, Rolf E. 330  
**T**aguchi, Akihiko 278  
Tainosho, Akira 306  
Takahashi, Nobukazu 388  
Takebayashi, Y. 106  
Tamagaki, Hiroko 298  
Tan, Maxilmilien Alaric O. 294  
Tang, Yat T. 292  
Taniguchi, Atsuhiko 195  
Tanokura, Masaru 345  
Tantry, Subramanyam J. 64  
Tateishi, Ukihide 388  
Taylor, Christina M. 357  
Teixeira, Luis G.D. 360  
Telles, Mônica M. 128  
Theeraladanon, Chumpol 388  
Thigpen, Antonio 15  
Timmerman, Peter 233  
Tolbert, Thomas J. 229  
Tolbert, Thomas J. 39, 177, 235  
Tong, Xiaohe 382  
Toniolo, Claudio 231, 284, 286, 370, 376, 378, 390  
Torre, Beatriz G. de la 268, 334  
Townsend, Jared 100  
Tregear, Geoffrey W. 139  
Treitl, Daniela 272  
Tsomaia, Natia 148  
Tulla-Puche, Judit 48  
Tumati, Suneeta 179  
**U**rbanc, Brigita 187  
**V**agner, Josef 325, 327, 332  
Valles-Miret, Mariona 268  
Vanier, Grace S. 17  
Varga, Eva 179  
Vasil, Adriana I. 266  
Vasil, Michael L. 266  
Veech, Sandralynn 211  
Veneziano, Maria 249  
Vicari, Daniele 252, 254  
Vijver, Pieter Van de 193  
Villardaga, Jean-Pierre 368  
Voburka, Zdeněk 282  
Vossmeier, D. 205, 207  
**W**ade, John D. 139  
Waheed, Abdul A. 102  
Wakselman, Michel 376  
Waldeck, W. 246  
Walker, Brian 135  
Walter, Sarah 217  
Wang, Jing 237  
Wang, Licheng 62  
Wang, Liping 62, 82, 262  
Wang, Wei 366  
Wang, Xiaobing 91  
Wang, Xueyun 237  
Wang, Yan 88, 91  
Wang, Ying-Jie 249  
Ward, Brian P. 153  
Wattenberg, Elizabeth 318, 362  
Weber, Craig S. 332  
Weidlich, Iwona 175  
Weltrowska, Grazyna 183  
Wester, H.-J. 205  
White, Rachel J. 239  
White, Richard 155  
White, Roger C. 201  
Whitehorn, Erik 169  
Wieczerek, Ewa 35  
Wiessler, M. 246  
Wilczynski, Andrzej 122  
Wilk, Sara 199  
Wilkes, Brian C. 183  
Williamson, Eric J. 17  
Winn, Melissa 27  
Witek, Rachel M. 122  
Wollack, James W. 318  
Woodburn, Kathryn 164  
Worthy, Karen M. 175  
Wortman, Matt 126, 384  
Woznica, Iwona 167  
Wright, Karen 376  
**X**iang, Zhimin 119, 126  
Xiao, Junpeng 229, 235  
Xiao, Kai 88  
Xiao, Wenwu 88  
Xing, Li 88  
Xu, Caiding 164  
Xu, Hua 300  
**Y**amazaki, Yuri 54  
Yang, Shijie 237  
Yao, Nianhuan 88  
Yin, Kevin 217  
Yoshiya, Taku 13  
Young, Anne W. 288  
Yu, Jiayi 237  
**Z**ahn, G. 205, 207  
Zeliadt, Nicholette 362  
Zeliadt, Nicholette A. 318  
Zemdeg, Juliana C. S. 128  
Zeng, Tao 213  
Zerbe, Oliver 64, 302  
Zhan, Jundong 148  
Zhang, Jingying 130  
Zhang, Shuhua 62, 262  
Zhang, Suode 139  
Zhang, Yingkai 288  
Zhong, Xiaofen 382  
Zhou, Chunhui 288  
Zhou, Jian 72  
Zhou, Tianhong 213  
Zhou, Xi 213  
Zhu, Ming 91  
Zingsheim, Morgan 310  
Zoelen, Dirk-Jan van 46  
Zotti, Marta De 231, 284, 286  
Zytka, Karolina 215



- $\alpha$ -amino  $\gamma$ -lactam (Agl) 86
- $\delta$  antagonist 179
- $\mu$  agonist 179
- 101.10 (rytvela) 86
- 2D NMR 384
- 5-TAMRA 382
- a**cid-catalyzed cyclization 54
- acute myocardial infarction 62
- acyclovir 227
- acyl-tetramate 60
- AFM 35
- aggregation 187,199
- aging 185
- AGRP 124
- a-helix mimetics 70, 72
- Aib 284, 355, 370
- albumin binding peptide 213, 219
- allosterism 76
- alpha-aminoisobutyric acid 290
- alpha-dystroglycan 40
- alpha-helical structures 282
- alpha-helix mimetics 66, 74
- alpha-methylalanine 290
- Alzheimer's disease 185,187, 189, 191,195,199
- amidation 46
- amide 160
- amphipathicity 282
- amphiphilic bis-benzamides 66
- amphiphilic tris-benzamides 70
- amylin 158, 171, 173, 193
- amyloid  $\beta$ -protein 185, 187, 189, 191,195, 197, 199
- Angiogenesis 252, 323
- angiotensin I 360
- angiotensin II 300, 360, 380
- angiotensin-converting enzyme 360
- anoplin 294
- anti-angiogenic 257
- anti-atherosclerosis peptides 137
- antibacterial activity 276, 292
- antibacterial peptide 284, 286
- antibiotics 60
- antibody 235
- antidiabetic 68
- antimicrobial activity 266, 268, 272, 274, 282, 290, 294
- antiparallel 308
- antitumor 257, 260
- antiviral 249, 296
- apoptosis 72
- arginine 44
- aromatic interactions 197
- asymmetric Michael addition 278
- Atomic Force Microscopy 35
- autofluorescence 100
- automated sorting 100
- automated synthesis 15
- aza amino acids 56
- Aza-peptides 58
- Aza-proline 56
- azido group 37
- b**acterial virulence 292
- BAFF 169
- BAFF antagonist 169
- Balb/c mice 169
- bee venom 282
- benzophenone 376
- beta amyloid 185
- beta hairpin 316, 349, 386
- Beta-Helix 308
- beta-turn 78, 370
- BH3 domains of Bak and Bad 72
- bile acids 227
- binding antagonist 104
- binding site 189
- Biopharmaceuticals 209
- Bisubstrate Inhibitors 264
- BMP-2 400
- bradykinin 181, 360, 380
- b-Sheets 351
- C**achexia 310
- CaCo-2 321
- Caenorhabditis elegans 262
- caged thiol 362
- calcitonin 153
- cancer 60, 323, 327, 337
- cancer targeting 88
- cancer therapeutic agent 388
- cancer therapy 252
- cancer vaccines 254
- candidacidal activity 270
- carbon nanotubes 392
- CD 86, 167
- CD36 56
- CDfss 19
- cell surface 91
- cell-penetrating peptide 52, 318, 334
- CFU-G colony assay 162
- chemical library synthesis 74
- chemical shift deviations (CSDs) 386
- chip-material 106
- circular dichroism 58, 78, 286, 384, 390

## Subject Index

- click chemistry 80, 195, 246, 400  
clinical trial 254  
*Clostridium difficile* 290  
CMC 114  
co-agonists 146  
coiled coil peptide 394  
collagen 396, 398  
combinatorial chemistry 88, 91, 97  
combinatorial library 100  
complement inhibitor 219  
compstatin 219  
computations 384  
COMU 15  
conformation 231, 233, 284, 286, 355, 384, 390  
conformational restriction 144  
conformational search 126  
conformational studies 280  
CPE peptide 29  
cross-linking 366  
crotamine 334  
cryptide 203  
C-terminal amide group 345  
C-terminal fragments 187, 189  
cyclic peptides 80  
Cysteine 19  
cytotoxicity 60, 268  
**d**e novo designed antimicrobial peptide 266  
DELFA 325  
delta opioid agonists 183  
delta opioid antagonists 183  
depot 155  
depsipeptide 48  
desulfurization 31  
DhHP-6 82, 262  
diabetes 130  
Diels-Alder 246  
diketopiperazine 54  
dimer of dimers 162  
dimerization 164  
dipeptide 54  
dipeptidic antibiotic 278  
dipeptidyl peptidase-IV 144  
discontinuous 233  
disulfides 351  
DL-peptides 308  
DNA binding 185, 296  
DNA-protein interaction 185  
docking 357  
DOPA 366  
DOTA 330, 332  
DPPH test 84  
drug delivery 88, 400  
drug design 111, 292  
Duchenne muscular dystrophy 278  
dye-sensitized solar cell 402  
dynorphin 181  
**E**lectrostatic interaction 398  
ELISA 98  
enzymatic stability 144, 355  
enzyme 46  
epitope 233  
epitope mimetic 244  
EPR 360  
ester 160  
exenatide 237  
Exendin-4 177  
exercise 119  
exosite 241  
ex-vivo colony assay 164  
**F**c fusion 177  
FK228 analogues 260  
fluorescent labeling 40  
Fmoc-AA-Wang Resin Quality 25  
FoF1-ATP Synthase 306  
Freidinger lactam 78, 86  
FRET 382  
frog 135  
fusaricidin A 272  
**γ** radiation 380  
GAP 388  
G-CSF 162, 164  
gene regulation 185  
gene transcription 185  
geranylgeranyltransferase-I 264  
GHRP-6 56, 78  
GHSR-1a 56  
Gi protein 203  
GLP-1 146, 153, 160, 177, 235, 321, 332  
GLP-1 Agonist 68  
GLP-1 analog 148  
glucagon 142, 146, 153  
glucagon-like peptide-1 66, 70, 142, 144, 148  
glucose 130  
glybeclamide 332  
glycopeptide 33, 37, 40, 106, 353  
glycoprotein 235  
GMP 114  
GnRH antagonist 155  
gomesin 274  
GPCR 76, 302  
growth hormone 150

- Growth Hormone-Releasing Factor 211
- GUV 274
- h**alf-life 213
- halictus sexcinctus 282
- HDAC inhibitors 260
- head-to-tail cyclization 17
- heart-type fatty acid-binding protein 62
- helical amphiphilicity 66, 70
- helical peptide 231, 390
- helix 284
- helix-loop-helix 343
- hemolytic activity 266
- Hemopressin 42
- hepatocyte targeting 150
- HER-2 254, 257
- heterobivalent ligands 327
- heteromultivalency 327
- high throughput screening 100
- hippuric acid 294
- histone 31
- HIV 235
- HIV entry inhibitor 229
- HIV-1 102
- HIV-integrase 231
- hormone 130
- HPV 296
- HPV16 296
- HSQC HR-MAS NMR 25
- Huisgen cycloaddition 264
- human islet amyloid polypeptide 158, 171, 173
- hydrolysis 46
- hydrophobic interactions 197
- hydroxyaspartic acid 276
- hydroxycinnamoyl amino acid amides 84
- hydroxyproline 231
- hyperstable 351
- hypoxia 82
- I**APP 193
- Id protein 343
- IgG 177
- imaging 205, 366
- imaging agent 388
- immunoglobulin G 177
- incretin 68
- inhibit 175
- inhibitor 98, 135, 158, 175, 235
- inhibitors of F11R/JAM-A 137
- insulin 150, 158, 171
- insulin resistance 237
- insulin superfamily 139
- integrin 205, 207
- Integrin  $\alpha v \beta 3$  337
- interleukin-1 receptor antagonist 86
- iso peptide 195
- isoprenoid 304
- K**atanosin B 276
- knockout mouse 119
- l**actam bridges 144
- lanthanide-based binding assay 325
- LC-MS 314
- Leishmania 268
- leptin fragments 128
- LHRH-II analogs 330
- library diversification 104
- lifespan 262
- ligands 91
- ligation 29, 298
- light-controlled binding 316
- lipidated peptidotriazoles 264
- lipidation 249
- lipodepsipeptides 272
- lipopeptaibol 284
- liver 130
- long duration 155
- lysine trimethylation 268
- m**acrocycles 376, 378
- matrix metalloproteinase 241
- MC1R selective 126
- MC4 117
- MC4R 119, 122, 124
- mechanism of action 274
- melanocortin 117, 119, 122, 124, 126, 270, 310
- melanocortin agonists 384
- melanocortin receptor 325
- membrane 158, 171, 173
- membrane protein 298
- metal-trigger 396
- micellar electrokinetic chromatography 318
- microarray 106
- microwave 17
- mini protein 349
- mitocryptide 203
- MMPs 382
- molecular imaging 323, 337
- molecular machines 378
- molecular modeling 126, 292
- monoclonal antibodies 233
- mouse models of neutropenia 164
- MTII 117
- MUC2 353
- mucin 353

- multivalent ligands 111
- muscle-eye-brain disease 40
- mutagenesis 164
- myocardial infarction 82
- N**-acylurea 33
- native chemical ligation 33, 35, 193
- N-capping 126
- NCL 35
- negamycin 278
- neuron 191
- neurotoxicity 187, 189
- neutral endopeptidase 24.11 144
- neutrophil 203
- neutrophilic activity 164
- NHE3 300
- NK1 antagonist 179
- N-linked glycopeptides 39
- NME 68
- N-methylation 48
- N-methylimidazole 296
- N-methylpyrrole 296
- NMR 117, 302, 345, 353
- NMR structure 148
- nocodazole 314
- non-covalent interactions 347
- N-terminal modification 17
- nucleolar localization 334
- nucleopeptides 355
- nucleus 191
- O**-acyl isodipeptide unit 13
- O-acyl isopeptide method 13
- O-acyl-isopeptide 343
- obesity 119, 122, 215
- OBOC 91
- on resin glycosylamine coupling 39
- one-bead-one-compound (OBOC) 93, 100
- opioid 181
- opioid peptides 183
- opsin 357
- oral peptide 150
- organic synthesis 378
- O-to-N intramolecular acyl migration 13
- ovarian cancer 330
- oxidation 19
- oxidative stress 191
- oxime ligation 205
- Oxyma 15
- P**ain 181
- PEG 35, 215
- PEGylated dimers 169
- PEGylation 162, 164, 209, 211, 217
- penicillamine 31
- peptaibiotic 286
- peptide agonist 162, 164
- peptide antagonists 169
- peptide conformation 370
- peptide conjugation 294
- peptide design 111, 244
- peptide drugs 111
- peptide library 62
- peptide mimetic 76, 78, 102, 104, 252, 257
- peptide purification 306
- peptide self-assembly 197
- peptide stability 111
- peptide synthesis 27, 270, 280, 298
- peptide therapeutic 215, 217, 249
- peptide thioester 29
- peptidomimetic 68, 167, 205
- peptoid 102, 175
- phage display 169
- pharmacokinetic 44, 209
- pharmacology 177
- phase 1 114
- pH-dependent 394
- phenylalanine analogues 183
- pheromone biosynthesis-activating neuropeptide (PBAN) 345
- PhoP/PhoQ 292
- phosphonium 15
- phosphopeptide 33
- phosphorylation 314
- photoactive 304
- photoaffinity-labeling 304
- photochemistry 376
- photocleavable-linker 306
- photolabile protecting group 362
- photoswitchable peptide 316
- phylogenetic analysis 139
- $\pi$  stacking 173
- plinabulin 54
- polo box domain 104
- polo-like kinase 1 104
- polyamide 296
- POMGnT1 40
- PPII helix; RCM macrocyclization 102
- prematurity 76
- prenylated peptide 318
- prenylation 304, 362
- privileged structure 60
- prodrugs 160, 227
- product specifications 114

## Subject Index

- proline 370
- prostate cancer 135, 155
- protease 135, 241
- protein design 244
- protein finger prints 106
- protein kinase C 221
- protein mimicry 233
- protein modification 229
- protein structure and stability 347
- proteinous microsphere 199
- protein-protein interactions 221
- proteins 114
- proteolysis 304
- proton channel 298
- PTH 167
- purification 27, 203
- pyrazinamide 294
- pyruvoyl group 37
- Quality** 114
- quantum dot 337
- quencher 382
- Racemization** 15
- racemization free 13
- radio-labelled 76
- radiotherapeutics 330
- ras converting enzyme 1 304
- ras protein 362
- RCE1 304
- receptor combination approach 327
- recombinant synthesis 27
- regulatory 114
- relaxin 139
- renal insufficient rat model 217
- reoxgenation 82
- rhodopsin 357
- ribonucleotide reductase inhibitors 80
- rotaxane 378
- SAR** 189
- screening 382
- segment condensation 13, 42
- self-assembly 396
- self-depoting 155
- SH2 domain 175
- Shc 175
- short peptides 384
- SHU9119 117
- side-chain chirality 390
- SII 300
- simplified peptide libraries 98
- Sir2.1 262
- Sirt1 237
- skin 135
- snake toxin 334
- solid phase 39
- solid phase peptide synthesis 17, 48, 74, 78, 139, 246, 260, 264, 294, 325, 332
- solution phase synthesis 42, 52
- specific targeting 327
- spectroscopy 349
- spiral countercurrent chromatography 27
- SPPS 15
- SPR 35
- stability 44
- stereoelectronic effects 347
- strand exchange 398
- structural minimization 334
- structural optimization 146
- structure 302, 349
- submonomer Aza-peptide synthesis 58
- SUR1 332
- surface plasmon resonance 35
- SynPhase lanterns 86
- synthetic peptides 254
- synthetic vaccine 244
- Taspoglutide** 148
- Tat 321
- temporal analysis 314
- temporins 280
- therapeutic index 266
- thioacid capture ligation 31
- thioester 33
- thioester method 37, 298
- three cysteines 162
- Thymosin  $\alpha$ 1 211
- TMPRSS2 135
- TMR 402
- Tn antigen 353
- TNF-  $\alpha$  310
- TOAC 360
- tolerance 179
- total synthesis 278
- toxic protein 106
- transcription factor 185, 191
- transducin 357
- transesterification 46
- transgenic 130
- transition state analog 241
- transmembrane 302
- transmembrane helices 306
- transport 321
- tripeptides 126

## *Subject Index*

triple-helical peptide 241  
tris-benzamides 72, 74  
TrNOE 357  
trypsin 44  
Tryptophan 351  
Tsg101 102  
tubulin 54  
two-component signal transduction 292  
type 2 diabetes 237  
type II transmembrane serine protease 135  
Tyrosine sulfation 93  
**U**ronium 15  
urotensin II-related peptide 133  
UT 133  
**V**accine 233  
VCD 349  
VEGF 252, 257  
vibrational circular dichroism 349  
virtual screening 292  
yeast 235  
**Z**Y-GLP-1 68

## *Subject Index*